to Pat C

PENNSTATE

DOE/PC/92162--T11-Vol.1

THE DEVELOPMENT OF COAL-BASED TECHNOLOGIES FOR DEPARTMENT OF DEFENSE FACILITIES

Phase I Final Report
Volume 1: Technical Report

By

Bruce G. Miller, Joel L. Morrison, Sarma V. Pisupati, Roger L. Poe, Reza Sharifi, Joseph F. Shepard, Peter M. Walsh, Jianyang Xie, and Alan W. Scaroni
Energy and Fuels Research Center
The Pennsylvania State University;
Richard Hogg, Subhash Chander, Heechan Cho, M. Thaddeus Ityokumbul, Mark S. Klima, and Peter T. Luckie
Mineral Processing Section
The Pennsylvania State University;
Adam Rose, Sam Addy, Timothy J. Considine, Richard L. Gordon, Jeffrey Lazo, Katherine McClain, and A. Michael Schaal
Department of Mineral Economics
The Pennsylvania State University;
Paul C. Painter and Boris Veytsman
Polymer Science Program
The Pennsylvania State University; and
Donald Morrison, Donald Englehardt, and Todd M. Sommer
Energy and Environmental Research Corporation

January 31, 1997

Work Performed Under Cooperative Agreement No. DE-FC22-92PC92162

For
U.S. Department of Energy
Federal Energy Technology Center
P.O. Box 10940
Pittsburgh, Pennsylvania 15236

By
The Consortium for Coal-Water Slurry Fuel Technology
The Pennsylvania State University
C211 Coal Utilization Laboratory
University Park, Pennsylvania 16802

THE DEVELOPMENT OF COAL-BASED TECHNOLOGIES FOR DEPARTMENT OF DEFENSE FACILITIES

Phase I Final Report
Volume 1: Technical Report

By

Bruce G. Miller, Joel L. Morrison, Sarma V. Pisupati, Roger L. Poe, Reza Sharifi, Joseph F. Shepard, Peter M. Walsh, Jianyang Xie, and Alan W. Scaroni
Energy and Fuels Research Center
The Pennsylvania State University;
Richard Hogg, Subhash Chander, Heechan Cho, M. Thaddeus Ityokumbul, Mark S. Klima, and Peter T. Luckie
Mineral Processing Section
The Pennsylvania State University;
Adam Rose, Sam Addy, Timothy J. Considine, Richard L. Gordon, Jeffrey Lazo, Katherine McClain, and A. Michael Schaal
Department of Mineral Economics
The Pennsylvania State University;
Paul C. Painter and Boris Veytsman
Polymer Science Program
The Pennsylvania State University; and
Donald Morrison, Donald Englehardt, and Todd M. Sommer
Energy and Environmental Research Corporation

January 31, 1997

Work Performed Under Cooperative Agreement No. DE-FC22-92PC92162

For
U.S. Department of Energy
Federal Energy Technology Center
P.O. Box 10940
Pittsburgh, Pennsylvania 15236

By
The Consortium for Coal-Water Slurry Fuel Technology
The Pennsylvania State University
C211 Coal Utilization Laboratory
University Park, Pennsylvania 16802

DISCLAIMER

EXECUTIVE SUMMARY

The first phase of a three-phase project investigating the development of coal-based technologies for Department of Defense facilities has been completed. The objectives of the project are to: decrease DOD's dependence on foreign oil and increase its use of coal; promote public and private sector deployment of technologies for utilizing coal-based fuels in oil-designed combustion equipment; and provide a continuing environment for research and development of coal-based fuel technologies for small-scale applications at a time when market conditions in the U.S. are not favorable for the introduction of coal-fired equipment in the commercial and industrial capacity ranges. The Phase I activities were focused on developing clean, coal-based combustion technologies for the utilization of both micronized coal-water mixtures (MCWMs) and dry, micronized coal (DMC) in fuel oil-designed industrial boilers. The specific objective in Phase I was to deliver fully engineered retrofit options for a fuel oil-designed watertube boiler located on a DOD installation to fire either MCWM or DMC. This was achieved through a project consisting of fundamental, pilot-scale, and demonstration-scale activities investigating coal beneficiation and preparation, and MCWM and DMC combustion performance. In addition, detailed engineering designs and an economic analysis were conducted for a boiler located at the Naval Surface Warfare Center, near Crane, Indiana.

Coal Beneficiation and Preparation Studies

Samples of six coals representing a range in the relative processing complexity required to meet sulfur and ash specifications for use in fuel oil-designed boilers have been procured. Each of the samples has been subjected to extensive characterization by float-sink analysis to determine the required level of cleaning. Some of these coals, and much of the potential reserve base, cannot be cleaned to the <5% ash, <1% sulfur specification by conventional means. Preliminary liberation models have been developed in order to establish appropriate (conventional) cleaning strategies. Fine-coal cleaning processes including fine gravity separations and surface-based processes such as froth flotation and selective agglomeration have been evaluated for their applicability to those coals which require fine grinding to achieve the necessary liberation. The factors which determine the size consist required for MCWM and the grinding/classification systems needed to obtain the desired size distribution have also been investigated. A dry coal cleaning system based on tribolelectrostatic separation has been evaluated particularly for DMC applications where dry cleaning would be preferred over wet cleaning.

MCWM and DMC Combustion Performance Evaluation

The combustion performance evaluation included conducting fundamental studies to determine the effect of the mineral matter on boiler tube erosion and deposition, identify the mechanism of atomizer wear (corrosion or erosion), and computationally model the burner and boiler. In addition, MCWMs and DMC produced from the candidate coals were fired in 1,000 and

15,000 lb steam/h watertube boilers. The fuels were fired in the 1,000 lb steam/h boiler in order to determine their relative performance while one of the coals was used in two demonstrations firing DMC and MCWM in the 15,000 lb steam/h boiler (which is of similar size to the retrofit candidate at Crane). The accomplishments on this aspect of the project include: modifying and optimizing a full-scale boiler system to fire DMC and MCWM; integrating the coal storage, handling, and micronization with the burner (for DMC firing); achieving 95% combustion efficiency (DMC); determining that erosion is not significant in the convective pass; and meeting targeted NO_x emissions of <0.6 lb/MM Btu.

Engineering Design

Two engineering studies were performed for the complete retrofit of a DOD boiler to fire either DMC or MCWM. Each design package includes a fuel preparation system (for the DMC option only; two conceptual MCWM processing circuits were prepared but not engineered), fuel delivery and handling systems, low-NO_x burner, baghouse, forced-draft fan, combustion air preheaters, induced-draft fan, ash silo, stack, and control system. The retrofit designs conform to accepted engineering practices and site requirements. The designs were based on the system in place at Penn State and the information that was learned from operating it. The design packages are intended to be used for soliciting bids from engineering/construction firms for completion of the detailed design, construction, and start-up of the candidate DOD boiler.

Cost/Economic Analysis

With respect to direct capital and operating cost considerations, *retrofit* DMC and MCWM technology boilers are not economically viable over a broad range of parameters for the Crane Site. For boiler retrofits to become economically viable, capital cost must be reduced, transportation costs of MCWM must be reduced, higher performance must be attained, and demand for slurry fuel in any given local area must be increased. Improving these parameters would increase the price differential of the DMC and MCWM with respect to fuel oil and natural gas.

With respect to direct capital and operating cost considerations, *new* DMC and MCWM technology boilers are not economically viable over a broad range of parameters for the Crane Site. There does not exist a sufficient critical mass of military boilers in one location to transform this into a viable option. For new DMC and MCWM technology boilers to become economically viable, capital costs and boiler derating must be reduced, higher performance must be attained, or fuel costs must be lowered.

Retrofit capital costs, followed by transportation costs, are the major inhibiting factors to the economic viability of MCWM technology at the Crane site. DMC delivered fuel costs are insensitive to fuel demand level. Transportation costs can be improved by developing a lower cost system of transportation dedicated solely to coal. With respect to environmental regulations, DMC and MCWM technologies are economically viable under a broad range of circumstances. Given

the small size of industrial boilers, existing pollution control devices will adequately meet environmental regulations. The regional multiplier effects of DMC and MCWM technologies are not significant for cases of less than 10 and 15 Crane size-equivalent installations, respectively, in a substate area. Regional multiplier effects can be significantly enhanced by purchasing more inputs from local vendors, though the sites where this is possible are limited.

TABLE OF CONTENTS
Volume 1: Technical Report

TABLE OF CONTENTS (cont.)

LIST OF FIGURES

LIST OF TABLES

1.0 INTRODUCTION

The U.S. Department of Defense (DOD), through an Interagency Agreement with the U.S. Department of Energy (DOE), initiated a three-phase project with the Consortium for Coal-Water Slurry Fuel Technology in September 1992, with the aim of decreasing DOD's reliance on imported oil by increasing its use of coal. The project is being conducted as a cooperative agreement between the Consortium and DOE. The first phase has been completed and is reported herein.

The introduction of the report consists of an outline of the DOD project and a brief discussion of two related and concurrent projects being conducted at Penn State.

1.1 DOD Project Outline

The general objectives of the cost-shared cooperative agreement are to:

1. Establish a National Center of Excellence for Coal Utilization to decrease DOD dependence on foreign oil and increase its use of coal by pursuing a program of research and development and actively participating in technology transfer;
2. Promote both the public and private sector deployment of technologies for utilizing coal-based fuels in oil-designed combustion equipment; and
3. Provide a continuing environment for research and development of coal-based fuel technologies for small-scale applications at a time when market conditions in the U.S. are not favorable for the introduction of coal-fired equipment in the commercial and industrial capacity ranges.

To achieve the objectives of the project, a team of researchers was assembled and the members of the Consortium for the Phase I activities were Penn State (Energy and Fuels Research Center (EFRC), Mineral Processing Section, Department of Mineral Economics, and Polymer Science Program) and the Energy and Environmental Research Corporation (EER). AMAX Research and Development Center was a member but withdrew.

Phase I activities were focused on developing clean, coal-based combustion technologies for the utilization of both micronized coal-water mixtures (MCWMs) and dry, micronized coal (DMC) in fuel oil-designed industrial boilers. These technologies were identified by the U.S. Corps of Engineers, Construction Engineering Research Laboratory as the two top priorities from a list of six topics for initial Center focus[1]. Phase II research and development continues to focus on industrial boiler retrofit technologies by addressing emissions control. Phase III activities expand upon emissions characterization and control from coal-fired boilers. Each phase includes an engineering cost analysis and technology assessment. The activities for Phase I are described below.

The specific objective in Phase I was to deliver fully engineered retrofit options for a fuel oil-designed watertube boiler located on a DOD installation to fire either MCWM or DMC. This was achieved through the following five tasks: 1) Coal Beneficiation/ Preparation; 2) Combustion

Performance Evaluation; 3) Engineering Design; 4) Engineering and Economic Analysis; and 5) Final Report/Submission of Design Package. Following is an outline of the tasks that comprised Phase I:

Task 1: Coal Beneficiation/Preparation

- Subtask 1.1 Identify/Procure Coals
- Subtask 1.2 Determine Liberation Potential
- Subtask 1.3 Produce Laboratory-Scale Quantities of MCWMs
- Subtask 1.4 Develop Dry Coal Cleaning Technique
- Subtask 1.5 Produce MCWMs and DMC From Dry Clean Coal
- Subtask 1.6 Produce MCWM and DMC for the Demonstration Boiler

Task 2: Combustion Performance Evaluation

- Subtask 2.1 Boiler Retrofit
- Subtask 2.2 Fuel Evaluation in the Research Boiler
- Subtask 2.3 Performance Evaluation of the MCWM and DMC in the Demonstration Boiler
- Subtask 2.4 Evaluate Emissions Reductions Strategies

Task 3: Engineering Design

- Subtask 3.1 MCWM/DMC Preparation Facilities
- Subtask 3.2 Fuel Handling
- Subtask 3.3 Burner System
- Subtask 3.4 Ash Removal, Handling, and Disposal
- Subtask 3.5 Air Pollution Control
- Subtask 3.6 Integrate Engineering Design

Task 4: Engineering and Economic Analysis

- Subtask 4.1 Survey Boiler Population/Identify Boilers for Conversion
- Subtask 4.2 Identify Appropriate Cost-Estimating Methodologies
- Subtask 4.3 Estimate Basic Costs of New Technologies
- Subtask 4.4 Process Analysis of MCWM and DMC
- Subtask 4.5 Analyze/Identify Transportation Cost of Commercial Sources of MCWM and Cleaned Coal for DMC Production
- Subtask 4.6 Determine Community Spillovers
- Subtask 4.7 Regional Market Considerations and Impacts
- Subtask 4.8 Integrate the Analysis

Task 5: Final Report/Submission of Design Package

1.2 Complementary Activities at Penn State

Penn State has been investigating the utilization of coal-based fuels in fuel oil-designed industrial boilers since 1983. Two projects which are related to the DOD project and are being conducted concurrently are the Superclean Coal-Water Slurry (SCCWS) and the ABB Combustion Engineering, Inc. (ABB CE) Dry Micronized Coal (DMC) projects.

The SCCWS project started in August 1989 with the DOE objective of developing a SCCWS infrastructure capable of providing the fuel auxiliary equipment, and the combustion systems needed to commercialize the technology of burning superclean coal-water slurry in oil-designed industrial boilers, when the economic justifications are realized[2]. The project was

completed in two phases. In the first phase, an oil-designed industrial boiler system was modified to handle and fire SCCWS[3]. The system was operated over eleven months (January to November 1992) using a modified heavy oil atomizer, and fired SCCWS for 500 hours, achieved 95% coal combustion efficiency (with 15% natural gas cofire based on thermal input), and established that erosion was not significant in the convective pass. The Phase II testing was conducted from February to July 1996 and included firing No. 6 fuel oil and evaluating the effect of coal particle size (produced through staged-grinding using coals with varying hardness) on combustion performance. Coal combustion efficiency increased as the coal particle size decreased[3].

Penn State was selected by ABB CE to be the host site in a DOE-funded project with the objective of developing and integrating all the system components for burning DMC in oil-designed industrial boilers, from fuel through total system controls, and then test the complete system in order to evaluate potential marketability[4]. The demonstration boiler testing started at Penn State in January 1993 and the proof-of-concept phase was conducted from July 1993 to April 1994. In this phase, an oil-designed industrial boiler system was modified to produce, handle, and fire DMC. The coal storage, handling, and micronizing was integrated with the burner and the system operated over ten months with 95% coal combustion efficiency and NO_x emissions below the target of <0.6 lb/million Btu[5]. A 1,000-hour demonstration was conducted from July 1995 to February 1996, which was after Phase I of the DOD project was completed, and addressed improved coal handling, ash deposition effects, and improved aerodynamic control of the fuel and air streams to improve the combustion efficiency and NO_x emissions. Coal combustion efficiency of >98% was achieved while maintaining the NO_x emissions target of 0.6 lb/million Btu.

In Phase I of the DOD program, the emphasis was to improve upon the burner/boiler performance obtained during Phase I of the SCCWS and ABB CE projects when using a commercial coal-designed burner that was identified for, and designed into, the DOD boiler retrofit. The DMC and MCWM demonstrations were conducted from May to December 1994 and from January to April 1995, respectively.

1.3 Phase I Final Report Presentation

The presentation of the results from Phase I begins with the DOD boiler survey and the selection of a boiler for the retrofit design. This is followed by a discussion of the coal beneficiation/preparation activities, combustion performance evaluation, engineering design, and an engineering and economic analysis. The coal beneficiation/preparation activities include identifying candidate coals for retrofit applications, fundamental beneficiation and preparation studies, and the preparation of DMC and MCWM for the combustion performance evaluation. The combustion performance evaluation includes burner/boiler modeling, fundamental atomizer erosion and boiler tube erosion/deposition studies, pilot-scale testing of DMC and MCWM, and demonstration-scale operation using DMC and MCWM. The engineering design summarizes the

key design aspects of the boiler conversion at the military site. An economic analysis of the DOD retrofitted boiler was also conducted.

2.0 BOILER SURVEY AND SELECTION

Penn State, working in conjunction with the U.S. Army Corps of Engineers, Construction Engineering Research Laboratory (CERL) and personnel at several military installations, identified candidate boilers for conducting the retrofit designs. The initial screening, which was based on a CERL computerized database and information received from civilian and military personnel, identified approximately 300 boilers as potential candidates. The initial screening was reduced to 32 boilers located at eleven military installations[6]. Upon further investigation, it was determined that several of the military installations were either closed or were on installation closure lists. In addition, others were in metropolitan areas or have stringent air quality/coal usage regulations. Consequently, the list was reduced to thirteen boilers located at the four military installations shown in Figure 2-1. Figure 2-1 is a map of the Eastern United States showing the locations of coal fields and the military installations.

Of the four sites shown in Figure 2-1, three were actively pursued as the candidate conversion site. They were: the Naval Surface Warfare Center Crane Division (Crane), the New Cumberland Defense Logistics Agency, and the Dover Air Force Base (Dover). Penn State visited all three of the sites to discuss the program and inspect the site and boilers. DOE attended the site visits at Crane and Dover, and CERL attended the site visit at Dover. A discussion of the boilers at each of the installations can be found elsewhere[6, 7].

As a consequence of the site visits and discussions with military personnel, Penn State recommended to DOE the Naval Surface Warfare Center at Crane, Indiana as the site for the retrofit designs. DOE and DOD (CERL) concurred with Penn State's selection.

The Crane facility has several boiler houses, one (Building 150) of which contains three boilers that are technically good candidates for conversion. There are three Cleaver Brooks D-type watertube boilers firing natural gas with No. 6 fuel oil backup. Two of the boilers were installed in 1989 and have a firing rate of 25.2 million Btu/h. The third boiler was installed in 1972 and has a firing rate of 18 million Btu/h. The boilers are good candidates for a retrofit design because there is space outside the building to accommodate coal (or MCWM) and ash storage and handling. In addition, there is a rail spur that services the building. Steam demand is based upon the number of orders for filling bombs.

The Crane facility was selected for the retrofit for the following reasons:

- The boilers are of a size which is representative of many military boilers. There are currently 266 natural gas, No. 2 fuel oil, or heavy fuel oil boilers in the inventory of the U.S. Army with capabilities ranging from 16 to 60 million Btu/h[1]. In addition, CERL states that these numbers would double if the Navy and Air Force are included[1].
- The boilers are good candidates from a technical viewpoint as discussed above.

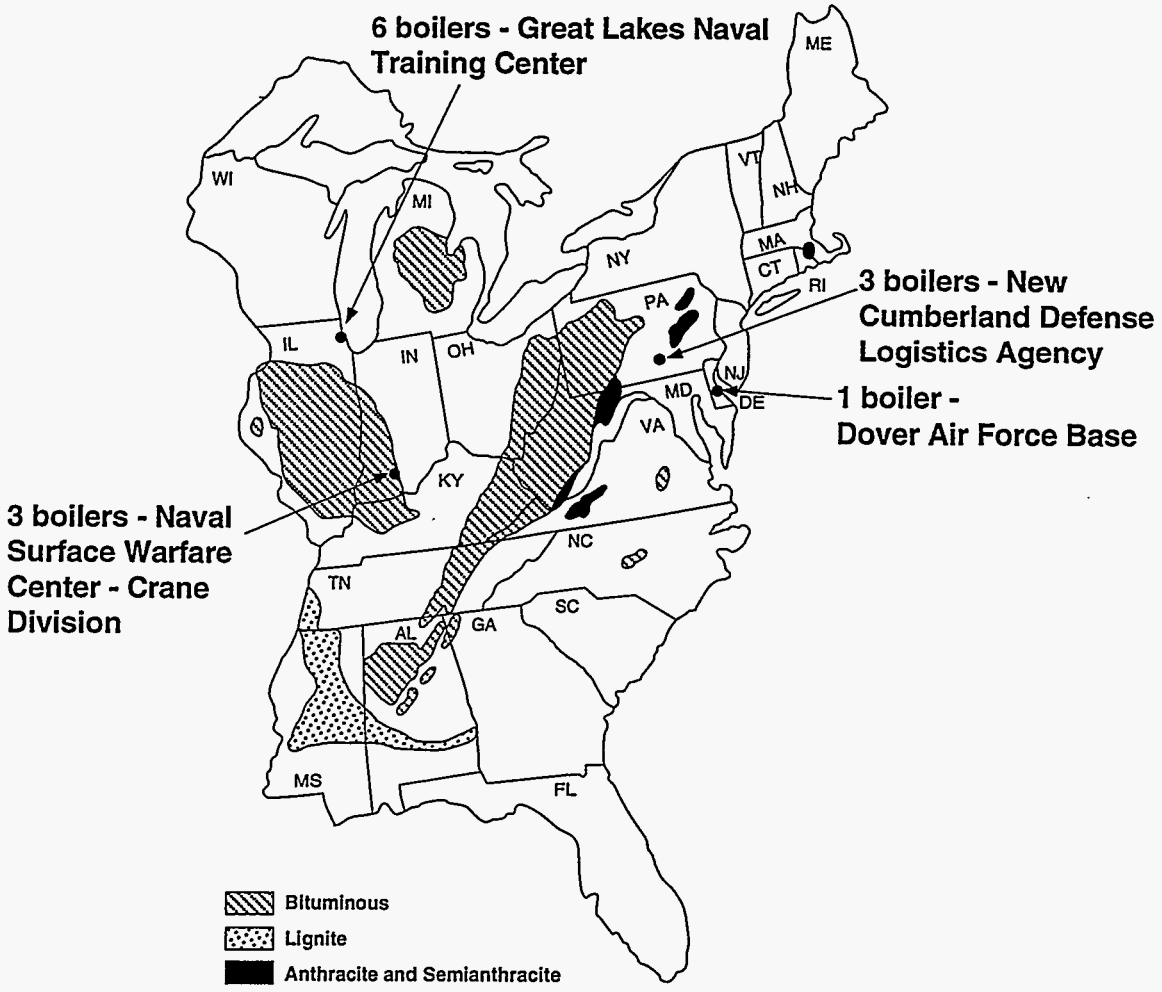

Figure 2-1. FINAL LIST OF CANDIDATE BOILERS

- The installation is located in the coal fields of a coal-producing state.

3.0 COAL BENEFICIATION AND PREPARATION

The initial objectives of this activity were to select appropriate coals which could meet the specific requirements of the project (specifically < 5.0 wt.% ash (to reduce deposition and boiler tube erosion), < 1.0 wt.% sulfur (to eliminate need for SO_2 emissions control), and > 30 wt.% volatile matter (to aid in ignition and flame stability)) and to prescribe the necessary cleaning steps to obtain these specifications. Longer-term objectives are to develop improved cleaning procedures which can be used to increase the yield of usable coal and to expand the reserve base of candidate fuels for retrofitted boilers.

Section 3.0 discusses the identification of candidate coals, and the results from fundamental, pilot-scale, and demonstration-scale coal cleaning and preparation studies. The fundamental beneficiation activities include modeling studies, coal cleaning processes, grinding investigations, and MCWM stabilization studies. Pilot-scale and demonstration-scale activities include coal cleaning, MCWM formulation, preparation, and characterization, and DMC preparation.

3.1 Coal Identification

Penn State, with assistance from AMAX Research & Development Center, identified a set of candidate coals. Based on the criteria given below, a final selection of six coals was made and samples were procured. The characteristics of the six test coals are presented in Table 3-1. The criteria used for the selection were as follows:

Availability. The test coals (except for the Taggart seam coal) were selected from seams containing significant reserves (> 300 million tons) and currently operating mines. Proximity to potential technology-demonstration boilers was also taken into account. Figure 3-1 shows the location of the coals relative to the candidate boilers for the retrofit design.

Cleanability. Test coals have been selected which fall into three broad categories based on relative ease of preparation to meet project specifications, i.e., less than 5.0 wt.% ash and 1.0 wt.% sulfur, and more than 30.0 wt.% volatile matter. The objective is to demonstrate the extent of the potential reserve base of coals which could be used in DOD facilities. The three categories are:

- Type I - coals which can meet the specifications at high yield with little or no cleaning;
- Type II - coals which can be cleaned by conventional means and can meet the specifications at fairly high yield; and
- Type III - coals which can be cleaned to meet the specifications but only at low yield using conventional cleaning technology.

The classification of each of the test coals is indicated in Table 3-1. Laboratory-scale quantities of MCWM were produced from Type II and III coals and used in the development of advanced coal cleaning procedures discussed in Section 3.2.

Table 3-1. Characteristics of the Test Coals.

Sample Designation	I-1	I-2	II-1	II-2	III-1	III-2
Seam	Taggart	Lower Block	Indiana VII	Lower Kittanning	Upper Freeport	Pittsburgh
State	Virginia	Indiana	Indiana	Pennsylvania	Pennsylvania	Pennsylvania
Counties	Wise, Lee	Greene, Knox	Sullivan, Knox	Armstrong, Clarion, Jefferson	Indiana, Armstrong, Jefferson	Greene, Washington
Estimated Reserves (Million tons)	50	3,500	400	480	8,000	6,000
Proximate Analysis						
Moisture %	1.6	11.9	12.7	2.1	1.4	2.6
Volatile Matter %	34.1	30.4	30.4	33.1	28.0	34.9
Fixed Carbon %	62.2	51.5	49.4	55.5	59.1	55.8
Ash %	2.1	6.1	7.5	9.4	11.5	6.7
Total Sulfur %	0.59	0.70	0.42	0.78	3.07	1.76
Hardgrove Grindability Index	47	45	51	68	76	56

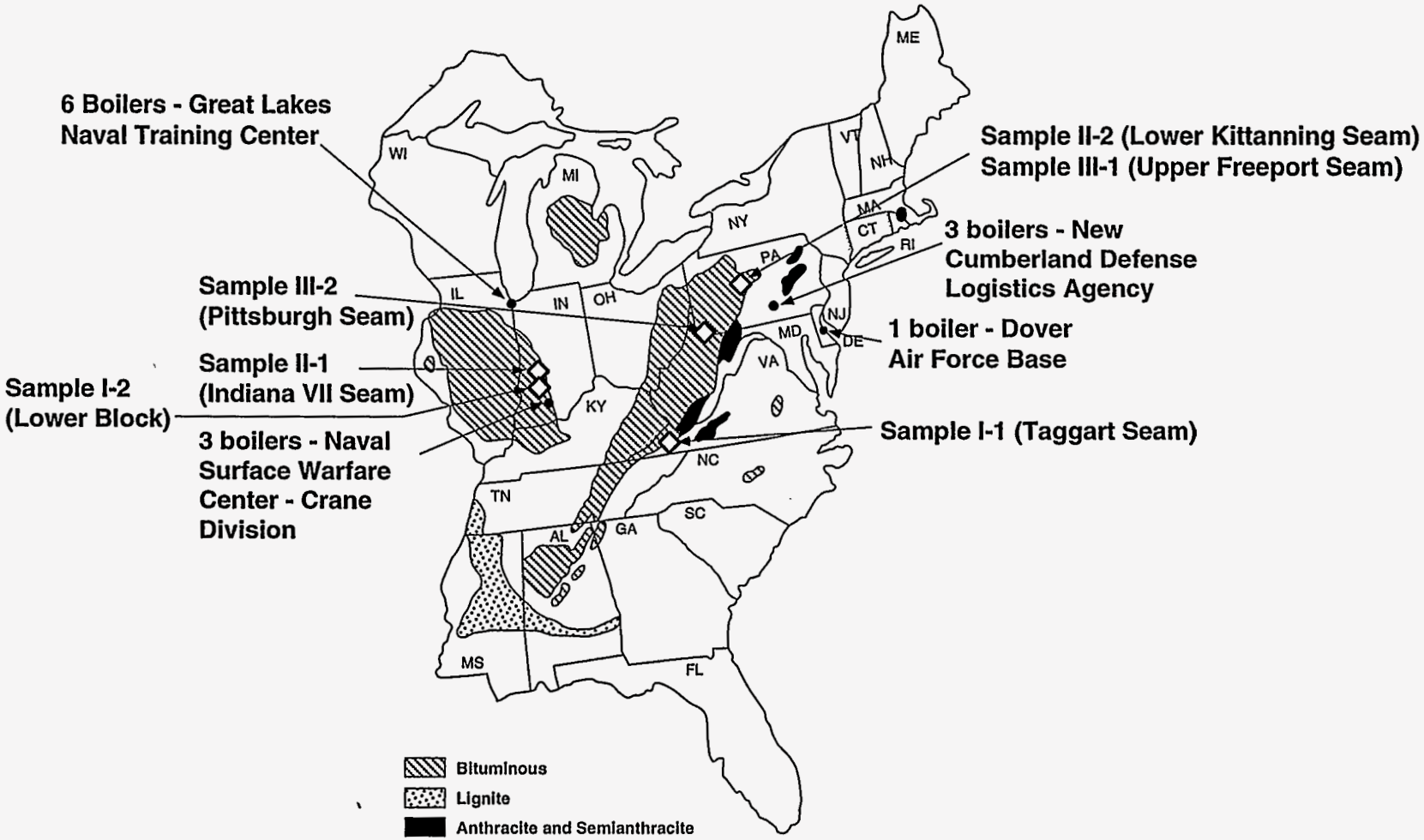

Figure 3-1. CANDIDATE BOILERS AND COALS

MCWM Characteristics. The test coals were selected from coal seams for which there is existing information and actual experience on MCWM formulation and preparation. More complete data was generated on the actual samples and was used to provide the basis for the grinding studies conducted in Sections 3.2 and 3.3.

3.1.1 Liberation Potential

Test coal samples were subjected to a series of float-sink tests to determine the level of cleaning to achieve the required grade of <5 wt.% ash and <1 wt.% total sulfur. Coal samples were crushed to a nominal -1/4" using a jaw crusher followed by screening at 1/4", 28 mesh, and 100 mesh. The +1/4", 1/4"x28 mesh, and 28x100 mesh size fractions were separated under gravity using Certigrav solutions of various relative densities, while the -100 mesh fraction was separated using a centrifuge. Separate samples of the Type II and III coals were crushed to a nominal -28 mesh. The ground products were then screened at 100 mesh. The +100 mesh size fraction was separated by gravity float-sink and the -100 mesh fraction was separated using centrifugal float-sink at the same relative densities. Each size/density fraction was analyzed for ash and sulfur content. The complete results are presented in Tables 3-2 to 3-7.

The Taggart seam coal can meet the product specification without any cleaning. However, float/sink separations were conducted on the -1/4" fraction for completeness. The results indicated that separating the coal at 1.3 relative density can reduce the ash content from 2.1 to 1.4 wt.% with 92% yield, while the sulfur reduction was minimal.

The Lower Block seam coal would require almost no cleaning to meet product specifications with 99% yield of less than 5 wt.% ash and 0.6 wt.% sulfur at a nominal size of -1/4". Hence, this coal could be classified as a Type I coal. If desired, a superclean coal of less than 3 wt.% ash can be produced with 70% yield. By reducing the top size to 28 mesh, the yield can be increased to 95% for the same ash content at a separation density of 1.60. The sulfur content of the product did not vary with the density of separation. However, this coal sample has a low sulfur content (0.7 wt.%) and can meet the sulfur specification at any density.

In order to produce a 5 wt.% ash product for the Indiana seam coal, crushing to -1/4" requires a subsequent separation at 1.37, giving a yield of 80%. By reducing the top size to 28 mesh, the yield can be increased to 93% for the same ash content at a separation density of 1.55. The sulfur content of the product did not vary with the density of separation. However, this coal sample also has a low sulfur content (0.45 wt.%) and can meet the sulfur specification without cleaning.

For the Lower Kittanning seam coal, the product specification can be met for the -1/4" coal at a separation density of 1.35 with about 75% yield (5 wt.% ash and 0.80 wt.% sulfur). The fine coal washability analysis indicates that by reducing the top size to 28 mesh, the yield can be increased to 82% (5 wt.% ash and 0.76 wt.% sulfur) at a separation density of 1.37.

Despite the high ash and sulfur content of the run-of-mine Upper Freeport seam coal, this

Table 3-2. Washability Analysis of the Taggart Seam Coal (Sample I-1) Crushed to a Nominal -1/4".

Rel. Den.	+1/4"			1/4"x28 Mesh			28x100 Mesh			-100 Mesh			Composite		
	Wt., %	Ash, %	T.S. %	Wt., %	Ash, %	T.S. %	Wt., %	Ash, %	T.S. %	Wt., %	Ash, %	T.S. %	Wt., %	Ash, %	T.S %
1.3 F	93.8	1.59	0.56	93.7	1.42	0.57	90.5	0.99	0.58	73.8	0.91	0.59	92.5	1.40	0.57
1.4 F	98.9	1.96	0.58	98.9	1.78	0.58	97.5	1.35	0.60	92.7	1.21	0.59	98.5	1.76	0.58
1.5 F	99.8	2.15	0.58	99.6	1.89	0.59	98.7	1.51	0.60	97.7	1.37	0.60	99.5	1.90	0.59
2.0 S	100.	2.18	0.60	100.	2.04	0.59	100.	2.02	0.61	100.	2.66	0.61	100.	2.10	0.60
Wt.,%	25.2			61.5			8.5			4.7			100.		

Table 3-3. Washability Analysis of the Lower Block Seam Coal (Sample I-2).

a) crushed to a nominal -1/4".

Rel. Den.	+1/4"			1/4"x28 Mesh			28x100 Mesh			-100 Mesh			Composite		
	Wt.,%	Ash,%	T.S.%	Wt.,%	Ash,%	T.S.%	Wt.,%	Ash,%	T.S %	Wt.,%	Ash,%	T.S %	Wt.,%	Ash,%	T.S %
1.3 F	59.3	2.15	0.64	12.7	1.47	0.64	0.22	-	0.73	0.10	-	0.70	33.1	1.64	0.62
1.4 F	87.2	3.54	0.62	65.9	2.54	0.60	13.3	1.34	0.62	14.8	1.40	0.43	70.6	2.89	0.58
1.5 F	94.1	4.34	0.62	89.0	3.29	0.59	81.4	3.26	0.61	65.3	2.12	0.46	89.8	3.72	0.58
1.6 F	95.2	4.50	0.62	94.6	3.84	0.59	87.3	3.97	0.60	82.9	2.69	0.40	94.0	4.09	0.58
2.0 F	99.4	5.40	0.65	98.3	4.56	0.62	94.6	4.32	0.53	95.7	4.40	0.43	98.5	4.93	0.60
2.0 S	100.	5.70	0.72	100.	5.40	0.71	100.	9.38	0.86	100.	7.75	0.65	100.	5.87	0.69
Wt.,%	46.5			43.5			5.2			4.7			100.0		

b) crushed to a nominal -28 mesh.

Rel. Den.	28x100 Mesh			-100 Mesh			Composite		
	Wt.,%	Ash,%	T.S.%	Wt.,%	Ash,%	T.S.%	Wt.,%	Ash,%	T.S %
1.3 F	60.3	2.45	0.62	9.3	0.61	0.59	44.7	1.71	0.61
1.4 F	83.5	2.57	0.63	83.8	1.89	0.59	83.6	2.10	0.62
1.5 F	92.5	3.30	0.62	91.5	2.54	0.59	92.2	2.77	0.61
1.6 F	96.1	4.06	0.60	94.8	2.10	0.58	95.7	2.70	0.59
2.0 F	98.8	5.07	0.61	97.7	4.32	0.68	98.4	4.53	0.63
2.0 S	100.	6.40	0.78	100.	5.87	0.91	100.	6.23	0.82
Wt.,%	69.5			30.5			100.0		

Table 3-4. Washability Analysis of the Indiana Seam Coal (Sample II-1).

a) crushed to a nominal -1/4".

Rel. Den.	+1/4"			1/4"x28 Mesh			28x100 Mesh			-100 Mesh			Composite		
	Wt.,%	Ash,%	T.S.%	Wt.,%	Ash,%	T.S.%	Wt.,%	Ash,%	T.S %	Wt.,%	Ash,%	T.S %	Wt.,%	Ash,%	T.S %
1.3 F	54.0	3.78	0.38	50.7	2.61	0.39	3.2	2.61	0.43	0.43	1.88	0.40	43.9	2.79	0.39
1.4 F	91.0	7.13	0.40	87.6	5.62	0.39	80.5	3.62	0.39	64.2	4.31	0.44	86.4	5.62	0.40
1.5 F	96.5	8.05	0.40	95.4	6.75	0.40	90.6	5.18	0.39	82.1	7.05	0.44	94.5	6.84	0.40
1.6 F	98.3	8.51	0.40	97.7	7.24	0.40	94.1	5.82	0.39	90.9	9.88	0.44	97.1	7.45	0.41
2.0 F	99.3	8.89	0.40	99.53	7.80	0.42	97.6	7.03	0.40	96.3	12.3	0.45	99.0	8.13	0.42
2.0 S	100.	9.48	0.40	100.	8.28	0.46	100.	8.60	0.49	100.	15.2	0.59	100.	8.86	0.46
Wt.,%	18.3			66.5			10.5			4.7			100.0		

b) crushed to a nominal -28 mesh.

Rel. Den.	28x100 Mesh			-100 Mesh			Composite		
	Wt., %	Ash, %	T.S. %	Wt.,%	Ash, %	T.S. %	Wt., %	Ash, %	T.S %
1.3 F	4.5	1.50	0.42	2.3	2.0	0.50	4.0	1.88	0.44
1.4 F	80.6	3.72	0.37	23.0	1.65	0.40	66.5	2.16	0.38
1.5 F	92.6	5.51	0.37	85.0	3.90	0.39	90.8	4.29	0.37
1.6 F	96.0	6.34	0.37	93.1	5.25	0.39	95.3	5.52	0.37
2.0 F	99.1	7.18	0.37	98.0	6.49	0.39	98.8	6.66	0.38
2.0 S	100.	8.06	0.42	100.	8.84	0.51	100.	8.20	0.44
Wt., %	75.5			24.5			100.0		

Table 3-5. Washability Analysis of the Lower Kittanning Seam Coal (Sample II-2).

a) crushed to a nominal -1/4".

Rel. Den.	+1/4"			1/4"x28 Mesh			28x100 Mesh			-100 Mesh			Composite		
	Wt.,%	Ash,%	T.S.%	Wt.,%	Ash,%	T.S.%	Wt.,%	Ash,%	T.S.%	Wt.,%	Ash,%	T.S.%	Wt.,%	Ash,%	T.S %
1.3 F	49.8	4.37	0.76	62.6	3.83	0.79	59.2	3.00	0.80	28.5	2.98	0.76	56.4	3.67	0.79
1.4 F	82.1	7.42	0.80	90.1	6.01	0.83	82.9	4.75	0.81	72.3	5.64	0.78	85.7	5.95	0.81
1.5 F	93.6	9.48	0.80	96.1	7.04	0.84	87.8	5.54	0.82	83.9	7.44	0.78	93.0	7.17	0.82
1.6 F	98.3	10.6	0.79	98.7	7.69	0.84	89.7	6.26	0.83	88.6	8.50	0.81	96.0	7.94	0.83
2.0 F	100.	11.2	0.79	99.5	7.98	0.84	92.7	7.00	0.86	91.6	9.56	0.84	97.6	8.43	0.84
2.0 S	100.	11.2	0.79	100.	8.31	0.84	100.	12.8	0.87	100.	16.1	0.99	100.	10.4	0.86
Wt.,%	13.7			58.1			16.8			11.4			100.		

b) crushed to a nominal -28 mesh.

Rel. Den.	28x100 Mesh			-100 Mesh			Composite		
	Wt., %	Ash, %	T.S. %	Wt.,%	Ash, %	T.S. %	Wt., %	Ash, %	T.S.%
1.3 F	64.4	3.13	0.75	48.6	2.45	0.75	59.8	2.65	0.75
1.4 F	86.8	5.15	0.76	84.3	5.47	0.77	86.1	5.38	0.76
1.5 F	91.9	6.24	0.76	89.4	6.33	0.79	91.2	6.30	0.76
1.6 F	95.7	7.29	0.76	93.8	7.12	0.79	95.2	7.17	0.77
2.0 F	98.1	8.24	0.76	96.3	7.95	0.79	97.6	8.03	0.77
2.0 S	100.	9.47	0.79	100.	10.9	0.90	100.	9.88	0.82
Wt., %	70.7			29.3			100.		

Table 3-6. Washability Analysis of the Upper Freeport Seam Coal (Sample III-1).

a) crushed to a nominal -1/4".

Rel. Den.	+1/4"			1/4"x28 Mesh			28x100 Mesh			-100 Mesh			Composite		
	Wt.,%	Ash,%	T.S.%	Wt.,%	Ash,%	T.S.%	Wt.,%	Ash,%	T.S.%	Wt.,%	Ash,%	T.S.%	Wt.,%	Ash,%	T.S %
1.3 F	33.6	4.61	0.96	57.2	3.62	0.87	63.3	2.64	0.85	45.4	2.83	0.80	53.4	3.57	0.87
1.4 F	74.0	7.05	1.50	85.1	5.26	1.09	83.3	4.00	0.98	73.9	4.64	0.90	82.2	5.30	1.12
1.5 F	80.2	8.10	1.52	89.1	5.80	1.22	87.6	4.61	1.07	83.2	5.42	0.95	87.0	5.95	1.22
1.6 F	85.7	9.41	1.58	91.3	6.24	1.32	89.9	5.07	1.18	89.6	6.85	1.21	90.1	6.61	1.33
2.0 F	93.1	11.7	1.95	94.1	7.02	1.60	92.5	5.86	1.34	93.8	7.90	1.63	93.7	7.64	1.62
2.0 S	100.	16.0	2.61	100.	10.5	2.80	100.	10.7	2.89	100.	12.2	3.21	100.	11.5	2.82
Wt.,%	14.9			62.9			13.2			9.0			100.		

b) crushed to a nominal -28 mesh.

Rel. Den.	28x100 Mesh			-100 Mesh			Composite		
	Wt., %	Ash, %	T.S. %	Wt., %	Ash, %	T.S. %	Wt., %	Ash, %	T.S %
1.3 F	68.0	3.10	0.80	50.0	2.36	0.76	62.5	2.58	0.78
1.4 F	86.0	4.60	0.87	76.7	4.43	0.95	83.2	4.48	0.89
1.5 F	89.5	5.10	0.94	84.4	5.39	1.02	87.9	5.30	0.96
1.6 F	91.7	5.82	0.98	89.1	6.78	1.41	90.9	6.49	1.11
2.0 F	94.0	6.60	1.13	90.6	6.86	1.24	93.0	6.62	1.14
2.0 S	100.	10.37	2.52	100.	12.84	3.66	100.	11.12	2.86
Wt.,%	69.6			30.4			100.		

Table 3-7. Washability Analysis of the Pittsburgh Seam Coal (Sample III-2).

a) crushed to a nominal -1/4".

Rel. Den.	+1/4"			1/4"x28 Mesh			28x100 Mesh			-100 Mesh			Composite		
	Wt.,%	Ash,%	T.S.%	Wt.,%	Ash,%	T.S.%	Wt.,%	Ash,%	T.S %	Wt.,%	Ash,%	T.S %	Wt.,%	Ash,%	T.S %
1.3 F	64.0	3.57	1.18	66.3	3.09	1.22	65.5	2.65	1.12	38.2	1.88	1.06	63.0	3.03	1.18
1.4 F	91.8	5.04	1.54	93.5	4.69	1.54	90.9	3.75	1.33	76.8	3.91	1.18	91.2	4.58	1.48
1.5 F	95.6	5.63	1.64	97.0	5.20	1.63	94.7	4.33	1.42	91.7	5.61	1.38	95.9	5.23	1.58
1.8 F	99.5	6.90	1.68	99.2	5.78	1.71	97.3	4.97	1.53	96.4	5.77	1.34	98.8	5.93	1.65
2.0 F	100.	7.09	1.74	99.5	5.91	1.73	97.8	5.30	1.56	98.4	7.42	1.60	99.3	6.24	1.70
2.0 S	100.	7.09	1.74	100.	6.23	1.79	100.	6.76	1.73	100.	8.55	1.89	100.	6.70	1.78
Wt.,%	21.6			57.3			11.5			9.6			100.0		

b) crushed to a nominal -28 mesh.

Rel. Den.	28x100 Mesh			-100 Mesh			Composite		
	Wt.,%	Ash,%	T.S.%	Wt.,%	Ash,%	T.S.%	Wt.,%	Ash,%	T.S %
1.3 F	72.2	2.67	1.11	53.3	1.80	1.00	66.5	2.06	1.08
1.4 F	94.8	4.45	1.32	89.1	4.22	1.27	93.1	4.29	1.30
1.5 F	95.5	4.65	1.35	94.5	4.80	1.29	95.2	4.75	1.33
1.6 F	97.4	5.00	1.39	96.4	5.01	1.31	97.1	5.01	1.36
2.0 F	98.8	5.48	1.46	97.5	5.18	1.31	98.4	5.27	1.42
2.0 S	100.	6.26	1.66	100.	6.93	1.77	100.	6.46	1.69
Wt.,%	69.4			30.6			100.0		

c) crushed to a nominal -100 mesh.

Rel. Den.	Wt.,%	Ash,%	T.S %
1.3 F	62.5	1.78	0.98
1.4 F	89.1	3.38	1.11
1.5 F	94.0	4.13	1.16
1.6 F	97.3	4.95	1.28
2.0 F	98.6	5.17	1.35
2.0 S	100.	6.20	1.64
Wt. %	100.0		

coal sample can be cleaned with a product of 5 wt.% ash and 0.98 wt.% sulfur at 1.37 separation density with a relatively high yield (76%). This suggests that the mineral matter of this coal sample can be well liberated by crushing. Further size reduction to -28 mesh can increase the yield to 85% with a cleaner product (5 wt.% ash and 0.92 wt.% sulfur) at a separation density of 1.45.

The results of the Pittsburgh seam coal showed that the ash specification can be easily met with over 90% yield at a separation density of 1.40. However, it would be difficult to obtain a product of <1 wt.% sulfur without a significant yield loss. Even with grinding to -100 mesh, this coal requires a low density separation at 1.3 to produce a 1 wt.% sulfur clean coal, with a theoretical yield of 62.5% and an ash content of 1.8 wt.%. In the actual coal cleaning operation, the yield will be further reduced considering the difficulty and the inefficiency of fine coal cleaning. Therefore, improvement in fine coal processing is needed to obtain an actual yield close to the theoretical.

3.1.2 Cleaning Strategies

Based on the analyses performed in Section 3.1.1, several alternative strategies for processing the six test coals to meet the sulfur and ash requirements have been identified. Specific examples are summarized below.

Coal I-1 (Taggart):	Specification can be met without further cleaning.
Coal I-2 (Lower Block):	Specification can be met without further cleaning.
Coal II-1 (Indiana VII):	Gravity separation of -1/4" coal at a density of 1.37 (80% theoretical yield at 5 wt.% ash and 0.45% sulfur).
Coal II-2 (Lower Kittanning)	Gravity separation of -1/4" coal at a density of 1.35 (75% theoretical yield at 5 wt.% ash and 0.8 wt.% sulfur).
Coal III-1 (Upper Freeport)*:	Gravity separation of -1/4" coal at a density of 1.37 (76% theoretical yield at 5 wt.% ash and 0.98 wt.% sulfur).
Coal III-2 (Pittsburgh):	5 wt.% ash requirement can be met by gravity separation of -1/4" material at a density of 1.40 (>90% theoretical yield). Grinding to -100 mesh and separation at 1.30 would be necessary to meet the 1 wt.% sulfur specification.

*Despite the high ash and sulfur content of the Upper Freeport coal, it should perhaps be reclassified as Type II because of relatively easy liberation.

3.2 Fundamental Beneficiation/Preparation Studies

The production of premium coal for use in the preparation of MCWM requires the removal of a large fraction of the mineral matter, including pyritic sulfur, from the raw coal. To obtain adequate liberation of the clean coal from the mineral matter, grinding to top sizes of 100 mesh and finer will usually be required. However, to take advantage of the liberation, a cleaning technology must be used, which is not only capable of processing such fine material, but can do so economically. For this reason, physical beneficiation processes such as flotation, selective

agglomeration or gravity concentration are the only viable options for near-term application. At the present time, flotation is the only one of these processes that is being used commercially to treat -100 mesh coal. Section 3.2 discusses activities that address coal cleaning processes and MCWM production.

3.2.1 Liberation Modeling

While the function of comminution is to produce an advantageous size distribution, in this case one that produces a highly concentrated slurry that combusts efficiently, a secondary aspect is the fact that additional liberation of undesirable materials in the coal - i.e., mineral matter that produces particulates and SO_x upon combustion - may also occur. If additional liberation can be achieved, then the undesirable materials should be removed prior to combustion. However, taking advantage of the liberation/separation aspect requires proper integration into the fuel preparation system. In order to do this optimally, it is necessary to be able to predict the liberation achieved, depending upon what devices are utilized.

Liberation modeling, unfortunately, is not a simple thing to do. From a comminution viewpoint, the liberation model needs to state what fraction of material of composition c_l and size x_k that breaks to size x_i will be of composition c_j. Then the liberation model combined with the appropriate comminution model will predict the washability analysis of the comminuted product -

SIZE INTERVAL:	1		2		..... n	
COMPOSITION	- mass fraction -					
INTERVAL	product	attribute				
1	p_{11}	ϕp_{11}	p_{21}	ϕp_{21}	p_{n1}	ϕp_{n1}
2	p_{12}	ϕp_{12}	p_{22}	ϕp_{22}	p_{n2}	ϕp_{n2}
.						
.						
.						
.						
m	p_{1m}	ϕp_{1m}	p_{2m}	ϕp_{2m}	p_{nm}	ϕp_{nm}

Now consider the comminution process shown in Figure 3-2, fracturing feed material of composition ℓ and size k, where

(1) the probability of fracture of the feed material is $a_{k\ell}$

(2) the distribution of the fractured feed material into size i is $b_{i;k\ell}$

(3) the probability of refracture of material is $a'_{k\ell}$

(4) the distribution of size i material into composition j is $m_{j;ik\ell}$

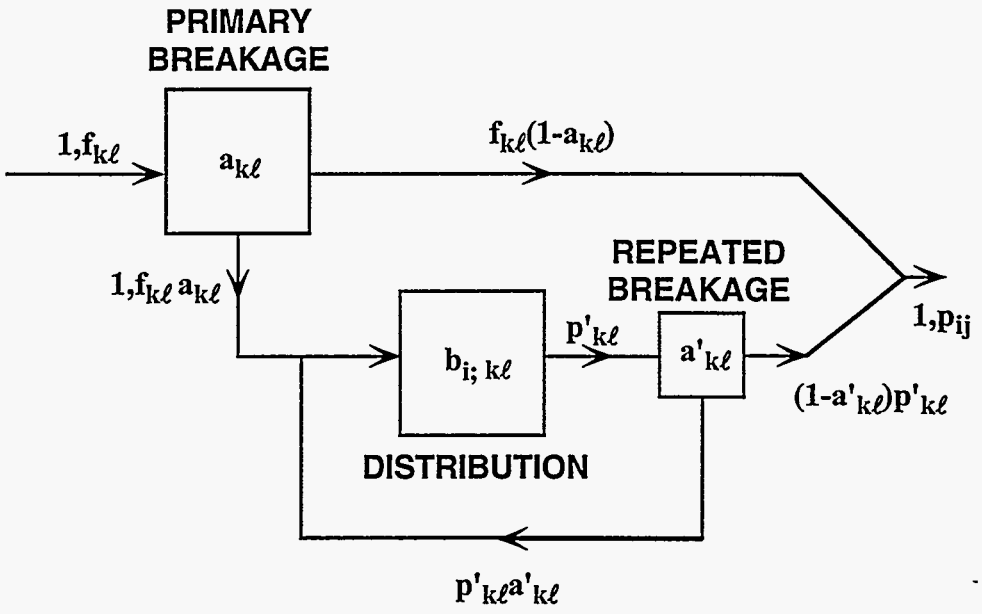

Figure 3-2. GENERAL COMMINUTION LIBERATION MODEL

(5) the distribution of rebroken size i material into composition j is $m'_{j;ik\ell}$

Thus the paths for the production of size 3, composition 1 class material from a 3x3 feed material are:

from the breakage of size 1 classes -

$f_{11} - (a_{11}b_{3;11}\, m_{1;311}) \rightarrow P'_{31} - (1-a'_{31}) \rightarrow P_{31}$
$f_{12} - (a_{12}b_{3;12}\, m_{1;312}) \rightarrow P'_{31} - (1-a'_{31}) \rightarrow P_{31}$
$f_{13} - (a_{13}b_{3;13}\, m_{1;313}) \rightarrow P'_{31} - (1-a'_{31}) \rightarrow P_{31}$

from the breakage of size 2 classes -

$f_{21} - (a_{21}b_{3;21}\, m_{1;321}) \rightarrow P'_{31} - (1-a'_{31}) \rightarrow P_{31}$
$f_{22} - (a_{22}b_{3;22}\, m_{1;322}) \rightarrow P'_{31} - (1-a'_{31}) \rightarrow P_{31}$
$f_{23} - (a_{23}b_{3;23}\, m_{1;323}) \rightarrow P'_{31} - (1-a'_{31}) \rightarrow P_{31}$

from the non-breakage of size 3, composition 1 feed -

$f_{31} - (1-a_{31}) \rightarrow P_{31}$

as well as from the breakage of size 2 classes from size 1 classes -

$f_{11} - (a_{11}b_{2;11}\, m_{1;211}) \rightarrow P'_{21} - (a'_{21}b_{3;21}\, m'_{1;321}) \rightarrow P'_{31} - (1-a'_{31}) \rightarrow P_{31}$
$f_{11} - (a_{11}b_{2;11}\, m_{2;211}) \rightarrow P'_{22} - (a'_{22}b_{3;22}\, m'_{1;322}) \rightarrow P'_{31} - (1-a'_{31}) \rightarrow P_{31}$
$f_{11} - (a_{11}b_{2;11}\, m_{3;211}) \rightarrow P'_{23} - (a'_{23}b_{3;23}\, m'_{1;323}) \rightarrow P'_{31} - (1-a'_{31}) \rightarrow P_{31}$
$f_{12} - (a_{12}b_{2;12}\, m_{1;212}) \rightarrow P'_{21} - (a'_{21}b_{3;21}\, m'_{1;321}) \rightarrow P'_{31} - (1-a'_{31}) \rightarrow P_{31}$
$f_{12} - (a_{12}b_{2;12}\, m_{2;212}) \rightarrow P'_{22} - (a'_{22}b_{3;22}\, m'_{1;322}) \rightarrow P'_{31} - (1-a'_{31}) \rightarrow P_{31}$
$f_{12} - (a_{12}b_{2;12}\, m_{3;212}) \rightarrow P'_{23} - (a'_{23}b_{3;23}\, m'_{1;323}) \rightarrow P'_{31} - (1-a'_{31}) \rightarrow P_{31}$
$f_{13} - (a_{13}b_{2;13}\, m_{1;213}) \rightarrow P'_{21} - (a'_{21}b_{3;21}\, m'_{1;321}) \rightarrow P'_{31} - (1-a'_{31}) \rightarrow P_{31}$
$f_{13} - (a_{13}b_{2;13}\, m_{2;213}) \rightarrow P'_{22} - (a'_{22}b_{3;22}\, m'_{1;322}) \rightarrow P'_{31} - (1-a'_{31}) \rightarrow P_{31}$
$f_{13} - (a_{13}b_{2;13}\, m_{3;213}) \rightarrow P'_{23} - (a'_{23}b_{3;23}\, m'_{1;323}) \rightarrow P'_{31} - (1-a'_{31}) \rightarrow P_{31}$

Thus, in general

$$p_{ij} = (1-a_{ij})\, f_{ij} + (1-a'_{ij})p'_{ij} \qquad (3\text{-}1)$$

where

$$p'_{ij} = \left\{ \sum_{k=1}^{i-j} \sum_{\ell} b_{i;k\ell}(m_{j;ik\ell}a_{k\ell}f_{k\ell} + m'_{j;ik\ell}a'_{k\ell}p'_{k\ell} \right.$$

The attribute units in the product are calculated from

$$Ap_{ij} = \sum_{k=1}^{i-1} \sum_{\ell} b_{i\,k\ell}(m_{j;ik\ell}\phi_{j;ik\ell}f_{k\ell} + m_{j;ik\ell}\phi_{j;ik\ell}a_{k\ell}p_{k\ell}) \tag{3-2}$$

where

$$Ap_{ij} = \sum_{k=1}^{i-1} \sum_{\ell} b_{i\,k\ell}(m_{j;ik\ell}\phi_{j;ik\ell}a_{k\ell}f_{k\ell} + m_{j;ik\ell}\phi_{j;ik\ell}a_{k\ell}p_{k\ell})$$

giving

$$\phi p_{ij} = Ap_{ij} / p_{ij}$$

The value of mj;ikℓ is given by $\int_{Cj-1}^{Cj} dM(c;ik\ell)$, while the product $m_{j;ik\ell}\phi_{j;ik\ell}$ is given by $\int_{Cj-1}^{Cj} c\,dM(c;ik\ell)$ where M(c;ikℓ) is the cumulative mass of material of size i, created by fracturing material of composition ℓ and size k, that is of composition c or less. A typical plot of M vs. c, for various degrees of liberation, is shown in Figure 3-3. This plot is known as the elementary attribute curve.

A plot of A vs. M, shown in Figure 3-4, is known as a Mayer Curve. Since dA/dM = c, the elementary attribute curve can be obtained by differentiating the Mayer Curve. Thus, if a functional form can be developed to represent the Mayer Curve, then a functional form can be derived for the liberation model. Now, by defining a Locking Index,

$$LI = \frac{\phi}{1-\phi} \int_0^{1-\phi} dA \tag{3-3}$$

where $\phi = \int_0^1 dA$, it is possible to perform a parameter search from which the elementary attribute curve can be obtained.

The combination of these phenomenological liberation equations with repetitive fracture in a crusher will be demonstrated in Phase II of the program.

3.2.2 Conventional Gravity Separations

The application of conventional gravity separations to the Type II and Type III coals has been evaluated using the washability data obtained for each of the test coals. The data were

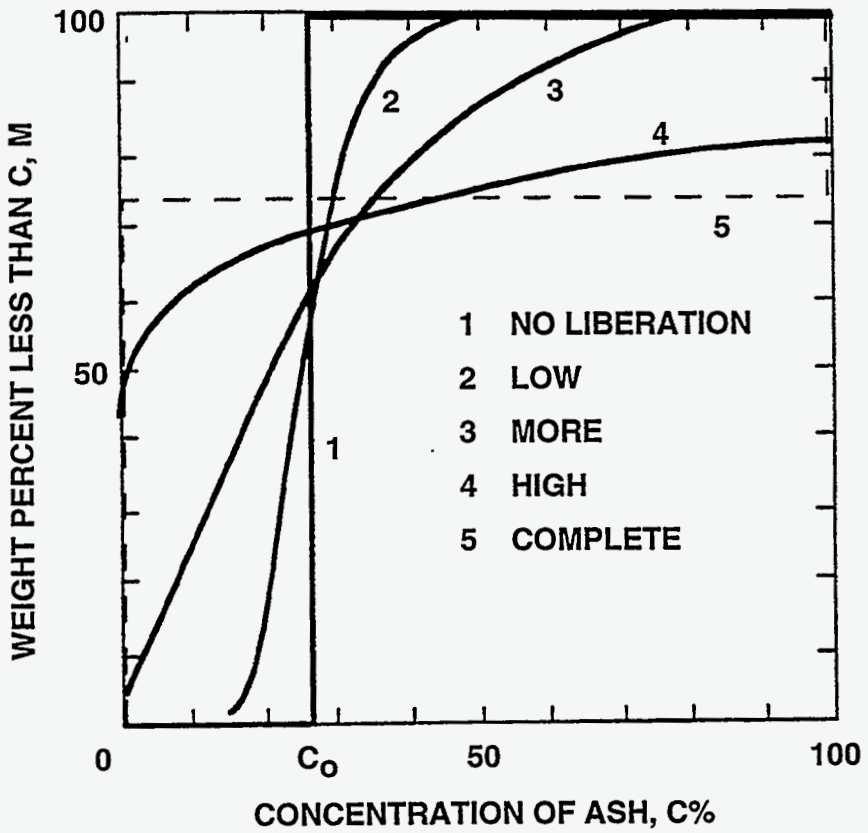

Figure 3-3. TYPICAL M-C PLOT FOR VARIOUS DEGREES OF LIBERATION

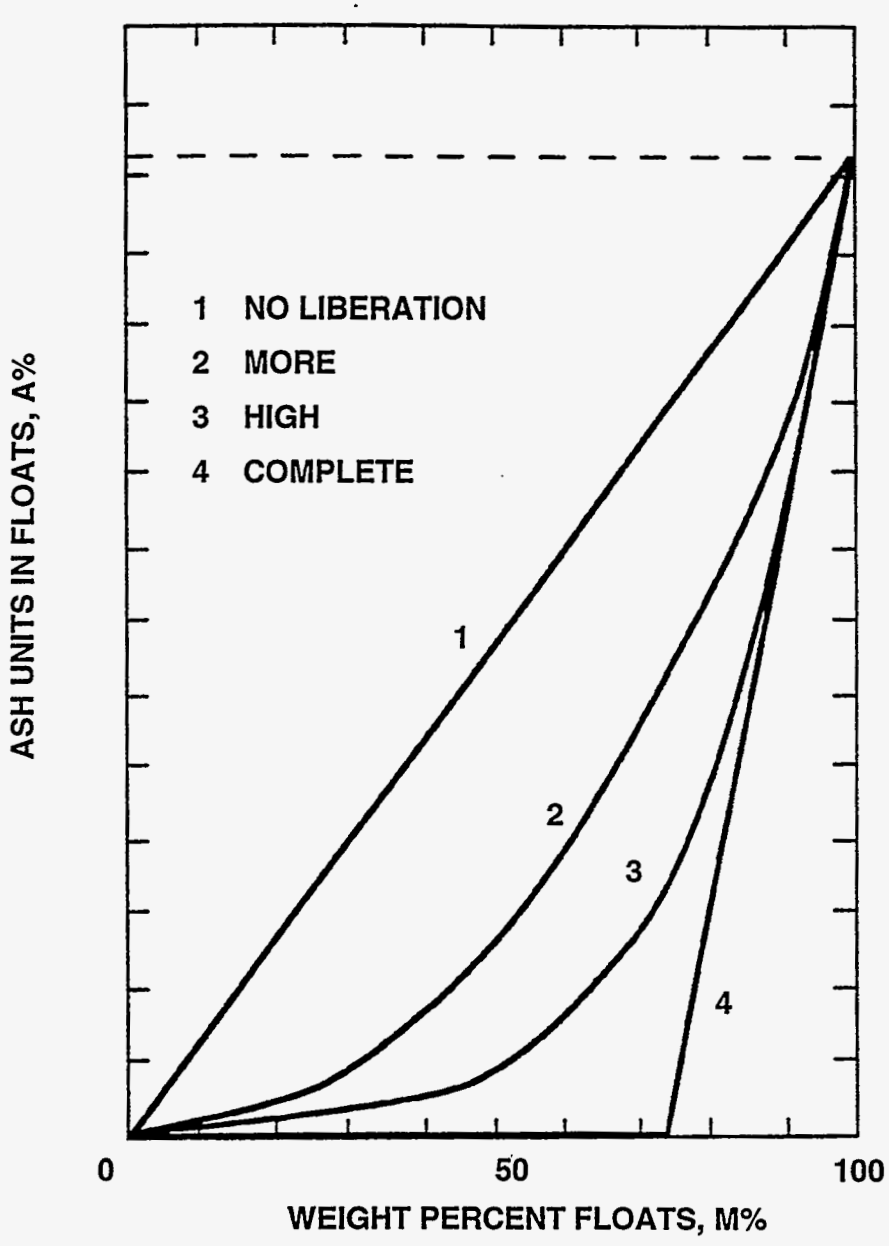

Figure 3-4. MAYER CURVES FOR VARIOUS DEGREES OF LIBERATION

interpolated as appropriate and then used in conjunction with existing computer simulation procedures[8]. The separations were made on the nominal 1/4"x28 mesh size fraction using performance data obtained by the U.S. Bureau of Mines for dense-medium cyclone operations.

Coal	Type	Relative Density of Separation	Yield, %	Ash, %	Total Sulfur, %
Indiana VII	II-1	1.35	59.2	4.9	0.39
Lower Kittanning	II-2	1.33	48.6	5.0	0.80
Upper Freeport	III-1	1.33	47.5	4.5	0.99
Pittsburgh	III-2	-	-	-	-

Conventional cleaning was able to produce between 50 and 60% of clean coal for three of the samples. For the Pittsburgh seam coal, the necessary sulfur reduction could not be obtained without crushing to -100 mesh. Therefore this coal was not evaluated, since the treatment of this size range would not be considered as conventional processing, at least for gravity concentration operations. For the Lower Kittanning and Indiana VII seam coals, the ash content was the limiting factor in producing a specification product, while the sulfur content of the clean coal prevented a higher yield for the Upper Freeport seam coal.

3.2.3 Fine Gravity Separations

Although flotation is quite effective in recovering fine coal and rejecting mineral matter impurities, it is not applicable to all coals (e.g., oxidized coal), and it is not always effective in rejecting pyritic sulfur. Similar problems are found for separations involving selective agglomeration, though not necessarily for the same coals. A gravity-based, fine-coal cleaning technique would provide an effective alternative for processing those coals not amenable to flotation or selective agglomeration. Gravity concentration processes are especially attractive since they are not affected by the surface properties of the coal and are particularly effective in rejecting pyritic sulfur because of its very high density.

Gravity concentration processes include water-only devices such as jigs, tables, spirals and hydrocyclones, and dense-medium devices such as baths and cyclones. For water-only devices, particles of mixed sizes and densities are separated from each other due to the differential settling of the particles in water under the influence of gravity or centrifugal force. The same separating principles apply to dense-medium processes although in this case, a suspension of fine solids (typically magnetite) and water is used. Dense-medium processes are capable of making separations over a wide range of relative densities and can be controlled with considerable

precision, making them the preferred approach for cleaning coals containing large amounts of near-gravity material. Furthermore, these are the only processes that are capable of making separations at very low (~1.30) relative densities, an important capability when attempting to meet the low-ash, low-sulfur requirement for preparing the coal to be used in a MCWM.

The production of a compliance product from a Type II or a Type III coal will require fine crushing or grinding to achieve additional liberation of the clean coal from the mineral matter, resulting in an increase in the quantity of material that must be treated by the fine-coal cleaning processes. As demonstrated above, this fraction may range from less than 50% for Type II coals to 100% for some Type III coals. In many cases, separations must be made at low relative densities to achieve the necessary ash and pyritic sulfur rejection. As such, dense-medium processes would be required.

Cyclone Separations

The separation of fine coal in dense-medium cyclones requires the generation of a greater separating force, i.e., a higher number of "g's", to obtain the same separation efficiency compared to coarser particles. At the present time, commercial preparation plants are cleaning coal down to 28 mesh and in some cases, 100 mesh, using dense-medium cyclones. The processing of finer coal has not been done, partly because of the decrease in separation efficiency with decreasing particle size. In an effort to extend the size range of coal treated by dense-medium separation, a micronized-magnetite cycloning process was developed at Department of Energy's Federal Energy Technology Center, Pittsburgh[9]. This process entails the use of an ultrafine (micronized) magnetite and water mixture as the separating medium in a cyclone for cleaning fine coal. It differs from commercial dense-medium cyclone operations in that the magnetite is much finer in size consist. The fineness of the micronized magnetite enables a higher number of "g's" to be employed during the separation. The result is a process that is capable of achieving separations of particles down to 400 mesh, which is not possible with current dense-medium cyclone technology.

Figure 3-5 shows the variation of the probable error as a function of the number of "g's" when separating nominal 28x100 mesh coal in different diameter cyclones[10]. When plotted on a log-log scale, the probable error decreased linearly as the cyclone diameter decreased (and the number of "g's" increased). Two additional data points, obtained from the DOE testing of a 76 mm diameter cyclone at two flow rates[9], correlated well with the data for the larger diameter cyclones.

However, in some cases, increasing the number of "g's" has led to results that were different than those in Figure 3-5. It was reported that the performance of a 150 mm diameter dense-medium cyclone was not influenced by changes in the volumetric feed rate when treating fine coal, at least at high medium-to-coal ratios[11]. In another case, the separation efficiency deteriorated when using smaller diameter cyclones to process fine coal[12].

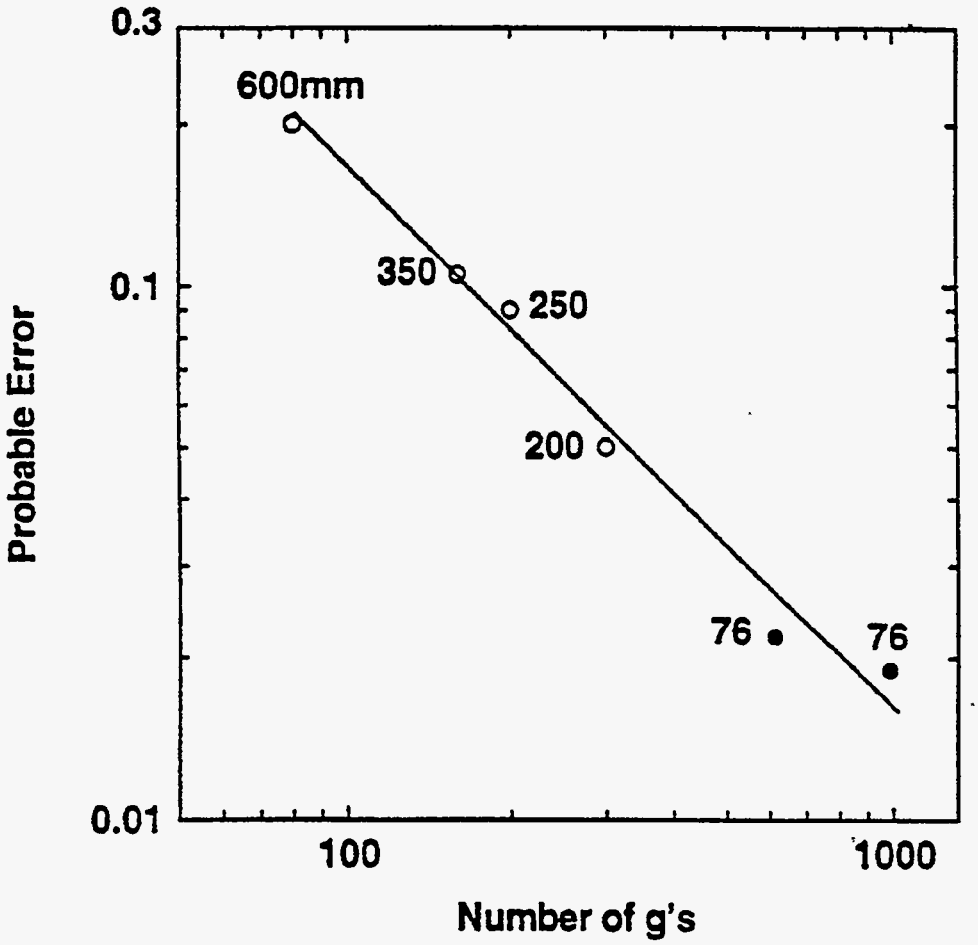

Figure 3-5. PROBABLE ERROR AS A FUNCTION OF THE NUMBER OF "g's" FOR VARIOUS DIAMETER CYCLONES

One explanation for these discrepancies relates to the stability and the rheology of the dense medium. He and Laskowski[13] showed that the separation efficiency of coarse particles increased when using finer magnetite because of the improved stability of the medium. However, for fine particles, the separation efficiency decreased because of the rheological effects of the dense medium. Similarly, Davis and Napier-Munn[14] showed that changes in medium viscosity impacted cyclone performance.

Another explanation relates to the interactions of the process variables. When the flow rate is increased, the overall retention time decreases. In addition, the turbulence would be expected to increase as the inlet velocity is increased. Both of these effects decrease the separation efficiency, potentially offsetting the expected improvement in cyclone performance. Also, a change in the cyclone flow rate changes the volumetric fraction of the feed slurry reporting to the overflow (i.e., pulp split). For dense-medium separation, an increase in the pulp split will lead to an increase in the density of separation, often with a decrease in the separation efficiency. Hence, it would be convenient to examine variable interactions using a mathematical model. One such approach is given in the next section.

Hindered-Settling Model

The prediction of the performance of dense-medium separation devices is difficult due in part to the interaction or compounding of operating variables such as the flow rate, the magnitude of the g-force, turbulence, and the characteristics of the dense medium. Recently, a batch hindered-settling model was developed and used to evaluate the classification behavior of a polydisperse particulate system[15]. This model was used to investigate the variation of the particle size distribution with time under different settling conditions. Dense-medium separation can be viewed in a similar fashion whereby the dense-medium solids, coal, and refuse, settle in water. Since the principle of separation also depends on the differential settling rate of these particles in the suspension, it should be possible to analyze dense-medium separation using the batch hindered-settling model[16].

Consider the settling column shown in Figure 3-6. In a hindered-settling regime, the movement of particles of a particular size and density, due to both settling (convection) and mixing (diffusion), would be a function of the concentration of these particles in the element within this device. It is possible to account for the movement of solids and liquid into and out of an element within the device such that the concentration at any height within the column can be calculated[17].

Representing Separations Using Fractional Recovery Curves

Although the solids concentration can be calculated at any point within the separator, it is more convenient to characterize the separation using fractional recovery (partition) curves. For example, consider the column in Figure 3-6 with particles uniformly dispersed in water. If these particles are allowed to settle for some time t and then the cylinder is cut at some fractional height L/H, the particles below this cut height can be defined as the refuse and the particles above the cut

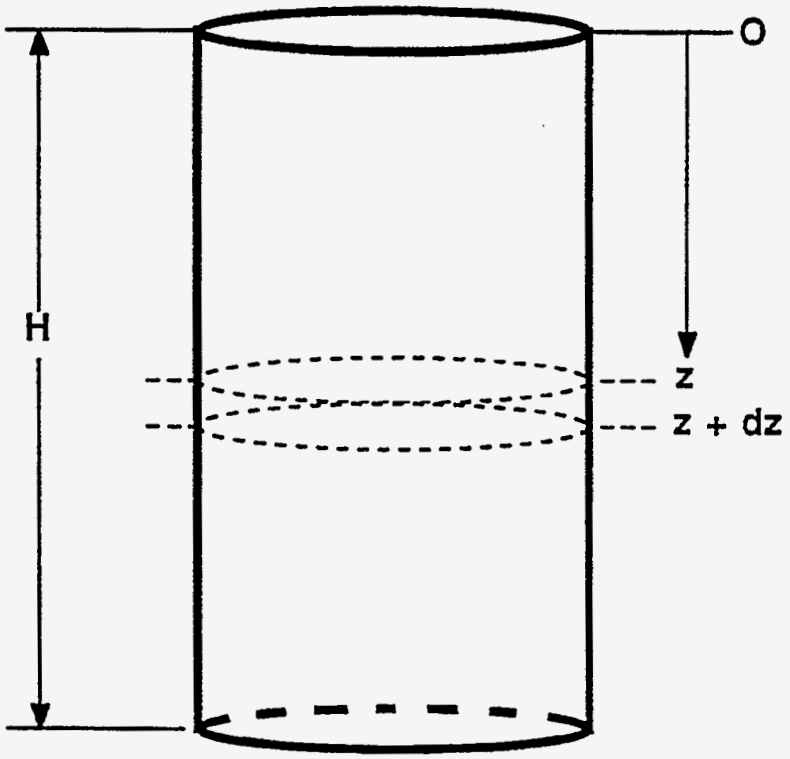

Figure 3-6. BATCH SETTLING COLUMN

height as the product. Since the particle size/density distribution at any location can be estimated from the hindered-settling model[15, 17], the fraction of feed particles of size x and density ρ which report to the product after time t is given by

$$K(\rho;x,t) = \frac{\int_0^{L/H} \phi(x,\rho,z,t)dz'}{\phi_0(x,\rho)} \qquad (3\text{-}4)$$

where $\phi_o(\rho,x)$ = initial volume fraction of particles of size x and density ρ, $\phi(\rho,x,z,t)$= volume fraction of particles of size χ and density ρ at location z of the settling column after time t, and z' = z/H.

A plot of a set of values from Equation 3-4 versus ρ for a given particle size is called a fractional recovery curve. As is common in gravity concentration, this curve can be characterized by a location modulus and a distribution modulus. The location modulus is defined as the density of those particles which have an equal probability of reporting to either the clean coal or to the refuse, i.e., the density corresponding to a fractional recovery value of 0.5. This location modulus for a given size is denoted by $\rho_{50(\chi)}$ and can be adopted as the separation density for that size. A distribution modulus is used to characterize the efficiency of separation. In this case, the probable error for a given size is defined as

$$Ep(x) = \frac{\rho_{25}(x) - \rho_{75}(x)}{2} \qquad (3\text{-}5)$$

where $\rho_{25}(x)$ = density corresponding to 0.25 on the fractional recovery curve, and $\rho_{75}(x)$ = density corresponding to 0.75 on the fractional curve.

Thus, as Ep(x) approaches one, the separation approaches ideal, while as Ep(x) approaches zero, no separation occurs, but rather the particles are split in the ratio L/H. The fractional recovery values can be fit to a mathematical function (model) from which the characteristic parameters can be obtained. One such model is the logistic function, which is given by

$$k(\rho;x) = \frac{1}{1+\exp\left[((1.099 / Ep(x))(\rho - \rho_{50}(x))\right]} \qquad (3\text{-}6)$$

The parameters $\rho_{50}(x)$ and Ep(x) can be found by using a nonlinear optimization routine.

Application to Cyclone Separations

In order to produce an acceptable yield for the Type II or Type III coals, the range of particle size to be processed must be extended to fine sizes. It is likely that cleaning of the 28x100

mesh size fraction would be required for a Type II coal to produce an acceptable yield of low ash and low sulfur material and even finer for a Type III coal. Using the hindered-settling model, an analysis of the change in the separation efficiency was made for various conditions. Appropriate parameters were used to describe the cyclone operation, the feed washability (i.e., the size and density distribution) and the dense medium characteristics. This involved the description of the parameters that impact the separation, including the number of "g's", the mean retention time, the amount of turbulence (mixing), and the pulp split.

The number of "g's" at some diameter, d, within the cyclone, can be estimated by[18]

$$Ng = \frac{27.4 D_i^2 Q_i^2}{A_i^2 D_c^3 g} \left(\frac{D_c}{d}\right) 2n + 1 \qquad (3\text{-}7)$$

where D_i = cyclone inlet diameter, D_C = cyclone diameter, Q_i = cyclone volumetric flow rate, A_i = inlet area, g= gravitational acceleration, and n= constant usually between 0.5 and 0.8. It can be seen from Equation 3-7 that increasing the cyclone flow rate, Q_i, for a fixed cyclone geometry, will increase the "g"-force, which should improve the overall separation. However, variable interactions may offset some of the expected improvement.

For example, as Q_i is increased, the retention time, t, decreases since

$$t = \frac{V_c}{Q_i} \qquad (3\text{-}8)$$

where V_c is the internal volume of the cyclone. In addition, the level of mixing would be expected to increase with an increase in the flow rate. Schubert and Neesse[19] give an equation for calculating a mixing coefficient in a cyclone as

$$D_m = k_1 Q_i \frac{D_i}{A_i} \qquad (3\text{-}9)$$

where k_1 = constant that depends on the units, and A_i = inlet area. Also, a change in the flow rate will also affect the pulp split, which will change the separation density. Therefore, in a cyclone, the number of "g's" cannot be increased independently by increasing the flow rate without causing a corresponding decrease in the mean retention time, and increase in mixing, and a change in the pulp split, all of which can offset the expected improvement in separation efficiency[20].

Simulations were performed to investigate the separation of 28x100 mesh coal in a conventional (36 cm) diameter cyclone using a suspension of magnetite and water with a medium density of 1.28g/cm^3. The corresponding set of simulation conditions are given in Table 3-8. The

Table 3-8. Simulation Conditions for the Dense-Medium Cyclone.

Total Height	18.0 cm
Relative Cut Height	0.6
Number of g's	120.0
Retention Time	1.75 s
Diffusion Coefficient	16.0 cm^2/s

Size/Density Distribution of the Coal Particles

	495µm	351µm	246µm	175µm	Composite
1.25 g/cm^3	0.145	0.204	0.185	0.142	0.676
1.35 g/cm^3	0.026	0.031	0.022	0.012	0.091
1.45 g/cm^3	0.014	0.014	0.010	0.007	0.045
1.55 g/cm^3	0.015	0.015	0.010	0.006	0.046
1.70 g/cm^3	0.010	0.010	0.007	0.004	0.031
2.30 g/cm^3	0.037	0.039	0.023	0.013	0.112
Composite	0.247	0.313	0.256	0.184	1.000

Characteristics of the Dense Medium

Medium Density	1.28 g/cm^3
Med.-to-Coal Ratio	5:1
Magnetite	
Density, g/cm^3	4.8
Size	95%<53µm
Vol. Fractions	
Solids	0.074
Water	0.926

fraction of each coal species, which reported to the product (Equation 3-4), was calculated by the hindered-settling model. Figure 3-7 shows the variation of the fractional recovery curves with particle size. As would be expected, sharper separations (i.e., lower Ep(x) values) were obtained for the coarser particles. If this treatment is extended to finer sizes, i.e., 100x325 mesh size fraction, the results as shown in Figure 3-8 are obtained. It can be seen that much flatter fractional recovery curves are obtained. Consequently, longer separation times and/or higher "g's" are needed to improve the separation. Work is continuing in this area (Phase II of the program) investigating the effects of variable interactions on separation efficiency, including the effects of medium characteristics.

Centrifuge Separations

Although dense-medium cyclones will likely be used to clean coal down to 100 mesh and perhaps even 400 mesh utilizing an ultrafine (micronized) magnetite-based process, the Type III coals will likely require grinding to top sizes of 100 mesh or finer to achieve liberation. Such grinding would invariably create a large fraction of -400 mesh material. Under these conditions, it may not be practical to utilize dense-medium cycloning since small diameter (i.e., lower capacity) units may be required to generate sufficient "g's". Also, because of the trade-off between the number of "g's" and retention time, it may not be possible to separate the -400 mesh coal efficiently using hydrocyclones.

As an alternative to a cyclone, it should be possible to use a solid-bowl centrifuge as a dense-medium separator, also employing an ultrafine-magnetite/water mixture as the dense-medium suspension. This device offers at least one major advantage over the cyclone for fine-coal cleaning: the ability to control independently the mean retention time and the number of "g's". As with the cyclone, the mean retention time can be increased (or decreased) simply by decreasing (or increasing) the flow rate through the device. However, unlike a cyclone, higher "g's" can be obtained at a constant flow rate by increasing the rotational speed of the centrifuge bowl.

The number of "g's" for a centrifuge can be calculated by

$$Ng = \frac{k_2 D_b N^2}{g} \tag{3-10}$$

where k_2 = constant that depends on the units, D_b = the bowl diameter, and N=rotational speed. Since Equation 3-10 does not depend on Q_i, the separating force can be increased, as required for the efficient separation of fine coal from refuse particles, without having to decrease the separation (retention) time. These devices are capable of operating at several thousand rpm to generate over 3,000 'g's'. In addition, the amount of turbulence that occurs in a centrifuge should be lower since high inlet pressures are not needed as is the case in the cyclone. Also, by changing the scroll speed and weir height, it should be possible to vary the pulp split independently, and hence,

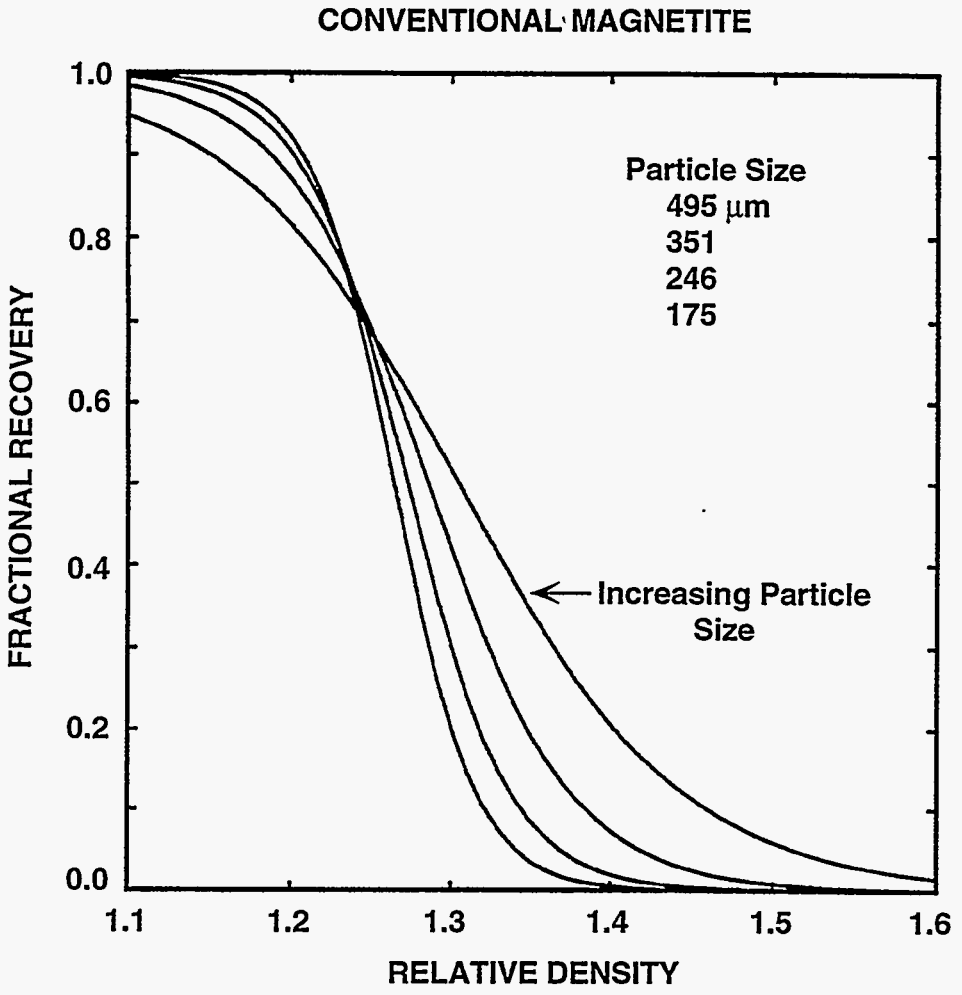

Figure 3-7. VARIATION OF THE FRACTIONAL RECOVERY CURVES WITH PARTICLE SIZE FOR THE 28 X 100 MESH SIZE FRACTION

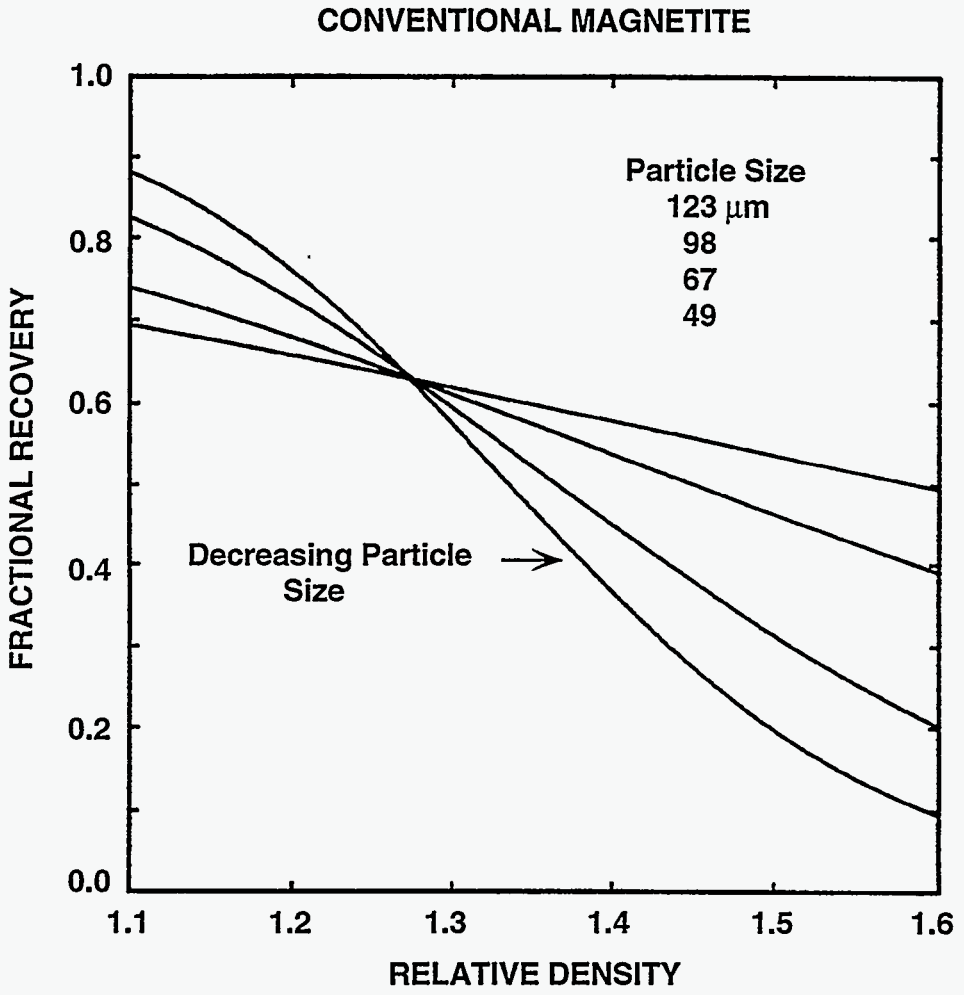

Figure 3-8. VARIATION OF THE FRACTIONAL RECOVERY CURVES WITH PARTICLE SIZE FOR THE 100 x 325 MESH SIZE FRACTION

regulate the separation density.

Another potential advantage of the solid-bowl centrifuge is that can be used to classify particles at very fine sizes. These devices have been used in the minerals industry to separate particles less than 5μm. The capability to classify in this range would be very valuable to produce the proper size distribution required for MCWM.

Batch Centrifuge

Preliminary testing was carried out using a "batch" centrifugal separator. The purpose of this testing was to examine the movement of solids and liquid in a centrifugal field. The primary test variables for this part of the study included rotational speed (i.e., N) and volumetric flow rate. The test unit, which was fabricated as part of a related study, consisted of a 152.4 mm diameter Plexiglas cylinder that was initially 152.4 mm long. However, preliminary tests utilizing the Upper Freeport (Type III) seam coal indicated that some of the higher-ash material was being retained in the separator during operation. To minimize this effect, the overall length of the separator was reduced to 76.2 mm (Figure 3-9).

The feed slurry enters at the top of the unit, near the center of the separator. As the slurry moves through the separator, the higher-density and/or coarser solids migrate towards the bowl wall and are withdrawn by a suction line located near the wall at the bottom of the centrifuge. The lower density and/or finer solids, which settle at a slower rate, are also removed by suction but at a location closer to the center of the bowl. By varying the location of the suction points, it is possible to withdraw lower or higher relative density fractions and hence, change the pulp split, without changing the medium density. The separator was mounted to an existing laboratory floor-model centrifuge to provide a means of controlling the rotational speed.

The test magnetite was obtained from the Pea Ridge Iron Ore Company of Sullivan, Missouri. This material was much finer than that used in commercial coal preparation facilities being nearly 100% < 15 μm, with approximately 75% < 5 μm. Nominal 100x500 mesh Upper Freeport seam coal was used throughout this study.

For each test, a suspension of the ultrafine magnetite and water was used at a relative density of 1.30 and a medium-to-coal ratio of 15-to-1. After the centrifuge speed was set, the sampling pumps were started. The feed pump was set to obtain the desired flow rate and retention time. Products were collected continuously over the duration of the test. It was not possible to perform long duration tests (i.e., >5 minutes) with the "batch" centrifuge because of a build up of solids on the separator wall. Consequently, a typical run lasted approximately 2 minutes. Also, the flow patterns of the slurry indicated that an internal recirculation was present, which became more pronounced as the centrifuge speed was increased. Different sampling locations were tried in an attempt to minimize this effect.

After each test, the samples were wet-screened at 500 mesh to remove the ultrafine magnetite. The +500 mesh coal and refuse were dried to determine the clean-coal yield. Ash and

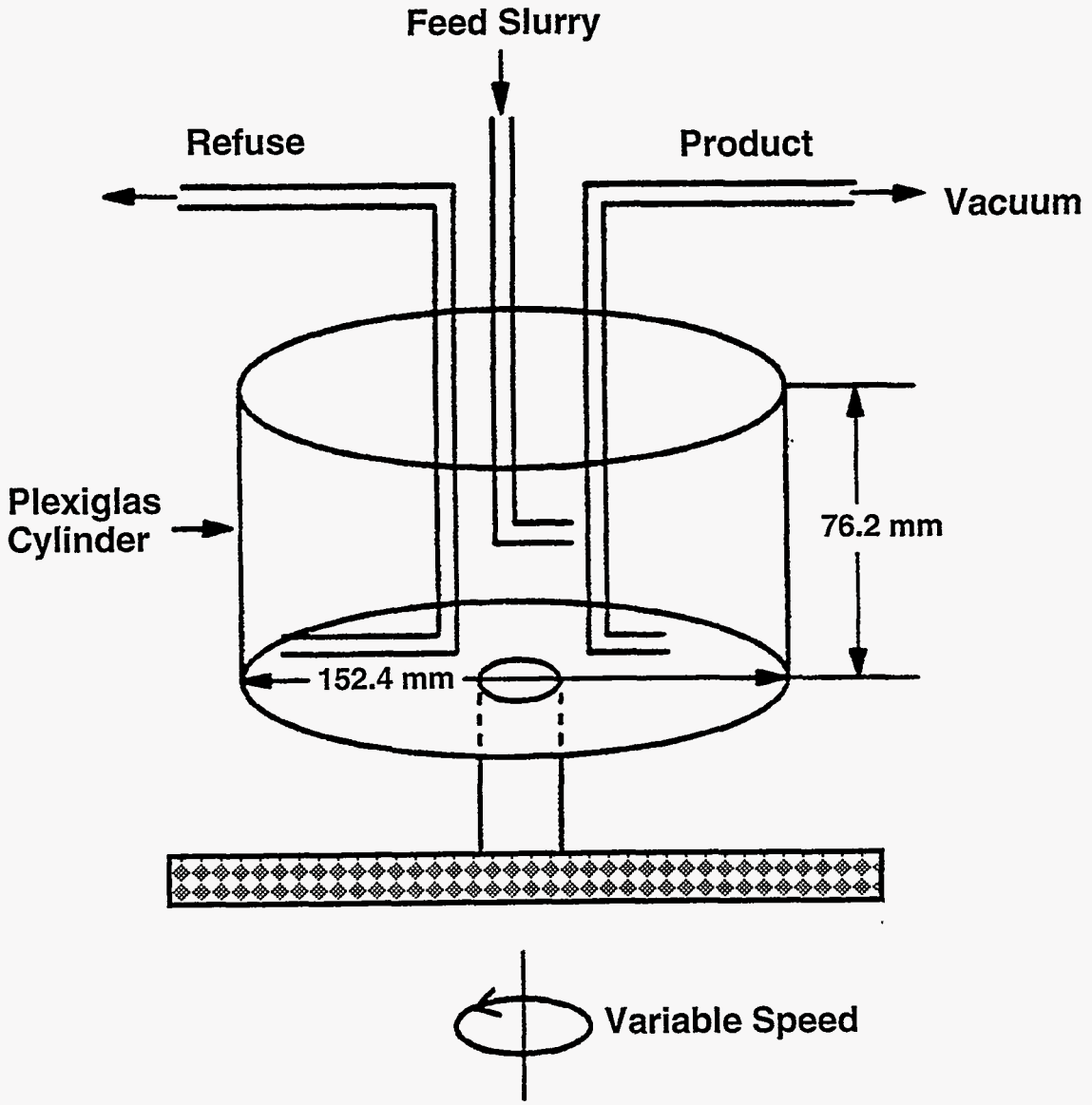

Figure 3-9. SCHEMATIC DIAGRAM OF THE "BATCH" CENTRIFUGAL SEPARATOR

total sulfur analyses were performed on each product. In some cases, float-sink separations were also performed on the 100x500 mesh size fraction at several relative densities from which the fractional recovery values were calculated.

Tests were made with the "batch" unit to demonstrate the advantage of using a dense-medium based separation system compared to a water-only system. When using the water-only system, a clean coal yield of 15.4% was obtained with an ash content of 4.9 wt.%. On the other hand, when using a dense medium of 1.30, the yield increased to 63.1% at an ash content of 4.7 wt.%. These results indicate that centrifugal dense-medium separation may be a viable alternative for producing the specification coal.

Additional tests were run to investigate changes in the rotational speed. The fractional recovery curves for these tests are shown in Figure 3-10. It can be seen that there is a shifting of the curves to lower values with an increase in the centrifuge speed. Also, the curves tend to level off around a relative density of 1.32, which may be the result of the internal recirculation. However, this recirculation is likely the result of the operation of the "batch" centrifuge and should not be present in a continuous centrifuge. The design of the unit limited an extensive investigation of the test conditions, in particular the effect of process variable interactions. However, a more detailed test program will be conducted in Phase II of the program using a continuous, high-speed, solid-bowl centrifuge.

Continuous Centrifuge

A continuous, high-g, solid bowl centrifuge was received and installed. This unit will be used in Phase II for continuous dense-medium centrifugation and for ultrafine coal classification. The results from this study can be used to scale to larger diameter units to be used in the production of MCWM.

The first phase of this study will involve testing a dense-medium slurry to determine the classification effects of the ultrafine magnetite. The key variables in this part include the volumetric feed rate, centrifuge speed, and solids concentration. In addition, the scroll speed and/or weir height will be varied to change the pulp split. Samples will be taken to determine the pulp splits and the effect on magnetite classification. Subsequent tests will use a dense medium and coal mixture to determine the separation efficiency when cleaning the -100 mesh coal. Float-sink separations of the products will be performed as appropriate.

Magnetic Fluid Separation

As an alternative to using a suspension of solids and water as a dense medium, it is possible to utilize a ferro (magnetic) fluid as the separating medium. These fluids consist of a colloidal suspension of sub-micron magnetite particles and dispersant in water. The fineness of the magnetite particles prevents the particles from settling in the fluid. This would be particularly useful when attempting to separate at a very high number of "g's", which are required for the separation of ultrafine coal. When a magnetic field is applied to the fluid, the particles align

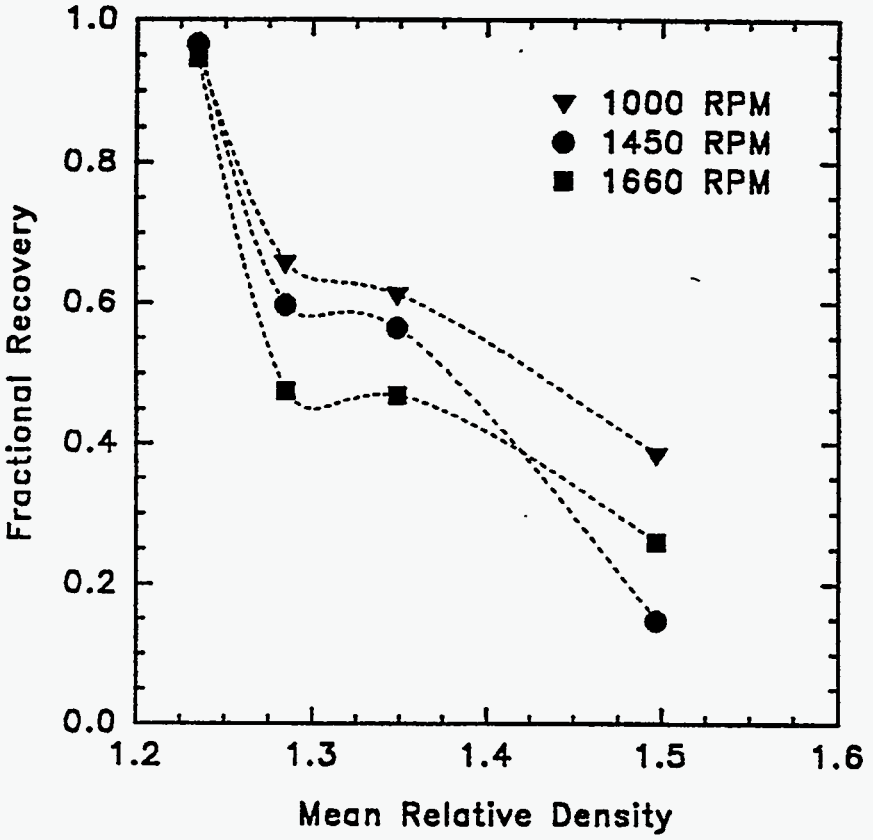

Figure 3-10. FRACTIONAL RECOVERY CURVES FOR THE 100 x 500 MESH SIZE FRACTION OBTAINED FOR THE "BATCH" CENTRIFUGE OPERATING AT VARIOUS ROTATIONAL SPEEDS

themselves in the direction of the field. The result of this alignment is that a "buoyant" or "levitation" force is produced. Particles that are placed in the fluid can be separated according to the density difference between the particles and the fluid, i.e., those "lighter" than the fluid will float, while those denser will sink. When the magnetic field is removed, the magnetite particles return to a random orientation, and no magnetic flocculation occurs. The strength of the buoyant force can be regulated by changing the strength of the magnetic field and/or concentration of the fluid.

A commercially available separator that uses a rotating magnetic fluid is the Magstream separator[21]. One of these units has been obtained on loan from DOE. This device seems to be limited to coal particle sizes greater than about 100 mesh. Testing is continuing in this area, in Phase II, to evaluate magnetic fluid technology for finer particle separations.

3.2.4 Surface-Based Cleaning Processes

In recent years, several surface-based advanced coal cleaning technologies have been developed, or are in various stages of development. These include:

- Advanced froth flotation;
- Column flotation; and
- Spherical or selective agglomeration.

As a part of this project these methods were used, individually or in combination, to clean coals from different sources.

Standard Flotation Tests

A WEMCO flotation machine, Model 71260-01, was used in the flotation experiments. A five-liter or a one-liter cell was used depending upon need. The stirrer speed was kept constant at 1,000 rpm. The solids concentration in the flotation feed was 10% by weight. The flotation pulp was conditioned for 3 minutes to disperse the coal, and dodecane was added in required amounts as the oily collector. The pulp was conditioned for an additional 3 minutes. In some tests, the desired quantity of a surfactant was added as a promotor to enhance flotation separation. After conditioning with the reagent and/or dodecane, methylisobutylcarbinol (MIBC) was added in the desired amount as the frother. The slurry was further conditioned for 2 more minutes prior to introduction of air into the cell. The froth was removed at preset time-intervals of 20, 40, 60, 120, 240 and 480 seconds. The natural pH of the pulp was used without any pH adjustments. The flotation products were filtered, dried, weighed and analyzed to determine their ash content.

To prepare the flotation feed, a rod mill was used to wet grind the sample to the nominal feed sizes of -600 and -150 μm. To prepare the -65 μm feed, a Blueler mill was employed. The grinding time was determined empirically. The baseline flotation tests were conducted for the Type II and Type III coals at three different feed sizes and the recovery versus ash curves are given in Figure 3-11. It can be seen that the effect of feed size was a function of coal type. The Lower Kittanning coal floated reasonably well but the ash content was much higher than the target. In

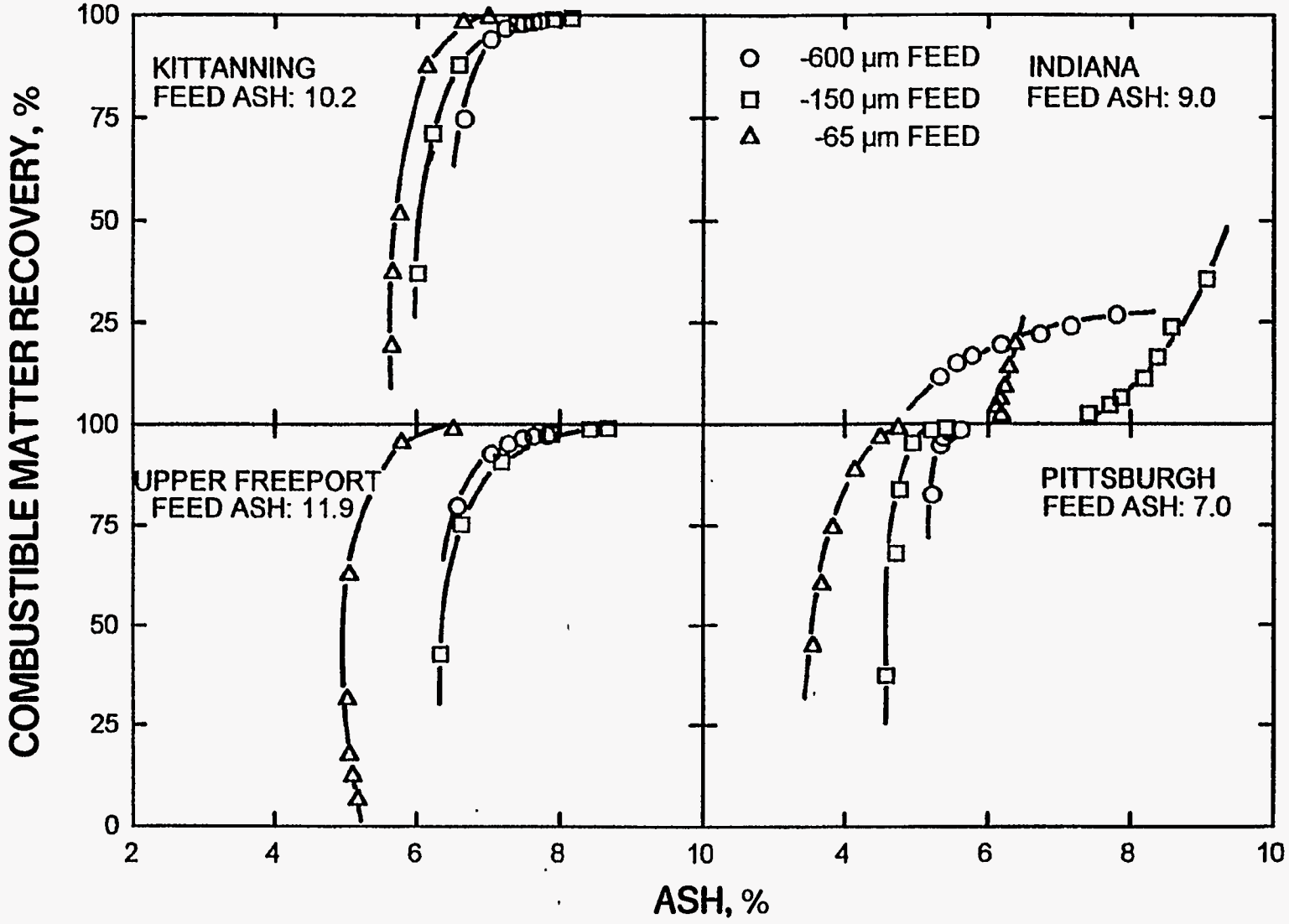

Figure 3-11. FLOTATION RESULTS FOR THE FOUR COALS TESTED AT THREE FEED SIZES OF NOMINAL -600 -150, AND -65 µm. The frother concentration was 0.15 kg/T for the -600 and -150 µm feed sizes, and 0.5 kg/T for the -65 µm feed. The collector concentration was 0.3 kg/T for the -600 and -150 µm feed sizes and 0.07 kg/T for the -65 µm feed (except for the Indiana VII coal for which it was 0.35 kg/T).

comparison, Indiana VII coal floated poorly, even at large amounts of oil. Both Type III coals had high floatability but further improvements were needed to reduce the ash and sulfur contents. To determine the effect of collector dosage, flotation tests were conducted at several concentrations of dodecane for -65 μm material and the results are presented in Figure 3-12 for the Pittsburgh seam and in Figure 3-13 for the Indiana VII seam coal. An increase in the collector increased the ash content for the Pittsburgh seam coal whereas it increased the recovery for the Indiana VII seam coal. The effect of collector concentration on the floatability of -600 and -150 μm materials can be seen in Table 3-9. It is obvious that alternate measures are needed to clean various coals.

Advanced Froth Flotation

Several methods are available to enhance separation efficiency. These include:

- Aid capture of fine particles by small bubbles;
- Increase hydrophobicity to increase rate of flotation - use of promotors;
- Increase hydrophobicity of particles which might increase the extent of hydrophobic aggregation;
- Aid capture of fine particles by oil droplets followed by flotation of aggregates; and
- Promote selective agglomeration to produce larger 'particles' which can be floated readily.

A comprehensive approach was used in this project to exploit some or all of the above methods.

Block co-polymeric surfactants, consisting of hydrophobic polypropylene oxide (PPO) and hydrophilic polyethylene oxide (PEO) groups were selected as promotors to improve the efficiency of separation. These reagents were selected based on previous experience in coal flotation. The criteria used for selection of these reagents were their commercial availability and ability to enhance the selectivity of separation. A list of the surfactants used in this investigation and their characteristics are given in Table 3-10. Standard flotation procedures were used to conduct tests. Suitable models were used to determine rate and ultimate recovery.

Role of Surfactants

Preliminary flotation tests conducted in the presence of selected reagents clearly demonstrated that substantial benefits are to be realized in coal cleaning when appropriate surfactants are used in small quantities. Prior studies have shown that block co-polymers containing ethylene and propylene oxide groups were found to be very effective in flotation of some coals. To determine their effectiveness for the coals chosen for this project, studies were carried out to determine the effect of surfactant concentration and surfactant type.

The results were analyzed using the total combustible matter recovery (CMR) and ash content in the clean product and the results are presented in Figure 3-14 for the Pittsburgh seam coal. A significant reduction in ash was observed in the presence of small quantities of the promotor. To further determine the effect of surfactant concentration, tests were performed at several concentrations and the combustible matter recoveries for the 2 minute product, along with

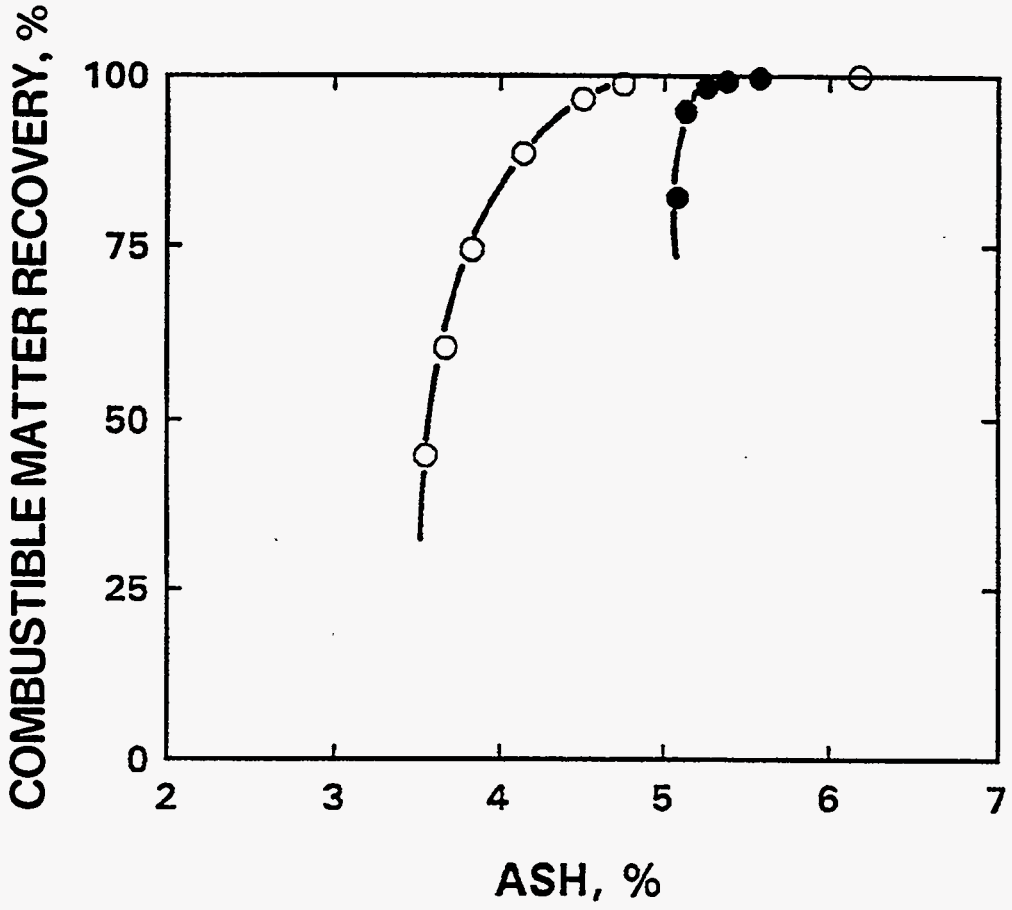

Figure 3-12. EFFECT OF DODECANE CONCENTRATION OF FLOTATION OF -65 μm PITTSBURGH SEAM COAL
(○-0.07 kg/T; ●-0.28 kg/T)

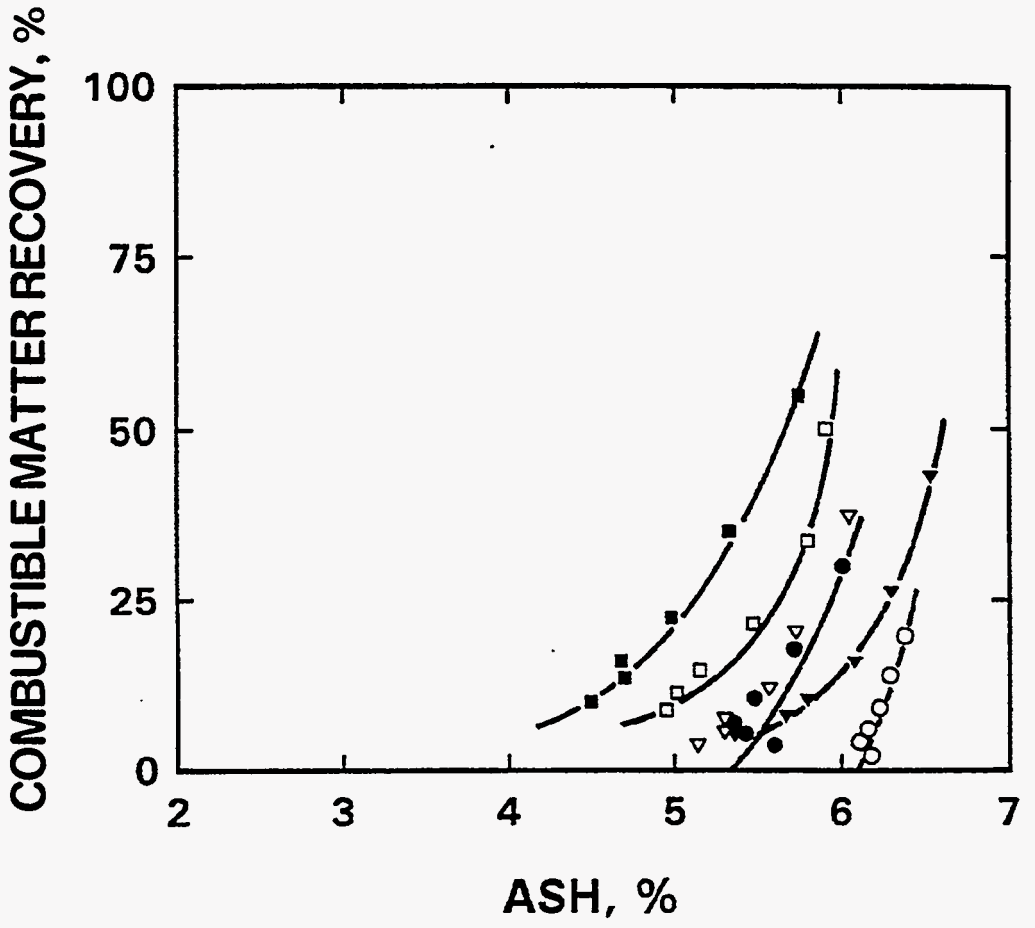

Figure 3-13. EFFECT OF DODECANE CONCENTRATION ON FLOTATION OF -65 μm INDIANA VII SEAM COAL (○-0.35 kg/T; ●-0.70 kg/T; ▽-1.40 kg/T; ▼-2.80 kg/T; □-5.60 kg/T; ■-11.20 kg/T)

Table 3-9. Combustible Matter Recovery and Ash Contents after 2 Minutes of Flotation as a Function of Oil Concentration for the Three Coal Samples.

Oil Conc. (kg/T)	-600 µm		-150 µm	
	$R_{2\ min.}$	$Ash_{2\ min.}$	$R_{2\ min.}$	$Ash_{2\ min.}$
Pittsburgh - Feed Ash: 7.0%				
0	91	5.0	85	4.8
0.15	98	5.8	97	5.5
0.30	99	6.1	98	5.7
0.60	99	5.9	99	5.9
Lower Kittanning - Feed Ash: 10.0%				
0	95	6.6	96	6.4
0.15	97	7.2	98	6.9
0.30	98	7.5	98	7.4
0.60	98	7.6	98	7.5
Indiana VII - Feed Ash: 9.2%				
0	6	9.0	9	10.1
0.15	13	7.1	12	9.0
0.30	20	6.2	11	8.2
0.60	25	5.9	12	7.3

Table 3-10. Selected Properties of the Surfactants Used in this Study

Surfactant	Surfactant Name: Pluronic -	Number of Hydrophobic PPO Groups	Number of Hydrophilic PEO Group	M.W.	HLB	Surface Tension @ cmc, dyne/cm
Ethylene PPO block copolymers	31R1			2,700	2.1	36.0
	L 64	30	26	2,900	14	43.0
	P 103	56	39	4,950	9	34.0
	P 104	56	60	5,900	13	33.0

PPO : Polypropylene oxide
PEO : Polyethylene oxide

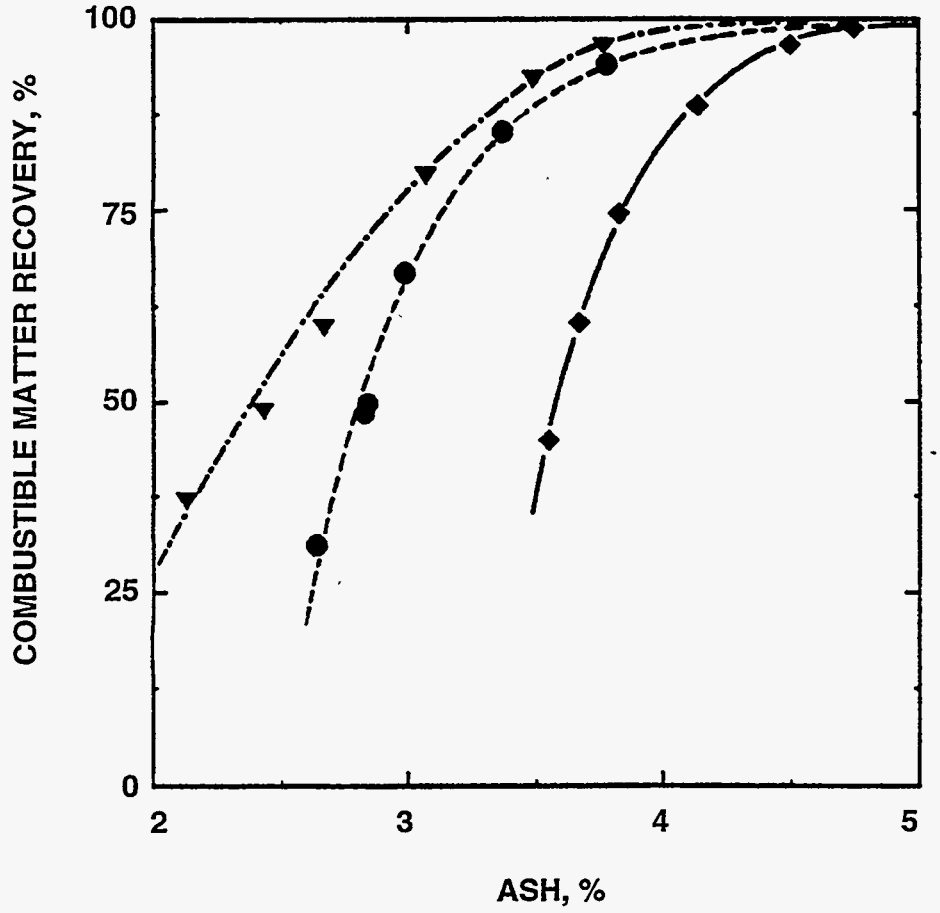

Figure 3-14. EFFECT OF PROMOTOR TYPE ON FLOTATION OF PITTSBURGH SEAM COAL
Frother: 0.5 kg/T MIBC; Collector: 0.07 kg/T Dodecane.
Promotor: ◆ - None; ▼ - 0.1 g/T L64; ● - 20 g/T P104.

the corresponding ash are presented in Figure 3-15. These results show that the effect of surfactant concentration is non-linear. At low concentrations, both the promotors reduced ash. It increased at intermediate concentrations, but decreased again when the surfactant concentration was about 0.02 kg/T. The data for flotation in the absence of surfactant were added for comparison. Based on these results the following observations were made:

- For the Pluronic L-64 surfactant, $1x10^{-4}$ kg/T (the lowest concentration tested) gave the best results with 80% CMR and 3.1 wt.% ash.
- For the Pluronic P-104 surfactant, a higher concentration was required to obtain low ash (3 wt.%) but the CMR decreased to 67%.
- At low surfactant concentrations, the surfactant with less number of ethylene oxide groups gave lower ash at a CMR of about 80%.
- Except at the lowest concentration, the increase in the number of ethylene oxide groups decreased the ash by about 0.5% and CMR by about 10%.

The surfactants might improve the efficiency of separation in two ways:

1. They make the coal more hydrophobic thereby increasing the rate of flotation.
2. They emulsify the oil to produce fine droplets. The fine droplets might act as collectors for coal or as liquid bridges. In both cases, an increase in flotation rate is expected but the effect on quality of the product might be more complex.

If 75% recovery is considered acceptable, the product ash is given as a function of surfactant concentration in Figure 3-16. These surfactants did not improve the flotation of the Upper Freeport seam coal.

The surfactants had somewhat different effect on the flotation of Indiana VII seam coal. The results are presented in Figure 3-17 for two reagents: Pluronic L-64 and 31R-1. Slightly different reagents were tested because this coal is relatively more hydrophilic. It can be readily seen that the amount of collector needed for this coal is considerably more than that for the Pittsburgh seam coal. The effect of reagent concentration varied with the type of surfactant. Target ash (< 5 wt.%) could be obtained for this coal using both the reagents at 90% recoveries. Surfactants did not improve the performance of the Lower Kittanning seam coal but some improvement was possible by using the surfactant in the second (cleaner) stage of flotation, as can be seen from the results in Figure 3-18. Based in these observations, alternate cleaning strategies were developed for this coal and will be discussed in the Phase II report.

To delineate the effect of surfactant type and concentration, contact angle and emulsification studies are being conducted and the results will also be addressed in Phase II.

Flotation Kinetics Models

Kinetics of flotation are important for the design of a flotation circuit and to evaluate the effect of reagents on flotation separations. Even though the rate of coal flotation has been studied by many investigators, there is no general agreement on the models to be used. Various investigators have been unable to select an appropriate model to describe the laboratory data for

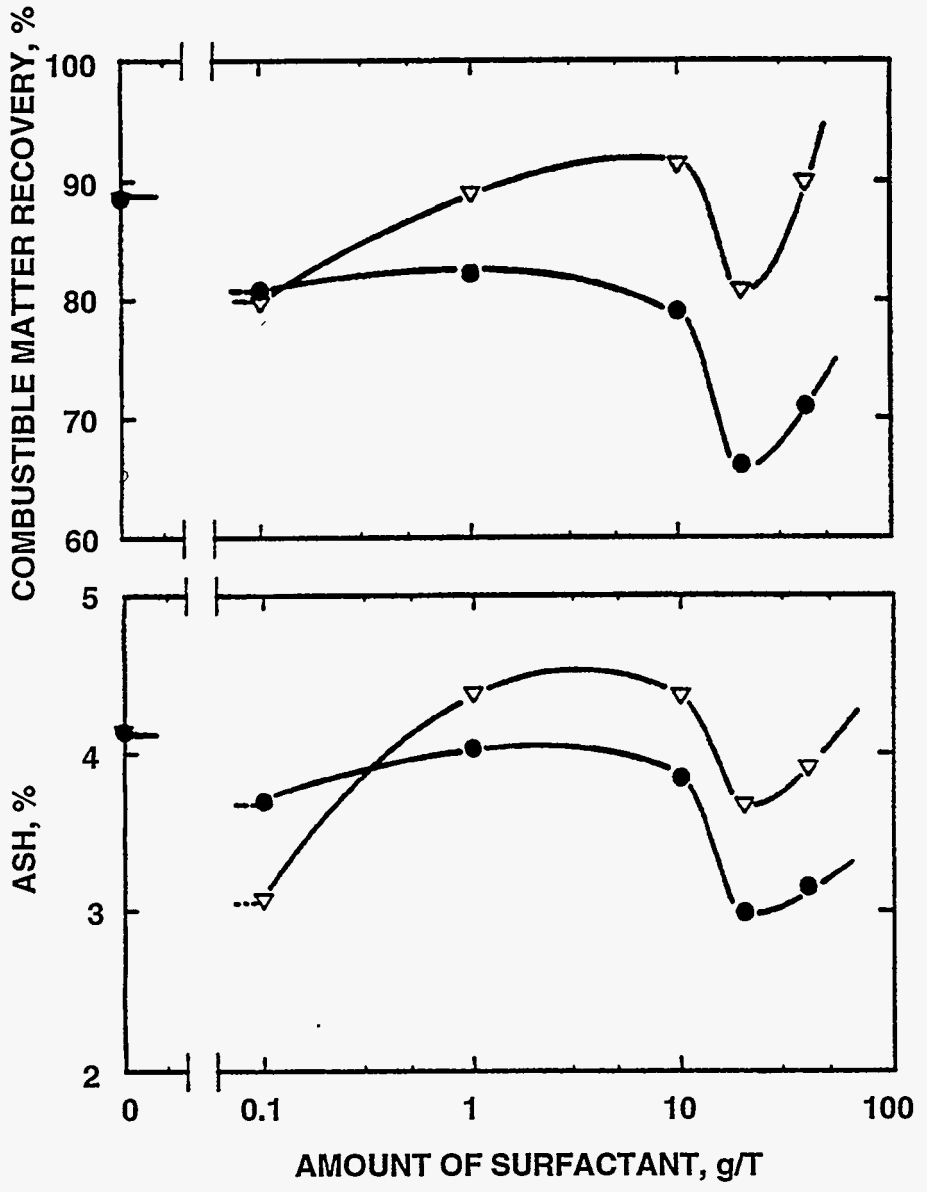

Figure 3-15. EFFECT OF SURFACTANT CONCENTRATION ON THE COMBUSTIBLE MATTER RECOVERY (CMR) AND ASH % FOR THE PITTSBURGH SEAM COAL
Frother: 0.5 kg/T MIBC; Collector: 0.07 kg/T Dodecane.
(▽ - L64; ● - P104)

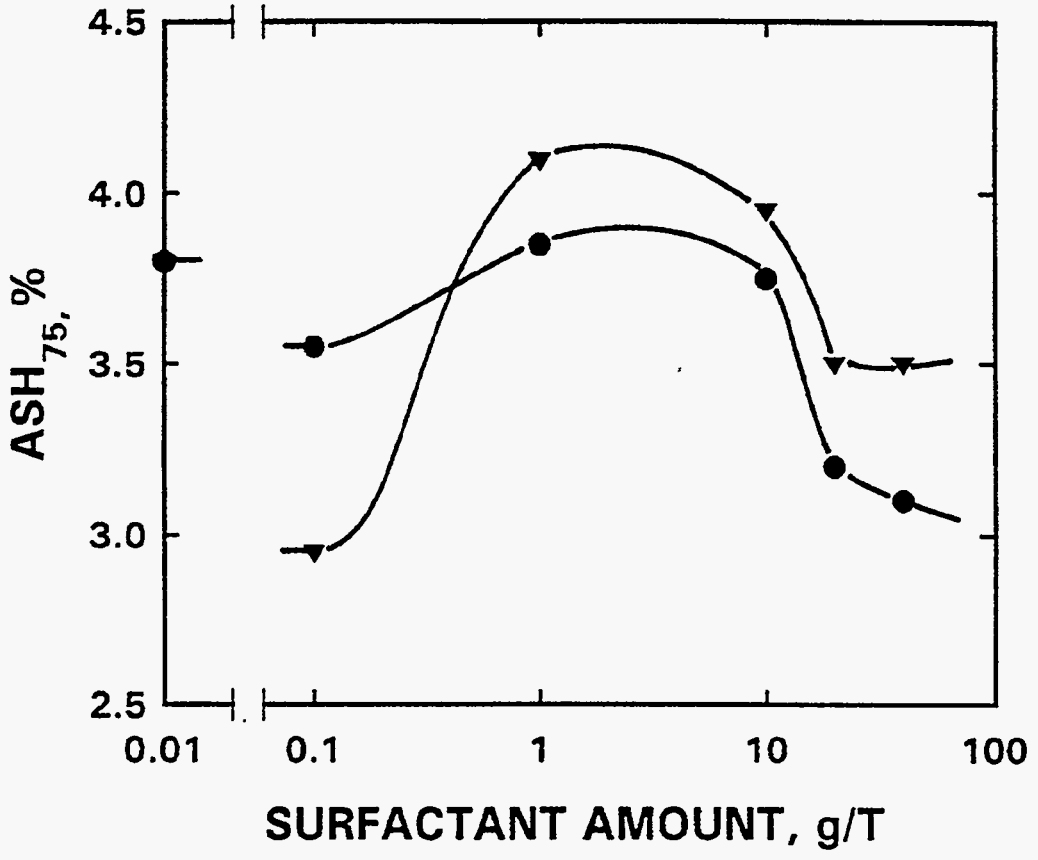

Figure 3-16. EFFECT OF SURFACTANT CONCENTRATION ON THE ASH % FOR 75% COMBUSTIBLE MATTER RECOVERY FOR THE PITTSBURGH SEAM COAL
Frother: 0.5 kg/T MIBC; Collector: 0.07 kg/T Dodecane.
(▼ - L64; ● - P104)

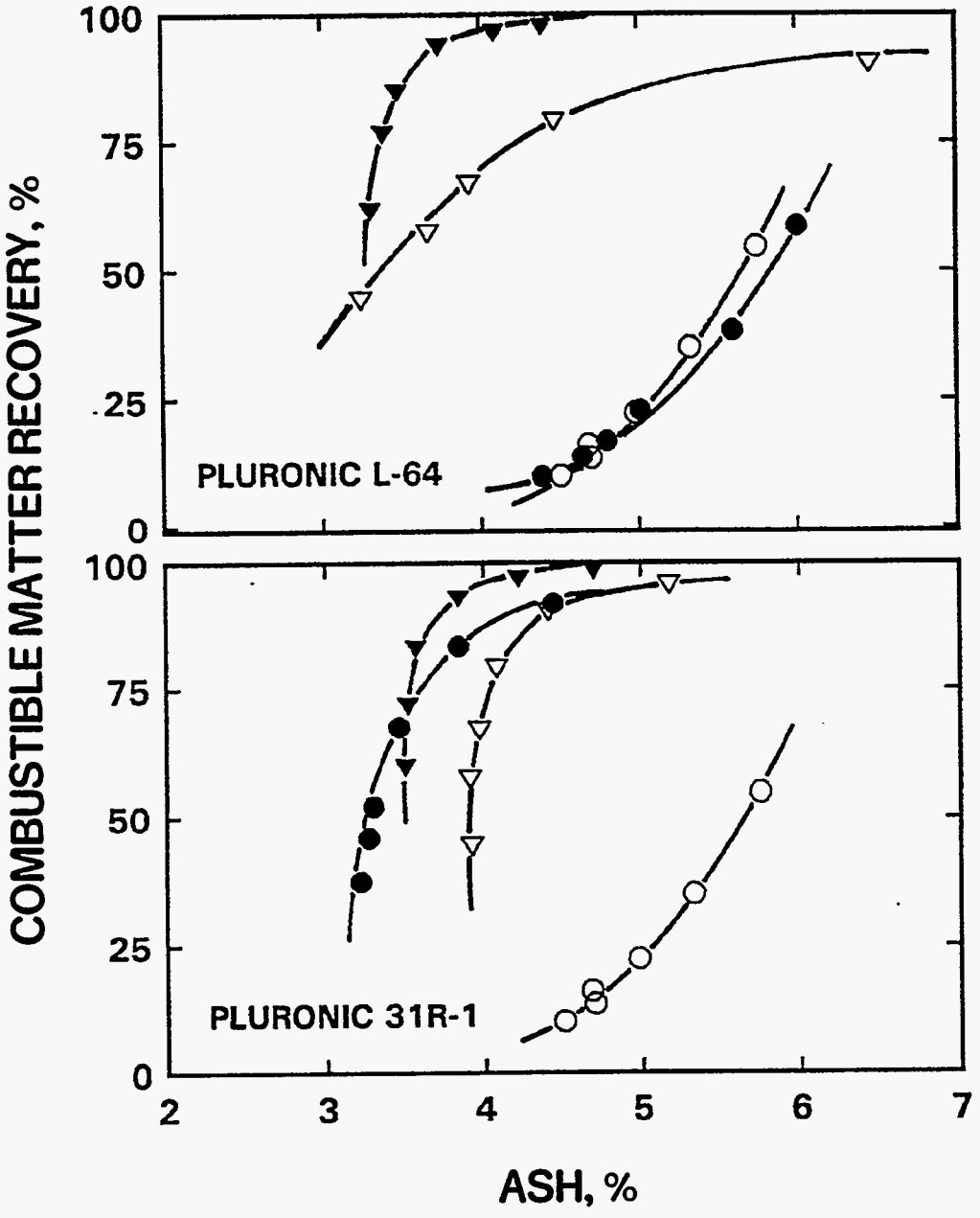

Figure 3-17. FLOTATION OF INDIANA VII SEAM COAL AT VARIOUS PROMOTOR ON CENTRATIONS IN THE PRESENCE OF 0.5 kg/T MIBC AND 11.20 kg/T DODECANE
(■ - no promotor; ● - 1.12 kg/T; ▽ - 5.60 kg/T; ▼ - 8.0 kg/T)

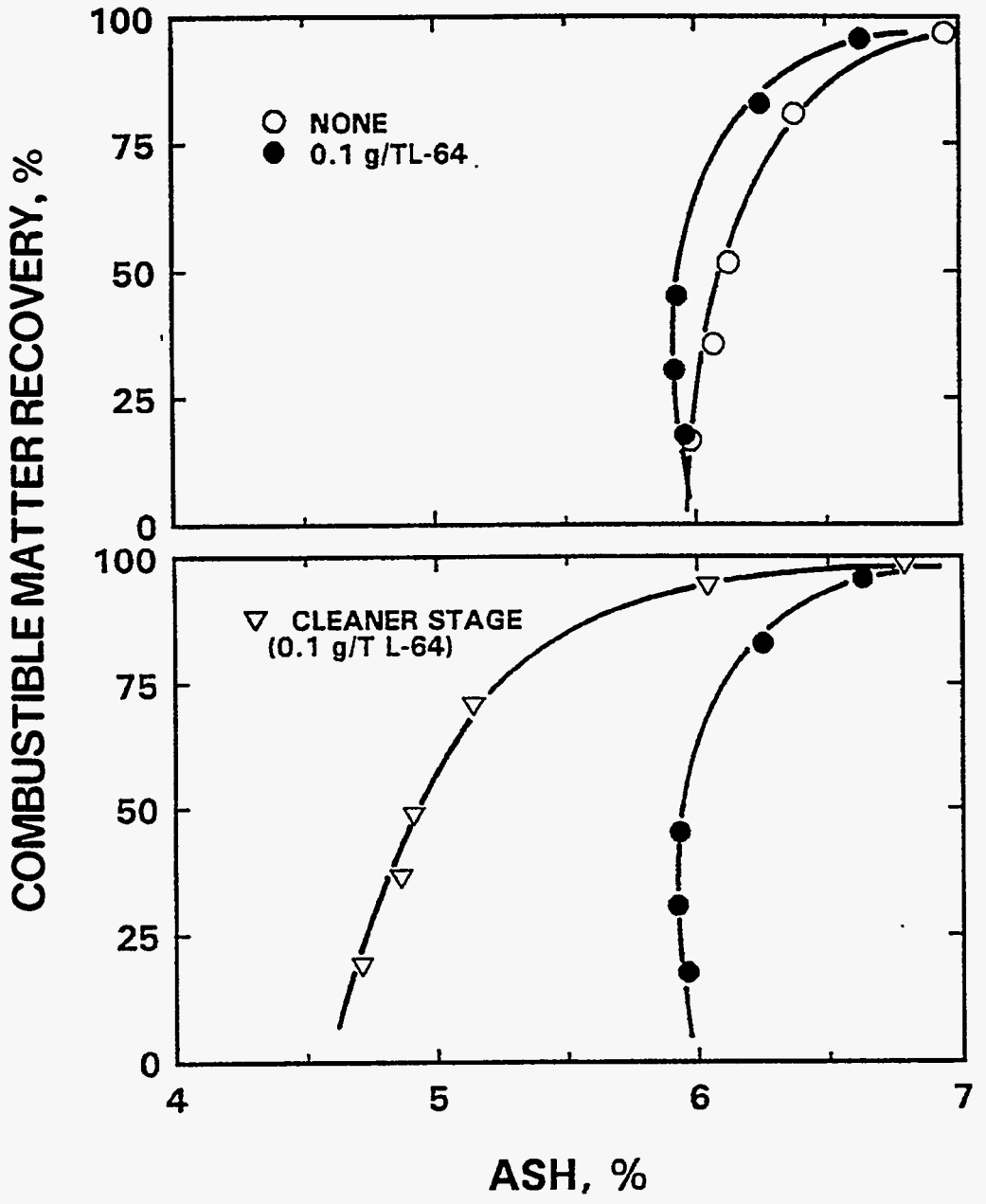

Figure 3-18. FLOTATION OF LOWER KITTANNING SEAM COAL IN THE PRESENCE OF SURFACTANT AND SECOND STAGE FLOTATION
Frother: 0.5 kg/T MIBC; Collector: 0.07 kg/T Dodecane
(○ - none; ● - 0.1 kg/T L-64; ▽ - second stage flotation with 0.1 g/T L-64)

kinetics of coal flotation. Since such data are essential for scale-up, studies were carried out to address this issue. Normal practice is to use a kinetic model to fit the coal yield (or recovery data). Two types of models have been considered in the past:

- Phenomenological Models: These models consider the process of flotation as analogous to a chemical reaction or other rate processes.
- Microscopic Models: In these models, the sub-processes occurring in flotation cell, such as bubble-particle collisions, attachment and detachment are considered.

While microscopic models provide a detailed insight of the processes occurring in the flotation cell, phenomenological models are simpler and adequate for scale-up and design. They are also suitable for evaluating the effect of various operating variables in laboratory experiments. Dowling et al.[22] evaluated several models, and found that all the models tested gave a reasonably good fit to the experimental data. Although some models were better than others the hierarchy of best models was expected to be a function of the material being floated. Since a suitable model is essential for evaluation of flotation kinetics data and to use the results for design and scale-up, a continued effort is needed for model evaluation and development. Therefore, several models were considered for this project and a few were selected for further evaluation. The criteria used were as follows:

- Minimum number of parameters to obtain a reasonable goodness of fit.
- Physical meaning of the model parameters. This aspect was deemed important for interpreting the effect of various operating variables on flotation performance.

The first step in evaluation of flotation results was to select a model to evaluate the results of flotation kinetics. Approximately 25 models in the literature were reviewed which were grouped as:

First-order models:	several models
Second-order models:	several models
Miscellaneous models:	froth flow, gas adsorption, two phase, law of proportionality, etc.

Various first-order flotation models and a few others were evaluated and a new model was developed because the existing models were deemed to be unsatisfactory. It was determined that some of the models gave a good fit in some conditions whereas others were better under different conditions. The reasons were not clear, however. On the basis of the literature survey, the following three models were selected for this project:

Classical First-Order Model (Model C)
First-Order Model with Rectangular Distribution of Floatabilities (Model R2)
First-Order Model with Sinusoidal Distribution of Floatabilities (Model S2)

Classical First Order Model

This is the basic model in which the flotation process is considered analogous to a first-order chemical reaction. The model is well known and used by many investigators to describe the kinetics of flotation in a laboratory cell. The mathematical form of this model can be written as

$$R(t) = R\infty[1-e^{-kct}] \tag{3-11}$$

where R is the recovery at time t, R_∞ is the recovery after long time (ultimate recovery), and k_C is the first-order rate constant.

First-Order Model with Rectangular Distribution of Floatabilities

This model was suggested by Huber-Panu et al.[23] and Klimpel[24] by considering a rectangular distribution of the rate constant in the first-order model. The model may be written as

$$R(t) = R_\infty\left[1-\frac{1-e^{k_{R2}t}}{k_{R2}t}\right] \tag{3-12}$$

This model was also derived by Meyer and Klimpel[25] by considering the effect of mechanical rate of froth removal from the cell.

First-Order Model with Sinusoidal Distribution of Floatabilities

This model was proposed by Fuerstenau and his co-workers[26]. The mathematical form of this model in which a sine function is considered to describe the distribution of floatabilities may be written as

$$R(t) = R_\infty\left[1-\frac{\left(\frac{2k_{s2}t}{\pi}\right)e^{-k_{s2}t}}{1+\left(\frac{2k_{s2}t}{\pi}\right)^2}\right] \tag{3-13}$$

Since none of the above models gave satisfactory fits to the experimental results, another model was developed as a part of this investigation and is discussed in the paragraphs that follow.

A First-Order Flotation Kinetics Model with Normal Distribution of Floatabilities

In this model, which is referred to as Model N3, the rate of flotation is assumed to be a normal distribution about a mean value. This model is capable of fitting the rate data under a wide variety of flotation conditions and the fitting errors were found to be small in the cases tested thus far.

The general form of the first-order rate equation with a floatability distribution f(k) is

$$R(t) = R_\infty\left[\int_o^\infty f(k)e^{-kt}\,dk\right] \tag{3-14}$$

Where (t) is the recovery at time t and R_∞ is the ultimate recovery. If a normal distribution of floatabilities is assumed

$$f(k) = \frac{1}{\sqrt{2\pi\sigma}}e^{-\frac{1}{2}\left[\frac{k-\mu}{\sigma}\right]^2} \quad \text{where } 0<k<2\mu \tag{3-15}$$

and

$$\int_o^{2\mu} f(k)dk \approx 1$$

The following first-order model is obtained

$$R(t) = R_\infty\left[\frac{e^A(erfB - erfC)}{2}\right] \tag{3-16}$$

The quantities A, B and C are defined by the following equations:

$$A = -\mu t + \frac{\sigma^2 t^2}{2} \tag{3-16a}$$

$$B = \frac{\sigma t + \mu/\sigma}{\sqrt{2}} \tag{3-16b}$$

$$C = \frac{\sigma t - \mu/\sigma}{\sqrt{2}} \tag{3-16c}$$

where μ is the mean and σ is the standard deviation of the normal distribution curve.

A two-parameter form of N3 can be derived if one assumes that the standard deviation is dependent on the mean. If we assume that $\mu=3\sigma$, the resulting two parameter model (which is referred to as Model N2) has the same form as given in Equation 3-16 where the quantities A, B and C are defined as

$$A = -\mu + \frac{\mu^2 t^2}{18}$$

$$B = \frac{\mu t + 9}{\sqrt{18}}$$

$$C = \frac{\mu t - 9}{\sqrt{18}}$$

Model Evaluation

The frequency distributions obtained from fitting the models to kinetics data are given in Figure 3-19 for the Upper Freeport and for the Pittsburgh seam coals. The experimental conditions are given in the figure caption. The results of fitting five different models are given. It can be seen that the predicted range of the floatabilities are strongly model dependent, making it necessary to select the model which most accurately represents the actual distribution of floatabilities. An accurate estimation of rate data is necessary for optimization, design, and scale-up of flotation. The floatability distributions vary with coal type and conditions of flotation, as expected. The model fitting errors are given in Figure 3-20 as mean residual squares (MRS). For the Upper Freeport seam coal the MRS increased in the order:

$$N3 < N2 < S2 < R2 < C \qquad (3\text{-}17)$$

and, for the Pittsburgh seam coal, it increased in the order:

$$N3 \sim C < N2 < S2 < R2 \qquad (3\text{-}18)$$

For both the coals, errors were least for the Model N3. The model is being evaluated further using the flotation results for other test conditions.

Effect of Particle Size on Flotation Kinetics

Studies conducted as a part of this project show that the statistics of fitting first-order models improved considerably when the flotation products were screened and analyzed individually, as can be seen from the results given in Figure 3-21 and Table 3-11. For the purpose of illustration, Model C was used to fit the flotation kinetic data. Evaluation of other models is in progress. This method (Method II) is a compromise between the traditional method of analyzing the flotation products collected at pre-selected time intervals (Method I) and a more elaborate method in which size-specific gravity fractionation on flotation products is done followed by analysis of individual fractions (Method III). The traditional method is well known and was used

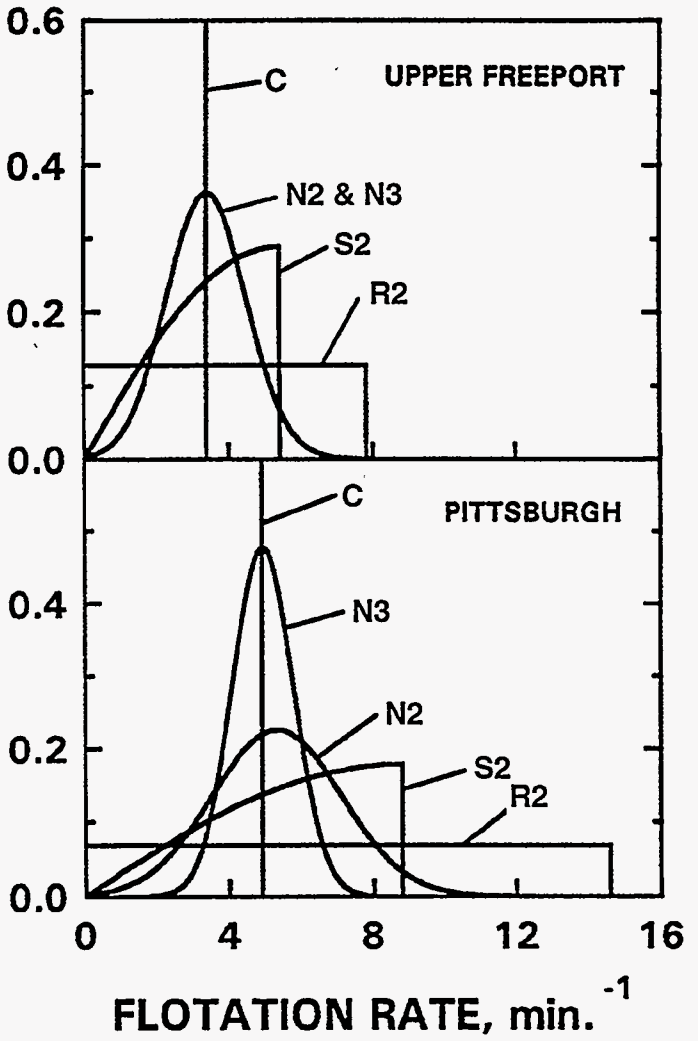

Figure 3-19. FREQUENCY DISTRIBUTIONS OF FLOTATION RATES OF THE OVERALL SAMPLE PREDICTED BY VARIOUS FIRST-ORDER FLOTATION KINETICS MODELS FOR THE UPPER FREEPORT AND PITTSBURGH SEAM COALS Experimental conditions: collector and frother conc. 0.3 kg/T, solids conc. 10%. See text for various model designations.

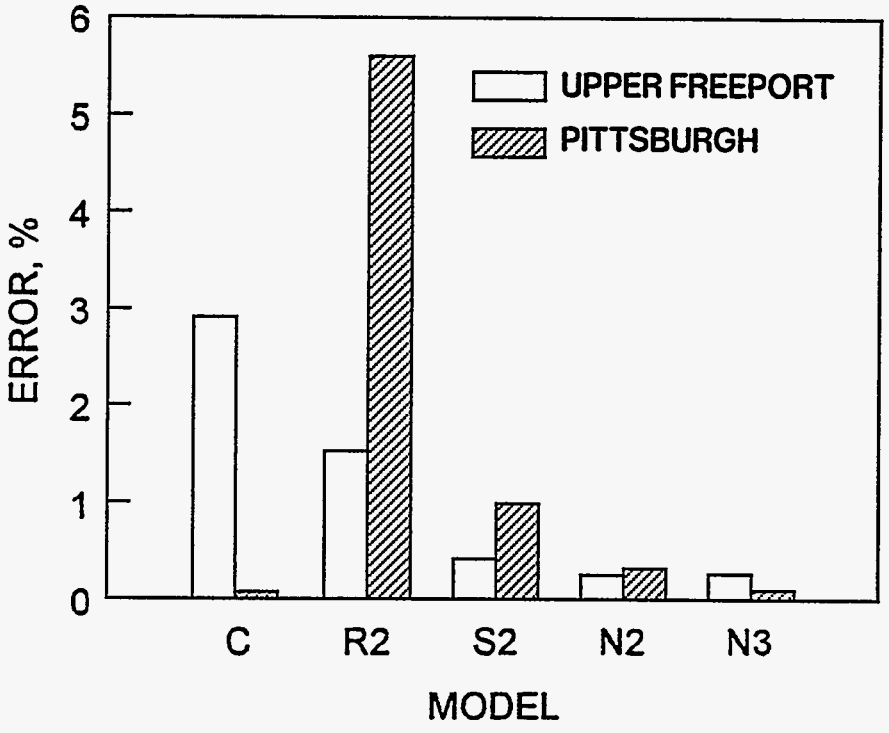

Figure 3-20. THE MEAN RESIDUAL SQUARE ERRORS OF VARIOUS MODELS FOR THE DISTRIBUTIONS GIVEN IN Figure 3-19

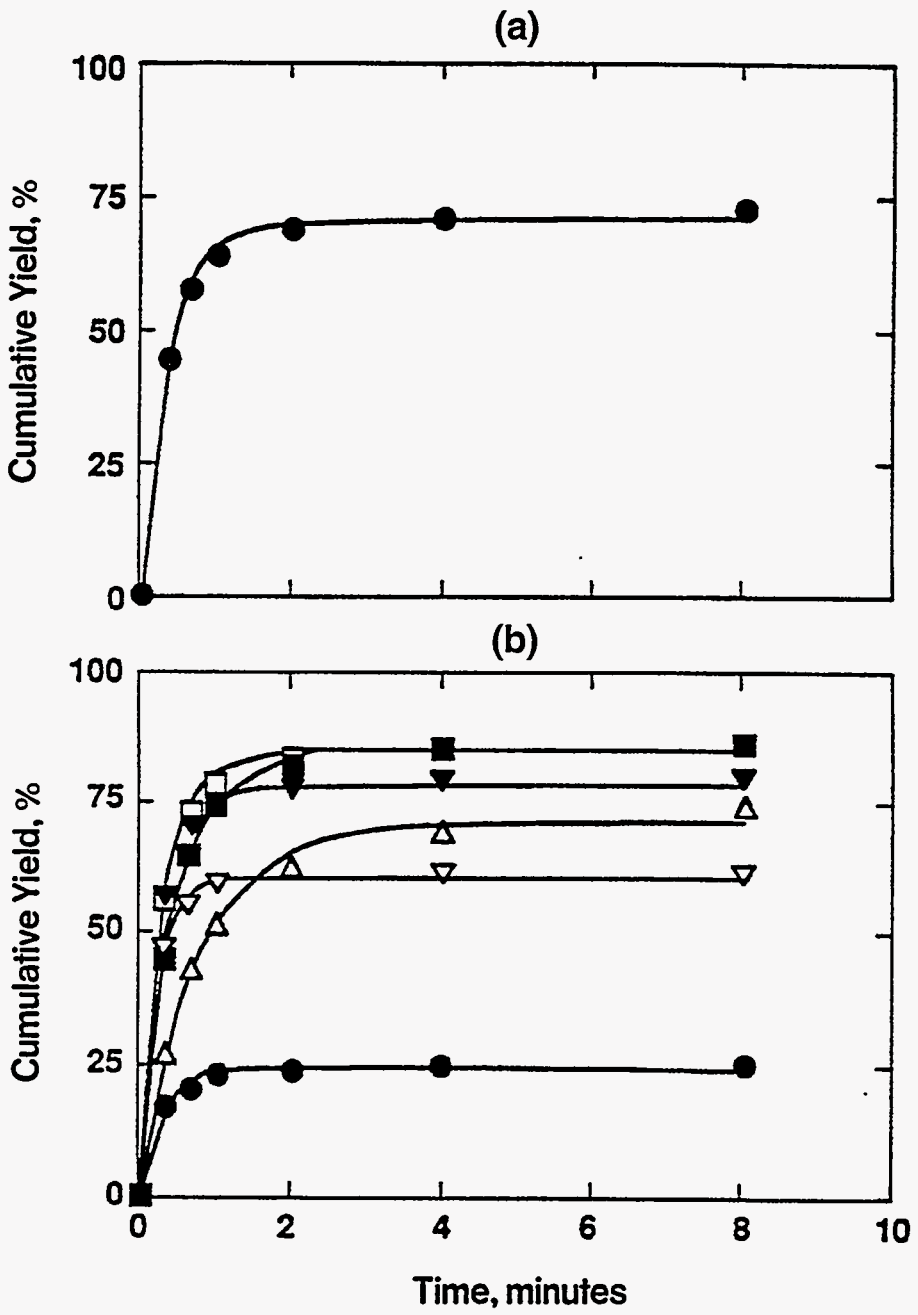

Figure 3-21. KINETICS OF FLOTATION OF hvA BITUMINOUS COAL FROM UPPER FREEPORT SEAM
Frother: 0.3 kg/T MIBC; Collector: 0.3 kg/T dodecane
a) Flotation kinetics of total material
b) Flotation kinetics of individual size fractions
(● +20 M; ▽ 28 x 48 M; ▼ 48 x 100 M; □ 100 x 200 M; ■ 200 x 400 M; △ -400 M)

Table 3-11. Statistical Parameters of Fitting Model C to Individual Size Fractions in Coal Flotation (Frother: 0.30 kg/T MIBC)

	SIZE FRACTION, μm						
	+600	**300x600**	**150x300**	**75x150**	**38x75**	**-38**	**Total**
a) No Collector							
R_∞	45	81	90	94	96	91	87
k_C	2.43	2.65	2.35	1.92	1.56	0.92	1.86
r^2	0.986	0.999	0.998	0.999	0.999	0.996	0.997
MRS	4.58	1.20	2.47	1.89	1.58	5.48	3.75
b) Collector: 0.15 kg/T							
R_∞	51	83	92	95	95	90	89
k_C	3.53	4.30	3.70	3.20	2.29	1.44	2.84
r^2	0.995	0.998	0.998	0.998	0.999	0.995	0.996
MRS	2.25	1.83	3.32	2.83	1.90	6.23	5.33
c) Collector: 0.30 kg/T							
R_∞	66	90	95	97	97	91	91
k_C	4.94	5.03	4.07	3.23	2.56	1.43	3.12
r^2	0.999	1.000	0.999	1.000	0.999	0.994	0.998
MRS	0.53	0.72	0.84	0.48	0.96	8.62	2.94
d) Collector: 0.60 kg/T							
R_∞	68	92	96	98	97	90	93
k_C	4.36	4.82	3.92	3.20	2.72	1.58	3.19
r^2	0.999	0.999	0.998	0.999	0.999	0.997	0.997
MRS	0.64	1.27	2.34	1.19	2.16	4.51	3.72

recently by researchers at the University of California, Berkeley, as part of a project sponsored by the DOE. The second approach was developed and used by Penn State's Mineral Processing Section (R. Hogg and S. Chander) as part of a project also funded by the DOE. Method I is not very satisfactory because the model discrimination is often poor whereas Method III provides more details but requires laborious experiments and data analysis. It should be noted that the size fractionation approach was used by Lay and Bell[27], Rastogi and Aplan[28], and later by others. Even though the method has been known for many years, its statistical advantages have not been discussed and it has not been used extensively in coal flotation research.

In the approach used in the present investigation, various flotation products were screened and the screen fractions were dried and weighed. The results were used to calculate the yields from which the rates of flotation of the individual size fractions were determined. The ash and sulfur analyses are also being conducted and will be reported later. The results are given in Figure 3-21 for a hvA bituminous coal from the Upper Freeport seam. The symbols represent the measured data and the lines were obtained by fitting the model. Figure 3-21a is for the unscreened material and Figure 3-21b is for various screen fractions. A careful examination of the experimental data and fitted results in Figure 3-21 shows a certain amount of 'systematic' error. The goodness of fit can be seen from the values of r^2 and MRS (mean residual squares). There was one exception, however, in that the -400 mesh fraction which gave larger errors. The reasons for this are being investigated.

Even though the effects of particle size and collector concentration on the rate of flotation and ultimate recovery appear to be reasonable, these results are considered to be preliminary until the validity of this approach has been tested using other models and tests with additional coal samples.

Column Flotation

A flotation column is a bubble column device in which separation between disperse phases is achieved using differences in their affinity for air bubbles. The concept of column flotation was first developed and patented in the mid 1910's by Flinn and Towne[29]. However, this early design was not commercially successful as it was plagued by solid settlement on the gas distributor. The success of the Boutin and Wheeler design of flotation column that was patented in the early 1960's[30] is attributed in part to its ability to overcome the solid settlement problem on the gas distributor.

At present, flotation columns are employed in a number of applications in the mineral processing industry[31]. Indeed flotation columns have been found to be effective in fine coal cleaning (e.g., [32-34]). In spite of the considerable research efforts and industrial applications of column flotation in the last seventy-seven years, the design and scale-up of flotation columns remains an empirical art. For example, all present designs are based on the use of analogy with chemical kinetics. According to this approach, the rate of recovery of hydrophobic particles in the

collection zone may be represented as a first order rate process. Thus, only the Damkohler number, kt_p, where k and t_p are the rate constant and particle residence time, respectively, and the mixing parameters of the process vessel or age distribution of the particles, are required for design and scale-up. Accordingly, the recovery is given by

$$(1 - X) = 4q \exp(Pe_p/2)/\{(1 + q)^2 \exp(Pe_p q/2) - (1 - q)^2 \exp(-Pe_p q/2)\} \quad (3\text{-}19)$$

where X is the fractional recovery and q is defined as

$$q = (1 + 4kt_p/Pe_p)^{0.5} \quad (3\text{-}20)$$

In Equation 3-19, Pe_p is the particle Peclet number, a measure of the particle mixing intensity in the sedimentation dispersion model. Some issues about this approach were recently raised by Ityokumbul[35, 36] which may lead to new perspectives in the design of flotation columns. Firstly, the use of Equation 3-19 in flotation column design and scale-up is predicated on the validity of the sedimentation-dispersion model in providing an accurate description of the solid particle behavior in the column. Unfortunately, solid tracer analysis using the sedimentation-dispersion model has consistently shown that the particle mixing intensity increases with size and in most instances, may even be larger than the corresponding value for the liquid[37-39]. Since the larger particles have a higher inertia, it is highly unlikely that they will be more mixed than the smaller ones under the same flow conditions. For the same reason, the dispersion coefficient of the solid particles cannot be larger than that of liquid molecules under the same flow condition. As indicated above, the results from the sedimentation-dispersion model are at variance with physical reality. The reasons for this observation (i.e., increased mixing with particle size) have been provided by Ityokumbul[35] and will not be repeated here, suffice to say that it clearly demonstrated that the sedimentation dispersion model does not provide an accurate description of the particle behavior in flotation columns. Ityokumbul[40] has recently shown that the behavior of solid particles in a flotation column may be described using the sedimentation-convection model.

Secondly, Equation 3-19 predicts that the recovery be independent of initial concentration of floatable particles. This is clearly not the case in flotation, especially at high concentrations for which the column carrying capacity is limited. Furthermore, Equation 3-19 suggests that increased mixing may result in lowering of the recovery. For typical column applications (where slugs of air bubbles are absent), intimate contact between the air bubbles and the hydrophobic particles is indeed required for separation to take place. This intimate contact only comes about as a result of mixing of the liquid phase which contains the hydrophobic particles. In fact the results of Espinosa-Gomez et al.[41] clearly indicate that with lead/zinc separation, the recovery/grade performance increases with mixing intensity.

In view of the inadequacies inherent in the present approach to flotation column design, a new approach based on fundamental principles was recently presented[35, 36]. The use of this approach to determine key design and scale-up parameters for column flotation has also been demonstrated[42] and will form the basis for the analysis of the flotation data in the present study.

Theory

The new approach to flotation column design is based on the consideration of the bubble loading rate, since it is this process that results in the separation. While the detailed theoretical formulation may be found elsewhere[35, 36], it was shown that the performance equation is given by

$$z = \frac{(U_R + V_p)}{ak\Gamma_m} \ln(1 - X) \qquad (3\text{-}21)$$

where z is height of recovery zone required for a given recovery, X, a is the bubble interfacial area, k the particle transfer rate constant, Γ_m is the maximum bubble load, U_R and V_p are the slurry velocity in the recovery zone and particle settling velocity, respectively. In Equation 3-21, the terms $k\Gamma_m$, $(U_R+V_p)/ak\Gamma_m$ and -ln(1 - X) are equivalent to the interface mass transfer coefficient, height of a transfer unit, HTU, and number of transfer units, NTU, respectively. As with other mass transfer operations in chemical engineering, the HTU is a measure of the difficulty of separation. A brief discussion of this follows.

The maximum NTU cannot be varied at will. It is determined by the maximum recovery which is a function of the degree of liberation of the mineral, reagent dosage, hydrophobicity of the particles, etc. The validity of this approach has been tested using literature data from a variety of applications (coal and mineral flotation in columns of different sizes). In addition, this approach has, for the first time, succeeded in demonstrating the detrimental effect of using excessively tall columns in some applications[35, 36, 42].

As indicated earlier, the term $(U_R + V_p)/ak\Gamma_m$ is a measure of the difficulty of the separation. It follows from this that the difficulty of separation increases with slurry velocity in the recovery zone and particle size. Intuitively, this is indeed a valid observation as the effect can be explained on the basis of reduced particle residence time in the recovery zone. The height of the transfer unit is inversely proportional to the quality of air dispersion in the system (through the interaction of a and to some extent, Γ_m). This is also a reasonable assumption insofar as flotation is an interfacial phenomenon: increasing the quality of air dispersion results in an increase in the bubble surface area available for flotation. The failure of the first column installations at Inspiration Copper Company was attributed to solid settlement on the gas distributor. Since bubble coalescence was reported with solid settlement on the gas distributor, it is obvious that the

available bubble surface for particle collection was reduced resulting in an increase in the HTU. It is obvious from the foregoing that knowledge of bubble characteristics (size, gas hold-up) will be required in the interpretation of flotation data. Unfortunately, information on bubble characteristics is rarely reported with flotation data. This makes comparison of flotation results in different vessels and/or with different spargers very difficult.

A comparison of estimates of the HTU from a number of applications in columns of different sizes was made recently and is summarized in Table 3-12. The results obtained indicated that coal cleaning generally gave lower HTUs in comparison to minerals made selectively hydrophobic[36]. This observation is expected since coal is naturally hydrophobic and the concentration of floatable particles is usually higher. From the data in Table 3-12, it is estimated that the maximum collection zone height required for coal cleaning should not exceed 2 m. This probably explains why Parekh et al.[34] did not observe any dependence of recovery on column height in the range 3-8 m.

The ensuing analysis has shown that the quality of air dispersion will have a strong effect on the column performance. Thus the availability of bubble surface does represent a useful design and scale-up parameter. However, the operational parameters controlling the bubble size are the gas velocity, bubble generator design, and solution chemistry. Xu and Finch[43] have shown that the bubble size varies with gas velocity according to

$$d_b = C(R_g U_g)^n \tag{3-22}$$

where C and n are constants and R_g is the ratio of column cross-sectional area to the area of sparger. For sparging through porous media, Xu and Finch[43] reported that n was in the range 0.2 to 0.5. It is therefore important to determine *a priori* the maximum gas velocity for effective column flotation. By using dimensional analysis, Ityokumbul[44] has shown that the maximum gas velocity for column flotation is related to the column diameter by the relationship

$$U_g, \max = 0.11 D_c^{0.5} \tag{3-23}$$

Analysis of published data show that in most large diameter columns ($D_c > 0.5$ m), the operational gas velocities were less than 40% of the maximum values predicted by Equation 3-23 (see Figure 3-22).

Future Test Plans

A laboratory flotation column was designed and built and will be used in Phase II testing. The column has an internal diameter of 0.076 m and an overall height of 5.5 m; however, its height can be readily varied due to its sectionalized nature. Cominco^R and Mott Metallurgical^R bubble

Table 3-12. Estimates of the Heights of Transfer Unit for the Different Column Applications.

Reference	Application	D_c, m	d_p, mm	U_R, m/s	HTU, m
Luttrel et al. (1988)	Coal	0.05	5	0.0067	0.29
Bensley et al. (1985)	Coal	0.10	-75	0.0039	0.28
Reddy et al. (1988)	Coal	0.10	-500	0.0043	0.43
Kho and Sohn (1989)	Talc	0.06	16	0.0066	0.26
Ounpuu and Tremblay (1991)	Sphalerite	1.20	-38	0.0063	0.48
Ynchausti et al. (1988)	Fluorite	0.06	-300	0.0114	0.70
	Pyrolusite	0.06	-210	0.0052	1.50

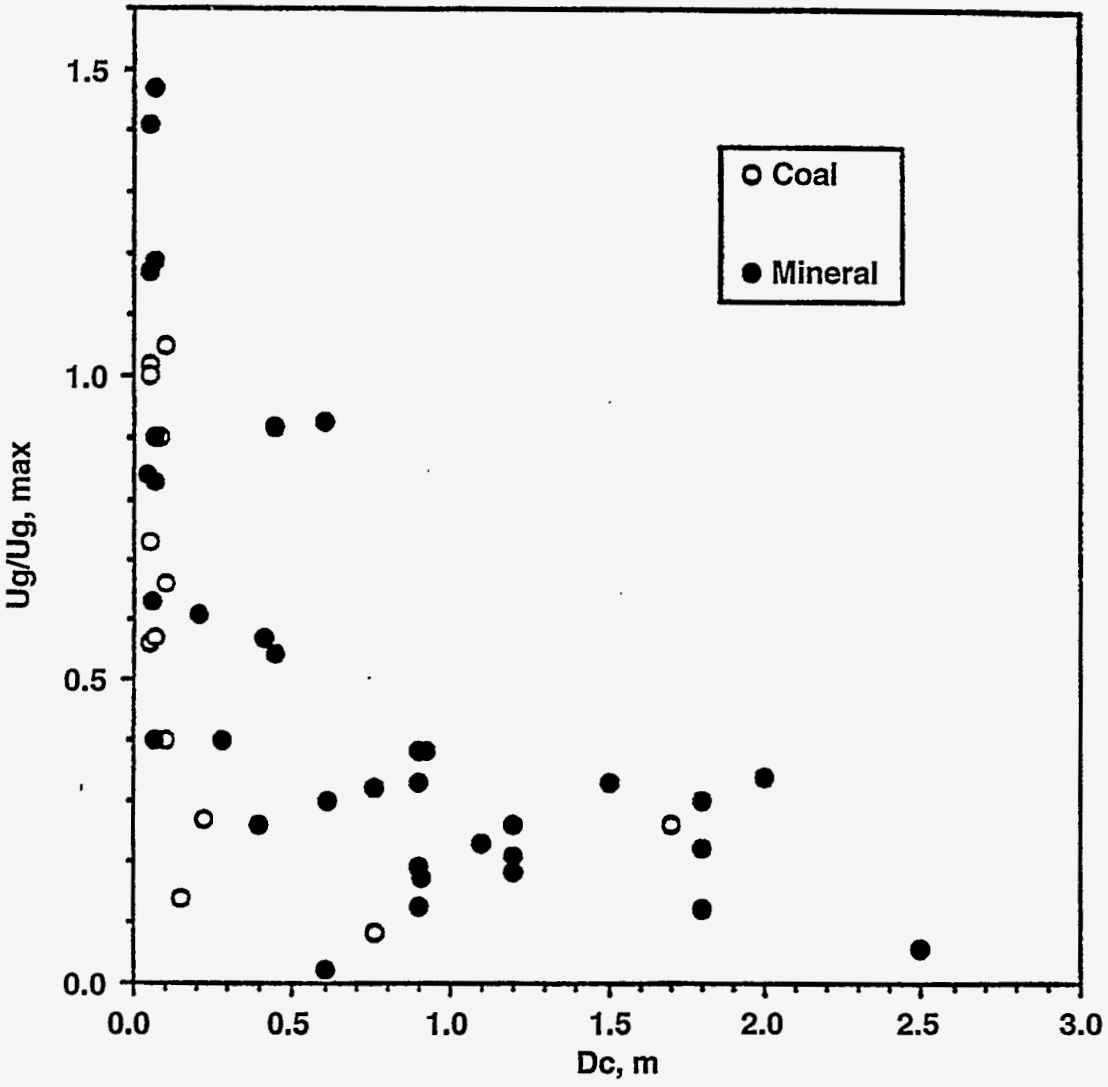

Figure 3-22. COMPARISON OF OPERATIONAL TO THE THEORETICAL MAXIMUM GAS VELOCITIES IN COLUMN FLOTATION

generators have been procured. The former employs high external shear to generate fine bubbles while the latter forces air through a porous medium with an average pore size of 2 mm. High-accuracy pressure transmitters (Cole-Palmer Model G-68971) installed along the column axis will be used to measure the static pressure profile. This profile will be used to determine the gas hold-up and the location of the pulp-froth interface. Schematic diagrams of the experimental set-up and the two bubble generators are shown in Figures 3-23 and 3-24.

In summary, the experimental work will consist of the following:

- bubble size/gas hold-up measurements with the different spargers;
- recovery/grade data with the different gas spargers; and
- analysis of the data to determine design parameters (terminal recovery, HTU, etc.).

Results of the Gas Hold-up Measurements

While the 0.076 m flotation column was under construction, gas hold-ups in a 0.063 m flotation column equipped with the static sparger were measured. The gas hold-up was estimated from static pressure measurements along the column axis. Since the behavior of air bubbles is influenced by the presence of frothers, the gas hold-up was determined as a function of gas velocity and frother concentration. For this study two frothers commonly used in flotation column work, methylisobutylcarbinol (MIBC), and Dowfroth 250C (DF250C), were selected. Figure 3-25 shows the gas hold-up data in the air-water and air-water-frother systems. For the same gas velocity, a higher gas hold-up is indicative of a higher bubble interfacial area in the column. These results show that the gas hold-up increases with the addition of frother which is consistent with the observation of others [45]. In addition, the results show that in comparison with MIBC, DF250C is a better frother.

Figure 3-26 shows the dependence of gas hold-up on the concentration of DF250C. It can be seen that the gas hold-up increases with frother concentration, however, the increase was not proportional to the frother concentration. Similar results were obtained with MIBC.

The drift-flux approach was used to estimate the terminal bubble rise velocity. Using correlations that have been developed by Ityokumbul et al.[46], the average bubble size in the presence of DF250C was estimated to be of the order of 1 mm. While the size of bubbles from the Mott Metallurgical sparger is suitable for fine coal flotation, it is not clear if clogging of the sparger will influence its performance. In order to study this phenomenon, the gas hold-up was determined at 100, 75, 50 and 25% of the total sparger surface area. The results obtained are shown in Figure 3-27. The results obtained show that for 25% reduction in the sparger surface area, the bubble characteristics are not significantly effected. Similar results were obtained with MIBC.

The 0.076 m column construction is completed and preliminary testing has been carried out. Systematic investigations of the effects of air, slurry and recovery zone heights will be conducted in Phases II and III.

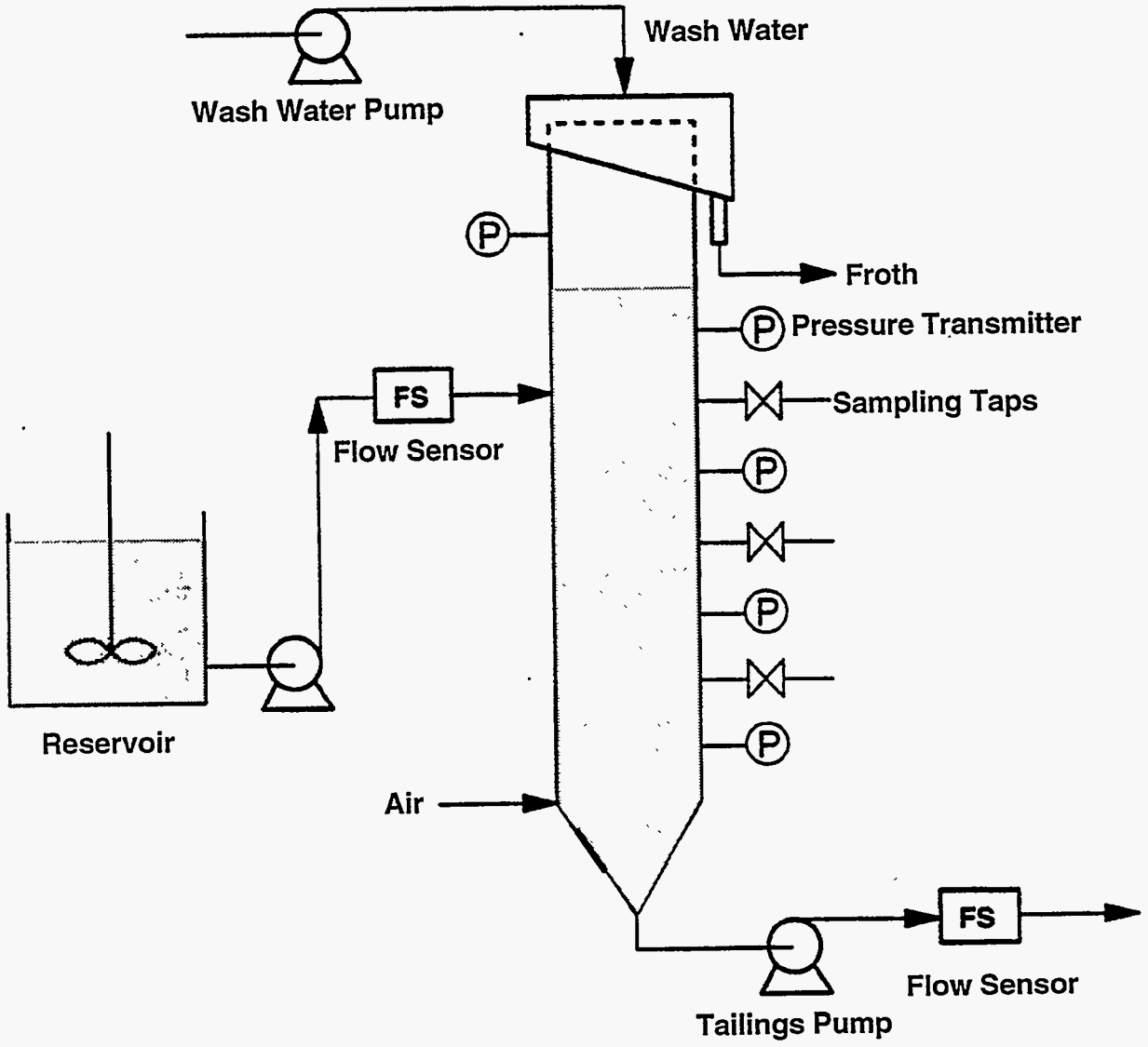

Figure 3-23. SCHEMATIC DIAGRAM OF THE FLOTATION COLUMN SET-UP

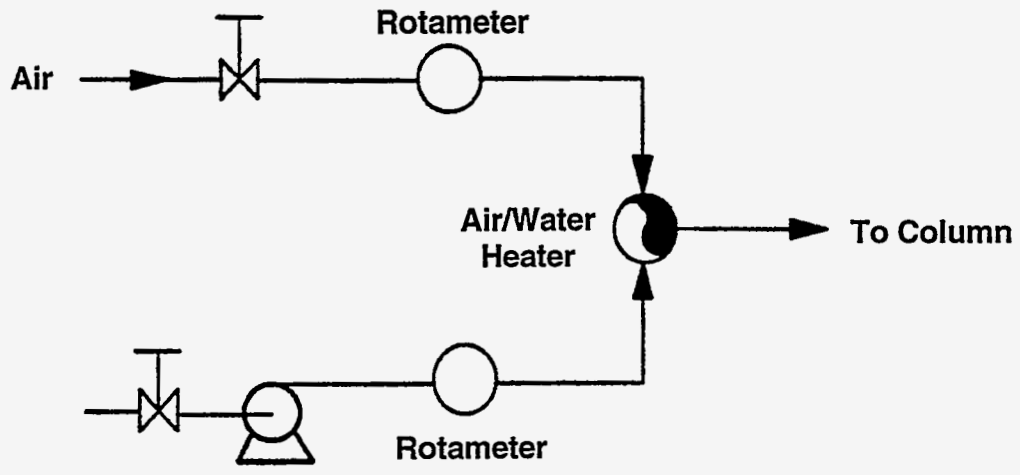

Cominco Sparger

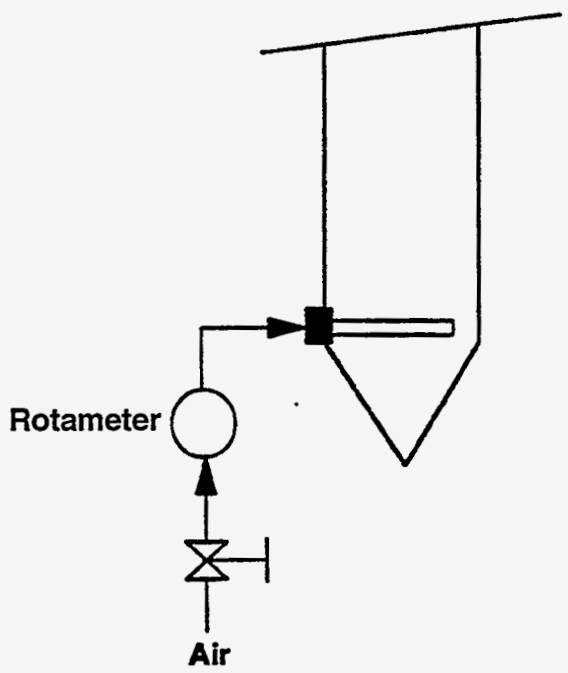

Static Sparger

Figure 3-24. SCHEMATIC DIAGRAM OF THE PROCURED BUBBLE GENERATORS

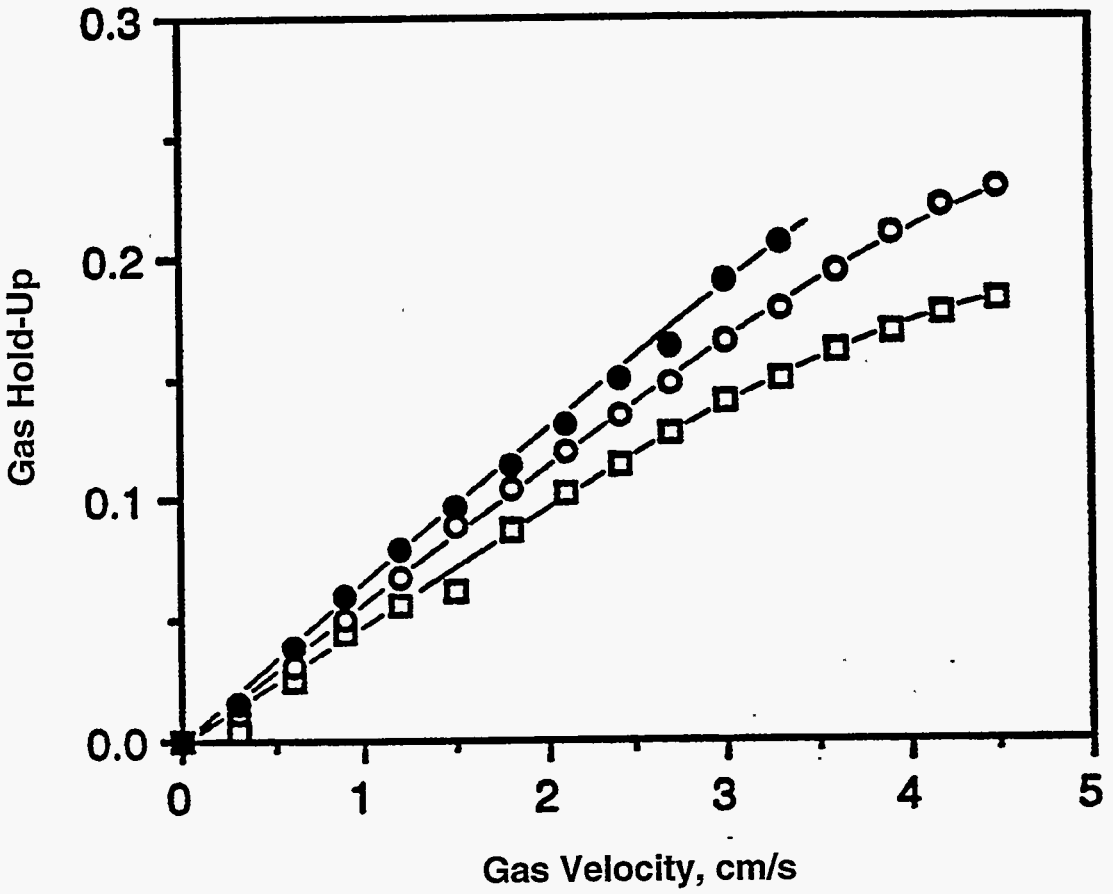

Figure 3-25. EFFECT OF FROTHER ADDITION ON GAS HOLD-UP
(●) 5 PPM DOWFROTH 250C; (○) 5PPM MIBC;
(□) NO FROTHER

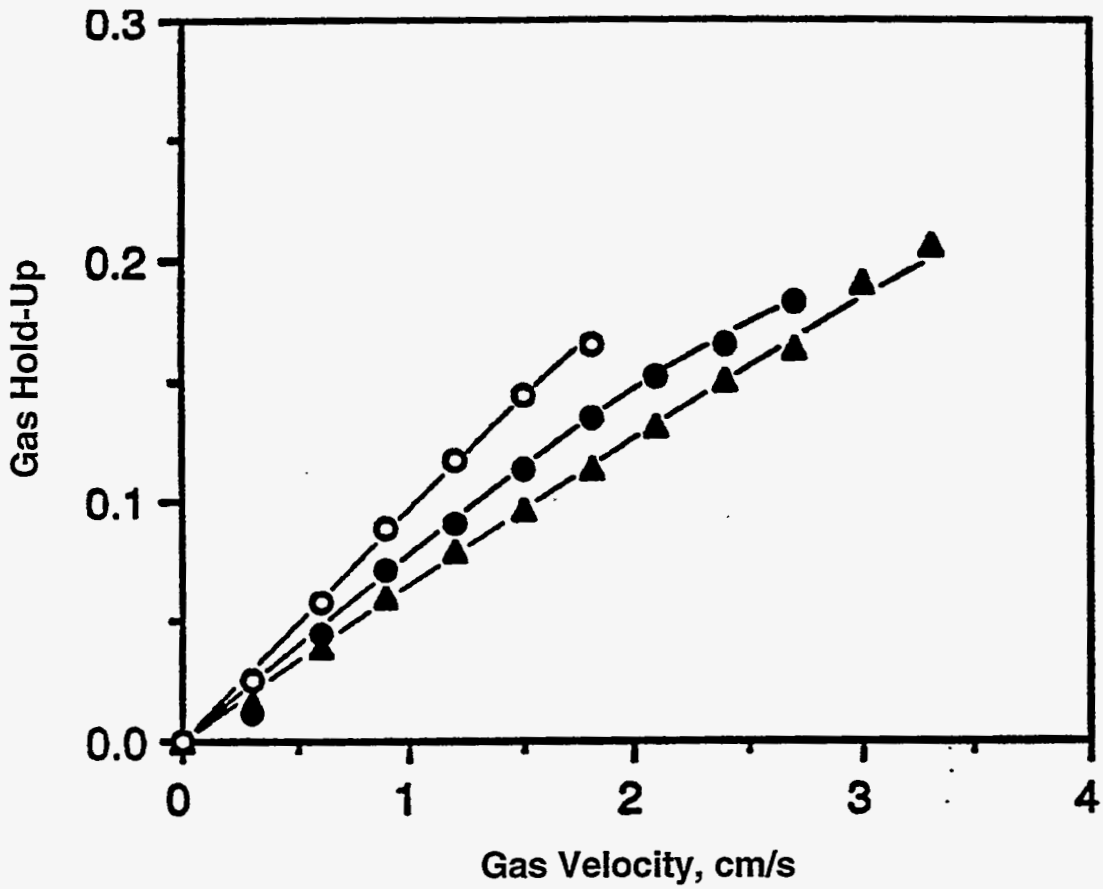

Figure 3-26. EFFECT OF DOWFROTH 250C CONCENTRATION ON GAS HOLD-UP (▲) 5PPM; (●) 7 PPM; (○) 10 PPM

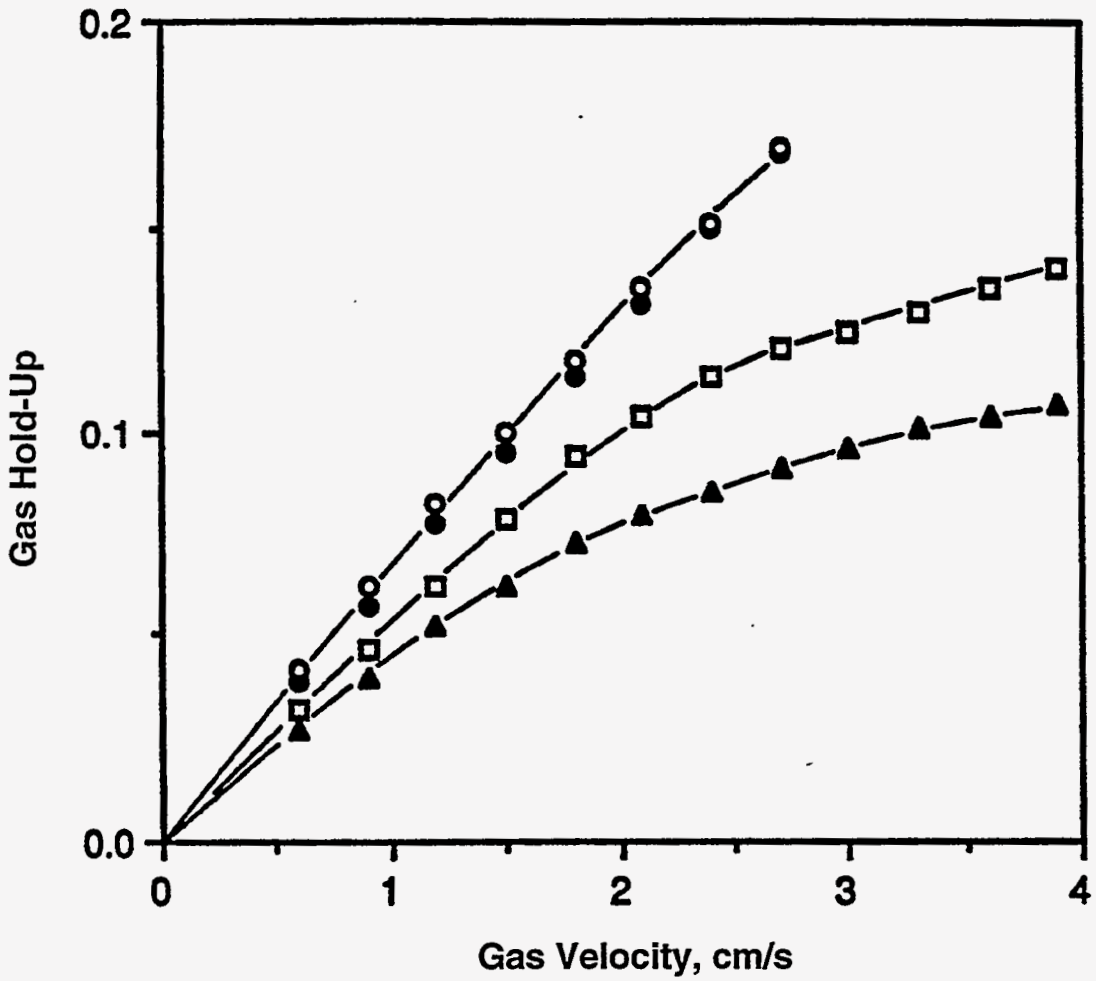

Figure 3-27. EFFECT OF SPARGER SURFACE AREA ON GAS HOLD-UP
(○) 100 %; (●) 75 %; (□) 50 %; (▲) 25%

Selective Agglomeration

The addition of small quantities of oil to a coal-water slurry promotes the selective agglomeration of hydrophobic coal particles leaving liberated (hydrophilic) ash minerals dispersed in the aqueous phases. The conventional oil-agglomeration (spherical agglomeration) process in which relatively large amounts of oil are used has been the subject of numerous laboratory and pilot-scale studies[47-50] but has not found wide commercial application. The main drawback is the high ash and moisture content of the product. The process does, however, have considerable potential for deep cleaning of coal at fine sizes, especially for applications in MCWM technology so as to avoid the problems of dewatering the fine, clean-coal product. The process is particularly attractive as a means of extending froth flotation to finer sizes. The objective is to use selective oil agglomeration to produce clean coal "particles" of size appropriate to the application of flotation separations. Investigations of the selective agglomeration process with an objective to produce micro-agglomerates of clean coal are being carried out in conjunction with a separately funded (DOE) project.

The use of oil agglomeration, at very low oil-addition levels, for sulfur and ash rejection in fine (-200 mesh) coal has been investigated. Wetting phenomena which provide the driving force for agglomerate formation and the growth of agglomerates in three-phase (oil-water-coal) systems have been evaluated in terms of the various contact angles (solid-liquid-liquid and solid-liquid-gas) which define the attachment of oil droplets to solid surfaces in an aqueous medium. Two different techniques for contact angle measurement have been used. The well-known captive bubble method has been used for direct measurements on polished surfaces. A recently developed "interface partitioning" technique[51] has been used for measurements on small particles at liquid-air and liquid-liquid interfaces.

Wetting behavior can be controlled through the appropriate use of surfactants. However, since these reagents can affect all of the interfaces present in an agglomeration system, reagent selection is by no means simple. Contact angle measurements can provide information of the specific effects of variables such as molecular weight and hydrophilic-liphilic balance (HLB). Such information can be used in the development of rational guidelines for reagent selection. An example of the effects of molecular weight and HLB on the wetting behavior of Pittsburgh seam coal (III-2) is shown in Figure 3-28 for two homologous series of ethylene oxide-propylene oxide block co-polymers. It can be seen that molecular weight has little effect at low HLB but that significant differences occur at an HLB of about 15. Further investigations of these effects are being carried out under Phase II of this project.

The dynamics of agglomerate formation and growth have been investigated by in-situ (laser diffraction) measurements of agglomerate size in agitated suspensions. The effects of the amount of added oil have been determined and indicate growth up to a limiting size of about 50 μm - which should be ideal for separation by flotation. Further analysis of the results suggests that the overall

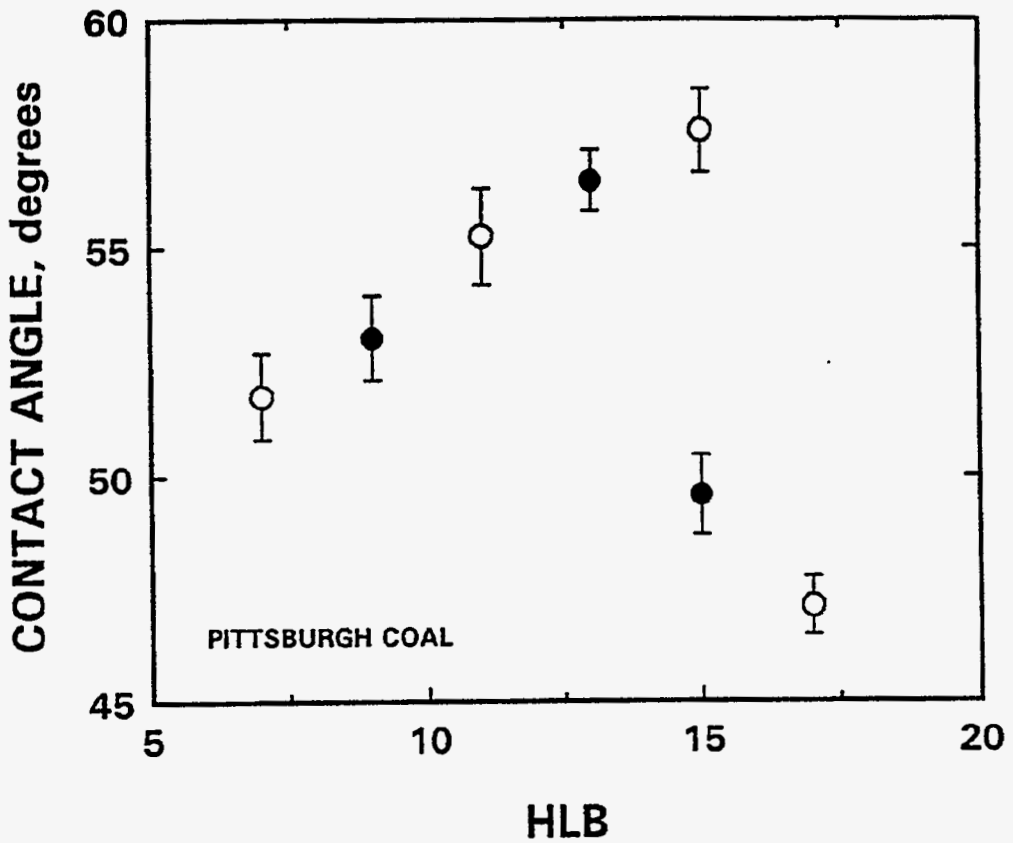

Figure 3-28. CONTACT ANGLE OF A PITTSBURGH SEAM COAL AS A FUNCTION OF HLB FOR TWO SERIES OF BLOCK CO-POLYMERS
● Pluronic P60 series; ○ Pluronic P100

process involves a complex combination of oil emulsification, agglomerate growth and agglomerate breakage. Pre-emulsification of the oil has been found to provide improved control over the agglomerate growth process and may enhance selectivity by eliminating large oil droplets from the coal-water slurry. Large droplets tend to form large, oil-rich agglomerates containing mineral particles as well as coal. Such agglomerates are resistant to subsequent breakage which may play an important role in preferential rejection of mineral matter.

Studies of combined agglomeration and flotation have also been carried out. The results shown in Figure 3-29 show that both the recovery and grade of coal are improved when particles were agglomerated prior to flotation. That is, pre-agglomeration of the fine coal leads to a substantial improvement in separation efficiency. These preliminary results indicate that agglomerate flotation has very considerable potential for fine-coal cleaning in the preparation of coal-water slurry, especially for Type III coals where fine grinding, prior to cleaning, is necessary for adequate liberation of the mineral matter. A systematic investigation of the effects of agitation, surfactant use etc., on selectivity in agglomerate flotation is included in the Phase II research.

Solid-Liquid Separations

A primary advantage of MCWM technology is that fine coal can be cleaned and utilized without the need for expensive, energy-consuming dewatering operations. However, there is likely to be some need for solid-liquid separation in order to control slurry density. Practical procedures for separating micronized coal from water generally involve flocculation of the particles prior to separation by sedimentation or filtration. Since flocculation is generally detrimental to MCWM production and utilization, its applicability to solid-liquid separation for increasing slurry density is rather limited. In many cases, however, it is possible to achieve some degree of flocculation in a reversible fashion - by pH control for example. For some applications, this may be sufficient to permit concentration of the slurry by sedimentation.

Test procedures for determining appropriate conditions for reversible flocculation of MCWM have been developed. Studies of the application to specific MCWM formulations have been carried out. The effects of pH on the surface charging characteristics have been evaluated using Electro-kinetic Sonic Amplitude (ESA) measurements. An example, for the Upper Freeport seam coal (III-1), is shown in Figure 3-30. Typically, the greatest need for slurry thickening is likely to occur subsequent to cleaning steps such as fine gravity separation or flotation but prior to final grinding. Based on available technology, these steps will generally be performed on coal ground to about -100 mesh. A series of sedimentation/clarification tests have been performed on -100 mesh samples of the Upper Freeport seam coal. Settling behavior was evaluated from measurements of suspension turbidity at fixed depths as a function of settling time. The results are shown in Figure 3-31. It is clear that rapid, efficient settling can be obtained at pH 7 which is close to the point of zero charge of this coal (see Figure 3-30). The results also indicate that the thickened coal can be readily redispersed simply by adjusting the slurry pH. Characterization of

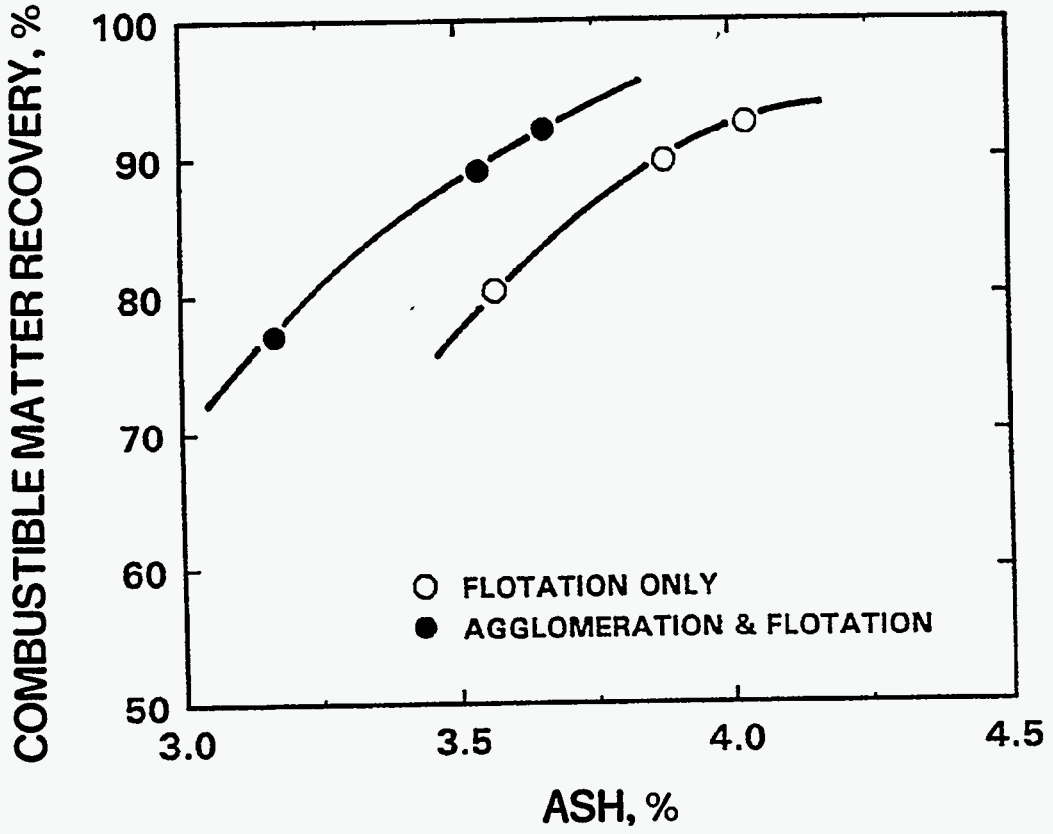

Figure 3-29. EFFECT OF PRE-AGGLOMERATION ON THE FLOTATION RESPONSE OF PITTSBURGH SEAM COAL
Frother = 0.5 kg/T MIBC; Collector = 0.035 kg/T Dodecane

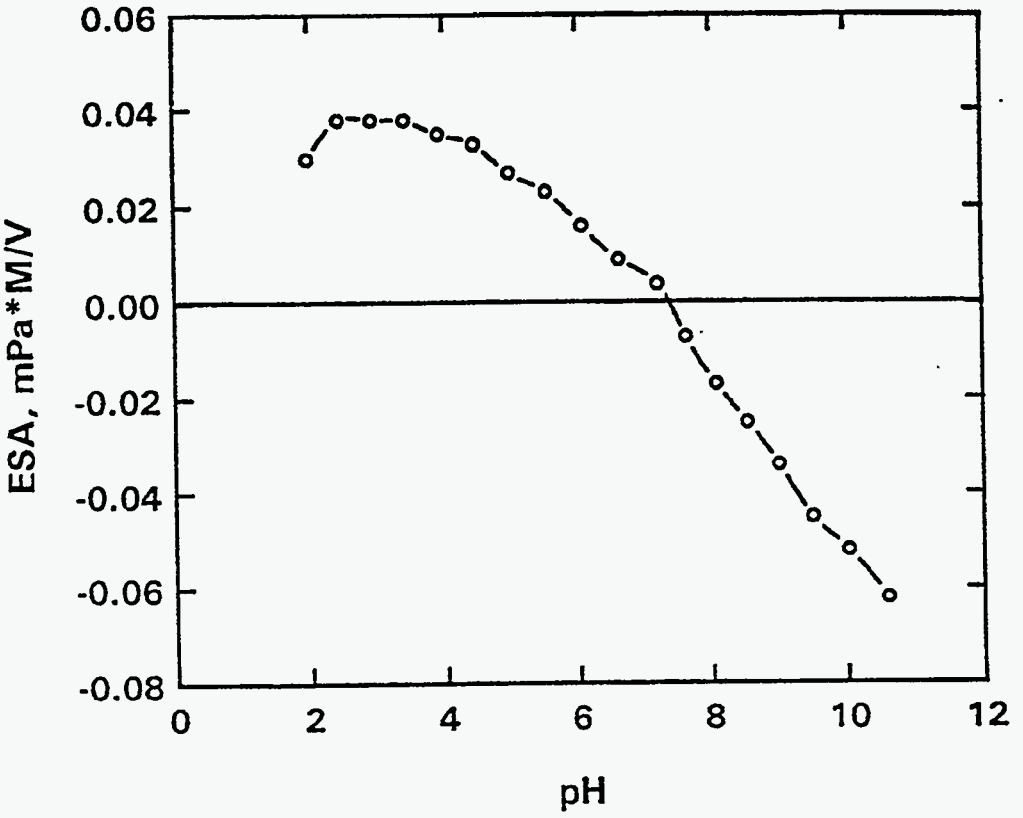

Figure 3-30. ELECTROKINETIC SONIC AMPLITUDE MEASUREMENTS FOR UPPER FREEPORT SEAM COAL

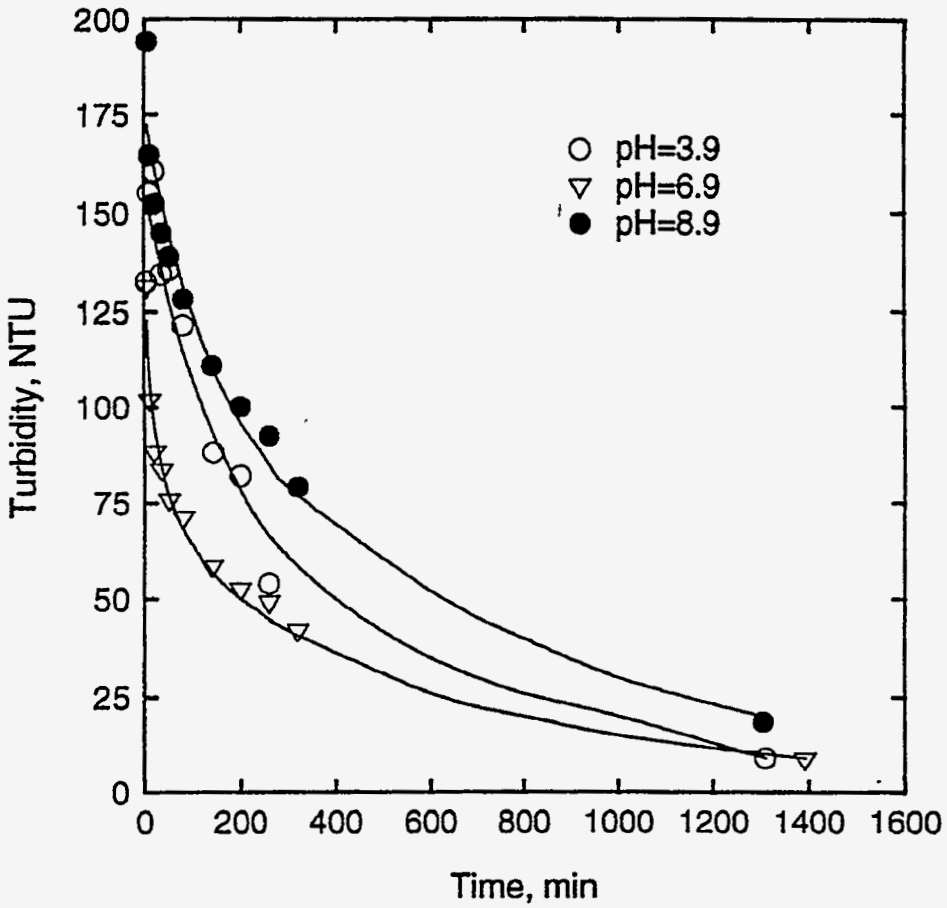

Figure 3-31. SEDIMENTATION/CLARIFICATION RESULTS FOR -100 MESH UPPER FREEPORT SEAM COAL

coal charging behavior through measurements of ESA is being used to provide the basis for predicting sedimentation behavior for different coals. The role of solid-liquid separations in the control of slurry density at the specific (often quite different) levels required for grinding and final coal-water slurry formulation is being evaluated as part of the Phase II research.

3.2.5 Establish Required Size Consist for Coal-Water Mixture Formulation

The basic requirements for coal-water mixtures are[52]:

- Maximum particle size less than about 150 μm to ensure complete combustion;
- High solids content (generally greater than 60% by weight);
- Stability with respect to settling and especially to the formation of hard-pack sediments; and
- Relatively low viscosity to facilitate handling, transport, and atomization.

The size distribution of the solid particles is a critical factor in the production of high-density MCWM with acceptable viscosity. It is generally accepted that broad size distributions are desirable since they afford the most opportunity for efficient packing of the particles. However, there seems to be little agreement over the "optimum" size distribution, and trial-and-error methods involving changes in the fine-grinding procedure are usually adopted. The size-consist requirements have been re-evaluated in the context of particle backing and particle interaction forces in the coal-water slurry.

Particle Interactions

Solid particles dispersed in water are subject to forces of interaction which become increasingly important as particle size is reduced. The principal forces of importance in coal-water slurry technology are:

- van der Waals-London dispersion forces which act between all particles and are always attractive for similar particles;
- Electrical double layer interactions between charged particles in suspension; and
- Solvation forces between structured layers of solvent molecules or adsorbed solute species such as polymers.

The nature and relative magnitudes of these forces were discussed elsewhere[53] and will not be repeated here.

Attractive, van der Waals' forces and repulsive, electrical double layer and steric interaction forces due to adsorbed, dispersant layers probably assume a dominant role in coal-water slurries. In the absence of repulsion, the attractive forces lead to particle aggregation and network formation with a corresponding increase in apparent viscosity. The presence of repulsive forces gives rise to the development of repulsive energy or force barriers between particles which prevent their coming into actual contact. Typically, these barriers lead to minimum particle separations in the range of 0.01 to 0.1 μm.

By preventing aggregation or network formation, the development of repulsive barriers

generally contributes to the reduction of slurry viscosity. On the other hand, the barrier itself represents an additional excluded volume which increases the effective solids volume in suspension. Such effects can become significant for very fine particles. For particles of size x with minimum separation H_m, the effective solids volume fraction ϕ is increased to

$$\phi_{eff} = \left(1 + \frac{Hm}{2X}\right)^3 \tag{3-24}$$

For 0.1 μm particles with a minimum separation of 0.05 μm, this would correspond to almost a doubling of the effective solids concentration.

Particle interactions also play a role in another important characteristic of coal-water slurries: sediment consolidation. Practical coal-water slurries are inevitably subject to some settling during long-term storage. This becomes a problem if the resulting sediments are highly consolidated ("hard-packed") and not easily redispersed by agitation. Network formation due to net attraction between particles generally promotes settling but opposes consolidation by forming rigid but relatively open structures which can easily be broken down by agitation. Very strong repulsive interactions can also inhibit consolidation by preventing close approach of particles. Both of these conditions can, however, contribute to increased slurry viscosity.

Particle Packing

It has long been recognized that particles of uniform size, arranged at random, pack to a solids volume fraction of about 0.6. These packing densities can be increased substantially by the addition of smaller particles which can fit into the interstices between the original particles. For slurry applications, it is convenient to consider the reverse (but entirely equivalent) situation of adding coarser material to a suspension of fine particles.

Consider a suspension of particles of size x_1 with solids concentration ϕ_1. If coarser particles (size x_2) are added, each particle (initially) adds its own solid volume to the suspension. Thus

$$V = V_1 / \phi_1 + V_2 \tag{3-25}$$

where V is the total slurry volume, V_1 and V_2 are the respective solid volumes.

By definition, the slurry concentration (volume fraction) is

$$\phi = \frac{V_1 + V_2}{V} \tag{3-26}$$

and the fraction of coarse particles is

$$Q = \frac{V_2}{V_1 + V_2} \tag{3-27}$$

It follows that

$$\phi = \frac{\phi_1}{1 - Q(1 - \phi_1)} \tag{3-28}$$

which describes the increase in solids loading due to the addition of coarse material. Obviously, such increase in loading cannot continue indefinitely. Eventually, the coarse particles cease to act independently; they begin to disturb the packing of the finer material and finally reach a packing limit of their own.

The maximum possible loading occurs when there is just enough fine-particle slurry to fill the voids in a bed of close-packed coarse particles. In this case,

$$V = V_2 / \phi_2^* \tag{3-29}$$

where ϕ_2^* is the maximum packing fraction for the coarse material (typically about 0.6). The void volume V_v (available to fine-particle slurry) is

$$V_v = \left(1 - \phi_2^*\right)V \tag{3-30}$$

It follows that the maximum loading occurs when the fraction of coarse particles in the mixtures is Q_m such that

$$Q_m = \frac{\phi_2^*}{\phi_1\left(1 - \phi_2^*\right) + \phi_2^*} \tag{3-31}$$

The corresponding maximum solids loading is

$$\phi_m = \phi_2^*\left(1 - \phi_1\right) + \phi \tag{3-32}$$

Some examples of calculated solids loadings for coarse-particle/fine-slurry mixtures are shown in Figure 3-32. The substantial increases in loading which can, potentially, be achieved can be seen clearly. It is also apparent that a range of options is available for producing a slurry with

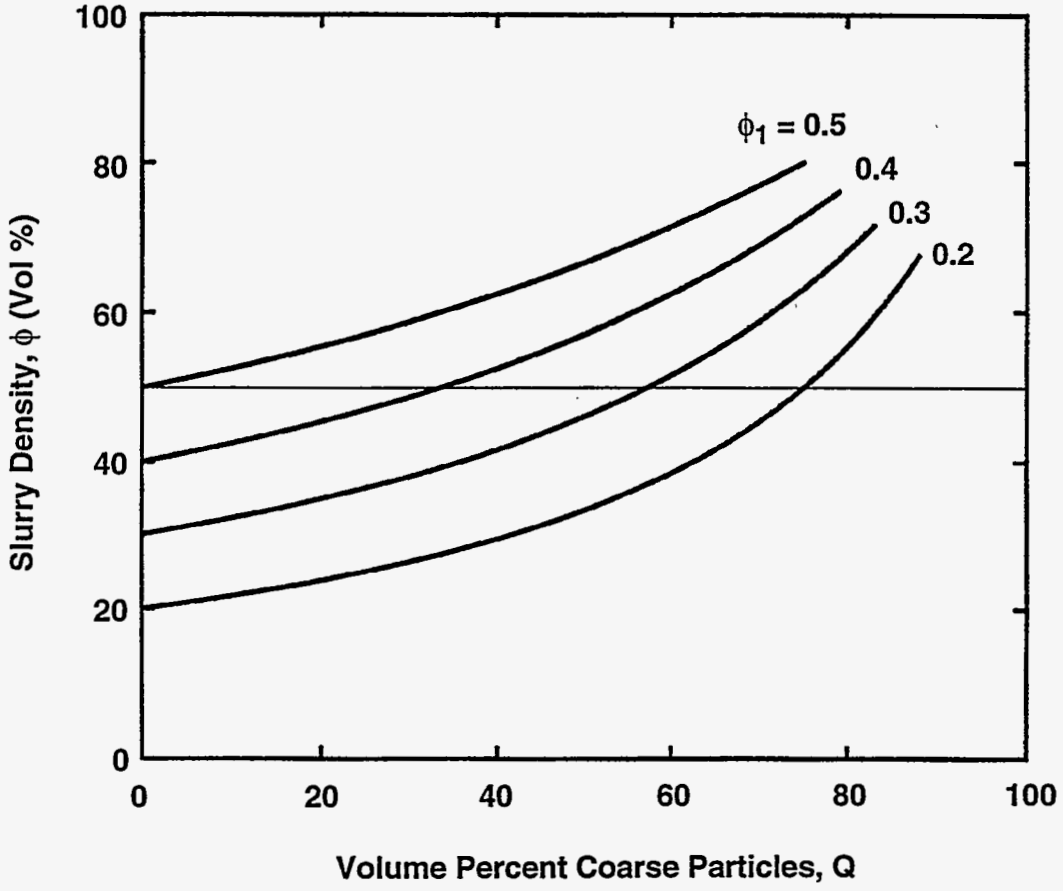

Figure 3-32. SLURRY PREPARATION FROM BINARY MIXTURES

given loading. Thus a loading of 50% solids overall can be accomplished by adding about 30% coarse particles to a 40% solids slurry or 70% coarse to a 20% solids slurry. Obviously, the rheological and settling characteristics of these different (but same-density) slurries would not be expected to be the same.

In principle, further increases in solids loading could be obtained by the addition of a third, still finer or coarser component in the appropriate amount. However, experience with powders suggests that such improvements are not generally achieved in practice[54].

In order to obtain the optimum packing from binary mixtures, it is necessary that the size ratio x_2/x_1 be as large as possible, In real coal-water mixtures, however, there are practical limits on this ratio. Combustion and burner requirements generally limit the upper size, x_2 to less than about 100 μm. Grinding costs and, to some extent, rheology constraints place limits on the finer size x_1.

The ability to achieve high packing density is largely determined by the ratio of the average separation H_2 of the large particles to the size of the fine material. For a "dilute" (non close-packed) coarse fraction, assuming an average cubic arrangement, the mean particle separation can be estimated as follows:

The volume of slurry associated with an average (size x) particle is

$$v_s = \frac{k_v x^3}{\phi} \tag{3-33}$$

where k_V is the column shape factor (=π/6 for spheres). For a cubic arrangement, the average center-to-center separation is

$$v_s^{1/3} = \left(k_V/\phi\right)^{1/3} x \tag{3-34}$$

and the average surface-to-surface separation for the coarse component is

$$H_2 = \left[\left(k_V/\phi_2\right)^{1/3} - 1\right] x_2 \tag{3-35}$$

The excluded-volume effect noted above restricts the size (x_1) of the fine-particle fraction. For stabilized particles, the minimum separation H_m (see Equation 3-24) is essentially constant, independent of particle size. Thus, as size x is reduced, the excluded volume effect described by Equation 3-24 becomes increasingly important and places an upper limit on the concentration ϕ_1.

The particle size limitations can be illustrated by considering a hypothetical slurry prepared at 50% solids, by weight, from various combinations of coarse and fine particles. The packing

effect is described by the ratio of the coarse-particle separation H_2 to the fine-particle size x_1. A large value indicates that the fine-particle slurry can readily fill the space between coarse particles. The excluded volume effect is reflected by the effective fine-particle concentration $(\phi_1)_{eff}$ as defined by Equation 3-24. High values would be expected to correspond to high slurry viscosity.

The results of such calculations, based on a coarse-particle size x_2 of 75 μm and a minimum separation of the fine particles of 0.05 μm, are given in Table 3-13. It can be seen that the packing effect becomes critical when the fine-particle component is dilute and relatively coarse. As expected, the excluded volume effect becomes significant when the fine-particle component is concentrated and extra fine.

These calculations also demonstrate the value of using a true bimodal size distribution for slurry formulation. The presence of intermediate sizes in a broad but continuous distribution will invariably lead to reduced values of H_2/x_1 and correspondingly reduced packing efficiency for a given solids loading.

The packing model can also be used to estimate the rheological behavior of binary (coarse+fine) coal-water mixtures. Provided the coarse particles are sufficiently widely spaced (dilute), such systems can be modeled as suspensions of coarse particles (concentration ϕ_2) in a medium consisting of fine particles at concentration ϕ_1. The advantage of this approach is that the relatively simple relationships which have been developed for suspensions of uniform particles can be used to estimate the viscosity of the fine-particle medium and the overall slurry. Typically, such expressions are of the form:

$$\mu = \mu_o f(\phi) \qquad (3\text{-}36)$$

where μ is the viscosity of the suspension and μ_o is that of the medium. Thus, for the binary coal-water mixture, the viscosity can be estimated by successively applying Equation 3-36, first to the fine-particle "medium", and then to the suspension of coarse particles in that medium. An example, using the Dougherty-Krieger relationship is given in Table 3-14. The results indicate an optimum composition (minimum viscosity) consisting of relatively coarse (> 2μm) fine particles at about 30% solids by volume with an appropriate addition of the coarse fraction (also about 30% by volume) in order to provide the desired overall solids content (50% in this example).

In practice, it is common to approximate the true bimodal distribution by a very broad, but continuous size distribution produced from a single-stage grinding operation. While this approach can provide slurry with acceptable characteristics, the compromises involved lead to several undesirable features. In addition to sub-optimum solids loading/stability/rheology characteristics, the grinding procedures used to produce such slurries tend to be quite inefficient. Since grinding costs are a major factor in the economics of coal-water slurry technology, it is obviously desirable to maximize grinding efficiency. On the other hand, a two-stage grinding process, designed to

Table 3-13. Packing Ratio and Excluded Volume Effect for Binary Slurries at 50% Solids by Volume (Based on 75 μm coarse particles). Figures in shaded blocks represent conditions where coarse-particle separation would be expected to limit fine-particle packing.

Fine-Particle Size X_1	Packing Ratio H_2/x_1				Excluded Volume Effect (Effective Fine-Particle Concentration)				
(μm)	f_1=0.1	0.2	0.3	0.4	f_1=0.1	0.2	0.3	0.4	0.5
0.5	8.4	17.7	33.6	69.7	0.116	0.232	0.347	0.463	0.579
1	4.2	8.8	16.8	34.8	0.108	0.215	0.323	0.431	0.538
2	2.1	4.4	8.4	17.4	0.104	0.208	0.311	0.415	0.519
5	0.8	1.8	3.4	7.0	0.102	0.203	0.305	0.406	0.508
10	0.4	0.9	1.7	3.5	0.101	0.202	0.302	0.403	0.504

Table 3-14. Estimated Viscosity for Binary Slurries at 50% Solids by Volume. Shaded figures represent impractical packing conditions (see Table 3-13).

Fine-Particle Size X_1 (μm)	Estimated Viscosity (cp)				
	f_1=0.1	0.2	0.3	0.4	0.5
0.5	12.3	10.5	11.3	18.0	211.9
1	11.9	9.8	9.7	12.8	38.4
2	11.8	9.5	9.1	11.1	24.7
5	11.7	9.3	8.8	10.3	20.0
10	11.7	9.3	8.7	10.0	18.8

provide an optimal bimodal distribution can, in principle, be operated so as to maximize grinding efficiency.

Perhaps the major potential advantage of coal-water mixture technology over conventional coal firing lies in the opportunity for advanced coal cleaning which is offered by the associated fine-grinding but is not offset by the need for expensive product dewatering. Integration of a multi-stage grinding operation with physical cleaning process such as flotation offers several opportunities for cost-effective deep cleaning of coal. With many coals, for example, it is possible to separate a clean fraction at a relatively coarse size, grinding of the remainder of the coal can then be used both to provide the sulfur and ash liberation and to produce the finer fractions needed for slurry preparation.

Within the constraints imposed by the basic requirements listed above, the required size consist for MCWM preparation is relatively independent of the nature of the feed coal. However, the procedure for obtaining that size consist will be highly coal-dependent. In particular, it is necessary to optimize the size-reduction processes used in the MCWM preparation.

3.2.6 Ball Mill Grinding

The use of coal-water mixtures in combustion requires high density slurries consistent with slurry handling and storage. Ball mills have been widely used for the preparation of coal-water mixtures because of their availability and capacity. Over last three decades, ball mill grinding has been studied extensively at Penn State and it is now possible to predict the performance of various ball mill grinding circuits based on laboratory grinding data. However, the grinding of high density slurries needs further study due to the complexity arising from the dependence of breakage rates on the slurry properties[55]. It is well-known that wet ball milling gives higher mill capacities than dry milling. However, as the slurry becomes thick and viscous, the grinding rate deteriorates.

According to Klimpel[56], grinding rates depend on several factors which affect the slurry rheology. These are: (i) the slurry density, (ii) the fineness of the size distribution, (iii) the shape of the size distribution, and (iv) the chemical environment. The work on the rheological properties of slurries and their effect on the breakage rates is summarized in the following:

(i) Many coals and mineral slurries exhibit dilatant character at relatively low slurry densities, less than 40 - 45% solids by volume for typical size distributions; closely sized solids give more dilatant character than broad distributions.

(ii) In this dilatant region, grinding is first-order, and absolute rates of breakage do not vary during the grinding or from one slurry density to another.

(iii) Increasing slurry density causes a trend toward pseudoplastic behavior. At a given slurry density, more pseudoplastic character can be developed by increasing the solids packing efficiency (by adding a proportion of fines or controlling the size distribution), by the use of a bulk thickening agent, or by the use of chemicals to modify viscosity.

(iv)When a slurry exhibits pseudoplastic behavior without a yield stress, then grinding is first-

order with higher absolute rates of breakage than in the corresponding dilatant systems.

(v) Grinding aid chemicals that work best in practice are those which maintain pseudoplastic behavior in the slurry without associated yield stress, or which reduce the yield stress in a dense pseudoplastic slurry.

(vi) When grinding is performed on a very dense slurry, the yield stress increases rapidly and leads to non-first-order breakage with a slowing-down of breakage rates.

Although this gives a general explanation of the change in the breakage rates as slurry condition is changed, the detailed variation is likely to be coal specific and must be determined experimentally. Therefore, a study of laboratory ball mill grinding of coal-water mixtures was carried out for five selected coals to identify and correlate different slurry conditions with grinding behavior. The effects of a dispersant (Coal Master A-23M) on grinding in dense suspensions were also analyzed for the modification of slurry rheology to increase mill output by taking advantage of high solids content.

Experimental Procedure and Results

The laboratory mill used was 200 mm i.d. with a volume of 5,230 cm^3, fitted with lifters. The mill was loaded to a bulk volume of 1,570 cm^3 (30% loading) with 25 mm diameter steel balls. All tests were run at 72 rpm (70% of critical speed) with a constant slurry volume loading of approximately 627 cm^3. Five of the coal samples (Taggart, Indiana, Lower Kittanning, Upper Freeport and Pittsburgh seam coal) were first crushed to -16 mesh using a hammer mill. Variations in the percent solids were achieved by changing the water-to-solids ratio to give 627 cm^3 total slurry volume assuming a coal density of 1.4 g/cm^3. Grinding tests were conducted for various times using a new sample for each test. The ground products were screened using a combination of wet and dry sieving.

Figure 3-33 shows a typical set of grinding data for various grinding times. Generally, as the grinding proceeds, the curves shift in a parallel manner to finer sizes. A convenient way to analyze the rate of grinding is the Weibull plot, which shows the variation of the percentage of material less than a certain size with time. Figure 3-34 is one such plot for 200 mesh at various solids concentration. It can be seen that the breakage rate decreases as the solids concentration increases, giving lower curves. Also, above 65% solids loading, the curve bends away from the straight line relationship as grinding proceeds. This indicates a slowing-down of the breakage rates for longer grind times. The addition of 0.5 wt.% dispersant increased the grinding rate and also removed the slowing-down effect, resulting in a higher production of fines as indicated by a higher curve in the figure. However, a further increase in reagent dosage did not improve the rate of grinding. Similar results were obtained for the other coals.

Figure 3-35 shows the time required to reach a product size of 80% passing 200 mesh. It is apparent that the time increases with increasing solids concentration. A rapid increase in the time was observed in the neighborhood of 60 wt.% for all coals except the Indiana seam coal, which

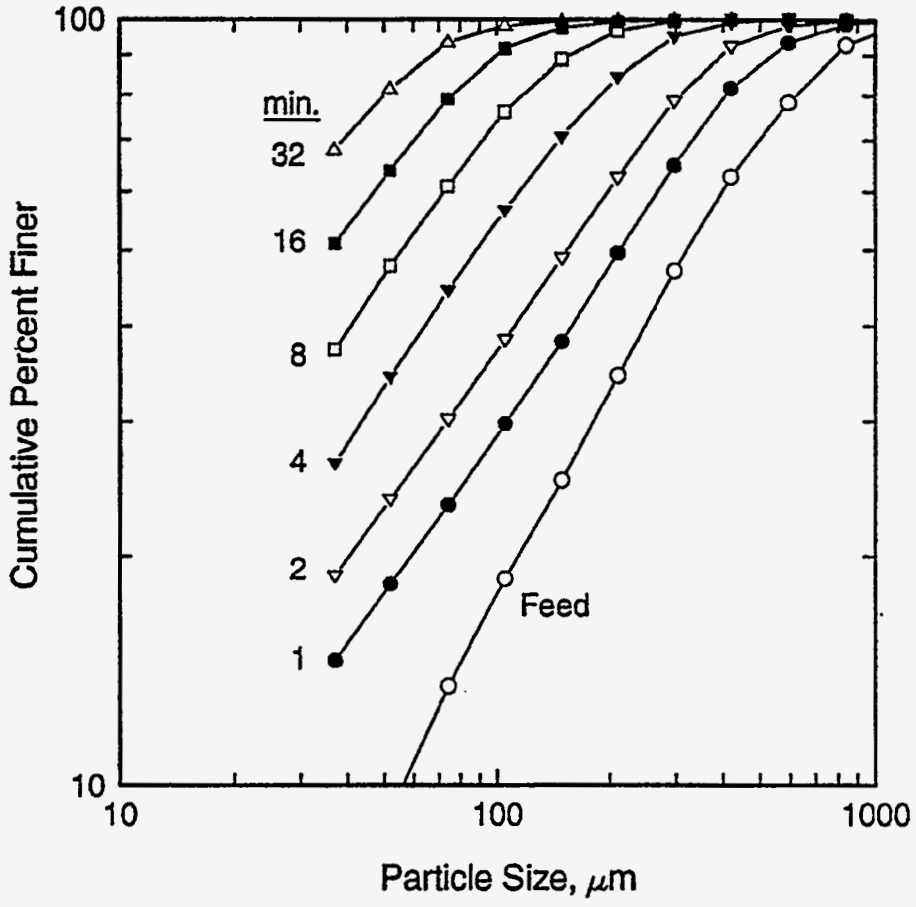

Figure 3-33. PRODUCT SIZE DISTRIBUTIONS FOR THE GRINDING OF –16 MESH UPPER FREEPORT SEAM COAL AT 50 WT. % SOLIDS WITHOUT DISPERSANT

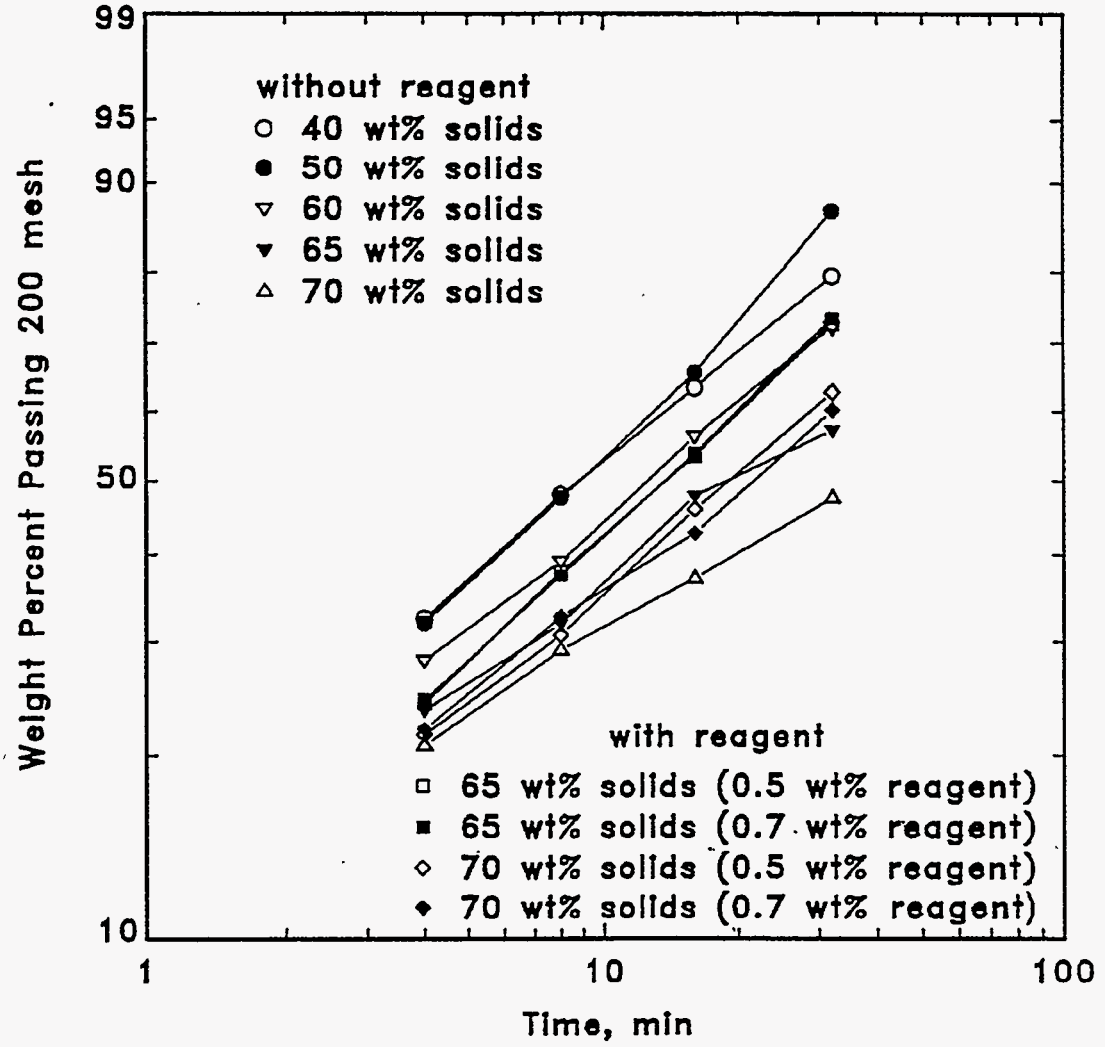

Figure 3-34. WEIBULL PLOTS OF THE TAGGART SEAM COAL AT VARIOUS SOLIDS CONCENTRATIONS

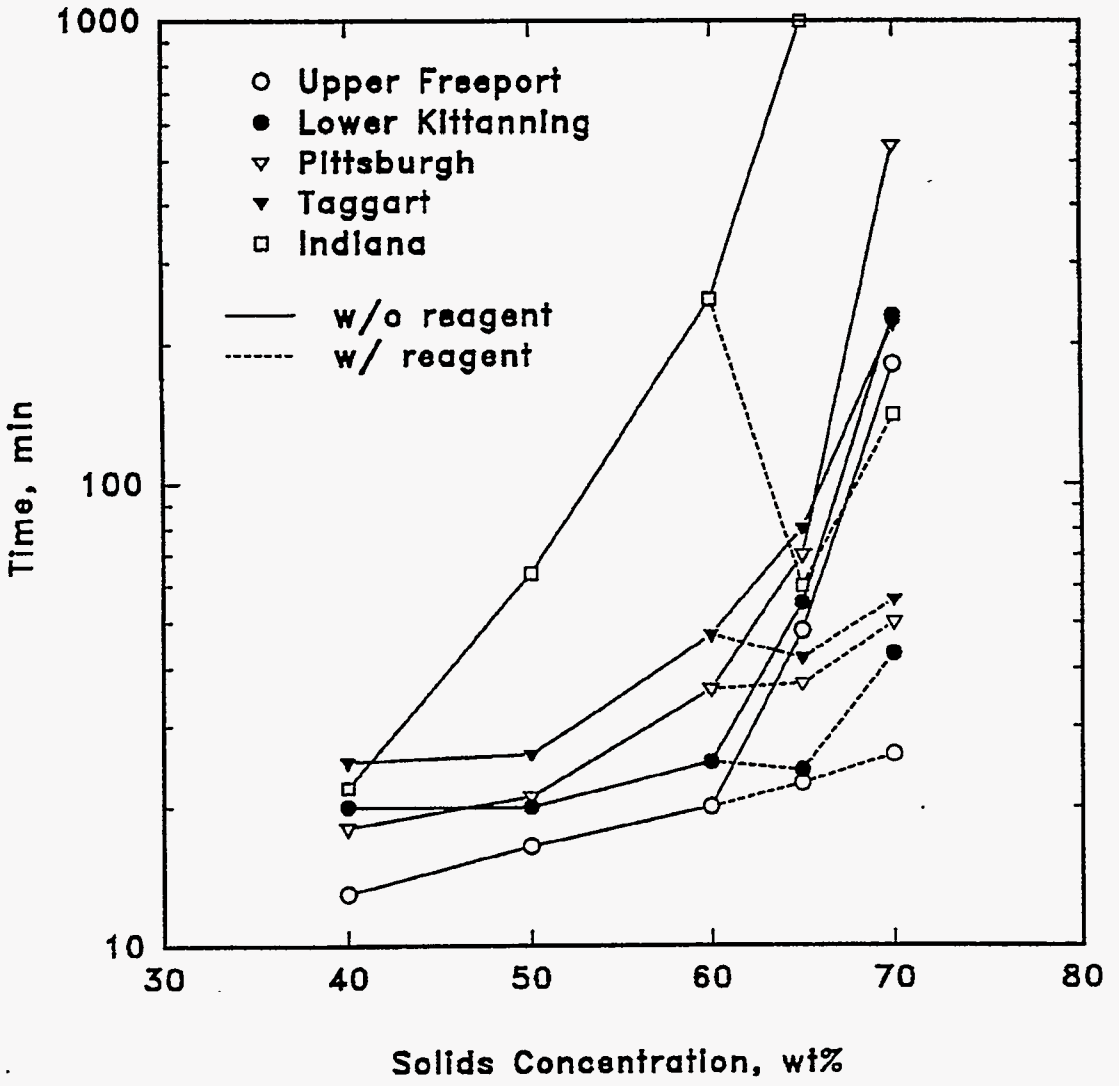

Figure 3-35. TIME REQUIRED TO REACH THE PRODUCT SIZE OF 80% PASSING 200 MESH FOR 5 COALS AT 65 WT. % SOLIDS WITH 0.5 WT. % DISPERSANT

increased at a much lower solids loading. This indicates that the Indiana seam coal exhibits the greatest tendency for a slowing-down of the breakage rate with increasing slurry concentration due to the increase in slurry viscosity. However, as with the other coals, the required grinding time can be significantly reduced by the addition of the reagent.

Figure 3-36 shows a plot of the grinding time required to achieve a product size of 80% passing versus HGI of coals. Except for the Indiana seam coal, a more or less straight line relationship can be seen. For these four coals, the HGI can be used as a criterion to determine the time required to produce a specific size.

Figure 3-37 shows net production of -400 mesh material versus solids concentration with and without chemicals for all coals. The decrease in the breakage rate at the higher solids concentration noted in Figure 3-34 is offset by the higher solids content, resulting in a net increase in the production rate of fines. However, beyond 60% solids, the slurry viscosity becomes too high, causing a slowing down of the breakage rate and a decrease in the net production rate. Nevertheless, grinding with the reagent resulted in a significant increase in the production rate for five coals. Figure 3-38 relates the production of fines after 32 minutes of grinding with HGI for all coals. Again, the production is well correlated linearly with HGI except for the Indiana seam coal. Obviously, the harder the coal, the longer the time needed to produce a specified size, therefore, the production will decrease accordingly.

Figure 3-39 shows a set of product size distributions for various solids concentrations. In order to compare the results, a grinding time was selected which gave a product size of 80% passing 200 mesh. It can be seen that the size distributions fall into three distinct groups, one for slurry densities of 50% and less, one for slurry densities of 60-65%, and one for the slurry density of 70%. The higher density slurries produce comparatively more fines. Similar trends were observed for all the other coals. This indicates that the mechanism of fracture changes when going from low to high pulp density.

Figure 3-40 shows the size distributions for the five coals ground at 70% solids with 0.5% dispersant. Typically, the softer (higher HGI) coals produce a flatter size distribution, containing a bigger portion of fines. However, this trend is not observed for this high solids loading. It seems that in addition to the solids content, the coal surface properties play a important role in determining the viscosity of the coal slurry, which in turn affects the shape of the size distribution. The solid line represents the optimum size distribution for a stable coal-water slurry as given by Henderson and Scheffee[57]. It can be seen that the size distributions for all coals do not follow the limiting size distribution. Generally, a natural breakdown of the particles does not produce the shape of the limiting size distribution under a simple grinding process. Therefore, a circuit arrangement involving staged grinding will be needed.

The simplest way to obtain the desired size distribution is by blending products from two mills. For this purpose, stirred ball milling can be used to produce the finer stream, which can be

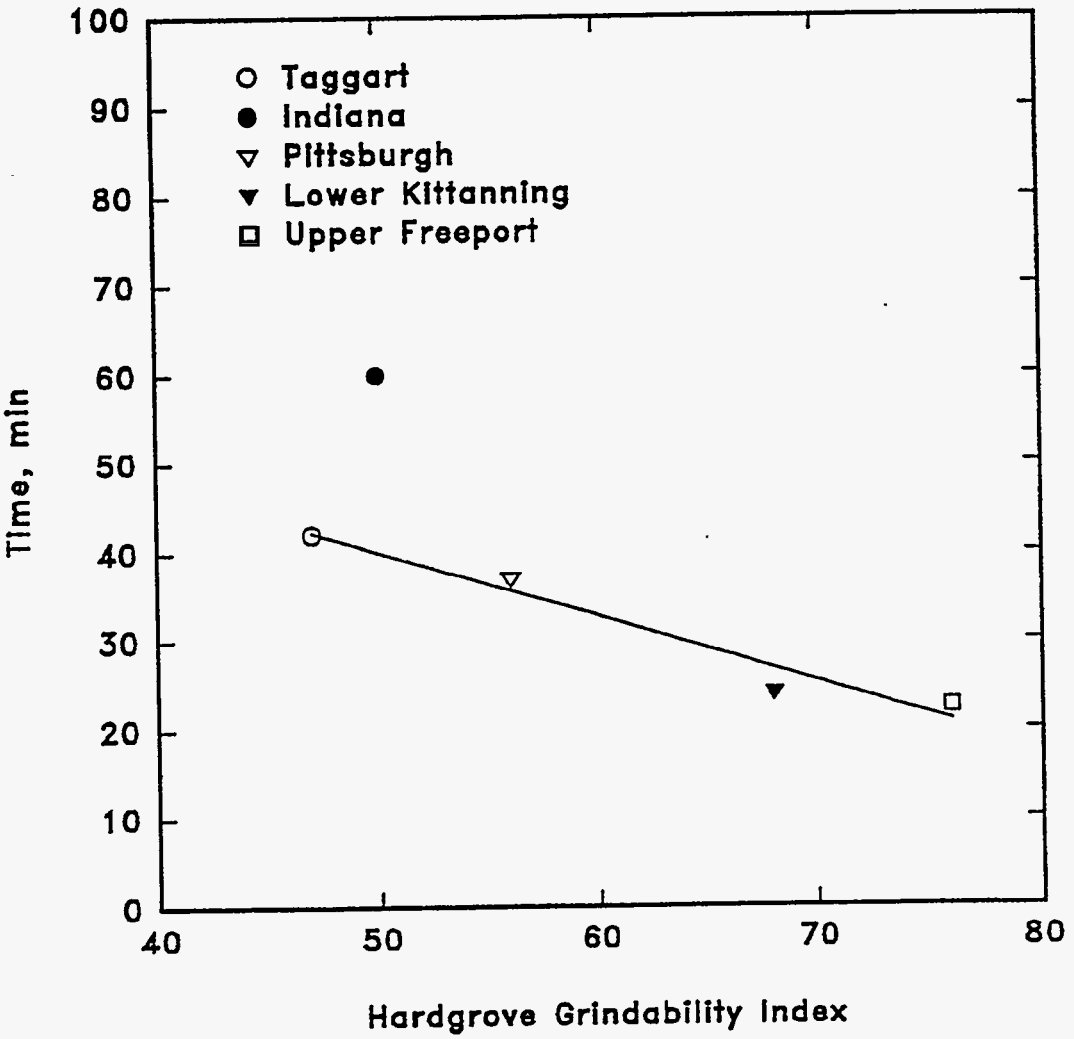

Figure 3-36. RELATIONSHIP BETWEEN THE TIME REQUIRED TO REACH A PRODUCT SIZE OF 80% PASSING 200 MESH AND HARDGROVE GRINDABILITY INDICES OF COALS

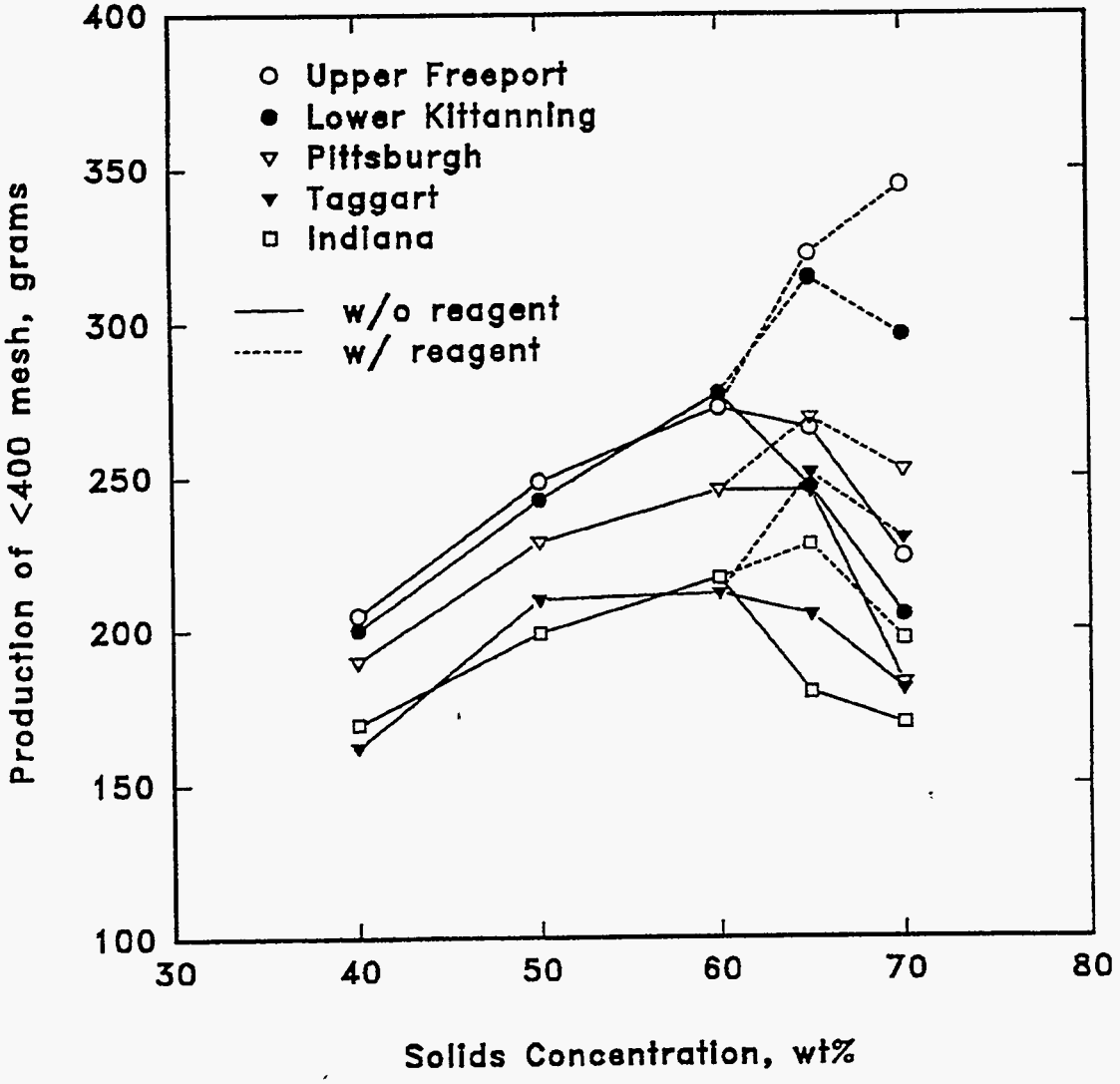

Figure 3-37. PRODUCTION OF THE -400 MESH MATERIAL FOR THE 5 COALS PRODUCED AFTER 32 MINUTES OF GRINDING AT VARIOUS SOLIDS CONCENTRATION

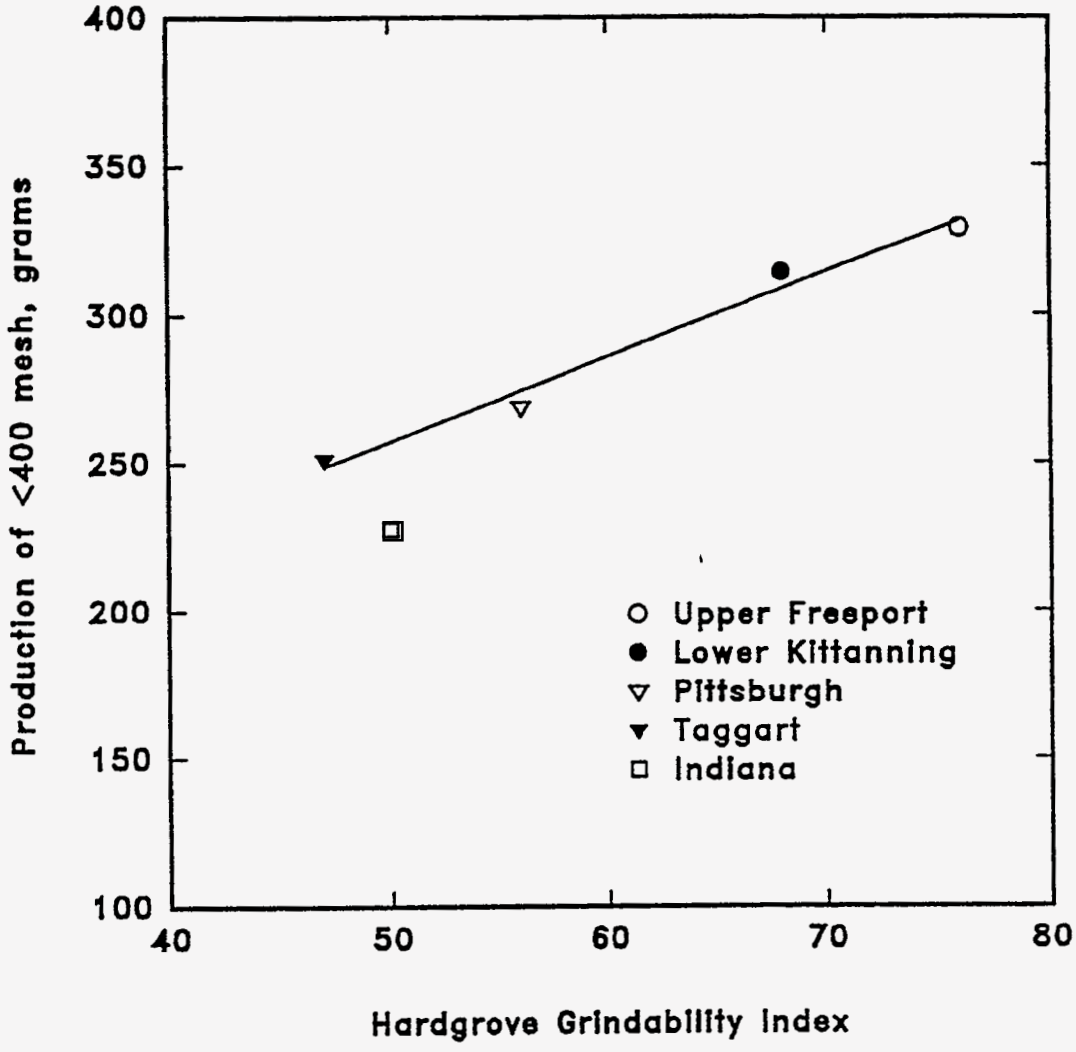

Figure 3-38. RELATIONSHIP BETWEEN HGI AND THE PRODUCTION OF –400 MESH MATERIAL AFTER 32 MINUTES OF GRINDING AT 65 WT. % SOLIDS WITH 0.5 WT. % DISPERSANT

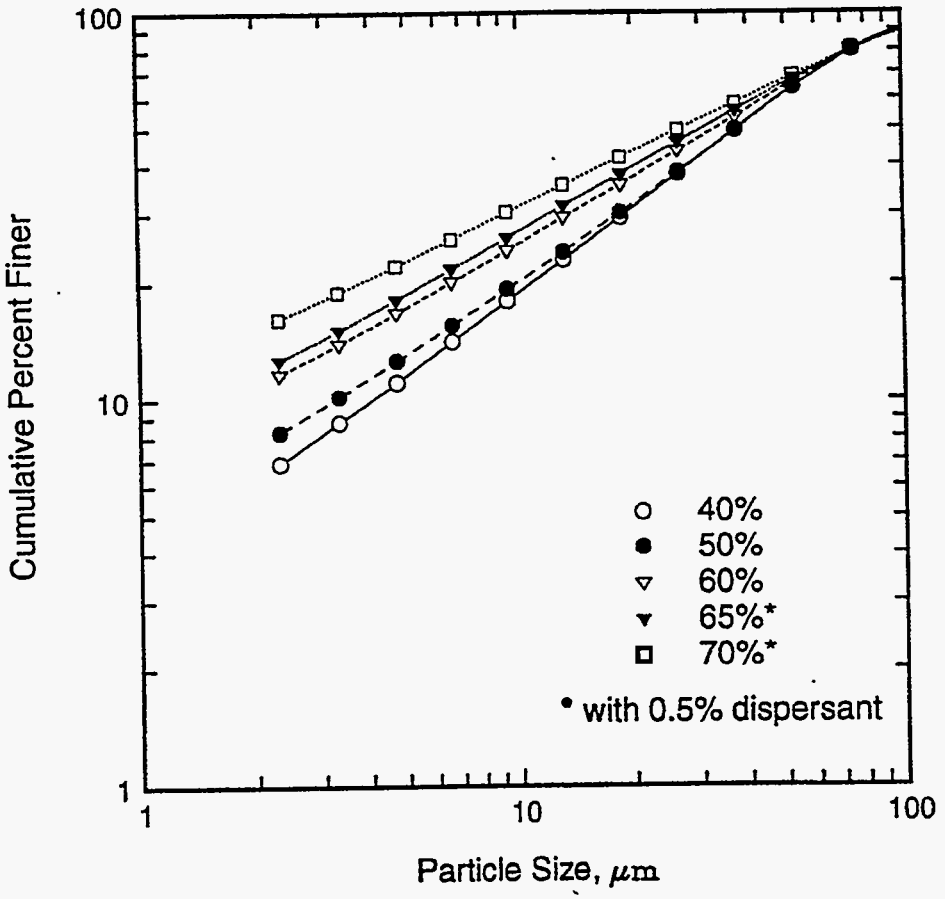

Figure 3-39. PRODUCT SIZE DISTRIBUTIONS OF 80% PASSING 200 MESH AT VARIOUS SOLIDS CONCENTRATIONS FOR THE TAGGART SEAM COAL

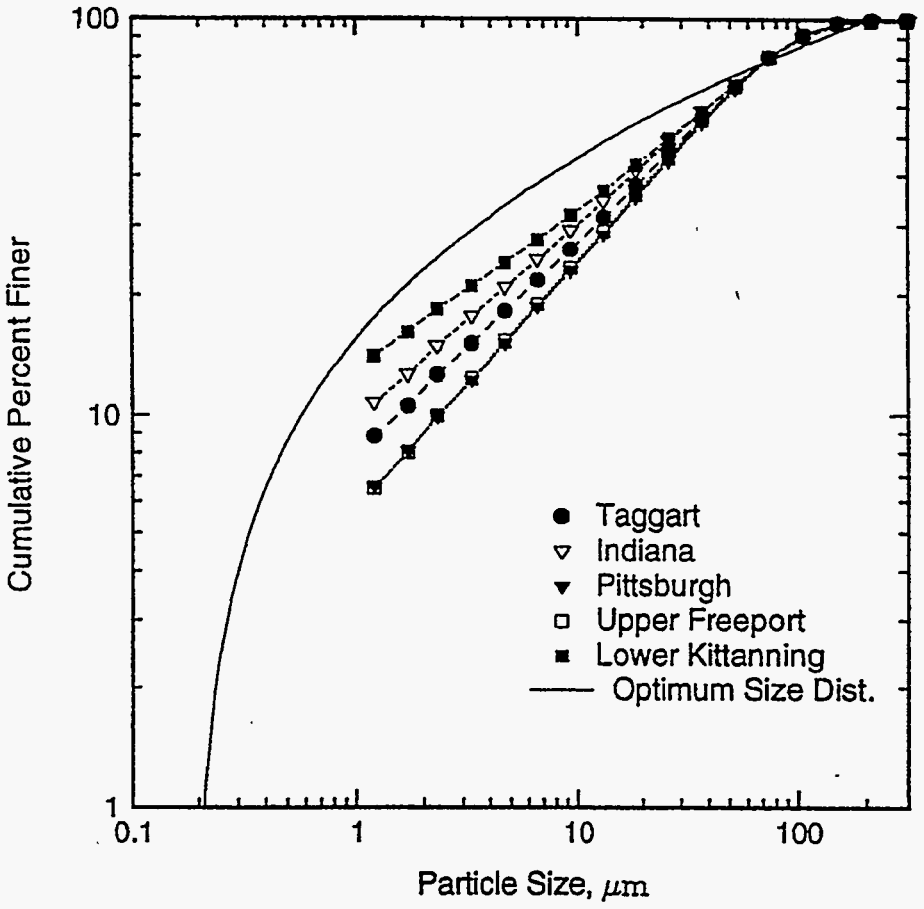

Figure 3-40. PRODUCT SIZE DISTRIBUTIONS OF 80% PASSING 200 MESH AT 70 WT. % SOLIDS FOR ALL COALS

mixed with the ball mill product to obtain the required size distribution.

3.2.7 Stirred Ball Milling

Stirred-media mills offer an attractive alternative for ultrafine grinding in the production of MCWM. Their use would be especially appropriate for preparing the fine component of a bimodal slurry for the relatively small-scale applications being evaluated in this project. However, while design and operation criteria for conventional ball mills are well established and widely applied, considerably less information is available for stirred-media milling.

In a separate, industrially-funded project, Penn State has been evaluating the performance of stirred-media mills. The results to date can be summarized as follows:

- Stirred-media mills can be used to grind to extremely fine sizes - as much as 100% less than 0.5 μm.
- Grinding behavior in stirred-media mills appears to follow a very similar pattern to conventional ball milling.
- Direct measurement of product size distributions by laser scattering/diffraction, dynamic light scattering, transmission electron microscopy and gas adsorption all support the approach to a limiting, minimum particle size in the 10-50 nm range.
- The results are consistent with primary breakage distributions which show progressive narrowing for sizes less than about 1 μm.
- The results also suggest that the specific rates of breakage follow a power-law relationship with size similar to that found for conventional (ball mill) grinding but show an enhanced decrease with size in the submicron range.

Based on the standard test procedures developed in these studies, an investigation of stirred-media milling of four coals was conducted.

The grinding tests were carried out using a laboratory horizontal stirred ball mill (Dyno-Mill). It consists of a water-jacketed stainless-steel grinding chamber of 0.6 liter volume and a stirrer shaft with four agitating disks. It is equipped with a feed inlet and outlet for continuous closed-loop operation, however, the tests were conducted in a batch mode without recirculation of the slurry. Stainless steel beads of 1/16 inch diameter were used as grinding media. The grinding tests were conducted with a 80% loading of media on a bulk volume basis and a slurry of 114 g of coal and 171 g of water (40% solids by weight). The mill was operated at a constant 3,000 rpm, although speed can be adjusted by a pulley arrangement.

The coal was ground for various times using a new sample for each test. The products were screened at 400 mesh. The +400 mesh size fractions were dried, followed by dry screening. Any -400 mesh material was combined with the wet-screened fines and then analyzed using a Microtrac SRA and SPA. The overall size distribution was calculated by combining the sieve size and Microtrac size based on the material balance and a sieving/Microtrac conversion factor.

Figures 3-41 to 3-44 show the size distributions of the four test coals obtained for various grinding times. It can be seen that the size distribution becomes progressively finer in a parallel manner, a trend very similar to the typical batch grinding data in a ball mill. However, the overall

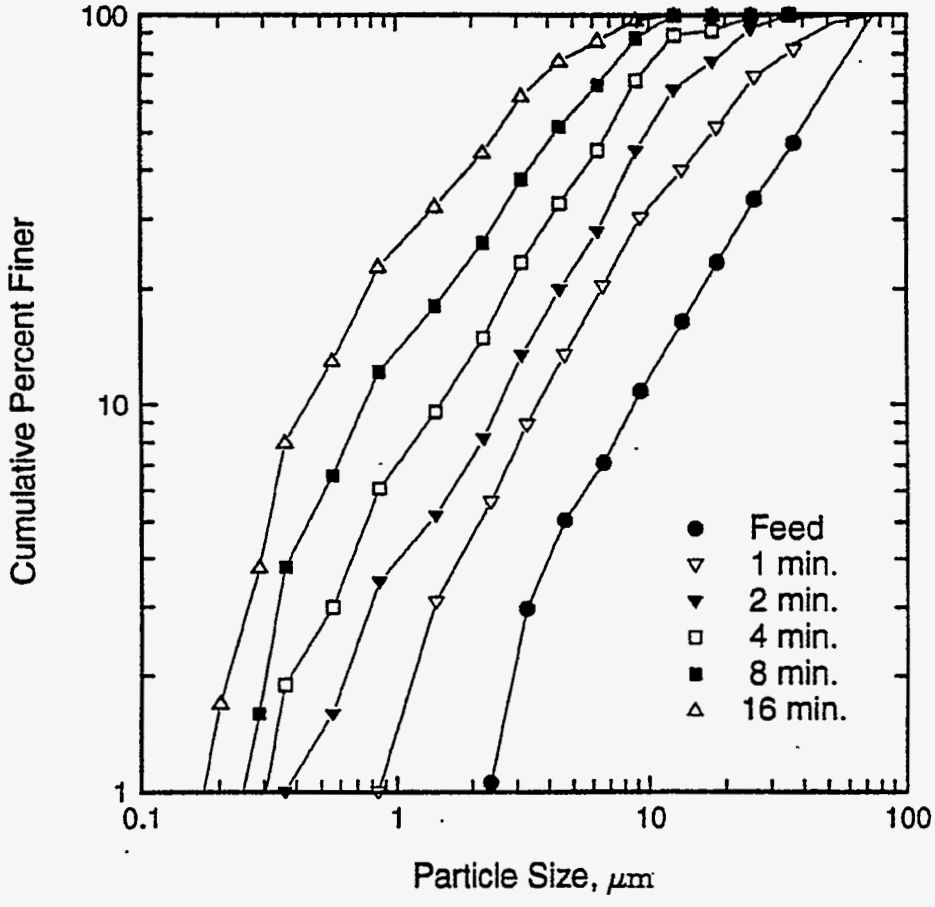

Figure 3-41. PRODUCT SIZE DISTRIBUTIONS AFTER GRINDING THE -200 MESH SAMPLE OF THE TAGGART SEAM COAL IN A STIRRED BALL MILL AT 40 WT. % SOLIDS FOR VARIOUS TIMES WITH 0.5 WT. % DISPERSANT

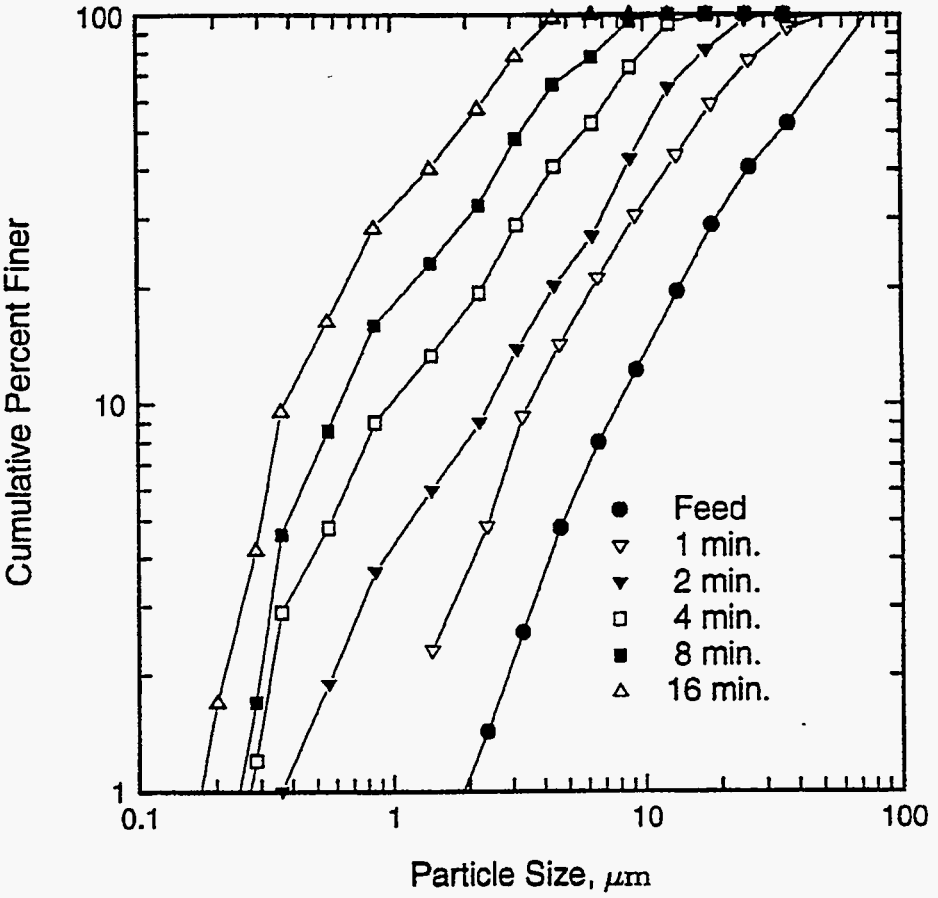

Figure 3-42. PRODUCT SIZE DISTRIBUTIONS AFTER GRINDING THE -200 MESH SAMPLE OF THE PITTSBURGH SEAM COAL IN A STIRRED BALL MILL AT 40 WT. % SOLIDS (BY WEIGHT) FOR VARIOUS TIMES WITH 0.5 WT. % DISPERSANT

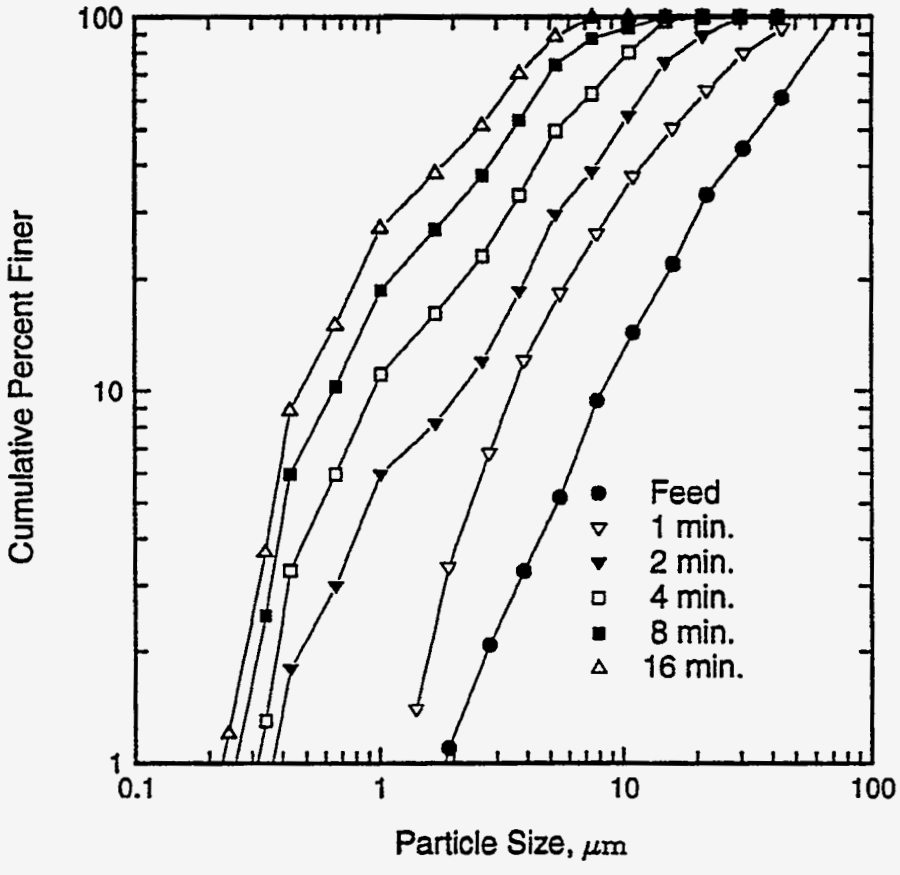

Figure 3-43. PRODUCT SIZE DISTRIBUTIONS AFTER GRINDING THE -200 MESH SAMPLE OF THE LOWER KITTANNING SEAM COAL IN A STIRRED BALL MILL AT 40 WT. % SOLIDS FOR VARIOUS TIMES WITH 0.5 WT. % DISPERSANT

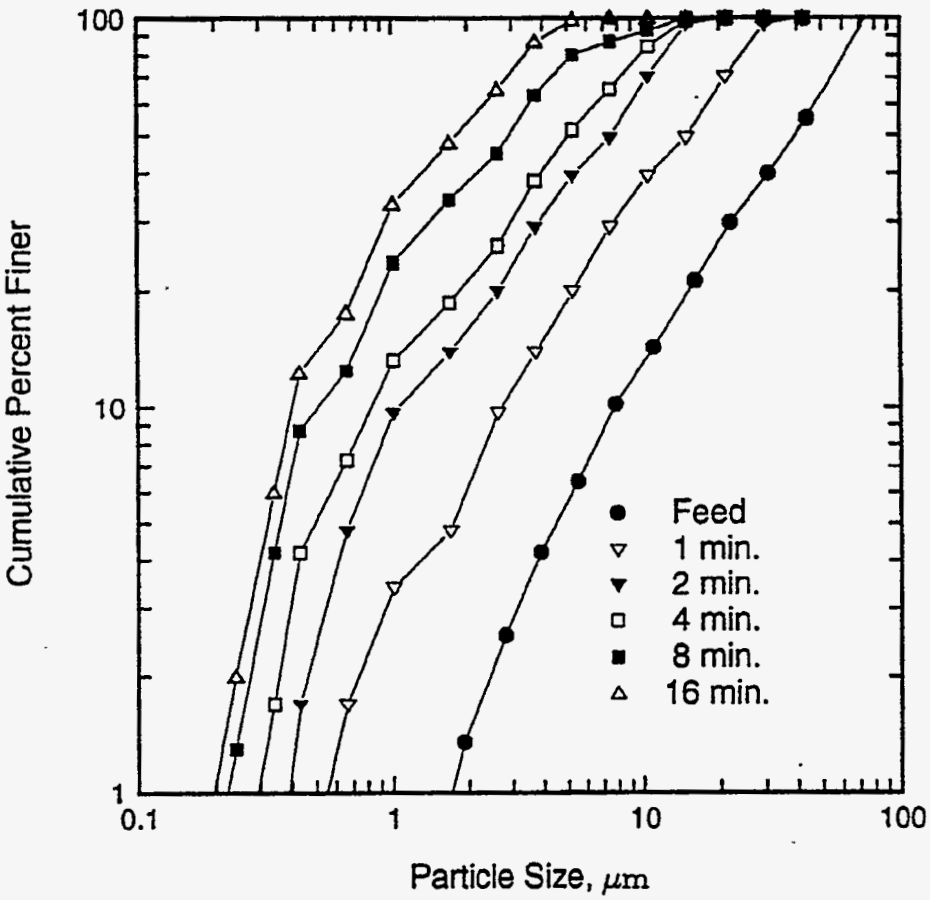

Figure 3-44. PRODUCT SIZE DISTRIBUTIONS AFTER GRINDING THE -200 MESH SAMPLE OF THE UPPER FREEPORT SEAM COAL IN A STIRRED BALL MILL AT 40 WT. % SOLIDS FOR VARIOUS TIMES WITH 0.5 WT. % DISPERSANT

shape of the size distribution is steeper than the ball mill grinding products at the same solids concentration. For example, the Gaudin-Schumann slope of the Taggart seam coal is about 0.8 for the stirred ball mill, compared to 0.72 for ball milling. Also, unlike the ball mill products, the shape of the size distribution is similar regardless of coal type. This is more evident in Figure 3-45 where the size distributions are plotted against the dimensionless size (x/x_{50}). It can be seen that all the size distribution data collapsed into a single curve. The implication is that the median size (x_{50}) can be used as a characteristic parameter to describe the grinding products.

Figure 3-46 shows the variation of median size with grinding time for the four coals. It can be seen that the median size decreased in a linear manner with grinding time when plotted on a log-log scale. Also, there is a general trend that for a given grinding time, the median size is smaller for the higher HGI coals. Figure 3-47 shows the power consumption over the grinding period for the Taggart seam coal. Except for the initial period of grinding, the power consumption remains fairly constant with a average value of 0.292 kW compared to 0.005 kW for the ball milling. Figure 3-48 relates the median particle size with the specific energy input for the ball mill and stirred ball mill. In this log-log plot, the size reduction is well correlated linearly with the energy input by a single line for both mills, known as the Charles' energy-size relationship. In this particular case, a size reduction ratio of 10 requires 80 times more energy.

Figure 3-49 shows the product size distributions after 16 minutes in the stirred ball mill and the ball mill products at various slurry conditions giving 70% passing 200 mesh. Since the calculated optimum size distribution of 80% passing 200 mesh lies between the two mill products, blending of the products should produce the desired size distribution. Indeed, 3:1 blending of the ball mill product and the stirred ball mill product produces a size distribution close to the optimum size distribution.

3.2.8 Attrition Milling

Attrition milling operates on the same basic principle as stirred-media milling, but the size reduction is accomplished by the using the coal itself as the media. However, there is a major difference between the stirred-media mills and attrition mills. First, the power input is substantially less for the attrition milling, since the coal is lighter than the media and hence, less energy is required to agitate the slurry. More importantly, the breakage process in attrition milling is totally different. Large coal particles acts as a grinding media for smaller particles, giving breakage mechanisms similar to those obtained by normal grinding media. But they also break themselves by particle-particle contact. The breakage in any grinding mills is generally achieved by the three different mechanism - fracture, chipping, and abrasion.

Fracture refers to complete disintegration of a particle by massive impact, while chipping refers to cutting off corners. Abrasion involves the wearing of surfaces by a rubbing action. The fragments produced by fracture spread over a broad range in size. On the other hand, chipping and abrasion lead to production of fine material and a residual "core" close to the original particle size.

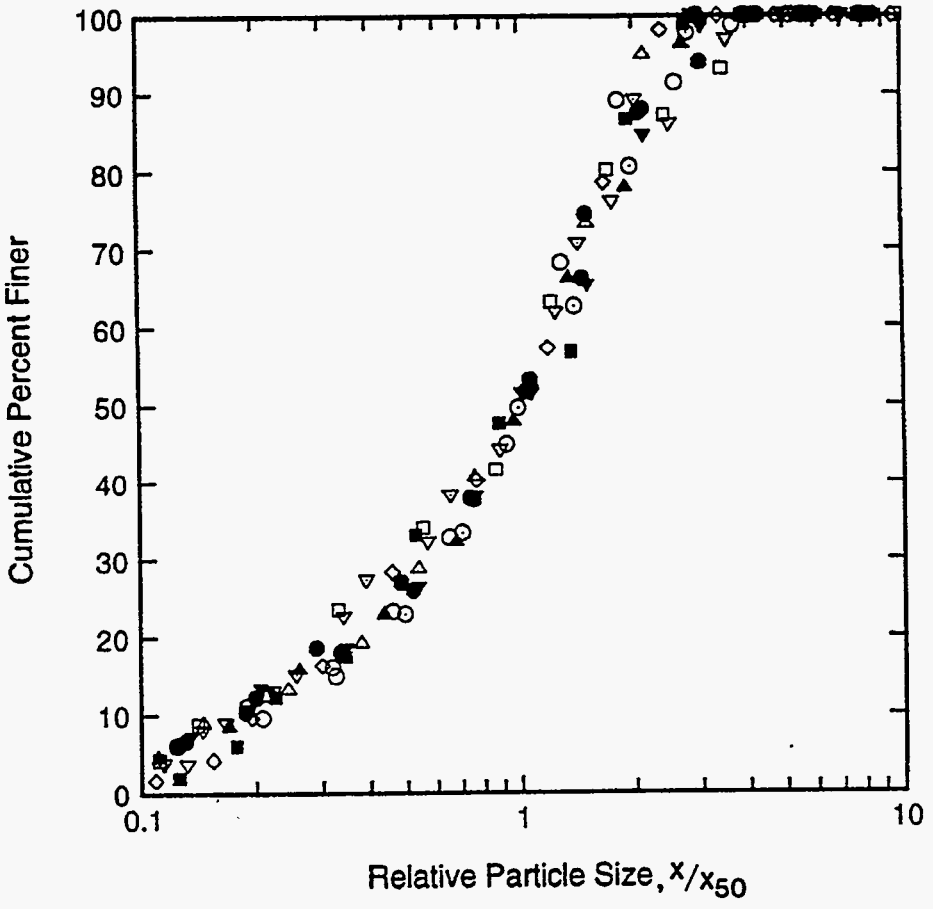

Figure 3-45. PRODUCT SIZE DISTRIBUTIONS AT VARIOUS GRINDING TIMES FOR THE FOUR COALS PLOTTED AGAINST THE DIMENSIONLESS SIZE

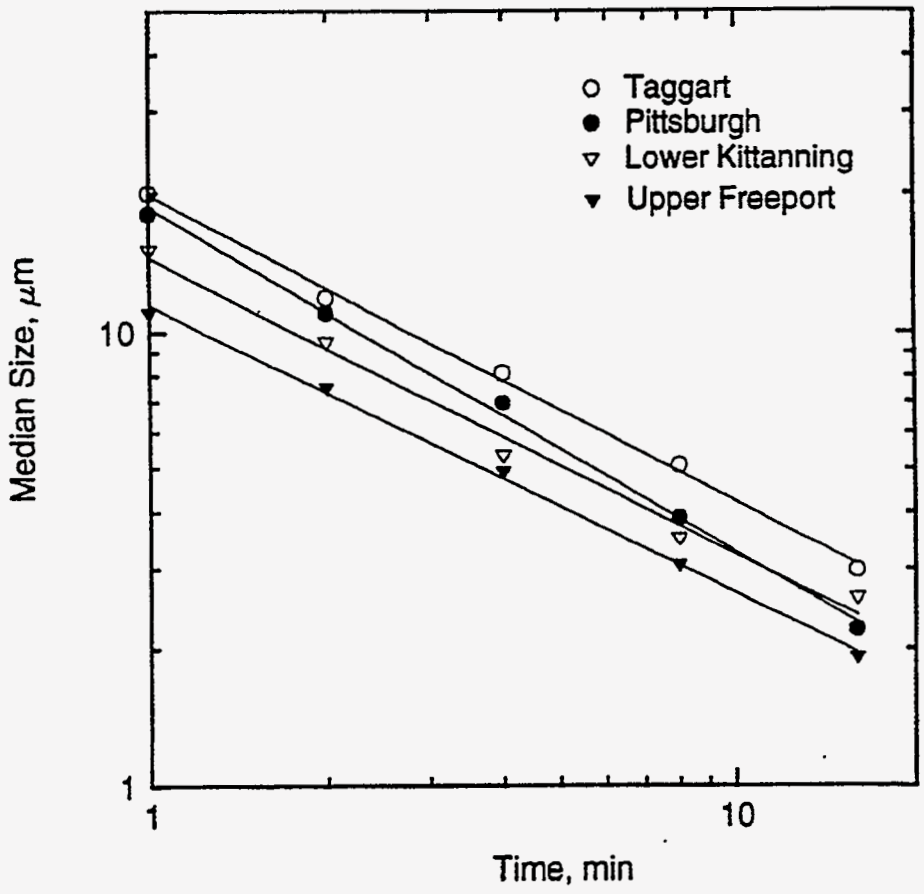

Figure 3-46. VARIATION OF THE MEDIAN SIZES WITH GRINDING TIME FOR THE FOUR COALS

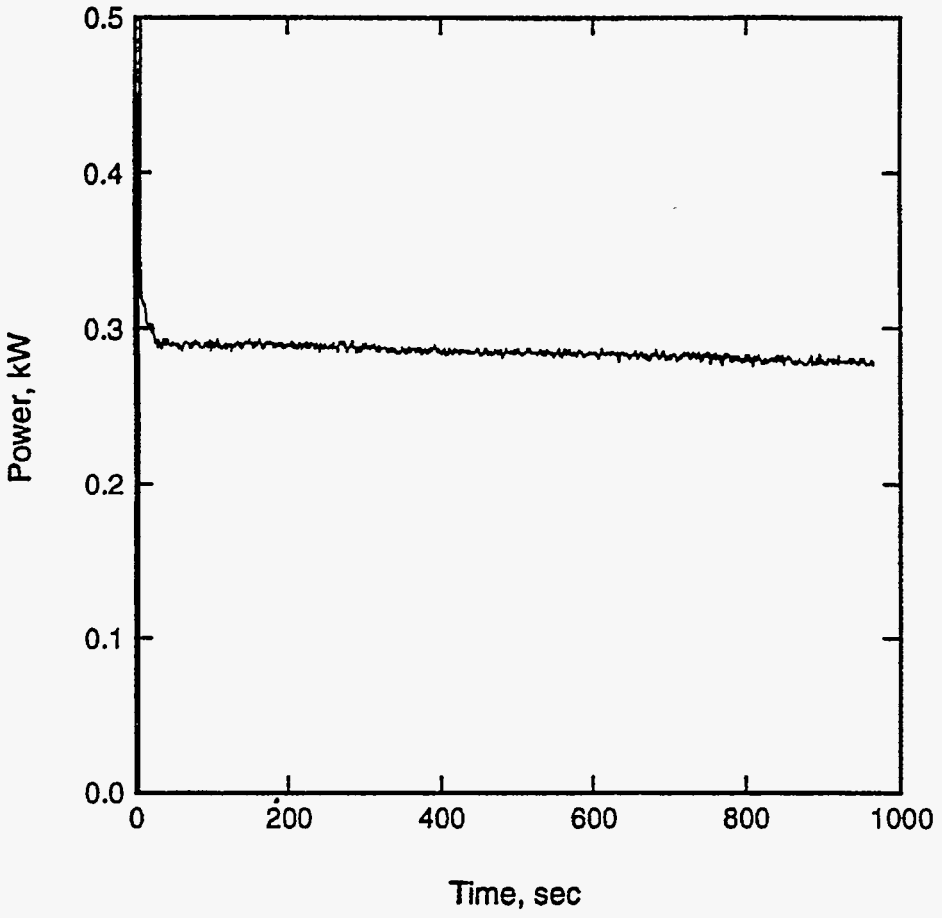

Figure 3-47. POWER CONSUMPTION FOR GRINDING THE TAGGART SEAM COAL IN A STIRRED BALL MILL AT 40 WT. % SOLIDS

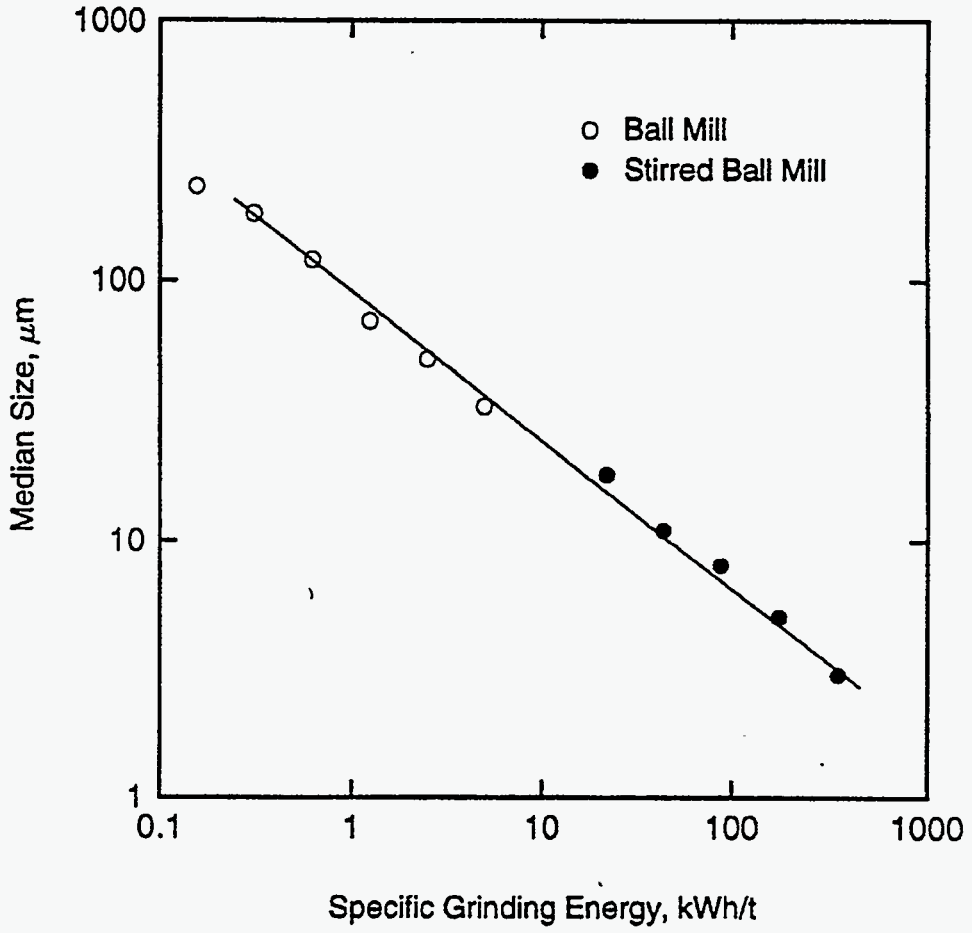

Figure 3-48. RELATIONSHIP BETWEEN THE SPECIFIC ENERGY INPUT AND THE PRODUCT MEDIAN SIZE FOR GRINDING THE TAGGART SEAM COAL IN A BALL MILL AND A STIRRED BALL MILL AT 40 WT. % SOLIDS

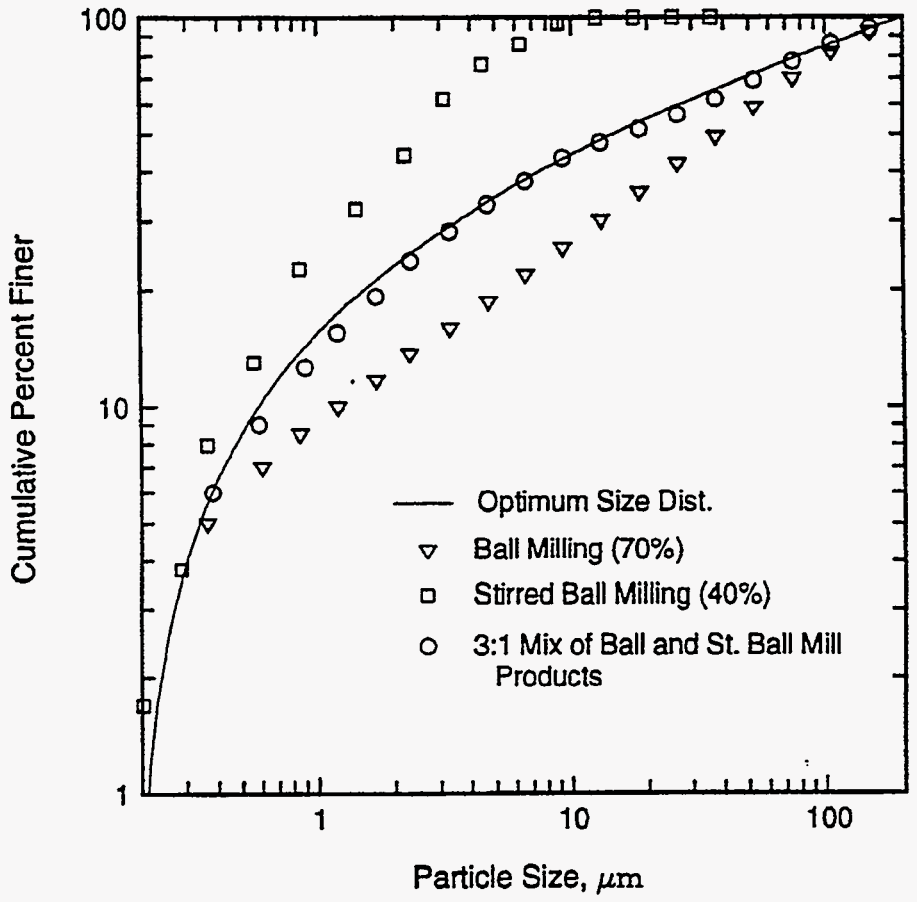

Figure 3-49. SIZE DISTRIBUTIONS FOR THE FOLLOWING CONDITIONS: ❑ after 16 minutes in a stirred ball mill; ▽ after 30 minutes in a conventional ball mill; ○ 3-to-1 mixture of the conventional and stirred ball mill products; and – optimum size distribution

Therefore, the shape of the product size distribution is greatly influenced by the type of the breakage mechanism. In attrition milling, chipping and abrasion will play a bigger role and the resulting product is likely to be composed of two main populations - coarse (remaining cores) and fines (chipped or abraded material). This is quite favorable for the production of coal-water slurry feedstock. Therefore, attrition milling potentially offers a great advantage for coal-water slurry preparation over other grinding device from both economic and engineering viewpoints.

Tests will be conducted as part of the Phase II research to explore such a potential advantage using a vertical type stirred-media mill.

3.2.9 A Dry Coal Cleaning

An alternative to wet cleaning is to utilize dry beneficiation. A dry process offers several advantages. The formulation of coal-water slurry can be controlled closely since no water has to be removed, which eliminates the need for dewatering equipment. It also offers a direct method of cleaning coal prior to micronized coal firing, again eliminating the need for extensive dewatering and drying of coal. One process that offers the potential for dry cleaning of fine coal on a commercial scale is triboelectrostatic separation[58]. This process involves the tribocharging and subsequent electrostatic separation of fine and ultrafine coal particles. Air-borne particles are charged by contacting them with some material such as copper. A common technique is to pass the particle stream through an in-line static mixer. The charged (positive) coal particles and charged (negative) mineral matter particles can then be separated electrostatically by passing them through an electric field.

The work by DOE showed that clean coal products with ash and pyritic sulfur contents of <2% and <0.3%, respectively, at yields of more than 40% were obtained when cleaning -400 mesh Pittsburgh and Upper Freeport seam coals. One of the goals for this project is to increase the overall yield for each coal, while still producing a product that meets the ash and sulfur requirements.

Dry Grinding

Prior to separation, the particles must be ground to produce the appropriate size distribution. This requires both size reduction and size classification. A grinding circuit was set-up, which consists of an opposing jet fluid-energy (jet) mill, in closed circuit with a Donaldson Acucut classifier (Figure 3-50). The compressed air (@~760 kPa) for the jet mill is supplied by a rotary screw compressor, while the flow of air through each jet is monitored with a differential pressure gauge. This circuit is capable of providing a wide range of particle size distributions for triboelectrostatic separation and is used primarily to produce micronized coal. The production of the coarser (pulverized coal-grind) material is done using staged size reduction with a hammer mill and high-speed pulverizer. A typical size distribution of the -100 mesh coal generated by the latter procedure is shown in Figure 3-51.

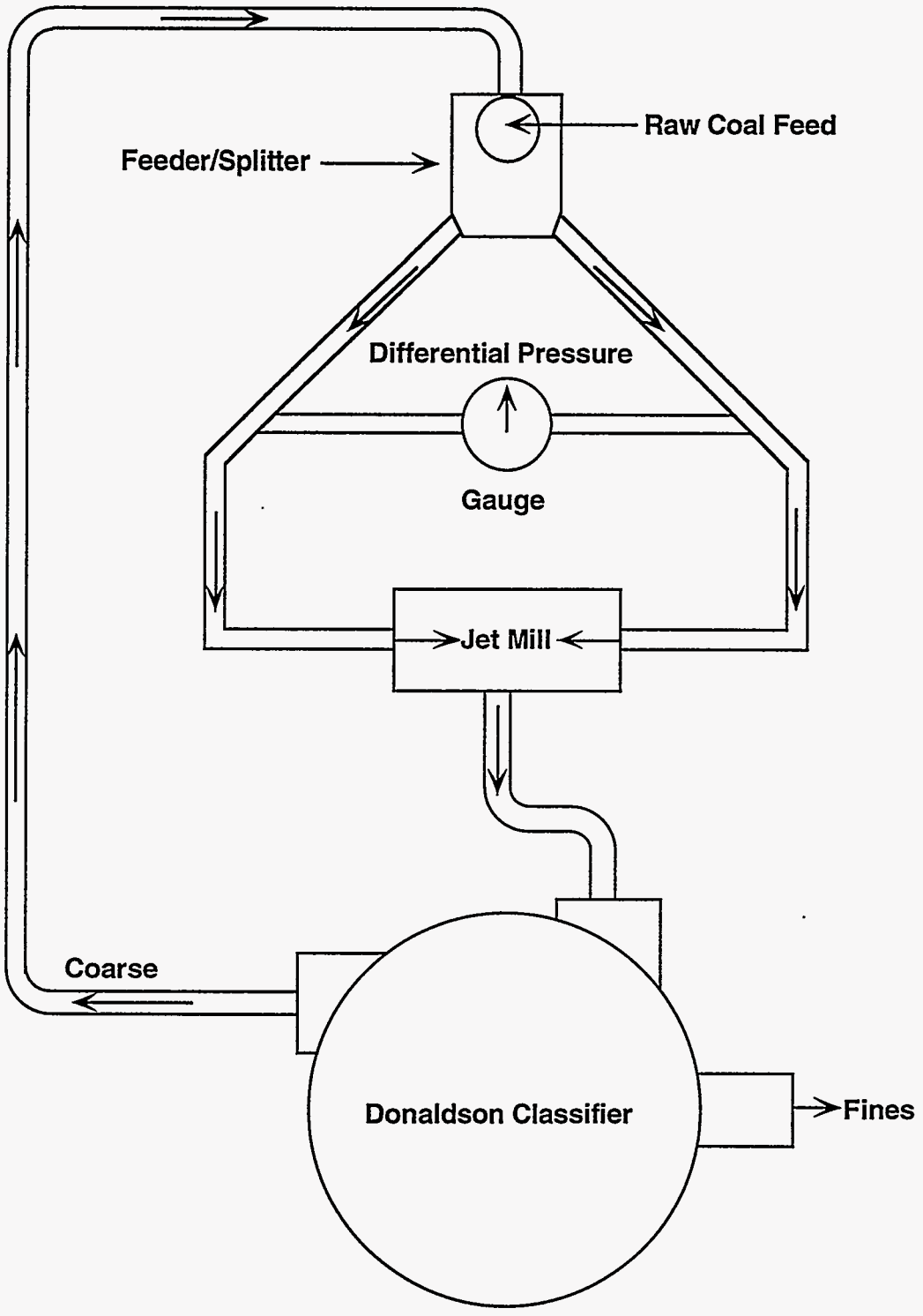

Figure 3-50. SCHEMATIC DIAGRAM OF THE DRY GRINDING CIRCUIT

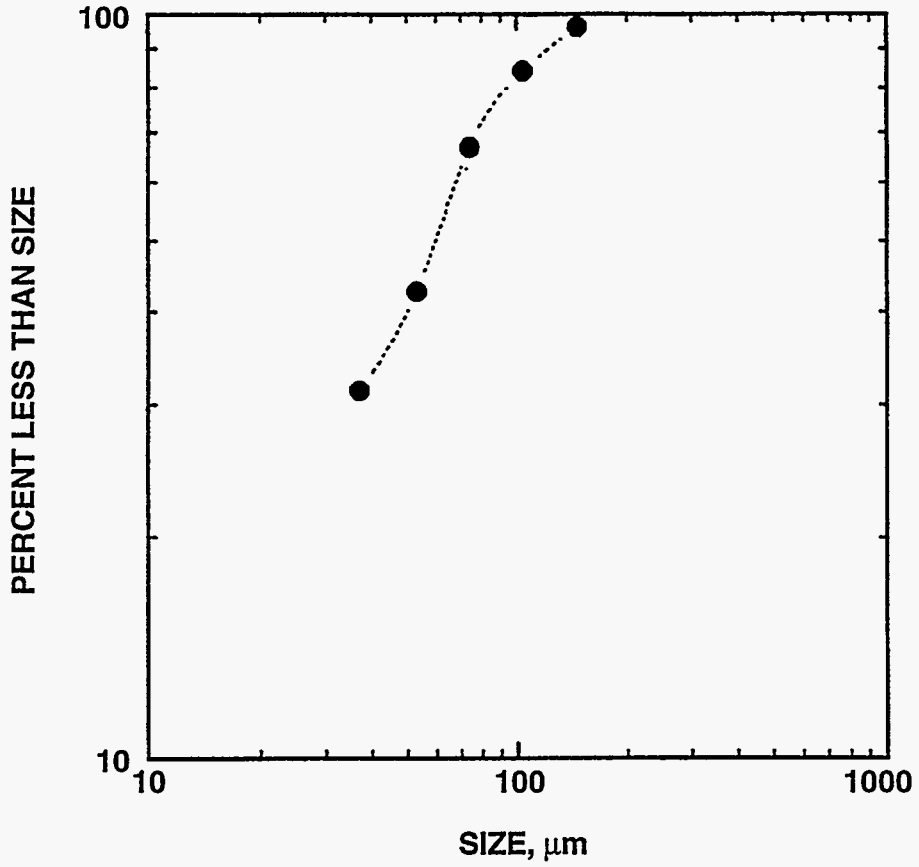

Figure 3-51. SIZE DISTRIBUTION OF THE -100 MESH COAL

Deagglomeration

One of the difficulties of separating fine coal is agglomeration. As particle size decreases, the tendency for particles to agglomerate increases. Hence fine coal may be carried to the refuse, decreasing recovery. Likewise, fine mineral matter may be carried to the clean coal, decreasing grade. Consequently, it is desirable that the coal be thoroughly dispersed before and after tribocharging, and that all particles appear in the gas stream as single particles rather than as agglomerates of two or more particles. It was reported[59-61] that the deagglomeration of particulates can be achieved by the use of a fluidized bed. In this technique, the powder to be dispersed is introduced into a fluidizing bed of beads (bronze or brass beads), which are larger than the powder. The fluidizing action of these beads disperses the powder as individual particles. A small test unit has been fabricated and will be tested during the subsequent phase of the study.

Dry Separations

An electrostatic separator, similar to that tested by DOE, was fabricated (Figure 3-52). A series of flow straighteners (~5 mm diameter by ~100 mm long plastic tubes) were added at the feed end to the separator so that sweep air could be drawn through the tubes. The coal was fed into the carrier gas stream by a vibrating feeder. Dried compressed air was initially used as the carrier gas, but was later replaced with nitrogen. Preliminary tests indicated that between 50 and 100 g of coal could be separated over a 5 to 10 minute period before the plates had to be removed for cleaning. It was also found that a separator gap of 115 mm was appropriate. Different baffling arrangements were used in the separator feed funnel in an attempt to improve the distribution of coal across the separator plates. Testing indicated that the best coal distributions were obtained when no feed funnel was used. These conditions were kept constant for subsequent tests.

A sample of the test coal was pulverized in stages to the desired product size (e.g., -100 mesh). This material was riffled into 50-100 g samples, which were stored in sealed bags under argon. Prior to each test, the coal sample was dried in an oven at 105°C for one to two hours. One sample was used per run. After the test was completed, the plates were removed and the coal and refuse were separated at spaced increments along the length of each plate. The samples were weighed to determine the yield at each increment and then analyzed for ash and total sulfur content.

A series of tests was performed using the Upper Freeport seam coal to investigate the effects of nitrogen flow rate, plate voltage, and coal feed size. Figure 3-53 shows the effects of changing the nitrogen flow rate. A change in the flow rate and hence, gas velocity through the feed tube and tribocharger (static mixer) had a minimal effect on the weight of coal (or refuse) reporting to the negative (or positive) plate. In both cases, approximately 60% of the feed reported to the clean coal. Likewise, the cumulative ash content as a function of distance along the plates was the same for both velocities, with ash contents less than 5 wt.% obtained in both cases. The total

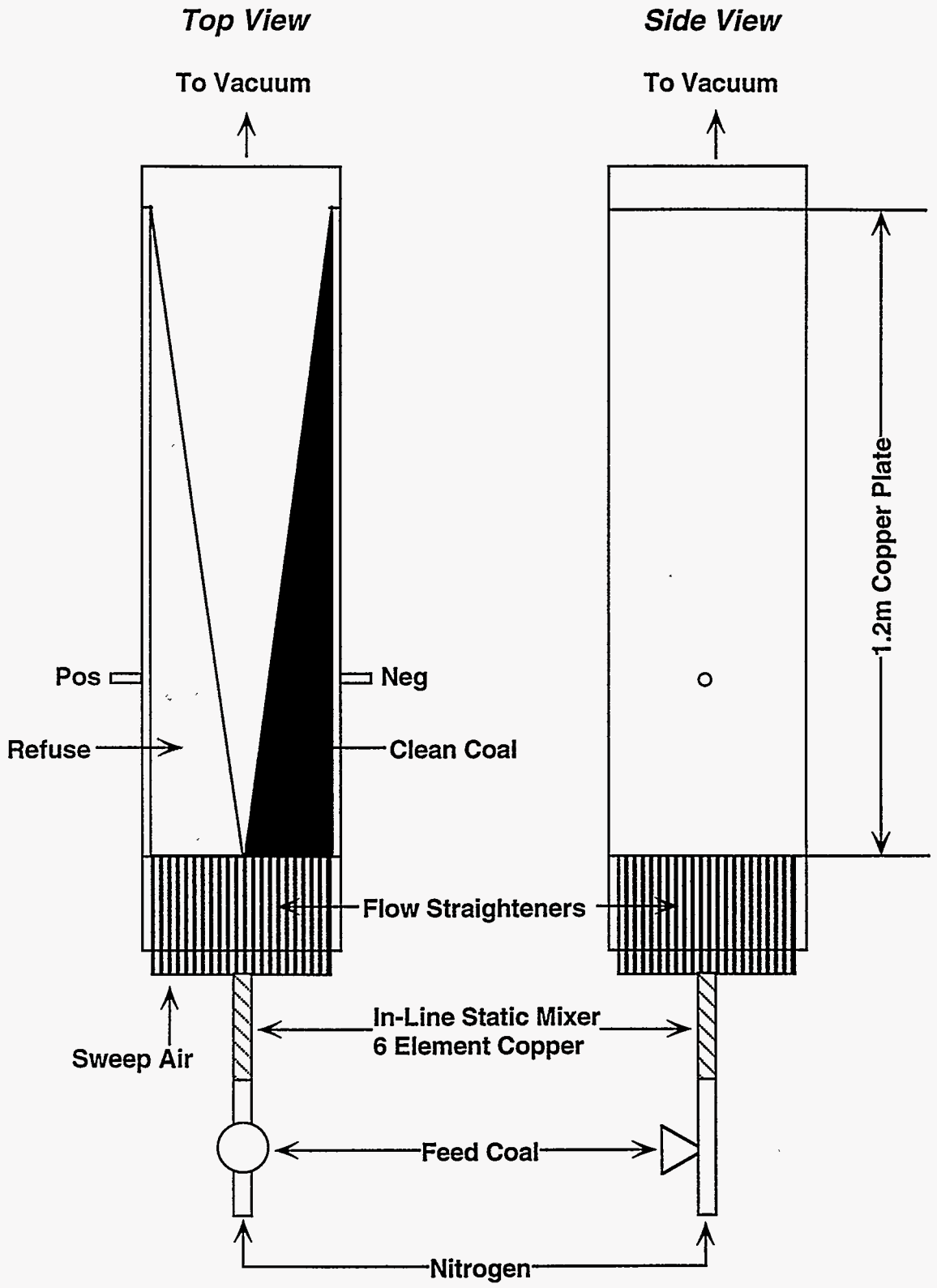

Figure 3-52. SCHEMATIC DIAGRAM OF THE TRIBOELECTROSTATIC SEPARATOR

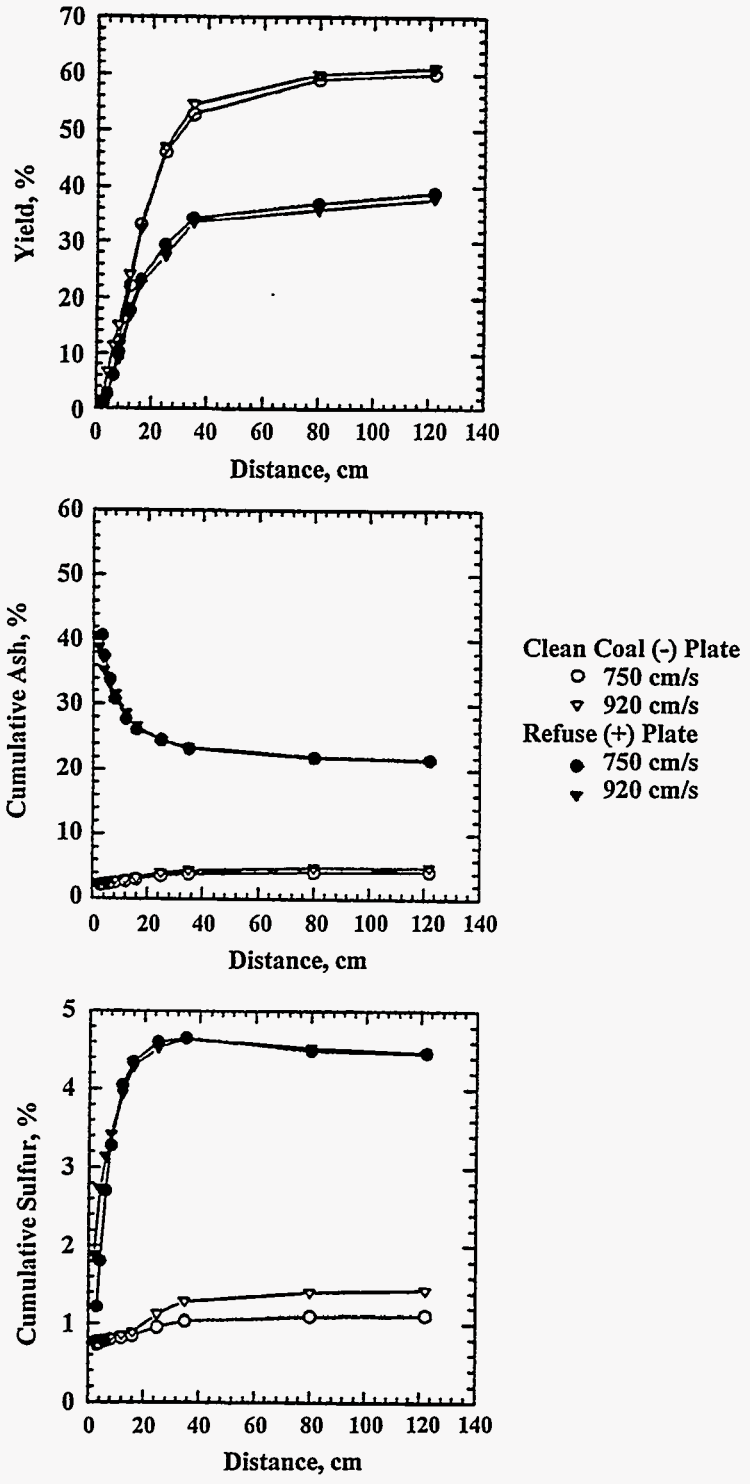

Figure 3-53. TRIBOELECTROSTATIC SEPARATION OF THE UPPER FREEPORT SEAM COAL (–100 mesh) AT DIFFERENT NITROGEN VELOCITIES
(voltage = ±26 kV; temperature = 29°C; humidity = 69%)

sulfur content was slightly lower for the lower aerosol velocity (~1.1 versus 1.4 wt.%). This is likely the result of the higher sulfur content of the feed sample used in the higher velocity test.

The effects of changing the voltage on the separator plates are shown in Figure 3-54. A decrease in the voltage drop across the plates decreased the coal yield over the first 40 cm of the plates. However, the final yield was the same (~60%) for both tests. The ash and sulfur contents on the refuse (positive) plate were higher when the higher voltage was used. On the other hand, these attributes were lower on the clean coal (negative) plate. This indicates better selectivity at the higher voltage.

For the next set of tests, the feed size fraction was varied. A sample of the -100 mesh coal was ground using the jet mill/Donaldson classifier circuit. A 6x12 μm fraction was prepared by grinding the entire sample down to a nominal -12 μm. The -6 μm material was then removed by classification. A separate -100 mesh sample was ground in closed circuit to a nominal -6 μm and then classified to remove the -3 μm material. A third fraction (1x3 μm) was also prepared in the same manner. Each of these size fractions was passed through the tribocharger/separator unit. For the finest size fraction, it was not possible to remove the material from the plates without causing excessive contamination and/or loss of coal. The resulting curves for the other two size fractions, along with the curves for the (-100 mesh) fraction, are given in Figure 3-55.

It can be seen that the yield of clean coal decreased with decreasing particle size. Likewise, the selectivity of the -100 mesh fraction was also the best, with the lowest and highest attributes obtained on the clean coal and refuse plates, respectively. One of the difficulties in processing the ultrafine size fractions is the agglomeration of the particles. There is a tendency for the fine mineral matter particles to coat the coal particles, destroying the ability to separate the particles selectively. This negates the advantages of grinding to ultrafine sizes to improve liberation. For this reason, testing of deagglomerating procedures is required if effective ultrafine coal separations are to be performed.

Another explanation may be associated with the material preparation during grinding and classification. Since the grinding/classification circuit is an air-swept system, the particles are continually being contacted with different materials within the devices (e.g., steel, ceramic, etc.). Such contact will resulting in some level of particle charging, which could have an effect on the final separation. This effect will also be examined.

Figure 3-56 compares separations for the Upper Freeport and the Pittsburgh seam coals. The clean coal yield was much higher for the Upper Freeport seam coal (60 versus 25%). Interestingly, the ash content of the clean coal was the same (~4 wt.%) for both coals, while the ash content of the refuse material for the Upper Freeport seam coal was much higher, indicating greater selectivity for this coal. However, the higher feed ash content of the Upper Freeport seam coal would also contribute to this effect. Similar results were also obtained for the sulfur content of each product.

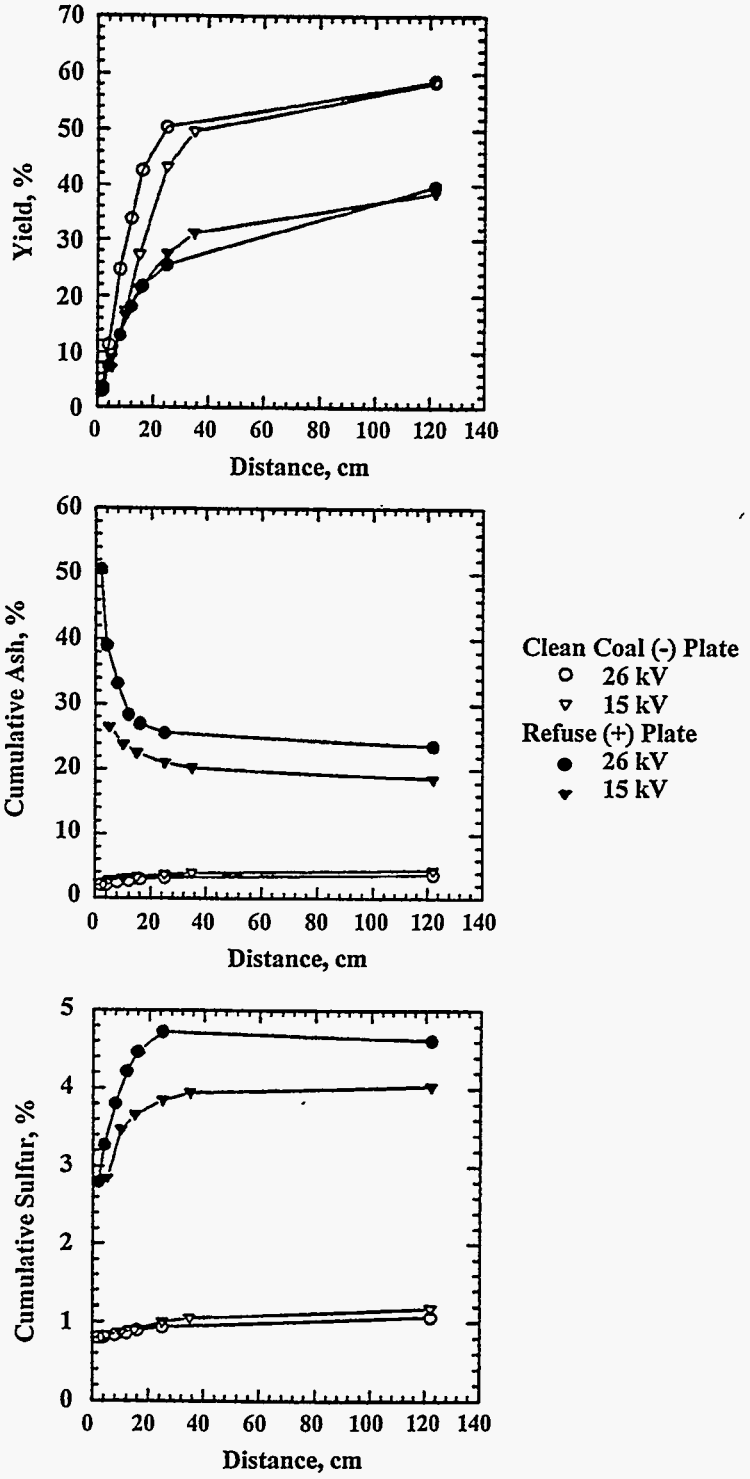

Figure 3-54. TRIBOELECTROSTATIC SEPARATION OF THE UPPER FREEPORT SEAM COAL (–100 mesh) AT DIFFERENT VOLTAGES (nitrogen velocity = 920 cm/s; temperature = 24°C; humidity = 38%)

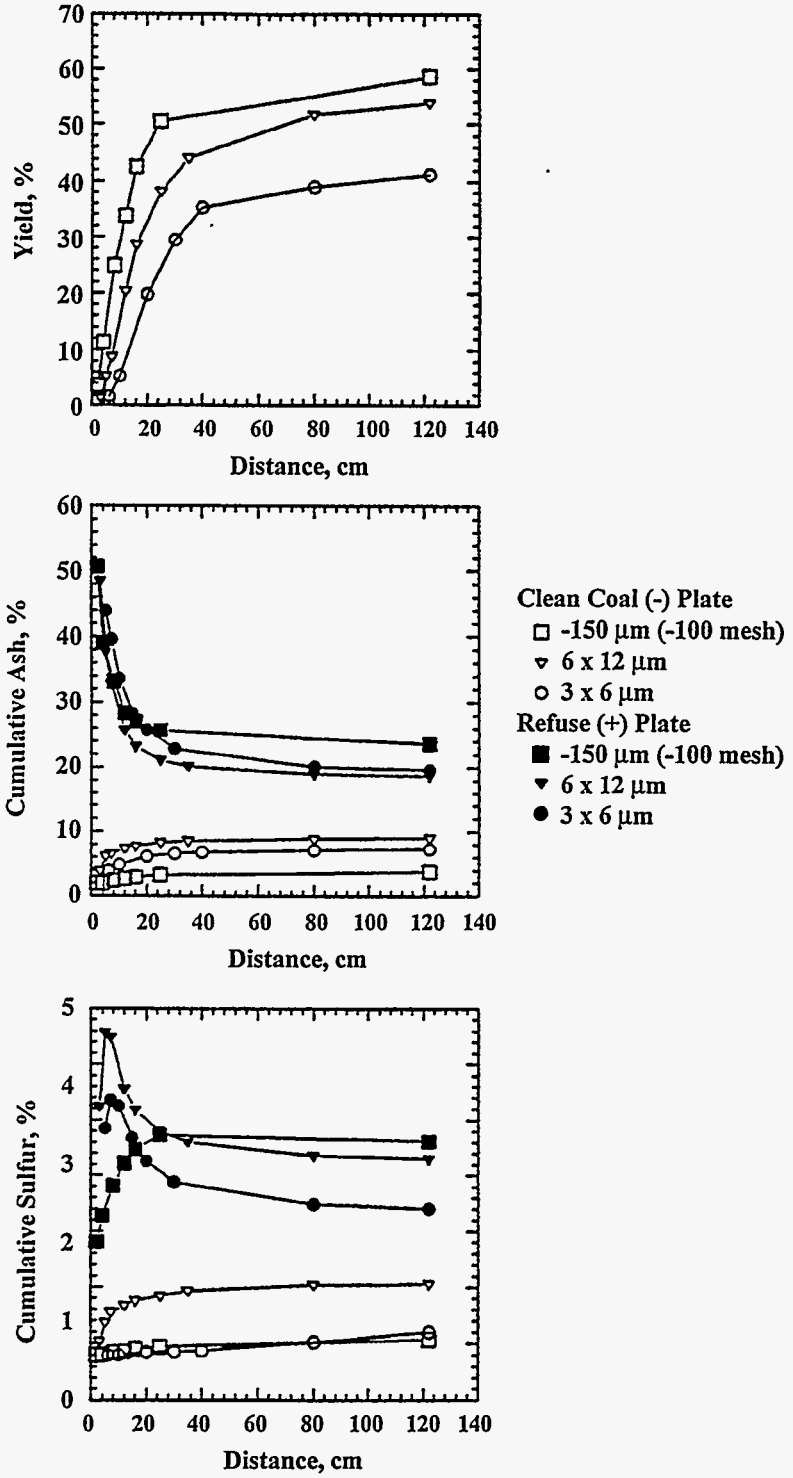

Figure 3-55. TRIBOELECTROSTATIC SEPARATION FOR DIFFERENT FEED SIZES OF THE UPPER FREEPORT SEAM COAL (nitrogen velocity = 920 cm/s; voltage = ±26 kV; temperature = 24°C; humidity = 22%)

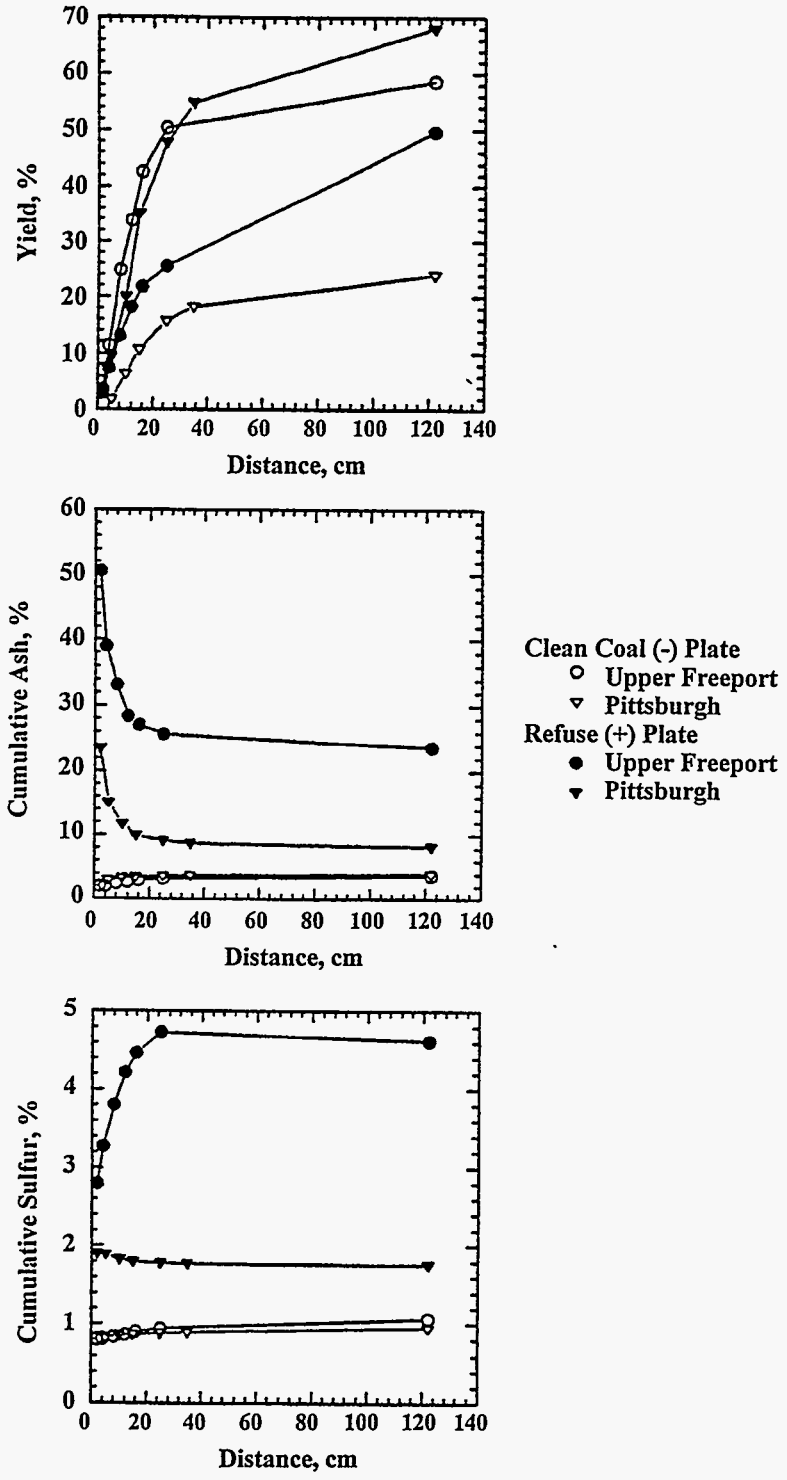

Figure 3-56. TRIBOELECTROSTATIC SEPARATION OF THE UPPER FREEPORT AND PITTSBURGH SEAM COALS
(coal feed size = –100 mesh; nitrogen velocity = 920 cm/s; voltage = ±26 kV; temperature = 21°C; humidity = 18%)

In an attempt to improve the yield of this coal, a longer in-line static mixer was tested. The new mixer was also constructed of copper. It was 61 cm long, with a nominal inside diameter of 1.25 cm. This mixer had 16 elements compared to the 6 element mixer used in the previous testing. The -100 mesh Pittsburgh seam coal was tested under the conditions as noted above. A comparison of the results from both mixers is given in Figure 3-57.

The longer mixer had a dramatic effect on the yield of the clean coal product, which increased to ~73%. This was achieved without an increase in the ash content of the clean coal (~4%), although the total sulfur content increased from 0.8% to approximately 1.1%. One explanation for the increase in yield would be the higher probability of coal to copper contact using the longer mixer. This would increase the opportunity for the coal particles to acquire a surface charge.

Tests were then run on the Upper Freeport seam coal using the 16 element mixer. In this case, the longer mixer had less of an impact on the separation but still increased the clean coal yield approximately 5% (Figure 3-58). Again the cumulative ash remained constant (~4.3 wt.%), while the total sulfur content of the clean coal increased slightly from 1.05 to 1.15 wt.%. The small increase in yield with the number of elements and length of the static mixer suggests that the Upper Freeport seam coal acquires a charge more readily than that of the Pittsburgh seam coal.

The results from using the Indiana VII seam coal are compared to those obtained for the Pittsburgh and Upper Freeport seam coals as shown in Figure 3-59. The yield for the three coals is constant up to a plate length of ~16 cm. Beyond 16 cm, the yield changes with the Pittsburgh seam coal having a final yield of 73%, followed by the Indiana VII seam coal at 68%, and the Upper Freeport seam coal at 64%. These results suggest that the surface charge is independent of coal type up to 16 cm. At the longer distances, the charge on the Indiana VII and Upper Freeport seam coals diminishes more quickly than that on the Pittsburgh seam coal. The ash content of all three coals was the same, while the total sulfur of the Pittsburgh seam coal was slightly less than that of the Upper Freeport seam coal. The sulfur content of the Indiana coal is not shown because of the low amount (~0.5 wt.%) in the feed. Work will continue in Phases II and III to investigate continuous triboelectrostatic separations.

3.2.10 The Optimal Packing of Particles in Coal-Water Mixtures

The problems of the optimal size distribution in the packing of powders was discussed in the classical work of Furnas[62] as early as 1931. During the last 55 years Furnas' theory, in its original form or with some modification[63], has been a major tool in particle packing theory. However, the Furnas theory has some drawbacks. First, there are some discrepancies with experimental data[64]. Second, it is necessary to calculate an integer constant n, which is a root of a rather complicated equation. Third, in this model the transition to a smooth size distribution is neither clear nor self-consistent. Fourth, it is not clear how the limiting cases of infinitely broad and infinitely narrow distributions may be derived from the Furnas' theory. These difficulties arise

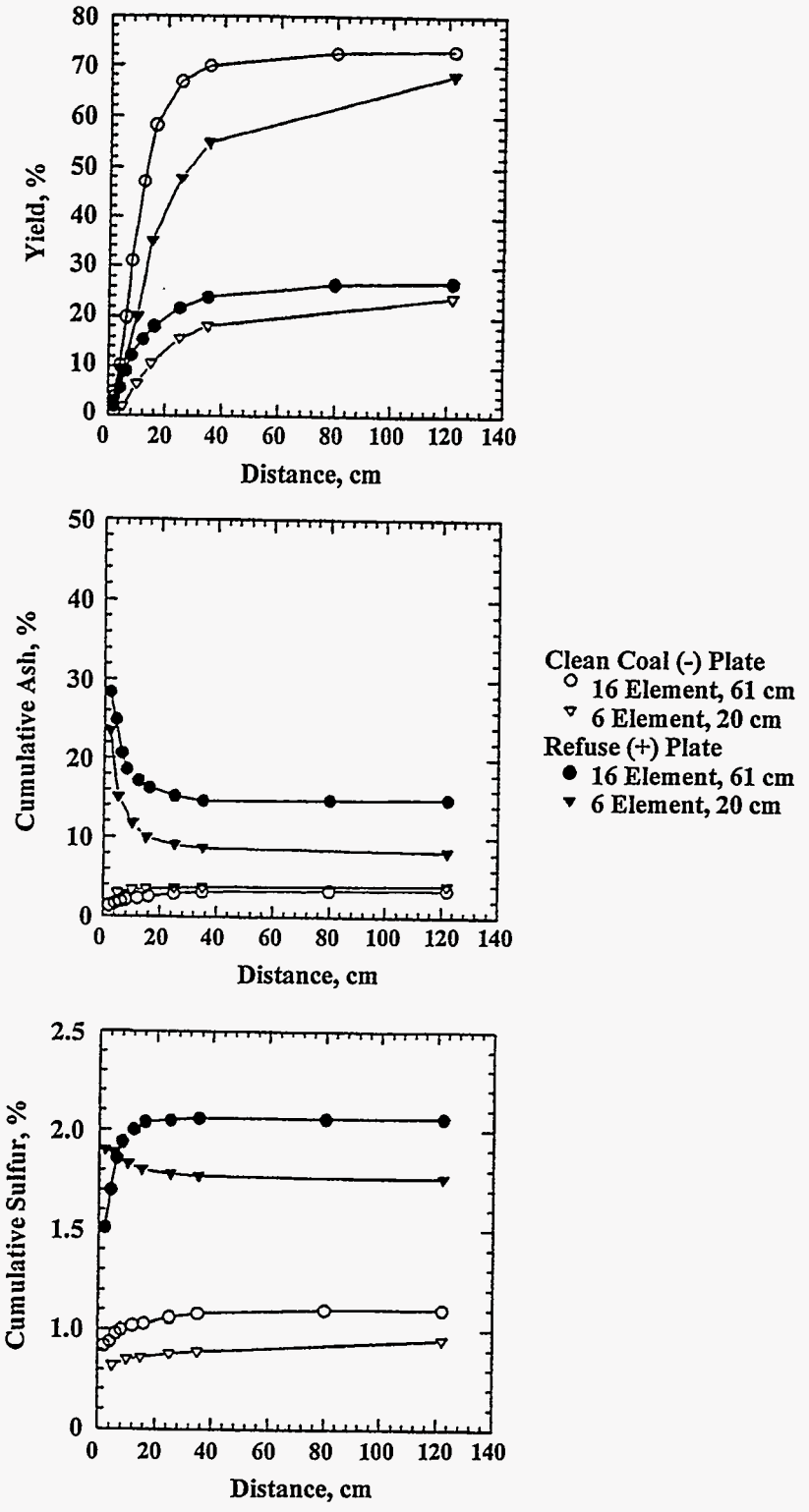

Figure 3-57. TRIBOELECTROSTATIC SEPARATION OF THE PITTSBURGH SEAM COAL (–100 mesh) USING DIFFERENT CHARGER LENGTHS
(nitrogen velocities = 920 cm/s; voltage = ±26 kV; temperature = 24°C; humidity = 26%)

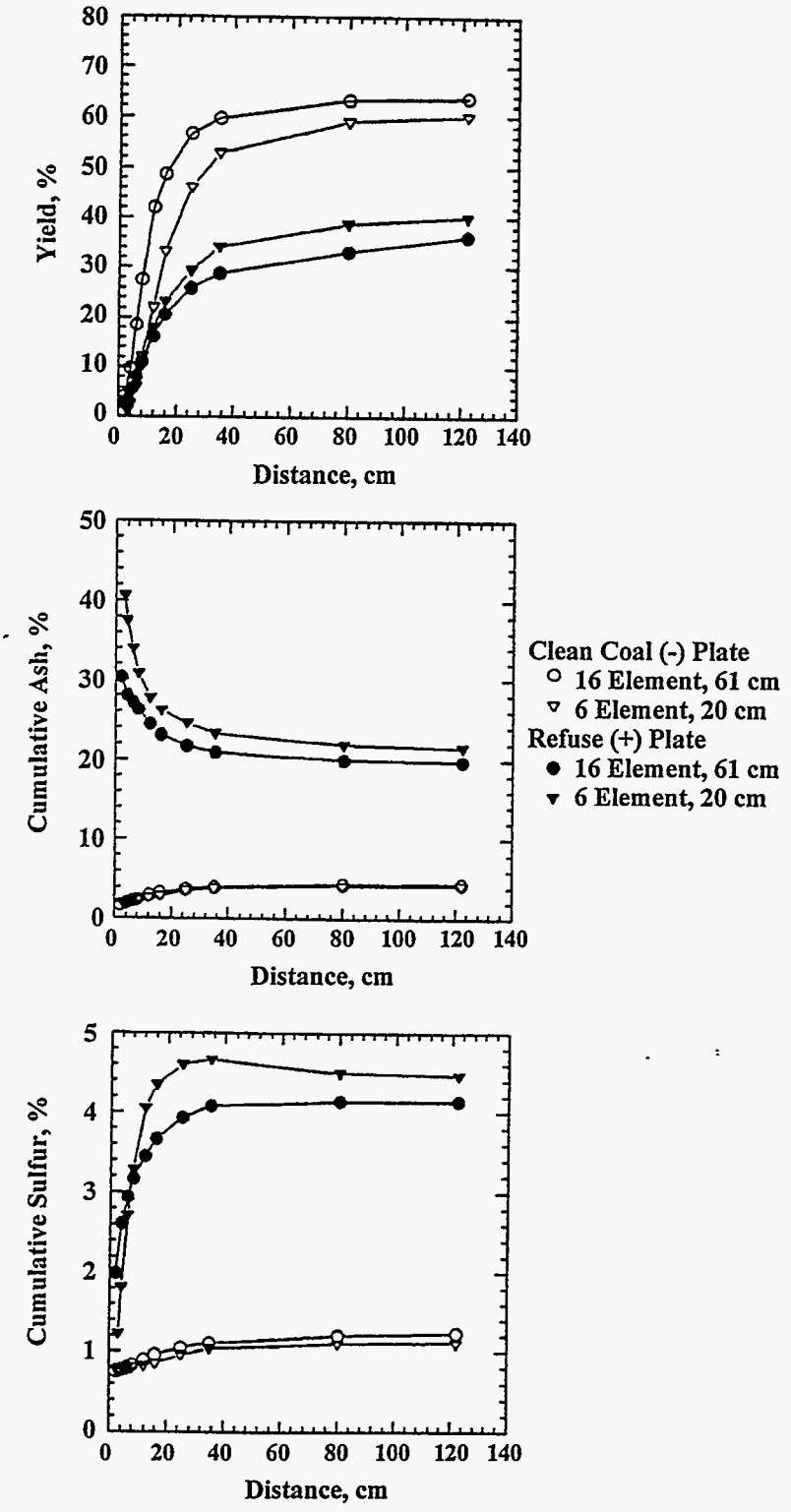

Figure 3-58. TRIBOELECTROSTATIC SEPARATION OF THE UPPER FREEPORT SEAM COAL (–100 mesh) USING DIFFERENT CHARGER LENGTHS (nitrogen velocity = 920 cm/s; voltage = ±26 kV; temperature = 23°C; humidity = 20%)

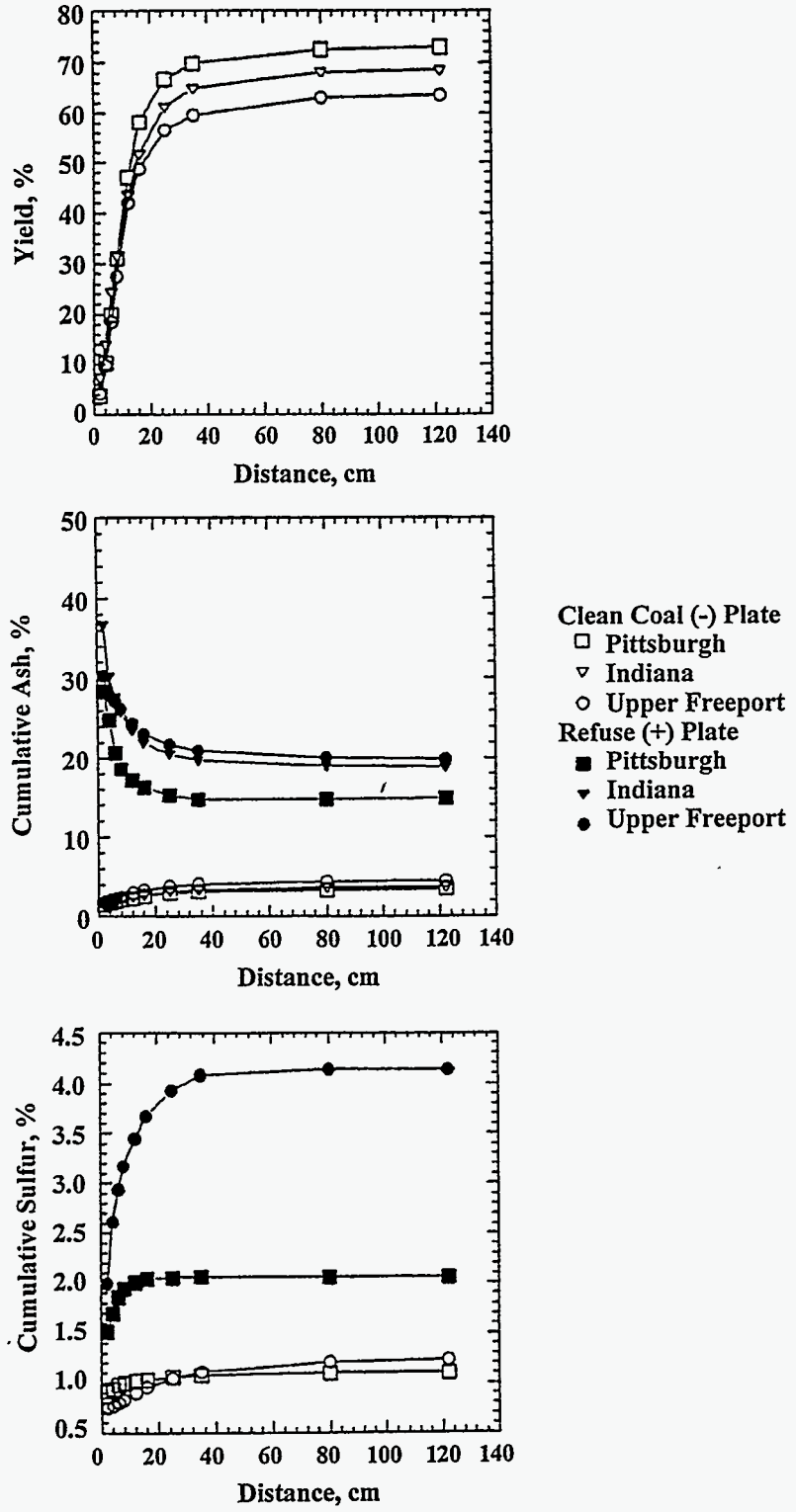

Figure 3-59. TRIBOELECTROSTATIC SEPARATION OF THE UPPER FREEPORT, PITTSBURGH, AND INDIANA VII SEAM COALS (coal feed size = -100 mesh; nitrogen velocity = 920 cm/s; voltage = ±26 kV; temperature = 23°C; humidity = 24%)

from the assumption that the particles are of very different size, such that small particles fill the "gaps" between the large particles. This leads to difficulties when introducing a "correction" factor to account for volume changes and in the transition to a smooth distribution.

Theory

Unlike the Furnas model, a distribution of particles where the successive size difference is small is used and it is assumed that there is a mixture of m spherical particles with sizes

$$D_L = D_1 > D_2 > \ldots > D_m = D_S \tag{3-37}$$

It is also assumed that the ratio

$$t = \frac{D_{i+1}}{D_i} = \text{constant} \tag{3-38}$$

for all i, so

$$t = \left(D_S/D_L\right)^{1/(m-1)} \tag{3-39}$$

The size distribution of balls that ensures optimal packing is to be determined.

Following the Furnas' treatment, a volume V is taken and filled with large spheres. Their volume fraction is:

$$f_1 = \phi_m \tag{3-40}$$

and the volume fraction of voids is

$$V_1 = 1-\phi_m \tag{3-41}$$

Now some spheres of diameter D_2 are added and it is assumed that the packing is changed in such a way that the total volume is unchanged (this assumption will be modified below). Suppose this is accomplished and the maximal volume of spheres of diameter D_2 is f_2V. The resulting fraction of voids is $V_2<V_1$. Then spheres of diameter D_3 are added, and so on.

After the i-th step, the fraction of voids is V_i. How many spheres of diameter D_{i+1} can be added at the (i+1)th step? If $t=\frac{D_{i+1}}{D_i}$ is small, spheres whose total volume, $f_{i+1} = \phi_m V_i$, can be added (because maximal packing is maintained) and the fraction of voids after (i+1)th step is $V_{i+1} = V_i (1-\phi_m)$. If, however, $t=\frac{D_{i+1}}{D_i}=1$, no additional spheres can be added because there is close

packing at each step! (So, in this case, $f_{i+1} = 0$, $V_{i+1} = V_i$.) In the intermediate case

$$f_{i+1} = s\phi_m V_i \tag{3-42}$$

$$V_{i+1} = V_i (1-s\phi_m) \tag{3-43}$$

$$f_1 = \phi_m;\ V_1 = (1-\phi_m) \tag{3-44}$$

where s is a "correction factor" that allows for volume change, analogous to the factor y in the Furnas theory.

In analogy to Furnas' treatment, the assumption was made that the factor s depends only on t , and does not depend on m. Then for the function s:

$$s(t) = \begin{cases} 1, t = 0 \\ 0, t = 1 \end{cases} \tag{3-45}$$

For t close to 1

$$s(t) = \alpha(1-t) \tag{3-46}$$

where it is assumed that α is a universal constant which does not depend on the size distribution.

The total volume fraction of voids is then:

$$V_m = (1-\phi_m) [1-\phi_m s(t)]^{m-1} \tag{3-47}$$

and the volume fraction occupied by the balls of diameter D_i is

$$f_i = s(t) \phi_m (1-\phi_m) [1-\phi_m s(t)]^{i-1} \tag{3-48}$$

The total volume fraction of spheres is given by

$$1-V_m = 1-(1-\phi_m) [1-\phi_m s(t)]^{m-1} \tag{3-49}$$

and it is possible to determine the cumulative distribution function, F_i, given by

$$dF_i = \frac{f_i}{\sum_{i=1}^{m} f_i} \tag{3-50}$$

and

$$dF_i = \frac{s(t)\,\phi_m(1-\phi_m)[1-\phi_m\,s(t)]^{i-1}}{1-(1-\phi_m)[1-\phi_m\,s(t)]^{m-1}} \tag{3-51}$$

The formula for the radii must be added:

$$D_i = D_L t^{i-1} = D_L K^{-(i-1)/(m-1)} \tag{3-52}$$

where $K = D_L/D_S$ is the width of the distribution.

Suppose now that m>>1. It must be assumed that m>>5 ~ 10 for most broad distributions. Then

$$t = K^{-\frac{1}{m-1}} = \exp\left(-\frac{\ln K}{m-1}\right) \approx 1-\frac{\ln K}{m-1} \tag{3-53}$$

and

$$s(t) \cong \frac{d}{m-1} \ln K \tag{3-54}$$

Using the limit $\lim_{m\to\infty}\left(1+\frac{1}{m}\right)^m = e$, the volume fraction of voids is given by

$$V_m = \frac{1-\phi_m}{K^{\alpha\phi_m}} \tag{3-55}$$

and the cumulative distribution function is determined by the equation

$$\frac{dF}{dD} = \frac{1}{D_L} \frac{\alpha\phi_m(1-\phi_m)}{(1-(1-\phi_m)K^{-\alpha\phi_m})} \left(\frac{D}{D_L}\right)^{K\phi_m-1} \tag{3-56}$$

Integrating this equation and using the boundary conditions

$$\lim_{D\to D_S-0} F(D) = 0 \tag{3-57a}$$

$$\lim_{D\to D_L+0} F(D) = 1 \tag{3-57b}$$

gives:

$$F_D = \begin{cases} 0, D < D_s \\ \dfrac{1-\phi_m}{K^r - 1 + \phi_m}\left[\left(\dfrac{D}{D_s}\right)^r - 1\right], D_S < D < D_L \\ 1, D > D_L \end{cases} \tag{3-58}$$

Analysis and Extension of the Model

The next step is to evaluate the constant r in Equation 3-58. A more thorough analysis reveals that the function s(t) coincides with the Furnas' function y ($K^{1/n}$). Unfortunately, Furnas was interested only in the limit t→0 while this analysis is interested in the limit t →1. (To reiterate, Furnas started with particles that have a large difference in radii, this study starts from small differences). Accordingly, his data considers only regions of small t. Strangely enough, during the 60 years since Furnas proposed his model, nobody appears to have reported comprehensive experiments in this area. For now, extrapolations of Furnas' data are used. A rough estimate gives

$\alpha \approx 0.3$, so that $r \approx 0.18 \sim 0.19$ (3-59)

The most interesting feature of the distribution described by Equation 3-58 is that it has a discontinuity at $D \to D_L$. This can be formally incorporated into the model in the following manner.

$$\lim_{D\to D_L-0} F(D) = \frac{(1-\phi_m)(K^r-1)}{K^r-1+\phi_m} \tag{3-60}$$

$$\lim_{D\to D_L+0} F(D) = 1 \tag{3-61}$$

There is a difference between these two limits, equal to

$$1-\frac{(1-\phi_m)(K^r-1)}{K^r-1+\phi_m} = \frac{K^r\phi_m}{K^r-1+\phi_m} \tag{3-62}$$

Therefore, the cumulative distribution function has the structure shown in Figure 3-60. To understand what this means, consider the differential size distribution,

$$f = dF/dD \tag{3-63}$$

where the volume fraction of balls with diameters between D and D+ dD is f(D)dD. Substituting from Equation 3-63, gives

$$f(D) = \frac{r(1-\phi_m)}{(K^r-1+\phi_m)D_L}\left(\frac{D}{D_s}\right)^{r-1} + \frac{K^r(1-\phi_m)}{K^r-1+\phi_m}\delta(D-D_L) \tag{3-64}$$

The distribution has two terms: a continuous distribution and a step function or δ-like peak. (See Figure 3-61)

The meaning of this peak is simple. The starting point was the volume filled by the balls of diameter D_L. This gives the δ - like initial distribution. By adding other balls, a continuous spectrum is introduced into the distribution, but the initially placed big balls remain, hence the calculated peak remains.

This result can also be obtained by starting from the "other end". The space could first be filled with small balls (of diameter D_S) followed by the gradual addition of balls of greater and greater radius. The final differential distribution will have the form shown on Figure 3-62.

$$f(D) = \frac{\phi_m K^r}{K^r-1+\phi_m}\delta(D-D_s) + \frac{r(1-\phi_m)}{(K^r-1+\phi_m)D_S}\left(\frac{D}{D_S}\right)^{r-1} \tag{3-65}$$

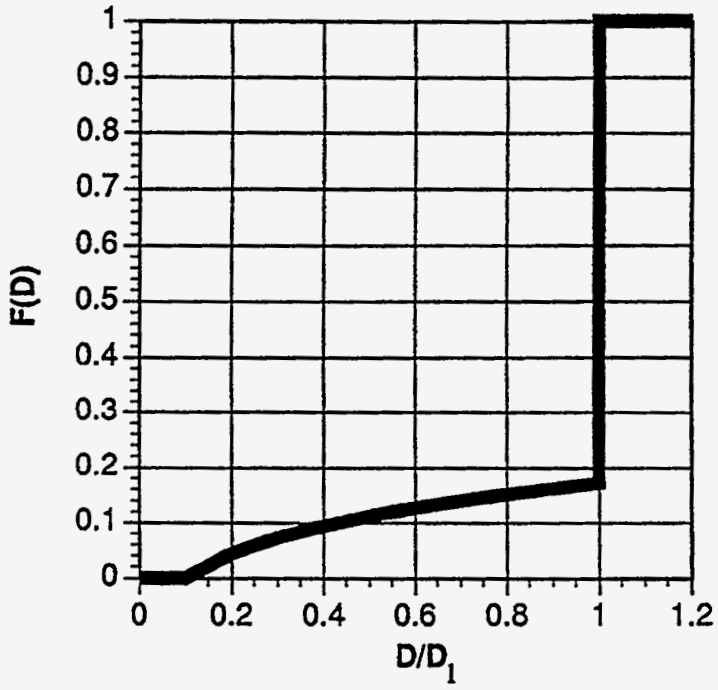

Figure 3-60. CUMULATIVE DISTRIBUTION FUNCTION FROM EQUATION 3-58, K = 10

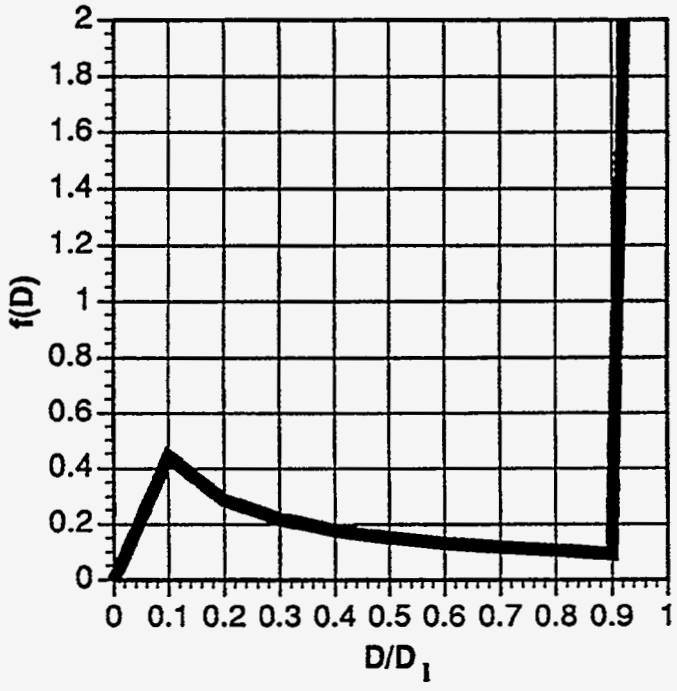

Figure 3-61. DIFFERENTIAL DISTRIBUTION FUNCTION FROM EQUATION 3-64 K = 10

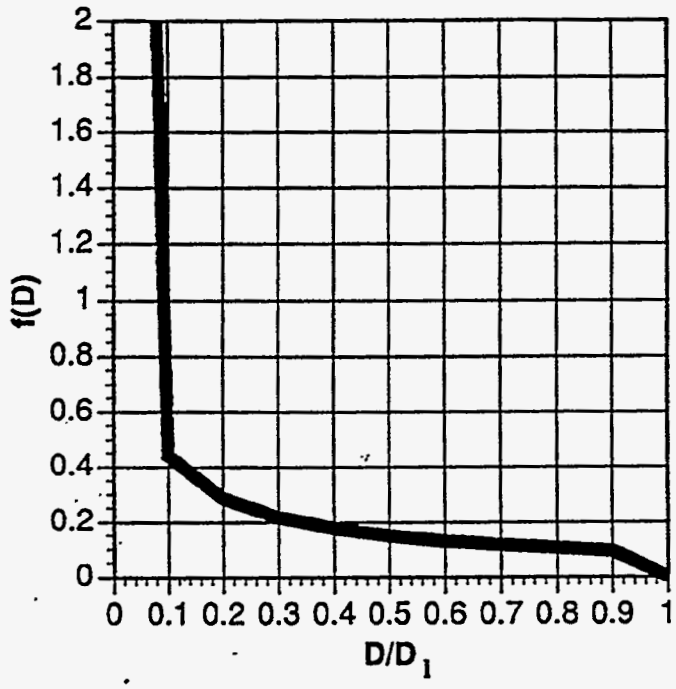

Figure 3-62. DIFFERENTIAL DISTRIBUTION FUNCTION FROM EQUATION 3-65, K = 10

with a peak at D_S. The cumulative distribution in this case will be:

$$F_D = \begin{cases} 0, D < D_S \\ \dfrac{1-\phi_m}{K^r - 1 + \phi_m}\left[\left(\dfrac{D}{D_S}\right)^r - 1\right] + \dfrac{\phi_m K^r}{K^r - 1 + \phi_m}, D_S < D < D_L \\ 1, D > D_L \end{cases} \quad (3\text{-}66)$$

So optimal packing can be approached in the following way: first the space is filled by either the smallest or biggest balls. Then the voids are filled with the continuously distributed balls. In both cases the continuous distribution and final fraction of voids are the same.

Now take some balls obeying the distribution described by Equation 3-58 and some balls obeying the distribution described by Equation 3-65 and mix them. The fraction of voids in both distributions is the same: $(1-\phi_m)K^{-r}$, so the fraction of voids in the mixture cannot be larger than this. It will probably not be less, although this is more difficult to prove. The following distribution is obtained:

$$F = \begin{cases} 0, D < D_S \\ \dfrac{1-\phi_m}{K^r - 1 + \phi_m}\left[\left(\dfrac{D}{Ds}\right)^r - 1\right] + \dfrac{\alpha\phi_m K^r}{K^r - 1 + \phi_m}, D_S < D < D_L \\ 1, D > D_L \end{cases} \quad (3\text{-}67)$$

where

$$0 \le \alpha \le 1 \quad (3\text{-}68)$$

Here α is an arbitrary constant. This distribution has the following characteristics, first there are big and small balls only, and the ratio of their volume fractions is $(1-\alpha):\alpha$. Then intermediate balls are added up to the value determined by Equation 3-67. The differential size distribution is

$$f(D) = \frac{\alpha\phi_m K^r}{K^r - 1 + \phi_m}\delta(D - D_S) + \frac{(1-\alpha)K^r(\phi_m)}{K^r - 1 + \phi_m}\delta(D - D_L) + \frac{r(1-\phi_m)}{(K^r - 1 + \phi_m)D_S}\left(\frac{D}{D_S}\right)^{r-1} \quad (3\text{-}69)$$

This distribution has two peaks, at D_S and D_L, with a peak height ratio α:(1-α) and an intermediate power-law curve linking them, as shown in Figure 3-63.

Limiting Cases

Consider some limiting cases of the distribution. The distribution depends only on the parameter $K = D_L/D_S$, so the limiting cases $K\to\infty$ and $K\to 1$ must be discussed.

a) $K\to 1$. In this case there is only one size of balls $D_S = D_L$.

Therefore:

$$F(D) = \begin{cases} 0, D < D_L \\ 1, D > D_L \end{cases} \tag{3-70}$$

The fraction of voids is:

$$\frac{(1-\phi_m)}{K^r} = 1-\phi_m \tag{3-71}$$

This is reasonable; this is the mono-disperse close-packing limit.

b) $K\to\infty$. In this case

$$F = \begin{cases} 0, D < D_s \\ \alpha\phi_m + (1-\phi_m)\left(\frac{D}{D_L}\right)^r, D_s < D < D_L \\ 1, D > D_L \end{cases} \tag{3-72}$$

The fraction of voids is

$$\frac{1-\phi_m}{K^r} = 0 \tag{3-73}$$

This means that there is a sufficiently broad particle size distribution, all available space can be filled with balls. The power-law continuous distribution does not depend on D_s only on D_L.

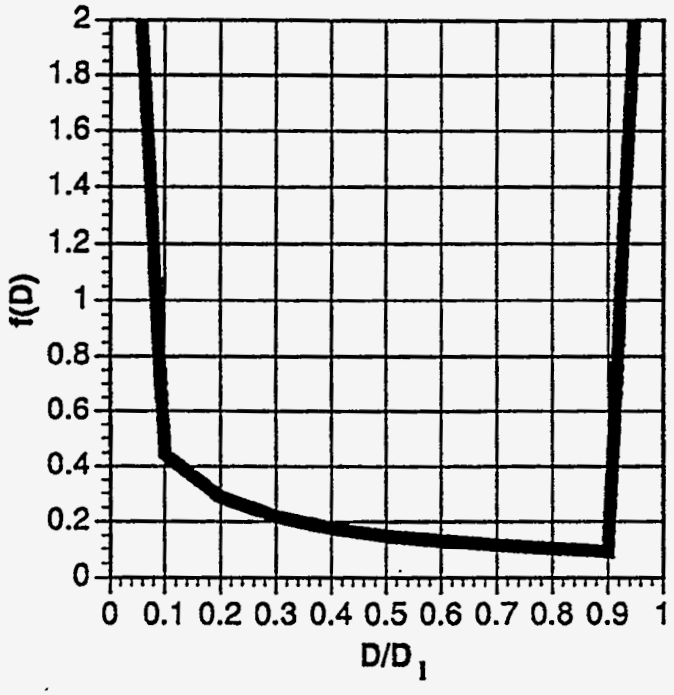

Figure 3-63. DIFFERENTIAL DISTRIBUTION FUNCTION FROM EQUATION 3-69
K = 10, α = 0.5

Accordingly, this theory predicts that if the particles that are sufficiently small, all the space can be filled and the distribution is not sensitive to the cut-off size (size of the smallest particle). This too seems to be intuitively reasonable.

3.3 Preparation of DMC and MCWM for the Combustion Performance Evaluation

The preparation of DMC and MCWM included pilot-scale and demonstration-scale activities. Pilot-scale activities include the cleaning of the coal feedstock to targeted coal specifications and the preparation of DMC and a stable, low viscosity MCWM from the cleaned coal feedstock which were tested in the research boiler (see Section 4.3 for combustion results). Demonstration-scale activities focused on producing DMC and MCWM from a cleaned coal feedstock for testing in Penn State's demonstration boiler (see Section 4.4 for combustion results).

Four coals were examined in the pilot-scale activities. They include the Taggart, Upper Freeport, Lower Kittanning, and Indiana VII seam coals. Of these, DMC was prepared from two of the coals while MCWM was prepared from all four. DMC was not prepared from Lower Kittanning and Indiana VII seam coals because they were cleaned using wet techniques and commercially they would not be dried for a DMC application; therefore, they were not tested as DMCs. In the demonstration-scale activities, the Upper Freeport seam coal was utilized.

3.3.1 Pilot-Scale Activities

MCWM Preparation

The targeted coal and MCWM specifications are presented in Table 3-15. The methodology by which the various coals were cleaned and prepared into a MCWM was coal specific and will be discussed on an individual basis. Despite the differences in the coal's physical properties (e.g., particle size) the methodology by which the slurryability of the coal is determined is similar. A systematic approach was undertaken for each of the four coals to determine how particle size, solids loading, slurry pH, and concentration of chemical additives (e.g., viscosity, pH, and stability modifiers) affected the rheology and stability of the MCWM. This approach is often referred to as the MCWM formulation methodology. A brief summary of the MCWM formulation for each of the four coals is summarized below.

Upper Freeport Seam Coal

The Upper Freeport seam coal was procured from Rawlee Fuels of Indiana, Pennsylvania. The coal was transported to a commercial coal cleaning facility located near Osceola Mills, Pennsylvania which is owned and operated by Power Operating Company, Inc.. The Upper Freeport seam coal was cleaned using heavy media cyclones operating at a media gravity of 1.30. The cleaned 1.5" x 0 Upper Freeport seam coal stockpile was sampled by taking approximately two fifty-gallon barrels of coal around the perimeter of the coal stockpile, and from the top, middle, and toe sections of the stockpile. The material was crushed and sample splits taken for chemical analysis and the MCWM formulation. A typical analysis of the cleaned Upper Freeport

Table 3-15. Targeted Coal and MCWM Specifications

Parameter	Targeted Specification
Coal Feedstock	
Total Sulfur	< 1.0 wt.% (d.b.)
Ash	< 5.0 wt.% (d.b.)
Volatile Matter	Maximize, > 30 wt.%
Micronized Coal-Water Mixture	
Coal Particle Size (Top Size)	100 wt.% passing 200 μm (~ 65 mesh)
Coal Particle Size Distribution	Broad, optimize using Farris-Furnas Equation
Apparent Viscosity	< 500 cp. at 100 sec^{-1} at 25° C
MCWM Flow Behavior	Yield psuedoplastic
Solids Loading	Maximize to targeted viscosity, < 50 wt. %)
Stability / Sedimentation Type	Maximize stability without the use of a stabilizer / softpack sedimentation

seam coal is presented in Table 3-16.

The coal was further reduced in size to a nominal top size of minus 1/8". Approximately 2.1 kg of coal was wet milled at a 68 wt.% solids loading in a 12" diameter by 12" long ball mill to determine the effect of grinding time on particle size. The coal, water, and chemical additives were mixed and introduced to the batch ball mill prior to grinding. Milling was performed in a batch mode at 65% of the critical speed. Hardened chrome alloy steel grinding media constituted approximately 35% of the mill volume and was comprised of 51 wt.% 1.5" balls and 49 wt.% 1.0" balls. The dispersant used in the pilot and demonstration-scale MCWM productions was an ammonia based sulfonated naphthalene condensate marketed under the trade name A-23-M by the Henkel Corporation. The dispersant concentration was adjusted to allow the MCWM to gravity discharge from the ball mill. In addition, ammonium hydroxide was used as a pH modifier in order to increase the slurry pH to 8.5 to 9.5. Solids loading was measured using a CEM AVC-80 microwave moisture analyzer. Particle size was measured using a Malvern 2600 Droplet and Particle Size Analyzer. Figure 3-64 illustrates the variation in particle size with grind time when the Upper Freeport seam coal was milled at approximately 68 wt.% solids, 0.6 wt.% dispersant, and slurry pH of approximately 9. To determine if the particle size distribution of the coal was near that required for optimum packing density, the particle size distributions were plotted against the calculated theoretical particle size distribution[64, 65] using the following mathematical expression:

$$CPP = (100)\,(D^n - Ds^n)/(Dl^n - Ds^n) \qquad (3\text{-}74)$$

where:

CPP = Cumulative weight percent of particles smaller than a given size
D = Particle diameter
Dl = Largest diameter coal particle
Ds = Smallest diameter coal particle
n = Distribution modulus (0.19 to 0.25)

The particle size distribution for the 30, 45, 60, 75, and 90 minute grinds were compared to the calculated theoretical particle size distribution needed to achieve optimum packing density. Figure 3-65 illustrates the "measured" vs. "calculated" particle size distribution for the 75 minute test grind. The 75 minute grind was used in the formulation work because it produced a top size less than the 100% passing 200 μm target specification while most closely approximating the theoretical particle size distribution.

The effect of slurry pH on the apparent viscosity was examined, after the determination of the grind time, to determine if additional reductions in apparent viscosity could be realized if slurry pH was modified. The slurry pH was varied from approximately 6.5 to 9.0. Slurry pH was measured using an Orion Model 420 pH meter. Apparent viscosity was measured using a using a

Table 3-16. Typical Analysis of the Cleaned Upper Freeport Seam Coal

Parameter		Wt.% (dry basis)
Particle Size		1.5" x 0
Coal Cleaning Methodology		Heavy Media Cyclone
Proximate Analysis		
	Volatile Matter	31.7
	Fixed Carbon	61.7
	Ash	6.6
Ultimate Analysis		
	Carbon	79.5
	Hydrogen	5.2
	Nitrogen	1.3
	Sulfur	0.5
	Oxygen	6.9
Higher Heating Value (Btu/lb)		14,062
Hardgrove Grindability Index		58.0
Alkali Extraction		94.3
Free Swelling Index		6.5
Equilibrium Moisture		3.37

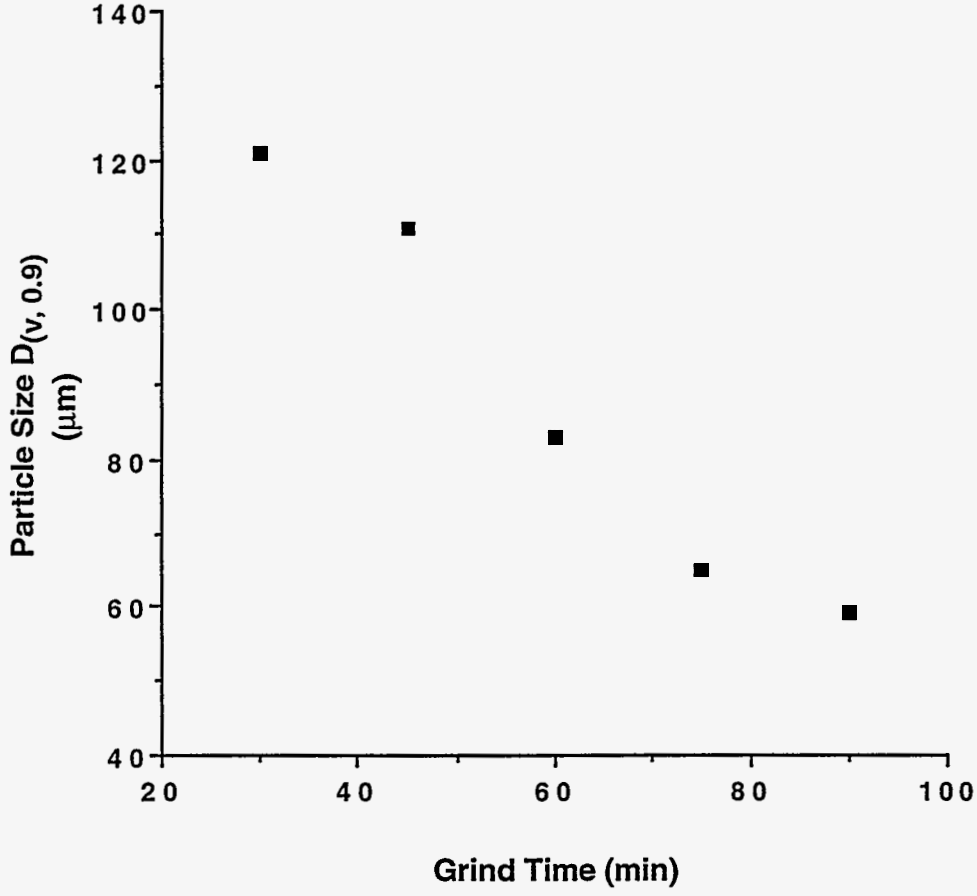

Figure 3-64. EFFECT OF GRINDING TIME ON PARTICLE SIZE FOR THE UPPER FREEPORT SEAM COAL

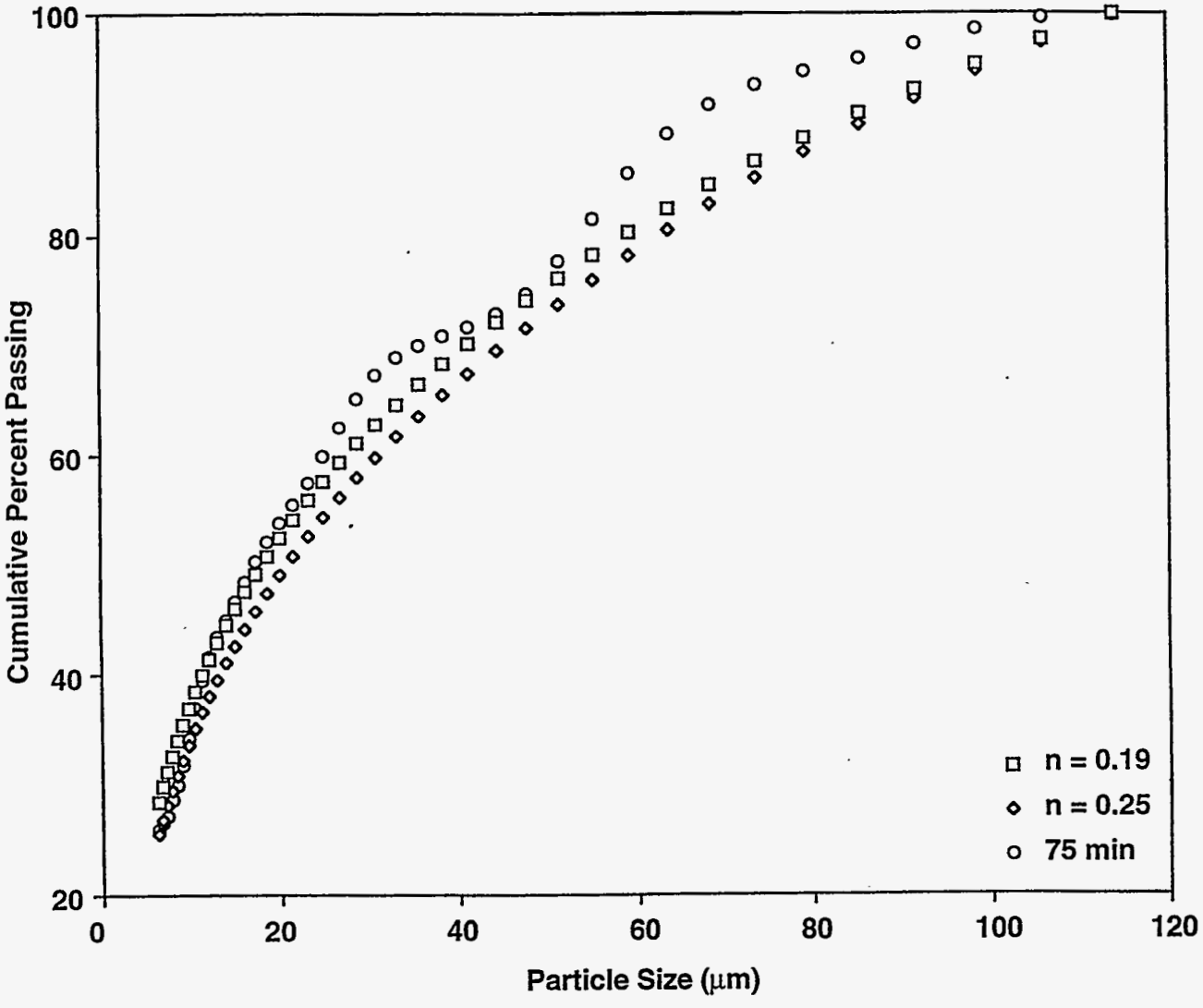

Figure 3-65. FARRIS-FURNAS DISTRIBUTION FOR A 75 MINUTE GRIND TIME FOR UPPER FREEPORT SEAM MCWM

Bohlin Visco-88 rotational viscometer. Figure 3-66 illustrates the effect of slurry pH on apparent viscosity. A marked decrease in apparent viscosity occurred as slurry pH increased.

The effect of dispersant level on the MCWM's apparent viscosity was determined by varying dispersant concentration from 0.6 to 1.2 wt.% (wt.% active solids, dry coal basis) while holding the solids loading at approximately 60 wt.%. Figure 3-67 illustrates the effect of dispersant concentration on apparent viscosity. A dramatic decrease in apparent viscosity can be clearly identified between the 0.6 to 0.7 wt.% dispersant levels. At a dispersant level greater than approximately 0.8 wt.%, there was little benefit of adding additional dispersant and would most likely over-disperse the MCWM eventually leading to the formation of "hardpack".

The effect of solids loading on the MCWM's apparent viscosity was determined by varying solids loading from approximately 59 to 66 wt.%. Dispersant concentration was held constant at 0.7 wt.%. Figure 3-68 illustrates the sudden increase in apparent viscosity when the solids loading exceeds approximately 63 to 64 wt.%.

The effect of stabilizer on the MCWM's apparent viscosity was determined by varying stabilizer concentration from 0 to 1,000 ppm (active solids, dry coal basis). The stabilizer used in the formulation and pilot-scale productions was a xanthan gum marketed under the trade name Flocon 4800C by the Pfizer Chemical Division. Dispersant concentration was held constant at 0.7 wt.% and solids loading was approximately 61 wt.%. The effect of stabilizer concentration on apparent viscosity is illustrated in Figure 3-69. Apparent viscosity increased as stabilizer concentration increased.

Based on the pilot-scale MCWM formulation data, the following criteria were targeted in the demonstration-scale MCWM production for the Upper Freeport seam coal:

Solids Loading: 62 wt.%
Slurry pH: 9.0 to 9.5
Dispersant Concentration: 0.7 wt.%
Stabilizer Concentration: 400 ppm

Barrel quantities of Upper Freeport seam MCWM were provided for pilot-scale atomization and combustion performance testing by taking several fifty-five gallon drums of MCWM from the process mix tanks at the demonstration-scale MCWM production facility.

Lower Kittanning Seam Coal

The Lower Kittanning seam coal was collected from Jefferson County, Pennsylvania. The Lower Kittanning seam coal was cleaned using the continuous, two-stage froth flotation circuit shown in Figure 3-70. A froth flotation feedstock was produced by crushing and sizing the parent coal into a 28x400 mesh size fraction. The 28x400 mesh size fraction was then slurried to a solids loading of approximately 25 wt.%. The feed slurry was pumped and stored in a 500 gallon tank which served as the main feed tank to the froth flotation circuit.

The Lower Kittanning seam feed slurry was pumped into a nominal 20 gallon conditioning tank where froth flotation reagents were introduced and slurry solids loading adjusted to

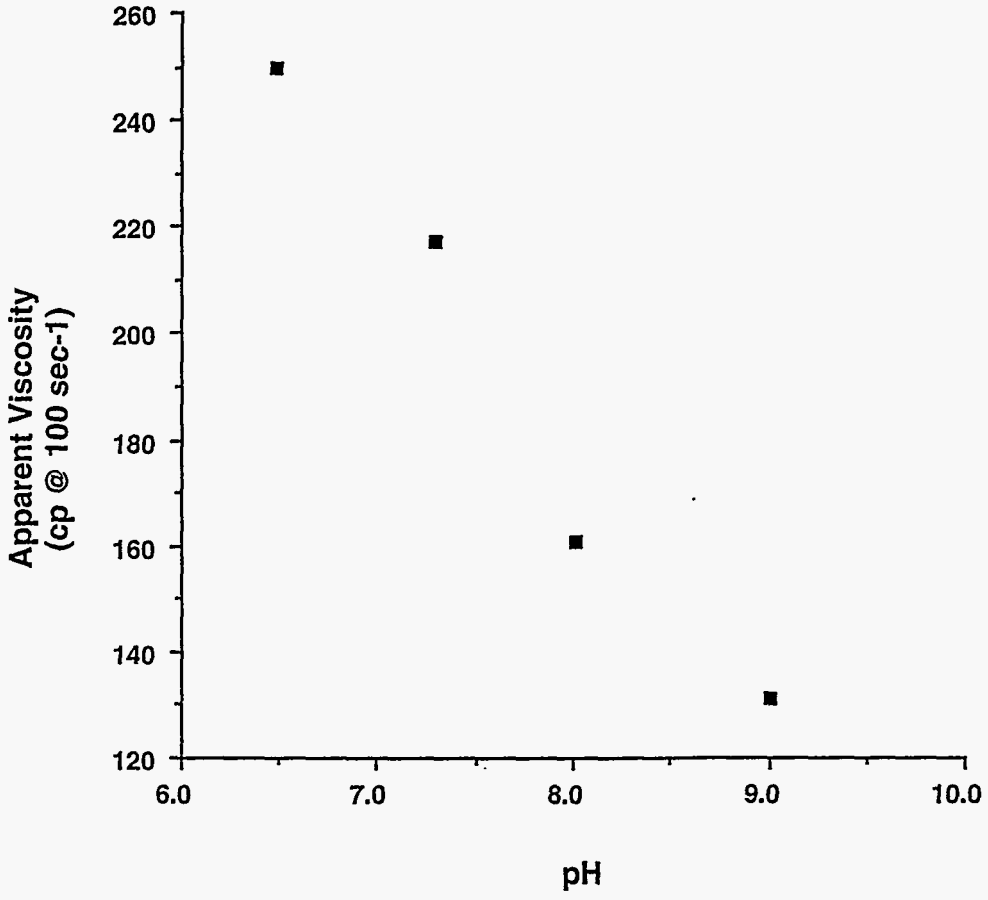

Figure 3-66. EFFECT OF SLURRY pH ON APPARENT VISCOSITY FOR THE UPPER FREEPORT SEAM COAL

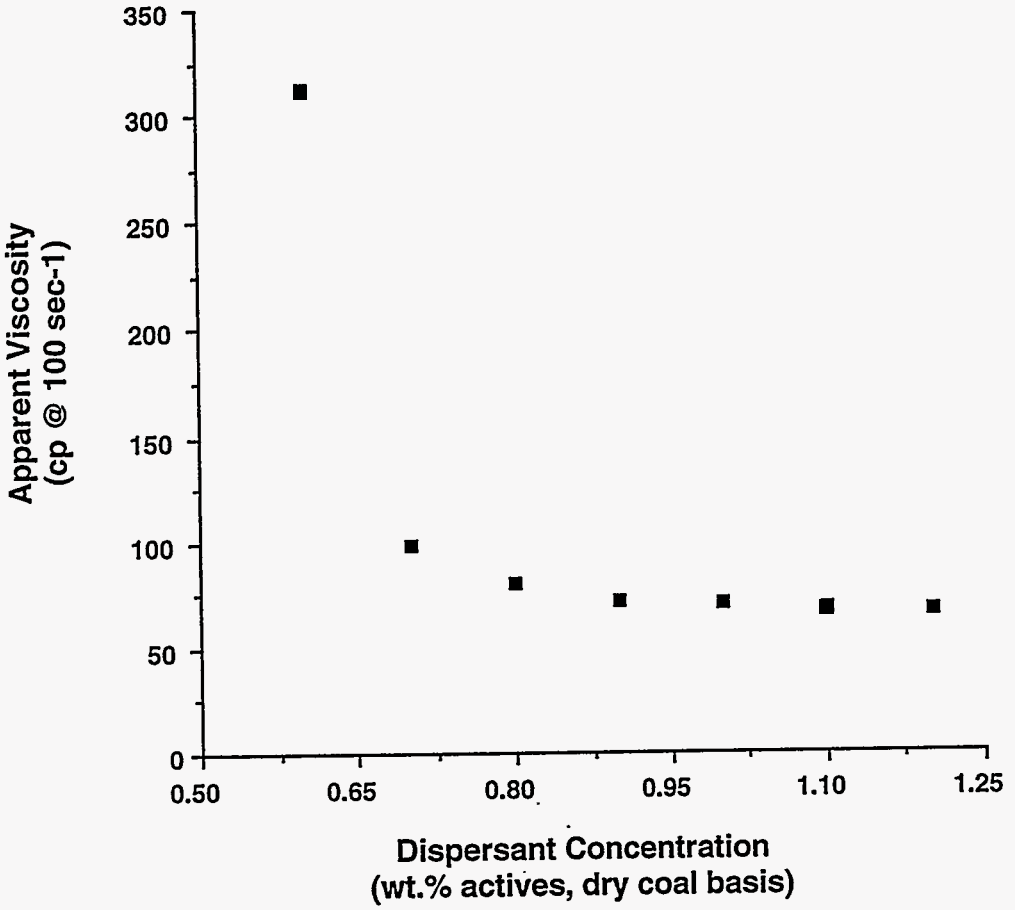

Figure 3-67. EFFECT OF DISPERSANT CONCENTRATION ON APPARENT VISCOSITY FOR THE UPPER FREEPORT SEAM COAL

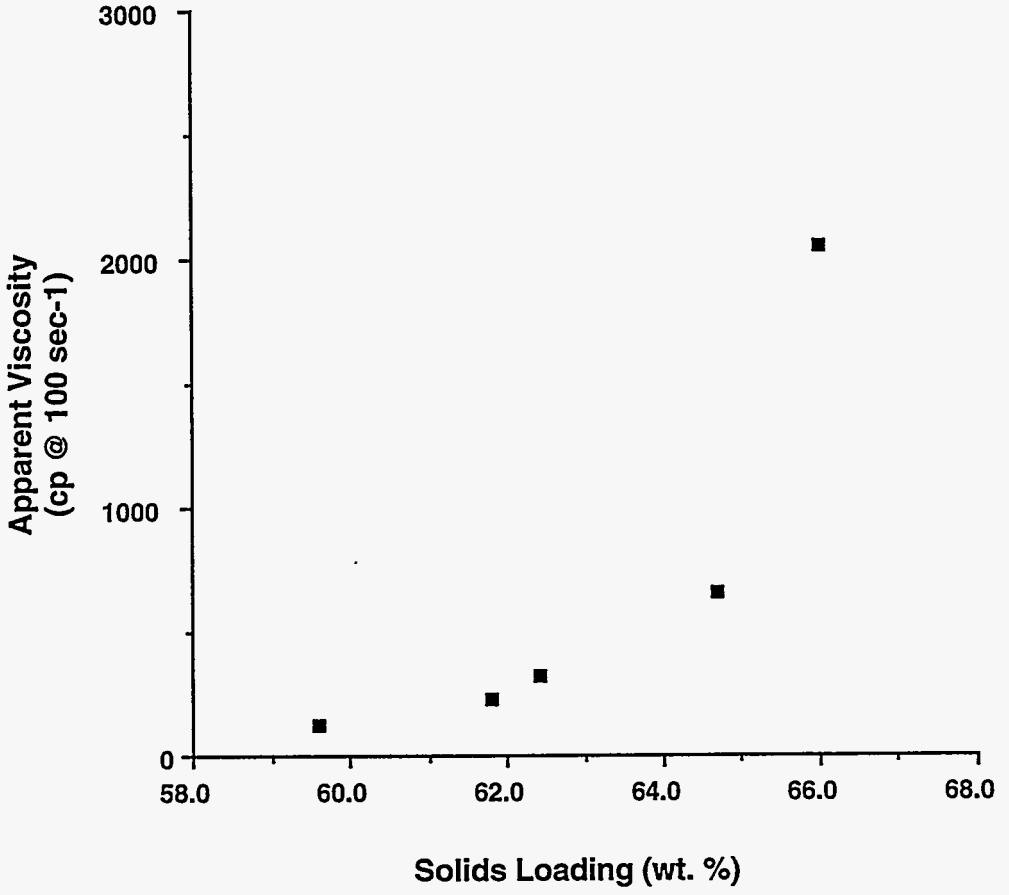

Figure 3-68. EFFECT OF SOLIDS LOADING ON APPARENT VISCOSITY FOR THE UPPER FREEPORT SEAM COAL

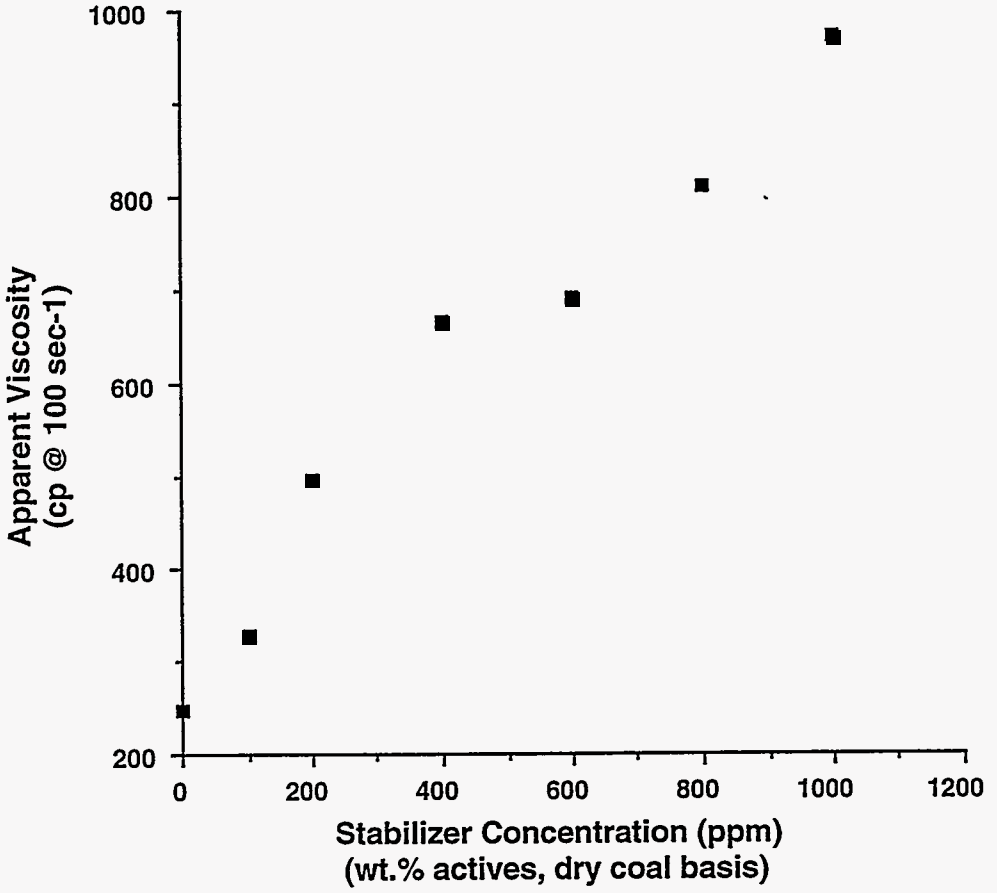

Figure 3-69. EFFECT OF STABILIZER CONCENTRATION ON APPARENT VISCOSITY FOR THE UPPER FREEPORT SEAM COAL

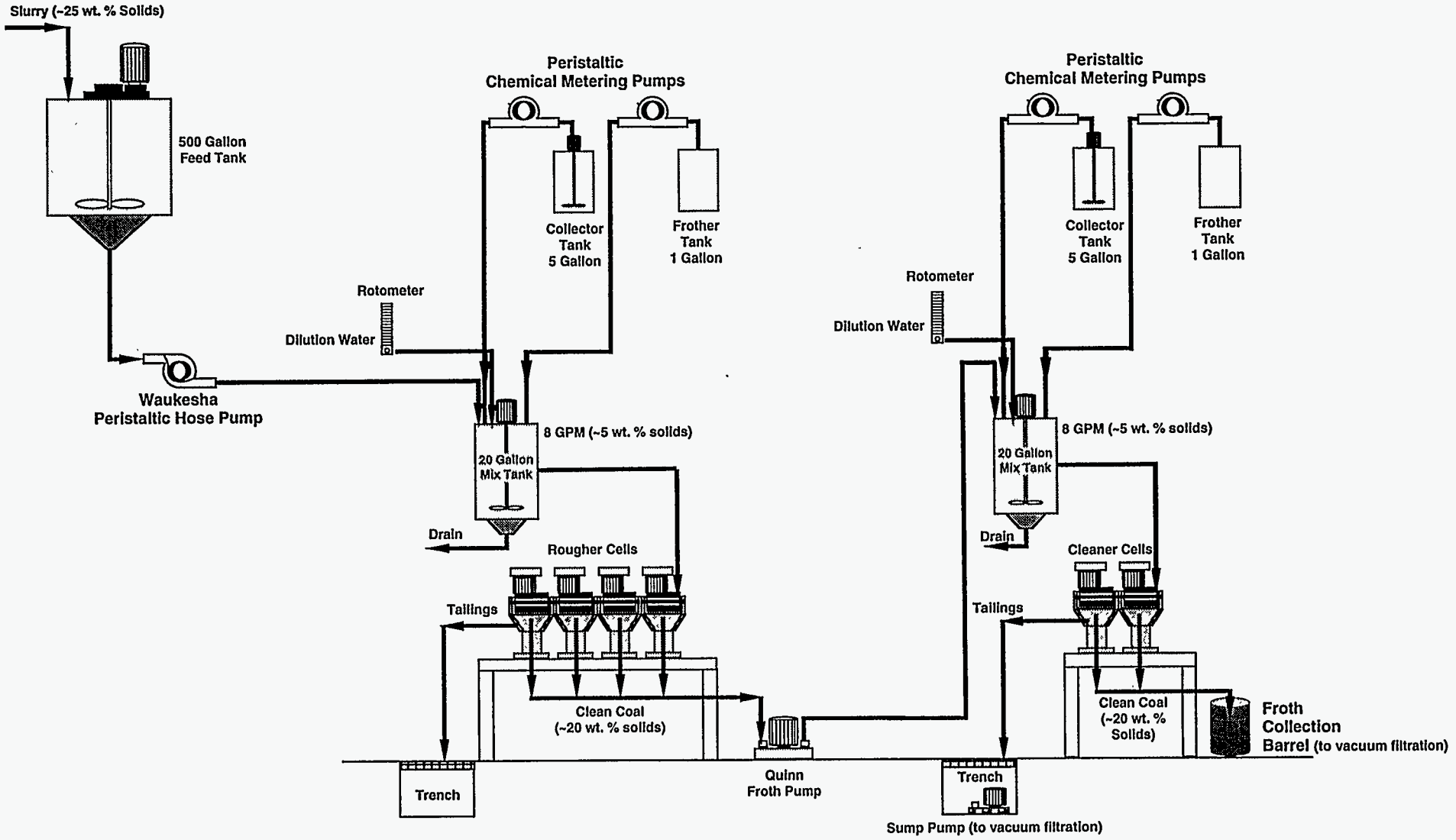

Figure 3-70. DOUBLE STAGE FROTH FLOTATION CIRCUIT

approximately 5 wt.%. MIBC was introduced to the conditioning tank as the frothing reagent at a dosage of 0.3 kg/ton of coal. Dodecane was introduced into the conditioning tank as the collector at a dosage of 0.05 kg/ton of coal. The conditioned slurry exited the conditioning tank through an overflow port at a rate of approximately 8 gpm into a single rougher flotation battery consisting of four Wemco flotation cells. The rougher concentrate then, if needed, underwent additional cleaning in a single cleaner flotation battery consisting of two Wemco flotation cells. The froth from the both the rougher and cleaner cells averaged approximately 20 wt.% solids. The froth was dewatered using a continuous Denver disk filter consisting of two 24 inch disks. After the initial shakedown and optimization of the froth flotation circuit, the cleaner cells were not operated because the targeted cleaned coal specification of < 1.0 wt.% sulfur and < 5.0 wt.% ash could be achieved by only cleaning the coal in the rougher circuit. A typical analysis of the cleaned Lower Kittanning seam coal filter cake is presented in Table 3-17.

Because the particle size of the froth flotation filter cake did not meet the particle size specifications for the MCWM, additional grinding in the 12 inch diameter batch ball mill was required. The MCWM formulation approach for the Lower Kittanning seam coal was identical to that for the Upper Freeport seam coal. Based on the formulation data, the following MCWM formulation was recommended for the Lower Kittanning seam coal:

Solids Loading: 63 wt.%
Slurry pH: 9.0 to 9.5
Dispersant Concentration: 0.8 wt.%
Stabilizer Concentration: 200 ppm

Taggart Seam Coal

The Taggart seam coal was collected from Wise County, Virginia. The as-received Taggart seam coal did not require cleaning to meet the clean coal specifications. A typical analysis of the Taggart seam coal is presented in Table 3-18. The MCWM formulation approach for the Taggart seam coal was identical to that for the Upper Freeport seam coal. Based on the formulation data, the following MCWM criteria were recommended for the Taggart seam coal:

Solids Loading: 61 wt.%
Slurry pH: 9.0 to 9.5
Dispersant Concentration: 0.4 wt.%
Stabilizer Concentration: 200 ppm

Barrel quantities of Taggart seam MCWM were provided for pilot-scale atomization and combustion performance testing by preparing the MCWM in a 2x4' ball mill. A generalized schematic diagram of the 2x4' ball mill MCWM preparation circuit is provided in Figure 3-71. The coal was crushed to minus 1/4" using a hammer mill and manually placed in a nominal 30 gallon stainless steel Acrison feed hopper. The minus 1/4" coal was fed to the 2x4' ball mill at a rate of approximately 125 lb/h. Water, dispersant (A-23M), and pH modifier (NH_4OH) was introduced into the ball mill feed screw as the coal was being fed into the ball mill. The coal was milled at a solids loading of approximately 68 to 72 wt.% while running the mill at 65% critical speed.

Table 3-17. Typical Analysis of the Cleaned Lower Kittanning Seam Coal

Parameter		Wt.% (dry basis)
Particle Size		28 x 400 mesh
Coal Cleaning Methodology		Conventional Froth Flotation
Proximate Analysis		
	Volatile Matter	30.6
	Fixed Carbon	65.8
	Ash	3.6
Ultimate Analysis		
	Carbon	84.5
	Hydrogen	5.2
	Nitrogen	1.6
	Sulfur	0.8
	Oxygen	4.4
Higher Heating Value (Btu/lb)		14,824
Alkali Extraction		91.3
Free Swelling Index		8.5

Table 3-18. Typical Analysis of the Taggart Seam Coal

Parameter		Wt.% (dry basis)
Particle Size		1.5" x 0
Coal Cleaning Methodology		Not Required
Proximate Analysis		
	Volatile Matter	34.5
	Fixed Carbon	61.9
	Ash	3.6
Ultimate Analysis		
	Carbon	84.1
	Hydrogen	5.6
	Nitrogen	1.5
	Sulfur	0.5
	Oxygen	4.7
Higher Heating Value (Btu/lb)		14,879
Hardgrove Grindability Index		55.0
Alkali Extraction		94.3
Free Swelling Index		7.5
Equilibrium Moisture		1.71

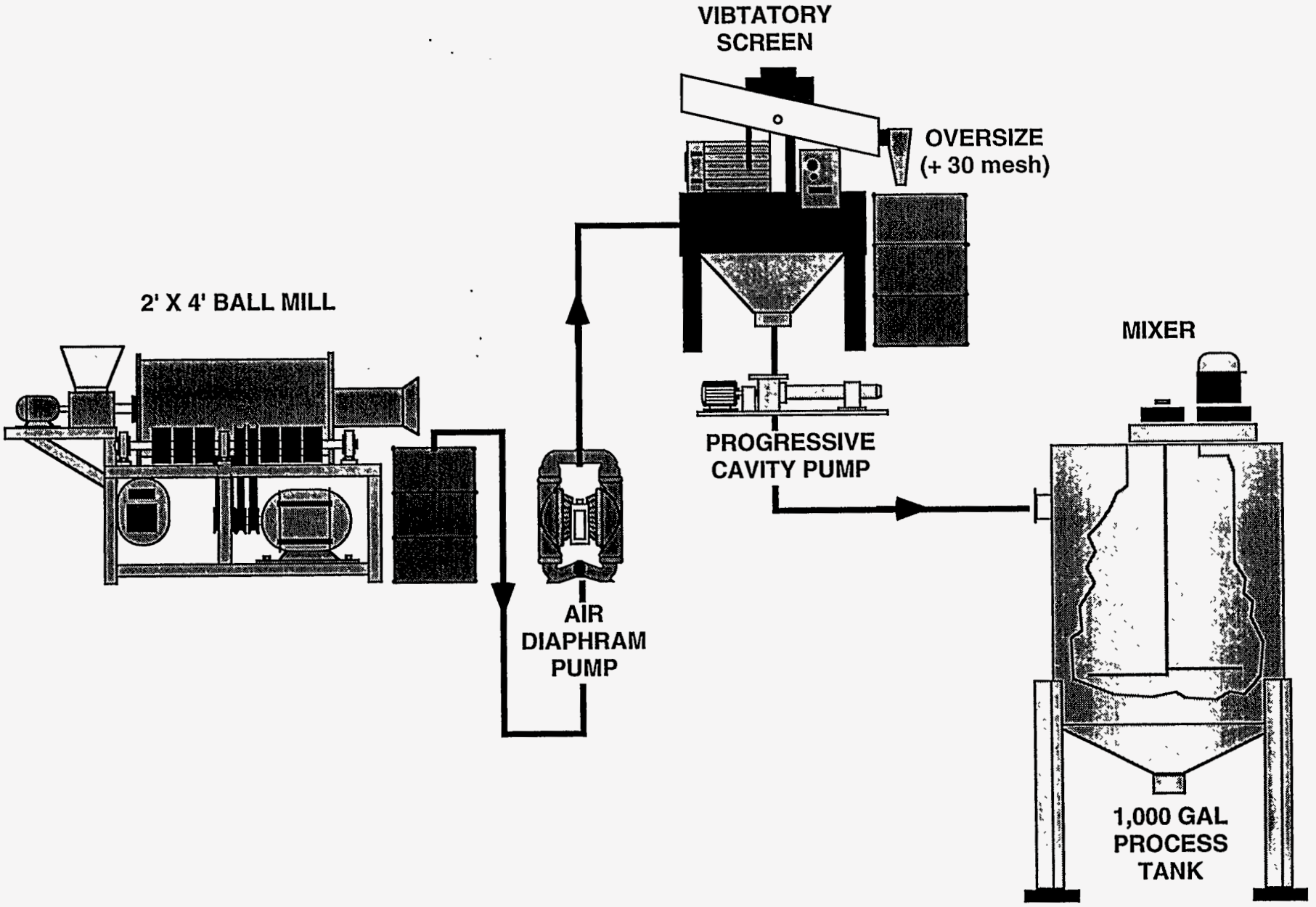

Figure 3-71. SCHEMATIC DIAGRAM OF THE 2 X 4' BALL MILL SYSTEM

Hardened chrome alloy steel grinding media constituted approximately 30% of the mill volume and was comprised of 40 wt.% 2.0", 45 wt.% 1.5", and 15 wt.% 1.0" balls. The MCWM was discharged into a nominal 55 gallon sump and then was screened using a 30 mesh screen to remove oversize particles. The MCWM was then pumped into a baffled 1,000 gallon, stainless steel mixing tank where the stabilizer was added. The MCWM was allowed to mix for approximately 12 to 24 hours.

Indiana VII Seam Coal

The Indiana VII seam coal was collected from Sullivan County, Indiana. A cleaned coal column flotation filter cake was supplied by Amax Research and Development Center. A typical analysis of the Indiana VII seam coal is presented in Table 3-19. Because the particle size of the column flotation filter cake met the MCWM particle size specifications additional grinding was not required. The MCWM formulation approach for the Indiana VII seam coal involved re-entraining the filter cake and then determining the effect of slurry pH, dispersant concentration, solids loading, and stabilizer concentration on the MCWM rheology and stability. Based on the pilot-scale MCWM formulation data, the following criteria were recommended for the Indiana VII seam coal:

Solids Loading: 49 wt.%
Slurry pH: 9.0 to 9.5
Dispersant Concentration: 2.0 wt.%
Stabilizer Concentration: 200 ppm

Barrel quantities of Indiana VII seam MCWM were provided for pilot-scale atomization and combustion performance testing by re-entraining the column flotation filter cake in a nominal 75-gallon ribbon mixer. Dispersant, pH modifier, and dilution water was added while the filter cake was being mixed. Once re-entrainment was achieved, the MCWM was pumped to a baffled 1,000 gallon, stainless steel mixing tank where the stabilizer was added. The MCWM was then allowed to mix for approximately 12 to 24 hours.

DMC Preparation

The DMC was prepared using a two-stage grinding approach. The as-received 2" x 0 coal was crushed using a laboratory-scale hammer mill to a nominal -1/4" product. The -1/4" material was then pulverized using a MikroPuhl Model 10 ACM Mikro-ACM-Pulverizer mill.

3.3.2 Demonstration-Scale Activities

MCWM

Demonstration-scale MCWM activities focused on preparing MCWM in a single-stage, wet grinding circuit. A generalized schematic diagram of this circuit is presented in Figure 3-72. The Upper Freeport seam coal was used in the demonstration as the coal feedstock from which the MCWM was produced. Production of Upper Freeport seam MCWM began on January 30, 1995 and was completed on April 14, 1995 with a total of approximately 210 tons of MCWM produced.

The Upper Freeport seam coal was transported from Power Operating Company Inc.'s coal

Table 3-19. Typical Analysis of the Indiana VII Seam Coal

Parameter	Wt.% (dry basis)
Particle Size	
Coal Cleaning Methodology	Column Flotation
Proximate Analysis	
Volatile Matter	30.4
Fixed Carbon	66.7
Ash	2.9
Ultimate Analysis	
Carbon	85.1
Hydrogen	5.5
Nitrogen	1.5
Sulfur	0.8
Oxygen	4.2
Higher Heating Value (Btu/lb)	13,876
Alkali Extraction	95.6
Free Swelling Index	8

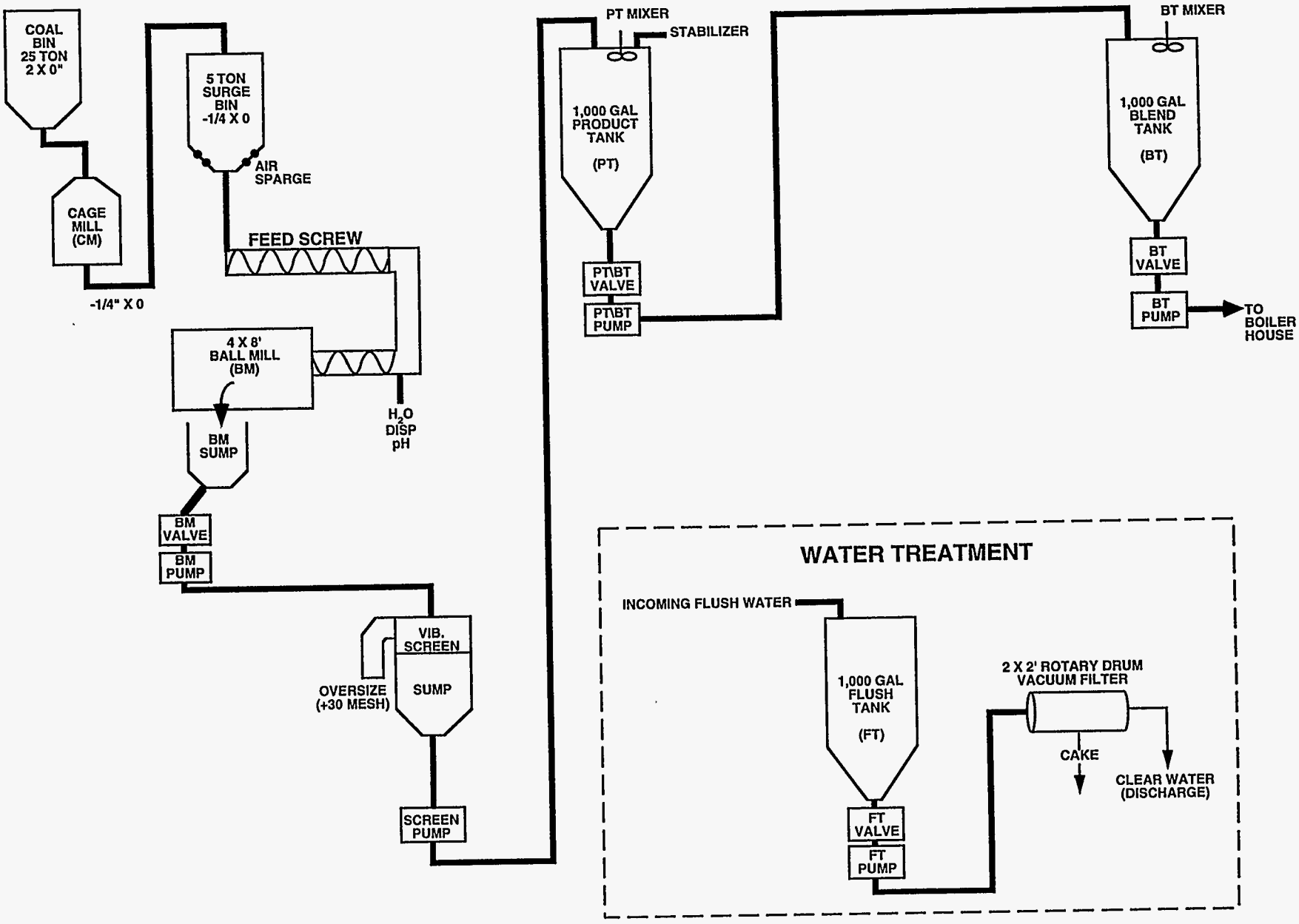

Figure 3-72. SCHEMATIC DIAGRAM OF THE MCWM PREPARATION CIRCUIT

cleaning facility in Osceola Mills, Pennsylvania to a covered outdoor storage area owned and operated by Bradford Coal Company in Bigler, Pennsylvania. The coal was trucked on an as-needed basis to the MCWM preparation facility. Incoming truck loads of coal were dumped into a covered 25 ton hopper. The coal was crushed to minus 1/4" using a cage mill and conveyed to a 5 ton surge bin. The minus 1/4" coal feed was fed to the 4x8' ball mill at a rate of approximately 600 to 650 lb/h. Water, dispersant (A-23M), and pH modifier (NH_4OH) was introduced into the ball mill feed screw as the coal was being fed into the ball mill. The coal was milled at a solids loading of approximately 68 to 72 wt.% while running the mill at 65% critical speed. Hardened chrome alloy steel grinding media constituted approximately 33% of the mill volume and was comprised of 40 wt.% 2.0 ", 45 wt.% 1.5", and 15 wt.% 1.0" balls. The MCWM was produced using a dispersant level target of 0.7 wt.% (percent actives, dry coal basis) and a pH target of 8.5 to 9.5. The MCWM discharged into a 175 gallon sump and was diluted to a solids loading of approximately 64 wt.%. The MCWM was agitated in the ball mill sump by an in-situ air sparge system. The MCWM was pumped from the ball mill sump to a Liquidtix vibratory screen where the MCWM was screened using a 30 mesh screen to remove any oversize particles. From the screen sump, the MCWM was pumped into a baffled 1,000 gallon, stainless steel mixing tank (identified as PT on Figure 3-72). Stabilizer (Flocon 4800 C) was added to the MCWM in the process tank at a dosage level of 400 ppm (percent actives, dry coal basis). The MCWM was allowed to mix in the process tank for 4 to 8 hours. Mixing was accomplished using a variable speed, center mounted, 5 Hp, Lightnin mixer (model 15Q5) equipped with a lower 18", 6-bladed, R-100 impeller and an upper 30", 3-bladed, A-305 impeller. The MCWM was pumped from the process tank (PT) to another baffled 1,000 gallon, stainless steel mixing tank (BT). This tank provided intermediate storage between the fuel production facility and the demonstration boiler. The MCWM was mixed in this tank using a fixed speed, center mounted, 5 Hp, Lightnin mixer (model 15Q5) equipped with a dual 30", 3-bladed, A-305 impeller. The MCWM was then pumped on an as-needed basis to the 2,000 gallon day tank located within the demonstration boiler room.

To maintain the targeted MCWM specifications, the MCWM was sampled at various sampling points within the circuit as it was being prepared. These sample points included: 1) the ball mill discharge, 2) the process tank inlet, 3) the blend tank inlet, and 4) the day tank inlet. The MCWM collected at the ball mill discharge was analyzed for temperature, pH, solids loading, and particle size distribution every 1 to 2 hours. The ball mill discharge sample was collected primarily to ensure that the MCWM's solids loading and particle size were acceptable and, if necessary, the coal feed rate and/or feed water to the ball mill would be adjusted accordingly. After the dilution water was added to the ball mill sump, another MCWM sample was collected from the process tank inlet and analyzed for pH, solids loading, particle size distribution, and apparent viscosity. This sample was collected primarily to determine if an adequate amount of dilution water was being

added to the ball mill sump to meet the targeted MCWM solids loading and also to measure the MCWM's apparent viscosity prior to adding the MCWM stabilizer. These samples were collected every 2 to 4 hours. After the stabilizer was added to the process tank, another MCWM sample was collected from the blend tank inlet and analyzed for pH, solids loading, particle size distribution, and apparent viscosity. This sample was collected every 2 to 4 hours and was primarily used for determining MCWM quality prior to pumping the MCWM to the 2,000 gallon day tank located in the demonstration boilerhouse. Day tank MCWM samples were taken prior to each test and on an as-needed basis throughout the combustion tests. Tables 3-20 and 3-21 are illustrative examples of these MCWM characterization data.

DMC Production

Similar to the MCWM preparation, the production of DMC started with Upper Freeport seam coal being transported from Power Operating Company Inc.'s coal cleaning facility in Osceola Mills, Pennsylvania to a covered outdoor storage area owned and operated by Bradford Coal Company in Bigler, Pennsylvania. The coal was trucked on an as-needed basis to the fuel preparation facility. Approximately 182 tons of coal were used in the demonstration. Incoming truck loads of coal were dumped into a covered 25 ton hopper. The coal was crushed to minus 1/4" using a cage mill and conveyed to a 5 ton surge bin. From the surge bin, the coal was screw fed to the TCS mill (See Figure 4-7, Section 4.1 for a layout of the DMC coal-fired system.) and transported to the burner via a booster fan.

4.0 COMBUSTION PERFORMANCE EVALUATION

As previously mentioned in Section 1.0, Penn State has been investigating the utilization of coal-based fuels in oil-designed industrial boilers since 1983. In the combustion performance evaluation, the emphasis was to improve upon the burner/boiler performance obtained in complementary programs when using a commercial coal-designed burner that was identified for, and designed into, the DOD boiler retrofit. Improving burner/boiler performance was addressed by conducting a fundamental, pilot-scale, and demonstration-scale combustion performance evaluation when firing coal-based fuels in a retrofitted oil-designed industrial boiler and determining flame stability, completeness of combustion, deposition, emissions, system derating, and erosion.

The presentation of the activities in Section 4.0 begins with a brief summary of previous burner activities in Penn State's demonstration boiler discussing the accomplishments made and the goals yet to be accomplished. This is followed by a discussion of the fundamental, pilot-scale, and demonstration-scale DOD activities.

4.1 Results from Previous Demonstration Boiler Activities

A summary of previous burner activities that preceded the DOD project is presented in Section 4.1. This section discusses previous accomplishments and sets the groundwork for the DOD demonstration-scale activities.

Table 3-20. Quality Assurance Data For the March 22, 1995 Ball Mill Discharge

Time	Sample Id	Temp (F)	pH	% Solids (wt.%)	Particle Size Distribution D (V,0.9)	D (V,0.5)	D (V,0.1)
0200	BM-01			65.0			
0220	BM-02			65.4			
0240	BM-03			65.8			
0325	BM-04		9.78	67.2	83.9	21.0	2.8
0440	BM-05	101	9.52	68.0	85.6	22.0	2.9
0530	BM-06	109	9.49	69.0	87.3	21.9	2.9
0630	BM-07	114	9.42	68.7	93.5	23.0	3.0
0800	BM-08	122	9.28	71.0	90.4	22.3	2.8
0930	BM-09	117	9.08	70.6	87.8	22.2	2.8
1030	BM-10	115	9.00	69.7	91.9	23.5	2.9
1130	BM-11	120	8.81	69.5	87.6	22.7	2.8
1230	BM-12	122	9.08	70.0	74.1	21.3	2.8
1345	BM-13	124	9.28	69.7	88.5	22.6	2.9
1430	BM-14	122	9.27	69.8	77.8	21.4	2.8
1530	BM-15	122	9.27	70.0	86.4	22.6	2.9
1730	BM-16	124	9.18	69.2	80.8	21.6	2.8
1930	BM-17	123	9.39	70.0	77.9	22.5	2.9
2130	BM-17	122	9.08	70.2	78.5	21.7	2.7
2330	BM-18	126	8.94	71.4	70.8	19.2	2.5

Table 3-21. Quality Assurance Data For the March 22, 1995 Process/Day Tank Samples

Time	Sample Id	pH	% Solids (wt.%)	Particle Size Distribution D (V,0.9)	D (V,0.5)	D (V,0.1)	Viscosity (100 sec^{-1})
0500	PT-01	9.28	64.6	88.2	21.9	2.9	357
0700	PT-02	9.38	64.7	82.4	21.4	2.9	381
1000	PT-03	9.36	66.0	85.5	21.2	2.7	568
1915	PT-04	9.50	61.5	87.4	23.3	3.0	180
2130	PT-05	9.53	62.4	83.7	22.5	2.9	212
0250	BT-01	8.78	63.3	97.3	23.0	2.9	298
0420	BT-02	8.96	63.2	90.3	22.4	2.9	247
0730	BT-03	9.25	64.1	94.8	22.4	2.9	296
1500	BT-04	9.30	64.6	83.5	22.4	2.8	377
2130	BT-05	9.44	62.6	89.0	23.0	3.0	196
0600	DT-01	9.08	62.4	83.8	21.4	2.8	174
0900	DT-02	9.03	63.2	90.5	23.0	2.8	212
1100	DT-03	9.02	63.5	94.9	23.2	2.9	215
1400	DT-04	9.05	63.5	78.0	21.7	2.8	241
1630	DT-05	9.15	62.5	89.0	22.6	2.9	239

4.1.1 SCCWS Project

Penn State and DOE entered into a cooperative agreement in 1989 with the purpose of determining if a MCWM prepared from a cleaned coal (containing approximately 3.0 wt.% ash and 0.9 wt.% sulfur) can be effectively burned in a heavy fuel oil-designed industrial boiler without adverse impact on boiler rating, maintainability, reliability, and availability. The project, called SCCWS (Superclean Coal-Water Slurry) will also provide information to help in the design of new systems specifically configured to fire these clean coal-based fuels. The first of two demonstrations was conducted, prior to conducting Phase I of the DOD project, to determine if the MCWM combustion characteristics, heat release rate, fouling and slagging behavior, corrosion and erosion tendencies, and fuel transport, storage, and handling characteristics can be accommodated in a boiler system designed to fire heavy fuel oil. A summary of the first phase of the SCCWS project is given; a complete discussion of the entire project and results can be found in the SCCWS final report to DOE[3].

A fuel oil-designed package boiler was installed at Penn State's East Campus Steam Plant. Equipment that was installed includes: a watertube package boiler of D-type design nominally rated for 15,000 lb saturated steam/h at 300 psig; forced draft and induced draft fans; a flue gas-to-combustion air heat pipe heat exchanger; a baghouse and an ash conditioning screw; a boiler feedwater pump; a MCWM unloading and pumping station; a 15,000 gallon storage tank, and a 2,000 gallon day tank; a MCWM preheater; control panels; automatic and manual boiler control systems and instrumentation; and associated ductwork and piping. Figure 4-1 is a layout of the ECSP showing the location of the boilerhouse addition, baghouse, MCWM unloading and pumping station, and 15,000 gallon storage tank. Figure 4-2 is a schematic diagram of the MCWM-fired system that was installed.

The first demonstration was conducted using the burner/atomizer system provided with the boiler and consisted of optimization testing and a combustion performance evaluation using MCWM preheat, a range of atomizing air pressures, steam as the atomizing medium, alternative atomizers, and minor burner modifications. Figures 4-3 and 4-4 are schematic diagrams of the burner and atomizer, respectively.

In summary, an oil-designed industrial boiler system was modified to handle and fire MCWM. The system was operated over eleven months from January to November 1992. Approximately 500 hours firing MCWM was obtained which translates into ~25% availability. The poor availability was due to poor fuel quality, component failure (e.g., MCWM preheater, in-duct burner, unloading station, boiler feed pump, condensate pump, draft control) and remediation, and system and burner modifications. The study indicated that deposition was not a problem under the conditions tested, erosion was not significant in the convective pass, and that MCWM could not be burned in the fuel oil-designed package boiler, using the fuel oil burner provided with the boiler, without cofiring natural gas. However, by optimizing the operating

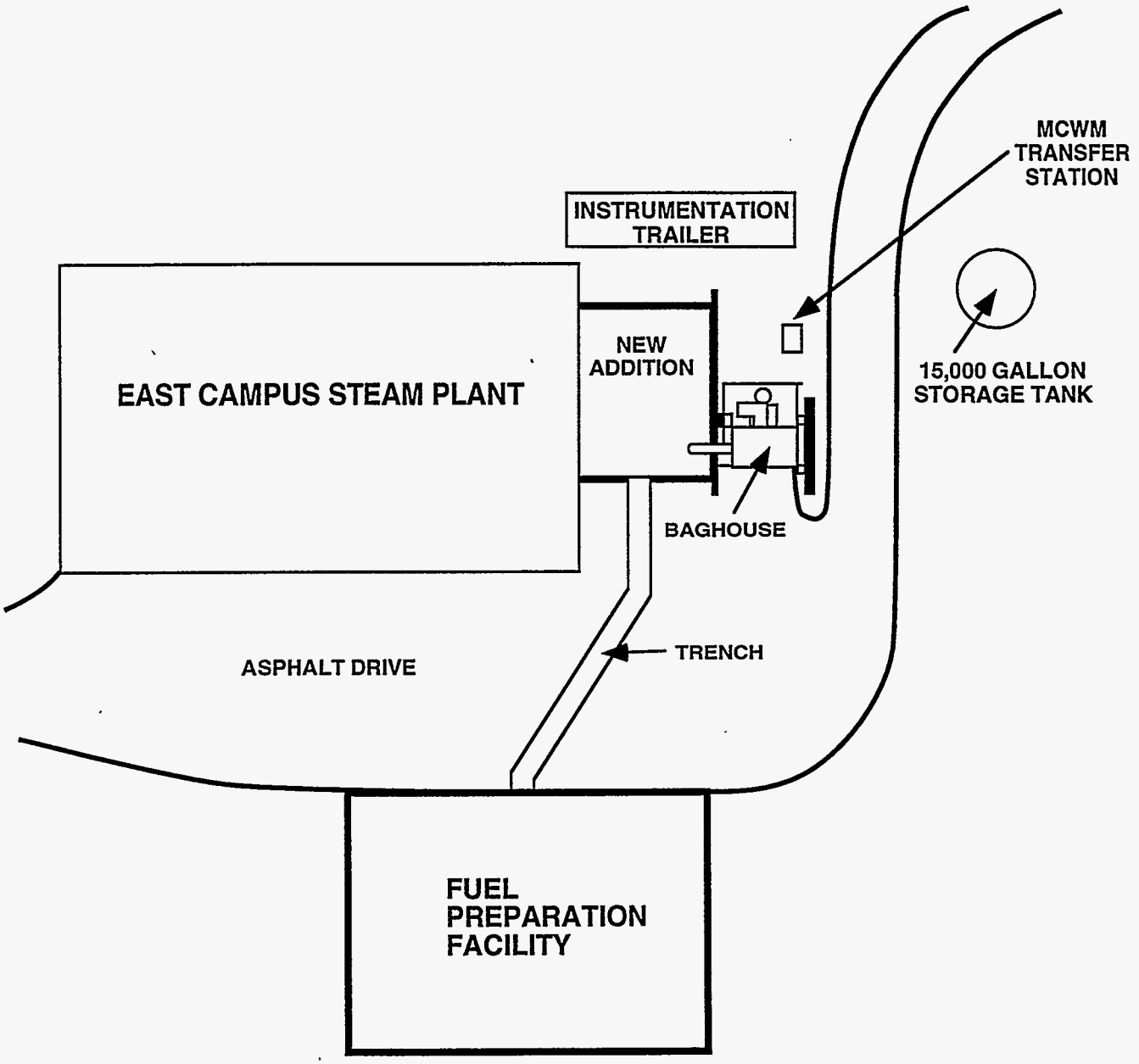

Figure 4-1. OVERALL SITE VIEW SHOWING THE LOCATION OF THE FUEL PREPARATION FACILITY AND NEW ADDITION WHICH HOUSES THE DEMONSTRATION BOILER

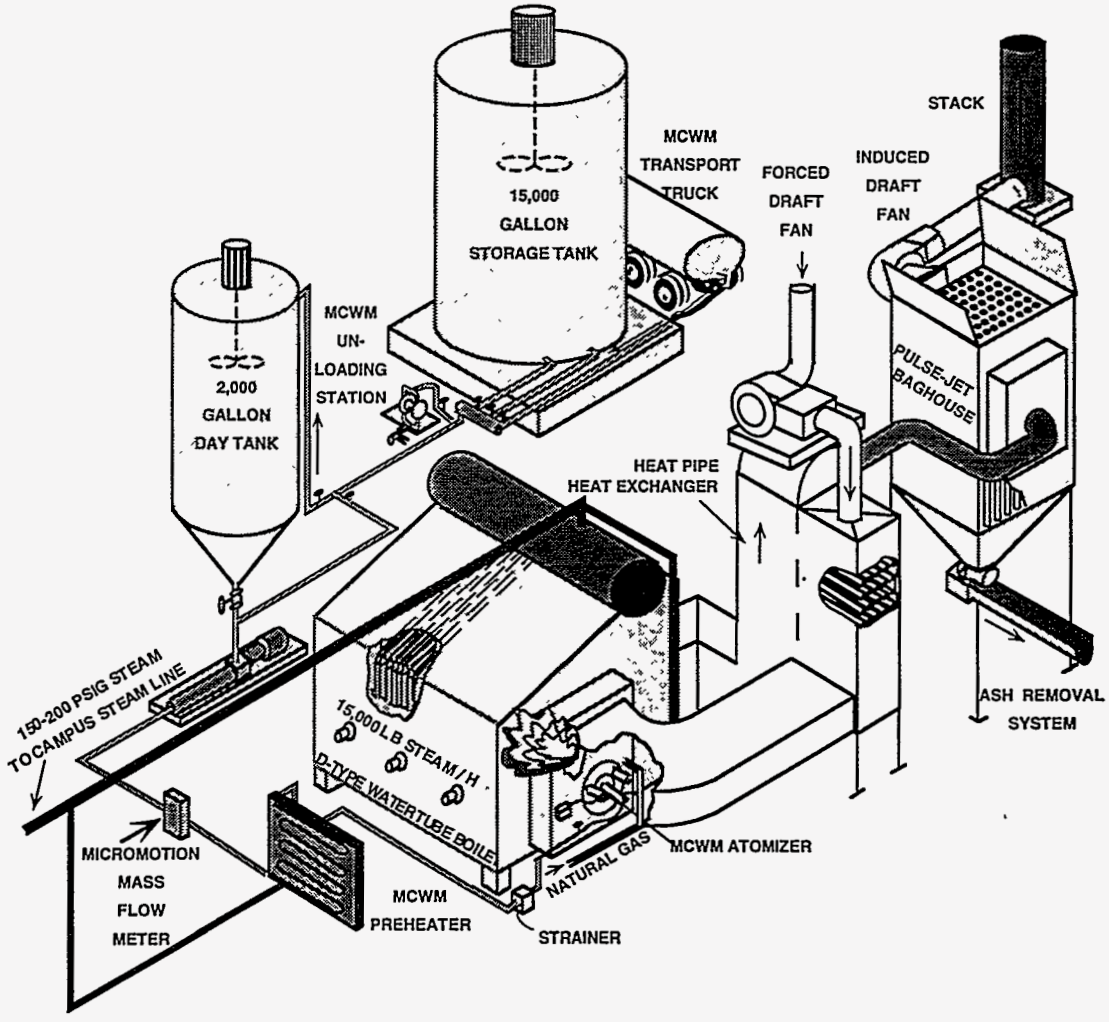

Figure 4-2. MCWM-FIRED BOILER SYSTEM

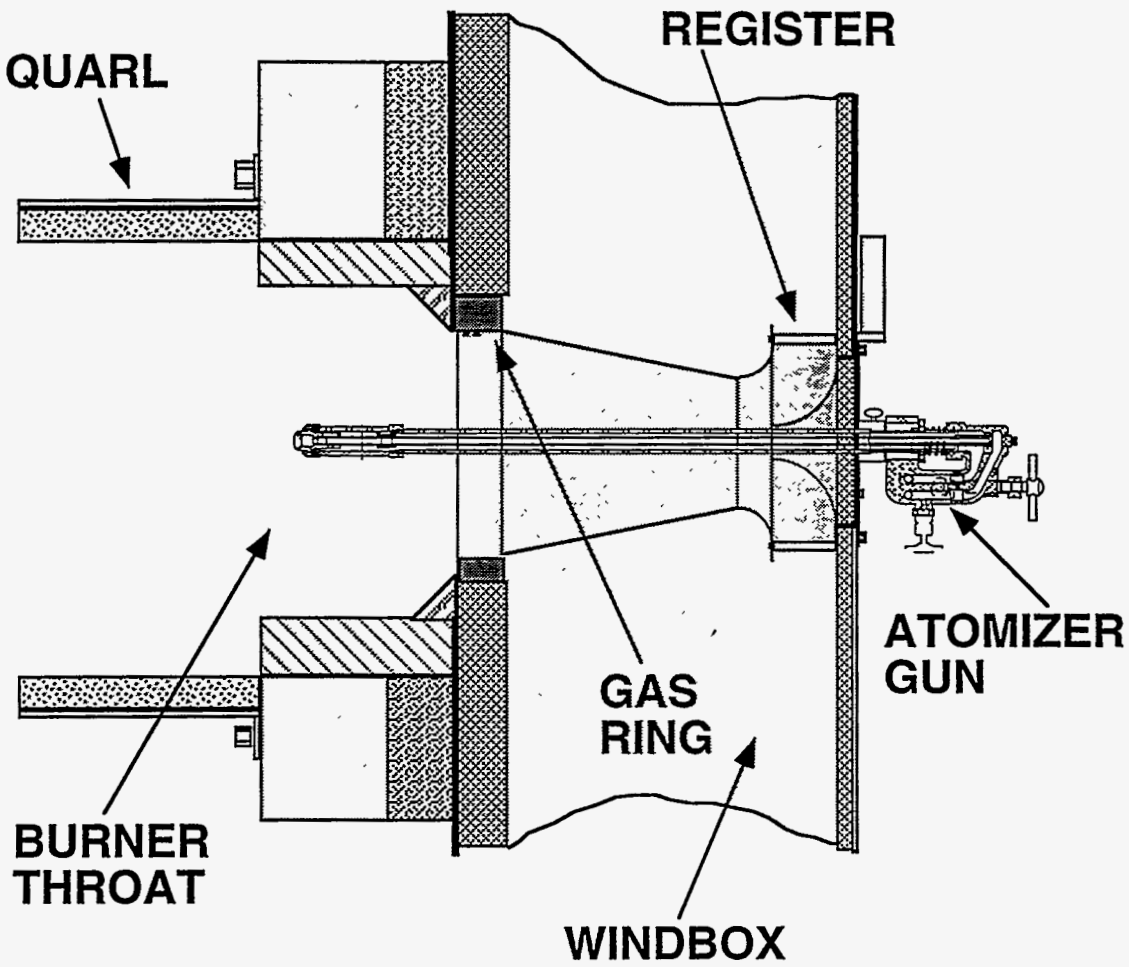

Figure 4-3. SCHEMATIC DIAGRAM OF THE FABER BURNER, WINDBOX, HEAVY OIL ATOMIZER, AND QUARL

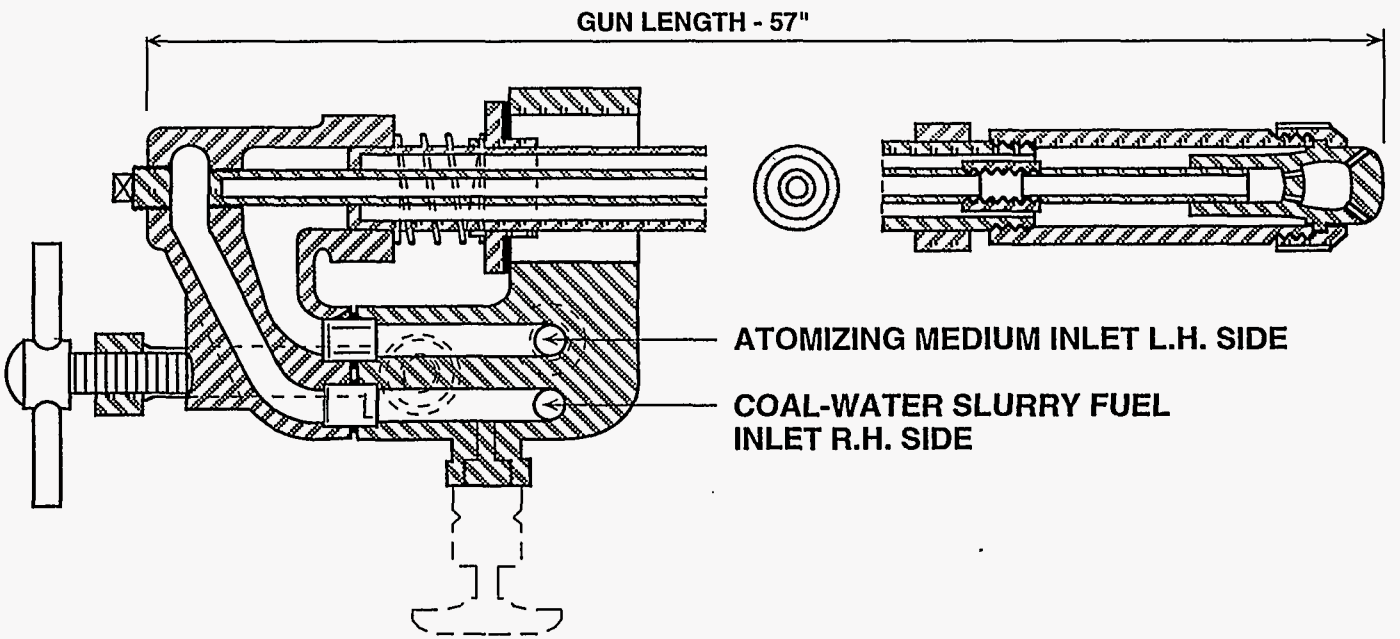

Figure 4-4. SCHEMATIC DIAGRAM OF THE FABER OIL GUN

parameters, and making minor modifications, the coal combustion efficiency was increased from 82 to 95% (see Figure 4-5). The reason for not achieving coal combustion efficiencies higher than 95% (with 15% natural gas support, based on thermal input) is believed to be the inability to stage the combustion air to promote recirculation of hot combustion products, thereby creating an optimum internal recirculation zone (IRZ). An IRZ enhances the convective heat transfer, which is the primary source of ignition energy, which reduces the time required for evaporation of water in the droplets, and thereby reduces the ignition delay. The goal was to be able to achieve fuel firing rates of 100% MCWM, 100% natural gas, or any combination of the two. In order to achieve this goal with acceptable coal combustion efficiencies (98%), it was determined that major modifications were necessary. Therefore, it was decided that a new burner with air staging capabilities would be installed prior to the next SCCWS demonstration.

4.1.2 ABB CE Project

In 1990, ABB Combustion Engineering (ABB CE) began a project funded by DOE to demonstrate the technical and economic feasibility of retrofitting a gas/oil-designed industrial boiler to burn micronized coal. In support of the overall objective, the following specific areas were targeted:

- A coal handling/preparation system that can meet the technical requirements for retrofitting microfine coal on a boiler designed for burning oil or natural gas;
- Maintaining boiler thermal performance in accordance with specifications when burning oil or natural gas;
- Maintaining NO_x emissions at or below 0.6 lb NO_2 per million Btu;
- Achieving combustion efficiencies of 98% or higher; and
- Calculating economic payback periods as a function of key variables.

A summary of the proof-of-concept testing is given; a complete discussion of the project and results has been presented elsewhere[5]. ABB CE designed a new burner, called the HEACC (High Efficiency Advanced Coal Combustor; see Figure 4-6), for burning micronized coal in an industrial boiler. After experimental testing of a prototype burner, Penn State acted as a host site for the installation and testing of a HEACC system in a retrofit application. Items installed for the HEACC system included: facility for housing coal storage, handling, and micronization; 25-ton coal hopper; vibratory feeder; crusher; conveyor; 5-ton surge bin; screw feeder; TCS mill; booster fan; magnets for removing tramp metal; HEACC; and associated piping and controls. Figure 4-7 is a schematic diagram of the micronized coal-fired system.

In summary, an oil-designed industrial boiler system was modified to produce, handle, and fire DMC. Coal storage, handling, and micronization were integrated with a burner. Proof-of-concept testing was conducted for ten months (from July 1993 through April 1994) firing DMC for ~600 hours (~25% availability). The poor availability was due to poor fuel quality, component failure (e.g., ignition system, control of fuel delivery, deposition and ash settling problems, and burner modifications for stability and flame shaping) and remediation. The testing indicated that the boiler thermal performance met requirements, combustion efficiency of 95% could be met on a

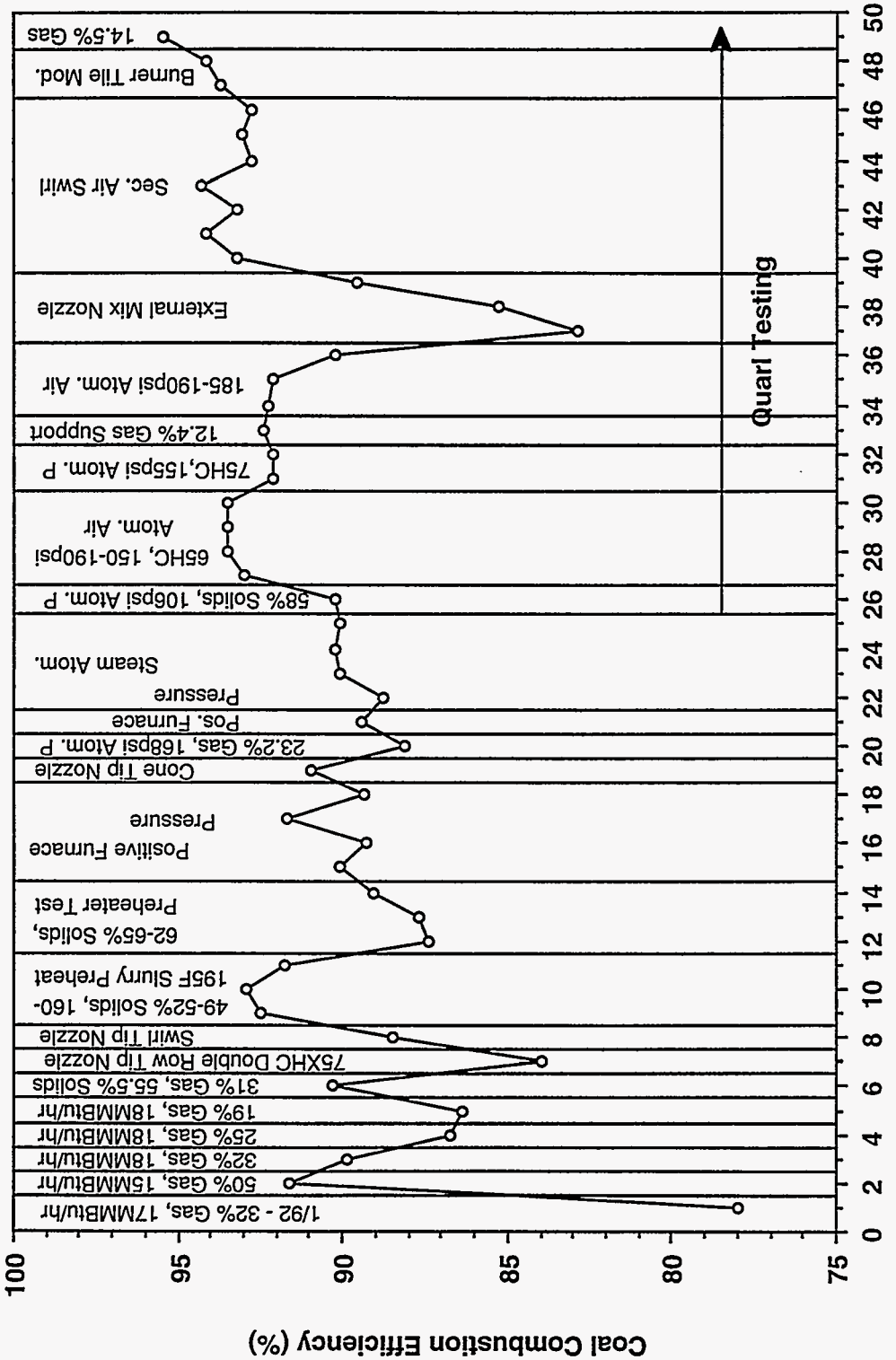

Figure 4-5. COAL COMBUSTION EFFICIENCIES FOR TESTING BETWEEN JANUARY AND NOVEMBER 1992

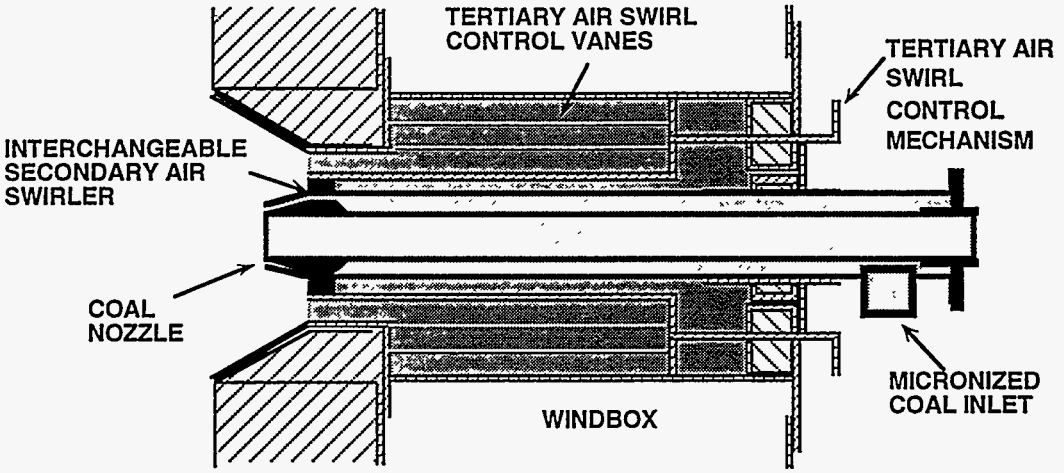

Figure 4-6. SCHEMATIC DIAGRAM OF THE HEACC

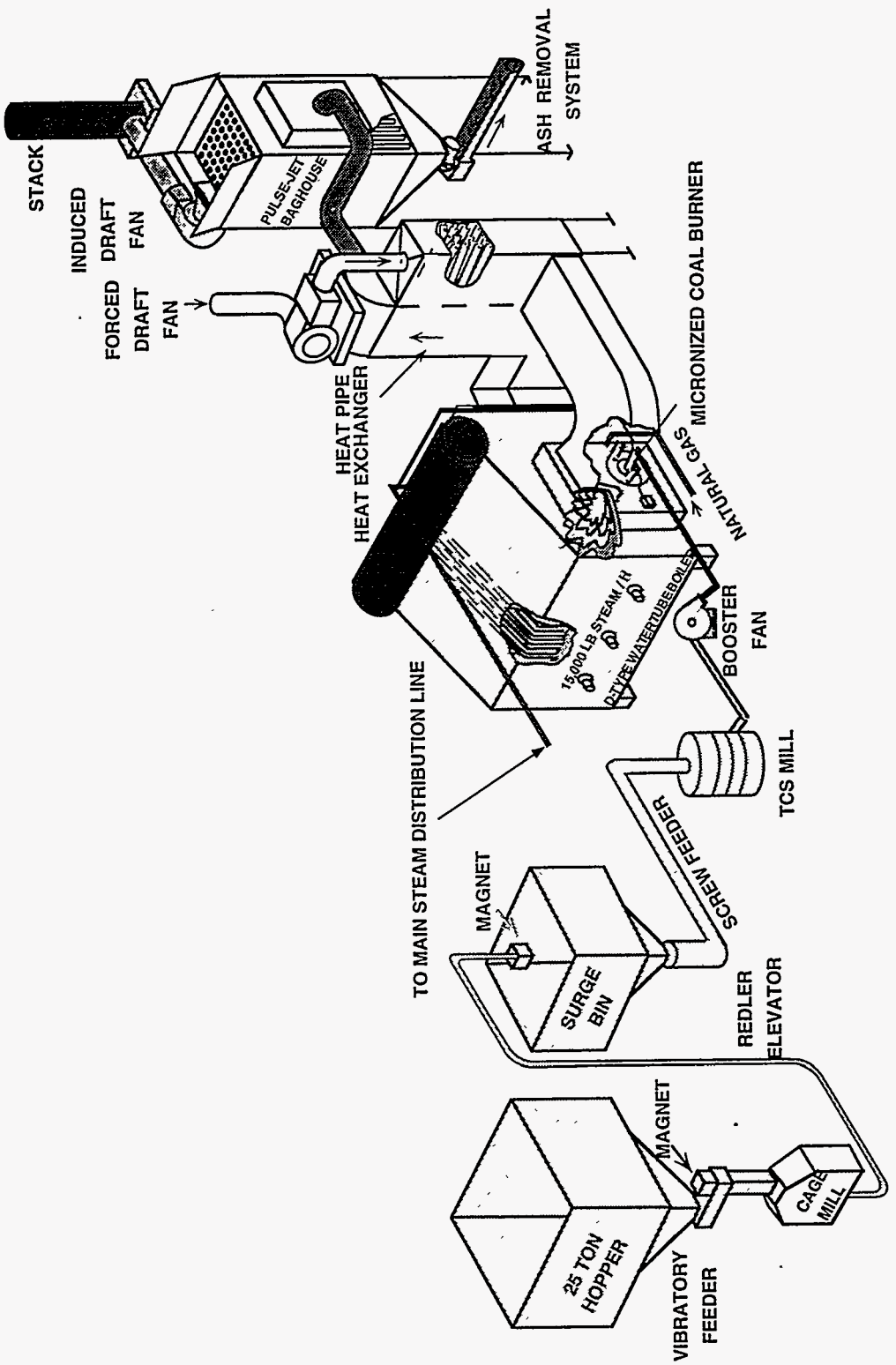

FIGURE 4-7. MICRONIZED COAL-FIRED BOILER SYSTEM

daily average basis, which is below the target of 98% (Figure 4-8 shows combustion efficiency as a function of test number as variables were being changed), and NO_x emissions can meet the target of 0.6 lb/million Btu.

As a result of problems encountered during the ABB CE project, improvements were made (upon conclusion of Phase I of the DOD project and prior to the ABB CE 1,000-hour demonstration) to the raw coal storage and transport. The surge bin was redesigned and will have a mass flow bottom. Also, a gravimetric feeder will be installed for better monitoring and control of coal feed to the TCS mill.

4.2 Fundamental Activities

Fundamental activities were performed in support of the combustion performance evaluation. These included burner/boiler modeling, an atomizer erosion investigation, and an erosion/deposition study. The burner/boiler modeling was performed to determine the effect of burner modifications on performance; the atomization study was conducted to determine the mechanism of atomizer wear (corrosion or erosion) by MCWM; and the erosion/deposition study was conducted to quantify the erosion/deposition interaction of convective pass tubes.

4.2.1 Burner/Boiler Modeling

Summary of the Modeling Work

The objective of the computer and numerical modeling effort carried out during the course of this project was to produce a computer model capable of predicting the combustion of natural gas and DMC in the demonstration boiler.

Computer codes used for modeling the combustion process can be divided into two broad categories:

1. **Kinetics Codes**, which model the kinetics and the chemistry of the combustion reactions while neglecting or simplifying the fluid mechanics of the combustion process; and
2. **Fluid Dynamics Codes**, which simplify the kinetics and the chemistry of combustion based on the assumption that the fluid mechanics, and the heat and mass transfer processes, determine the overall process of combustion in industrial-scale combustors.

For this work, it was assumed that the fluid mechanics of the combustion process, which determine the rate of mixing of air and coal and hence the rate of combustion, dominated the overall combustion process. Consequently, a computational fluid dynamics (CFD) code was chosen. Further support for this decision was based on the fact that the fluid mechanics in an industrial boiler are in turn determined by the burner design, and hence to investigate the fluid mechanics of a burner it is important for the burner geometry and the burner operating parameters to be characterized. Only the second category of code allows the investigator to model a burner[66].

As there are a number of CFD codes available on the market, a set of guidelines had to be

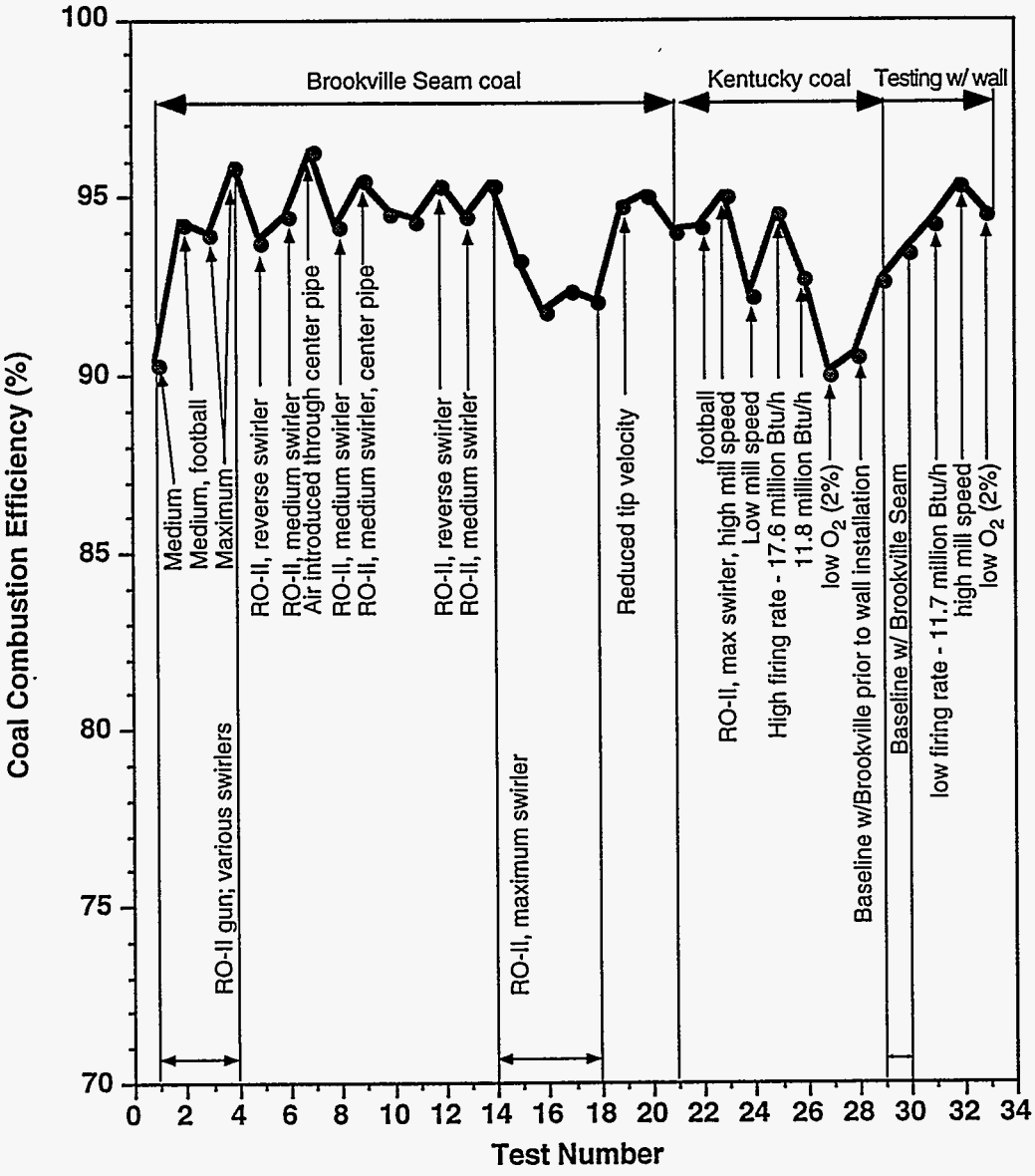

Figure 4-8. COAL COMBUSTION EFFICIENCIES FOR DMC TESTING FROM AUGUST 1993 TO APRIL 1994 USING THE HEACC

defined in order to choose the most appropriate code. These guidelines include the following:

- It must be convenient to define and change both the geometry and the simulated operating conditions;
- The governing equations which are solved must correctly represent the physical and chemical processes which take place in the practical system; and
- The results must be communicated in an easily assimilated form[67].

A number of the commercially available CFD codes were investigated: PCGC-2 (Brigham Young University, UT), FLOW 3D (Flow Science, New Mexico), FLUENT (FLUENT Inc., New Hampshire), NEKTON (FLUENT Inc., New Hampshire), SIMPLE (Imperial College, United Kingdom), FLOTRAN (Swanson Analysis Systems Inc., Pennsylvania). Based on the above guidelines, FLUENT 4.2 was chosen[67].

The numerical modeling effort was divided into two main areas -- the burner and the boiler. The reason for this division was that with state-of-the-art CFD codes, it is impossible to model both the geometry of the burner and that of the boiler with any degree of accuracy. A sound approach is to model the burner separately and use the results of the computations as input boundary conditions for the model of the boiler. A brief history of the development of the model is:

- The modeling of natural gas combustion with the Faber burner for a simplified 2-dimensional geometry in the absence of swirl[53];
- The modeling of natural gas combustion with in a 3-dimensional geometry in the presence of swirl for a range of operating conditions and geometries[67];
- The isothermal modeling of the HEACC and the EER burner for generic, simplified, and two dimensional geometries in the presence of swirl under a range of operating conditions[68]; and
- The modeling of micronized coal combustion in a 3-dimensional geometry, in the presence of swirl, for a range of operating conditions and geometries.

The modeling efforts progressed to the point that the following phenomena can be modeled successfully in the boiler:

- swirling turbulent flow;
- combustion of natural gas;
- combustion of micronized coal; and
- heat and mass transfer processes associated with the combustion process (including radiative heat transfer).

Furthermore, the model that was produced can be applied to other combustors with similar geometries with minor modifications. The theory embodied in FLUENT, along with some of the validation studies, have been reported previously. Consequently, the focus of this section will be on some of the more salient features of the results and the predictions obtained from the modeling effort. The predictions of temperature and velocity fields in the boiler during the combustion of natural gas and DMC will be discussed and compared with experimental data.

Comparison of Modeling Predictions with Experimental Measurements

Figures 4-9 and 4-10 depict the numerical modeling predictions of gas temperatures and velocities respectively for natural gas firing at 17.3 MM Btu/h with the HEACC. In order to assess

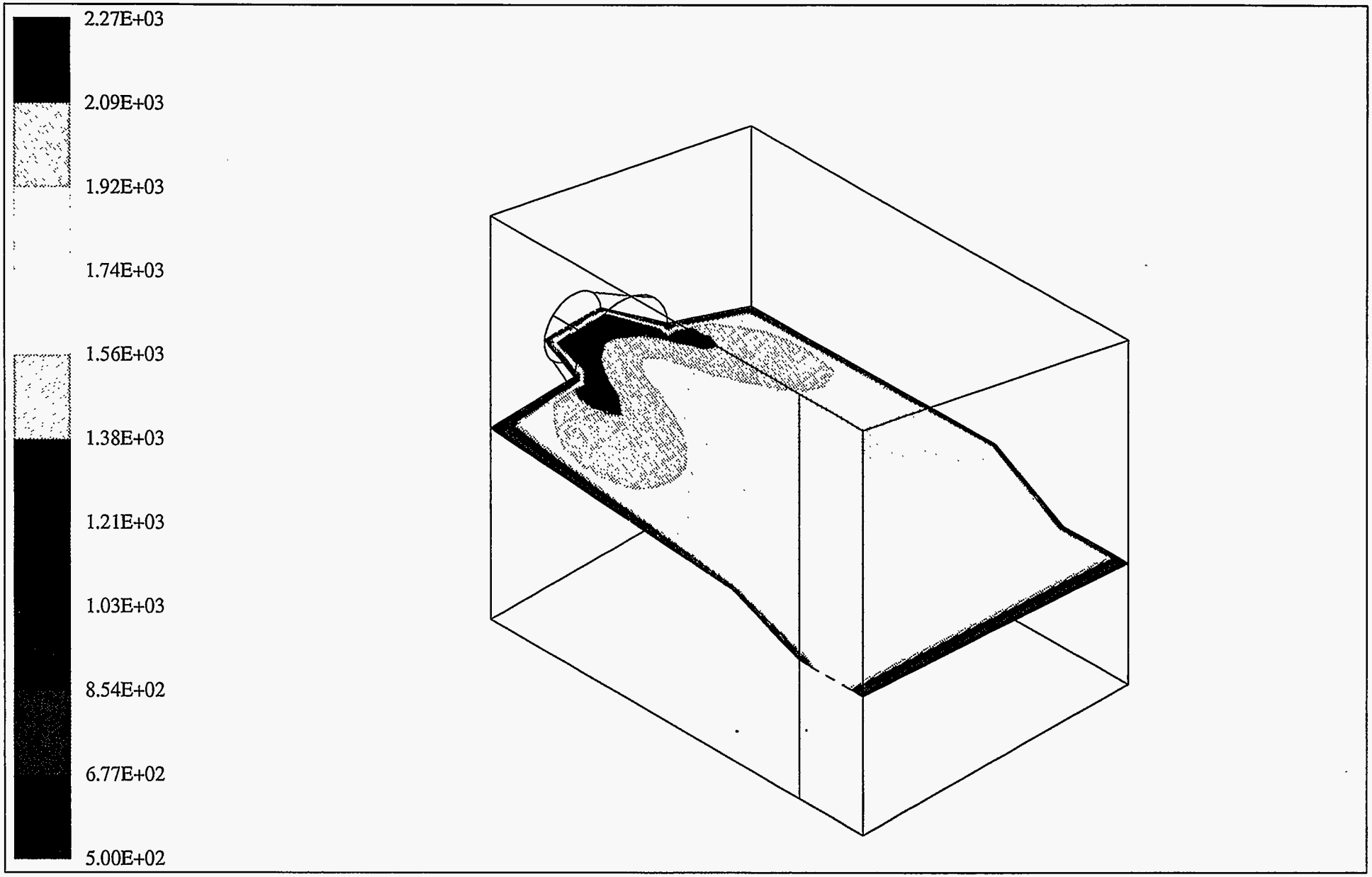

Figure 4-9. GAS TEMPERATURE (K) PROFILE IN THE DEMONSTRATION BOILER WHEN FIRING NATURAL GAS AT 17.3 MM Btu/h USING THE HEACC

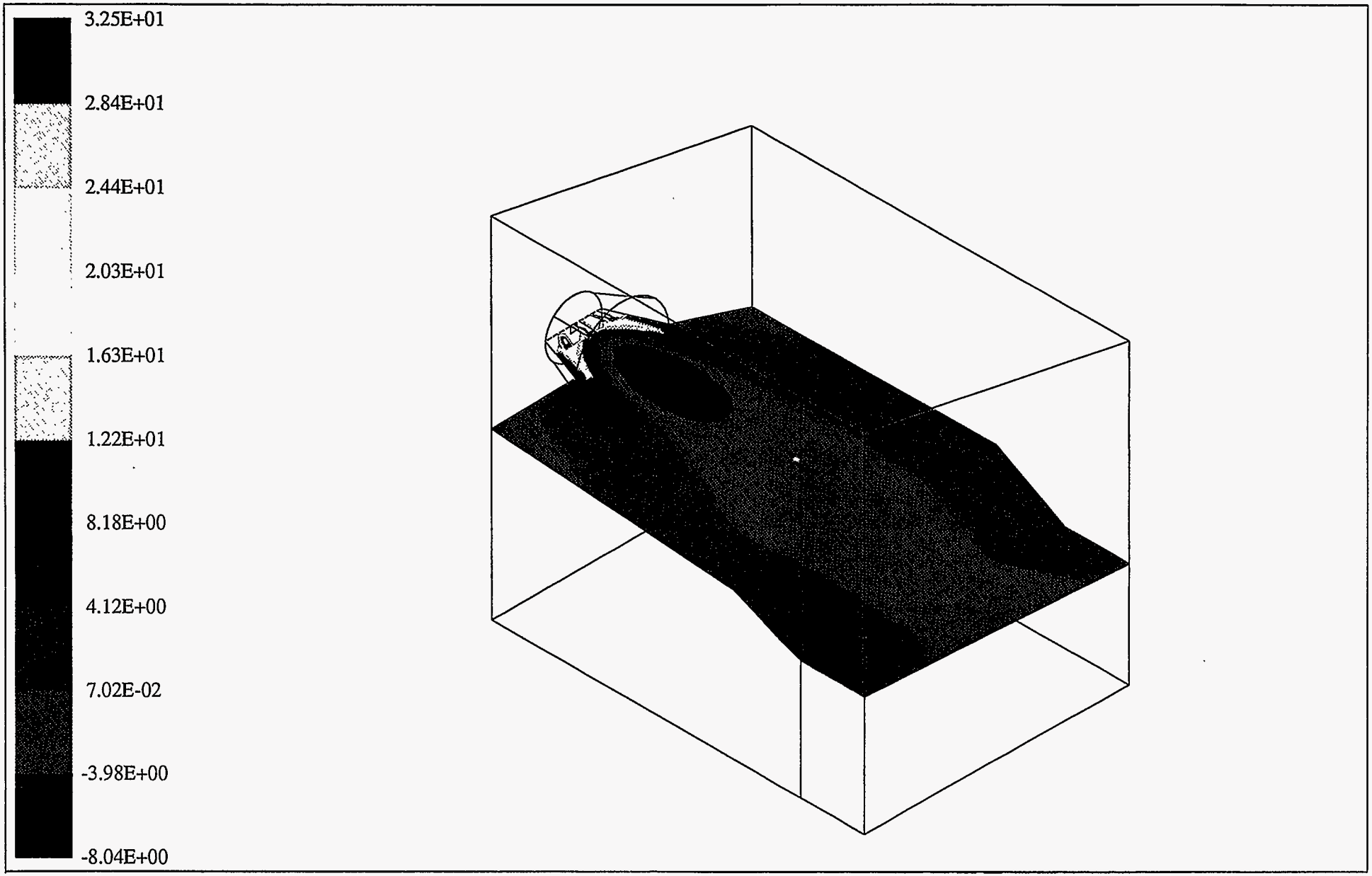

Figure 4-10. GAS VELOCITY (m/s) PROFILE IN THE DEMONSTRATION BOILER WHEN FIRING NATURAL GAS AT 17.3 MM Btu/h USING THE HEACC

the accuracy of the predictions, experimental measurements of gas temperature were taken. Figure 4-11 shows the locations in the boiler where the temperature measurements were taken by means of suction pyrometry. Six observation ports (Ports A-F in Figure 4-11) provide access to a central slice of the boiler (in the x-z plane) located at a distance equal to approximately half of the height of the boiler.

The accuracy of a suction pyrometer depends on the flow rate over the thermocouple. An experimental determination of the accuracy involves plotting the values of observed temperature against the volumetric flow rate through the suction pyrometer. The efficiency of a particular design, operating under given conditions, can then be estimated from a knowledge of heat transfer and of the geometry of the shield system. The theory of operation has been published previously and some of the relevant results are quoted here[69-74].

Accuracy of the Experimental Measurements

The temperature reported by a pyrometer falls between the true temperature of the gas, T, and the temperature ($T - \theta_0$) indicated by a simple sheathed thermocouple. The suction pyrometer indicates a temperature ($T - \theta$) which falls to ($T - \theta_0$) when the gas velocity is reduced to zero. The ratio $(\theta_0 - \theta)/\theta_0$ has been termed the "efficiency" of the pyrometer and this definition is used here. From theoretical considerations[73]:

$$\frac{\theta_o - \theta}{\theta_o} = 1 - \frac{1}{I_o\left[N\sqrt{\frac{h}{2\sigma T^3}}\right]} \qquad (4\text{-}1)$$

where, h, is the convective heat transfer coefficient, σ, is the Stefan-Boltzman constant, N is the number of radiation shields and I_0, is the modified Bessel function of the first kind (zero order). It can be seen from the above equation that the efficiency depends on the term

$$N\sqrt{\frac{h}{2\sigma T^3}} \qquad (4\text{-}2)$$

which is, in effect, a ratio of the convective to radiative heat transfer coefficients. In addition to the above theoretical definition of the efficiency, there are two other methods of determining the accuracy of a suction pyrometer; estimation of efficiency from the ratio of time constants, and estimation of efficiency from the shape of temperature/velocity curve [73]. The efficiency of the suction pyrometer used in this investigation was estimated by all three methods and was found to be greater than 92%.

Figure 4-12 illustrates the experimental measurements when firing the boiler at 17.3 MM Btu/h. From Figure 4-12 the Furnace Exit Gas Temperature (FEGT) was determined to be

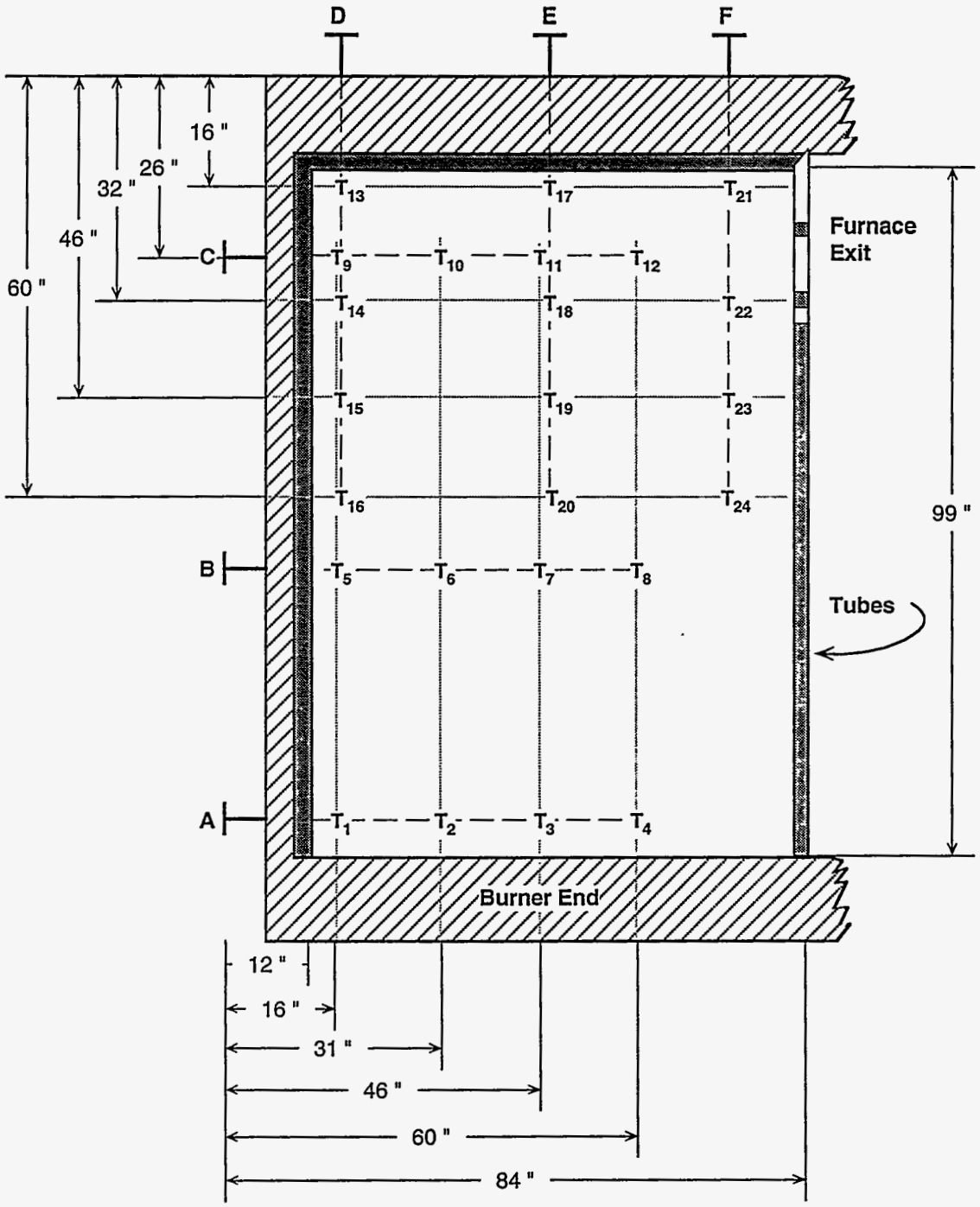

Figure 4-11. PLAN VIEW OF THE DEMONSTRATION BOILER SHOWING THE LOCATION OF THE 24 TEMPERATURE MEASUREMENTS

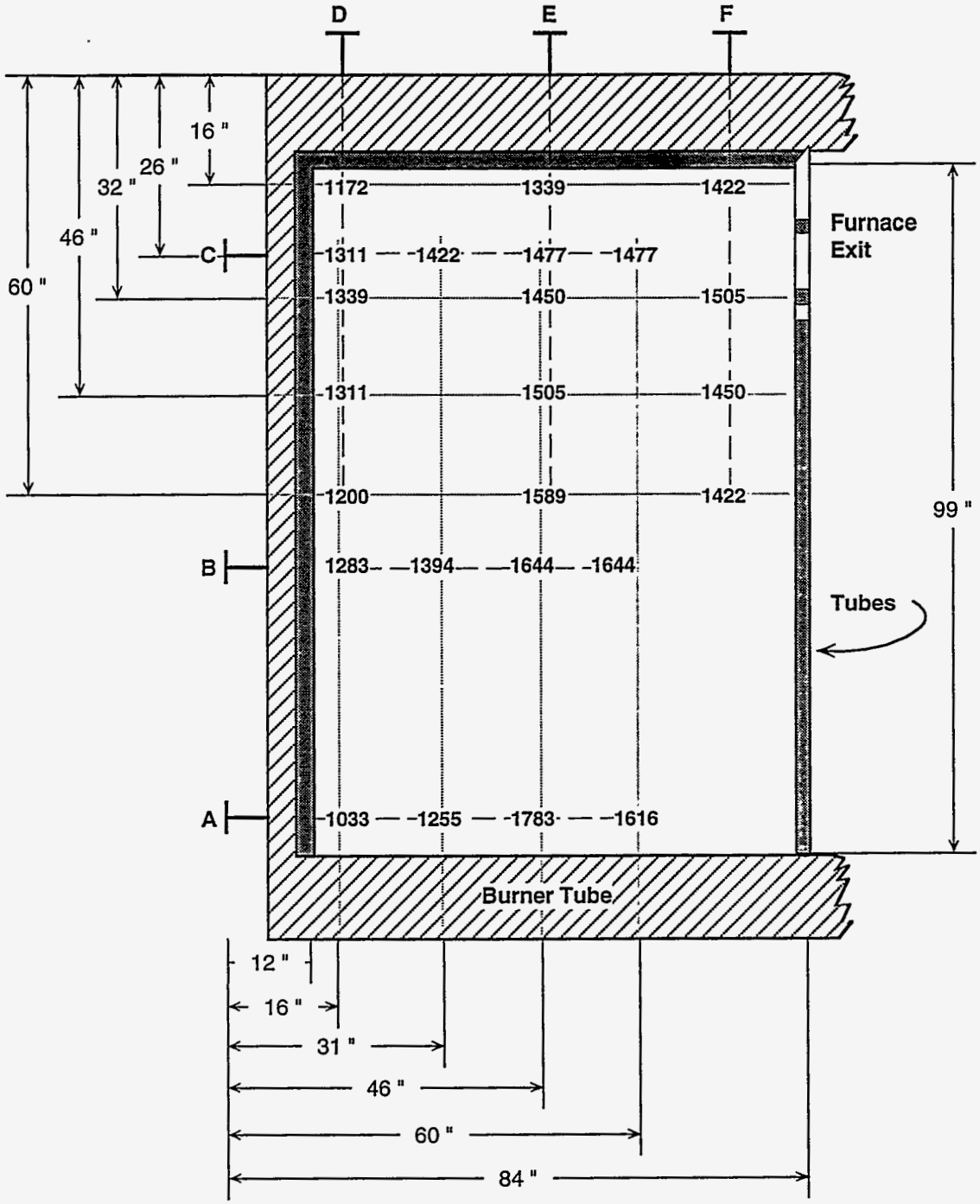

Figure 4-12. GAS TEMPERATURES (K) IN THE DEMONSTRATION BOILER WHEN FIRING NATURAL GAS AT 17.3 MIILLION BTU/H

between 1,422 and 1,505 K. The FEGT from the numerical predictions was 1,560 K (Figure 4-9). The maximum temperature measured was 1,783 K at an axial distance of one burner diameter, on the centerline of the boiler (Figure 4-12). The corresponding value of temperature obtained from the numerical predictions was 1,740 K (Figure 4-9). Hence, there is relatively good agreement between the predictions made by the model and the experimental temperature measurements.

Figures 4-13 and 4-14 illustrate the temperature and flow fields, respectively, for DMC combustion using the HEACC. Comparison of the predicted temperatures (Figure 4-13) with the experimental measurements (Figure 4-15) reveals the following: The maximum temperature predicted was 1,210 K and the FEGT was 1,060 K (Figure 4-13). The maximum temperature measured was 1,533 K and was at a location close to the centerline of the boiler with a slight bias to the right side of the boiler volume (Figure 4-15). The measured FEGT was approximately 1,144 K. Consequently, while the magnitudes of predicted temperatures seem realistic, the distribution of the temperatures does not. Furthermore, in Figure 4-13 the ignition and the subsequent release and combustion of the volatiles from the micronized coal particles are not characterized by a rapid rise in temperature. The reasons for some of these differences are discussed next.

As mentioned previously, by choosing a CFD code to model the combustion behavior in a boiler, by definition, the investigator is making gross oversimplifications of the kinetics of the combustion process in general, and the kinetics of the ignition process in particular. This means that while the gas flow fields (as shown by Figures 4-10 and 4-14) were computed accurately for natural gas and micronized coal combustion, the predicted temperature field for micronized coal combustion will contain some inaccuracies. The implications of such simplifications become even more significant in the case of a heterogeneous combustion process such as micronized coal combustion and result in some of the differences between the measurements and the predictions.

Classification of the Scientific and Engineering Methodologies Employed for Furnace Analysis

In general, there are three methods of analyzing and predicting the behavior of swirling turbulent reacting and 3-dimensional flows [75]:

- Numerical modeling and subsequent solution of the relevant set of partial differential equations of conservation of mass, momentum and energy for turbulent flow;
- The use of simplified statistical models of flow in furnaces such as combinations of well-stirred and plug-flow sections to describe the mixing pattern in the combustors. This includes physical modeling for the determination of the residence time distributions; and
- Predictions based on the laws of similarity of turbulent jets.

Clearly, the computer modeling effort carried out so far falls under the first category. However, for the sake of thoroughness the second methodology was also utilized. The theory

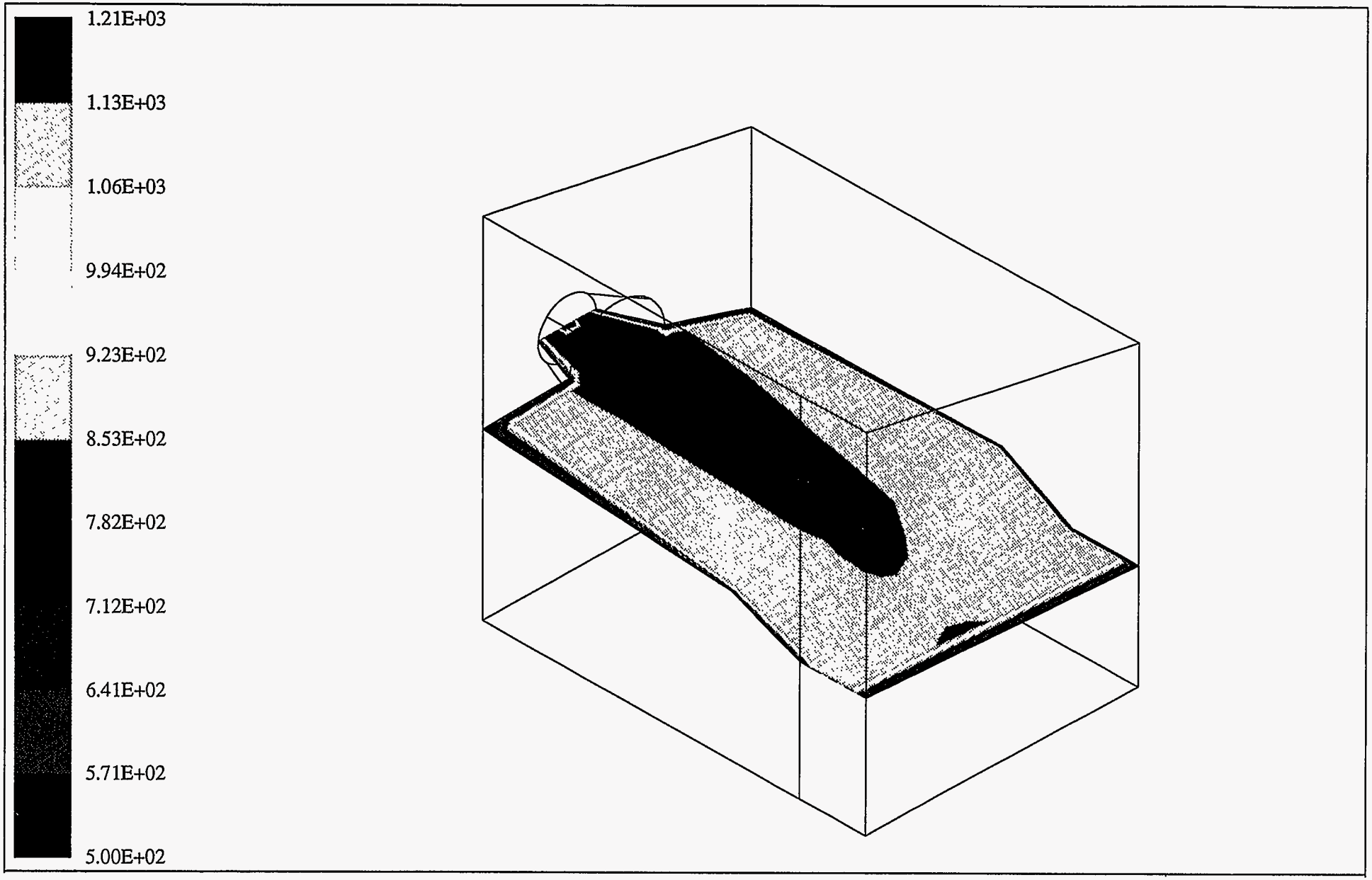

Figure 4-13. GAS TEMPERATURE (K) PROFILE IN THE DEMONSTRATION BOILER WHEN FIRING DMC AT 15 MM Btu/h USING THE HEACC

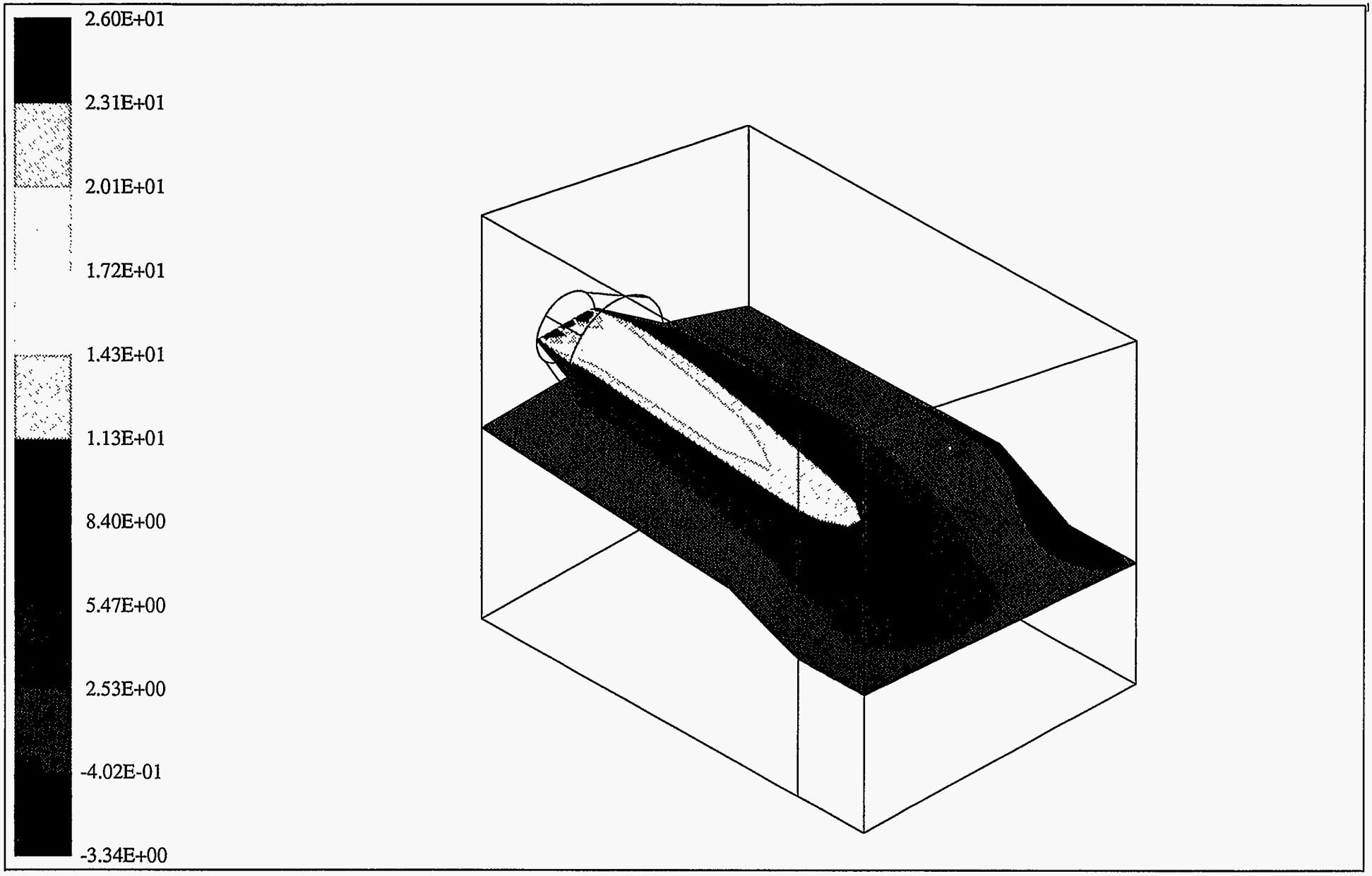

Figure 4-14. GAS VELOCITY (m/s) IN THE DEMONSTRATION BOILER WHEN FIRING DMC AT 15 MM Btu/h USING THE HEACC

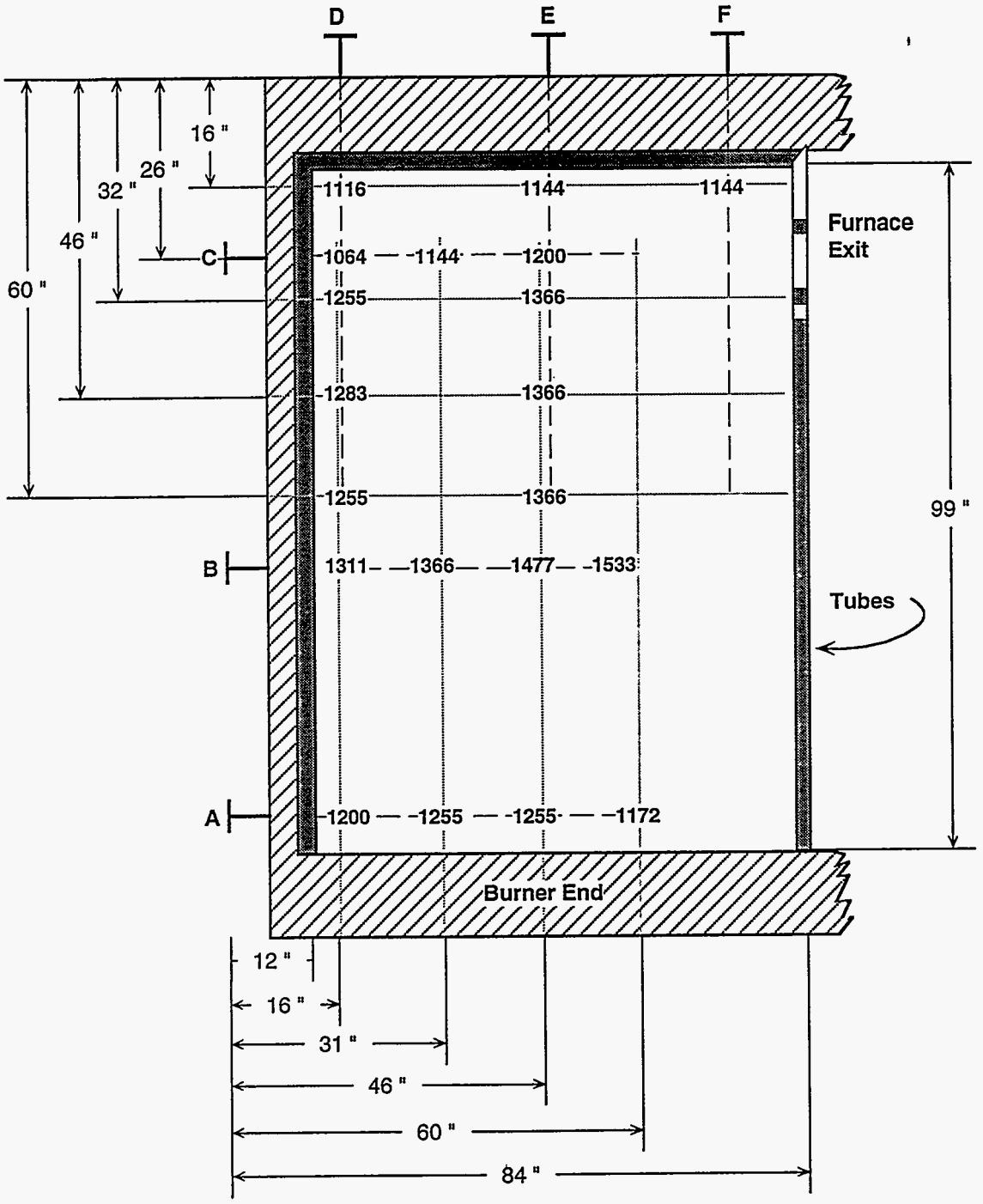

Figure 4-15. GAS TEMPERATURES (K) IN THE DEMONSTRATION BOILER WHEN FIRING DMC AT 15 MILLION BTU/H

behind this second methodology is explained briefly and some of the predictions are compared with experimental measurements of particle speed, number density and size distribution.

Distribution of Residence Times in Watertube Boilers

The key to this approach is the concept of residence-time-distribution (RTD) which has a long history deriving largely from chemical engineering [76]. The RTD is often determined by tracer experiments, in which the age distribution functions of molecules or particles injected into a reactor at some certain time are monitored either inside the reactor or at the exit. In essence, the RTD provides information on how long different parcels of gas or particles of fuel (in this case micronized coal) spend traveling through the volume of the combustion chamber.

To determine the RTD, two Standard Response curves and Two Age Distribution Function curves are employed [76, 77]. These four curves include:

- C- the exit response from a pulse input;
- F- the exit response from a step function start-up input;
- I- the internal age distribution function; and
- E- the exit age distribution function.

Following a slightly different approach, a fifth curve, G_∞, the exit response from a step function cutoff input, is added to the above family of curves. These functions can be related to the probability distribution functions $P(\varepsilon,\theta_i)$ where P is the probability of finding a particle injected some time between θ_i and $\theta_i + d\theta_i$ earlier in a normalized volume element $d\varepsilon(x,y,z)$ inside the reactor, and θ is the normalized time, that is $\theta = t / \tau_s$. The probability of finding the particles in the exit volume, which is the only way for them to leave the boiler, is $P(e, \theta_i)$. The following relationships between the different functions are thus obtained[77]:

$$I(\theta_i) = 1 - F(\theta_i) = G_\infty(\theta_i) \tag{4-3}$$

$$= \int_\varepsilon^? P(\varepsilon,\theta_i)\, d\varepsilon \tag{4-4}$$

$$= \int_0^{\theta_i} E(\theta)\, d\theta \tag{4-5}$$

$$= \int_0^{\theta_i} C(\theta)\, d\theta \tag{4-6}$$

$$= 1 - \int_0^{\theta_i} P(e,\theta)\, d\theta = \int_{\theta_i}^{\infty} P(e,\theta)\, d\theta \tag{4-7}$$

Previous studies and experiments have employed the step function cutoff [78-80]. The response was then compared to the expected behavior for a perfectly stirred reactor (PSR) condition [77]. The PSR response was obtained from the equations above by assuming that the probability of finding a fluid particle was equal at all points, including the exit volume. Inserting this condition yields [77]:

$$G_{\infty} = \exp\left(-\frac{t}{\tau_s}\right) \tag{4-8}$$

In practice, the response generally includes an initial period of constant concentration (the mixing period τ_D) before the exponential decay begins. Conceptual models have been developed to explain this delay behavior, and primarily it appears to be due to the finite transit time through the reactor. The exponential decay highlights the distribution of residence times that exists in a stirred reactor that is frequently ignored in combustion equations by employing an average residence time.

Another reason for using a residence time distribution in the current analysis is the swirling nature of the flow field. In general, the existence of swirl in a flow field gives rise to variations in the degree of swirl due to decay of the kinetic energy in the swirling flow as a function of time or distance. As a result of the decay in the degree and intensity of swirl, there is a distribution of residence times for the different fluid-particles in the flow field. In a turbulent swirling flow-field the path of travel for the fluid is no longer linear. The fluid as a whole follows a spiral path and as a result, different particles of the fluid sweep through unequal distances. The direct result of this behavior is a distribution of residence times for the various fluid-particles. Fluid particles in this context refer to infinitesimal parcels of fluid and not physical particles. Solid particles will be referred to as coal particles, char particles and ash particles. It is because of the existence of a distribution of residence times in turbulent swirling flows that swirl affects the combustion efficiency [75, 81].

Based on the above discussion it was decided to monitor the behavior of DMC particles employing a laser-based particle analyzer to determine the importance of the RTD on the combustion history of the particles. Measurements of particle number density, size distribution, and speed were taken at set intervals starting at the boiler wall and traversing the width of the boiler, by employing the central side port (Port B in Figure 4-11). The purpose of these measurements was twofold; firstly, to determine the impact of various operating parameters on the speed of the particles and secondly, to determine changes in the particle size distribution and number density with time and distance in the boiler. The experimental technique utilized is based on the particle counting, sizing, and velocimetry technology that has been explained previously [53, 82-86].

Measurements of Particle Number Density and Speed

Particle size distributions and average particle speeds obtained from the PCSV-P (Particle Counter-Sizer-Velocimeter-Probe) are depicted in Figures 4-16 through 4-19. Distance (depicted in the legend box of each graph) refers to the length of penetration of the probe into the boiler while traversing the width of the boiler through the middle observation port.

Figure 4-16 illustrates the variations in the number density (particles per cubic centimeter) of the burning micronized-coal particles as a function of distance from the boiler wall toward the center line. The measurements shown in Figure 4-16 were made at a constant firing rate of 13.2 MM Btu/h. Measurements were also taken for firing rates of 14.3 and 15.1 MM Btu/h (Figures 4-17 and 4-18, respectively). The most noticeable trend in the data was a shift in the particle size distribution to larger sizes with increasing distance from the boiler wall. This was attributed to swelling as well as the combustion history of the DMC particles. The particles close to the boiler wall have undergone more complete combustion than the particles close to the centerline of the boiler.

Figure 4-19 depicts the variation in particle speed with distance from the boiler wall for three different firing rates (13.2, 14.3 and 15.1 MM Btu/h). The highest particle speeds were observed at the highest firing rate. Additional measurements of particle speed were made and are expressed as a function of the mass flow rate of the total combustion air in Figure 4-20.

Before any further discussion of Figure 4-20, it is important to point out that the detected changes in the particles' speed were too significant to be attributed to factors such as the reproducibility of the measurements taken by the PCSV-P, beam steering and measurement errors. The two key parameters that determine the RTD of micronized coal particles for a given size distribution are the speed and the trajectory of the particles. Both parameters are in turn influenced by the fluid dynamics of the boiler. Consequently, Figure 4-20 establishes the variations of the particle speed as a function of the mass flow rate of combustion air. It is clear from Figure 4-20 that as the mass flow rate of combustion air was increased the average speed of the particles was also increased. Consequently, the RTD of the particles, as influenced by their speed was changed.

The above measurements have provided a body of evidence for changes in speed of the micronized coal particles and hence in their RTD.

The Modifications to the EER Burner

Pulverized coal burners are mixing devices. The functions of such burners are:

- To inject the pulverized coal and combustion air into the combustion chamber (in this case an industrial boiler);
- To mix the pulverized coal with the combustion air or the hot gases present in the combustion chamber appropriately;
- To provide good flame stability by promoting back-mixing of hot gases; and
- To ensure that combustion efficiency is met at satisfactory levels with a minimum of excess air (usually 15%)[81].

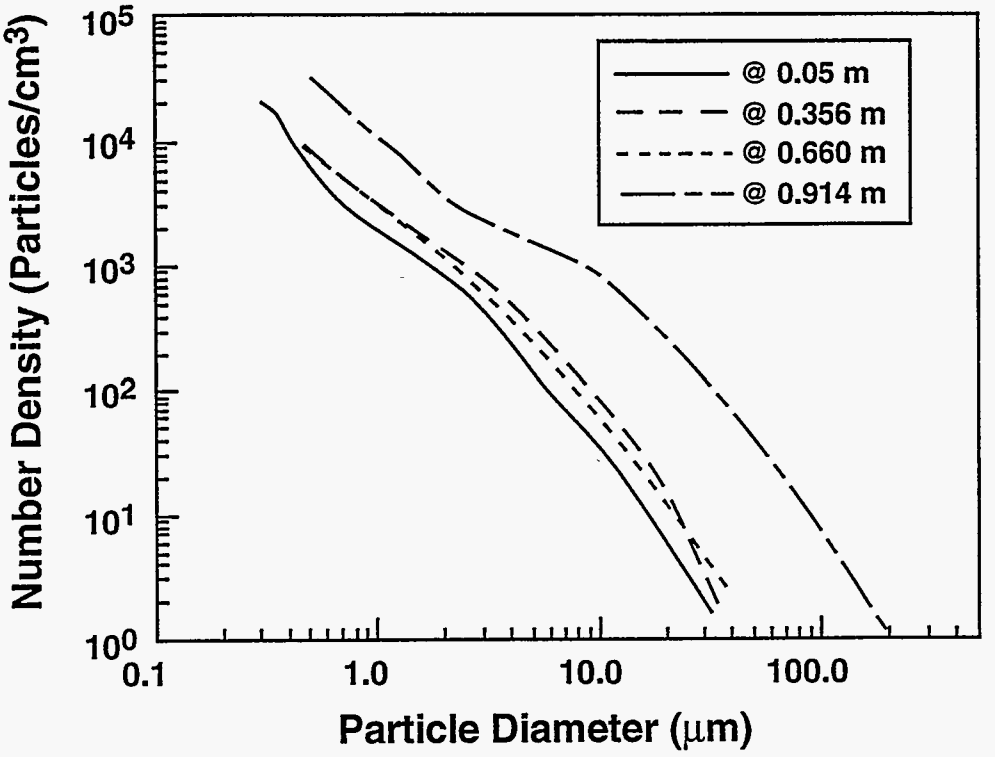

Figure 4-16. NUMBER DENSITY AS A FUNCTION OF DISTANCE FROM THE BOILER WALL WHEN FIRING DMC AT 13.2 MM Btu/h

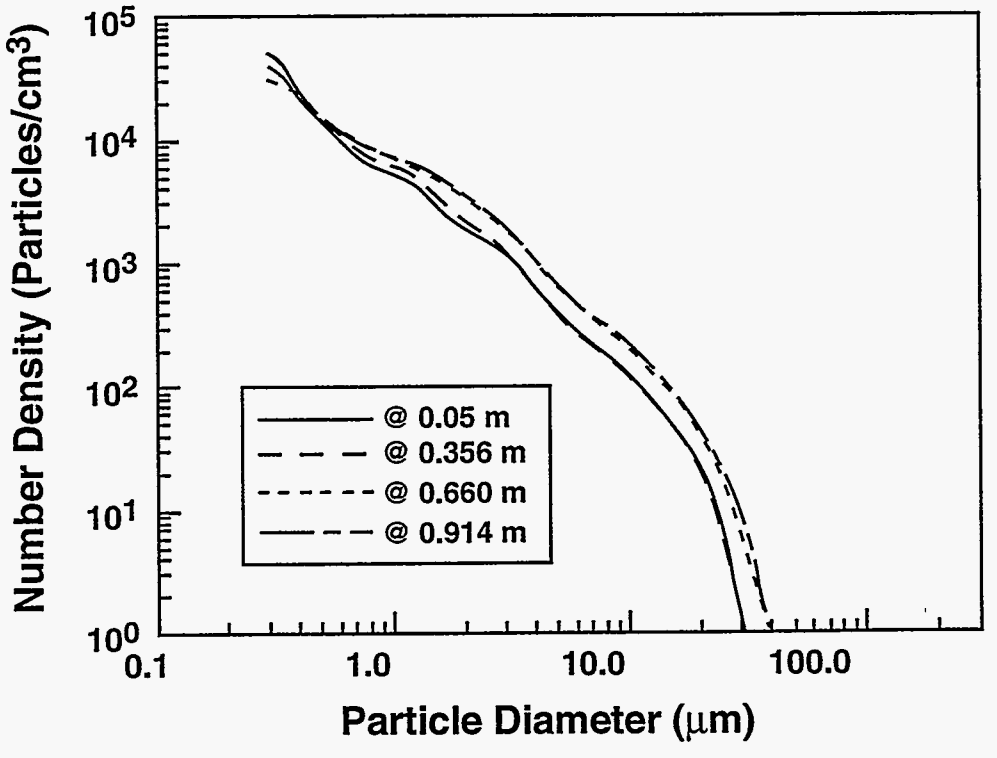

Figure 4-17. NUMBER DENSITY AS A FUNCTION OF DISTANCE FROM THE BOILER WALL WHEN FIRING DMC AT 14.3 MM Btu/h

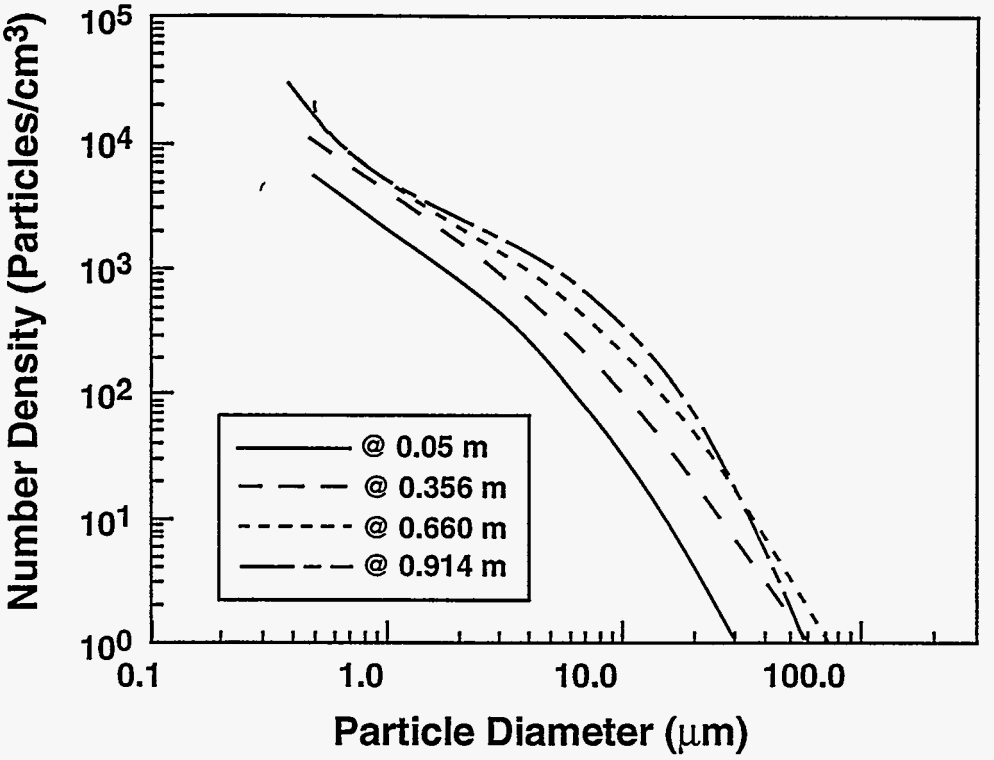

Figure 4-18. NUMBER DENSITY AS A FUNCTION OF DISTANCE FROM THE BOILER WALL WHEN FIRING DMC AT 15.1 MM Btu/h

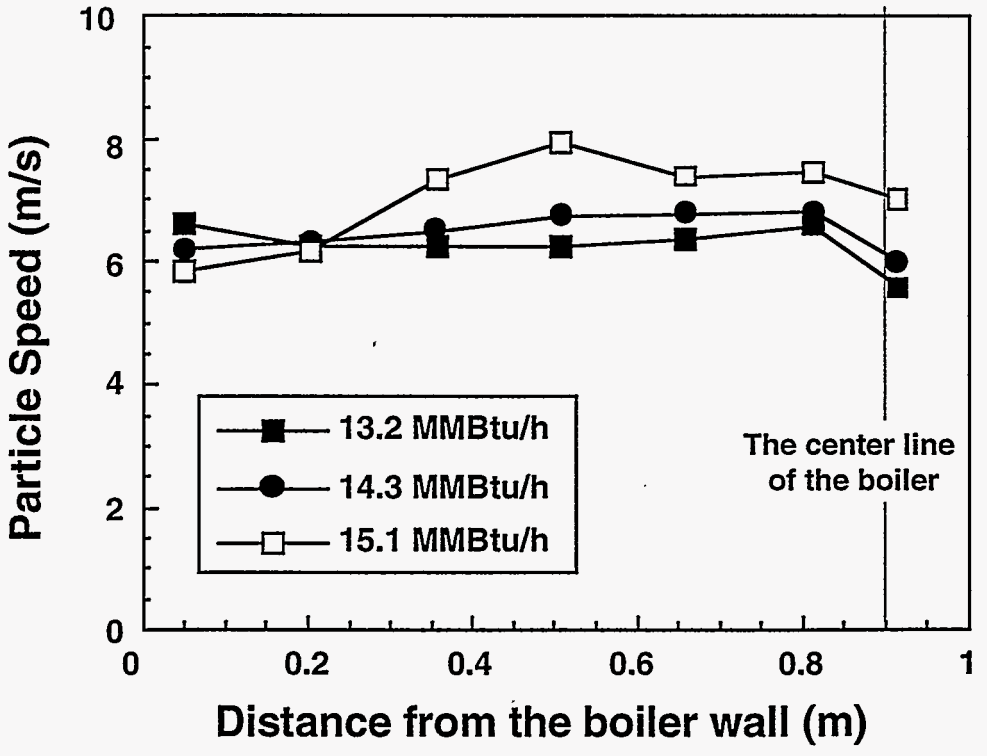

Figure 4-19. AVERAGE PARTICLE SPEED AS A FUNCTION OF DISTANCE FROM THE BOILER WALL FOR DIFFERENT FIRING RATES

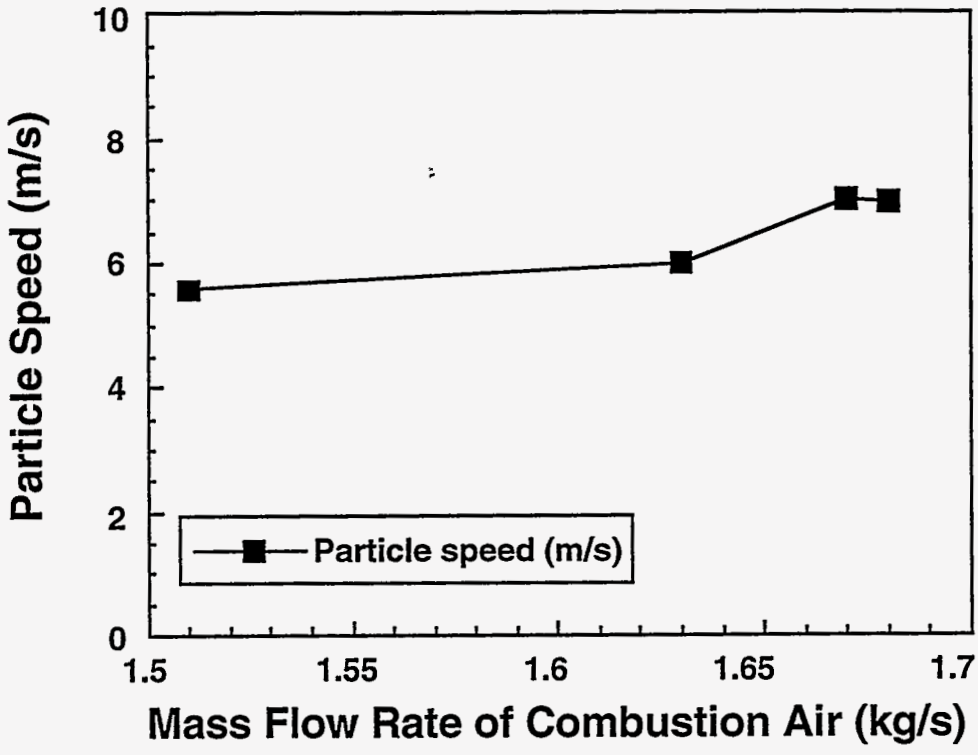

Figure 4-20. AVERAGE PARTICLE SPEED AS A FUNCTION OF DISTANCE FROM THE BOILER WALL FOR DIFFERENT MASS FLOW RATES OF COMBUSTION AIR

While satisfying the above functions it is essential that the burner and its surrounding walls do not collect excessive amounts of slag, and that the pressure drop across the burner does not exceed prohibitively high levels in terms of pumping air power requirements. It is with these guidelines that the HEACC and the EER burner were tested and compared.

Previously, a comparison between the fluid mechanics of the flows issued by the HEACC and the EER burner was carried out and the results were reported. Based on some of the results of this work and further computational modeling work done on the EER burner, it was determined that the flame issued by the EER burner was a Type I or Type III flame. What this means is that the flame has two main characteristics:

1. The primary jet of coal and air penetrates the IRZ of the burner either completely (Type I) or partially (Type III); and
2. It is a fairly long flame and has the potential to impinge on the back wall of the industrial boiler in which it is being tested.

The flame shape and type for the EER burner remained as described above over the range of operating parameters used. For a full comparison of the aerodynamics of the two aforementioned burners, the reader is referred to Sharifi and Scaroni,[87]; and Miller et al.[68].

It is important to point out that an ideal flame for a retrofit application should have the following characteristics:

1. A large IRZ;
2. A wide angle of spread; and
3. Relatively low values of axial velocity.

Clearly, a long Type I or Type III flame is not desirable in a retrofit application. Since it is the burner design that determines the fluid mechanics of the burner, it was postulated that by modifying the geometry of the EER burner, improvements in the flame shape and type might result. The main reason for the long flame issued by the EER burner was the staging of secondary and tertiary air streams. In order to create an IRZ with a rich stoichiometry, the tertiary air stream is kept separated from the secondary air stream and the natural gas or coal (in this case MCWM). This separation is achieved by means of a membrane. Consequently, it is only after a certain time period when both secondary air, fuel (natural gas or MCWM) and tertiary air are issued into the boiler that they can mix thoroughly. This delayed mixing, while beneficial for creating a rich stoichiometric zone, results in a long flame. It was postulated that by removing a portion of the m embrane the rate of mixing between the secondary and tertiary air streams could be enhanced. In effect, the objective was to produce a wider and shorter flame by causing the secondary air, fuel, and tertiary air to mix closer to the burner throat. The main steps of this task were:

1. Numerical modeling of the burner;
2. Measurements of gas temperature and velocity; and
3. Modifications to the burner geometry.

The logical sequence of the steps involved in the above analysis of the burner are depicted in Figure 4-21. Upon making modifications to the burner, it was found that when firing natural

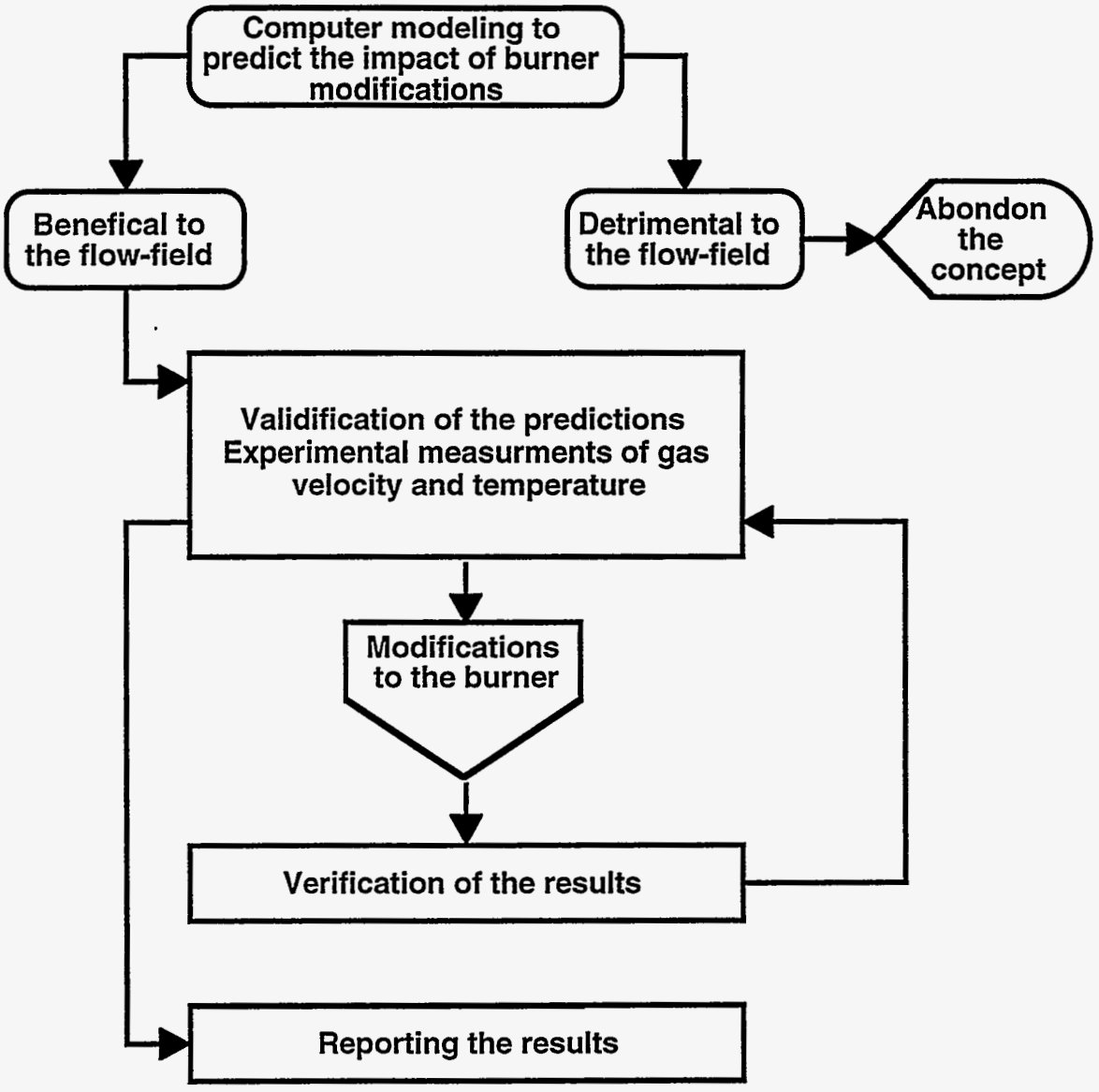

Figure 4-21. LOGIC SEQUENCE TO MODIFY THE EER BURNER GEOMETRY

gas at different rates the flame issued by the burner did indeed become shorter and wider. The direct impact of this was to make the burner quarl highly radiant. Furthermore, the modifications to the burner caused the flame to stay closer to the quarl. Hence, the quarl served as a preliminary firebox. The modified burner discharges the fuel and air into the quarl and a flame is established within the quarl. This enhances the combustion process downstream of the boiler when firing natural gas.

However, when firing MCWM (the burner modifications were made near the end of the MCWM demonstration) the coal combustion efficiency was lowered. See Section 4.4.4 for a discussion of the combustion results.

4.2.2 Investigation and Prediction of Atomizer Nozzle Erosion

Introduction

Rapid failure of atomizer nozzles in coal-slurry systems is commonly attributed to mechanical erosion by the constituent coal particles[88-91]. The fundamental mechanisms and theoretical considerations of the underlying erosion processes have been extensively studied[92-97] but systematic investigations of atomizer wear are limited to candidate materials evaluation [88, 89]. Prototype analyses do not provide adequate predictive capabilities; consequently, a fundamental study, using a modified atomizer and dilute silica-water slurry (SWS), was undertaken to develop a modeling technique and theoretical prediction of the erosion rate.

The computational fluid dynamics (CFD) code FLUENT 4.2, which was used in the burner/boiler modeling, was also used to numerically model the flow field and silica particle trajectories within the mixing region of a modified fuel oil atomizer. Data obtained from the simulation were then input into Sundararajan's comprehensive erosion equation [98] and the numerical results compared with experimentally determined values.

The objective of the study was to adapt modeling techniques for the prediction of the erosion rate in a *simplified* (no airblast, dilute silica-water slurry) atomizer/slurry system. Procedures developed and information gained can be expanded to aid in the design and performance prediction of the more complex twin-fluid (airblast) atomizers commonly used in MCWM applications.

Experimental Procedure

Atomizer Modification

The atomizer used in the study was a Delavan Variflo Nozzle originally designed to fire #2 fuel oil. Modifications to the original design are illustrated in Figures 4-22 (original design) and 4-23 (modified design) and included removal of the swirler and isolation of the mixing chamber.

Damage to the atomizer and subsequent erosion analyses were limited to the nozzle's removable orifice disk (Figure 4-24). Disks were constructed of 416 martensitic stainless steel. Material properties of the stainless steel are:

- Tensile Strength 97.5 ksi, and
- Vickers Hardness 205.0 kg/mm^3.

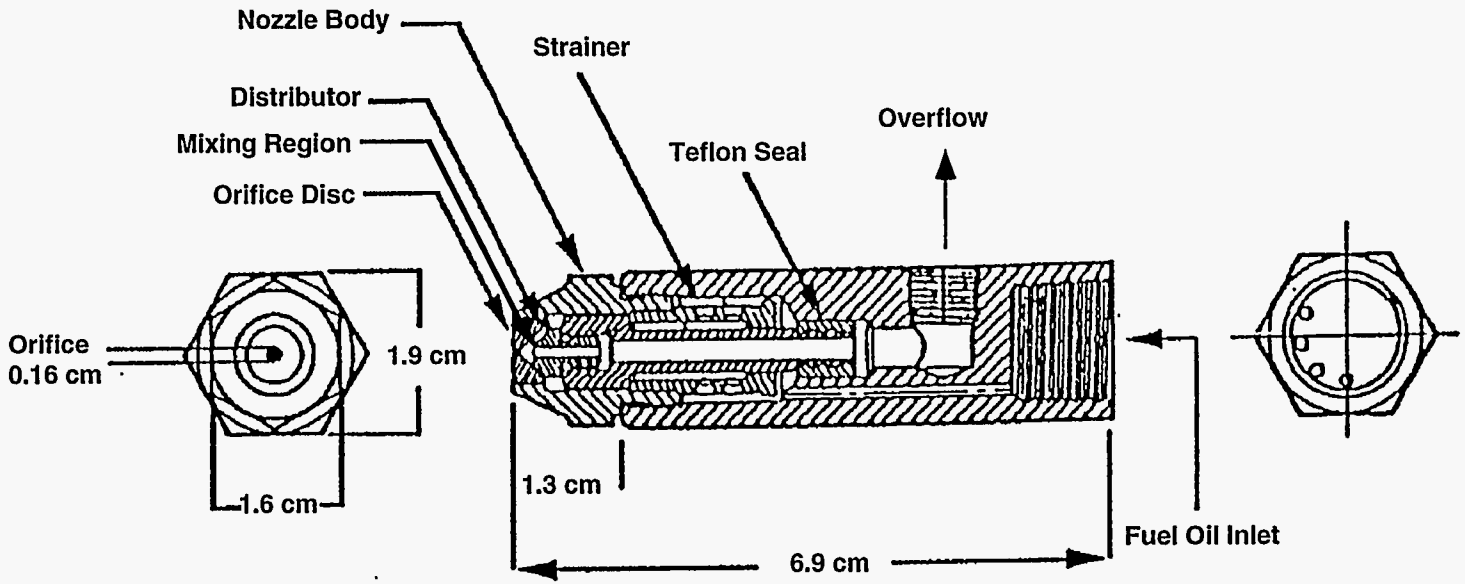

Figure 4-22. DELAVAN VARIFLO NOZZLE

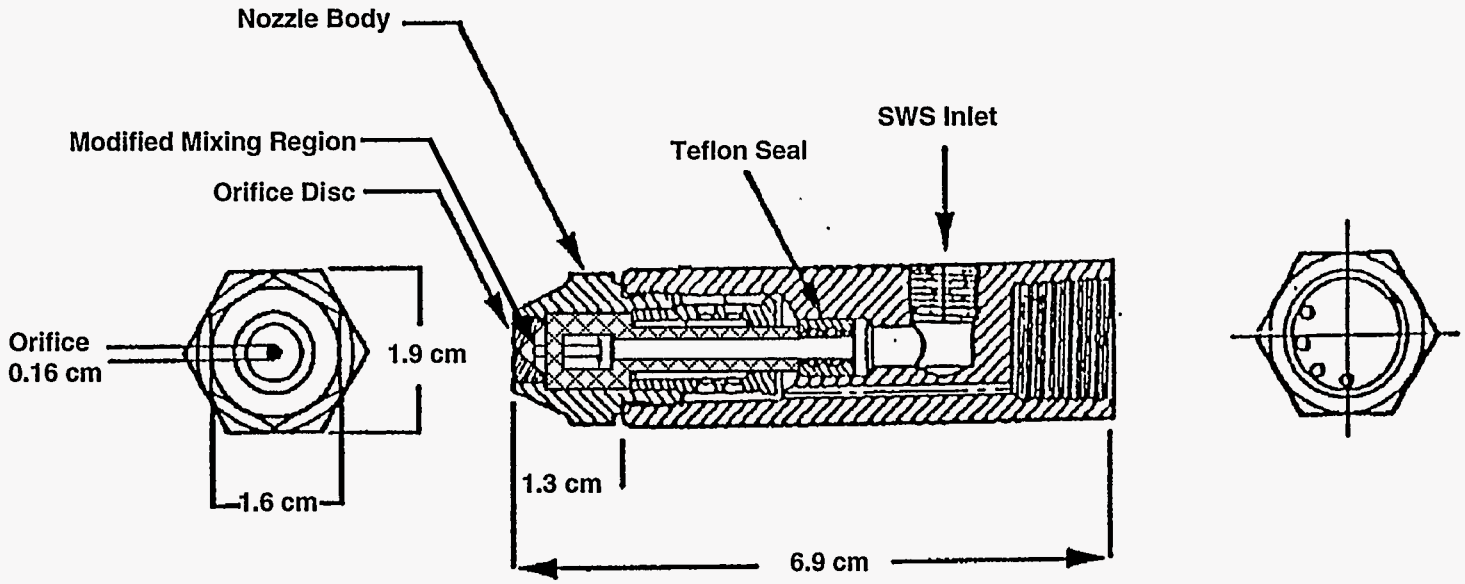

Figure 4-23. MODIFIED DELAVAN NOZZLE

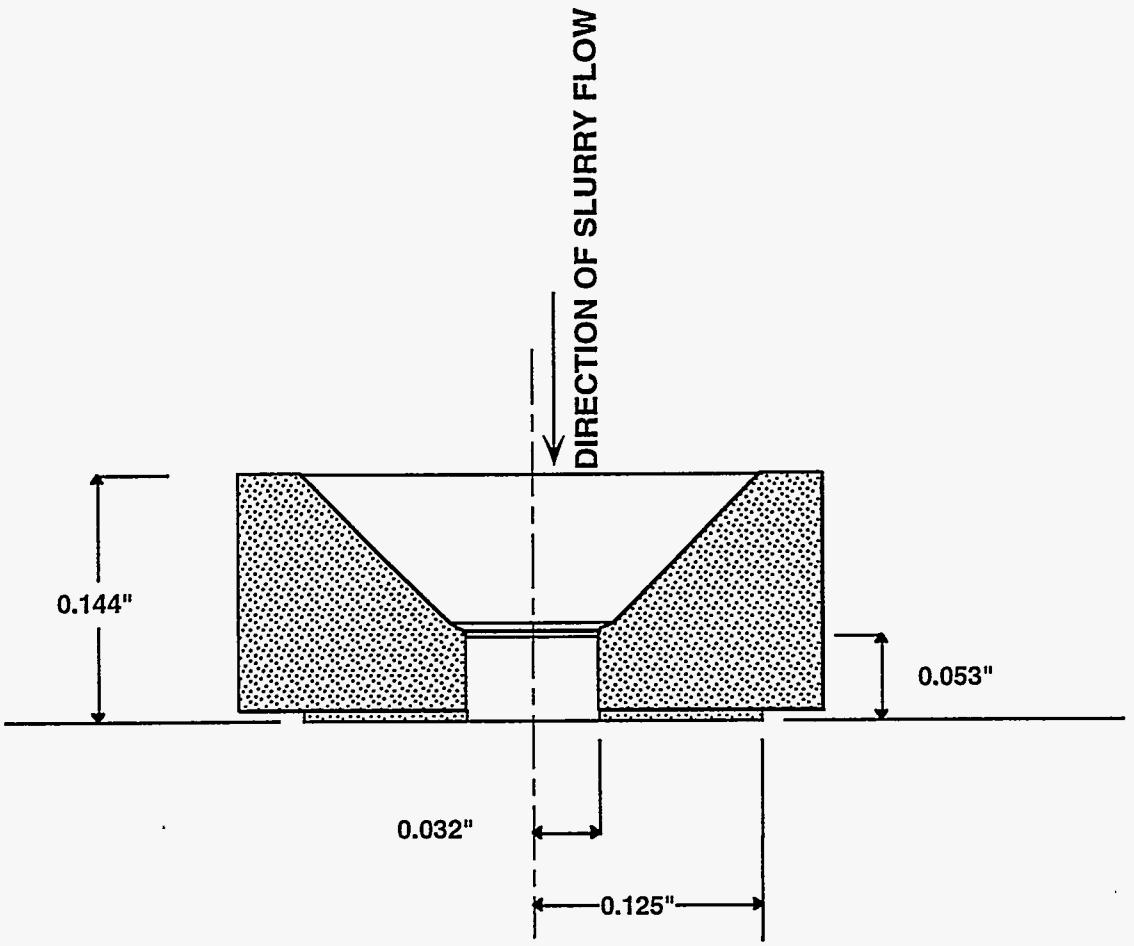

Figure 4-24. ORIFICE DISK CROSS SECTION

The chemical composition of the stainless steel is (weight basis): C, 0.10%; Mn, 0.42%; Si, 0.62%; P, 0.014%; S, 0.35%; Cr, 13.14%; Ni, 0.24%; Mo, 0.04%; Cu, 0.04; and Fe, balance.

Silica-Water Slurry

The silica-water slurry used in the experimental investigation was produced in 5 gallon charges from 2.1 kg of powdered silica and 5 gallons of distilled water. The silica concentration was formulated to be 10% by weight.

Silica Specifications

The physical and chemical specifications of Sil-Co-Sil 250, which was obtained from U.S. Silica of Ottawa, Illinois, are:

- Median size ($D_{v,0.5}$) -- ~ 42 μm;
- Density[99] -- 2.2 g cm^{-3};
- Vickers Hardness[90] -- 1,100 kg mm^{-2}; and
- Chemical Composition (U.S. Silica Corp.) -- > 99.9 % SiO_2.

Figure 4-25 shows the particle size distribution obtained using a Malvern 2600 Droplet and Particle sizer.

Operating Conditions

Experimental and theoretical erosion rates were calculated for a mass flow rate of ~500 lb/h and a SWS composition of 10 wt.% silica.

Experimental Setup

The experimental setup is shown in Figure 4-26 and consists of two separate components, the spray chamber and the slurry train.

Spray Chamber

The spray chamber is a 2' x 2' x 2' cube constructed of 0.5" thick 6061-T651 aluminum plate. Although originally designed for the analysis of unrestricted MCWM sprays[53], the study discussed here used the chamber as a nozzle housing, with minor alterations made to facilitate collection and reuse of SWS.

Slurry Train

SWS was mixed and stored in a five gallon, plain carbon steel storage tank. The tank was painted to discourage corrosion and fabricated from a 12 3/4" diameter 16" long A53 steel pipe and 12 3/4" butt weld cap. A 1/4 hp, 1,725 rpm Reliance agitator was mounted on the housing frame above the slurry tank and used to keep the slurry charge suspended.

The fuel tank is mounted at the inlet port of a Robbins and Myers 6P3-CDQ progressive cavity Moyno pump. Power is supplied to the pump by a 1 hp Reeves Motodrive connected to a Cutler Hammer 3-phase magnetic starter and 30 amp, 230V disconnect.

SWS is carried from the pump exit through 3/8" diameter high pressure (< 200 psig) hose through a Micro Motion model D25 mass flow meter. At the flow meter outlet, 1/4" high pressure hose transports SWS into the spray chamber, through a check valve, and into the atomizer.

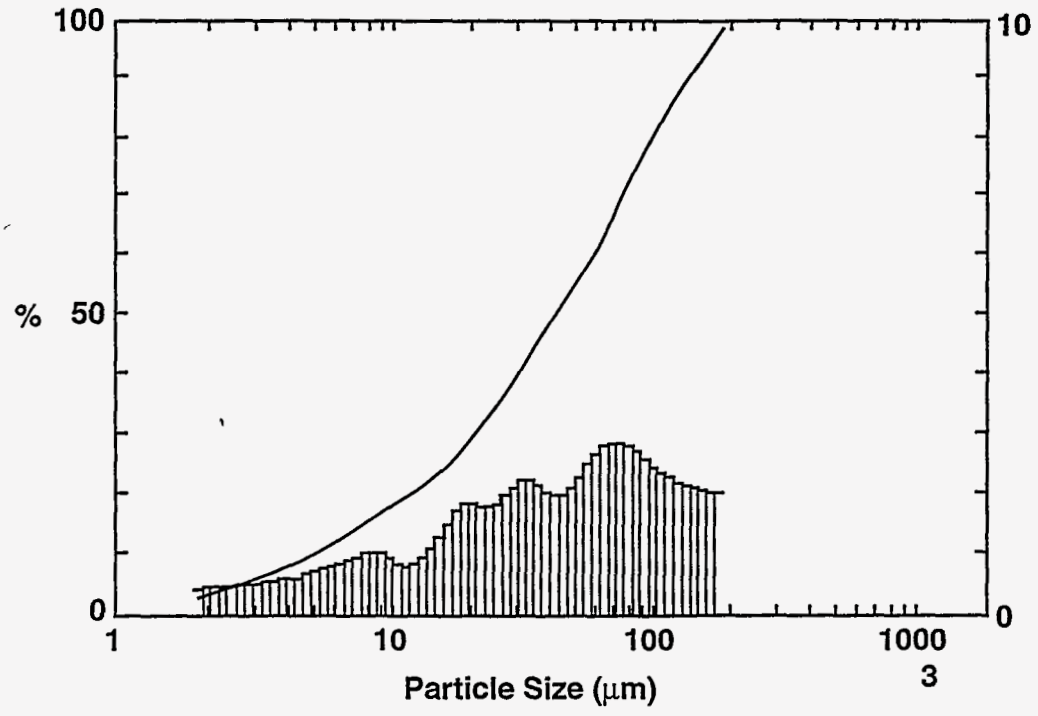

High Size	Under %	High Size	Under %	High Size	Under %	High Size	Under %	High Size	Under %	High Size	Under %
188	100	84.5	74.7	38.0	47.5	17.1	25.7	7.69	14.4	3.46	6.5
175	98.0	78.6	71.9	35.4	45.3	15.9	24.2	7.15	13.5	3.21	6.0
163	95.9	73.1	69.0	32.9	43.1	14.8	22.9	6.65	12.6	2.99	5.5
151	93.8	68.0	66.1	30.6	40.8	13.7	21.8	6.18	11.7	2.78	5.0
141	91.7	63.2	63.2	28.4	38.7	12.8	20.9	5.75	10.9	2.59	4.5
131	89.5	58.8	60.5	26.4	36.7	11.9	20.1	5.35	10.1	2.40	4.1
122	87.3	54.7	58.0	24.6	34.9	11.1	19.2	4.97	9.4	2.24	3.6
113	85.0	50.8	55.7	22.9	33.1	10.3	18.4	4.62	8.8	2.08	3.2
105	82.6	47.3	53.5	21.3	31.2	9.56	17.5	4.30	8.2	1.93	2.7
97.8	80.1	44.0	51.5	19.8	29.3	8.89	16.4	4.00	7.6		
90.9	77.5	40.9	49.5	18.4	27.5	8.27	15.4	3.72	7.1		

Medium Particle Size ($D_{v,50}$) = 41.57 μm

Figure 4-25. Sil-Co-Sil 250 PARTICLE SIZE DISTRIBUTION

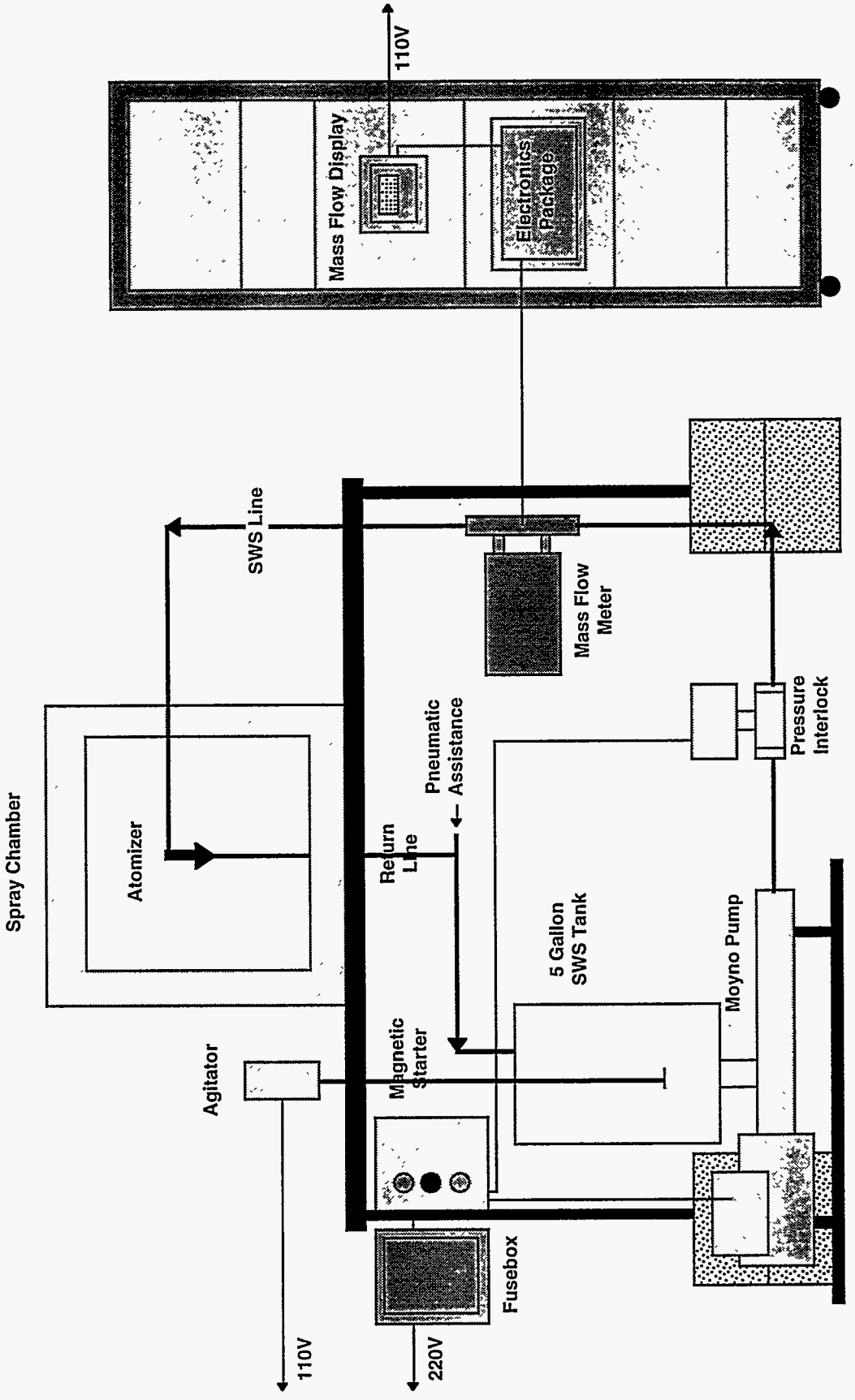

Figure 4-26. EXPERIMENTAL SETUP

After atomization, spent slurry is collected in 1/2" diameter Tygon tubing fastened to the atomizer tip with a hose clamp. The tubing feeds a return line at the bottom of the chamber in which slurry is conveyed back to the slurry tank for reuse.

Fluid Flow Modeling

FLUENT 4.2 was used to model individual particle impacts within the atomizer nozzle for a SWS mass flow rate of ~500 lb/h. Impact velocities and impingement angles (to be used in the erosion equations) were obtained for a range of 10 particle diameters (10-200 μm) taken to represent specific size fractions contained within the experimental silica distribution (Figure 4-25).

Explicit details of the numerical modeling process and the underlying theory may be found elsewhere[100] and[101].

Erosion Rate Calculation

Experimental

Experimental values of erosion rate were calculated by dividing the mass lost from an orifice disk after 30 minutes of slurry exposure by the mass of SWS which *resulted* (not all slurry that moves through the nozzle contains silica that does damage) in the erosion. Erosion rate is therefore expressed as:

$$E_{\exp} = \frac{\Delta m}{m_{SWS}} \tag{4-9}$$

where Δm is the total mass lost from the orifice (kg), and m_{SWS} is the mass of slurry which caused material loss (kg).

The mass of SWS passing through the atomizer with potential to cause erosion (m_{SWS}) was estimated from the CFD calculations to be 30% of the total mass throughput by noting an inlet location (inlet to the mixing region) which separated an area of no predicted impact from an area of potential particle impact. Equation 4-9 may then be rewritten as follows:

$$E_{\exp} = \frac{\Delta m}{0.3 M_{tot}} \tag{4-10}$$

where Δm is the change in orifice mass (kg), and M_{tot} is the total mass of SWS throughput (kg).

Theoretical

The dimensionless erosion rate E (kg/kg) of a ductile target impacted by a mass of particles having a velocity V and an angle α is predicted by Sundararajan[98] to be

$$E = \left(2^n C V^2 \sin^2\alpha F(t) / n C_p\right)\left[1 + \left\{(n+1)(\psi/\mu_c)(2-\psi/\mu_c) / 4(1+\lambda)\tan^2\alpha F(t)\right\} - e^2\right]. \tag{4-11}$$

All nomenclature used in Equation 4-11 is described in Section 8.0. The equations used to derive numerical quantities for nomenclature given in Section 8.0 are extensive and the interested reader is referred to references[98, 102-107].

The theoretical considerations from which the model was derived account for erosive attack by a homogenous abrasive particle stream, i.e. uniform impact characteristics (velocity and angle). Actual erosive environments, e.g. atomizers, are not homogenous and Sundararajan's original equations must therefore be modified to predict the erosion rate of a surface exposed to an ensemble of impact conditions.

The calculation of erosion rate by a particle distribution is performed by numerically integrating Equation 4-11 over the range of conditions experienced by the eroding surface. Integration requires that the equation be rewritten in terms of the impact variables V and α (velocity and angle, respectively). Expansion and simplification yields a three term equation for E having the form:

$$E = E_1 + E_2 + E_3 \tag{4-12}$$

where

$$E_1 = \frac{2^n C F(t)}{n C_p} V^2 \sin^2 \alpha \tag{4-13}$$

$$E_2 = 0.95 \frac{2^n C H^{5/8} \mu (n+1)}{n C_p E_e^{1/2} \rho_p^{1/8}} V^{1.75} \frac{\sin^2 \alpha}{\tan \alpha} \tag{4-14}$$

and

$$E_3 = -1.9 \frac{2^n C F(t) H^{5/8}}{E_e^{1/2} \rho_p^{1/8}} \left[\frac{\mu^2 (1+\lambda)(n+1)}{4F(t)} + 1.9 \frac{H^{5/8}}{E_e^{1/2} \rho_p^{1/8}} \right] V^{1.5} \sin^2 \alpha. \tag{4-15}$$

The calculation of mass lost from the atomizer's orifice disk required that Equations 4-13 to 4-15 be evaluated for each particle size at every impact location. Analysis of the erosion equations was simplified from double integration (velocity and angle) to single integration (velocity) by noting that results of the CFD simulations predicted only small fluctuations (typically ± 1°) in impact angle within the boundaries of reported particle impact. Calculations were therefore performed by designating three surface regions of the orifice, illustrated in Figure 4-27, where fluctuations of impact angle were assumed negligible.

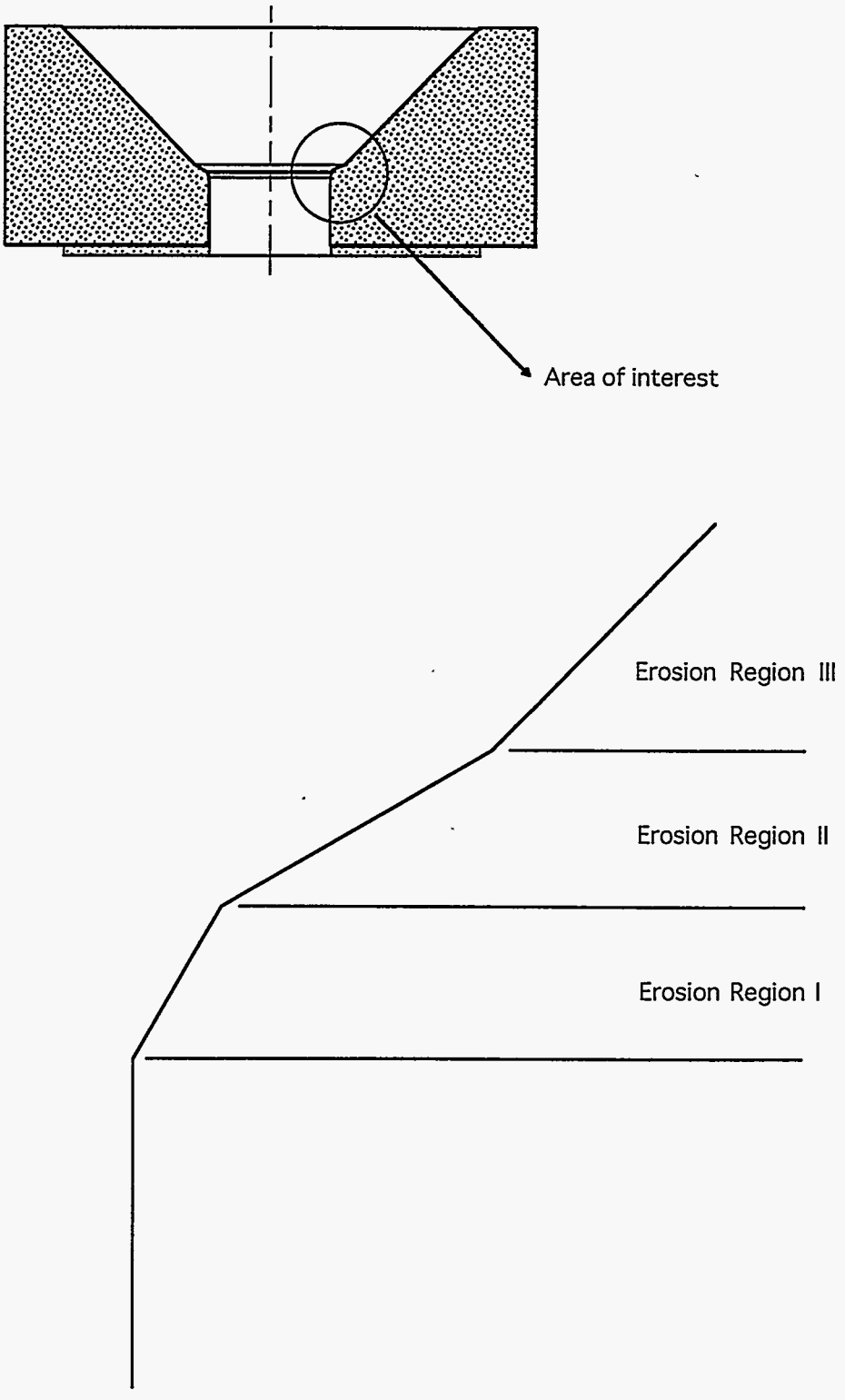

Figure 4-27. EROSION ZONES

Impact angle was taken to be constant and velocity was treated as a linear function of position within the boundaries of each erosion region. Equations 4-13 to 4-15 were then integrated with respect to the axial (z) position using velocity functions derived from a least squares curve fit of the CFD data. Rewriting:

$$E_1 = \frac{2^n CF(t)\sin^2\alpha}{nC_p}\int_{z1}^{z2} V^2 dz \tag{4-16}$$

$$E_2 = 0.95\frac{2^n CH^{5/8}\mu(n+1)\sin^2\alpha}{nC_p E_e^{1/2}\rho_p^{1/8}\tan\alpha}\int_{z1}^{z2} V^{1.75} dz \tag{4-17}$$

$$E_3 = -1.9\frac{2^n CF(t)H^{5/8}\sin^2\alpha}{E_e^{1/2}\rho_p^{1/8}}\left[\frac{\mu^2(1+\lambda)(n+1)}{4F(t)} + 1.9\frac{H^{5/8}}{E_e^{1/2}\rho_p^{1/8}}\right]\int_{z1}^{z2} V^{1.5} dz\,. \tag{4-18}$$

The limits of integration for Regions I and II were taken to be the geometric boundaries of each erosion zone. Integration limits for Region III were defined for each particle size based on the lower boundary (between Regions II and III) and the uppermost impact position, obtained from CFD impact predictions of the type presented in Figure 4-28.

The computational software Mathcad 3.1[108] was used to evaluate erosion integrals in each of the three erosion zones for each of the ten particle sizes modeled. Total erosion attributed to each particle size was calculated from the sum of the erosion rates produced in each zone, e.g.,

$$E^{tot}_{100\mu m} = E_1 + E_2 + E_3\,. \tag{4-19}$$

Erosion rate was predicted for the complete particle size distribution by assuming the results for the ten sizes modeled could be weighted to include the effects of any species not explicitly considered in previous calculations. Weighting factors were derived based on inspection of the experimentally determined size distribution (Figure 4-25) and the assignment of a percentage of that distribution to be represented by one of the modeled sizes (It was assumed that particle distribution was constant throughout the slurry.). The percentage of the distribution assigned to each particle size was then divided by the percentage contained in the smallest size fraction yielding a value for relative impaction frequency.

Data obtained from the procedure described above predicts the theoretical mass loss from a rectangular scar on the orifice surface. Results are based on the two dimensional particle tracks produced by the CFD simulations and therefore neglect particle impact on the complete circumference of the orifice face. The comprehensive erosion rate was calculated by assuming symmetric particle

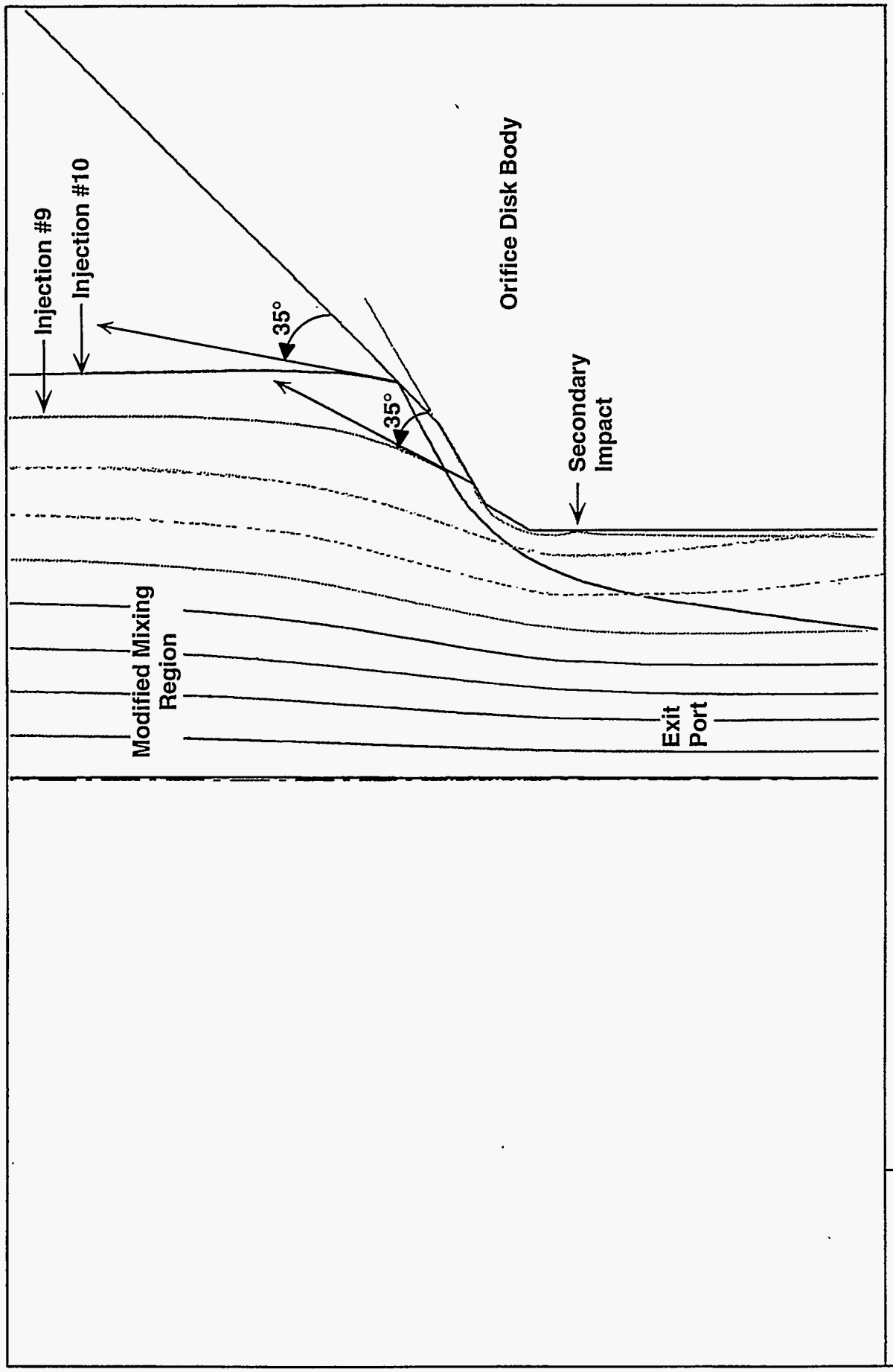

Figure 4-28. PARTICLE TRAJECTORIES
Diameter = 181.5 μm

behavior within the mixing region and determining the number of scars contained on the eroding surface. Multiplying erosion rate of the scar by the total number of theoretical scars yielded the comprehensive erosion rate of the surface in terms of kg/(kg SiO_2).

Multiplication of the predicted erosion rate by the solids loading of the slurry, as measured at the nozzle exit (~8 %), converted kg/(kg SiO_2) to kg/(kg SWS) and allowed direct comparison of theory with experiment.

Results

The 95% confidence interval (adjusted using Student's t statistic[102]) obtained from six experimental erosion calculations and the corresponding theoretical prediction are $3.44 \times 10^{-7} \pm 2.04 \times 10^{-8}$ and 1.8×10^{-7} respectively, for 10% silica-water slurry delivered to the atomizer nozzle at 500 lb/h for 30 minutes. The theoretical model predicts a value of erosion rate approximately two times smaller than the experimentally determined average. In an attempt to simplify erosion calculations, the modeling procedure ignored the possibility of multiple impact (per particle) and erosion within the cylindrical region of the orifice disk (i.e., the exit port). Inspection of numerical data obtained from CFD simulations (Figure 4-28) and SEM micrographs of the eroded surface (Figure 4-29) indicate both assumptions to be an oversimplification of the problem resulting in the underestimation of erosion rate.

Conclusions

The comprehensive erosion model of Sundararajan has been extended from the conditions of its derivation (homogenous particle stream, identical surface characteristics) and applied to the practical problem of atomizer nozzle erosion. FLUENT 4.2 was used to model the dilute two-phase flow field and predict silica particle trajectories within a modified fuel oil atomizer at ~500 lb SWS/h. Information obtained from particle trajectory analysis was input into the modified erosion equations and the results weighted to account for silica species not explicitly treated. Summation of the weighted erosion results and integration over the orifice surface yielded a value of the theoretical erosion rate which was a factor of two smaller than the experimental average obtained at similar conditions.

The agreement between theory and experiment is considered satisfactory and represents a significant advance in atomizer erosion analysis. Extension of analytical techniques developed in this study to coal-liquid systems and twin-fluid atomizers is a promising area of future research and will require fundamental treatments of three-phase fluid mechanics and non-Newtonian slurry flows.

4.2.3 Erosion/Deposition Study

This component of the research program addresses the impact of ash and unburned char particles on the performance of heat exchanger tubes in the convective section of the demonstration boiler. Since carbon steel is the material universally used for convective heat exchangers in package boilers, the investigation is centered on the performance of this material. A plan of the boiler showing the location of the erosion test probe is given in Figure 4-30. The erosion test

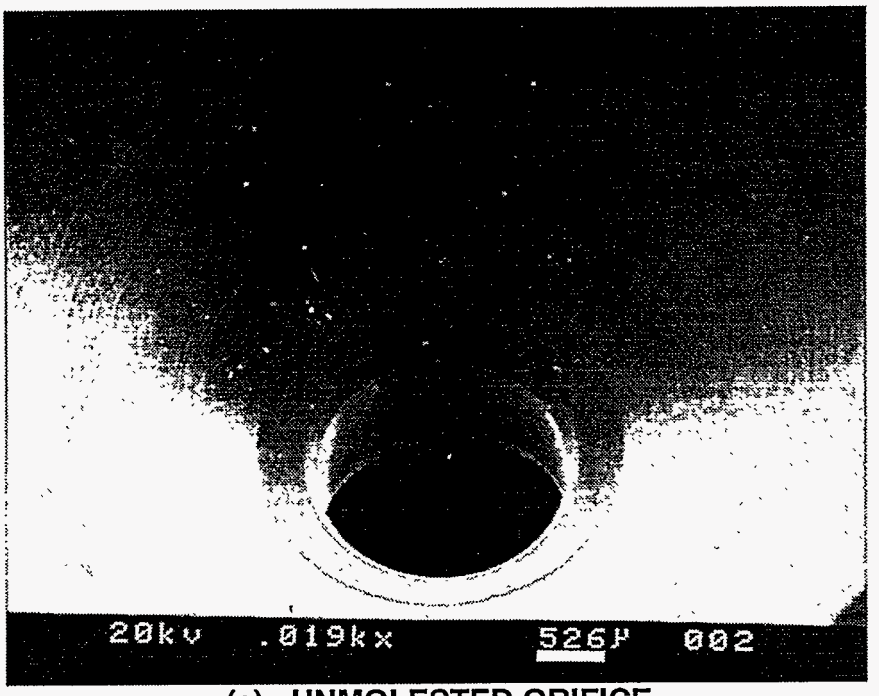

(a). UNMOLESTED ORIFICE

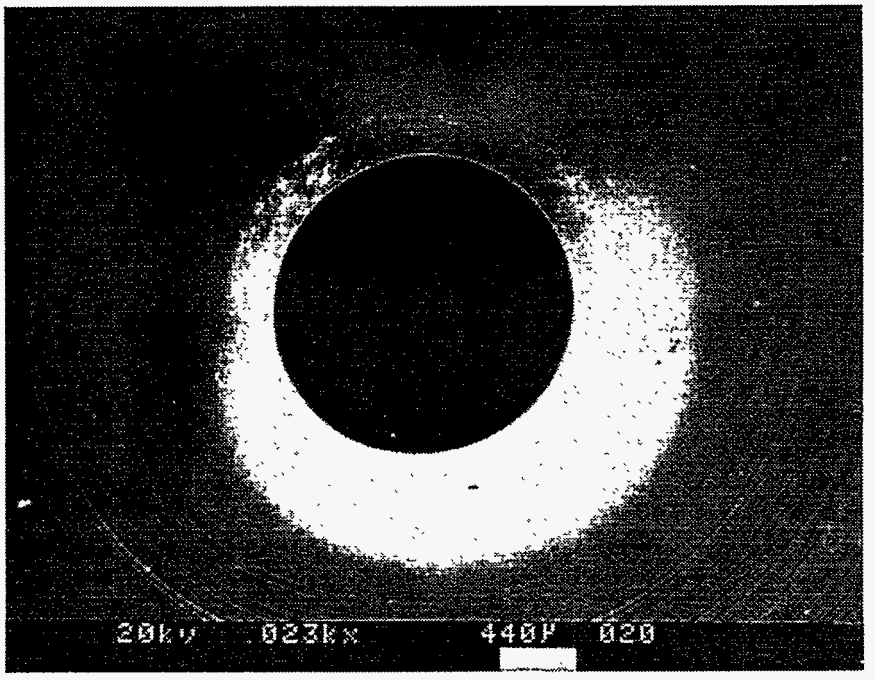

(b). ERODED ORIFICE SHOWING DAMAGED EXIT PORT

Figure 4-29. ELECTRON MICROGRAPHS OF UNMOLESTED SURFACE (a) AND ERODED ORIFICE SHOWING DAMAGED EXIT PORT (b)

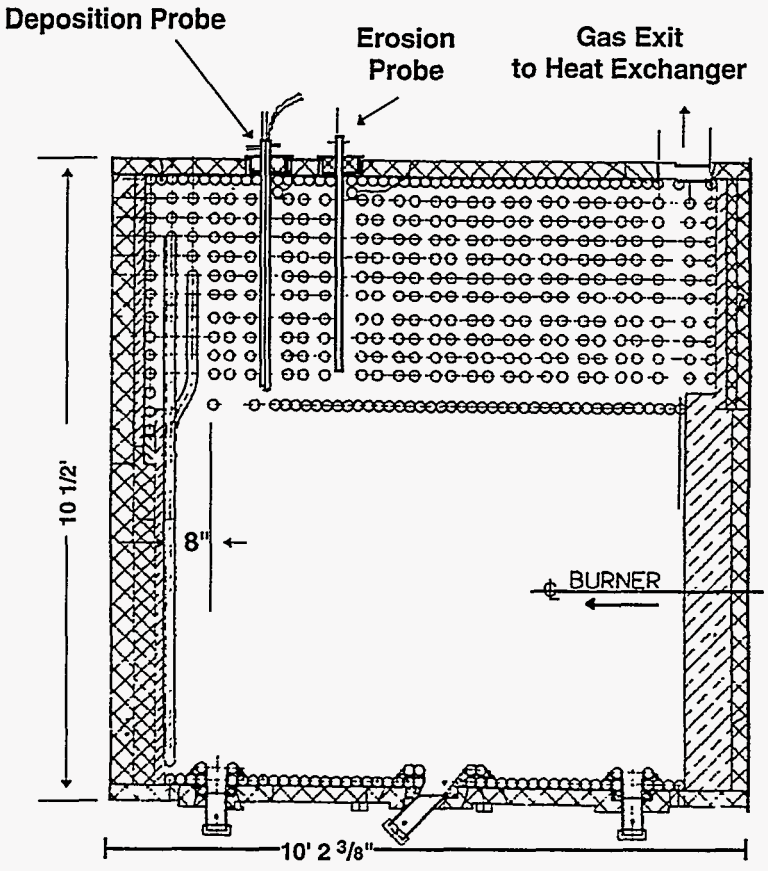

Figure 4-30. PLAN VIEW OF THE FURNACE AND CONVECTIVE SECTION OF THE BOILER AND ARRANGEMENT OF THE PROBE FOR EROSION TESTS

probe was used for this erosion/deposition study.

Test Conditions

Measurements on erosion and deposition have been completed for two candidate fuels, MCWM and DMC, both prepared using high volatile A bituminous coal from the Brookville seam in Lawrence County, Pennsylvania. The properties of the MCWM and DMC are listed in Table 4-1. The MCWM contained 58.4% solids having a mean coal particle size of 23 μm. The DMC had a mean diameter of 22 μm. The experimental measurements were obtained during MCWM and DMC testing during the SCCWS and ABB CE programs, respectively, along with preliminary model development. The final model development and its interpretation were done in Phase I of this program.

The combustion conditions under which the measurements were made are listed in Table 4-2. When the boiler was cofiring MCWM and natural gas, the latter provided 31.5% of the heat input[109]. Modifications were made to accommodate the HEACC[87, 110, 111], and the boiler was able to fire 100% DMC. Table 4-2 shows the boiler heat input, carbon conversion, and NO_x/SO_2 emissions for MCWM and DMC.

Conditions at the location of the probe are listed in Table 4-3. The flue gas temperature was averaged over the test period. Convective section gas velocity and particle concentration were calculated using boiler dimensions and material balances. The particles collected in the baghouse contained residual combustibles and ash. The apparent density of the particles was determined from their settled volume, assuming a voidage of 0.42[112]. The volume-based size distributions of particles in the baghouse catch are shown in Figure 4-31.

Erosion-Corrosion

Specifics of the probe may be found elsewhere[109]. A small orifice, 1.7 mm inside diameter, was supported on a sidearm attached to the probe and supplied with compressed gas from a cylinder outside the boiler. The rate of erosion was enhanced by directing a small jet of clean gas to accelerate the particles toward the surface of a test coupon. Details of the jet and metal sample, with some examples of particle trajectories, are shown in Figure 4-32.

The initial jet velocity at the orifice was 200 m/s during all of the measurements reported. The jet issuing from the nozzle was oriented with its axis parallel to the flue gas flow and perpendicular to the surface of the sample. Specimens of carbon steel were cut from 25.4 mm outside diameter ASTM A179 tube having the following composition (weight basis): C, 0.08%; Mn, 0.42%; P, 0.027%; S, 0.017%; Si, 0.030%; Al, 0.048%; and Fe, balance. A flat area, 38 x 10 mm, was machined, ground, and polished to roughness less than 0.05 μm on the outside of each test piece, for the erosion measurements.

The samples were mounted in the opening formed by cutting an identical section from the air-cooled support. The temperature of the target was controlled by adjusting the cooling air flowrate and measured using two thermocouples located in recesses drilled into the back side of the

Table 4-1. Properties of the MCWM and DMC

Fuel Type	MCWM	DMC
Proximate Analysis (wt%, as-received)		
Moisture	41.6	6.4
Ash	2.1	3.3
Volatile Matter	21.1	33.5
Fixed Carbon (difference)	35.2	56.8
Ultimate Analysis (wt%, as-received)		
Moisture	41.6	6.4
Ash	2.1	3.3
Carbon (C)	46.6	74.5
Hydrogen (H)	3.2	5.0
Nitrogen (N)	0.9	1.5
Sulfur (S)	0.5	0.7
Oxygen (O) (difference)	5.1	8.6
Higher Heating Value (MJ/kg, as-received)	19.3	31.0
Particle Size Distribution: Fraction under the Size (μm, volume-based)		
10 %	4	6
50 %	23	22
90 %	78	62

Table 4-2. Operating Conditions and Flue Gas Composition

Fuel Type	MCWM	DMC
Fuel Firing Rate (MWth)		
Coal	3.8	4.4
Gas	1.7	-
Total	5.5	4.4
Carbon Conversion (wt%)		
Coal	87	94
Gas	100[a]	-
Total	91	94
Flue Gas Composition[b]		
N_2 (vol %)	68.3[c]	75.4[c]
H_2O (vol %)	14.3[c]	6.9[c]
CO_2 (vol %)	13.6	14.2
O_2 (vol %)	3.7	3.4
CO (vol ppm)	190	480
SO_2 (vol ppm)	430	430
NO_x (vol ppm)	570	410

[a]Assuming the combustion to be complete.
[b]At the exit of the boiler.
[c]Calculated.

Table 4-3. Conditions in the Convective Section and Composition of the Particles

Fuel Type	MCWM	DMC
Parameters of Flue Gas near the Erosion Probe		
Temperature (K)	850	890
Velocity (m/s)	4.0[a]	3.1[a]
Particle Loading (g/m^3)	2.7[a]	3.0[a]
Fly Ash and Unburned Char Particles (wt%, dry)		
Ash	23	37
Combustible	77[a]	63[a]
Ash Composition[b] (wt%, dry, SO_3 free)		
SiO_2	49.4	50.3
Al_2O_3	35.7	35.2
TiO_2	1.2	1.4
Fe_2O_3	7.3	6.6
CaO	2.7	3.2
MgO	0.6	0.7
Na_2O	0.5	0.4
K_2O	1.3	1.5
Other (difference)	1.3[a]	0.7[a]

[a]Calculated.

[b]Sample from baghouse.

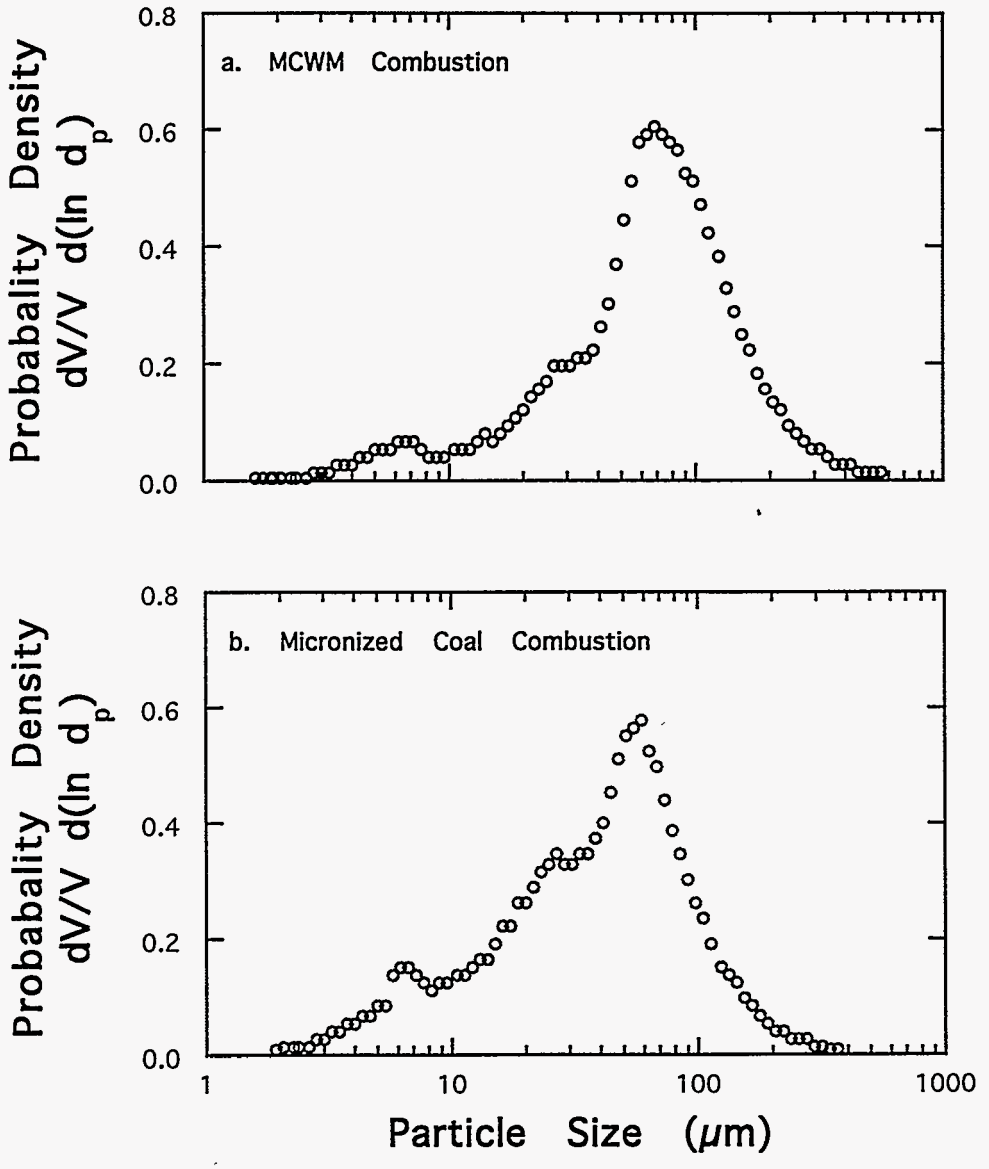

Figure 4-31. TYPICAL VOLUME-BASED SIZE DISTRIBUTIONS OF PARTICLES COLLECTED IN THE BAGHOUSE, DETERMINED USING A MALVERN DROPLET AND PARTICLE SIZER

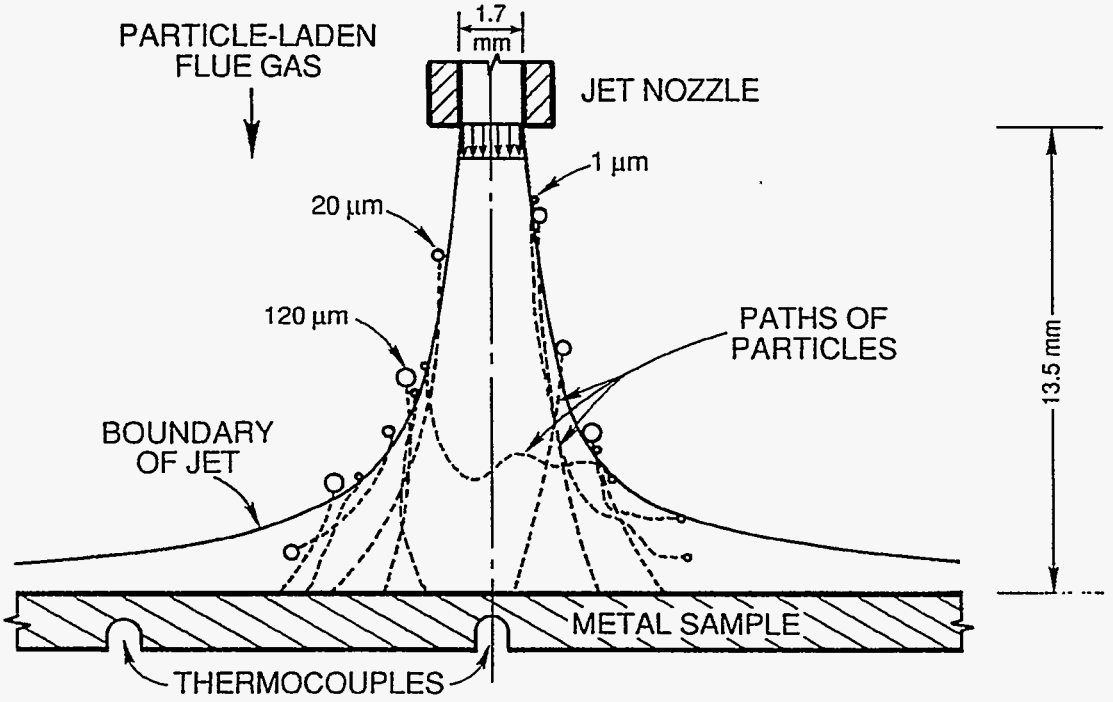

Figure 4-32. ARRANGEMENT OF THE METAL SPECIMEN, THERMOCOUPLES, AND GAS JET USED TO ACCELERATE PARTICLES TOWARD THE SAMPLE SURFACE

sample, one on the axis of the jet and the other 10 mm away. The difference in temperature indicated by the thermocouples was 10 K at the highest sample temperature.

Conditions which were varied during the tests were metal temperature and jet gas oxygen content. Measurements were made at metal temperatures of 450, 550, and 650 K. The jet gases were: nitrogen, dry air, and pure oxygen for the measurements of erosion during MCWM combustion; and nitrogen, a mixture of 3 vol.% oxygen in nitrogen, and dry air for the erosion measurements during DMC combustion. Some oxygen was present as an impurity in the nitrogen gas, at a typical level of 3 ppm.

Each sample was exposed to the effects of the jet and particles for 2 hours. After a test, the shape of the surface of the sample was measured using a profiler and the erosion craters and surface structure were examined using a scanning electron microscope. The profiles and electron micrographs of samples treated under all of the combinations may be found elsewhere[109, 113]. The maximum erosion depths in each surface profile were converted to time-averaged rates, assuming constant rate of material loss over the 2-hour exposure period. The averages of these maximum rates, with estimates of their uncertainty, are plotted as a function of temperature for each jet gas in Figures 4-33 and 4-34.

The dependence of the erosion rate on temperature and oxygen partial pressure is summarized as follows: the rate of metal loss was lowest at low temperature, regardless of the oxygen concentration; it was also slow under strongly oxidizing conditions, at high temperature and high oxygen concentration; and erosion was most rapid at high temperature in the presence of very low oxygen concentration.

A model for simultaneous erosion and oxidation of carbon steel has been developed[113-115]. In the model, metal undergoes ductile erosion, increasing with increasing temperature, while oxide exhibits brittle erosion, at a rate independent of temperature. Oxide and metal are removed in series, their proportions depending upon their relative resistance to erosion and the steady average thickness of the scale. Over most of the range of temperatures investigated, oxide scale was more resistant to erosion than the carbon steel substrate.

Four parameters were adjusted to fit the model to the measurements: 1) Erosivity of the particles toward the metal; 2) Erosivity of the particles toward the metal oxide; 3) Effective order of the metal oxidation process with respect to oxygen; 4) Average area of scale removed by a single impact. A procedure for determination of erosion rate coefficients from the measurements may be found elsewhere[113]. Comparisons between the calculated and measured results are shown in Figures 4-33 and 4-34.

The characteristic dependence of erosion on temperature arises from the model calculations as follows. At the low end of the temperature range, the oxidation rate of carbon steel is slow, the oxide layer is very thin, the erosion behavior is that of bare metal, and the erosion rate therefore increases with increasing temperature. Because the oxidation rate is so slow, oxygen partial

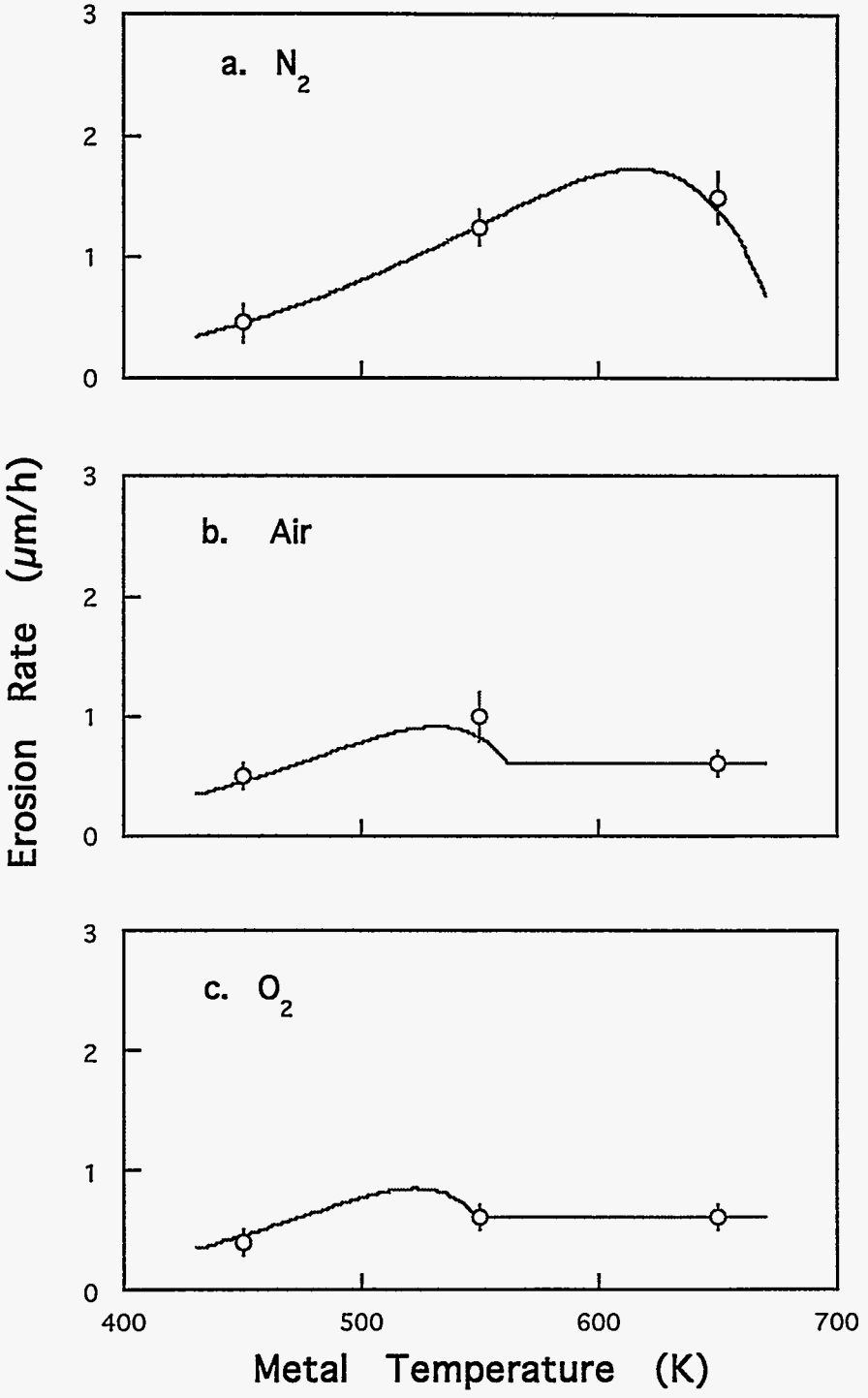

Figure 4-33. MEASURED AND CALCULATED EROSION RATES OF CARBON STEEL AS FUNCTIONS OF TEMPERATURE AND THE JET GAS OXYGEN CONTENT UNDER THE CONDITIONS OF MCWM COMBUSTION

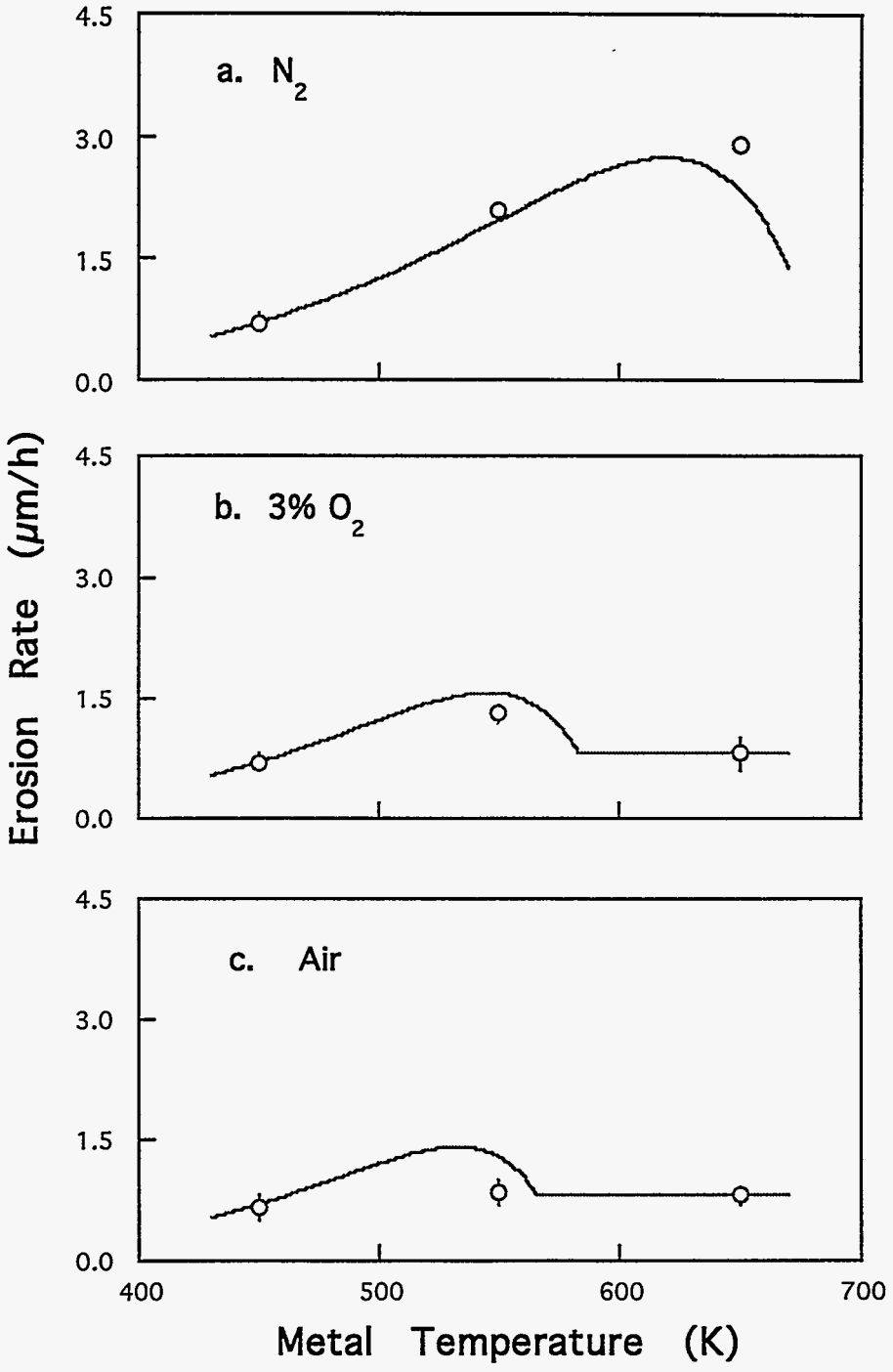

Figure 4-34. MEASURED AND CALCULATED EROSION RATES OF CARBON STEEL AS FUNCTIONS OF TEMPERATURE AND THE JET GAS OXYGEN CONTENT UNDER THE CONDITIONS OF DMC COMBUSTION

pressure has little effect on the steady oxide thickness or erosion rate, as shown by comparison of the measurements at 450 K in nitrogen, air, and oxygen.

As temperature is increased, the oxidation rate increases, with a corresponding increase in the steady thickness of oxide scale. As the thickness of scale increases, the fraction of oxide in the eroded material increases, and the influence of the oxide on erosion behavior increases. Over most of the temperature range investigated, the oxide is more resistant to erosion than the metal, therefore, as the contribution of oxide to eroded volume increases with increasing oxygen partial pressure, the erosion rate declines.

When the oxidation rate is sufficiently high, the scale on the metal surface is large enough that the erosion rate is that which is characteristic of pure oxide, which is independent of temperature. This is the situation under the most oxidizing conditions, on the right hand sides of Figures 4-33b, 4-33c, 4-34b, and 4-34c. As shown by the calculations for air and oxygen gases, increasing oxygen partial pressure shifts the transition from metal to oxide erosion toward lower temperature.

Using the experimentally determined values for the erosion rate coefficients and the oxidation rate coefficient which fit the measurements, the erosion-oxidation loss was calculated for a tube having a diameter of 51 mm and metal temperature of 550 K. The typical conditions in the convective section of the boiler during MCWM combustion were: gas temperature 850 K, excess oxygen 3.7 vol.%, particle loading 2.7 g/m^3, particle density 870 kg/m^3, and particle size of 65 μm. During DMC combustion, gas temperature was 890 K, excess oxygen 3.4 vol.%, particle loading 3.0 g/m^3, particle density 835 kg/m^3, and particle size 43 μm. The impaction efficiency on the tube was obtained using the correlations of Israel and Rosner[116] and Serafini[117], as described by Walsh et al.[118]. Ductile erosion of metal and brittle erosion of oxide are expected to be most rapid at impaction angles of 30° and 90°, respectively. The erosion rates at these locations, as functions of the convection section gas velocity, are shown in Figures 4-35 and 4-36.

At low velocity the erosion rate is low, and erosion occurs only from the oxide layer. Increasing the gas velocity increases the rate of oxide removal and decreases the steady thickness of the scale. At a critical velocity, the oxide layer becomes thin enough that erosion removes both oxide and metal, and the rate begins to increase markedly. The critical velocities are 21 m/s for MCWM and 25 m/s for DMC at an impaction angle of 30°, but these values decrease to 12 m/s and 16 m/s, respectively, for impaction at 90°, the angle at which brittle erosion of oxide is greatest.

Raask[90] considered 0.05 μm/h to be the highest acceptable rate of tube thickness loss. According to the model, erosion at collision angles near 30° is below 0.05 μm/h for gas velocities up to approximately 12 m/s for MCWM and 15 m/s for DMC. However, erosion at an impaction angle of 90°, on the upstream stagnation line of the tube, is only expected to be less than this rate at flue gas velocities below approximately 8 m/s for MCWM and 10 m/s for DMC. These are the estimated upper limits on gas velocity when firing MCWM with natural gas and when firing DMC

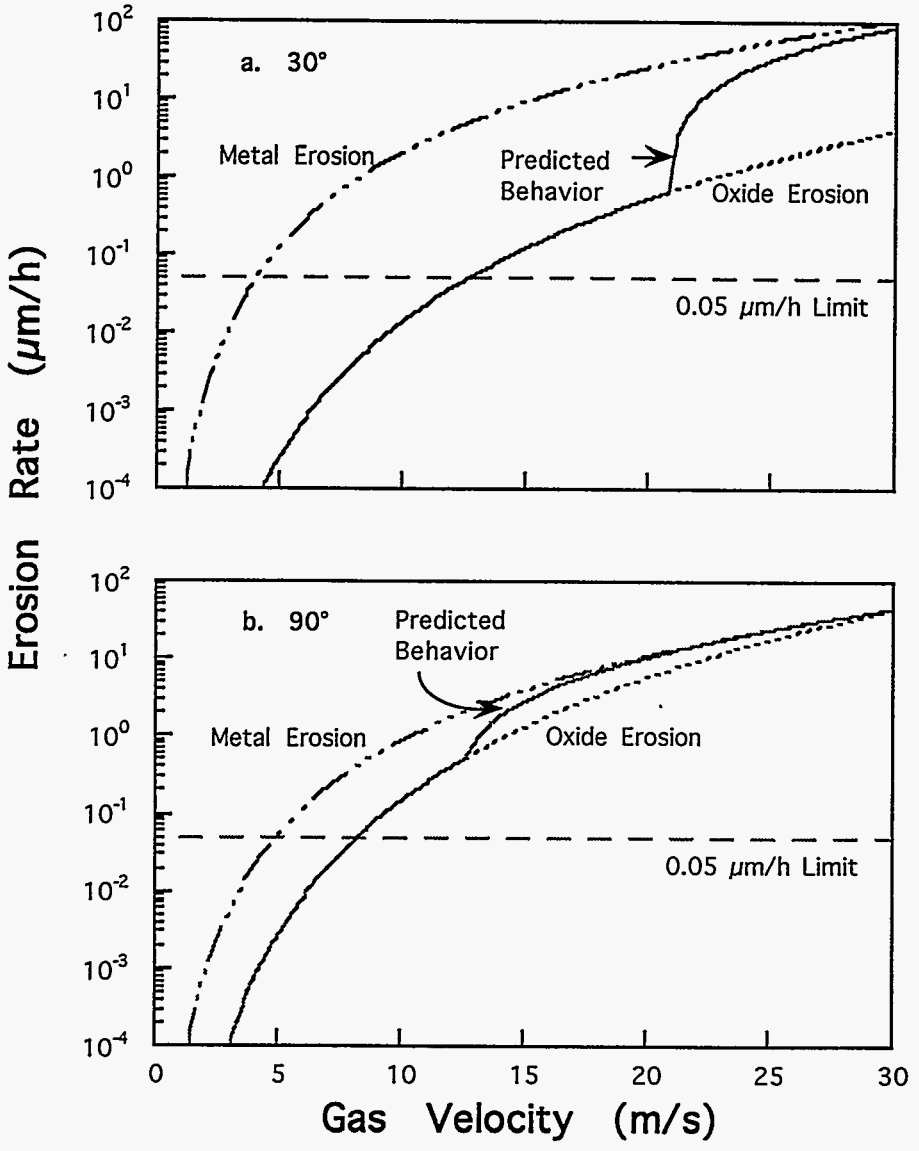

Figure 4-35. ESTIMATE OF THE EROSION RATE OF CARBON STEEL BY PRODUCTS OF MCWM COMBUSTION AT IMPACTION ANGLES 30° AND 90°

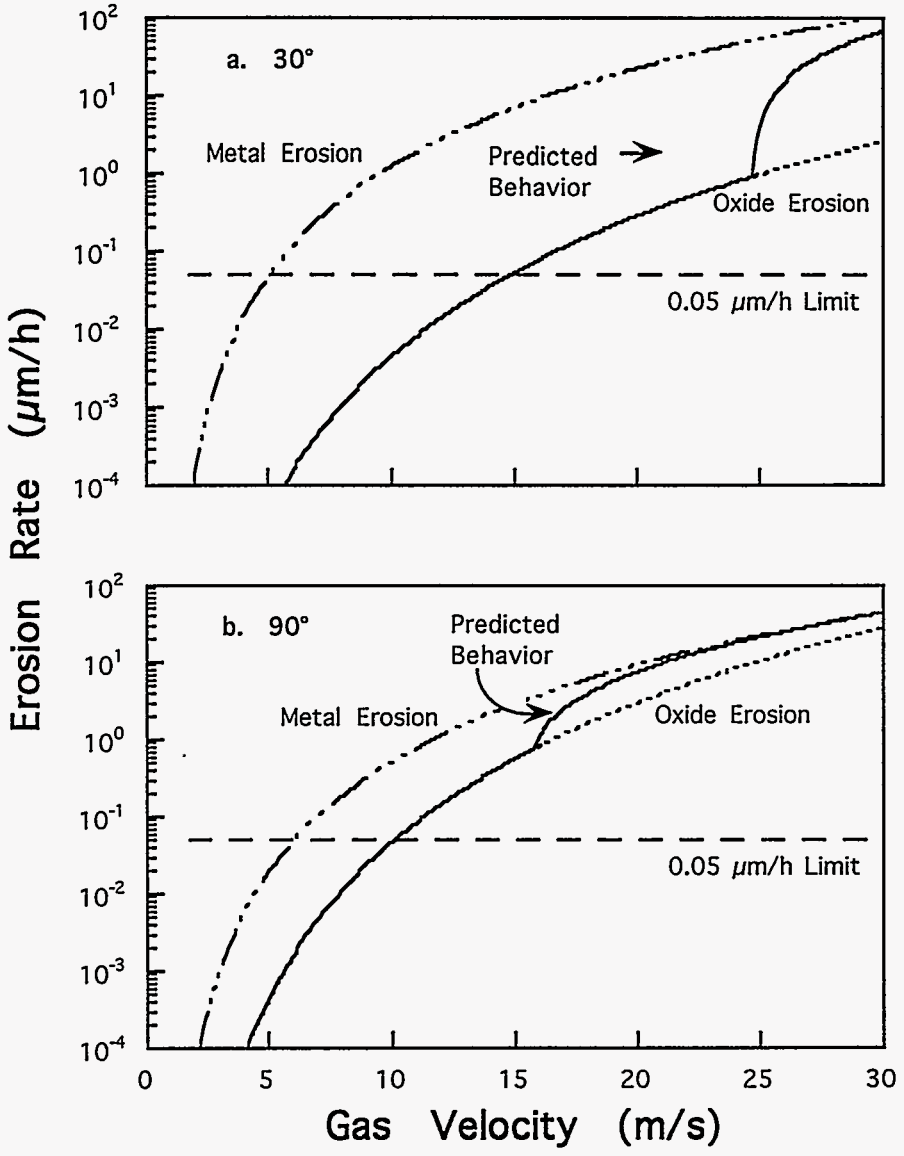

Figure 4-36. ESTIMATE OF THE EROSION RATE OF CARBON STEEL BY PRODUCTS OF DMC COMBUSTION AT IMPACTION ANGLES 30° AND 90°

alone, under the conditions of metal temperature, particle size, particle composition, and particle loading investigated.

Deposition of Ash

Deposition of ash on heat exchanger tubes has direct impact on the boiler rating and maintainability. Measurements of ash deposition in the convective section of the boiler were presented in previous reports[67, 68]. A test probe of 25.4 mm diameter was air-cooled to maintain its temperature level and placed in the convective section for a period of time within the sootblowing interval. Removal of the accumulated ash covering the circumference of the probe showed patterns of deposition versus angle with respect to the flow direction, as shown in Figure 4-37. The mass amount of ash deposit, collected from 12 sectors at the circumference of the probe, was converted to time-averaged rates, assuming constant rate of deposition over the exposure period.

Figure 4-37a shows the rate of ash deposition during combustion of MCWM. The deposits were found on the downstream side of the tube, but they were very thin over almost the entire upstream half of the tube. A maximum rate of about 4.4 g/m^2-h was found in the region from 90° to 135° away from the upstream stagnation line. The probe temperature was 450 K. At higher tube temperatures, less deposits or clean tubes were observed. The fine dashed lines in Figure 37a correspond to the sectors where ash deposits were collected.

During combustion of DMC, the deposits were found over all the sectors at the circumference of the probe, as shown in Figure 4-37b. The maximum rate of 26 g/m^2-h (at temperature of 450 K) was 6 times of that in Figure 4-37a. As the probe temperature rose from 450 to 650 K, the temperature gradient between the probe and flue gas decreased, and deposition declined. The deposits on the probe at temperature of 450 K were relative thin at angular positions from -45° to 45°.

The trajectories of particles suspended in the gas around the probe in crossflow, described elsewhere[119], are shown in Figure 4-38. Small particles ($\leq$ 10 μm) respond to the changes in direction of the gas flow and pass around the tube under the aerodynamic drag on the particles. However, in the presence of a temperature gradient within the boundary layer around the heat exchanger tubes, the thermophoretic force causes diffusion toward the lower temperature region, and deposition of fine particles occurs on the surface of the tube. Most of the particles found in the deposits collected during combustion of MCWM have sizes between 0.5 and 5 μm. The sizes of the particles in the deposits collected during combustion of DMC were up to 20 μm.

Because the thermophoretic velocity of particles is proportional to the gradient in the gas temperature perpendicular to the tube surface, and because the gradient is steepest on the upstream stagnation line of the tube, deposition by this mechanism is expected to be greatest on the upstream side. The measurements, shown in Figure 4-37, indicate that the opposite was the case; the deposit was thickest on the downstream side, suggesting that deposition is offset by erosion. As

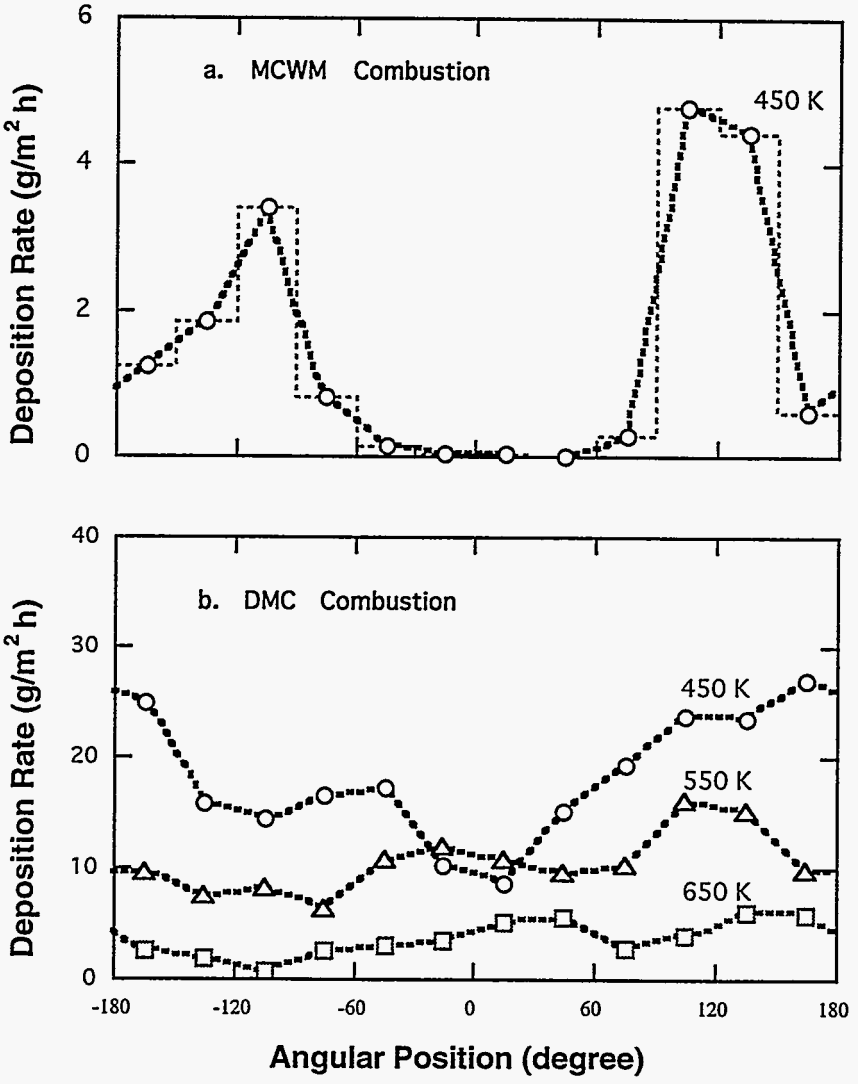

Figure 4-37. DEPOSITION OF ASH ON AN AIR-COOLED TUBE EXPOSED TO THE CONVECTIVE SECTION FLOW AT 4.0 m/s FOR MCWM AND 3.1 m/s FOR DMC

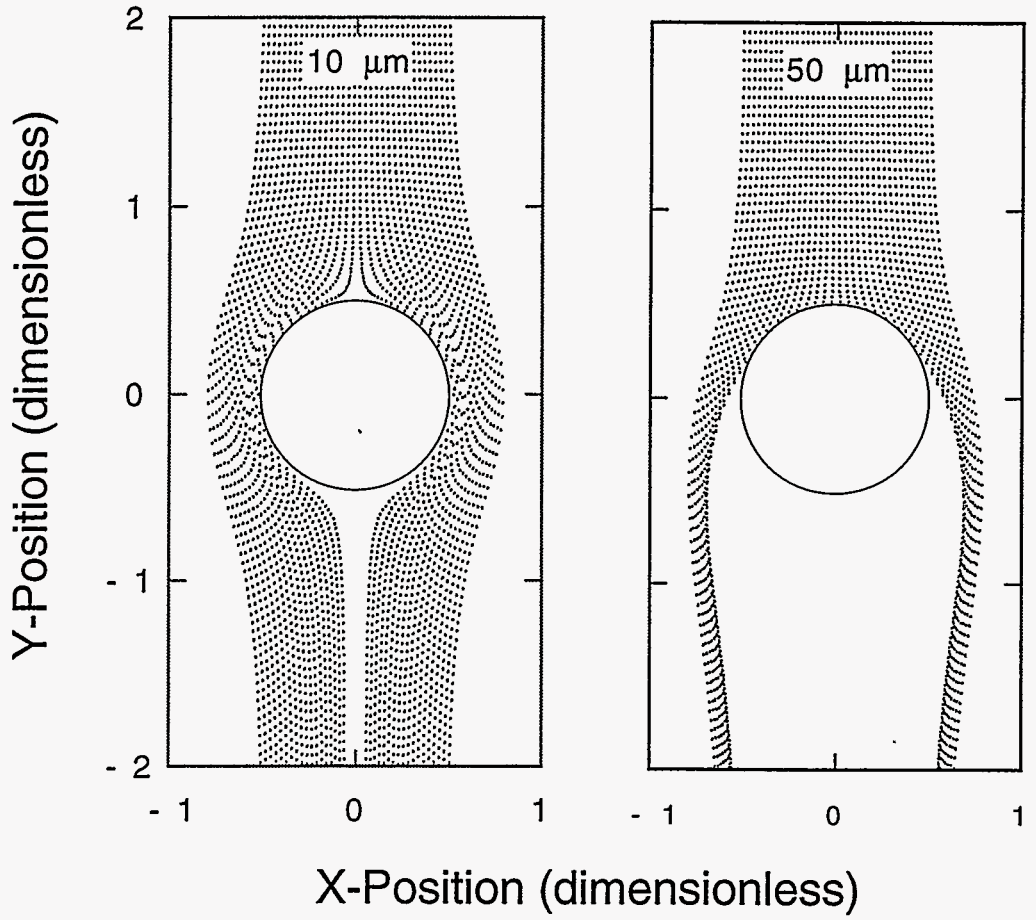

Figure 4-38. TRAJECTORIES OF PARTICLES AROUND A SINGLE TUBE UNDER TYPICAL CONDITIONS IN THE CONVECTIVE SECTION OF THE BOILER

shown in Figure 4-38, large particles (≥ 50 μm), whose behavior is dominated by inertia, collide with the front surface and cause the removal of deposit. Therefore, the observed deposition rate is the difference between the deposition and removal rates.

Details for simulation of ash deposition may be found in a previous report[67]. An increase in gas velocity has two effects: 1) it decreases the thickness of the thermal boundary layer of the tube and increases the temperature gradient and thermophoretic velocity, and 2) it increases the rate of erosion of the ash deposit by impacting particles. The total effect of gas velocity on deposit growth on the upstream stagnation line is that: at velocities higher than approximately 3 m/s deposition is offset by inertia impaction, and erosion is the dominant process; at very low velocities (say, less than 3 m/s), where erosion becomes negligible, the deposit will build up rapidly.

The largest local Nusselt number around the circumference of the tube is near the upstream stagnation line. Formation of deposit on the upstream side of heat exchanger tubes cause a significant derating of heat transfer in the convective section of the boiler. When the boiler is firing DMC, the gas velocity in the convective section is about 3 m/s. When firing DMC, deposition of ash caused an increase in the flue gas temperature at the boiler outlet, therefore, sootblowing was frequently used to clean the heat exchanger tubes to maintain the temperature of the gas entering the baghouse[67].

Conclusions

Formation of ash deposit and erosion of tube material by fly ash and unburned char were studied in the convective section of the boiler while firing MCWM and DMC (Brookville Seam coal). Deposition is favored by the relatively low convective section gas velocity and high temperature gradient around a heat exchanger tube. When the demonstration boiler was firing MCWM with natural gas and DMC alone, the rate of deposition was measured in the convective section at gas velocities 4.0 m/s and 3.1 m/s, respectively. Deposition was the dominant process occurring on heat exchanger tubes in the boiler, particularly, while firing DMC.

Erosion of tube material by impaction of particles is expected at high convective section gas velocities. The transition from metal erosion to oxide erosion, with increasing temperature or oxygen concentration, was accompanied by a decrease in the erosion rate. Using experimentally determined values for the erosion rate coefficients, a model for simultaneous erosion and oxidation provided estimates of the erosion rate as a function of the gas velocity in the convective section of the boiler. Under the conditions of metal temperature, flue gas oxygen concentration, particle size distribution, and particle loading investigated, erosion of carbon steel is expected to be slower than 0.05 μm/hour when the gas velocity in the convective section is less than 8 m/s for MCWM combustion and approximately 10 m/s for DMC combustion.

4.3 Pilot-Scale Activities

Pilot-scale atomization and combustion tests were performed in support of the combustion

performance evaluation. The candidate coals identified in Section 3.1 were fired in Penn State's research boiler. All were fired as MCWM, most were fired as DMC. Those that required cleaning by froth flotation, and hence formed a filter cake, were not fired as DMC because they would not be dried for a commercial application. Atomization studies were conducted for each of the MCWMs.

The combustion test matrix was:

- Test #1 Upper Freeport seam DMC;
- Test #2 Upper Freeport seam DMC;
- Test #3 Upper Freeport seam DMC;
- Test #4 Upper Freeport seam DMC;
- Test #5 Taggart seam DMC;
- Test #6 Taggart seam DMC;
- Test #7 Upper Freeport seam MCWM;
- Test #8 Upper Freeport seam MCWM;
- Test #9 Indiana VII seam MCWM;
- Test #10 Taggart seam MCWM;
- Test #11 Taggart seam MCWM;
- Test #12 Upper Freeport seam DMC;
- Test #13 Upper Freeport seam MCWM;
- Test #14 Upper Freeport seam MCWM;
- Test #15 Upper Freeport seam MCWM;
- Test #16 Upper Freeport seam MCWM;
- Test #17 Lower Kittanning seam MCWM; and
- Test #18 Indiana VII seam MCWM.

The Indiana VII and Lower Kittanning seam coals were not tested in dry micronized coal form because of the fine wet cleaning methods that are employed to clean the coals. The fine coal product from wet cleaning circuits is in the form of a cake, and from an economics stand point, would only be utilized in slurry form. The slurry tests were limited to one or two tests with a maximum of about 6 hours duration because of the availability of MCWM (except for the Upper Freeport MCWM).

The combustion behavior was characterized in terms of combustion efficiency, temperature profiles resulting from heat release rates, and char/ash morphology. The gas temperature profiles were measured inside the boiler using a Land suction pyrometer. The combustion gas profile was measured with a Lancom portable gas analyzer. The total heat flux measurements were made using a Total Heat Flux meter from Land Combustion. Radiation heat flux measurements were made using an ellipsoidal radiometer from Land Combustion.

The compositional analysis of the as-fired coal was determined using Leco proximate and ultimate analyzers. Calorific values of the fuels were determined using a Parr Adiabatic Calorimeter. Table 4-4 provides the analysis of the coals tested.

The fuels were fired in the 1,000 lb/h watertube research boiler. A description of the research boiler system has been given elsewhere[68]. A ceramic quarl was preheated by a natural gas flame until the surface temperature was approximately 900°F for DMC. DMC was then

Table 4-4. Proximate Analysis of the Coals Tested in the Research Boiler

Coal Seam:	Upper Freeport	Taggart	Lower Kittanning	Indiana VII
Volatile Matter (wt.% dry basis)	31.68	34.47	30.62	30.43
Fixed Carbon (wt.% dry basis)	61.72	61.91	65.82	66.70
Ash (wt.% dry basis)	6.60	3.62	3.56	2.87
Heating Value (Btu/lb dry basis)	14,062	14,879	14,824	13,876

admitted slowly (1 lb of air/lb of coal). The coal firing rate was increased gradually while reducing simultaneously the natural gas rate until the desired load was obtained on coal. A thermal input of approximately 1.6 million Btu/h (MM Btu/h) was held constant throughout the testing with DMC and about 1.9 MM Btu/h for MCWM testing. A higher firing rate when firing MCWM was necessary to maintain a self-sustaining flame. The boiler was operated on coal for about half an hour before ash samples were collected from the hoppers and baghouse. A test was continued thereafter for about four to six hours while collecting ash samples from the hoppers and the baghouse every fifteen minutes. Data were collected at 30 second intervals on pressures, temperatures, emissions, and air flow rates. The data during steady-state operation were then averaged. The ash samples were analyzed for moisture and ash to calculate the combustion efficiency using the ash tracer technique as follows:

$$\text{Combustion Efficiency (\%)} = \left[1 - \frac{A_c\left(100 - A_r\right)}{A_r\left(100 - A_c\right)}\right] \text{x } 100$$

where, A_c = weight percent ash in the coal (dry) and A_r = weight percent ash in the residue (dry).

The flue gas analysis was obtained by a continuous emissions monitoring system interfaced to a data acquisition system (DAS). The flue gas analyzers and the data acquisition system used are listed below. The analyzers included: Beckman Oxygen Analyzer, model 755; Beckman Carbon Dioxide Analyzer, model 864 infrared; Thermo Electron Pulsed Fluorescent SO_2 Analyzer, series 40; Thermo Electron Chemiluminescent NO-NO_2-NO_x Analyzer. A computer was used to collect the temperatures, flow rates, and the flue gas concentration at the economizer outlet. All the signals were relayed to a Texas Microsystems industrial grade computer and processed through a Viewdac software package. The Viewdac display was updated every second and data were recorded from each signal every 30 seconds.

Test Results

Table 4-5 gives a summary of the test conditions, including air and fuel flow rates, flue gas composition, temperatures and combustion efficiencies for each test. In addition to 7-8 hours of heating time burning natural gas, each combustion test lasted between 2 to 6 hours. During this test period, data on temperature profiles, heat flux, gas composition, etc. were obtained using various probes. Since the Upper Freeport and Taggart seams were the only two coals burned both as DMC and MCWM, most of the comparison of data was made with these coals. Indiana VII MCWM tests were conducted with natural gas support because of the limitation of the pump to handle the required flow to achieve 100% thermal load. Therefore, it does not reflect the combustion behavior of the MCWM. Combustion efficiency data of the Indiana VII seam MCWM therefore, was not directly comparable with other slurry data.

Table 4-5. Summary of the Research Boiler Combustion Test Results

Coal Seam:		Upper Freeport	Upper Freeport	Upper Freeport	Upper Freeport	Taggart	Taggart	Upper Freeport
Test No.		1	2	3	4	5	6	7
Fuel Type		DMC	DMC	DMC	DMC	DMC	DMC	MCWM
Test Duration (hours)		2.25	6.00	6.00	5.25	4.00	4.50	4.50
Firing Rate (MMBtu/h)		1.56	1.58	1.78	1.48	1.69	1.52	1.89
Comb. Air Flow (lb/h)		901	863	997	807	919	855	1,020
Atom. Air Flow (lb/h)		Not App.(NA)	NA	NA	NA	NA	NA	113
Atom. Air Pres.(psig)		Not App.(NA)	NA	NA	NA	NA	NA	100
Transport Air (lb/h)		107	114	118	112	112	112	NA
Cooling Air Flow(lb/h)		31	31	31	31	31	31	31
Tertiary Air Flow(lb/h)		324	316	316	324	316	316	391
Steam Flow(lb/h)		Not Meas.(NM)	NM	NM	NM	NM	NM	1,094
MCWM Feed(lb/h)		NA	NA	NA	NA	NA	NA	214
MCWM Solids(%)		NA	NA	NA	NA	NA	NA	63
Comb. Air Temp.(F)		183	258	217	237	161	202	324
Quarl Temp.(F)		1,266	1,349	1,425	1,279	1,330	1,318	1,354
O2 (%)		7.5	6.8	5.8	6.9	5.9	7.0	6.1
Boiler O2 (%)		NM	NM	NM	NM	NM	NM	NM
CO (ppm)		24	174	179	171	123	74	508
CO2 (%)		11.9	15.6	16.3	14.1	13.9	12.7	* 9.6
SO2 (ppm, corr)		241	299	312	247	273	248	314
SO2@3%O2 (ppm)		322	380	371	317	327	319	380
NOx@3%O2 (ppm)		860	844	778	823	748	781	610
Comb. Eff. (based on ash colleted,%)		97.4	100.9	94.9	100.1	95.9	98.8	NA
Ave BH Comb. Eff.(%)		NA	NA	NA	NA	NA	NA	87.6
Ave Hop. Comb Eff.(%)		NA	NA	NA	NA	NA	NA	67.0

* CO2 analyzer was not functioning properly just before Test 8. Since the CO2 concentration during Test 7 is suspect, the problem may have started during Test 7.

** NOx analyzer stopped fuctioning during Test 8, the average concentration given is the average before the problem is encountered.

*** Had to run Test 18 with ~26%(.5 MM Btu/h) gas support.

Table 4-5. Summary of the Research Boiler Combustion Test Results

Coal Seam:	Upper Freeport	Indiana 7	Taggart	Taggart	Upper Freeport	Upper Freeport	Upper Freeport	Upper Freeport	Lower Kittanning	Indiana 7
Test No.	8	9	10	11	13	14	15	16	17	18
Fuel Type	MCWM	MCWM	MCWM	MCWM	MCWM	MCWM	MCWM	MCWM	MCWM	MCWM
Test Duration (hours)	4.00	0.42	6.00	0.83	2.75	3.75	3.75	4.20	3.17	2.37
Firing Rate (MM Btu/h)	1.92	1.47	1.97	1.91	1.92	1.89	1.91	1.77	1.92	*** 1.94
Comb. Air Flow (lb/h)	1,089	868	1,150	1,058	1,019	1,090	1,103	838	1,110	1,032
Atom. Air Flow (lb/h)	111	115	115	115	110	112	109	110	111	113
Atom. Air Pres.(psig)	100	100	100	100	100	100	100	100	100	100
Transport Air (lb/h)	NA	NA	NA	NA	NA	NA	NA	NA	NA	NA
Cooling Air Flow(lb/h)	31	31	31	31	31	31	31	31	31	31
Tertiary Air Flow(lb/h)	391	328	320	328	222	254	260	260	260	260
Steam Flow(lb/h)	1,101	823	1,184	1,181	1,110	1,100	1,084	1,006	1,171	1,119
MCWM Feed(lb/h)	214	225	217	210	207	202	215	230	205	223
MCWM Solids(%)	64	47	61	61	66	67	64	55	65	47
Comb. Air Temp.(F)	304	342	303	299	330	302	309	340	303	315
Quarl Temp.(F)	1,282	1,377	1,255	1,251	1,311	1,230	1,231	1,235	1,275	1,211
O2 (%)	6.5	7.3	5.6	4.8	6.0	6.5	6.4	5.3	5.5	5.3
Boiler O2 (%)	NM	4.89	3.13	3.12	3.66	4.1	3.8	2.3	3.1	2.5
CO (ppm)	520	627	264	264	349	492	459	523	379	762
CO2 (%)	14.9	13.1	14.5	15.5	13.9	13.1	13.3	14.3	14.2	14.0
SO2 (ppm, corr)	310	391	417	416	370	351	320	333	341	308
SO2@3%O2 (ppm)	386	514	488	463	450	437	395	380	397	353
NOx@3%O2 (ppm)	** 619	545	856	832	761	754	695	648	743	668
Comb. Eff. (based on ash colleted,%)	NA	NA	NA	NA	NA	NA	NA	NA	NA	NA
Ave BH Comb. Eff.(%)	88.4	96.2	97.9	97.3	91.5	86.4	87.8	89.1	93.9	95.2
Ave Hop. Comb Eff.(%)	70.0	87.1	81.9	73.2	74.7	74.1	59.4	72.0	83.6	74.3

* CO2 analyzer was not functioning properly just before Test 8. Since the CO2 concentration during Test 7 is suspect, the problem may have started during Test 7.

** NOx analyzer stopped fuctioning during Test 8, the average concentration given is the average before the problem is encountered.

*** Had to run Test 18 with ~26%(.5 MM Btu/h) gas support.

Atomization Characteristics of the MCWMs

Atomization studies were carried out in EFRC's atomization test facility. The characteristics were measured by atomizing the MCWM either from the same batch that was burned in the research boiler or a MCWM that was prepared simulating the properties of the MCWM that was burned. The MCWMs that were used for this study were Upper Freeport, Taggart, and Indiana VII seam MCWMs. Upper Freeport seam MCWM was also used to study the effect of variation of solids loading on the atomization and combustion characteristics. Tables 4-6 to 4-8 and Figure 4-39 give a summary of the atomization characteristics for an Upper Freeport seam MCWM. Since the solids loading was varied in the study for the Upper Freeport seam MCWM, the flow rate had to be varied to obtain constant thermal outputs of 1.5 and 1.9 MM Btu/h. Flows required for 1.5 and 1.9 MM Btu/h were termed low and high fire flow rates, respectively. The data indicate that the atomization becomes coarser (based on D_{50}) as the air to fuel ratio is decreased (from low to high fire) at any given atomization air pressure. A decrease in solids loading (dilute slurries) decreased the mean droplet size for any air to fuel ratio. However, the decrease in the mean droplet size is more significant for the low air to fuel ratio case. Similar trends were also observed for D_{10} for all the atomization pressures tested. However, no significant effect was seen on the D_{90} of the spray of the air to fuel ratios tested in the study.

Temperature Profiles

Figures 4-40 and 4-41 provide the gas temperature profiles as measured by a suction pyrometer for the Upper Freeport and Taggart seam DMCs and MCWMs, respectively. The temperature data for the MCWMs are given in parentheses.

The gas temperature, when firing DMC, was higher than that when firing MCWM. This is due to evaporation of the water in the MCWM. The average difference in the temperature measured across a vertical plane in front of the boiler for the Upper Freeport seam DMC and MCWM is about 337°F. The temperature difference remained about the same from the front of the boiler (exit of the quarl) to the back of the radiant section (313°F). Similar measurements for the Taggart seam DMC and MCWMs shown in Figure 4-41 indicate that the difference in the average temperature in the front section of the boiler is about 260°F, whereas at the back of the boiler (radiant section) it is only 30°F. The higher mean temperatures in the front of the boiler indicate quicker ignition and higher rates of combustion and heat release. Higher combustion efficiencies were obtained in the micronized Taggart tests (both DMC and MCWM) compared to those for the Upper Freeport seam coal. Higher gas temperatures for similar particle size distributions of the starting coal resulted in relatively lower combustion efficiencies for the Upper Freeport seam coal.

For the MCWM tests, the solids loading for the Upper Freeport seam coal was slightly higher than that for the Taggart seam coal on the days these measurements were made. However, it should be noted that for all the tests with Upper Freeport seam MCWM (with varying solids contents and viscosities), the combustion efficiency was lower than during the Taggart seam

Table 4-6. Summary of the Atomization Characteristics of an Upper Freeport Seam MCWM at 60 Psig Atomization Air Pressure

Slurry	D_{90} (μm)		D_{50} (μm)		D_{10} (μm)	
	Low fire flow	High fire flow	Low fire flow	High fire flow	Low fire flow	High fire flow
Upper Freeport	1,034	1,353	86	102	30	31
(67% Solids)	1,054	1,337	83	105	29	32
Upper Freeport	784	1,416	84	107	30	31
(65% Solids)	1,085	1,344	85	100	30	30
Upper Freeport	1,336	879	83	78	29	29
(63% Solids)	1,235	1,274	77	84	28	29
Upper Freeport	1,274	1,260	73	73	29	29
(60% Solids)	1,170	1,274	69	76	30	30
Upper Freeport	1,185	983	53	55	29	27
(55% Solids)	1,142	947	54	55	29	27
Upper Freeport	1,453	1,312	47	54	27	28
(51% Solids)	1,386	1,358	49	51	27	27

Table 4-7. Summary of the Atomization Characteristics of an Upper Freeport Seam MCWM at 80 Psig Atomization Air Pressure

Slurry	D_{90} (μm)		D_{50} (μm)		D_{10} (μm)	
	Low fire flow	High fire flow	Low fire flow	High fire flow	Low fire flow	High fire flow
Upper Freeport	1,223	1,563	82	115	30	31
(67% Solids)	995	1,567	76	112	29	31
Upper Freeport	1,105	998	77	81	28	28
(65% Solids)	1,514	881	83	76	28	27
Upper Freeport	1,429	1,507	77	90	29	29
(63% Solids)	1,480	1,220	81	77	29	30
Upper Freeport	1,416	1,454	70	76	29	30
(60% Solids)	1,557	1,445	82	74	30	29
Upper Freeport	1,405	1,269	47	51	28	29
(55% Solids)	1,391	1,382	46	48	27	28
Upper Freeport	1,543	1,479	43	46	24	26
(51% Solids)	1,607	1,485	53	47	24	26

Table 4-8. Summary of the Atomization Characteristics of an Upper Freeport Seam MCWM at 100 Psig Atomization Air Pressure

Slurry	D90 (μm)		D50 (μm)		D10 (μm)	
	Low fire flow	High fire flow	Low fire flow	High fire flow	Low fire flow	High fire flow
Upper Freeport	1,316	1,439	78	83	30	29
(67% Solids)	230	1,356	68	79	29	29
Upper Freeport	1,425	251	78	75	30	29
(65% Solids)	1,530	1,468	86	85	30	30
Upper Freeport	1,532	1,553	82	82	29	30
(63% Solids)	1,582	1,563	82	81	29	29
Upper Freeport	1,561	1,521	69	70	27	28
(60% Solids)	1,649	1,512	88	66	28	28
Upper Freeport	1,370	1,425	40	47	26	27
(55% Solids)	1,531	1,424	51	44	26	27
Upper Freeport	1,676	1,569	94	48	21	24
(51% Solids)	1,651	1,611	75	54	24	24

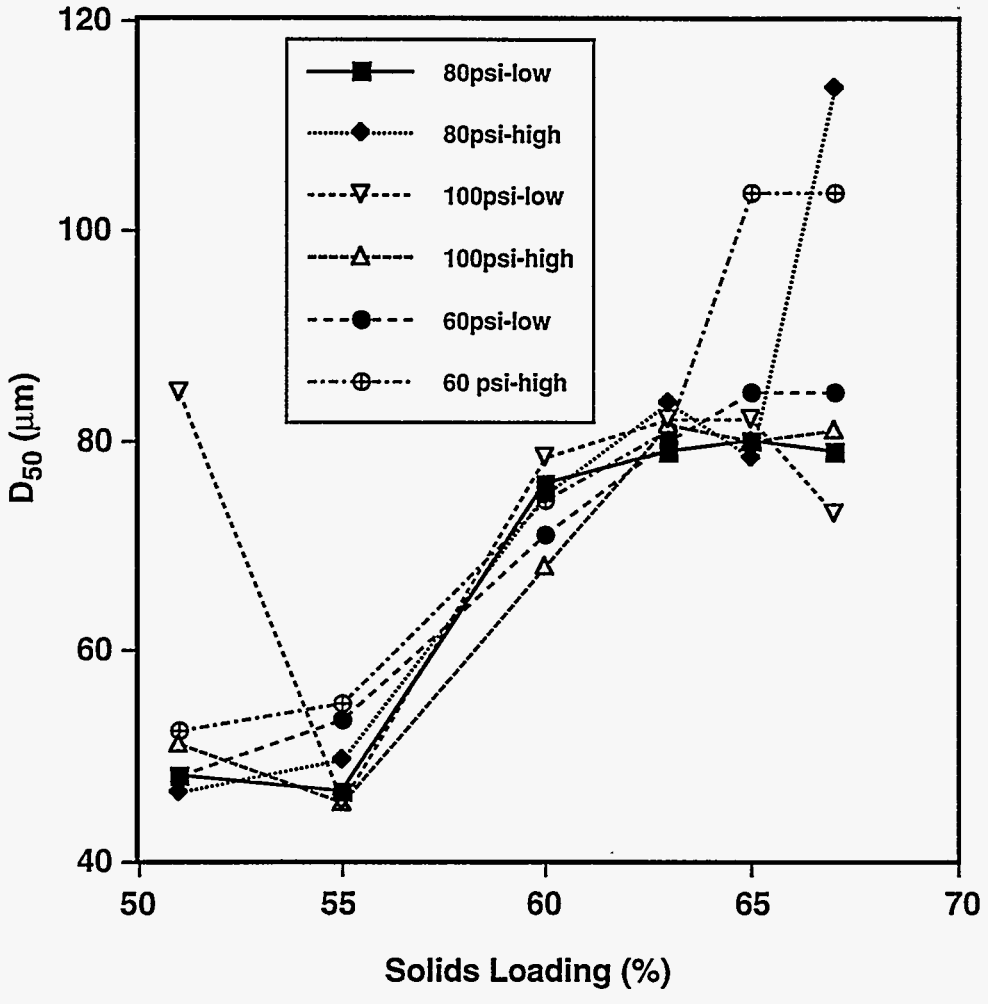

Figure 4-39. EFFECT OF SOLIDS LOADING ON THE D_{50} OF UPPER FREEPORT SEAM MCWM

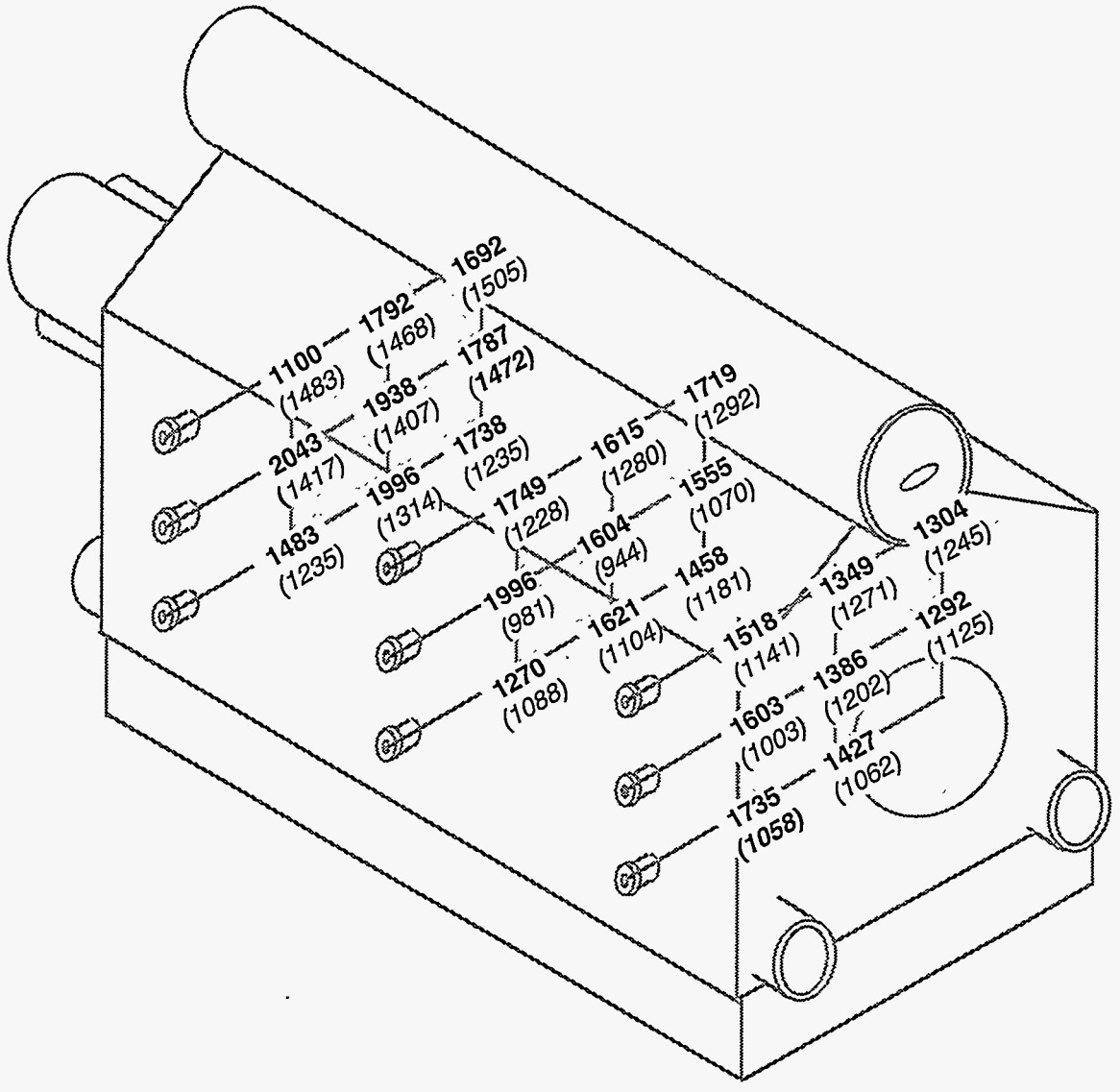

Figure 4-40. GAS TEMPERATURE MEASUREMENTS (°F) IN THE RESEARCH BOILER FOR UPPER FREEPORT SEAM DMC AND MCWM AT VARIOUS LOCATIONS (MCWM value in parentheses)

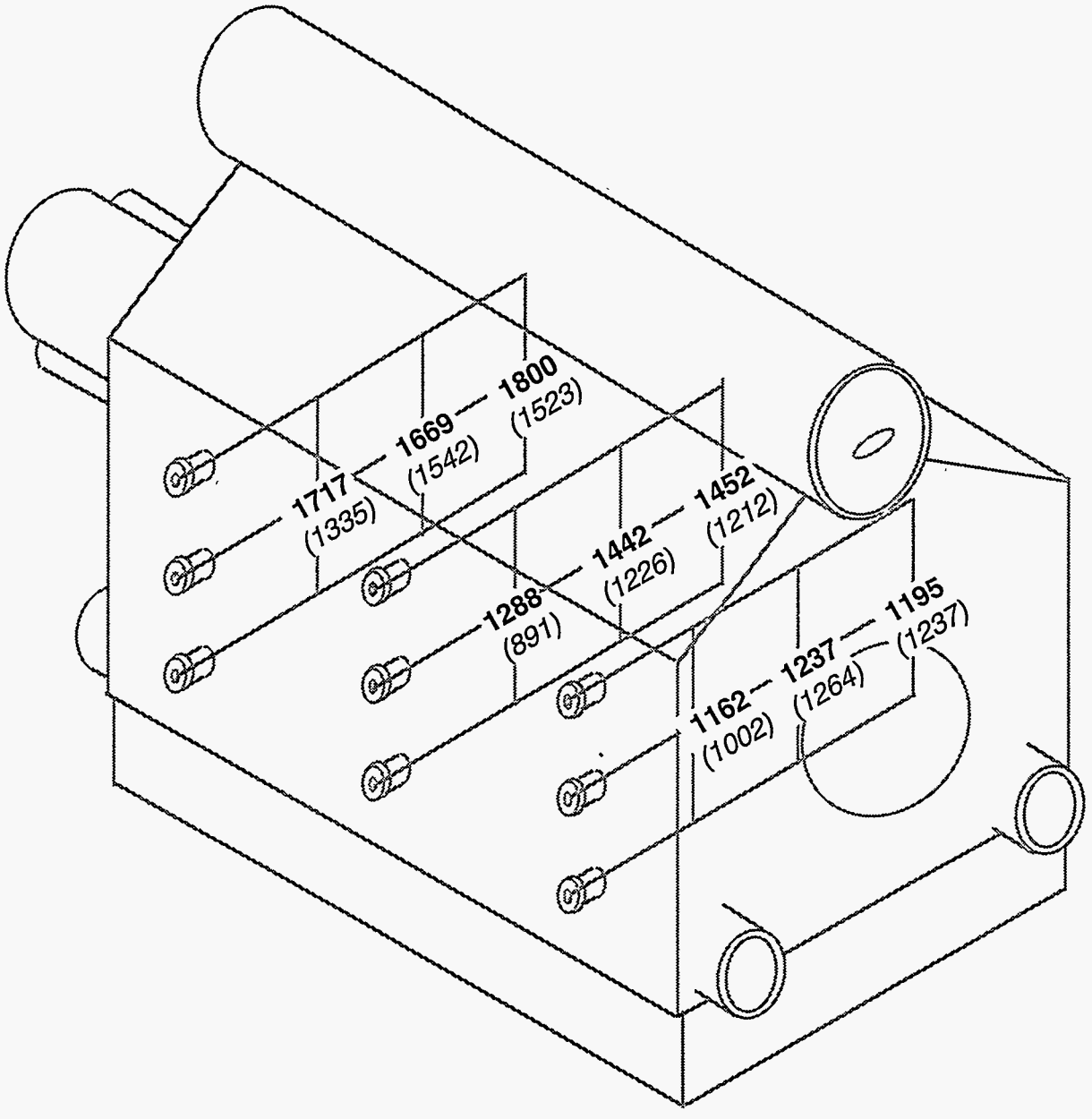

Figure 4-41. COMPARISON OF TEMPERATURE (°F) PROFILES FIRING TAGGART SEAM DMC AND MCWM AT VARIOUS LOCATIONS (MCWM Values in parentheses)

MCWM tests. A more detailed analysis of the combustion efficiencies is presented in a later section.

Heat Flux Measurements

Heat flux measurements were made to examine and compare the heat release rates for the various fuels. Figure 4-42 shows a comparison of total heat flux (radiant and convective) profiles for the Upper Freeport and Taggart seam coals. These profiles indicate that there are differences in the heat fluxes at a given location in the boiler. Total heat flux, in general, is lower for the Taggart seam coal at most locations than for the Upper Freeport seam coal, which is consistent with the temperature profile data. The asymmetry in the heat flux distribution is likely caused by the asymmetrical firing or maldistribution of fuel.

Figures 4-43 and 4-44 show a comparison of the total heat fluxes at various planes in the boiler for Upper Freeport and Taggart seam DMC and MCWM tests, respectively. The heat fluxes in the front portion of the firebox are higher than those in the back portion, which is a similar trend to the temperature measurements at those locations. Heat fluxes for the Upper Freeport seam MCWM are lower than those for the DMC at most of the locations. This is also consistent with the temperature profiles. The differences in the total heat fluxes become smaller with axial distance from the burner. The mean total heat fluxes along the vertical plane (ports closer to the burner) for the Upper Freeport seam DMC and MCWM tests were 52,205 and 29,350 Btu/h-ft^2, respectively. The mean heat fluxes at the back of the boiler along the farthest vertical plane for the Upper Freeport seam DMC and MCWM tests were 22,199 and 18,321 Btu/h-ft^2, respectively. It is important to note that in spite of higher thermal input rates (~1.9 MM Btu/h) for the MCWM tests than for the DMC tests (~1.5 MM Btu/h), the total heat fluxes are lower for the MCWM tests.

Figures 4-45 and 4-46 compare the total and radiant heat fluxes at given locations for the Upper Freeport and Taggart seam MCWM tests. The average total heat flux in the ports closer to the burner wall for the Upper Freeport seam MCWM was 29,350 Btu/h ft^2, whereas the radiant heat flux was 10,303 Btu/h ft^2. The total and the radiant heat fluxes in the farthest ports (closer to the back wall) were 18,321 and 6,198 Btu/h ft^2, respectively. The radiant heat flux was, therefore a third of the total heat flux for the Upper Freeport seam MCWM.

The total and radiant heat fluxes for the Taggart seam MCWM test at the ports closer to the burner wall were 31,598 and 2,044 Btu/h ft^2, respectively; whereas, at the farthest ports from the wall they were 16,510, and 3,237 Btu/h ft^2, respectively. The radiant heat flux in the case of the Taggart seam MCWM was significantly lower than the total heat flux. For the Taggart seam MCWM test, the radiant heat flux was significantly lower than that measured for the Upper Freeport seam MCWM in spite of slightly higher mean gas temperature for the Taggart seam MCWM. Recall that the combustion efficiency for the Taggart seam MCWM was higher than that for the Upper Freeport seam MCWM. This points to a balance between an increase in the emissivity of the flame due to the moisture content and the overall temperature decrease due to

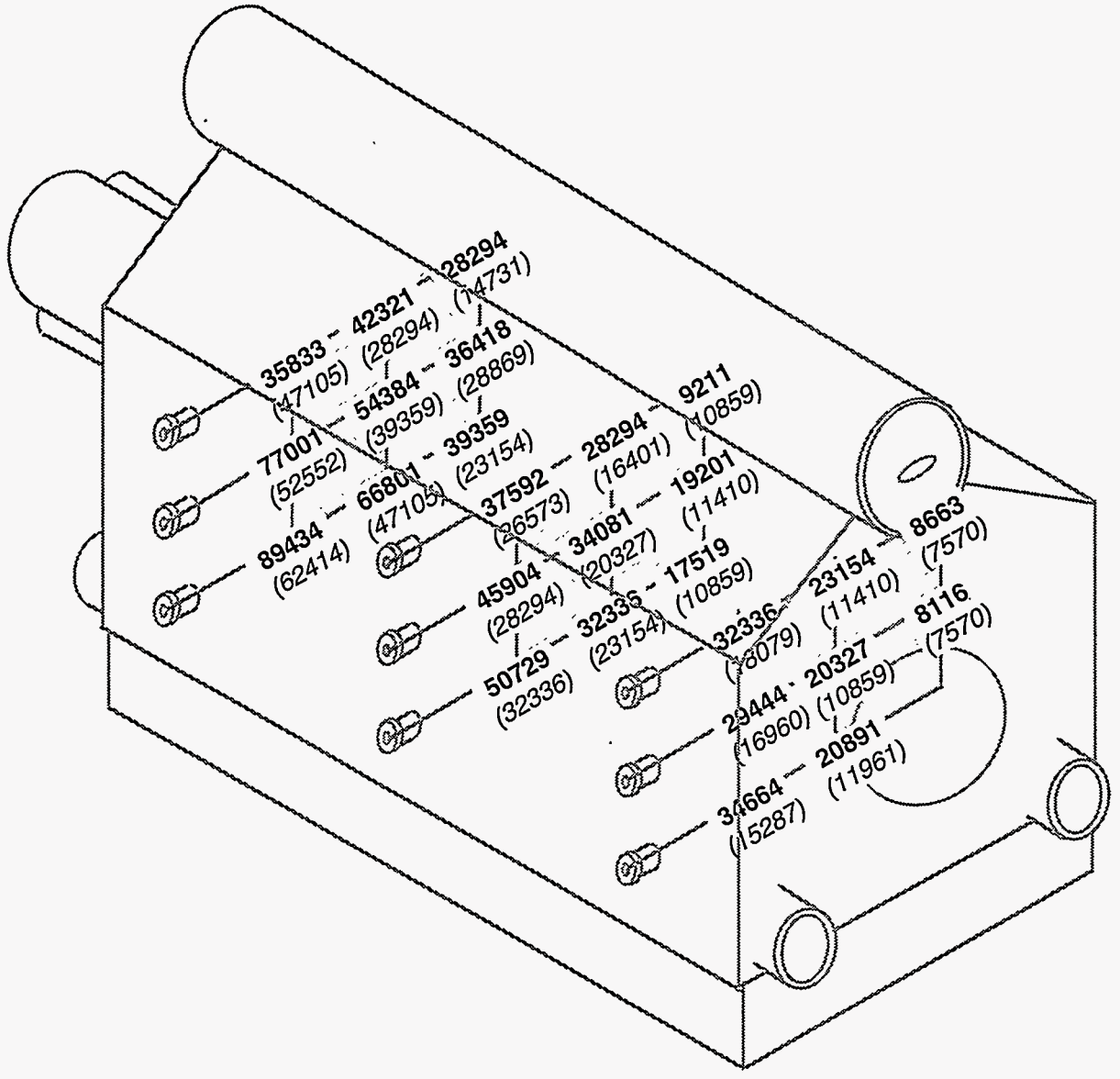

Figure 4-42. COMPARISON OF TOTAL HEAT FLUX (Btu/h ft^2) MEASUREMENTS DURING THE UPPER FREEPORT AND TAGGART SEAM DMC TESTS (Taggart seam values in parentheses)

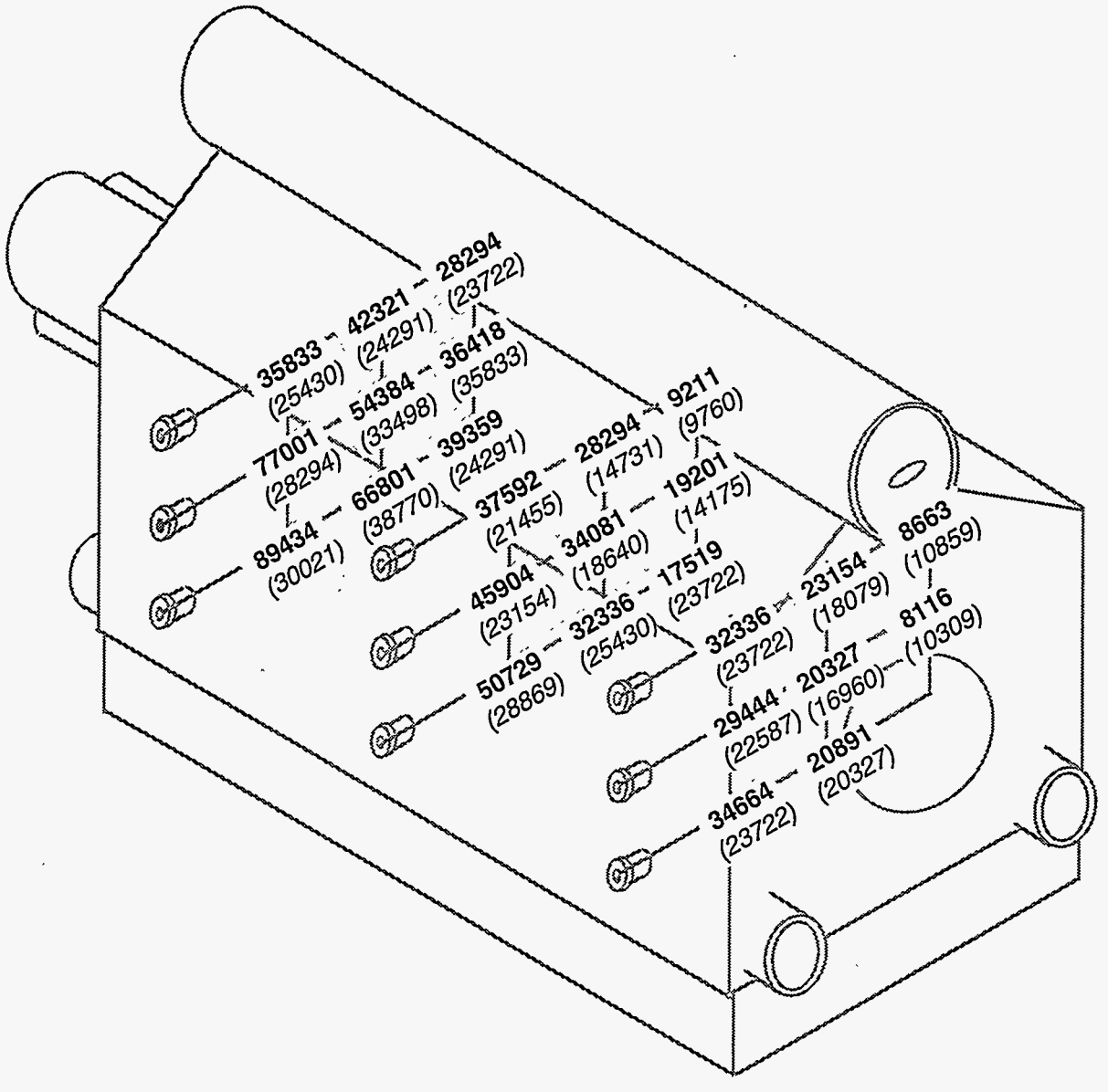

Figure 4-43. COMPARISON OF TOTAL HEAT FLUX MEASUREMENTS (Btu/h ft^2) FOR THE UPPER FREEPORT SEAM DMC AND MCWM (MCWM values in parentheses)

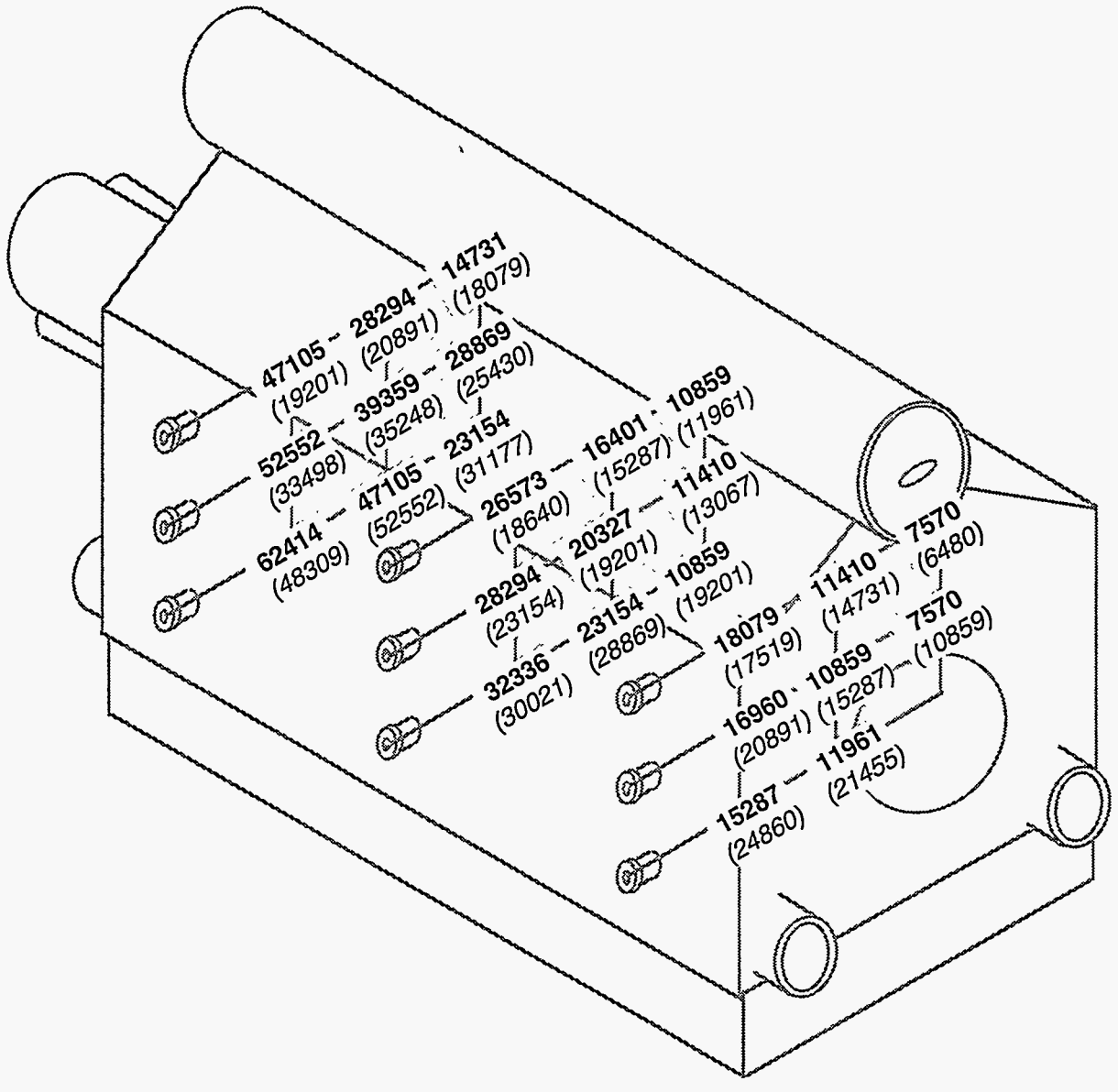

Figure 4-44. COMPARISON OF TOTAL HEAT FLUX MEASUREMENTS (Btu/h ft^2) FOR THE TAGGART SEAM DMC AND MCWM (MCWM values in parentheses)

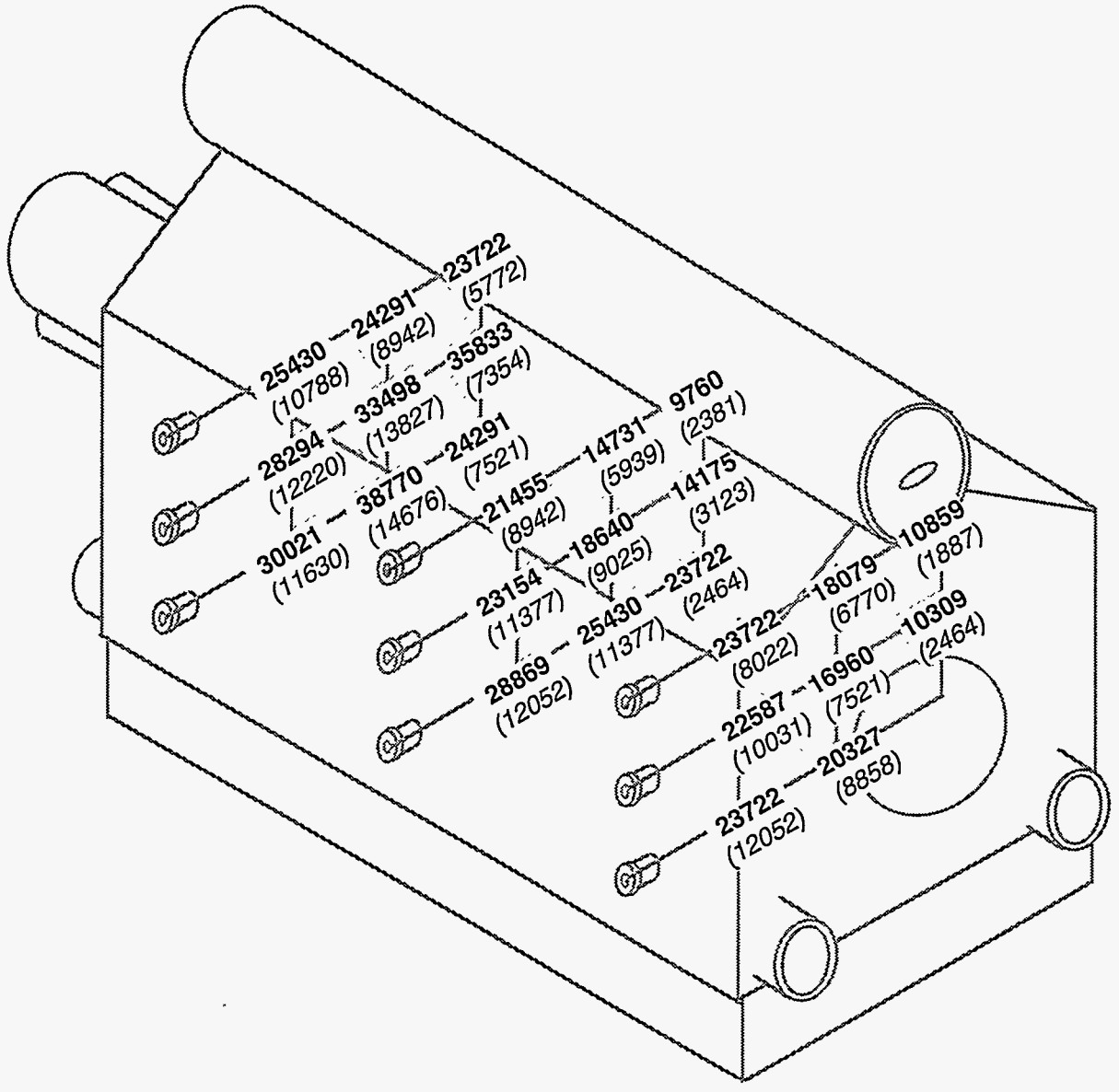

Figure 4-45. COMPARISON OF TOTAL AND RADIANT HEAT FLUX MEASUREMENTS (Btu/h ft^2) FOR THE UPPER FREEPORT SEAM MCWM TEST (Radiant heat flux in parentheses)

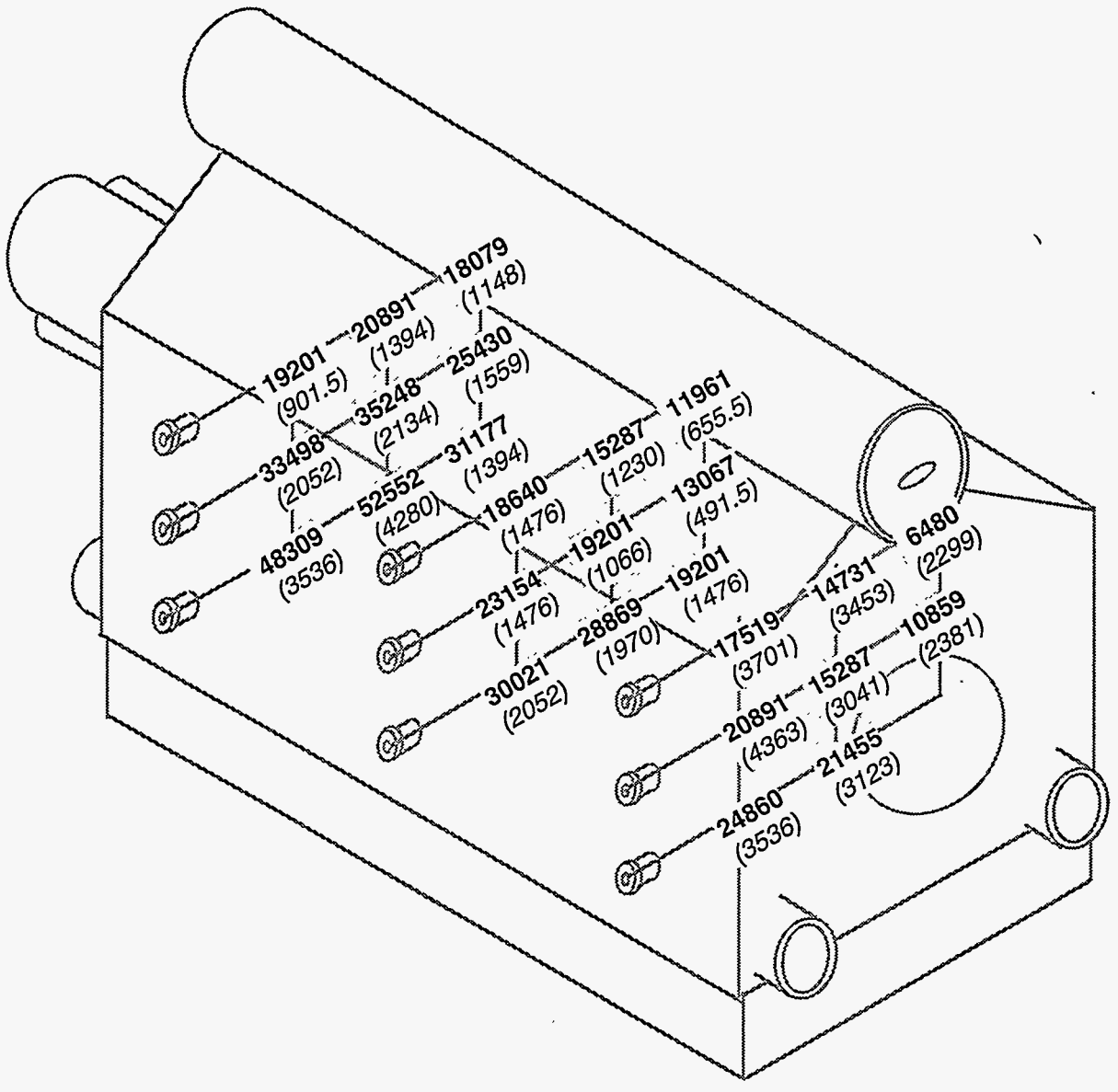

Figure 4-46. COMPARISON OF TOTAL AND RADIANT HEAT FLUX MEASUREMENTS (Btu/h ft^2) FOR THE TAGGART SEAM MCWM (Radiant heat flux values in parentheses)

higher moisture content on the radiant heat flux.

All bodies continuously emit radiant energy in amounts which are determined by the temperature and nature of the surface. The maximum theoretical radiant energy emitted by a Black Body is given by:

$$q_r = A\sigma T_s^4 \qquad (4\text{-}20)$$

where, σ is the Stefan Boltzman constant (0.1713×10^{-8} Btu/h ft^2 R^4) and T_s= absolute temperature (R).

A real body absorbs (or emits) less than 100% of the energy that is incident on the surface. Therefore, the energy that is absorbed by a real body (gray body) is expressed by:

$$q_r = A\varepsilon\sigma T_s^4 \qquad (4\text{-}21)$$

where, ε is the emissivity of the surface. Emissivities of substances depend on the surface composition, surface finish, and wavelength of radiation. Emissivity values range between 0.2 and 0.9. The higher the value, the closer the surface is to a blackbody. A number of commercial surfaces, particularly at high temperature, have emissivities of 0.8 to 0.95 and behave much like blackbodies. In addition to solid surfaces, many gases absorb and emit radiation. Diatomic gases such as oxygen and nitrogen, which are present in boiler furnace gases, absorb and emit insignificant quantities. However, triatomic gases such as water vapor, carbon dioxide, sulfur dioxide etc., absorb and emit radiation in significant quantities. Although both water vapor and carbon dioxide are important constituents of combustion gases and contribute to nonluminous radiation, for a comparison of the flue gases from DMC and MCWM firing, the role of water vapor is particularly important. Although the radiation to and from the furnace wall is a surface phenomenon, flue gas radiates and absorbs at every point throughout the furnace chamber. Furthermore, the emissivity of the flue gas changes with temperature and composition, and the presence of one radiating gas has an effect on the radiating characteristics of another gas with which it is mixed. Since the temperature and gas composition change from point to point in a furnace, it should be noted that a multi zone analysis is required. In this section, first order estimates are used to evaluate the magnitude of the influence of these factors.

The energy emitted by a radiating gas mixture depends on the temperature, partial pressures of the components in the mixture, and the beam length, L, which depends on the shape and dimensions of the furnace (gas enclosure). An estimate of beam length can be made using:

$$L = 3.6\ (V/A) \qquad (4\text{-}22)$$

where V and A are the volume and surface area of the enclosure, respectively.

In the research boiler, the volume of the radiant section is 53.5 ft^3, and the surface area of the four walls is 83.3 ft^2. For a typical pulverized coal fired unit, the flue gases would contain 6.0% (by volume) water vapor and 14.3% CO_2. For a unit operating at atmospheric pressure, p_w = 0.06 atm;, L= 2.31 and therefore, emissivity (ε_{H2O}) at 1,500°F (1,960 R) = 0.07. Similarly, p_c= 0.143 atm, and at L=2.31 emissivity (ε_{CO2}) at 1500°F (1960 R) = 0.12. The correction factor $\Delta\varepsilon$ = 0.008[120]; and hence $\varepsilon = \varepsilon_{H2O} + \varepsilon_{CO2} - \Delta\varepsilon = 0.07 + 0.12 - 0.008 = 0.182$.

For a MCWM unit, the flue gases would contain approximately 14% water vapor and 13% CO_2 and p_w = 0.14 atm, L=2.31 and therefore, emissivity (ε_{H2O}) at 1,200°F (1,640 R) = 0.16. Similarly, p_c= 0.13 atm and at L = 2.31 emissivity (ε_{CO2}) at 1,200°F (1,640 R) = 0.11. The correction factor, $\Delta\varepsilon$, is 0.025[120]; and hence $\varepsilon = \varepsilon_{H2O} + \varepsilon_{CO2} - \Delta\varepsilon = 0.16 + 0.11 - 0.025 = 0.245$.

Assuming that the emissivity of the boiler water walls and the view factor are the same for both DMC and MCWM systems:

$$q'' = \sigma F_e (T_1^4 - T_2^4) \qquad (4\text{-}23)$$

where q"= heat flux, Btu/h ft^2;

F_e = 0.9 (assumed effectiveness factor excluding the emissivity of gases);

T_1= Furnace gas temperature (average temperature of eight measurements in the radiant section); and

T_2= Wall temperature (approximately saturation temperature).

For Upper Freeport seam DMC firing, q" = 0.171 x 10^{-8} Btu/h ft^2 x 0.9 x 0.182 x $((1591+460)^4 - (358+460)^4)$= 4,831 Btu/h ft^2. For Upper Freeport seam MCWM firing, q" = 0.171 x 10^{-8} Btu/h ft^2 x 0.9 x 0.245 x $((1,265+460)^4 - (358+460)^4)$ = 3,169 Btu/h ft^2.

This analysis shows that in spite of a 30% increase in the gas emissivity for the MCWM flame due to increased water vapor content, a gas temperature drop of about 300°F caused a 30% overall drop in the radiative heat flux in the boiler. However, this may slightly change if the beam length of the boiler changes. These calculations also indicate that the average radiant heat flux measurements made are slightly lower than the calculations for the Taggart seam MCWM, whereas the measurements are higher than the calculations for the Upper Freeport seam MCWM. It should be noted that the ash content of the Upper Freeport seam coal is 6.6% whereas that of the Taggart seam coal is 3.6%. The char/ash particles carried by the flue gases receive heat from the flue gases by radiation, convection, and conduction and emit radiation to the furnace enclosure. The extent of this process depends on the particle temperature, which depends on the extent of combustion. Deposits on the furnace walls also change the emissivity and the radiation heat flux.

Char Characteristics

Particle Size Distribution

Chars produced in the boiler from DMC and MCWM firing were significantly different in appearance both in terms of size and surface texture. Figures 4-47 and 4-48 compare the particle size distribution of the feed coal and the char collected from the baghouse and hoppers for the Upper Freeport and Taggart seam DMCs, respectively. Figures 4-49 and 4-50 provide the size distribution of coals and chars from the baghouse and hoppers for the Upper Freeport and Taggart seam MCWMs, respectively. These size distributions were obtained using a Malvern Droplet and Particle Size Analyzer.

It should be noted that the values for $D_{(v,\ 0.9)}$ etc., are for the coal and not for the MCWM droplets. The data suggest that larger particles drop out in the hoppers. A higher $D_{(v,\ 0.9)}$ is observed because the hopper char is not representative of the total char that is passing though the convective section of the boiler. It is also observed that the mean sizes of the hopper and baghouse samples from Taggart seam MCWM are lower than those of the Upper Freeport seam MCWM. This could be a result of finer atomization of the former. Although the mean size of the baghouse ash samples generated from a MCWM test is higher than that from a dry coal test, the combustion efficiency of the samples is very close. This suggests that although for larger particles oxygen penetration into the particle is difficult, size alone may not be a limiting factor for oxygen penetration. Irrespective of the viscosity, particle size and temperature profile, Taggart seam MCWMs had higher combustion efficiencies in the baghouse than the Upper Freeport seam MCWMs.

In Situ Droplet / Particle Size Analysis

The objective of this work was to obtain in situ measurements of size distribution, number density, and speed of the particles in an industrial boiler firing DMC and MCWM using the PCSV-P.

Results and Discussion

The locations of the measurements taken in the boiler are shown in the Figure 4-51. The operating parameters were:

Operating Parameter	DMC	MCWM
Firing rate (MM Btu/h)	1.60	1.92
Combustion air flow (lb/h)	1,019	819
Atomizing air flow (lb/h)	0	110
Primary air (lb/h)	109	0
Tertiary air (lb/h)	320	222
Steam flow (lb/h)	1,071	1,110

The data collected from mapping a plane of the boiler is voluminous and instead of reporting the entire size distributions and number densities of the particles, a number of key parameters were used to summarize the data. These parameters are:

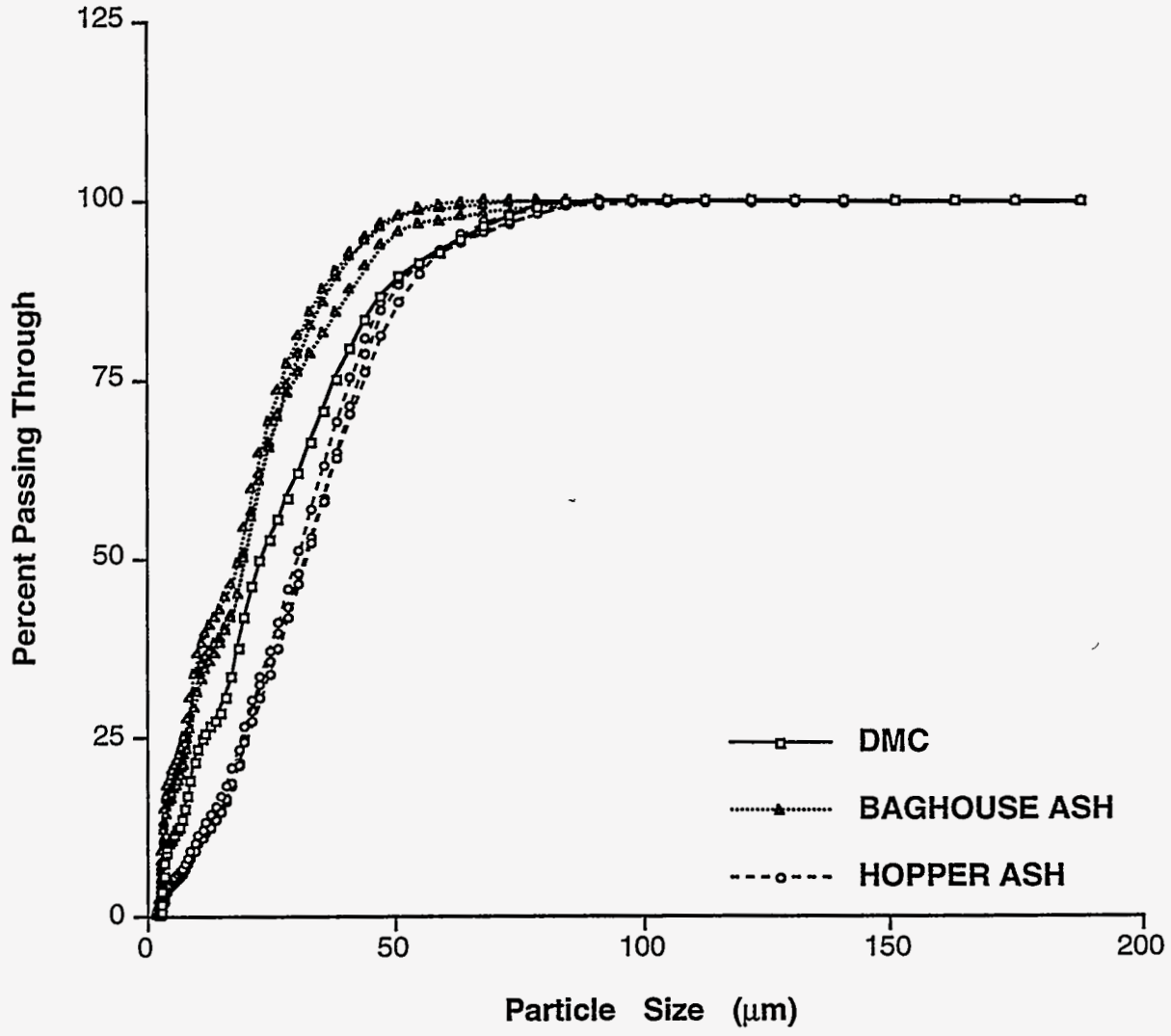

Figure 4-47. PARTICLE SIZE DISTRIBUTION OF COAL AND CHAR SAMPLES COLLECTED AT VARIOUS TIMES DURING THE TEST PERIOD FOR THE UPPER FREEPORT SEAM DMC

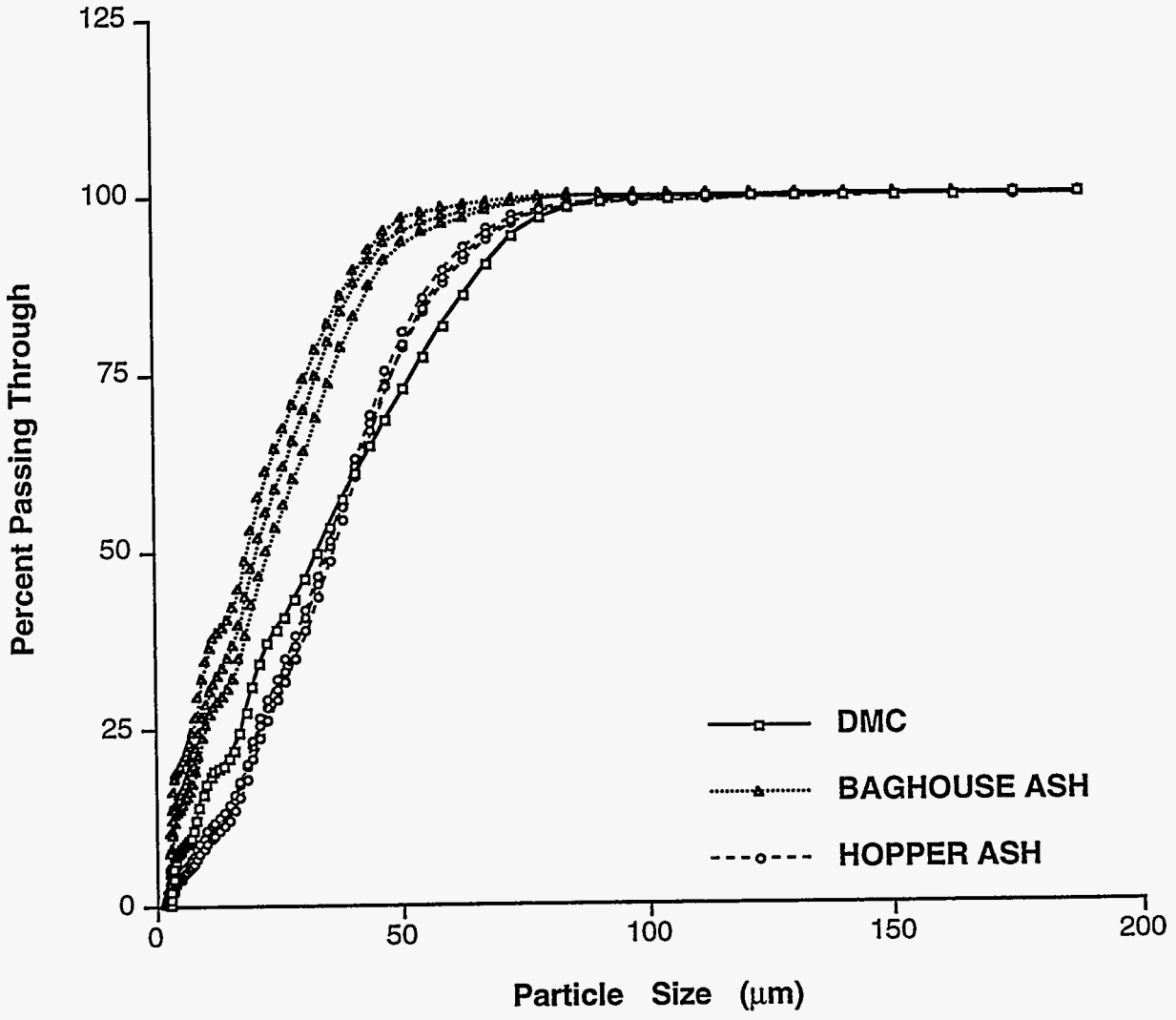

Figure 4-48. PARTICLE SIZE DISTRIBUTION OF COAL AND CHAR SAMPLES COLLECTED AT VARIOUS TIMES DURING THE TEST PERIOD FOR THE TAGGART SEAM DMC

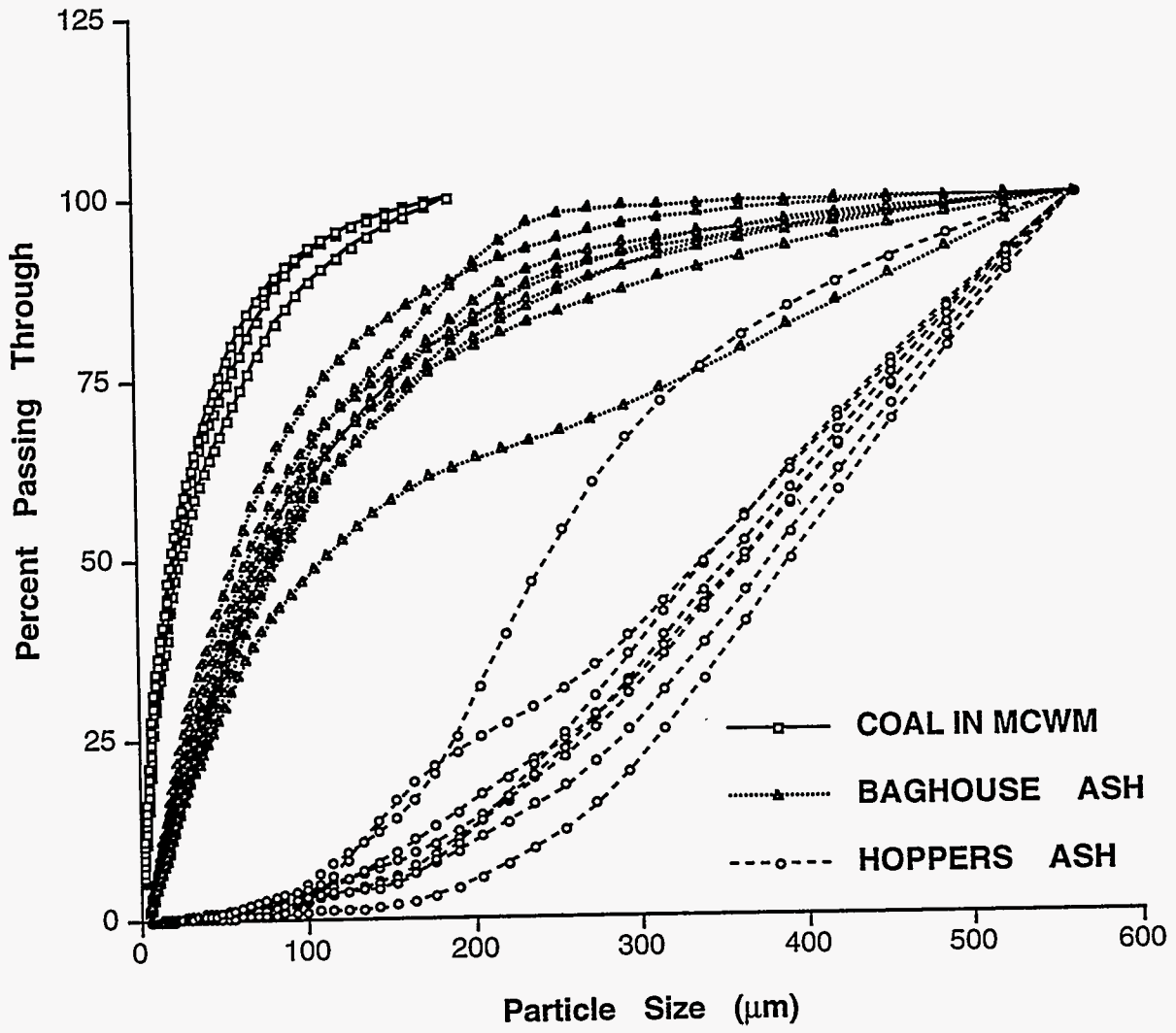

Figure 4-49. PARTICLE SIZE DISTRIBUTION OF COAL IN THE MCWM AND CHAR SAMPLES COLLECTED AT VARIOUS TIMES DURING THE TEST PERIOD FOR THE UPPER FREEPORT SEAM MCWM

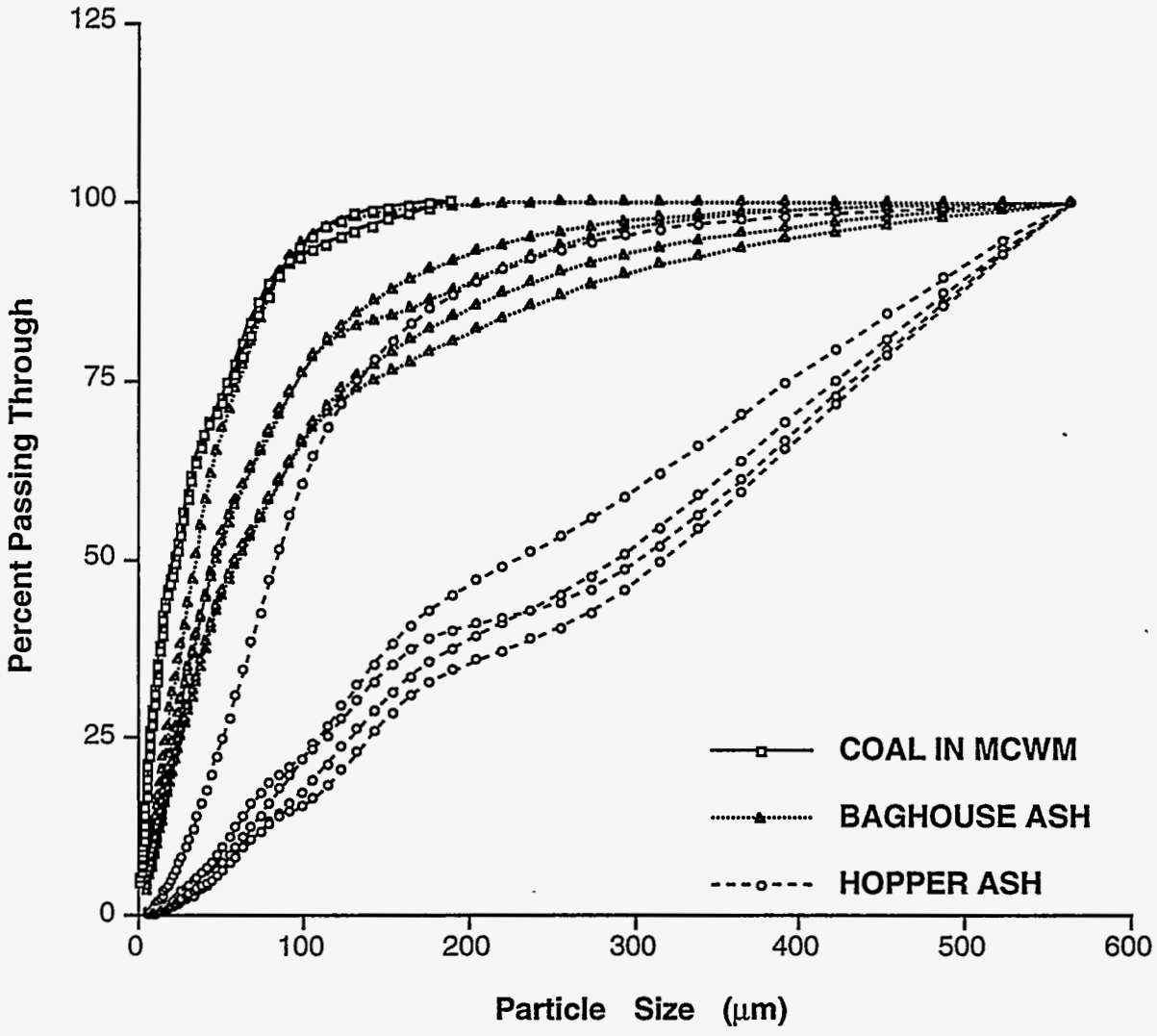

Figure 4-50. PARTICLE SIZE DISTRIBUTION OF COAL IN THE MCWM AND CHAR SAMPLES COLLECTED AT VARIOUS TIMES DURING THE TEST PERIOD FOR THE TAGGART SEAM MCWM

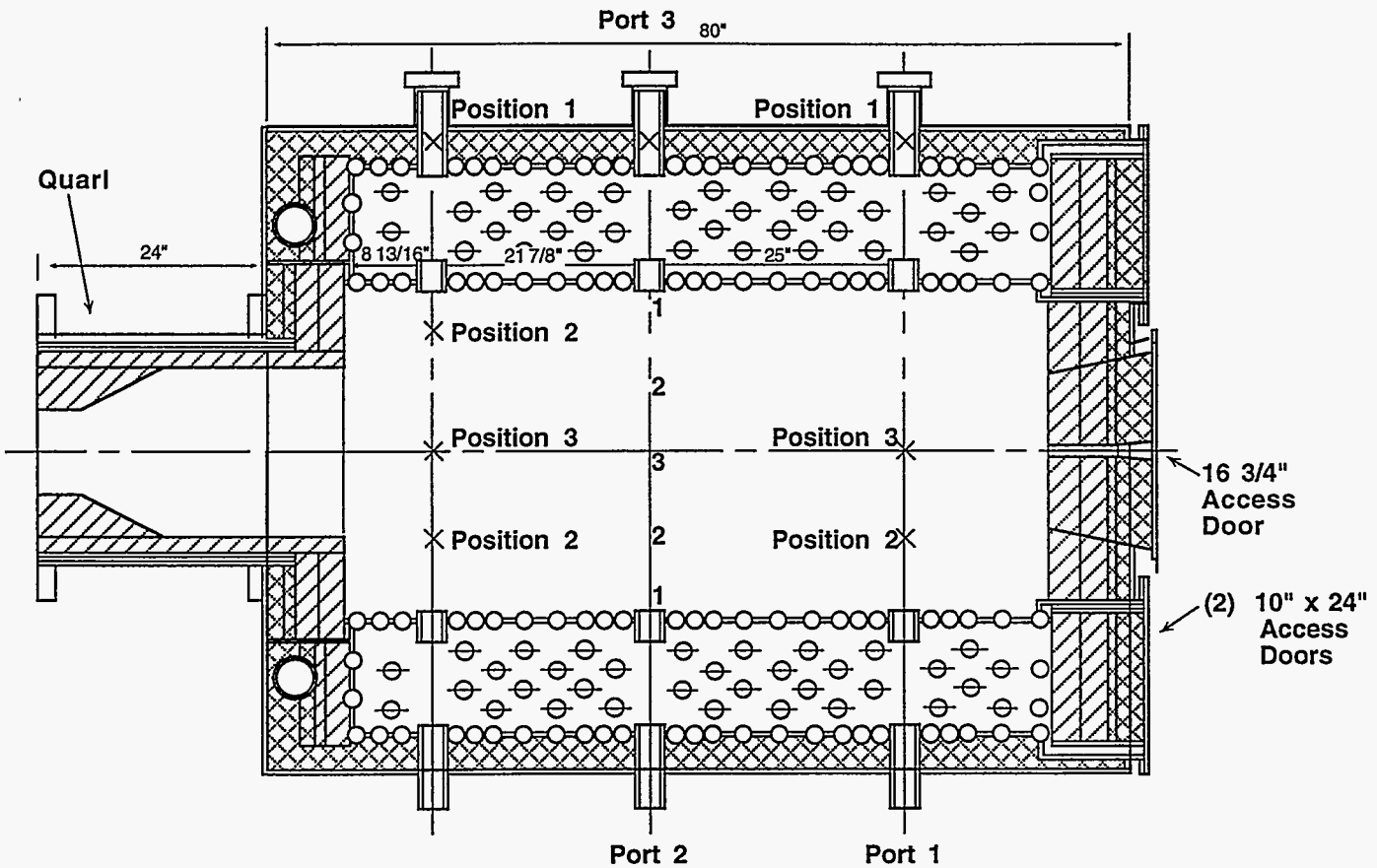

Figure 4-51. LOCATION OF MEASUREMENTS TAKEN IN THE RESEARCH BOILER

- d_{10} 10% of the particles sampled having diameters larger than this value;
- d_{50} 50% of the particles sampled having diameters larger than this value;
- d_{90} 90% of the particles sampled having diameters larger than this value;
- u_m the mean speed of the particles sampled; and
- ΣN_i the total number of particles sampled at a specific node within the boiler.

It is important to emphasize that the above listed measurements were taken using the PCSV-P, a single particle counter, and are all number based (i.e., they are expressed on the basis of the number of particles measured). Hence, the subscripts with the numbers 10, 50 and 90 refer to number based measurements, as opposed to the measurements with the Malvern Particle and Droplet Analyzer, which are volume based.

A summary of the data when firing DMC is given in Table 4-9. Particle size distributions were characterized by high number densities in the small size classes (0.4-2 μm) followed by a logarithmic increase to larger particle sizes. For the data collected from Port 1, the largest d_{50} measured was at a position midway between the boiler wall and the centerline of the boiler (Position 2). The PCSV technology does not distinguish between coal, char, and ash particles and therefore it is very difficult to infer direct information on the combustion history of the coal particles as they are issued by the burner into the boiler. In other words, every time a particle passes through the control volume of the laser analyzer, it gives rise to a light scattering signal, the magnitude of which depends primarily on the size of the particle, regardless of whether it is a coal, char or ash particle. Other factors influencing the size of this scattered signal include variations in the particle morphology (characterized by the porosity and density) and opacity (characterized by the particle's refractive index). Translucent particles, such as char cenospheres or those particles with low light absorption coefficients tend to scatter more light. Consequently, despite the fact that the complex light scattering interrelations between absorption, sphericity and porosity of ash particles are not well understood, an increase in the amount of scattered light will ultimately result in particle oversizing by the PCSV technology, which in turn results in high calculated mass loadings. Despite this shortcoming of the instrument, it still provides indirect evidence of the fate of the particles in the boiler. If the particles are burning under Regime II conditions (i.e., mixed control), their density and their size should be changing and the overall shift in the particle size distribution toward smaller sizes can be attributed to fragmentation and ash formation: processes that are likely to occur during char combustion and toward the end of the travel of coal particles in the boiler. The implication of this is that it is likely that by the time the particles have reached those regions of the boiler accessible by Port 1, they have already undergone devolatilization, and the process of char burnout is well underway.

From the data collected from Port 2 (which is the port closer to the front of the combustor where the burner is located), the d_{50} measured on the centerline of the boiler (Position 3) was 1.08 μm, which indicates the existence of larger particles. Traversing the width of the boiler from Port

Table 4-9. Summary of the PCSV-P Data When Firing DMC

Parameter	ΣN_i	d_{90} (μm)	d_{50} (μm)	d_{10} (μm)	u_m (m/s)
Port 1					
Position 1	9,600	0.51	0.83	2.26	4.18
Position 2	12,000	0.51	0.90	2.31	4.32
Position 3	12,000	0.50	0.74	2.13	4.25
Con-Pass[a]	6,000	0.50	0.79	2.05	4.15
Port 2					
Position 1	29,000	0.50	0.77	2.05	4.88
Position 2	10,000	0.50	0.73	1.86	4.37
Position 3	12,000	0.53	1.08	2.45	4.22
Con-Pass[a]	7,200	0.52	0.90	2.17	4.14
Port 3					
Position 1	11,000	0.51	0.77	1.93	4.01
Position 2	9,300	0.50	0.76	2.17	4.04
Position 3	12,000	0.53	1.08	2.45	4.22
Con-Pass[a]	8,400	0.50	0.71	1.72	4.07

[a] Convective section of the boiler

3 (i.e., the port opposite Port 2) the values of d_{10}, d_{50} and d_{90} did not differ significantly from those measured in Port 2. This observation provides indirect evidence for "homogeneous mixing" caused by the swirl burner. "Homogeneous mixing" in this context refers to the symmetry of the mixed jets of air and coal around the centerline of the boiler. "Homogeneous mixing" does not refer to the "efficiency" with which the burner is mixing fuel and air. It is common in mathematical modeling to assume a line of symmetry running through the center of the combustor and if the flow has a swirling component, by employing symmetrical cylindrical coordinates, the task of numerical modeling can be facilitated and simplified significantly. These measurements provide support for this approach when firing DMC. In other words, because of the aforementioned symmetry observed in the concentration, size distribution and speed of the particles in the near burner region, if numerical modeling of the burner and/or the boiler were to be carried out, then by employing a two dimensional cylindrical coordinate system, considerable computer time could be saved. However, as will be discussed shortly, this was not the case when firing MCWM. Finally, the data collected in the convective pass of the boiler can be used to complement the modeling work carried out on erosion and corrosion phenomena, as both are strong functions of particle dynamics.

A summary of the data when firing MCWM is given in Table 4-10. The most noticeable change was the asymmetrical spread of the data points. Measurements obtained from ports located opposite each other, i.e., Ports 2 and 3, show distinct differences in particle loadings and speeds. For instance, traversing the width of the boiler with the PCSV-P through Port 2, the total number of particles counted was 23,000 at Position 1 and went up to 100,000 for the corresponding position reached from Port 3. Similar trends were observed for the mean speeds of the particles. That is, the particles sampled close to Port 3 showed considerably higher speeds than those sampled close to Port 2. It was concluded that the atomized spray of MCWM in the boiler was not homogeneous, with a much higher loading closer to Port 3.

As mentioned previously, instead of reporting the entire particle size distribution functions, a number of key parameters were used to characterize each data set. For example, 10% of the particles measured had diameters larger than the diameter specified d_{10}. At this stage, an additional parameter, the top size measured at each node within the boiler, is reported for comparison. This diameter refers to the diameter of the largest particles detected by the PCSV-P. It should be pointed out that for the sake of consistency, the measurement time was kept constant when firing DMC and MCWM. Longer measurement times may have allowed the detection of larger particles. Nonetheless, the maximum diameters measured are given in Table 4-11.

The most obvious feature of Table 4-11 is a shift to larger top sizes detected by the instrument when firing MCWM. The particle size distributions of the coal fired as DMC and the parent coal from which MCWM was produced were identical, hence there should be other explanations for the observed differences in the top sizes. Some causes are explained briefly here. Coal particles are hydrophobic and tend to agglomerate in the presence of water molecules, which

Table 4-10. Summary of the PCSV-P Data When Firing MCWM

Parameter	ΣN_i	d_{90} (μm)	d_{50} (μm)	d_{10} (μm)	u_m (m/s)
Port 1					
Position 1	41,000	0.50	0.69	1.56	4.77
Position 2	27,000	0.51	0.71	1.65	4.74
Position 3	22,000	0.51	0.79	2.22	4.56
Con-Pass[a]	16,000	0.52	0.82	2.22	4.43
Port 2					
Position 1	23,000	0.51	0.71	1.90	4.46
Position 2	20,000	0.51	0.79	2.22	4.25
Position 3	31,000	0.51	0.73	2.13	4.40
Con-Pass[a]	13,000	0.51	0.70	1.86	4.17
Port 3					
Position 1	100,000	0.50	0.69	1.62	8.59
Position 2	51,000	0.50	0.70	1.62	6.14
Position 3	22,000	0.51	0.77	2.35	4.41
Con-Pass[a]	10,000	0.51	0.76	6.90	4.38

[a] Convective section of the boiler

Table 4-11. Maximum Particle Diameters Measured in the Research Boiler Using the PCSV-P When Firing DMC and MCWM

Fuel Fired	**DMC**	**MCWM**
Top Size	**d (μm)**	**d (μm)**
Port 1		
Position 1	17.29	22.74
Position 2	17.29	23.19
Position 3	15.99	20.62
Con-Pass[a]	14.22	17.63
Port 2		
Position 1	19.07	21.03
Position 2	15.99	22.30
Position 3	15.08	25.57
Con-Pass[a]	13.15	17.98
Port 3		
Position 1	12.90	31.10
Position 2	17.98	27.65
Position 3	15.08	25.08
Con-Pass[a]	12.16	16.63

[a] Convective section of the boiler

means no matter how efficient the process of atomization, it is virtually impossible to produce droplets containing a single coal particle. Furthermore, since there is an additional step of evaporation of the water involved in the sequential combustion process, the overall time for combustion becomes longer and, therefore, for a given boiler mean residence time the char particles produced from MCWM tend to be larger as they may not burn out.

Finally, the measured speeds of the droplets issued by the atomizer were high, which can be the only explanation for the particulate matter from MCWM combustion having higher speeds than the particulate matter from DMC combustion.

Char Structure

Figures 4-52 to 4-57 are scanning electron micrographs which highlight some fundamental differences in the morphology of the chars that were generated from the same coal when fired as DMC and MCWM. The char particles from the Upper Freeport seam MCWM are large in diameter, almost spherical, and most importantly have passed through a plastic phase and formed large cenospheres. The char particles from DMC combustion are smaller in size, very porous and do not appear to have gone though a plastic phase. The char particles from the MCWM droplets experience different conditions than those burned as DMC because of the differences in their size, speed and temperature. DMC and MCWM particles have similar mean diameters (D_{50} of 20 and 23 μm for the MCWM and DMC, respectively). However, the atomization study showed that the mean droplet size for the MCWM ranged from 48-95 μm (2.5 - 5.0) times the mean particle size) depending on the solids loading. These droplets have gone through the processes of evaporation of water, devolatilization, swelling, agglomeration and fragmentation during combustion. Ash/char from the hoppers in the case of the MCWM test runs was larger in mean size and quantity than that from the DMC tests. A summary of the amount of ash/char collected from the hopper and the baghouse was compared for the two DMC and MCWM tests is given in Table 4-12.

It appears as if the char particles have undergone plastic transformations only during the MCWM firing. As char and cenosphere formation depends on the plastic and swelling properties of the parent coal, the Free Swelling Index (FSI) of the parent coal was determined as per ASTM D720. A one gram sample of the DMC (minus 60 mesh) was loaded into a standard crucible. The crucible was placed in a standard furnace and was heated as per the prescribed procedure. The resulting coke button was then compared to the ASTM standard profile scale and assigned an index number. An average number based on three tests was reported as per the standard. The procedure was the same for the MCWM except that one gram of water was added to the coal sample.

Gieseler fluidity was determined as per ASTM standard D2639. Five grams of the micronized coal sample was prepared to pass through a U.S. No. 40 sieve with a minimum of fines. The retort with the sample was lowered into the solder bath and the test began as the bath came to equilibrium. An impeller shaft was imbedded in the coal. As the coal became fluid the impeller was turned by the application of a constant torque from the head of the plastomer and the

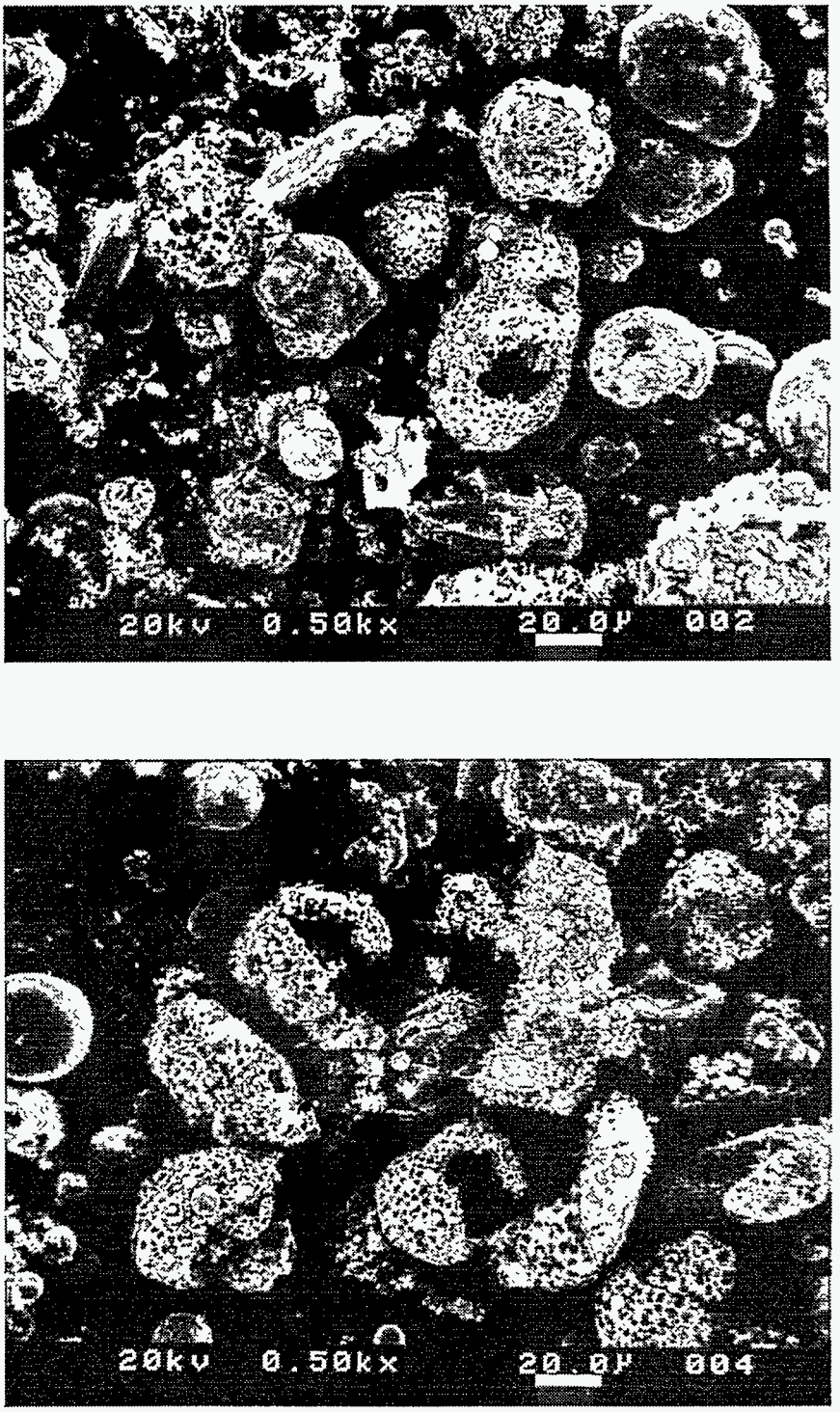

Figure 4-52. SEM MICROGRAPHS (0.5 k Magnification) OF CHAR COLLECTED FROM THE RESEARCH BOILER HOPPER WHEN FIRING UPPER FREEPORT SEAM DMC

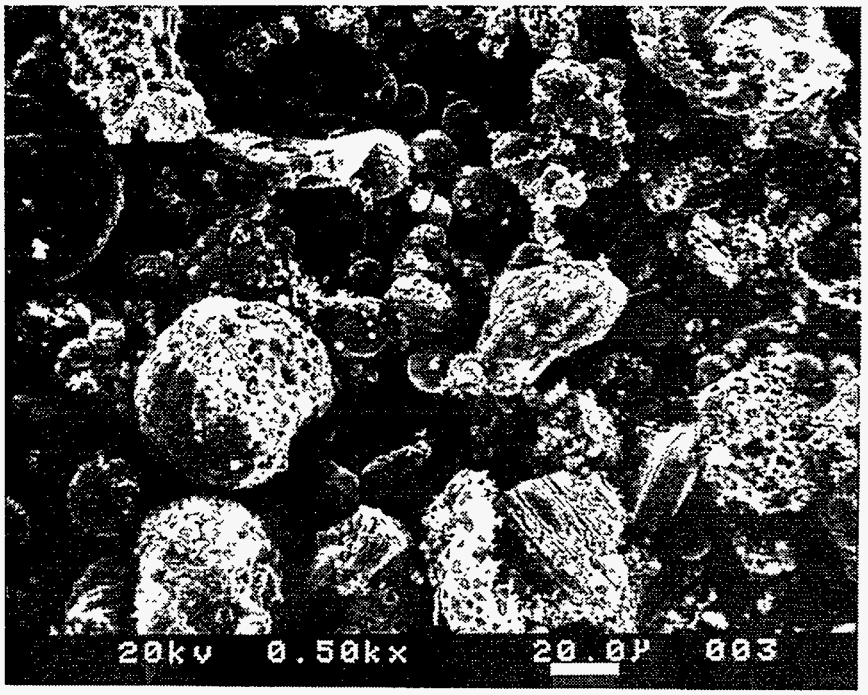

(a)

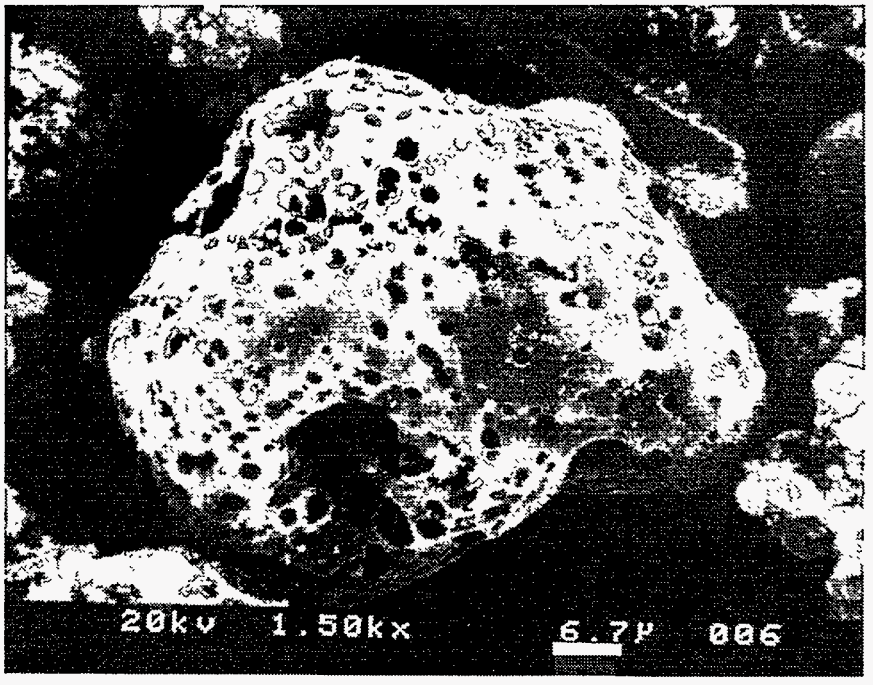

(b)

Figure 4-53. SEM MICROGRAPHS OF CHAR COLLECTED FROM THE RESEARCH BOILER HOPPER WHEN FIRING UPPER FREEPORT SEAM DMC
(a) 0.5 k Magnification; (b) 1.5 k Magnification

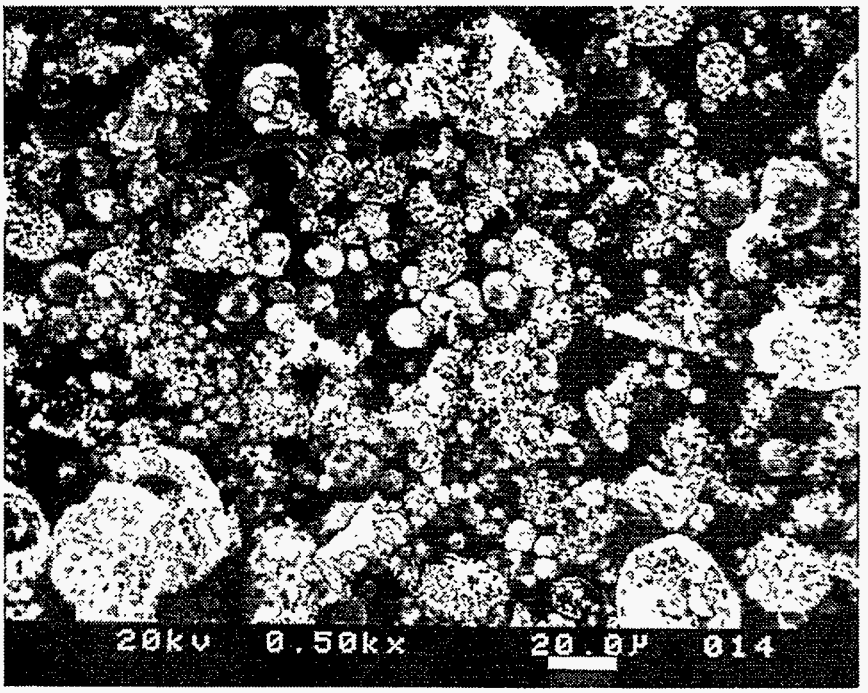

(a)

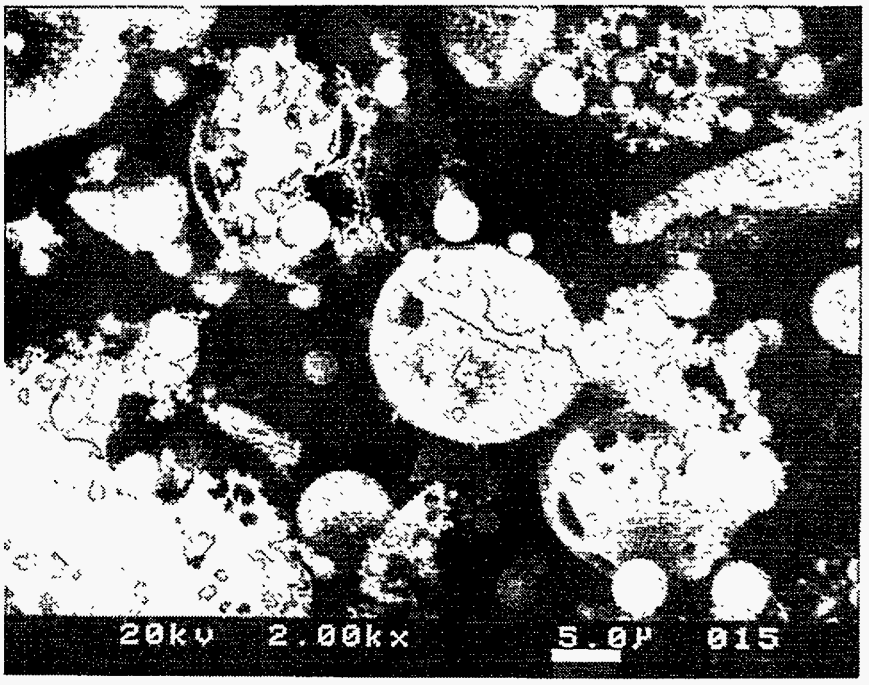

(b)

Figure 4-54. SEM MICROGRAPHS OF CHAR COLLECTED FROM THE RESEARCH BOILER BAGHOUSE WHEN FIRING UPPER FREEPORT SEAM DMC
(a) 0.5 k Magnification; (b) 2.0 k Magnification

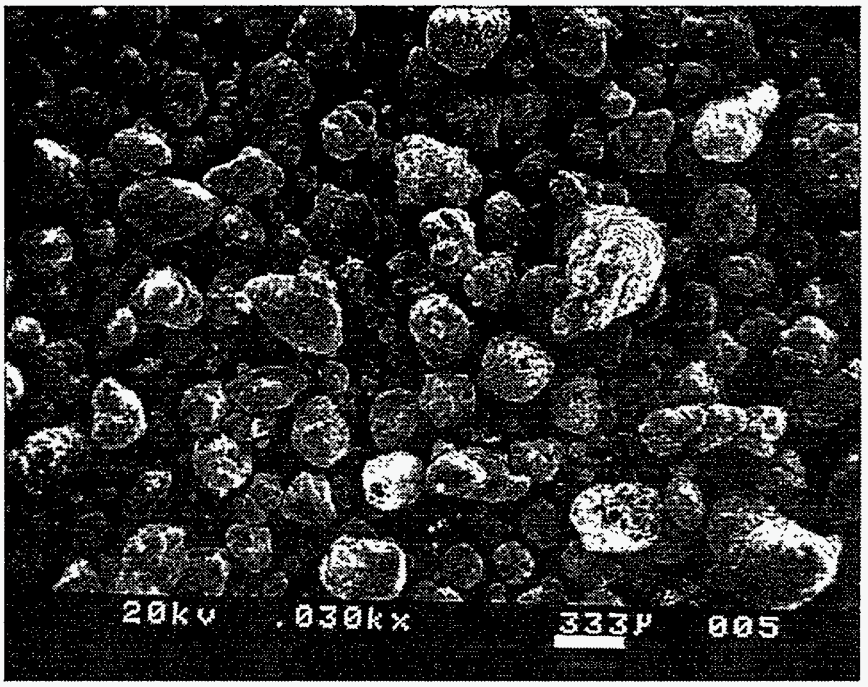

(a)

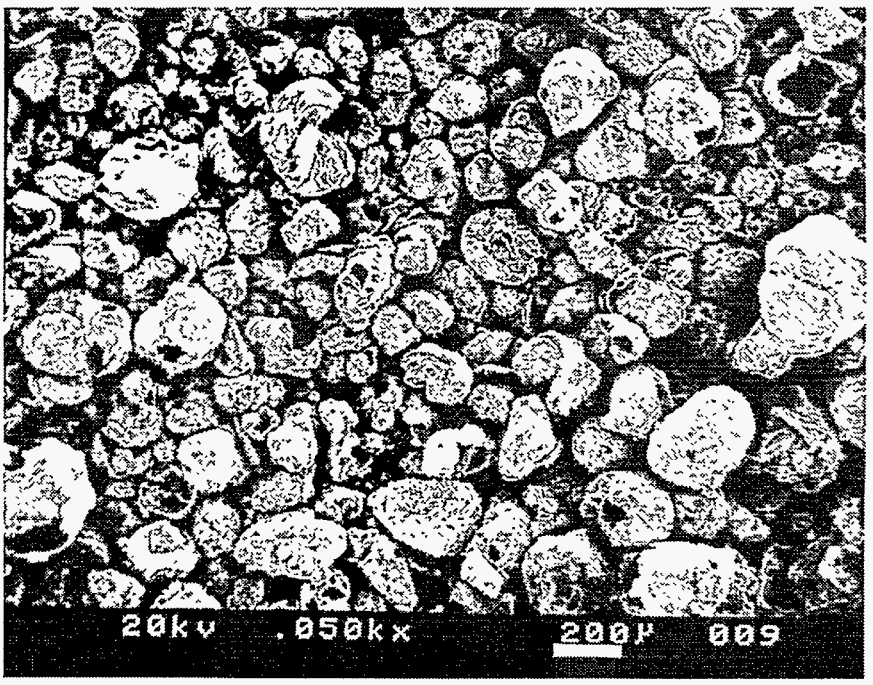

(b)

Figure 4-55. SEM MICROGRAPHS OF CHAR COLLECTED FROM THE RESEARCH BOILER HOPPER WHEN FIRING UPPER FREEPORT SEAM MCWM
(a) 0.03 k Magnification; (b) 0.05 k Magnification

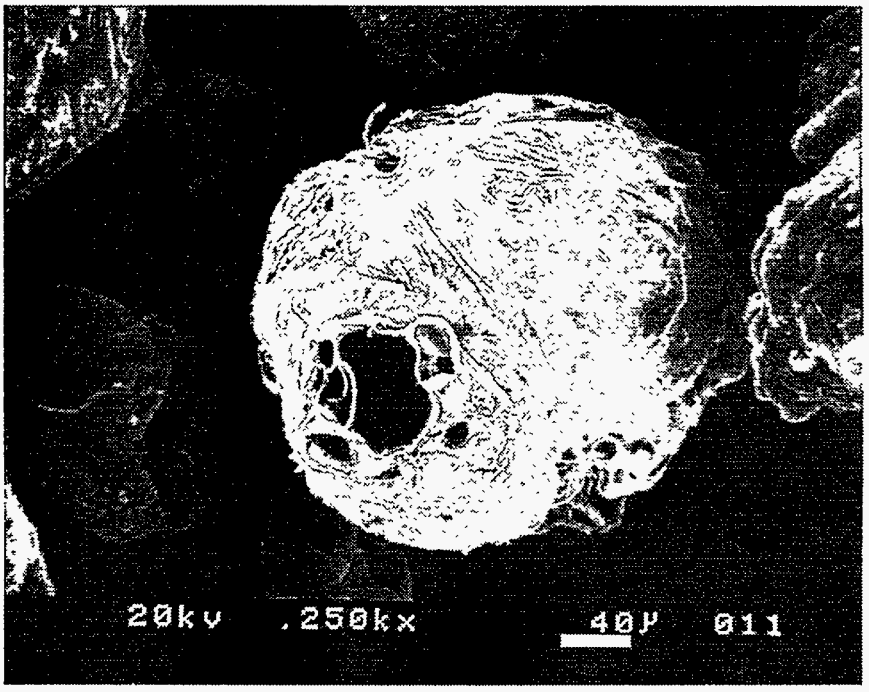

(a)

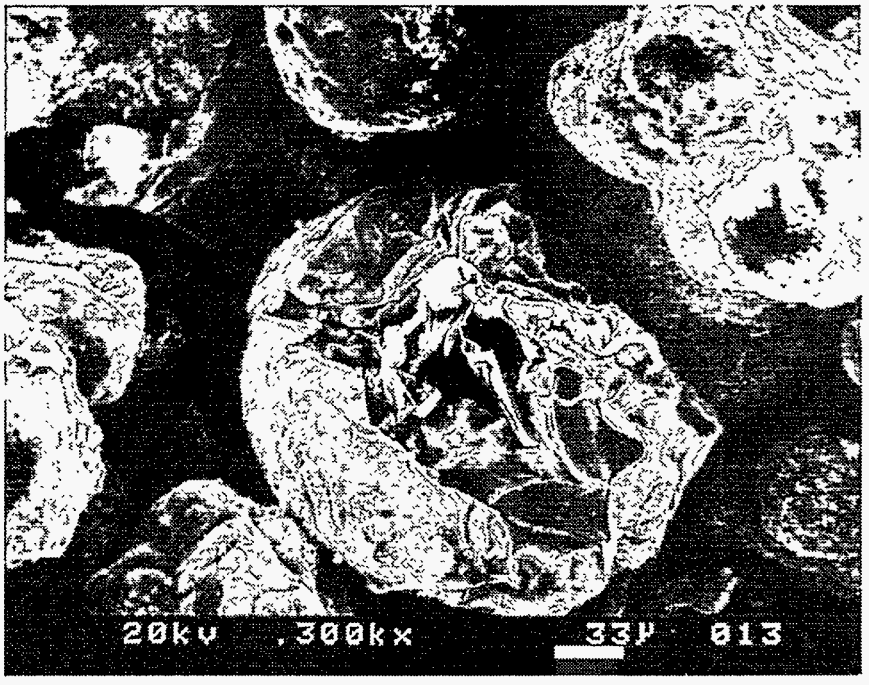

(b)

Figure 4-56. SEM MICROGRAPHS OF CHAR COLLECTED FROM THE RESEARCH BOILER HOPPER WHEN FIRING UPPER FREEPORT SEAM MCWM
(a) 0.25 k Magnification; (b) 0.30 k Magnification

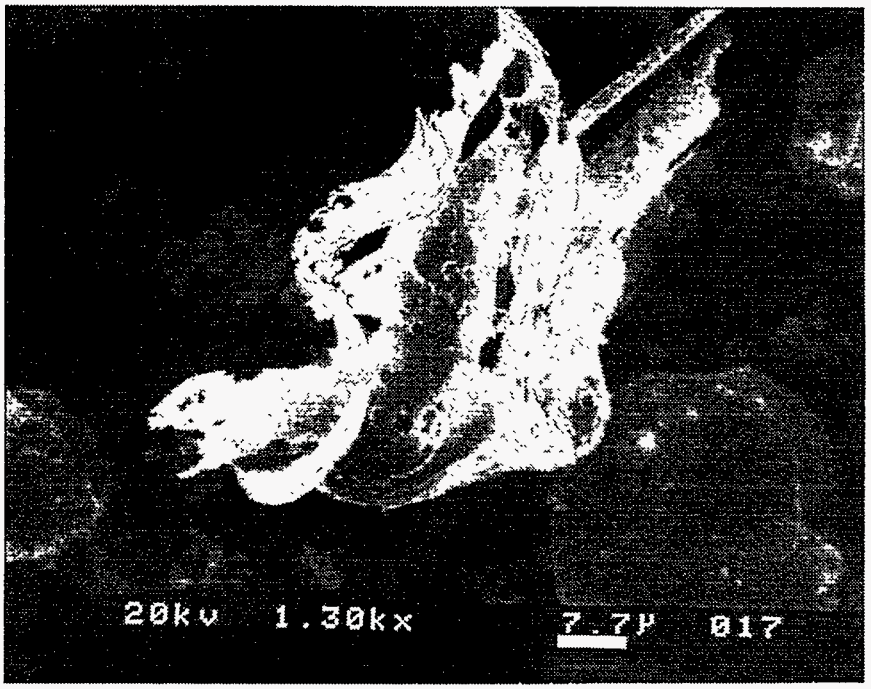

(a)

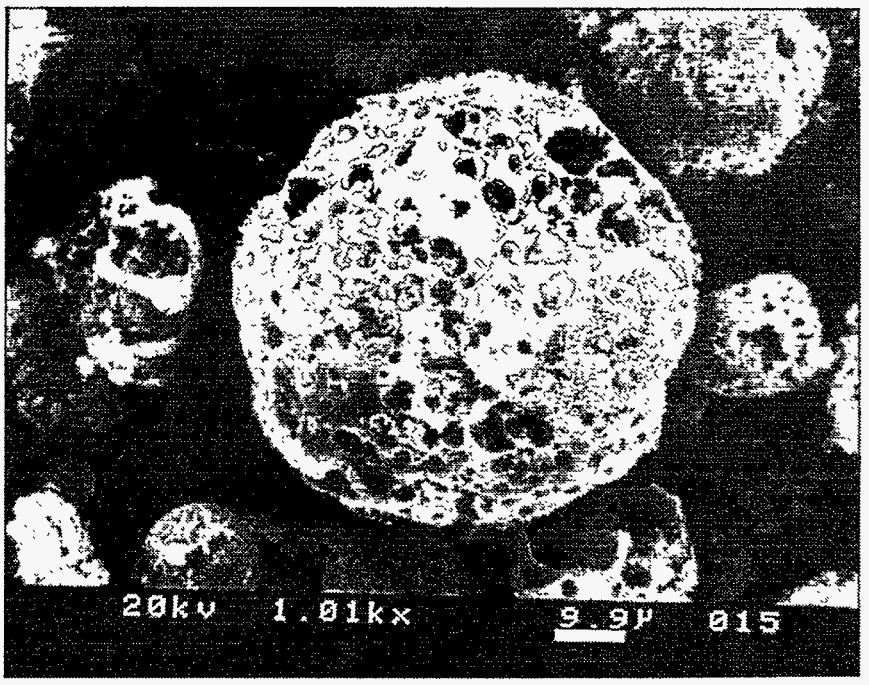

(b)

Figure 4-57. SEM MICROGRAPHS OF CHAR COLLECTED FROM THE RESEARCH BOILER BAGHOUSE WHEN FIRING UPPER FREEPORT SEAM MCWM
(a) 1.01 k Magnification; (b) 1.30 k Magnification

Table 4-12. Summary of Char/Ash Collected in the Hopper and Baghouse When Firing Upper Freeport and Taggart Seam DMCs and MCWMs

	Upper Freeport DMC	**Upper Freeport MCWM**	**Taggart DMC**	**Taggart MCWM**
Total ash fed from coal (lbs)	38.1	43.3	12.6	30.4
Char/ash collected from baghouse (lbs)	26.0	121.1	11.4	66.9
Char/ash collected in hoppers (lbs)	2.1	22.8	2.9	18.6
Char/ash collected from the boiler floor (lbs)	9.4	9.1	4.0	5.4

temperature at which movement occurred was recorded as the initial (softening) temperature. The solder bath was heated at a constant rate of 3°C/minute from the starting temperature (330°C) to 600°C. The fluidity (dial divisions per minute, ddpm) and temperature were recorded every minute to determine the temperature of maximum fluidity, the maximum fluidity, the initial softening temperature and the final resolidification temperature.

A summary of the influence of water addition on these properties is:

Coal	FSI	Maximum Fluidity (ddpm)
Upper Freeport Coal	3	70
Upper Freeport Coal (with water)	3	48
Taggart Coal	3	3,698
Taggart Coal (with water)	3	2,101

Water addition did not enhance the swelling or fluidity of the coals, in fact, the maximum fluidity decreased. Therefore, the cenosphere formation must be a result of the differences in combustion conditions. It should be noted that the maximum gas temperatures in the boiler by suction pyrometry were approximately 300°F lower when firing MCWM than when firing DMC. The mean size of the MCWM droplets issuing from the atomizer was 3-4 times larger than the mean particle size observed during DMC firing. These two factors decrease the droplet heating rate and therefore, the time required to reach the maximum temperature. This increases the duration over which the particles remain fluid, thus providing enough time for the carbon atoms to rearrange before resolidification. For the DMC particles, the heating rate was so rapid that the time during which the particles were fluid was short and this resulted in resolidification before the molecules rearranged.

Combustion Efficiency

The combustion efficiency results are tabulated in Table 4-5. The combustion efficiency for the DMC was higher than that for the MCWM (Figure 4-58). The average baghouse combustion efficiency for the Taggart seam MCWM was 97.6% whereas it was 88.5% for the Upper Freeport seam MCWM. The combustion efficiency for the Taggart seam DMC was 98.5% whereas it was 97.6% for the Upper Freeport seam DMC. The difference in combustion efficiency between the DMC and MCWM tests for the Taggart seam coal was only 0.9% (based on average results from multiple tests). On the other hand, the difference in combustion efficiency between the DMC and MCWM tests for the Upper Freeport seam coal was 9.1%. The mean particle size of the Taggart seam MCWM char was almost twice that of the DMC char but the combustion efficiency was only 0.9% lower; whereas the mean particle size of the Upper Freeport seam MCWM char was also twice than that of the DMC char but the combustion efficiency was 0.1%

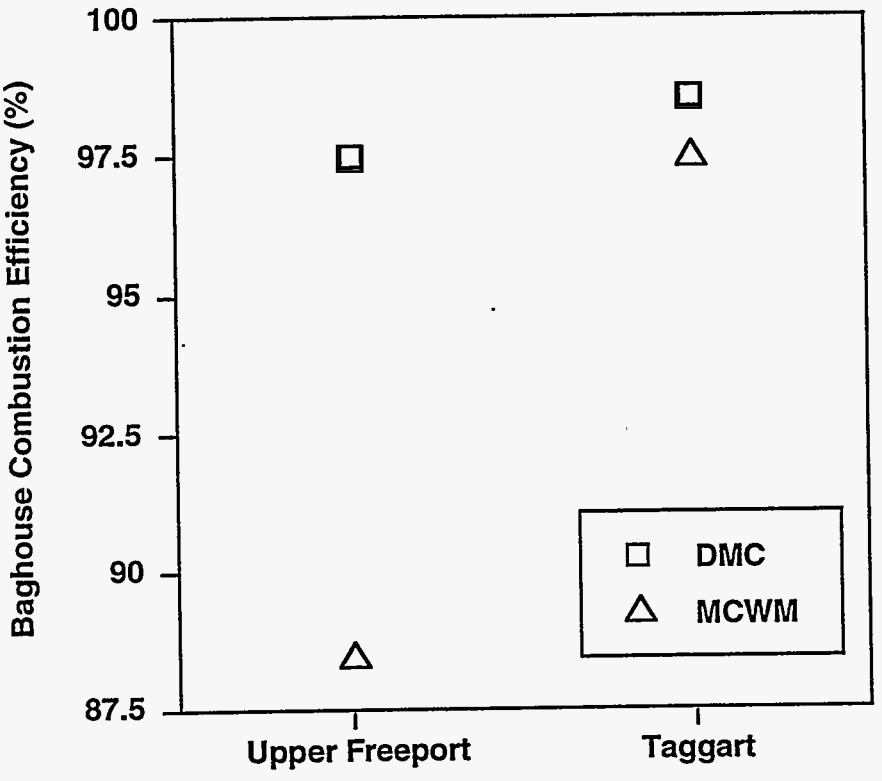

Figure 4-58. DIFFERENCES IN COMBUSTION EFFICIENCY BETWEEN DMC AND MCWM TESTS

lower. These data suggest that in addition to the larger particle size, which reduces the oxygen penetration, ash also physically hinders the penetration of oxygen in the case of MCWM droplets. This effect due to ash is also evident in the case of DMC but is lower in magnitude because of the smaller particle size.

Figure 4-59 is a plot of combustion efficiency as a function of ash content for all the MCWM tests performed. Irrespective of the solids loading or viscosity of the MCWM, the Upper Freeport seam MCWM consistently had lower combustion efficiencies than the Taggart seam MCWMs. This supports the hypothesis that ash hinders the oxygen availability or penetration.

4.4 Demonstration-Scale Activities

The demonstration-scale activities included procuring a coal-based burner, burner and boiler characterization firing natural gas, a DMC demonstration, and a MCWM demonstration. Each is discussed in detail in the following sections. The procurement of the burner, and tests firing natural gas, DMC, and MCWM were conducted in the order listed.

4.4.1 Burner Procurement

A commercial low-NO_x burner capable of firing natural gas and DMC or MCWM was designed and constructed by EER for Penn State's 15,000 lb steam/h demonstration boiler. A side view of the burner is shown in Figure 4-60 and a sectional view is shown in Figure 4-61. The specifications for which the burner was designed are:

DMC

- >3:1 turndown
- < 8" H_2O pressure drop
- Dual fuel capable (Natural gas and DMC)
- No support fuel required for flame stability
- < 400°F combustion air preheat temperature
- > 98% coal combustion efficiency
- < 200 ppm CO @ 3%O_2 (~0.17 lb/million Btu)
- < 475 ppm NO_x @ 3%O_2 (~0.6 lb/million Btu)
- 25% excess air

MCWM

- >3:1 turndown
- < 8" H_2O pressure drop
- Dual fuel capable (Natural gas and MCWM)
- No support fuel required for flame stability
- < 400°F combustion air preheat temperature
- > 98% coal combustion efficiency
- < 200 ppm CO @ 3%O_2 (~0.17 lb/million Btu)
- < 475 ppm NO_x @ 3%O_2 (~0.60 lb/million Btu)
- 25% excess air
- > 4,000 h atomizer tip life
- < 0.2 atomizing air/fuel ratio
- 90 psig atomizing air pressure
- air or steam as the atomizing medium

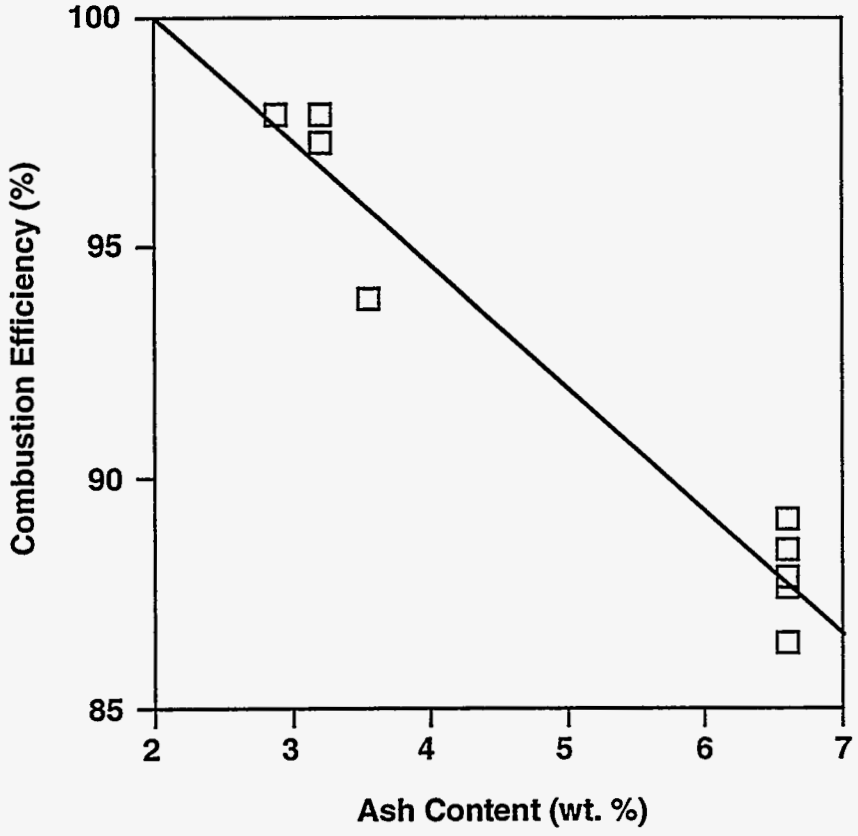

Figure 4-59. EFFECT OF ASH CONTENT ON THE COMBUSTION EFFICIENCY OF THE MCWM TESTS

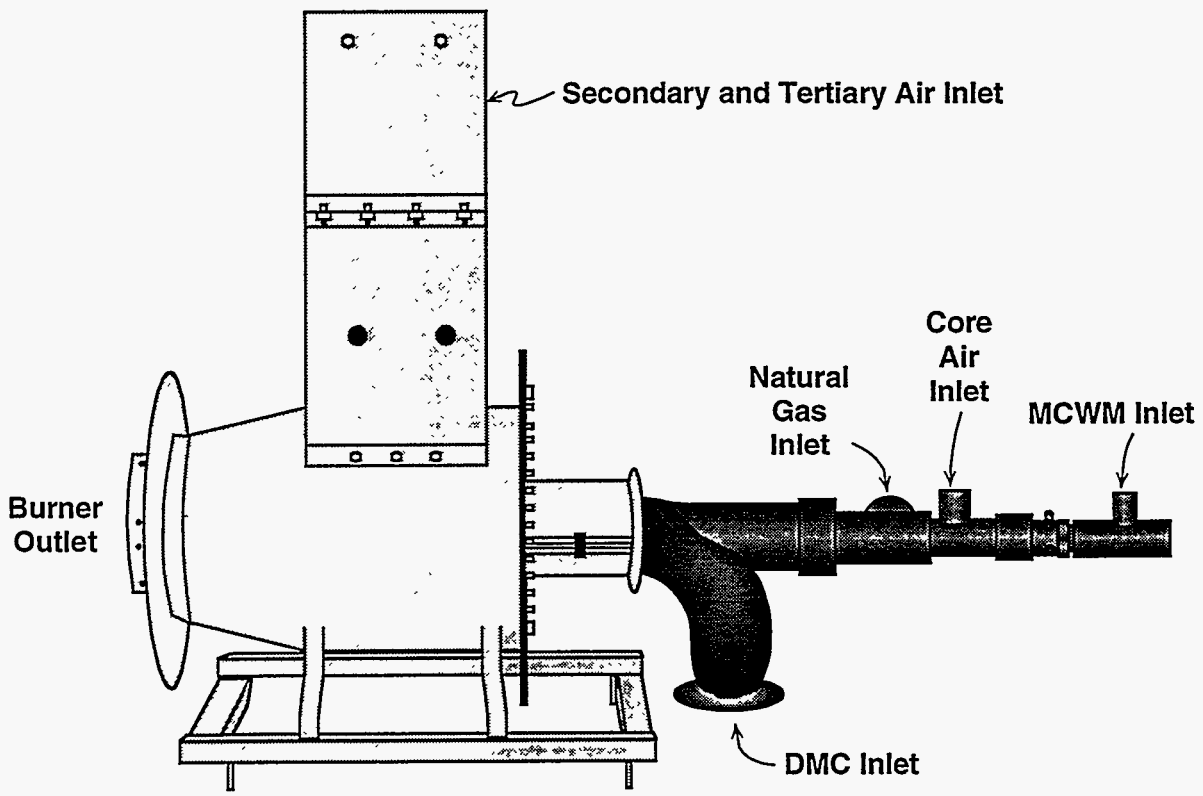

Figure 4-60. SIDE VIEW OF ASSEMBLED BURNER PRIOR TO INSTALLATION INTO THE DEMONSTRATION BOILER

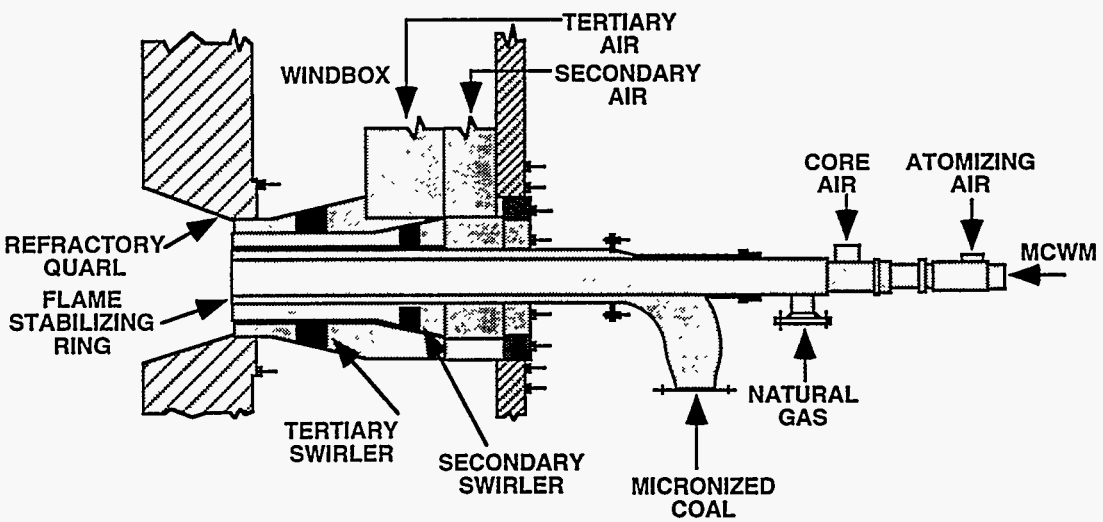

Figure 4-61. EER BURNER SECTIONAL VIEW

4.4.2 Burner/Boiler Characterization Firing Natural Gas

After the burner was installed, it was shaken down and evaluated firing natural gas prior to the first (DMC) demonstration. This was done to ensure proper performance firing natural gas, to obtain comparative data to previous burners, and to provide baseline data prior to firing coal.

Burner Optimization

Difficulties were initially experienced upon firing natural gas. The burner was unstable and high CO emissions were observed. Modifications to the burner were necessary in order to maintain a stable flame. The modifications consisted of systematically plugging axial natural gas ports and drilling radial ports until a stable flame was obtained. Details of the burner modifications are given elsewhere[121]. In addition, modifications to the ultra violet (u.v.) scanner tube and refractory rework were necessary for flame detection. Figure 4-62 is a schematic diagram of the natural gas burner prior to, and after, the modifications.

Baseline Data Firing Natural Gas

A series of tests was conducted to evaluate the performance of the burner firing natural gas. This was done to verify natural gas firing capabilities and characterize the burner on natural gas prior to beginning coal firing. The objective of the testing was to evaluate the effect of excess oxygen, firing rate, and tertiary and secondary air swirl on boiler efficiency and emissions, and to determine the burner stability as a function of tertiary and secondary air degree of swirl and flow.

Table 4-13 contains a summary of the tests (boiler performance/emissions) except for the stability tests which are presented later. Each boiler performance/emissions test was conducted over a five to six hour period with maximum tertiary and secondary air swirl. The tests are presented in chronological order and the planned test conditions are briefly described below.

- Test No. 1 -- High firing rate; 2% O_2
- Test No. 2 -- High firing rate; 3% O_2
- Test No. 3 -- High firing rate; 2% O_2; repeat of Test No. 1 (reproducibility test)
- Test No. 4 -- High firing rate; 1% O_2
- Test No. 5 -- ~60% firing rate; 2% O_2
- Test No. 6 -- ~80% firing rate; 2% O_2
- Test No. 7 -- Lowest firing rate achievable when firing at 3% O_2
- Test No. 8 -- High firing rate; 2% O_2; 2-hour test
- Test No. 9 -- Lowest firing rate achievable when firing at 1% O_2
- Test No. 10 -- High firing rate; 3% O_2; heat flux and suction pyrometry data obtained
- Test No. 11 -- High firing rate; 2% O_2; minimal transport air
- Test No. 12 -- High firing rate; 3% O_2; heat flux data obtained (This test was a repeat of Test No. 10 after it was observed that the steam drum pressure was 183 psig instead of ~200 psig which is the normal operating pressure.)
- Test No. 13 -- High firing rate; 2% O_2; minimum tertiary and secondary air swirl
- Test No. 14 -- High firing rate; 2% O_2; medium tertiary and secondary air swirl
- Test No. 15 -- High firing rate; 2% O_2; minimal transport air (This test was a repeat of Test No. 11 after it was observed that the steam drum pressure was 178 psig instead of ~200 psig which is the normal operating pressure.)

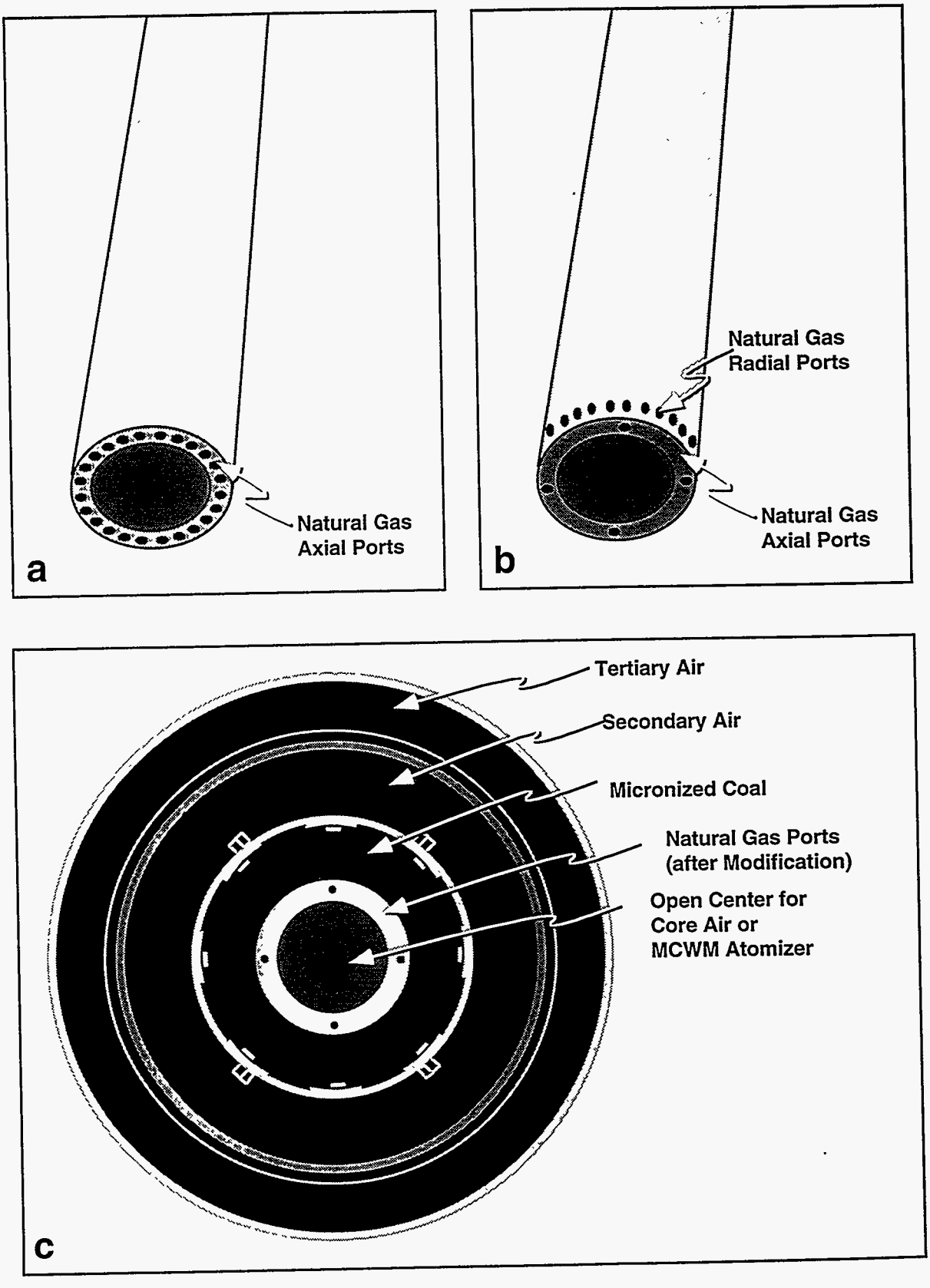

Figure 4-62. SCHEMATIC DIAGRAMS OF THE NATURAL GAS BURNER PRIOR TO (a) AND AFTER MODIFICATION (b) AND THE FRONT VIEW OF THE BURNER (c)

Table 4-13. Summary of Results for Boiler Performance/Emissions Testing When Firing Natural Gas

Summary Sheet																
	Test No. 1	Test No. 2	Test No. 3	Test No. 4	Test No. 5	Test No. 6	Test No. 7	Test No. 8	Test No. 9	Test No. 10	Test No. 11	Test No. 12	Test No. 13	Test No. 14	Test No. 15
	20-Jun	21-Jun	21-Jun	22-Jun	22-Jun	23-Jun	23-Jun	24-Jun	24-Jun	28-Jun	29-Jun	6-Jul	7-Jul	7-Jul	8-Jul
TEST/DESCRIPTION:		A	B	A	B	A	B	A	B				A	B	
	2% O2;	3% O2;	2% O2;	1% O2;	2% O2;	2% O2;	3% O2;	2% O2;	1% O2;	3% O2;	2% O2;	3% O2;	2% O2;	2% O2;	2% O2;
	100% load	100% load	100% load	100% load	~60% load	~80% load	lowest load	100% load;	lowest load	100% load;	100% load;	100% load;	100% load;	100% load;	100% load;
								2h test		probes	low mill air	probes	Min Swirl	Med Swirl	low mill air
WATER/STEAM SIDE															
Steam flow rate; lb/h	15,290	15,088	15,138	15,429	10,131	14,249	11,788	15,446	11,328	16,232	16,778	14,556	14,871	13,895	15,015
Water temperature into boiler; °F	208	201	206	204	208	209	208	206	207	165	162	204	208	208	208
Drum pressure; psig	205	205	203	204	190	175	171	200	194	183	178	213	212	209	208
Calorimeter temperature; °F	Not Measured (NM)	NM	307	308	302	300	296	307	303	302	301	309	304	308	302
Steam temperature; °F	383	381	382	382	377	370	368	381	378	373	370	385	385	384	383
Steam quality; %	Not Determined (ND)	ND	99.66	99.73	99.39	99.25	99.05	99.63	99.44	99.38	99.29	99.74	99.48	99.71	99.37
Blowdown rate; lb/h	3,136	3,139	3,125	3,126	3,019	2,899	2,864	3,098	3,054	2,968	2,925	3,199	3,187	3,167	3,156
AIR, FUEL, FLUE GAS SIDE															
Natural gas flow rate; lb/h;MMBtu/h	704;16.5	708;16.6	706;16.6	707;16.6	433;10.2	559;13.1	461;10.8	706;16.6	499;11.7	705;16.6	705;16.6	704;16.6	705;16.6	654;15.4	703;16.5
Air temperature entering air heater; °F	160	98	114	118	154	127	125	93	102	155	159	173	163	167	170
Air temperature leaving air heater; °F	401	373	380	376	364	357	348	364	348	392	387	405	397	393	400
Air temperature into boiler; °F	375	347	355	350	338	335	325	339	323	366	362	379	372	369	374
Boiler outlet temperature; °F	561	557	556	555	481	511	484	554	497	554	552	562	566	561	556
Gas temperature leaving air heater; °F	386	363	366	361	316	330	308	352	305	379	373	389	385	377	385
Baghilter inlet temperature; °F	380	357	359	355	312	325	305	346	300	373	368	384	381	373	381
Baghilter outlet temperature; °F	344	327	330	323	281	294	275	310	269	343	334	352	346	342	347
Combustion air flow; lb/h	13,119	13,666	13,105	12,654	8,081	10,520	8,965	13,123	8,909	13,225	12,830	13,260	13,077	12,740	12,925
Boiler *draft; in* H2O	-0.04	-0.05	-0.04	-0.01	-0.04	-0.02	-0.03	-0.05	-0.04	-0.06	-0.06	-0.04	-0.01	-0.02	-0.03
Boiler efficiency; %	83.08	83.44	83.60	83.55	84.25	83.87	84.22	82.49	84.01	82.86	83.24	82.87	82.80	82.98	82.87
Mill air flow rate; ACFM;lbs/hr	228;1148	308;1552	306;1546	150;752	156;787	148;742	153;773	155;781	158;793	311;1561	186;935	345;1750	156;785	176;891	284;1432
Mill inlet temperature; °F	81	80	82	78	81	77	80	81	80	78	78	84	81	82	80
Mill outlet temperature; °F	79	78	80	77	79	76	78	79	77	76	76	82	79	80	79
Burner inlet temperature; °F	86	83	86	81	85	82	86	85	84	81	80	90	83	86	86
Natural gas temperature; °F	74	70	74	71	79	73	78	75	76	69	69	76	73	75	74
EMISSIONS															
O2; %	2.05	2.80	1.98	1.22	2.07	2.24	2.90	2.07	1.15	2.21	1.55	2.27	1.96	2.95	1.79
CO; ppm	33	28	44	303	34	20	19	36	138	30	6	17	32	22	40
CO2; %	11.43	11.08	11.48	11.63	11.44	11.00	10.77	8.75	9.97	10.63	11.29	10.79	10.77	10.78	10.84
SO2; ppm	Not Applicable (NA)	NA	NA	NA	NA	NA	NA	NA	NA	NA	NA	NA	NA	NA	NA
NOx; ppm	40	91	91	92	101	87	85	88	78	108	103	97	86	86	86

Boiler Performance

The effects of the oxygen concentration in the flue gas (excess air), mill (coal transport) air flow rate, firing rate, and secondary and tertiary air swirl on boiler efficiency were determined. A detailed discussion of the results are given elsewhere[121]. In summary, the boiler efficiencies ranged from ~82.5 to 83.6% and exhibited a decreasing trend in boiler efficiency as O_2 concentration was increased (as would be expected) from ~1.2 to 1.8%, but was variable from 1.8 to ~3.0% O_2; no relationship between boiler efficiency and mill air (coal transport) flow was observed; the boiler efficiency exhibited a decreasing trend as the firing rate was increased from ~10.2 to 15.2 MM Btu/h but was very variable as it ranged from ~82.5 to 83.6% when firing at 16.5 MM Btu/h; and there was a minor effect of swirl on boiler efficiency as it increased as swirl increased.

Emissions

The effects of excess air (O_2 concentration), firing rate, and secondary and tertiary air swirl on CO and NO_x emissions were determined. None of these operating conditions affected the emissions significantly except for very low O_2 concentration (~1.1%) where the CO concentration increased from the typical <40 to 140 to 300 ppm. The concentration of NO_x was consistently in the 90 to 100 ppm range.

Burner Stability

A series of eight tests was conducted to evaluate the stability of the burner when varying the secondary and tertiary air dampers and swirl. This was done to characterize the burner prior to firing coal. The tests that were conducted were:

Matrix Number	Tertiary Air Damper Setting	Secondary Air Damper Setting	Tertiary Air Swirl	Secondary Air Swirl
1	Maximum	*Varied*	Maximum	Maximum
2	*Varied*	Maximum	Maximum	Maximum
3	Maximum	Maximum	Maximum	*Varied*
4	Maximum	Maximum	*Varied*	Maximum
5	*Varied*	Maximum	Minimum	Minimum
6	Maximum	*Varied*	Maximum	Minimum
7	*Varied*	Maximum	Maximum	Minimum
8	Maximum	*Varied*	Maximum	Minimum

A detailed discussion of the results of the stability testing is found elsewhere [122]. In summary, the burner was very stable regardless of secondary and tertiary air swirl or the amount of secondary air introduced into the boiler. Only when closing the tertiary air damper, and hence limiting the quantity of combustion air into the boiler, did the burner become unstable. The burner

exhibited flexibility in damper and swirl settings.

4.4.3 DMC Demonstration

A DMC demonstration was conducted with the objectives of determining burner and boiler performance, improving burner performance (increasing combustion efficiency) firing coal, examining furnace and convective pass deposition, and determining the effect of deposition on continuous operation. A day-to-day synopsis can be found elsewhere[67, 121]. A total of 2,028.5 hours of operation were accumulated from May through December 1994, of which 396.1 hours were with coal firing (5.1 hours of operation per 1.0 hour of coal firing). The DMC demonstration included coal firing, baseline testing (natural gas), burner optimization (natural gas and DMC), system modification, and component repair.

Table 4-14 contains a boiler performance and emissions summary (which are averaged over half hour periods) for the DMC demonstration. Most of the testing was conducted with two shifts per day except for the testing from November 21 to 22, 1994 and from December 5 to 7, 1994. These tests were continuous (24 h/day) but the results have been reported for either twelve or eight hour periods for the November and December testing, respectively.

Two coals were used during the demonstration. The first was Brookville seam coal (from July to September 1994) which had been tested in the SCCWS and HEACC projects. The second was an Upper Freeport seam coal (October through December). Table 4-15 contains the coal analysis of weekly composites produced from daily samples collected at the screw feeder outlet.

Combustion and Boiler Performance

The combustion and boiler efficiencies, when firing DMC, ranged from 86 to 95% and from 76 to 84%, respectively. Figure 4-63 shows the combustion efficiency for the testing conducted from July to December 1994. Most of the DMC operation resulted in combustion efficiencies ranging from 92 to 94%, which were below the target of 98%.

In an attempt to increase combustion efficiency, the quantity of secondary and tertiary air and their degrees of swirl were varied, a coal diverger piece (cone) was installed, and air was introduced into the center of the burner. The installation of the cone and introducing air into the center of the burner had a negative impact on combustion efficiency; varying the quantity of secondary and tertiary air and their degrees of swirl did not result in combustion efficiencies greater than approximately 94%.

One goal of this testing was to improve upon the combustion efficiencies obtained during previous testing[5]. As can be seen from Figure 4-64, where the combustion efficiency results from the two series of DMC testing are overlaid, the combustion efficiencies obtained with the EER burner were slightly less than those obtained with the HEACC.

Deposition/Accumulation

A concern when firing coal in a boiler designed for fuel oil is the effect of the inorganic portion of the coal on deposition and erosion. This section describes the effect of deposition.

Table 4-14. Summary of Results for the DMC Demonstration

Summary Sheet

TEST/DESCRIPTION:	13-Jul #1 Gas Support	13-Jul #2 Coal Only	14-Jul #3 Gas Support	14-Jul #4 Coal Only	15-Jul #5 Coal Only	18-Jul #6 Coal Only	19-Jul 7 Coal Only	20-Jul 8 0800 hrs Gas Support	20-Jul 9 0945 hrs Gas Support	21-Jul 10 Coal Only	27-Jul 11 Coal Only
WATER/STEAM SIDE											
Steam flow rate; lb/h	11,830	8,868	12,877	12,446	11,164	12,063	12,269	12,048	11,956	11,754	12,486
Water temperature into boiler; °F	209	207	208	209	207	209	209	209	204	209	210
Drum pressure; psig	209	204	213	211	209	208	206	208	206	200	204
Calorimeter temperature; °F	215	305	203	294	288	307	306	203	203	306	306
Steam temperature; °F	384	381	385	385	384	384	383	384	383	383	382
Steam quality; %	94.39	99.51	93.72	98.93	98.58	99.66	99.59	93.74	93.73	99.62	99.62
Blowdown rate; lb/h	3,170	3,131	3,196	3,182	3,171	3,159	3,142	3,159	3,142	3,118	3,126
AIR,FUEL, FLUE GAS SIDE											
Natural gas flow rate: lb/h;MMBtu/h	280;6.58	0;0	140;3.29	0;0	0;0	0;0	0;0	313;7.35	326;7.66	0;0	0;0
Coal flow rate; lb/h,MMBtu/h	534;7.62	977;13.95	780;11.14	1,113;15.9	1,120;15.9	1,117;15.8	1,294;18.1	639;8.92	639;8.92	1,172;16.2	1,174;16.6
Air temperature entering air heater; °F	93	154	137	135	172	87	92	84	89	88	75
Air temperature leaving air heater; °F	366	392	405	411	417	409	403	383	392	402	397
Air temperature into boiler; °F	338	362	373	381	387	378	374	353	363	372	365
Furnace outlet temperature; °F	529	528	577	565	553	587	585	563	572	584	571
Gas temperature leaving air heater; °F	336	352	387	377	383	372	370	356	364	369	361
Bagfilter inlet temperature; °F	328	346	379	371	376	362	360	346	353	359	353
Bagfilter outlet temperature; °F	299	310	330	325	339	324	322	304	315	318	314
Combustion air flow; lb/h	12,880	12,646	13,180	13,571	14,221	13,601	15,818	15,415	15,783	14,388	14,220
Boiler draft; in H2O	0.01	-0.03	0.01	-0.01	-0.02	0.02	0.01	-0.01	-0.01	-0.09	-0.02
Boiler efficiency; %	84.1	82.1	83.5	83.9	83.5	83.6	84.0	83.3	83.3	80.7	82.9
Mill air flow rate: ACFM;lbs/hr	354;1,608	317;1,432	350;1,599	348;1,576	380;1,728	353;1,591	361;1,627	352;1,619	362;1,657	386;1,744	418;1,916
Mill inlet temperature; °F	94	98	93	96	95	99	99	88	90	98	89
Mill outlet temperature; °F	185	215	205	208	201	209	208	184	185	189	179
Burner inlet temperature; °F	152	181	172	174	182	180	183	148	153	170	166
Natural gas temperature; °F	82	97	82	79	94	90	92	80	82	90	77
Coal combustion efficiency; %	97.00	86.90	94.40	94.00	94.62	93.77	94.34	90.12	90.12	90.49	92.80
EMISSIONS											
O2; %	3.2	4.3	3.6	3.2	3.9	3.3	3.3	3.7	3.8	3.4	3.3
CO; ppm	52	1,454	122	193	123	286	161	34	28	192	158
CO2; %	13.4	14.7	14.7	16.0	15.1	16.0	16.0	15.5	15.5	15.6	16.1
SO2; ppm	219	479	354	496	514	499	481	121	125	490	456
NOx; ppm	446	298	540	536	538	541	573	444	404	553	594
Land Analyzer (in bold)											

Table 4-14. Summary of Results for the DMC Demonstration

Summary Sheet

TEST/DESCRIPTION:	28-Jul 12 Coal Only	29-Jul 13 Coal Only	1-Aug 14 Coal Only	3-Aug 15 Coal only	4-Aug 16 Coal only	4-Aug 17 Coal only	5-Aug 18 Coal only	10-Aug 19 Coal Only	11-Aug 20 Coal Only	25-Aug 21 Coal Only
WATER/STEAM SIDE										
Steam flow rate; lb/h	11,888	11,679	11,471	12,074	12,194	12,656	9,686	11,993	13,097	11,526
Water temperature into boiler; °F	209	209	210	209	206	205	117	220	215	217
Drum pressure; psig	199	196	204	197	201	191	209	206	207	211
Calorimeter temperature; °F	305	304	306	306	305	302	304	306	306	208
Steam temperature; °F	380	379	382	380	380	375	382	382	383	383
Steam quality; %	99.55	99.51	99.61	99.59	99.53	99.39	99.49	99.61	99.61	93.99
Blowdown rate; lb/h	3,087	3,064	3,126	3,077	3,110	3,028	3,170	3,145	3,149	3,187
AIR,FUEL, FLUE GAS SIDE										
Natural gas flow rate: lb/h;MMBtu/h	0;0	0;0	0;0	0;0	0;0	0;0	0;0	0;0	0;0	0;0
Coal flow rate; lb/h,MMBtu/h	1,174;16.7	1,174;16.5	1,174;16.6	1,129;15.9	1,129;16.0	1,129;16.0	1,170;16.4	1,166;16.7	1,165;16.5	1,135;16.1
Air temperature entering air heater; °F	110	119	118	132	132	131	98	128	128	144
Air temperature leaving air heater; °F	424	433	428	417	412	408	403	414	411	419
Air temperature into boiler; °F	394	403	394	390	386	385	375	382	385	386
Furnace outlet temperature; °F	582	582	578	578	581	575	572	142	159	570
Gas temperature leaving air heater; °F	385	393	388	385	386	382	368	382	387	381
Bagfilter inlet temperature; °F	379	388	382	378	377	375	364	376	380	374
Bagfilter outlet temperature; °F	335	344	342	338	337	334	326	335	339	331
Combustion air flow; lb/h	14,221	14,540	14,353	13,535	13,741	13,475	15,196	14,344	13,908	14,001
Boiler draft; in H2O	-0.01	-0.01	-0.01	-0.01	0.00	0.00	0.00	-0.01	0.01	0.02
Boiler efficiency; %	81.1	81.1	82.9	82.8	84.0	84.0	83.7	83.2	82.7	81.2
Mill air flow rate: ACFM;lbs/hr	424;1,927	488;2,214	489;2,222	294;1,327	324;1,467	308;1,383	311;1,409	303;1,389	283;1432	343;1569
Mill inlet temperature; °F	94	96	95	99	96	101	97	90	95	90
Mill outlet temperature; °F	181	171	171	213	201	208	205	195	210	212
Burner inlet temperature; °F	169	165	166	179	177	179	175	172	182	178
Natural gas temperature; °F	82	89	89	92	87	93	74	83	81	81
Coal combustion efficiency; %	91.32	91.72	93.76	93.46	95.29	94.90	94.62	94.16	93.77	91.92
EMISSIONS										
O2; %	3.2	3.6	3.8	3.5	4.0	3.7	4.7	3.6	3.3	3.8
CO; ppm	1,070	1,121	536	260	132	277	165	509	496	473
CO2; %	15.9	15.8	15.3	15.4	15.1	15.3	14.6	15.5	15.8	15.1
SO2; ppm	426	426	291	400	368	442	535	376	401	322
NOx; ppm	512	529	554	618	651	671	610	583	665	494
Land Analyzer (in bold)										

Table 4-14. Summary of Results for the DMC Demonstration

Summary Sheet

TEST/DESCRIPTION:	30-Aug 22 w/o gun	30-Aug 23 w/ gun	31-Aug 24 w/ gun	31-Aug 25 w/o gun	2-Sep 26 Coal Only w/ gun	13-Oct 27 cone installed	19-Oct 28	20-Oct 29	7-Nov 30 Coal Only
WATER/STEAM SIDE									
Steam flow rate; lb/h	12,016	11,439	11,462	11,271	11,600	11,835	13,289	15,508	13,167
Water temperature into boiler; °F	218	218	196	164	189	209	161	218	195
Drum pressure; psig	212	211	213	212	212	209	206	203	212
Calorimeter temperature; °F	208	211	215	230	203	161	308	203	305
Steam temperature; °F	386	385	385	385	384	385	384	383	382
Steam quality; %	93.98	94.17	94.41	95.27	93.73	91.31	99.68	93.69	99.56
Blowdown rate; lb/h	3,190	3,180	3,196	3,191	3,192	3,166	3,142	3,123	3,189
AIR,FUEL, FLUE GAS SIDE									
Natural gas flow rate: lb/h;MMBtu/h	0;0	0;0	0;0	0;0	0;0	0;0	0	0;0	0;0
Coal flow rate; lb/h,MMBtu/h	1,134;16.0	1,134;16.0	1,134;16.1	1,134;16.1	1,132;15.9	1,135;16.0	1,102;15.2	1,120;15.4	906;12.5
Air temperature entering air heater; °F	158	171	167	166	160	170	155	159	155
Air temperature leaving air heater; °F	415	420	420	426	417	422	414	415	399
Air temperature into boiler; °F	384	393	391	401	386	388	387	390	365
Furnace outlet temperature; °F	554	559	559	578	555	560	82	91	72
Gas temperature leaving air heater; °F	382	381	382	392	380	381	397	402	376
Bagfilter inlet temperature; °F	378	376	376	385	378	378	389	395	379
Bagfilter outlet temperature; °F	337	332	331	341	334	330	345	355	332
Combustion air flow; lb/h	13,468	13,790	13,860	13,894	13,005	13,806	14,160	13,759	11,134
Boiler draft; in H2O	0.02	-0.03	-0.02	-0.03	0.05	0.03	-0.02	0.00	-0.03
Boiler efficiency; %	82.6	80.3	80.6	83.1	82.4	80.1	81.8	80.7	79.6
Mill air flow rate: ACFM;lbs/hr	327;1494	333;1505	333;1517	333;1518	289;1316	345;1602	360;1663	365;1677	366;1705
Mill inlet temperature; °F	91	98	93	94	93	83	85	89	81
Mill outlet temperature; °F	204	208	203	204	217	194	216	219	207
Burner inlet temperature; °F	173	180	171	176	177	162	183	191	174
Natural gas temperature; °F	79	85	81	85	71	70	74	82	66
Coal combustion efficiency; %	93.16	90.17	90.39	93.81	92.71	91.50	93.28	91.71	89.71
EMISSIONS									
O2; %	3.1	3.5	3.4	3.5	2.7	3.6	4.0	3.3	3.7
CO; ppm	439	332	462	234	420	127	164	397	187
CO2; %	16.4	15.9	16.2	16.2	17.1	15.7	15.3	15.8	15.6
SO2; ppm	NM	NM	NM	NM	NM	60	337	334	96
NOx; ppm	507	427	416	544	639	519	338	364	299

Land Analyzer (in bold)

Table 4-14. Summary of Results for the DMC Demonstration

Summary Sheet

TEST/DESCRIPTION:	16-Nov 31 Coal Only	17-Nov 32 Coal Only	18-Nov 33 Coal Only	21-Nov 34 AM Cont. Testing	21-Nov 35 PM Cont. Testing	22-Nov 36 Coal Only Cont. Testing	28-Nov 37 Baseline prior to Cont. Test.	30-Nov 38 Baseline prior to Cont. Test.	1-Dec 39 Baseline prior to Cont. Test.
WATER/STEAM SIDE									
Steam flow rate; lb/h	12,454	13,650	12,748	13,448	14,851	15,027	9,252	10,409	11,052
Water temperature into boiler; °F	193	206	209	197	211	214	214	216	217
Drum pressure; psig	207	209	207	205	186	184	206	208	188
Calorimeter temperature; °F	305	304	303	302	300	302	200	300	278
Steam temperature; °F	381	382	381	380	373	373	380	382	374
Steam quality; %	99.53	99.50	99.42	99.38	99.25	99.38	93.55	99.25	98.01
Blowdown rate; lb/h	3,156	3,168	3,154	3,134	2,990	2,974	3,148	3,162	3,006
AIR,FUEL, FLUE GAS SIDE									
Natural gas flow rate: lb/h;MMBtu/h	0;0	0;0	0;0	0;0	0;0	0;0	0;0	0;0	0;0
Coal flow rate; lb/h,MMBtu/h	1,080;14.89	1,147;16.0	1,147;15.8	1,174;15.7	1,174;15.7	1,174;16.4	910;12.81	910;12.81	910;12.81
Air temperature entering air heater; °F	161	154	157	144	145	139	167	150	153
Air temperature leaving air heater; °F	428	417	416	410	414	408	415	411	413
Air temperature into boiler; °F	392	389	391	383	396	390	367	377	383
Furnace outlet temperature; °F	573	109	114	120	587	595	549	561	109
Gas temperature leaving air heater; °F	393	389	389	391	397	397	370	375	380
Bagfilter inlet temperature; °F	389	384	385	389	394	392	371	374	377
Bagfilter outlet temperature; °F	332	333	339	338	352	350	308	324	328
Combustion air flow; lb/h	13,995	16,783	15,721	14,780	14,359	15,287	11,514	11,841	11,900
Boiler draft; in H2O	-0.10	-0.04	-0.03	-0.02	-0.02	-0.02	-0.01	-0.03	-0.04
Boiler efficiency; %	76.2	48.6	59.7	79.6	79.7	82.1	78.8	79.9	80.5
Mill air flow rate: ACFM;lbs/hr	358;1673	353;1630	361;1670	360;1675	349;1613	358;1,658	359;1689	351;1625	357;1639
Mill inlet temperature; °F	80	86	85	81	86	84	75	85	89
Mill outlet temperature; °F	214	214	207	205	212	210	195	210	217
Burner inlet temperature; °F	176	181	175	172	185	183	169	178	179
Natural gas temperature; °F	61	68	70	56	67	68	62	69	65
Coal combustion efficiency; %	86.35	90.48	93.98	91.50	91.50	93.68	88.72	89.70	90.93
EMISSIONS									
O2; %	4.4	7.0	5.8	4.2	3.7	4.5	4.1	4.4	4.6
CO; ppm	1,339	115	-4	225	256	301	987	526	782
CO2; %	14.8	10.5	10.8	15.0	15.3	14.5	14.8	14.6	14.2
SO2; ppm	270	360	311	NM	NM	NM	NM	378	393
NOx; ppm	323	312	349	344	403	317	NM	224	242
Land Analyzer (in bold)									

Table 4-14. Summary of Results for the DMC Demonstration

Summary Sheet

TEST/DESCRIPTION:	2-Dec 40 Baseline prior to Cont. Test.	5-Dec 41 A Cont. Testing	5-Dec 42 B Cont. Testing	5-Dec 43 C Cont. Testing	6-Dec 44 A Cont. Testing	6-Dec 45 B Cont. Testing	6-Dec 46 C Cont. Testing	7-Dec 47 A Cont. Testing	7-Dec 48 B Cont. Testing
WATER/STEAM SIDE									
Steam flow rate; lb/h	10,639	10,895	11,155	12,148	11,573	11,914	11,855	12,031	11,682
Water temperature into boiler; °F	213	182	206	207	207	207	207	207	207
Drum pressure; psig	204	204	201	194	191	186	188	185	186
Calorimeter temperature; °F	304	304	302	302	301	300	300	301	300
Steam temperature; °F	381	380	378	376	375	373	374	374	373
Steam quality; %	99.48	99.49	99.38	99.37	99.30	99.23	99.27	99.31	99.25
Blowdown rate; lb/h	3,131	3,133	3,104	3,050	3,025	2,989	3,004	2,979	2,985
AIR,FUEL, FLUE GAS SIDE									
Natural gas flow rate: lb/h;MMBtu/h	0;0	0;0	0;0	0;0	0;0	0;0	0;0	0;0	0;0
Coal flow rate; lb/h,MMBtu/h	904;12.72	904;12.72	904;12.72	904;12.72	904;12.72	904;12.72	904;12.72	904;12.72	904;12.72
Air temperature entering air heater; °F	163	160	165	162	163	162	165	160	156
Air temperature leaving air heater; °F	434	425	425	425	423	421	421	417	413
Air temperature into boiler; °F	402	393	400	399	400	400	402	401	398
Furnace outlet temperature; °F	593	585	582	596	585	583	585	583	579
Gas temperature leaving air heater; °F	394	390	392	398	393	392	392	389	386
Bagfilter inlet temperature; °F	390	386	388	393	389	389	390	388	384
Bagfilter outlet temperature; °F	338	334	342	350	343	342	343	339	335
Combustion air flow; lb/h	11,875	11,692	12,092	12,159	12,423	12,020	12,119	11,974	12,370
Boiler draft; in H2O	-0.03	-0.04	-0.04	-0.08	-0.06	-0.06	-0.06	-0.06	-0.06
Boiler efficiency; %	82.7	82.5	82.1	81.2	82.1	81.0	82.6	83.2	80.9
Mill air flow rate: ACFM;lbs/hr	369;1710	350;1625	358;1657	358;1657	359;1650	350;1610	351;1613	348;1593	350;1611
Mill inlet temperature; °F	84	84	84	86	89	88	89	91	87
Mill outlet temperature; °F	207	212	208	198	209	212	214	215	209
Burner inlet temperature; °F	171	171	171	168	176	178	178	179	172
Natural gas temperature; °F	74	68	71	71	70	66	71	70	72
Coal combustion efficiency; %	94.11	94.11	93.98	93.00	93.92	92.34	94.41	94.84	92.43
EMISSIONS									
O2; %	4.6	4.2	4.8	4.9	5.3	4.8	4.9	4.5	5.3
CO; ppm	5	287	279	183	217	339	240	257	540
CO2; %	14.3	14.4	13.8	13.7	13.7	14.1	13.9	14.1	13.4
SO2; ppm	475	430	375	402	386	391	502	516	480
NOx; ppm	287	304	300	364	354	345	330	327	276
Land Analyzer (in bold)									

Table 4-15. Coal Analysis of Composite Samples Collected During the DMC Demonstration

Date	Screw Composite	Full Proximate Analysis				Ultimate Analysis					Cal Value (Dry)
		% Moist (Dried)	% V.M. (Dry)	% Ash (Dry)	% F.C. (Dry)	% C (Dry)	% H (Dry)	% N (Dry)	% S (Dry)	% O (Dry)	
11 Jul - 15 Jul	screw	02.66 ±0.04	35.81 ±0.00	03.66 ±0.01	60.53	81.19 ±0.04	05.34 ±0.05	01.55 ±0.01	00.68 ±0.01	07.58	14229 ±19
18 Jul - 22 Jul	screw	02.39 00.00	34.84 ±0.19	04.76 ±0.09	60.40	80.24 ±0.15	05.30 ±0.01	01.51 ±0.01	00.73 ±0.01	07.46	14084 ±7
25 Jul - 29 Jul	screw	02.39 ±0.01	34.45 ±0.03	04.62 ±0.01	60.93	80.54 ±0.02	05.28 ±0.04	01.51 ±0.03	00.77 ±0.01	07.28	14070 ±16
01 Aug - 05 Aug	screw	03.06 ±0.05	34.41 ±0.21	05.72 ±0.04	59.87	79.48 ±0.03	05.24 ±0.01	01.52 ±0.03	00.64 ±0.01	07.40	13883 ±3
08 Aug - 12 Aug	screw	02.83 ±0.01	34.65 ±0.01	04.19 ±0.01	61.16	80.86 ±0.01	05.32 ±0.01	01.53 ±0.01	00.56 ±0.01	07.54	14143 ±22
25 Aug - 02 Sep	screw	02.72 ±0.04	34.37 ±0.01	04.36 ±0.01	61.27	80.73 ±0.01	05.27 ±0.04	01.53 ±0.00	00.61 ±0.00	07.50	14163 ±11
19 Oct - 21 Oct	screw	01.63 ±0.03	32.03 ±0.04	06.57 ±0.03	61.40	79.51 ±0.01	05.38 ±0.08	01.50 ±0.02	00.53 ±0.01	06.51	13771 ± 1
07 Nov - 18 Nov	screw	01.72 ±0.03	31.91 ±0.03	06.93 ±0.03	61.16	79.13 ± 0.12	05.09 ± 0.00	01.50 ± 0.01	00.52 ± 0.01	06.83	13915 ± 6
21 Nov - 22 Nov	screw	01.48 ±0.03	31.79 ±0.09	06.65 ±0.03	61.56	79.47 ± 0.06	05.10 ± 0.09	01.49 ± 0.02	00.44 ± 0.00	06.85	13909 ± 1
28 Nov - 02 Dec	screw	01.46 ±0.01	31.54 ±0.01	06.61 ±0.05	61.85	79.26 ± 0.20	05.00 ± 0.08	01.49 ± 0.03	00.48 ± 0.01	07.16	13852 ± 4
05 Dec - 07 Dec	screw	01.52 ±0.04	31.75 ±0.15	06.51 ±0.00	61.74	79.69 ±0.11	05.21 ± 0.01	01.44 ± 0.03	00.45 ± 0.01	06.70	14033 ± 1

Brookville Seam coal - July 11 through September 2
Upper Freeport Seam Coal - October 19 through December 7

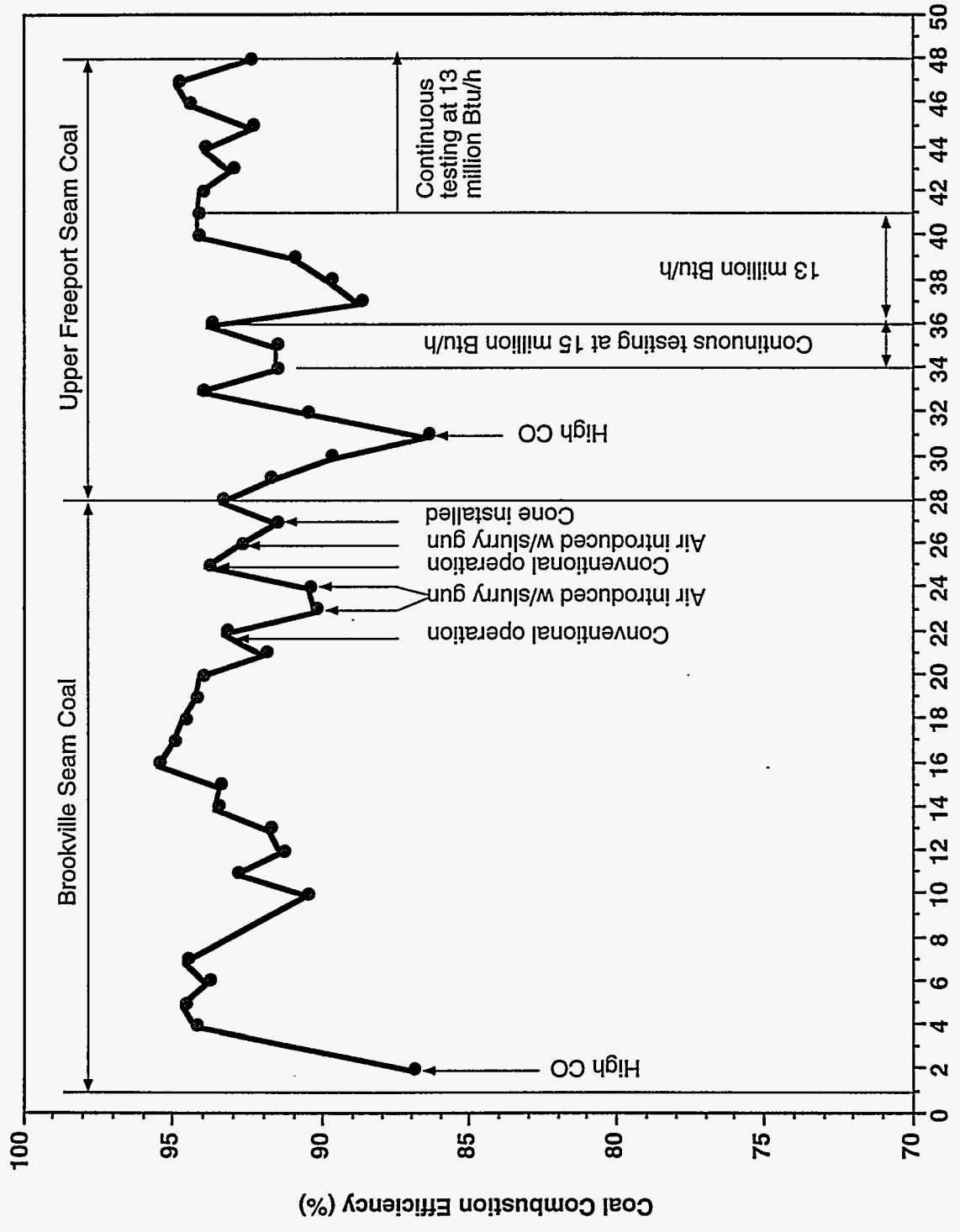

Figure 4-63. COAL COMBUSTION EFFICIENCIES FOR DMC TESTING FROM JULY TO DECEMBER 1994 USING THE EER BURNER

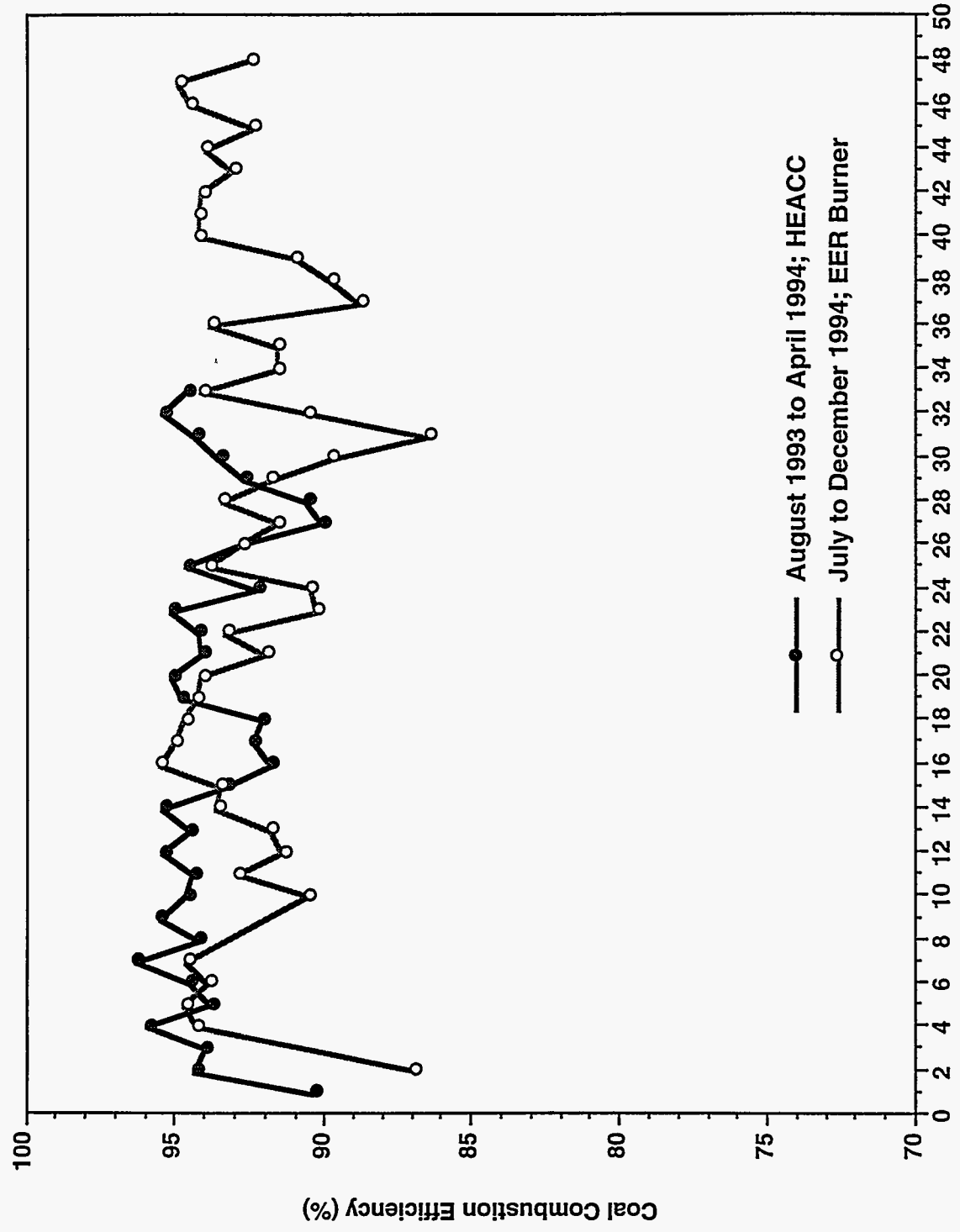

Figure 4-64. COAL COMBUSTION EFFICIENCIES FOR DMC TESTING

Erosion was previously addressed.

The boiler outlet and baghouse inlet temperatures were monitored and the convective pass steam sootblower was operated when the boiler outlet temperature was ~600°F. The baghouse inlet temperature would approach 400°F as the boiler outlet temperature reached 600°F and this is the upper limit set for comfortable operation.

Figure 4-65 is a typical plot of the boiler outlet temperature history for a day of operation. Figure 4-65 is a plot of boiler outlet temperature as a function of data acquisition time and shows when the coal feed was started (time 50), the period of cofiring coal and natural gas where the total firing rate was held constant and the coal feed was increased as the natural gas was decreased (approximately the next 100 data points), the switch to 100% coal (approximately time 175), four convective pass and furnace floor blowdowns, and the termination of the test (approximately time 800).

Plots such as Figure 4-65 illustrate the time/temperature history of the boiler outlet temperature but do not give a quantitative indication of the severity of deposition. Figure 4-66 is a plot of coal consumed since the last soot blowdown when using the Brookville seam coal. It must be noted that soot blowing routinely occurred at the beginning and end of most days and was not strictly a function of boiler outlet temperature. Noting this, between 2,000 and 3,000 lb of coal were fired between sootblowing events. This is similar to testing that occurred during the previous program firing DMC.

During the previous burner demonstration, testing was stopped because a significant quantity of ash was building up on the floor and walls of the furnace, and this had to be removed. As a consequence of this buildup, a manufacturer of commercial soot blowing systems was approached for options to keep the ash entrained. Their recommendation of retractable soot blowers was not adopted and Penn State designed a floor blast system. A schematic diagram of a prototype system is shown in Figure 4-67. The system consists of two pipes that are located on the furnace floor with a series of holes directed towards the furnace floor. A small quantity of air is constantly passed through the pipe to keep it cool. Whenever the sootblower in the convective pass is operated, the floor is also blown down. Several variations of the system have been tested where the hole size, height of the pipes above the floor, and the compressed air impact area on the floor have been varied. The results were encouraging; most of the ash was entrained and the boiler has not been shut down due to excessive ash accumulation on the furnace floor. The prototypes were constructed out of carbon steel (to use an inexpensive material of construction) while determining optimum design and operating conditions.

The demonstration boiler was operated on a 2-shift/day and a continuous (24 hour) basis during November and December 1994 to evaluate the effect of ash deposition on boiler performance. A detailed discussion of the results can be found elsewhere[121].

The boiler was operated at two firing rates -- approximately 16 and 13 million Btu/h. Prior

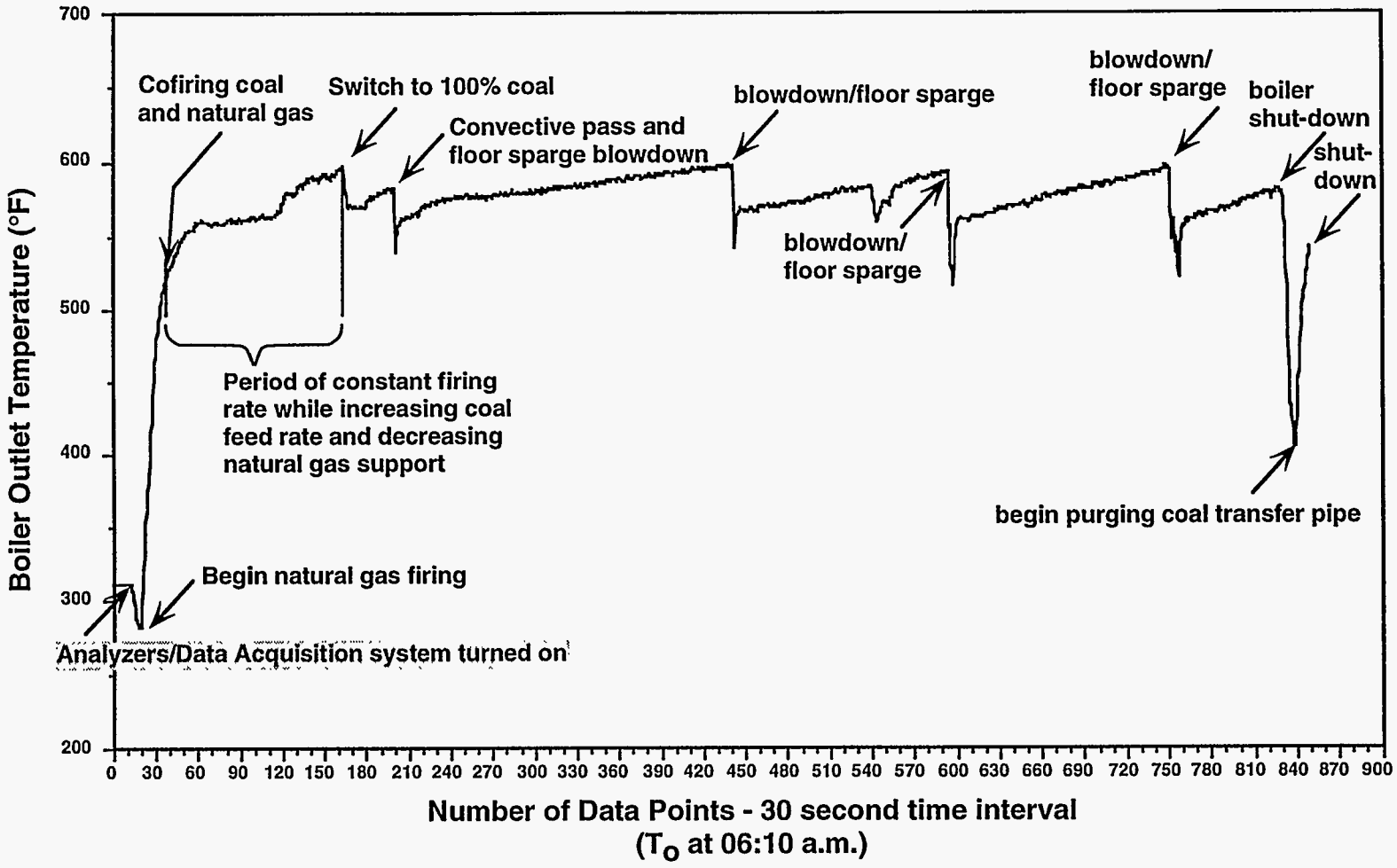

Figure 4-65. EXAMPLE OF BOILER OUTLET TEMPERATURE (°F) *vs* TIME FOR MICRONIZED COAL TESTING ON 08/04/94

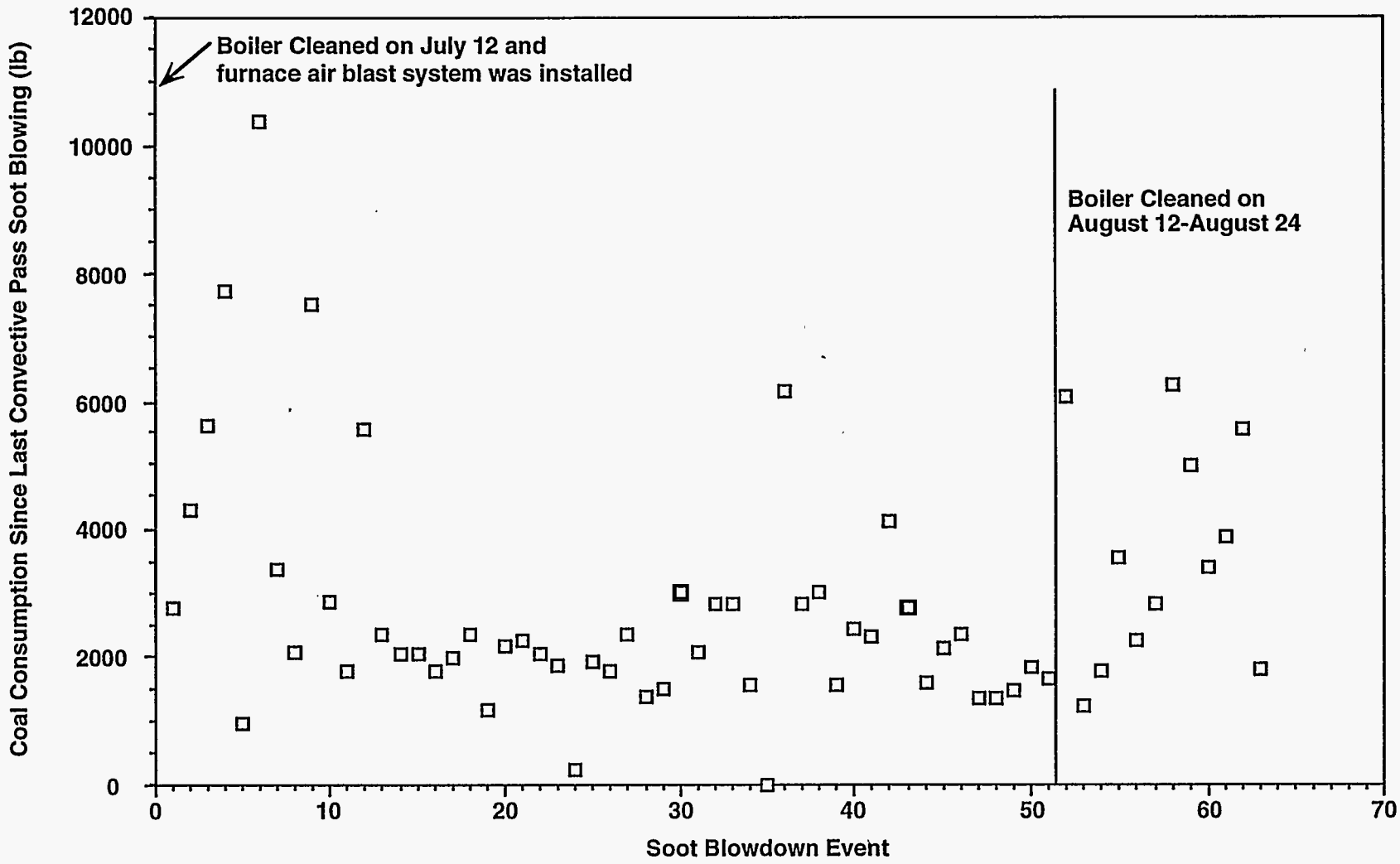

Figure 4-66. QUANTITY OF COAL CONSUMED SINCE LAST CONVECTIVE PASS SOOT BLOWING WHEN OPERATING FROM 07/13/94 TO 09/02/94

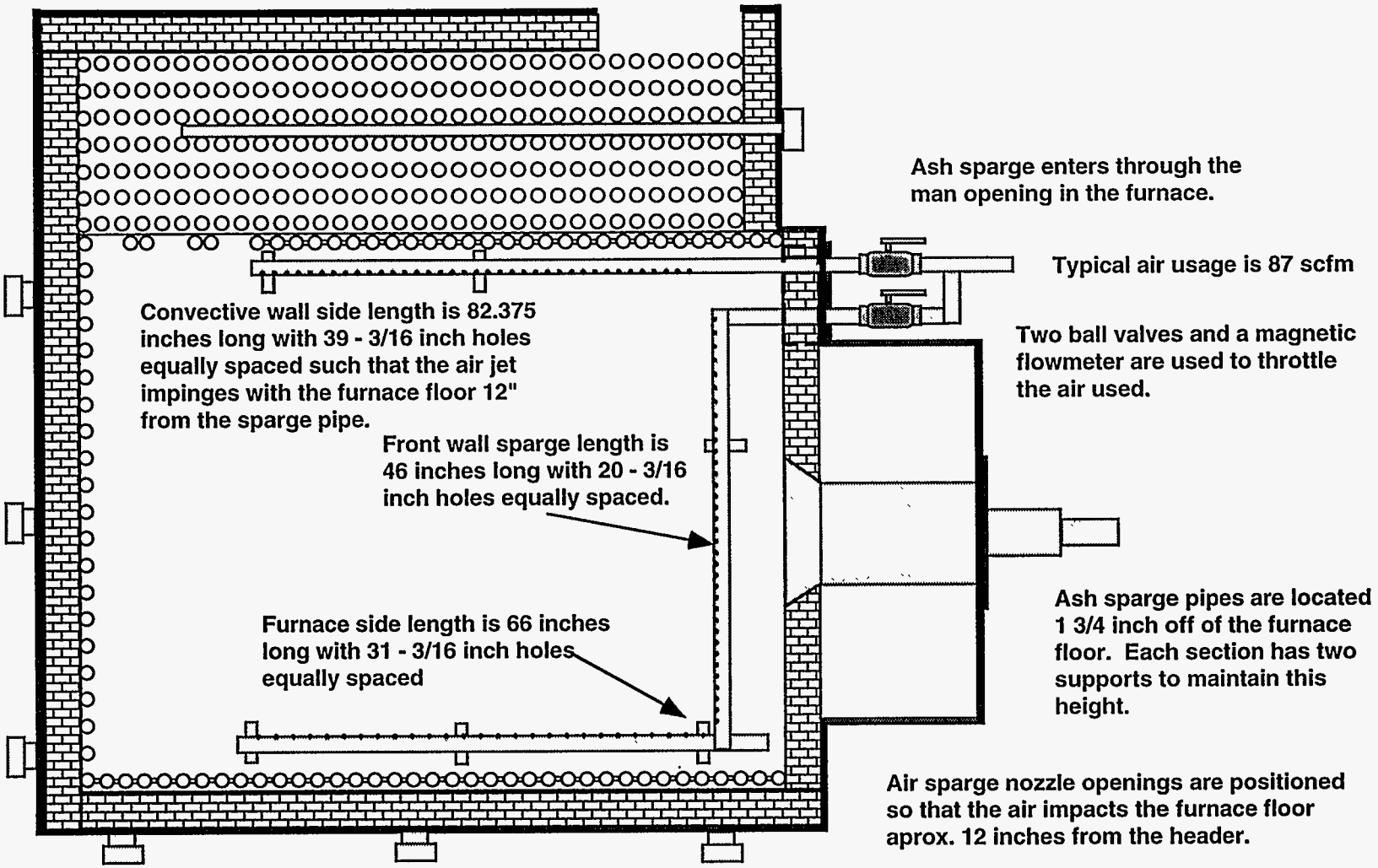

Figure 4-67. FURNACE ASH BLOWDOWN SYSTEM

to testing in November, the boiler was cleaned on November 4, 1994 and ash was removed from the furnace, the entrance to the convective pass, and the breaching (interconnection between the boiler and the heat-pipe heat exchanger). Tests conducted on November 16, 17, and 18, 1994 were performed while operating the boiler on two shifts per day and at 14.9 to 16.0 million Btu/h. The test conducted from November 21 to 22, 1994 was performed while operating the boiler 24-hours/day at a firing rate of 15.7 million Btu/h. The 15.7 firing rate increased from 15.7 (for two twelve hour periods) to 16.4 MM Btu/h (for one twelve hour period) because the feed rate was held constant but the heating value of the coal increased.

The boiler was cleaned on November 23, 1994 and ash was removed from the furnace, entrance to the convective pass, and the breaching. Tests were then conducted on November 28 and 30, 1994 and December 1 and 2, 1994 while operating the boiler on two shifts per day at 12.7 to 12.8 million Btu/h. A test was conducted from December 5 to 7, 1994 while continuously operating the boiler and firing at a rate of 12.7 million Btu/h.

Table 4-16 summarizes the results of the tests conducted at the two firing rates. It should be noted that there were not any operational problems observed when operating the boiler on a two-shift per day basis. The tests conducted when operating on a continuous basis were terminated when significant deposition was noted in the entrance to the convective pass (when firing at ~16 million Btu/h) and when the rear side panels of the boiler warped and discoloration was noted on the back wall (when firing at 12.7 million Btu/h).

Table 4-17 summarizes the results of the two continuous tests conducted at the two firing rates. As previously mentioned, the tests were terminated when significant deposition was noted in the entrance to the convective pass when firing at ~16 million Btu/h (11/21-11/22/94), and when the rear side panels of the boiler warped and discoloration was noted on the back wall when firing at 12.7 million Btu/h (12/05-12/07/94). The boiler was shut down on November 22, 1994 because it was the first time that such significant deposition was observed at the entrance into the convective pass. The shutdown on December 7, 1994 was a forced shutdown due to the sidewall (metal) warping allowing burning between the refractory rear wall and the insulation/metal skin interface.

Summary

No operational problems were encountered when operating the boiler on a two-shift per day basis. There was no significant deposition on the boiler walls or accumulation at the convective pass entrance, and the floor blast system entrained the majority of the ash (after a steady-state layer was deposited) that accumulated on the floor. It appears that the ash that deposited on the walls sloughed off due to the cyclic nature of the operation. Conversely, the tests conducted when operating on a continuous basis were terminated when significant deposition occurred at the entrance to the convective pass (when firing at ~16 MM Btu/h) and when refractory failure around a sight port on the sidewall occurred (when firing at 12.7 MM Btu/h). As a

Table 4-16. Deposition Summary -- Two Firing Rates

15.7 - 16.4 Million Btu/h	12.7 Million Btu/h
• 61,216 lb of coal were consumed at a rate of 1,148 lb/h for 53 h of operation.	• 74,606 lb of coal were consumed at a rate of 904 lb/h for 83 h of operation. (22% more coal was consumed and 57% more operating time was accumulated.)
• The boiler outlet pressure (B.O.P.) maxed out (<-2.2" W.C.) after consuming 57,000 lb of coal.	• The B.O.P. maxed out after consuming 64,000 lb of coal (12% more coal was consumed.).
• The B.O.P. started at -0.8" W.C. and began decreasing at 47,000 lb of coal consumed. There was 10,000 lb of coal consumed between the time the B.O.P. started to decrease and when the gauge maxed out. This is equivalent to 8.7 h of operation.	• The B.O.P. started at -0.8" W.C. and began decreasing at 56,000 lb of coal consumed. There was 8,000 lb of coal consumed between the time the B.O.P. started to decrease and when the gauge maxed out. This is equivalent to 8.9 h of operation.
• The sootblowing frequency was typically every half hour and increased to 1.5 and then 2h before boiler shutdown (during the continuous test).	• After the B.O.P. maxed out, the soot blowing frequency increased to 2, 2.75 2.5, and 2h before the forced shutdown.
• The boiler was cleaned out on 11/23/94 and 855 lb of ash were removed from the furnace/convective pass entrance and 180 lb of ash were removed from the breaching for a total of 1,035 lb. There was 3,979 lb of ash introduced into the boiler (6.50% ash as-rec.; 61,216 lb of coal fired); 26.0% of the ash was retained in the system.	• The boiler was cleaned out on 12/09/94 and 740 lb of ash were removed from the furnace/convective pass entrance and 175 lb of ash were removed from the breaching for a total of 915 lb. There was 4,693 lb of ash introduced into the boiler (6.29% ash as-rec.; 74,606 lb of coal fired); 19.5% of the ash was retained in the system.

Table 4-17. Deposition Summary -- Two Continuous Tests

11/21/-11/22/94 -- 15.7-16.4 Million Btu/h	12/05-12/07/94 -- 12.7 Million Btu/h
• 37,945 lb of coal were consumed at a rate of 1,148 lb/h for 33 h of operation	• 53,476 lb of coal were consumed at a rate of 904 lb/h for 59 h of operation. (41% more coal was consumed and 79% more operating time was accumulated.)
• The boiler outlet pressure (B.O.P.) maxed out (<-2.2" W.C.) after consuming 33,927 lb of coal	• The B.O.P. maxed out after consuming 43,080 lb of coal (27% more coal was consumed.)
• The B.O.P. started at -0.8" W.C. and began decreasing at 24,000 lb of coal consumed. There was 10,000 lb of coal consumed between the time the B.O.P. started to decrease and when the gauge maxed out. This is equivalent to 8.7 h of operation.	• The B.O.P. started at -0.8" W.C. and began decreasing at 35,000 lb of coal consumed. There was 8,000 lb of coal consumed between the time the B.O.P. started to decrease and when the gauge maxed out. This is equivalent to 8.9 h of operation.
• The sootblowing frequency was typically every half hour and increased to 1.5 and then 2h before boiler shutdown (during the continuous test).	• After the B.O.P. maxed out, the soot blowing frequency increased to 2, 2.75 2.5, and 2h before the forced shutdown.
• The ID fan amperage exhibited a decrease from ~31.5 amps to 30.0 amps after consuming ~1,000 lb of coal. The amperage then slowly increased to ~32.5 over the consumption of ~27,000 lb of coal.	• The ID fan amperage was less than that observed during the 15 million Btu/h tests because of the decreased volume of flue gas and was ~28 amps as compared to 30 to 32.5 amps. The amperage was relatively constant at ~28.5 with an increase to ~29.5 at the time of shut down.
• The convective pass temperature decreased from ~1,300 to 1,000°F while the B.O.P. was decreasing.	• No temperature data was collected.
• Steam production increased as the test progressed.	• Steam production remained relatively constant during the test.

consequence of the excessive ash deposition at the convective pass entrance during continuous testing, a sootblower is being designed for this region and will be used during the next series of testing.

Emissions

Table 4-18 contains the emissions data from the DMC demonstration. The flue gas analysis has been converted to a lb/MM Btu (corrected to 3% O_2) basis. The SO_2 and NO_x emissions ranged from 0.6 to 1.2 lb/MM Btu and from 0.3 to 1.0 lb/MM Btu, respectively. The targeted NO_x level was met at firing rates from 12.7 to 15.7 MM Btu/h but was not met at firing rates greater than 15.8 MM Btu/h.

The carbon monoxide emissions varied considerably during the testing. Very high CO emissions (sometimes in excess of 4,000 ppm) were observed when coal feed variability and maldistribution were encountered, and during the natural gas/coal cofiring period when transiting to 100% coal firing.

Derating

The original rated capacity of the DS-15 package boiler was 15,000 lb saturated steam/h at 300 psig; however, the design capacity was decreased to 14,900 lb steam/h (at a natural gas firing rate of ~19.8 MM Btu/h) when two rows of tubes were removed from the convective pass to accommodate test probes. Natural gas testing that was conducted for the boiler performance guarantees in January 1992 resulted in 14,700 lb steam/h produced when firing at 18.5 MM Btu/h[3].

Steam production during this reporting period ranged from 9,300 to 15,500 lb/h at firing rates from 12.5 to 16.4 MM Btu/h. Testing was conducted primarily over two ranges of firing rates, 15.0 to 16.5 MM Btu/h and 12.5 to 13.0 MM Btu/h. Typically, the boiler was not fired over 16 MM Btu/h because increases in the boiler outlet temperature (and hence the baghouse entrance temperature) were observed. At the higher firing rate range, 15.0 to 16.5 MM Btu/h, the mean steam production was 13,600 lb/h or 93% of design capacity and the standard deviation of 1,200 lb steam/h.

Operability

Redesign of Coal Storage and Handling Facilities

One objective of the DMC testing was to determine the operating characteristics of a complete, integrated firing system. Although all of the system components (e.g., coal hoppers, crushers, conveyors, and mill) have been used commercially, an integrated system from coal preparation to steam production has not been proved, trouble free, at this scale.

Severe coal handling problems were encountered during DMC testing that was conducted during the winter of December 1993 to March 1994[5]. Because of the relatively small quantities of low ash coal required for the testing, the coals were cleaned in a batch mode by heavy media cyclones and stored in a local coal yard. During testing in the winter, snow and ice were included

Table 4-18. Emissions Levels During the DMC Demonstration

Date	Test #	Firing Rate (MMBtu/h)	SO2 Conc. (moles)	NOx Conc. (moles)	CO Conc. (moles)	O2 Conc. (%)	SO2 Conc. (lb/MMBtu Corrected to 3% O2)	NOx Conc. (lb/MMBtu Corrected to 3% O2)	CO Conc. (lb/MMBtu Corrected to 3% O2)
7/13/94	2	14.0	0.000479	0.000298	0.001454	4.26	0.99	0.44	1.32
7/14/94	4	15.9	0.000496	0.000536	0.000193	3.19	0.91	0.71	0.16
7/15/94	5	15.9	0.000514	0.000538	0.000123	3.92	1.03	0.78	0.11
7/18/94	6	15.8	0.000499	0.000541	0.000286	3.26	0.93	0.72	0.23
7/19/94	7	18.1	0.000481	0.000573	0.000161	3.28	0.91	0.78	0.13
7/21/94	10	16.2	0.000490	0.000553	0.000192	3.36	0.94	0.77	0.16
7/27/94	11	16.6	0.000456	0.000594	0.000158	3.27	0.84	0.79	0.13
7/28/94	12	16.7	0.000426	0.000512	0.001070	3.24	0.78	0.68	0.86
7/29/94	13	16.5	0.000426	0.000529	0.001121	3.63	0.83	0.74	0.95
8/1/94	14	16.6	0.000291	0.000554	0.000536	3.77	0.56	0.77	0.45
8/3/94	15	15.9	0.000400	0.000618	0.000260	3.47	0.74	0.83	0.21
8/4/94	16	16.0	0.000368	0.000651	0.000132	4.01	0.71	0.91	0.11
8/4/94	17	16.0	0.000442	0.000671	0.000277	3.68	0.82	0.90	0.23
8/5/94	18	16.4	0.000535	0.000610	0.000165	4.75	1.17	0.96	0.16
8/10/94	19	16.7	0.000376	0.000583	0.000509	3.58	0.71	0.79	0.42
8/11/94	20	16.5	0.000401	0.000665	0.000496	3.34	0.73	0.87	0.40
8/25/94	21	16.1	0.000322	0.000494	0.000473	3.78	0.62	0.69	0.40
8/30/94	22	16.0	NM	0.000507	0.000439	3.10	NA	0.66	0.35
8/30/94	23	16.0	NM	0.000427	0.000332	3.52	NA	0.58	0.27
8/31/94	24	16.1	NM	0.000416	0.000462	3.44	NA	0.56	0.38
8/31/94	25	16.1	NM	0.000544	0.000234	3.47	NA	0.74	0.19
9/2/94	26	15.9	NM	0.000639	0.000420	2.67	NA	0.78	0.31
10/13/94	27	16.0	NM	0.000519	0.000127	3.55	NA	0.72	0.11
10/19/94	28	15.2	0.000337	0.000338	0.000164	4.03	0.71	0.51	0.15
10/20/94	29	15.4	0.000334	0.000364	0.000397	3.29	0.64	0.50	0.34
11/7/94	30	12.5	NM	0.000299	0.000187	3.68	NA	0.42	0.16
11/16/94	31	14.9	0.000270	0.000323	0.001339	4.44	0.59	0.50	1.28
11/17/94	32	16.0	0.000360	0.000312	0.000115	7.00	1.08	0.67	0.15
11/18/94	33	15.8	0.000311	0.000349	0.000274	5.84	0.81	0.65	0.31
11/21/94	34	15.7	NM	0.000344	0.000225	4.16	NA	0.53	0.21
11/21/94	35	15.7	NM	0.000403	0.000256	3.66	NA	0.58	0.23
11/22/94	36	16.4	NM	0.000317	0.000301	4.53	NA	0.49	0.29
11/28/94	37	12.8	NM	NM	0.000987	4.12	NA	NA	0.88
11/30/94	38	12.8	0.000378	0.000224	0.000526	4.43	0.81	0.34	0.49
12/1/94	39	12.8	0.000393	0.000242	0.000782	4.59	0.85	0.38	0.74
12/2/94	40	12.7	0.000475	0.000287	NM	4.64	1.04	0.45	NA
12/5/94	41	12.7	0.000430	0.000304	0.000287	4.20	0.90	0.46	0.26
12/5/94	42	12.7	0.000375	0.000300	0.000279	4.78	0.84	0.48	0.27
12/5/94	43	15.7	0.000402	0.000364	0.000183	4.92	0.74	0.48	0.15
12/6/94	44	12.7	0.000386	0.000354	0.000217	5.28	0.92	0.61	0.23
12/6/94	45	12.7	0.000391	0.000345	0.000339	4.75	0.87	0.55	0.33
12/6/94	46	12.7	0.000502	0.000330	0.000240	4.88	1.14	0.54	0.24
12/7/94	47	12.7	0.000516	0.000327	0.000257	4.54	1.13	0.51	0.25
12/7/94	48	12.7	0.000480	0.000276	0.000540	5.26	1.14	0.37	0.56

NM - Not measured
NA - Not applicable

in the shipments. The wet coal (often with moisture content in excess of 12%) tended to bridge and rathole in the hoppers, especially the surge bin. This required constant operator attention and corrective action and resulted in erratic coal feed. This inconsistent coal feed, coupled with the variability introduced by varying coal size and moisture content, made it difficult to maintain a constant feed to the burner. The moisture content was inconsistent because of drying in the heated building and by an air sparge system that was installed on the surge bin.

The operating problems encountered due to high moisture content of the fine coal and fuel transport oscillations led to a reevaluation of the system design and coal storage logistics. For winter testing conducted during the period December 1994 to March 1995 (DMC testing for the DOD program), the moisture content of the coal was limited by storing it in a protected environment after cleaning. Less coal handling problems were encountered during the present winter; however, snowfall was significantly less than that during the previous winter (a few inches compared to several feet).

Since most of the coal feed problems occurred in the surge bin, its design was evaluated and it was found that the bin outlet dimensions and hopper sidewall angle should be modified to improve coal handling. The original surge bin has a circular opening with a bin angle of 60°. It was recommended that the bin outlet should be pyramidal with a length to width ratio of 3:1 and the sidewall angle should be 70°.

A test hopper was fabricated based on the recommended design criteria and tested with the as-received coal at various moisture levels. This was done to test the flowability of the coal in a new hopper before reengineering the coal handling and feeding system. The pyramidal test hopper was constructed from carbon steel, had a discharge opening of 16 by 48" (3:1 ratio), had sidewall angles of 70°, and was a full-scale model of the bottom portion of a proposed surge bin. The discharge width (16") was maximized based on the width of candidate weigh-belt feeder belt sizes.

Flowability tests were conducted by first adding water to the coal (-1/4" in size) at various moisture levels in a barrel. A barrel roller was then used to achieve homogeneous moisture levels. The coal was then transferred into the test hopper and left to settle prior to the flow test. Moisture levels of approximately 8.0, 12.0, 14.1, and 17.8% were tested. The moisture content would vary from 2-4% from the top to the bottom of the hopper. The highest percentage of moisture noted at the bottom of the hopper was approximately 21%. The flow test was conducted by lifting the hopper with a forktruck and allowing the coal to flow from the hopper onto the ground. The test hopper was lifted at a rate of one inch per minute which translates into a coal flow rate of 18.5 lb/min. At each of the conditions tested, there was little or no coal left in the hopper at the end of each test.

As a result of the system design reevaluation and study, a new coal storage and handling system was reengineered. A pyramidal bin with a length to width discharge outlet of 3:1 and a steeper angle (70 vs 60°) was designed and installed in April/May 1995 (after testing was

completed for Phase I of the DOD project and prior to the ABB CE 1,000-hour demonstration). An isometric view of the new hopper is shown in Figure 4-68. The new surge bin will be constructed out of stainless-steel to eliminate scaling. In addition, the screw feeder will be replaced with a weigh-belt feeder to eliminate fuel feed oscillations. Figure 4-69 is a schematic diagram of the new coal storage and handling system.

4.4.4 MCWM Demonstration

A MCWM demonstration was conducted with the objectives of determining burner and boiler performance, achieving high coal combustion efficiency firing MCWM without natural gas support, examining furnace and convective pass deposition, and determining the effect of continuous operation on deposition. A day-to-day synopsis can be found elsewhere[121]. A total of 1,461.5 hours of operation were accumulated from January to mid-April, 1995, of which 244.5 hours were with MCWM firing (6.0 hours of operation per 1.0 hour of MCWM firing). The MCWM demonstration included firing MCWM, completing the construction of MCWM preparation circuit (see Section 3.3.2 for a discussion of the circuit), component repair, and making minor modifications to the burner.

Table 4-19 contains a boiler performance and emissions summary (which are averaged over half-hour periods) of the MCWM demonstration. Most of the testing was conducted with two shifts per day except for the testing on March 22 and 23, 1995 which were continuous (24 h/day).

One coal was used during the MCWM demonstration. It was the Upper Freeport seam coal which was also used during the DMC demonstration. Table 4-20 contains the coal analysis of weekly composites produced from daily samples of MCWM collected at the burner pump.

Combustion and Boiler Performance

The combustion and boiler performance, when firing MCWM, ranged from 72 to 86% (with ~30% natural gas support based on total heat input) and from 64 to 76%, respectively. Figure 4-70 shows the combustion efficiency for the testing conducted from January 31, 1995 to April 13, 1995. Most of the MCWM operation resulted in combustion efficiencies ranging from 80 to 85%, with ~30% natural gas support. This did not meet the program target of 98% combustion efficiency without natural gas support, and the results were poorer than those obtained during the SCCWS testing in which 95% combustion efficiency with 15% natural gas support was obtained. The combustion efficiency results from the two programs are overlaid in Figure 4-71. Items that were different between the two demonstrations include:

1. A fully-swirled burner (EER) was used in the latest test program compared to a partially-swirled burner (oil-burner; Faber) in the previous testing;
2. A quarl (34" dia. x 18" long) for flame stabilization was installed in the boiler (on the front wall) for the SCCWS testing; and
3. The best results during the SCCWS testing were observed when using 186 psig atomizing air pressure (from a portable air compressor) compared to ~90 psig (typical

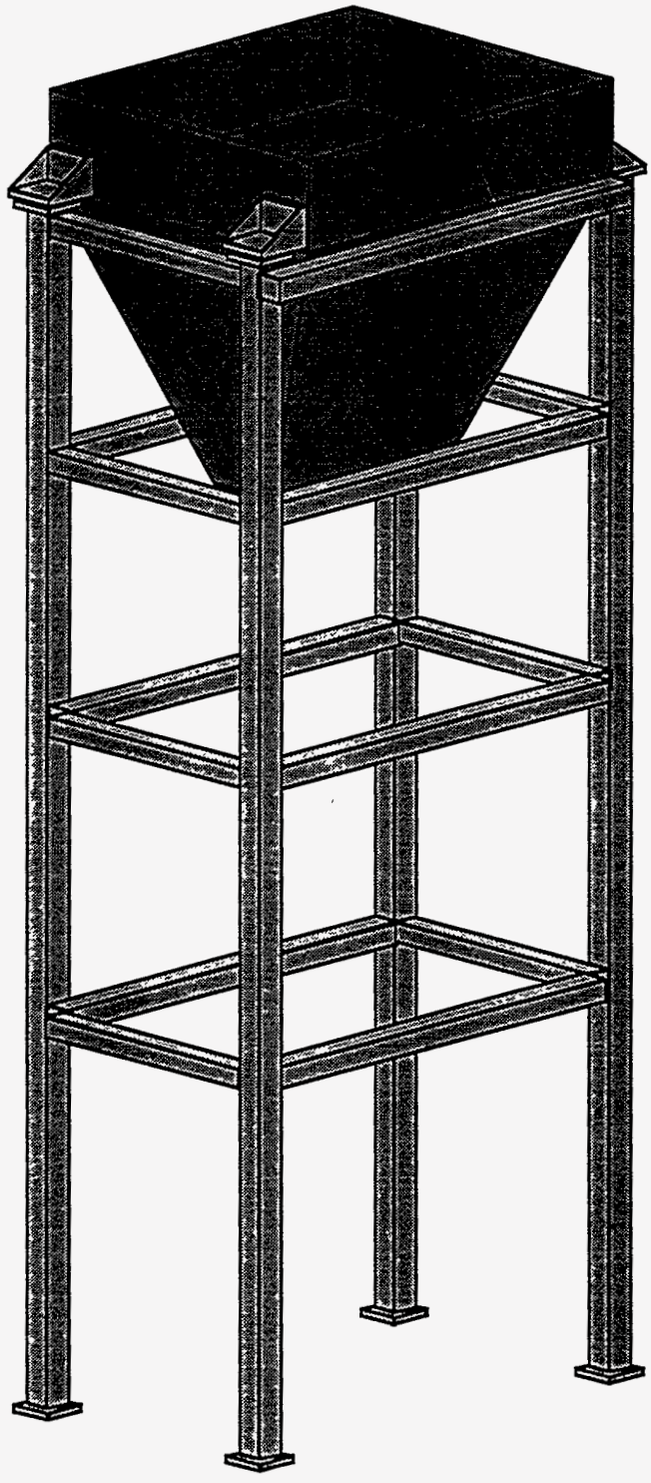

Figure 4-68. ISOMETRIC VIEW OF NEW HOPPER

Figure 4-69. SCHEMATIC DIAGRAM OF THE NEW COAL HANDLING SYSTEM

Table 4-19. Summary of Results for the MCWM Demonstration

Summary Sheet															
	8-Feb	14-Feb	15-Feb	16-Feb	17-Feb	17-Feb	21-Feb	23-Feb	24-Feb	28-Feb	28-Feb	1-Mar	2-Mar	6-Mar
TEST/DESCRIPTION:					No Preheat	Preheat	Preheat	Preheat	Preheat	No Preheat	Preheat	No Preheat	Preheat	Preheat
	65XHC-cap	65XHC-cap	65XHC-cap	65XHC-cap	65XHC-cap	65XHC-cap	swirl nozzle	75XHC-c	75XHC-c	m-75XHC-c	m-75XHC-c	m-75XHC-c	m-75XHC-c	75XHC-c
	XHC-plug	XHC-plug	XHC-plug	XHC-plug	XHC-plug	XHC-plug		XHC-p	XHC-p	m-XHC-p	m-XHC-p	m-XHC-p	m-XHC-p	m-XHC-p
Test No.:	3	4	5	6	7	8	9	10	11	12	13	14	15	16
WATER/STEAM SIDE														
Steam flow rate; lb/h	10,523	11,611	11,539	11,284	10,943	11,014	10,737	12,856	12,728	12,523	12,883	12,415	13,231	13,093
Water temperature into boiler; °F	216	214	214	204	196	191	209	215	210	208	207	211	215	212
Drum pressure; psig	215	199	207	206	211	210	228	229	228	219	220	216	217	219
Calorimeter temperature; °F	306	305	306	305	306	305	306	309	309	307	307	308	309	308
Steam temperature; °F	385	379	382	380	382	381	388	390	390	385	385	385	386	385
Steam quality; %	99.60	99.54	99.59	99.54	99.59	99.53	99.62	99.77	99.75	99.65	99.65	99.70	99.76	99.70
Blowdown rate; lb/h	3,215	3,092	3,153	3,148	3,180	3,175	3,307	3,317	3,312	3,243	3,247	3,218	3,229	3,241
AIR,FUEL, FLUE GAS SIDE														
Total Firing Rate; MMBtu/h	15.7	15.3	15.2	15.3	15.1	15.0	18.7	18.7	18.8	18.4	18.5	18.4	18.5	18.0
Natural gas flow rate; lb/h;MMBtu/H	139;3.3	188;4.4	192;4.5	194;4.5	185;4.3	188;4.4	227;5.3	220;5.1	210;4.9	216;5.0	216;5.0	243;5.7	228;5.3	230;5.4
MCWM flow rate; lb/h;MMBtu/h	1,473;12.4	1,246;10.9	1,290;10.8	1,322;10.8	1,273;10.7	1,257;10.6	1,663;13.4	1,644;13.6	1,590;13.9	1,552;13.4	1,559;13.4	1,480;12.7	1,540;13.2	1,446;12.6
Air temperature entering air heater; °F	119	119	132	137	141	148	140	136	118	129	135	132	117	136
Air temperature leaving air heater; °F	386	386	395	397	389	396	397	410	399	389	394	392	390	401
Air temperature into boiler; °F	363	363	372	375	367	375	373	386	374	364	370	369	364	377
Furnace outlet temperature; °F	550	538	547	560	548	556	562	600	590	561	566	562	571	581
Gas temperature leaving air heater; °F	352	358	365	366	361	367	372	395	381	370	375	370	371	384
Baghilter inlet temperature; °F	353	358	364	364	360	364	373	392	380	369	372	368	370	381
Baghilter outlet temperature; °F	311	318	313	322	319	324	331	346	336	322	327	329	323	335
Combustion air flow; lb/h	13,955	13,538	13,478	13,672	13,589	13,352	16,439	16,432	16,665	16,403	16,136	16,751	16,340	16,260
Boiler draft; in H2O	0.03	-0.04	-0.13	-0.12	-0.12	-0.13	-0.04	-0.08	-0.07	-0.12	-0.11	-0.12	-0.12	-0.16
Boiler efficiency; %	70.84	73.50	73.25	71.59	72.83	74.54	64.31	72.31	72.12	69.60	70.62	69.92	71.53	73.11
Atomizing Air Pressure; psig	87	85	83	84	88	88	84	NR	81	78	78	75	85	NR
Atomizing air flow rate;lbs/hr	460	463	456	525	468	468	518	392	407	535	539	535	525	NR
A/F ratio;lb/lb	0.32	0.37	0.35	0.40	0.37	0.37	0.32	0.25	0.26	0.35	0.35	0.37	0.35	NR
MCWM temperature; °F	95	95	95	95	95	168	95	134	138	95	131	95	154	148
Natural gas temperature; °F	80	86	81	78	83	83	70	71.33	70.03	83.67	83	84	77	85
Excess air used (%)	17.3	16.6	16.2	17.3	18.5	17.0	15.7	15.1	16.6	17.0	14.7	19.9	16.0	19.3
Coal combustion efficiency;%	83.1	85.6	86.1	83.7	85.3	86.8	72.3	85.2	83.6	79.7	80.7	79.9	81.6	84.7
Overall combustion efficiency;%	84.6	87.5	87.9	85.8	87.2	88.5	75.6	86.9	85.5	82.2	83.0	82.7	84.0	86.8
EMISSIONS (Dry Basis)														
O2; %	3.25	3.13	3.07	3.25	3.43	3.43	3.04	2.90	3.13	3.19	2.82	3.66	3.04	3.55
CO; ppm;lb/MMBtu (3% O2)	226;0.19	167;0.19	180;0.15	208;0.17	204;0.17	181;0.15	961;0.80	167;0.13	246;0.20	199;0.16	188;0.15	172;0.15	136;0.11	149;0.13
CO2; %;lb/MMbtu (3% O2)	14.0;177	14.0;173	13.7;179	13.7;178	13.5;179	13.8;180	13.2;172	13.8;173	13.9;178	13.7;177	14.0;174	13.0;176	13.8;175	13.5;180
SO2; ppm;lb/MMBtu (3% O2)	412;0.78	323;.60	328;0.61	338;0.64	313;0.6	308;0.59	309;0.58	323;0.59	342;0.64	346;0.65	354;0.64	306;0.60	329;0.61	328;0.64
NOx; ppm;lb/MMBtu (3% O2)	402;0.55	462;0.62	393;0.53	344;0.47	358;0.5	395;0.54	292;0.40	423;0.56	526;0.71	339;0.46	334;0.43	319;0.45	328;0.44	402;0.56
FUEL ANALYSIS DATA														
Solids Content (%)	60.1	62.5	59.9	59.0	60.5	60.5	57.5	59.2	62.6	61.8	61.8	61.6	61.4	62.5
Top size (µm)														
D90 (µm)					98.4		87.3			103.3		103.2		
D50 (µm)					28.6		24.6			26.3		24.6		
D10 (µm)					2.9		3.1			3.3		3.1		
Viscosity@100/s (cp)					93		73			110		85		
ph					9.3		8.8			9.0		9.3		

Table 4-19. Summary of Results for the MCWM Demonstration

Summary Sheet														
TEST/DESCRIPTION:	7-Mar Preheat 75XHC-c m-XHC-p	9-Mar No Preheat 75XHC-c m-XHC-p	9-Mar Preheat 75XHC-c m-XHC-p	10-Mar No Preheat 75XHC-c m-XHC-p	10-Mar Preheat 75XHC-c m-XHC-p	13-Mar 75XHC-c m-XHC-p	14-Mar 75XHC-c m-XHC-p	22-Mar AM I ceramic-cap m-XHC-p	22-Mar AM II 75XHC-c m-XHC-p	22-Mar PM 75XHC-c m-XHC-p	23-Mar 75XHC-c m-XHC-p	27-Mar No Preheat m-75XHC-c m-XHC-p	27-Mar Preheat m-75XHC-c m-XHC-p
Test No.:	17	18	19	20	21	22	23	24	25	26	27	28	29
WATER/STEAM SIDE													
Steam flow rate; lb/h	12,898	12,834	12,992	12,348	12,719	13,130	13,317	13,364	13,693	13,991	13,617	12,379	12,532
Water temperature into boiler; °F	211	216	214	215	213	211	212	208	197	202	208	209	208
Drum pressure; psig	216	214	213	212	214	218	217	217	217	217	219	227	227
Calorimeter temperature; °F	308	307	306	308	305	310	310	246	248	220	232	307	307
Steam temperature; °F	385	386	384	384	383	387	387	385	385	385	385	387	387
Steam quality; %	99.69	99.68	99.59	99.69	99.57	99.81	99.83	96.20	96.26	94.71	95.38	99.67	99.66
Blowdown rate; lb/h	3,223	3,207	3,199	3,192	3,209	3,235	3,227	3,232	3,231	3,229	3,243	3,300	3,299
AIR,FUEL, FLUE GAS SIDE													
Total Firing Rate; MMBtu/h	19.1	17.7	18.2	18.1	18.2	18.3	18.2	18.0	18.6	18.5	18.4	18.1	18.5
Natural gas flow rate; lb/h;MMBtu/H	227;5.3	218;5.1	232;5.4	226;5.3	225;5.3	229;5.4	227;5.3	217;5.1	234;5.5	229;5.4	229;5.4	218;5.1	233;5.4
MCWM flow rate; lb/h;MMBtu/h	1,583;13.8	1,553;12.6	1,504;12.3	156,112.80	1,573;12.9	1,510;13.0	1,497;12.9	1,500;13.0	1,500;13.2	1,500;13.1	1,507;13.1	1,527;13.1	1,527;13.0
Air temperature entering air heater; °F	147	123	125	122	137	141	137	137	131	131	131	145	146
Air temperature leaving air heater; °F	404	392	397	391	395	402	406	405	411	407	402	397	399
Air temperature into boiler; °F	379	368	373	368	374	374	383	379	387	385	382	370	376
Furnace outlet temperature; °F	575	564	577	558	559	575	582	575	593	583	570	554	556
Gas temperature leaving air heater; °F	387	368	375	363	367	382	385	380	386	382	375	369	370
Bagfilter inlet temperature; °F	382	367	373	361	366	371	375	373	379	377	372	364	366
Bagfilter outlet temperature; °F	337	324	328	320	325	326	333	331	335	337	333	323	324
Combustion air flow; lb/h	17,278	15,420	16,466	15,748	15,534	15,954	15,846	15,820	16,392	16,281	16,276	15,980	16,216
Boiler draft; in H2O	-0.13	-0.13	-0.09	-0.13	-0.13	-0.14	-0.14	-0.12	-0.14	-0.16	-0.16	-0.14	-0.14
Boiler efficiency; %	71.74	69.61	72.27	71.82	72.89	71.14	71.34	71.74	68.26	71.86	70.79	71.11	70.79
Atomizing Air Pressure; psig	NR	83	81	81	81	80	80	80	81	81	80	82	82
Atomizing air flow rate;lbs/hr	467	482	485	483	481	480	483	478	485	485	487	469	467
A/F ratio;lb/lb	0.31	0.31	0.32	0.31	0.31	0.32	0.32	0.32	0.33	0.33	0.32	0.31	0.31
MCWM temperature; °F	137	95	130	95	132	95	95	95	95	95	95	95	124
Natural gas temperature; °F	89	71	63.24	79	75	73	74	76	76	77	79	65	67
Excess air used (%)	19.3	15.0	19.0	14.8	12.7	14.6	14.4	14.8	15.4	15.5	15.8	16.1	15.7
Coal combustion efficiency;%	83.3	80.2	83.8	83.5	84.6	82.4	83.3	83.6	77.2	83.4	81.4	82.3	80.9
Overall combustion efficiency;%	85.4	82.6	86.0	85.6	86.5	84.7	85.1	85.7	80.3	85.6	83.9	84.5	83.4
EMISSIONS (Dry Basis)													
O2; %	3.57	2.87	3.52	2.84	2.49	2.82	2.78	2.86	2.95	2.96	3.01	3.06	3.00
CO; ppm;lb/MMBtu (3% O2)	281;0.24	200;0.16	407;0.35	197;0.16	208;0.16	149;0.12	256;0.2	352;0.28	236;0.19	248;0.20	209;0.17	160;0.13	234;0.19
CO2; %;lb/MMbtu (3% O2)	13.2;177	14.0;173	13.3;179	13.9;172	14.2;169	13.7;170	13.7;169	13.8;173	13.6;172	13.8;174	13.8;175	13.6;173	13.5;170
SO2; ppm;lb/MMBtu (3% O2)	326;0.64	331;0.60	323;0.63	318;0.57	329;0.57	313;0.56	303;0.54	349;0.64	342;0.63	338;0.62	340;0.63	332;0.61	328;0.60
NOx; ppm;lb/MMBtu (3% O2)	341;0.48	429;0.56	472;0.66	409;0.53	433;0.54	443;0.57	429;0.55	449;0.59	454;0.60	449;0.59	417;0.55	383;0.51	361;0.47
FUEL ANALYSIS DATA													
Solids Content (%)	62.5	60.6	61.2	58.9	58.9	61.6	61.5	62.3	63.2	63.0	62.4	61.0	61.0
Top size (µm)													
D90 (µm)		95.2	95.2	88.1			98.9	96.3	83.8		81.5	81.5	81.5
D50 (µm)		23.9	23.9	21.6			23.8	23.6	21.4		21.9	21.4	21.4
D10 (µm)		2.9	2.9	2.8			2.9	3.0	2.8		2.8	2.8	2.8
Viscosity@100/s (cp)				148				176	174		178	113	113
ph		8.8	8.8	9.3			9.6	9.2	9.1		9.4	9.3	9.3

Table 4-19. Summary of Results for the MCWM Demonstration

Summary Sheet											
TEST/DESCRIPTION:	28-Mar No Preheat m-75XHC-c m-XHC-p	28-Mar Preheat m-75XHC-c m-XHC-p	29-Mar No Preheat m-75XHC-c m-XHC-p	29-Mar Preheat m-75XHC-c m-XHC-p	31-Mar Preheat m-75XHC-c m-XHC-p	3-Apr m-75XHC-c m-XHC-p	4-Apr Coal m-75XHC-c m-XHC-p	10-Apr RM m-75XHC-c m-XHC-p	11-Apr AM m-75XHC-c m-XHC-p	13-Apr 65XHC-c m-XHC-p
Test No.:	30	31	32	33	50% gas supp. 34	35	Burner modified after 4/3/95 36	37	test 38	core air 39
WATER/STEAM SIDE										
Steam flow rate; lb/h	12,396	12,623	12,742	13,116	13,201	12,382	12,538	11,608	11,685	12,764
Water temperature into boiler; °F	209	208	216	213	214	213	214	218	218	216
Drum pressure; psig	224	226	228	229	224	224	219	238	232	208
Calorimeter temperature; °F	307	308	308	308	309	309	214	218	218	216
Steam temperature; °F	387	387	388	388	388	389	78	64	67	68
Steam quality; %	99.68	99.69	99.71	99.69	99.76	99.79	94.33	94.56	94.57	94.45
Blowdown rate; lb/h	3,280	3,297	3,310	3,317	3,279	3,284	3,244	3,383	3,338	3,158
AIR,FUEL, FLUE GAS SIDE										
Total Firing Rate; MMBtu/h	18.1	18.2	18.0	17.9	17.2	18.1	18.3	18.7	18.3	17.9
Natural gas flow rate; lb/h;MMBtu/H	221;5.2	224;5.2	223;5.2	218;5.1	349;8.2	219;5.1	221;5.2	219;5.1	230;5.4	249;5.8
MCWM flow rate; lb/h;MMBtu/h	1,507;13.0	1,507;12.9	1,573;12.8	1,573;12.8	1,050;9.1	1,516;13.0	1,561;13.1	1,557;13.6	1,445;12.9	1,444;12.1
Air temperature entering air heater; °F	141	150	145	141	133	144	130	148	153	151
Air temperature leaving air heater; °F	399	408	410	410	411	408	404	401	396	396
Air temperature into boiler; °F	374	384	382	384	384	382	383	381	379	373
Furnace outlet temperature; °F	558	568	577	582	592	566	561	543	532	525
Gas temperature leaving air heater; °F	368	378	381	383	383	375	369	369	362	360
Baghilter inlet temperature; °F	360	369	373	373	376	370	365	365	358	354
Baghilter outlet temperature; °F	313	328	328	332	336	323	322	320	312	314
Combustion air flow; lb/h	15,914	15,848	15,753	15,651	15,269	15,989	16,535	16,677	17,713	16,097
Boiler draft; In H2O	-0.14	-0.14	-0.15	-0.14	-0.13	-0.13	-0.11	-0.11	-0.10	-0.05
Boiler efficiency; %	69.47	71.00	69.84	71.89	75.82	71.15	68.85	68.84	67.81	68.40
Atomizing Air Pressure; psig	84	81	80	79	82	82	82	75	NR	66
Atomizing air flow rate;lbs/hr	481	491	473	488	498	469	489	469	NR	420
A/F ratio;lb/lb	0.32	0.33	0.30	0.31	0.52	0.31	0.31	0.30	NR	0.29
MCWM temperature; °F	95	143	95	139	160	147	95	95	95	95
Natural gas temperature; °F	65	70	63	63	69	81	91	89	83	86
Excess air used (%)	15.8	14.9	15.0	15.0	18.1	16.1	18.7	17.8	27.8	19.1
Coal combustion efficiency;%	79.2	81.2	81.2	84.0	86.9	81.7	78.7	78.2	76.2	76.8
Overall combustion efficiency;%	81.9	83.6	83.5	85.9	90.2	84.0	81.4	80.9	79.5	80.2
EMISSIONS (Dry Basis)										
O2; %	3.01	2.87	2.88	2.87	3.40	3.07	3.46	3.34	4.79	3.56
CO; ppm;lb/MMBtu (3% O2)	199;0.16	283;0.22	169;0.13	151;0.12	124;0.1	340;0.28	290;0.25	339;0.28	247;0.24	356;0.30
CO2; %;lb/MMbtu (3% O2)	13.6;172	13.7;170	13.7;171	13.8;172	12.6;161	13.6;173	13.6;181	13.3;174	11.9;164	12.9;171
SO2; ppm;lb/MMBtu (3% O2)	322;0.59	341;0.62	347;0.63	3530;.64	240;0.45	344;0.64	362;0.70	371;0.71	345;0.78	344;0.67
NOx; ppm;lb/MMBtu (3% O2)	326;0.43	385;0.50	409;0.53	419;0.55	377;0.51	400;0.53	440;0.61	258;0.35	223;0.36	389;0.54
FUEL ANALYSIS DATA										
Solids Content (%)	61.3	61.3	58.3	58.3	61.8	61.2	60.1	62.5	64.0	59.8
Top size (µm)										
D90 (µm)	74.1		71.9	71.9	85.2	83.1	74.7			
D50 (µm)	19.6		20.6	20.6	21.5	20.7	20.0			
D10 (µm)	2.7		2.8	2.8	2.8	2.7	2.8			
Viscosity@100/s (cp)	239		94	94	181	119	108			
ph			9.3	9.3	9.4		9.5			

Table 4-20. Coal Analysis of Composite Samples Collected During the MCWM Demonstration

Date	Screw Composite	Full Proximate Analysis				Ultimate Analysis					Cal Value (Dry)
		% Moist (Prepped)	% V.M. (Dry)	% Ash (Dry)	% F.C. (Dry)	% C (Dry)	% H (Dry)	% N (Dry)	% S (Dry)	% O (Dry)	
1/30-2/3/95		1.38 ± 0.02	31.96 ± 0.20	6.36 ± 0.04	61.68	79.40 ± 0.14	5.01 ±0.02	1.60 ± 0.01	0.72 ± 0.00	6.91	13957 ± 4
2/6-10/95		1.39 ± 0.01	31.93 ± 0.03	6.33 ± 0.02	61.74	79.17 ± 0.21	5.07 ± 0.03	1.63 ± 0.02	0.71 ± 0.01	7.09	13954 ± 7
2/13-17/95		1.62 ± 0.02	31.49 ± 0.10	6.35 ± 0.03	62.16	79.66 ± 0.14	5.07 ± 0.03	1.64 ± 0.03	0.69 ± 0.01	6.59	13945 ± 1
2/20-24/95		1.76 ± 0.06	32.00 ± 0.01	6.37 ± 0.04	61.63	79.52 ± 0.06	5.17 ± 0.10	1.61 ± 0.01	0.69 ± 0.01	6.64	13984 ± 3
2/27-3/3/95		1.57 ± 0.03	31.89 ± 0.02	6.22 ± 0.01	61.89	79.50 ± 0.06	5.12 ± 0.01	1.63 ± 0.00	0.71 ± 0.01	6.82	13947 ± 8
3/6-10/95		1.31 ± 0.02	31.86 ± 0.01	6.29 ± 0.01	61.85	79.43 ± 0.20	5.04 ± 0.06	1.56 ± 0.07	0.69 ± 0.00	6.99	13940 ± 3
3/13-17/95		1.74 ± 0.02	31.36 ± 0.06	6.31 ± 0.02	62.33	79.49 ± 0.11	5.06 ± 0.04	1.61 ± 0.00	0.68 ± 0.01	6.85	13910 ± 4
3/20-24/95		0.96 ± 0.00	31.49 ± 0.05	6.23 ± 0.00	62.28	79.42 ± 0.01	5.15 ± 0.03	1.66 ± 0.00	0.68 ± 0.00	6.86	13878 ± 8
3/27-31/95		1.80 ± 0.00	32.04 ± 0.03	6.30 ± 0.01	61.66	79.41 ± 0.12	5.17 ± 0.02	1.64 ± 0.01	0.70 ± 0.00	6.78	13979 ± 2
4/3-7/95		1.65 ± 0.02	32.14 ± 0.10	6.24 ± 0.01	61.62	79.82 ± 0.32	5.07 ± 0.01	1.61 ± 0.00	0.73 ± 0.00	6.53	13979 ± 2
4/10-14/95		1.67 ± 0.01	31.99 ± 0.00	6.22 ± 0.02	61.79	79.25 ± 0.04	5.10 ± 0.01	1.61 ± 0.02	0.76 ± 0.00	7.06	13966 ± 2

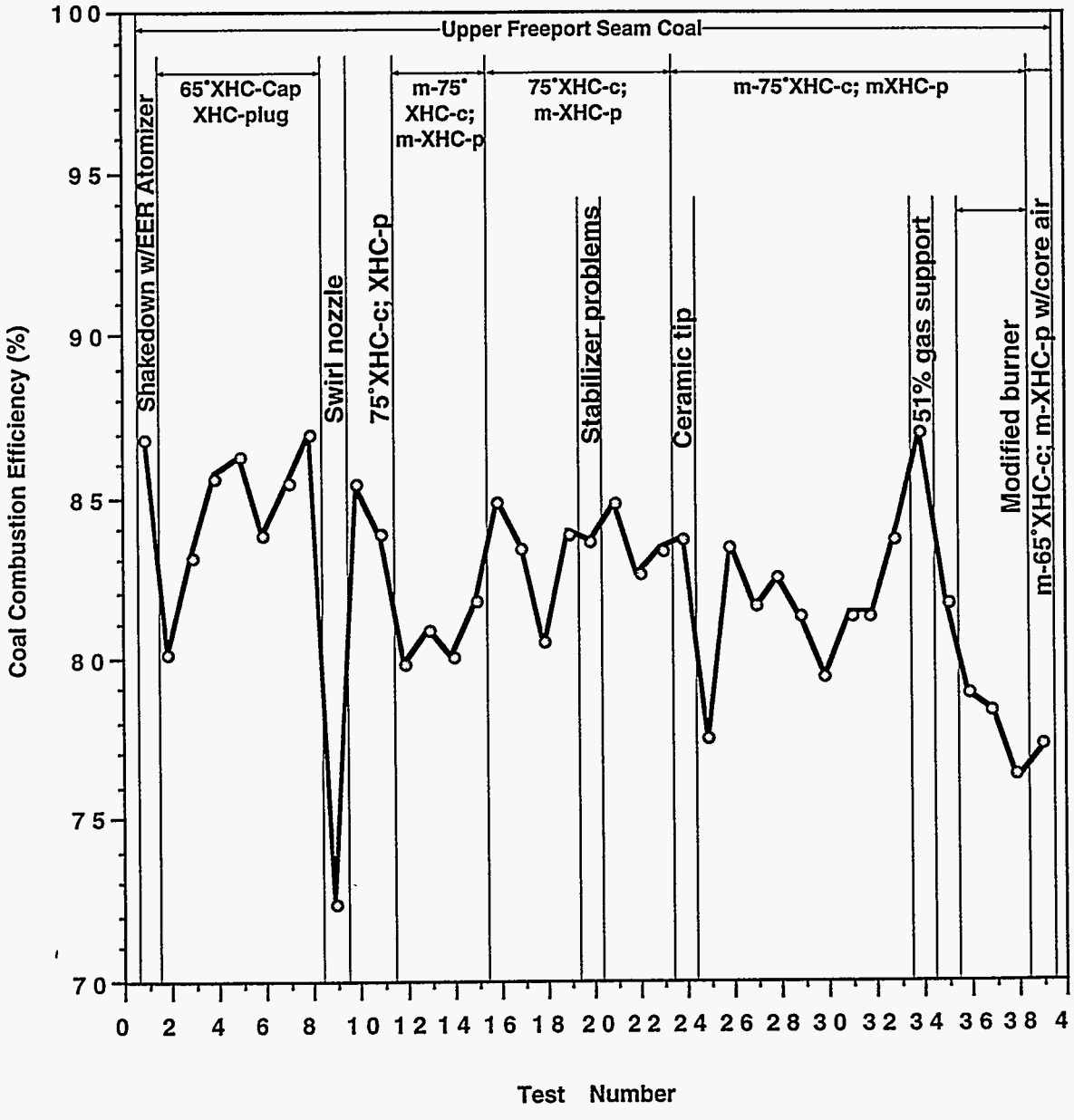

Figure 4-70. COAL COMBUSTION EFFICIENCIES FOR MCWM TESTING FROM JANUARY TO APRIL 1995 USING THE EER BURNER

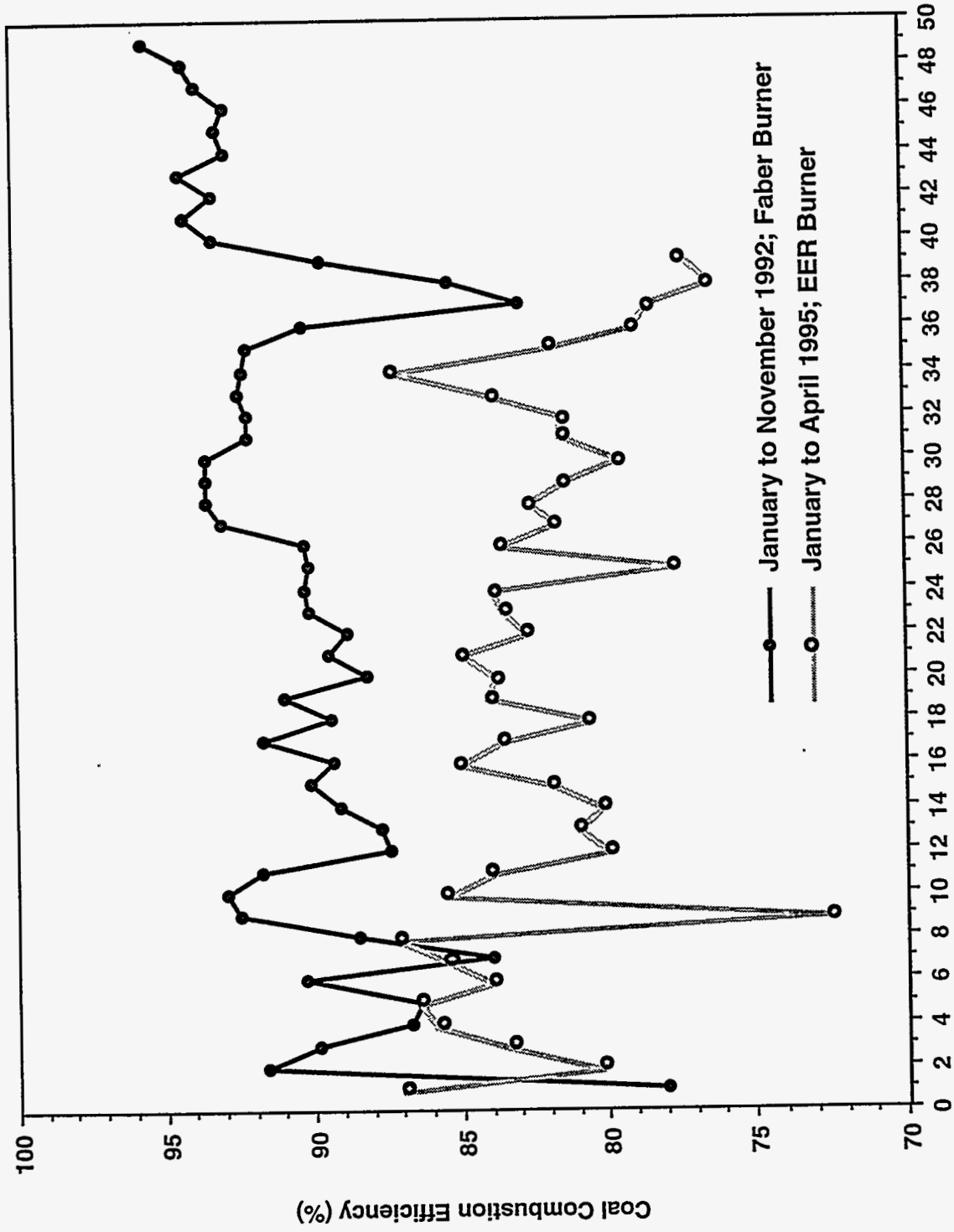

Figure 4-71. COAL COMBUSTION EFFICIENCIES FOR MCWM TESTING

University compressed air pressure) during the EER burner test program.

In an attempt to improve the combustion efficiency, several operating parameters were varied and minor modifications to the burner were made. The atomizer that was provided with the burner produced a long, narrow flame that impinged on the back wall. It was replaced with the Faber nozzle during MCWM/burner shakedown in January. Subsequent testing was conducted using various nozzle combinations, MCWM preheat temperatures, and solids loading, and burner modifications to initiate earlier tertiary and secondary air mixing. A discussion of each of these is provided in the following subsections.

Error Analysis

A series of tests was used to determine reproducibility of the coal combustion efficiency. Table 4-21 contains three sets of data listing the primary operating parameters and coal combustion and boiler efficiencies. Most of the testing was conducted with three atomizer tip configurations (see next section) and each is represented in the error analysis. The sets of data were assembled using tests without MCWM preheat, and with firing rate, solids loading, percent natural gas support, and excess air as similar as possible. The set of data for the 65°XHC cap/modified XHC plug combination had the most variability; these were the three closest data points as most of the testing with this nozzle combination was conducted with MCWM preheat.

The coal combustion efficiency differed by 0.9, 2.4, and 3.1% for the three sets of tests. Hence, coal combustion efficiency reproducibility is determined to be ±1.5% and was used to determine significance when evaluating the results from the parametric analysis presented in the following subsections. This is larger than the error in the previous SCCWS testing where the coal combustion efficiency significance was determined to be ±0.25%[3].

Nozzle Configuration

The primary components of the internal mix, twin-fluid Faber atomizer consist of a plug and cap combination. An example of one combination, a XHC (extra-high capacity) plug and 75°XHC cap, is shown in Figure 4-72. The 75° in the cap designation refers to the spray angle produced, the capacity descriptor refers to the MCWM flow. Table 4-22 lists the caps and plugs that were used and their characteristic air and MCWM passage openings.

Five primary nozzle combinations were used. Table 4-23 lists selected results from the MCWM demonstration. Test group A used a 65°XHC cap: Tests 3 through 8 used a XHC plug; Test 39 used a modified XHC plug (air openings enlarged to 0.141"; this was the only test with the plug modified to this dimension); and Test 24 used a ceramic cap with a modified XHC plug (air openings enlarged to 0.125"; all modified XHC plug refers to this dimension except for Test 39). Test group B used a swirl nozzle. Test group C used a 75°XHC cap with a XHC plug. Test group D used a modified 75°XHC cap (holes were jetted to 0.188") and a modified XHC plug. Test group E used a 75°XHC cap and a modified XHC plug.

Table 4-21. Comparison of Test Results for Determining Significance

Test No.	Nozzle Cap/Plug	Firing Rate MM Btu/h	Solids Loading (%)	CWF Temp. (°F)	Pct. Gas Support	Excess Air (%)	Coal Combustion Efficiency (%)	Boiler Efficiency (%)
February 15, 1995	65°XHC/	15.2	59.9	95	29.5	16.2	86.1	73.3
February 16, 1995	XHC	15.3	59.0	95	29.6	17.3	83.7	71.6
March 13, 1995	75°XHC/	18.3	61.6	95	29.5	14.6	82.4	71.1
March 14, 1995	m-XHC	18.2	61.5	95	29.1	14.4	83.3	71.3
March 27, 1995	m-75°XHC/	18.1	61.0	95	28.1	16.1	82.3	71.1
March 28, 1995	m-XHC	18.2	61.3	95	28.5	15.8	79.2	69.5

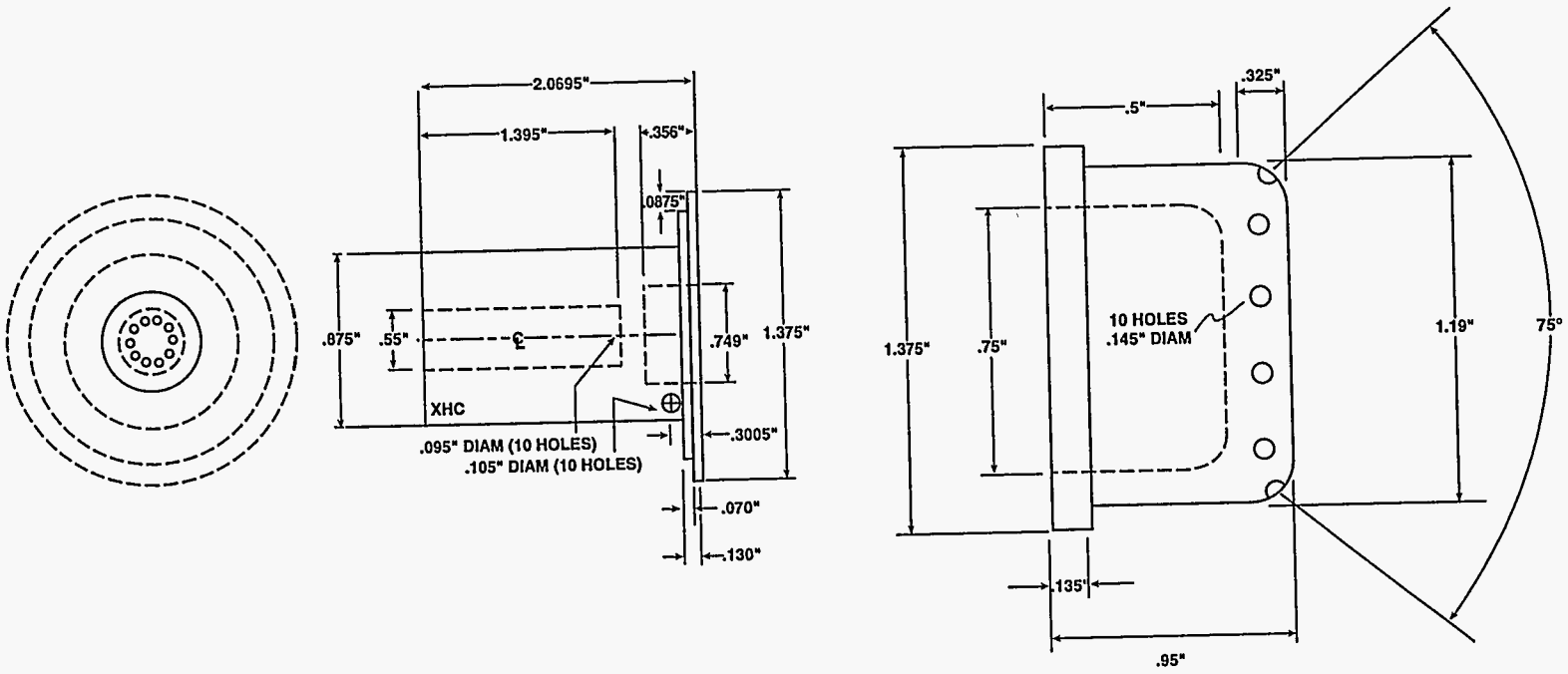

Figure 4-72. SCHEMATIC DIAGRAM OF THE FABER XHC PLUG AND CAP

Table 4-22. Hole Diameters of the Faber Plugs and Caps Used in the Demonstration

Swirl Plug Opening Diameters (175 gal/h):	
Slurry Openings	1/16"
Axial Air Openings	7/64"
Tangential Air Openings	1/8"
Standard Plug Opening Diameters:	
Extra High Capacity (XHC)	
Axial Slurry Opening	0.109"
Radial Air Opening	0.125"
Standard Cap Opening Diameters:	
Extra High Capacity	5/32"

Table 4-23. Selected MCWM Data

Date	Test Group	Test No.	Firing Rate (MM Btu/h)	Pct Gas Support	Pct Solids	Coal Combustion Efficiency (%)	Boiler Efficiency (%)	MCWM Temperature (F)	Atomizing Air to Fuel Ratio (lb/lb)	Steam Production (lb/h)	SO2 (lb/MM Btu)	NOx (lb/MM Btu)	CO (lb/MM Btu)	O2 (%)
2/8/95	A	3	15.7	20.7	60.1	83.1	70.84	95	0.32	10,523	0.78	0.55	0.19	3.25
2/14/95	A	4	15.3	28.7	62.5	85.6	73.50	95	0.37	11,611	0.60	0.62	0.19	3.13
2/15/95	A	5	15.2	29.5	59.9	86.1	73.25	95	0.35	11,539	0.61	0.53	0.15	3.07
2/16/95	A	6	15.3	29.6	59.0	83.7	71.59	95	0.40	11,284	0.64	0.47	0.17	3.25
2/17/95-NP	A	7	15.1	28.6	60.5	85.3	72.83	95	0.37	10,943	0.60	0.50	0.17	3.43
2/17/95-P	A	8	15.0	29.3	60.5	86.8	74.54	168	0.37	11,014	0.59	0.54	0.15	3.43
3/22/95-AMI	A	24	18.0	28.2	62.3	83.6	71.74	95	0.32	13,364	0.64	0.59	0.28	2.86
4/13/95	A	39	17.9	32.5	59.8	76.8	68.40	95	0.29	12,764	0.67	0.54	0.30	3.56
2/21/95	B	9	18.7	28.3	57.5	72.3	64.31	95	0.32	10,737	0.58	0.40	0.80	3.04
2/23/95	C	10	18.7	27.5	59.2	85.2	72.31	134	0.25	12,856	0.59	0.56	0.13	2.90
2/24/95	C	11	18.8	26.1	62.6	83.6	72.12	138	0.26	12,728	0.64	0.71	0.20	3.13
2/28/95-NP	D	12	18.4	27.4	61.8	79.7	69.60	95	0.35	12,523	0.65	0.46	0.16	3.19
2/28/95-P	D	13	18.5	27.2	61.8	80.7	70.62	131	0.35	12,883	0.64	0.43	0.15	2.82
3/1/95	D	14	18.4	30.8	61.6	79.9	69.92	95	0.37	12,415	0.60	0.45	0.15	3.66
3/2/95	D	15	18.5	28.8	61.4	81.6	71.53	154	0.35	13,231	0.61	0.44	0.11	3.04
3/27/95-NP	D	28	18.1	28.1	61.0	82.3	71.11	95	0.31	12,379	0.61	0.51	0.13	3.06
3/27/95-P	D	29	18.5	29.4	61.0	80.9	70.79	124	0.31	12,532	0.60	0.47	0.19	3.00
3/28/95-NP	D	30	18.1	28.5	61.3	79.2	69.47	95	0.32	12,396	0.59	0.43	0.16	3.01
3/28/95-P	D	31	18.2	28.7	61.3	81.2	71.00	143	0.33	12,623	0.62	0.50	0.22	2.87
3/29/95-NP	D	32	18.0	28.9	58.3	81.2	69.84	95	0.30	12,742	0.63	0.53	0.13	2.88
3/29/95-P	D	33	17.9	28.4	58.3	84	71.89	139	0.31	13,116	0.64	0.55	0.12	2.87
3/31/95	D	34	17.2	47.4	61.8	86.9	75.82	160	0.52	13,201	0.45	0.51	0.10	3.40
4/3/95	D	35	18.1	28.3	61.2	81.7	71.15	147	0.31	12,382	0.64	0.53	0.28	3.07
4/4/95	D	36	18.3	28.3	60.1	78.7	68.85	95	0.31	12,538	0.70	0.61	0.25	3.46
4/10/95	D	37	18.7	27.4	62.5	78.2	68.84	95	0.30	11,608	0.71	0.35	0.28	3.34
4/11/95	D	38	18.3	29.4	64.0	76.2	67.81	95	NR	11,685	0.78	0.36	0.24	4.79
3/6/95	E	16	18.0	30.0	62.5	84.7	73.11	148	NR	13,093	0.64	0.56	0.13	3.55
3/7/95	E	17	19.1	27.8	62.5	83.3	71.74	137	0.31	12,898	0.64	0.48	0.24	3.57
3/9/95-NP	E	18	17.7	28.8	60.8	80.2	69.61	95	0.31	12,834	0.60	0.56	0.16	2.87
3/9/95-P	E	19	18.2	29.7	61.2	83.8	72.27	130	0.32	12,992	0.63	0.66	0.35	3.52
3/10/95-NP	E	20	18.1	29.3	58.9	83.5	71.82	95	0.31	12,348	0.57	0.53	0.16	2.84
3/10/95-P	E	21	18.2	29.1	58.9	84.6	72.89	132	0.31	12,719	0.57	0.54	0.16	2.49
3/13/95	E	22	18.3	29.5	61.6	82.4	71.14	95	0.32	13,130	0.56	0.57	0.12	2.82
3/14/95	E	23	18.2	29.1	61.5	83.3	71.34	95	0.32	13,317	0.54	0.55	0.20	2.78
3/22/95-AM2	E	25	18.6	29.6	63.2	77.2	68.26	95	0.33	13,693	0.63	0.60	0.19	2.95
3/22/95-PM	E	26	18.5	29.2	63.0	83.4	71.86	95	0.33	13,991	0.62	0.59	0.20	2.96
3/23/95	E	27	18.7	27.3	59.2	85.2	72.31	134	0.25	12,856	0.59	0.56	0.13	2.90

Group Description:
A - 65°XHC cap/ XHC plug; except for Test #24 which used a ceramic cap and Test 39 which used a modified XHC plug (9/16" openings)
B - Swirl nozzle
C - 75°XHC cap/XHC plug
D - modified 75°XHC cap/modified XHC plug
E - 75°XHC cap/modified XHC plug

Previous testing during the SCCWS program determined that 65° was the optimum spray angle after investigating spray angles from 50 to 75°[3]. Consequently, the testing was started using the 65°XHC cap. The 65° angle cap was replaced with the 75° angle caps in order to widen the flame and attempt to make the quarl radiant. The quarl never became radiant during the MCWM demonstration. The caps and plugs were later modified to vary the atomizing air-to-fuel ratio.

As a group, the tests conducted with the 65°XHC cap/XHC plug at firing rates from 15.0 to 15.7 MM Btu/h performed the best with an average of 84.8% coal combustion efficiency without MCWM preheat, and 86.8% coal combustion efficiency with MCWM preheat. These results are similar to the SCCWS testing[3].

The tests conducted with the 75°XHC cap and with either the XHC or modified XHC plug at firing rates from 17.2 to 19.2 MM Btu/h worked slightly better than the modified 75°XHC cap/modified XHC plug combination. The average coal combustion efficiencies were 84 and 82%, respectively, with MCWM preheat. No tests were conducted using the 75°XHC cap/XHC plug combination without MCWM preheat.

The swirl nozzle performed very poorly with a coal combustion efficiency of 72.3% and resulted in a narrow flame that impinged on the back wall. Similarly, the ceramic cap was used for approximately eight hours with 83.6% coal combustion efficiency before it lost structural integrity and the center of the cap broke resulting in a narrow flame that impinged on the rear wall. The ceramic tip was a prototype that was produced for the atomizer corrosion/erosion testing but was used in the boiler because it was too large for the fundamental study.

MCWM Preheat

Tests were conducted to determine the effect of MCWM temperature on coal combustion efficiency. Figure 4-73 shows the effect of MCWM on coal combustion efficiency for a series of side-by-side tests. Seven tests were conducted where several hours of operation were conducted without MCWM preheat which was followed by several hours of operation with MCWM preheat. In six of the seven tests there was an increase in coal combustion efficiency of 1.0 to 3.6%; in one test there was a decrease in coal combustion efficiency of 1.4%. Using 1.5% as the significance level, four of the tests indicated that preheating the MCWM had a positive effect on coal combustion efficiency. Previous testing had shown that preheating the slurry from 95 to 160°F resulted in only a minor increase of 1.0% in coal combustion efficiency[3]. In the current test program, increases in coal combustion efficiency as high as 3.6% were observed when preheating the MCWM to 130°F.

When evaluating the data as a whole, the effect of MCWM temperature on coal combustion efficiency is not clear. Figure 4-74 is plot of coal combustion efficiency as a function of MCWM temperature for the 65°XHC cap/modified XHC plug combination (15.0 to 15.7 MM Btu/h firing rate) and for the 75°XHC cap/XHC and modified XHC plugs combinations (17.7 to 19.1 MM

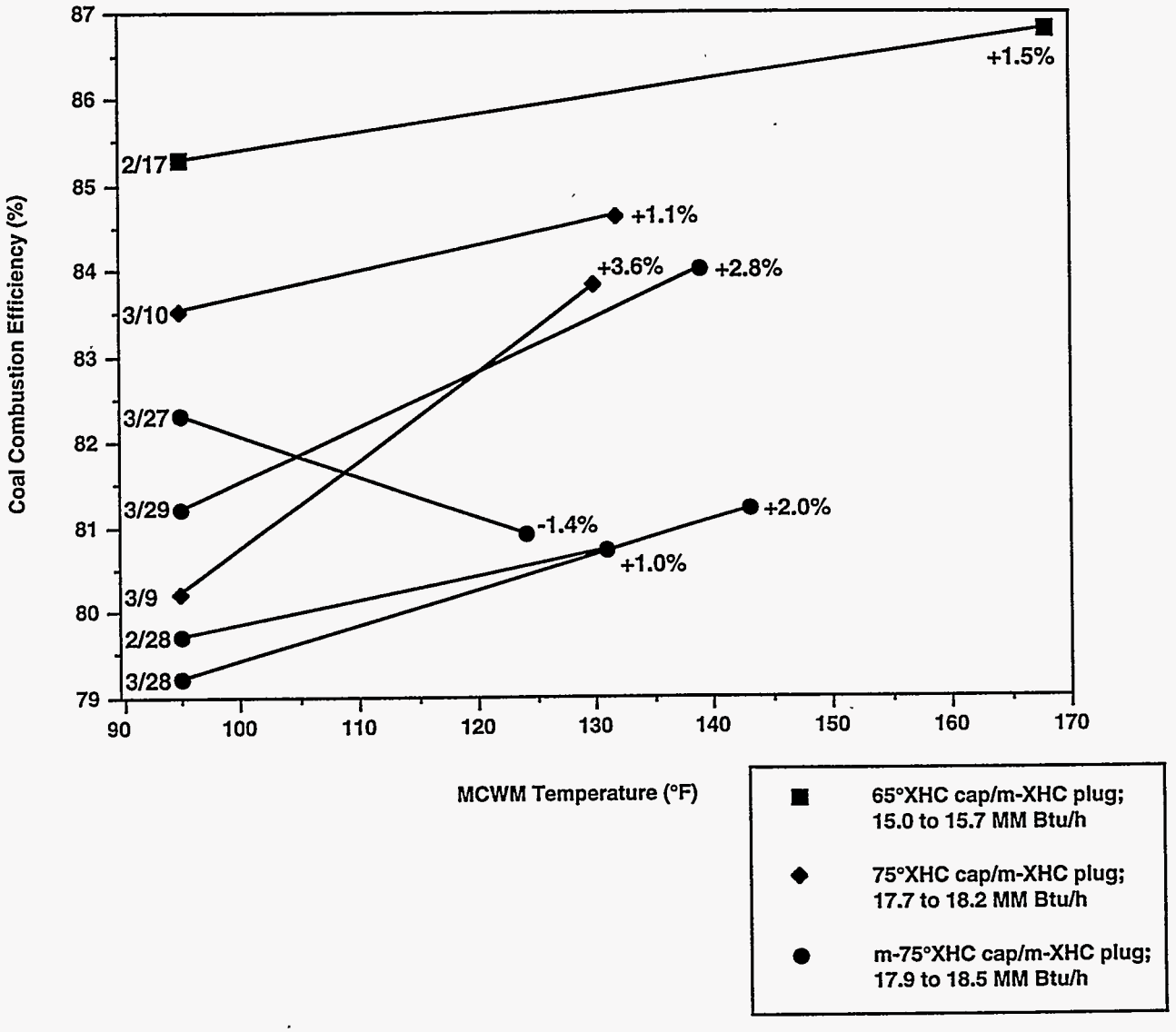

Figure 4-73. EFFECT OF MCWM PREHEAT TEMPERATURE ON COAL COMBUSTION EFFICIENCY FOR THREE NOZZLE COMBINATIONS

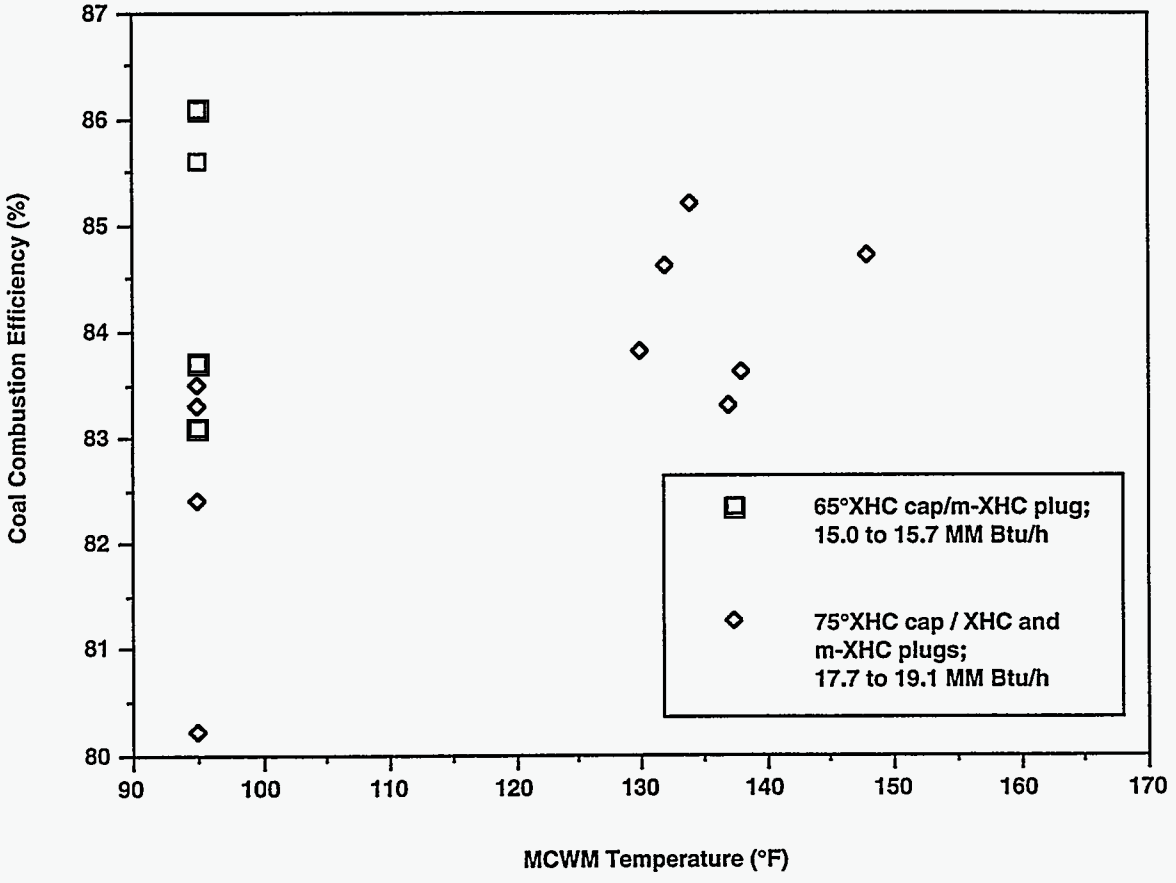

Figure 4-74. THE EFFECT OF MCWM PREHEAT TEMPERATURE ON COAL COMBUSTION EFFICIENCY FOR THREE NOZZLE COMBINATIONS

Btu/h firing rate). The modified 75°XHC cap was not included in the data because it was a poorer performer than the unmodified 75°XHC cap. There is much scatter in the data and no trends are evident.

MCWM Solids Loading

The effect of MCWM solids loading on coal combustion efficiency was influenced by the nozzle combination. Figure 4-75 shows the effect of solids concentration on coal combustion efficiency. The solids loading varied from 58.3 to 64.0 wt.% during the test program. The coal combustion efficiency showed a decreasing trend as the solids loading was increased from ~58.5 to 64.0 wt.% when using the modified 75°XHC cap/modified XHC plug combination. Similarly, there was a decrease in coal combustion efficiency as solids content increased from 59.2 to 62.6% when using the 75°XHC cap/XHC plug combination. Apparently, poorer atomization was obtained with these nozzles. Full-scale atomization studies were not conducted to determine the atomization characteristics of these nozzles.

No trends were discernible when using the 65°XHC cap/XHC plug and 75°XHC cap/modified XHC plug combinations. Previous testing showed a slight increase (1.0%) when increasing the SCCWS solids content from 59 to 62 wt.%[3].

Burner Modifications

Throughout the MCWM demonstration prior to the burner modifications, CO excursions were experienced and the quarl never became radiant (quarl is shown in Figure 4-61). This may have contributed to poor coal combustion efficiency and the need for natural gas to maintain a stable flame. Minor modifications were made to the burner to address this issue. First, the section of the membrane that separates the tertiary and secondary air streams was shortened to alter the flame shape in order to widen the base of the flame and transfer more heat to the quarl. The goal was to make the quarl more radiant to stabilize the flame. The Fluent CFD code was used to model the burner before and after the modifications when firing natural gas (see Section 4.2.1). The code results indicated that the alteration would have a minor affect on the temperature and gas velocity in the near burner region, and consequently, the modifications were made after the April 3, 1995 test. The tests conducted after this date were with the modified burner. As can be seen from Table 4-19, the modifications had a negative effect on the coal combustion efficiency even though the quarl became radiant. The momentum of the MCWM/atomizing air stream may have negated the effect of the modifications.

The final test of the program was conducted with air introduced through the annular section around the atomizer (core air). Previous work firing DMC and cofiring DMC and MCWM with air introduced into the center of the flame improved flame stability and increased coal combustion efficiency. However, the test on April 13, 1995 resulted in poor coal combustion efficiency.

Deposition/Accumulation

No depositional problems were experienced when firing MCWM. Most of the testing was

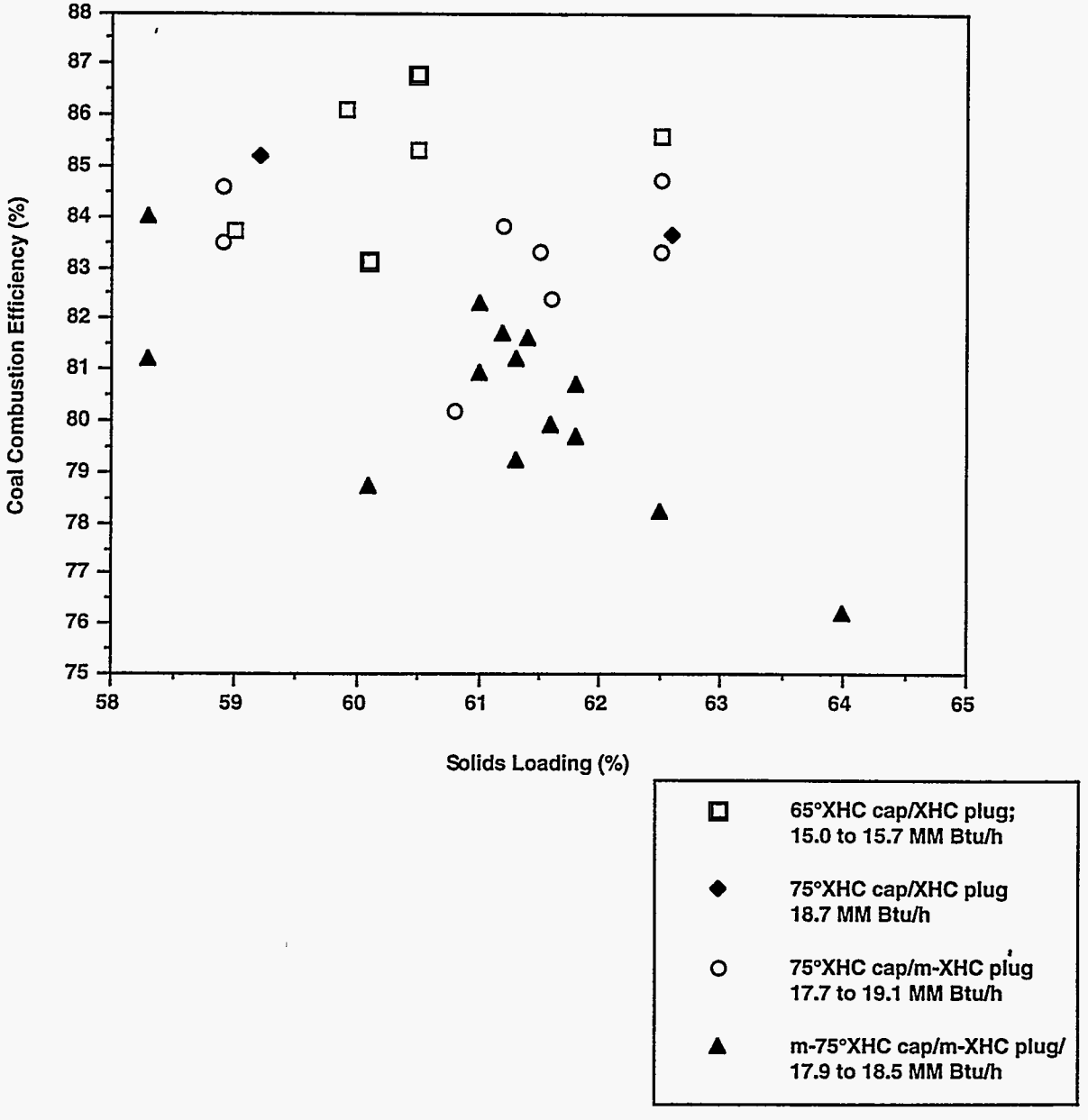

Figure 4-75. THE EFFECT OF SOLIDS LOADING ON COAL COMBUSTION EFFICIENCY

two shifts per day and test lengths were typically 3 to 10 hours in length except for the testing on March 22 and 23, 1995 which was 24 hours in length. No buildup on the furnace wall tubes was observed and no sootblowing was necessary. The boiler outlet temperature remained constant during the testing and did not exceed 600°F and was typically 560 to 580°F.

Emissions

Table 4-24 contains the emissions data from the MCWM demonstration. The flue gas analysis has been converted to lb/MM Btu corrected to 3% O_2 basis. The SO_2 and NO_x emissions ranged from 0.5 to 0.8 lb/MM Btu and from 0.4 to 0.7 lb/MM Btu, respectively. The SO_2 emissions were lower than the DMC testing and previous SCCWS testing (the coals all had similar sulfur levels) due to the level of natural gas support and probably the lower coal combustion efficiency. For the most part, the targeted NO_x level were met over the range of firing rates tested.

The carbon monoxide emissions varied during the testing. The CO emissions were more stable during the MCWM operation and, on average, were lower than those observed during the DMC operation; however, high CO excursions were encountered.

Derating

As previously discussed, the capacity of the boiler is 14,700 lb steam/h when firing at 18.5 MM Btu/h. Steam production during the MCWM demonstration ranged from 10,500 to 13,400 lb/h at firing rates from 15.0 to 19.1 MM Btu/h. Testing was conducted primarily over two ranges of firing rates, 15.1 to 15.7 MM Btu/h and 17.2 to 19.1 MM Btu/h. At the higher firing rate range, 17.2 to 19.1 MM Btu/h (26 out of 28 tests were in the range 18 to 19 MM Btu/h), the mean steam production was 12,600 lb/h or 86% of design capacity with a standard deviation of 600 lb steam/h.

4.4.5 Summary

In summary, two demonstrations firing DMC and MCWM were conducted. The accomplishments of this aspect of the program include: modifying and optimizing a boiler system to fire DMC and MCWM; integrating the coal storage, handling, and micronizing with the burner (for DMC firing); achieving 95% combustion efficiency (DMC); determining that erosion is not significant in the convective pass; and meeting targeted NO_x emissions of <0.6 lb/MM Btu. Items not accomplished were: establishing the effect of long-term continuous operation on deposition, firing 100% MCWM; achieving 98% coal combustion efficiency; and eliminating CO fluctuations. These items will be addressed in future testing.

5.0 ENGINEERING DESIGN

Two engineering studies were performed for the complete retrofit of a DOD boiler to fire either DMC or MCWM. Each design package includes a fuel preparation system (for the DMC option only), fuel delivery and handling systems, low-NO_x burner, baghouse, forced-draft (FD) fan, combustion air preheaters, induced-draft (ID) fan, ash silo, stack, and control system. The retrofit designs conform to accepted engineering practices and site requirements. The designs were

Table 4-24. Emissions Levels When Firing MCWM

Date	Test #	Firing Rate (MMBtu/h)	SO2 Conc. (moles)	NOx Conc. (moles)	CO Conc. (moles)	O2 Conc. (%)	SO2 Conc. (lb/MMBtu Corrected to 3% O2)	NOx Conc. (lb/MMBtu Corrected to 3% O2)	CO Conc. (lb/MMBtu Corrected to 3% O2)
2/8/95	3	15.6	0.000412	0.000402	0.000226	3.25	0.78	0.55	0.19
2/14/95	4	15.3	0.000323	0.000462	0.000167	3.13	0.60	0.62	0.14
2/15/95	5	15.2	0.000328	0.000393	0.000180	3.07	0.61	0.53	0.15
2/16/95	6	15.3	0.000338	0.000344	0.000208	3.25	0.64	0.47	0.17
2/17/95	7	15.1	0.000313	0.000358	0.000204	3.43	0.60	0.50	0.17
2/17/95	8	15.0	0.000308	0.000395	0.000181	3.43	0.59	0.54	0.15
2/21/95	9	18.7	0.000309	0.000292	0.000961	3.04	0.58	0.40	0.80
2/23/95	10	18.7	0.000323	0.000423	0.000167	2.90	0.59	0.58	0.13
2/24/95	11	18.8	0.000342	0.000526	0.000246	3.13	0.64	0.71	0.20
2/28/95	12	18.4	0.000346	0.000339	0.000199	3.19	0.65	0.46	0.16
2/28/95	13	18.5	0.000354	0.000334	0.000188	2.82	0.64	0.43	0.15
3/1/95	14	18.4	0.000306	0.000319	0.000172	3.66	0.60	0.45	0.15
3/2/95	15	18.5	0.000329	0.000328	0.000136	3.04	0.61	0.44	0.11
3/6/95	16	18.0	0.000328	0.000402	0.000149	3.55	0.64	0.56	0.13
3/7/95	17	19.1	0.000326	0.000341	0.000281	3.57	0.64	0.48	0.24
3/9/95	18	17.7	0.000331	0.000429	0.000200	2.87	0.60	0.56	0.16
3/9/95	19	18.2	0.000323	0.000472	0.000407	3.52	0.63	0.66	0.35
3/10/95	20	18.1	0.000318	0.000409	0.000197	2.84	0.57	0.53	0.16
3/10/95	21	18.2	0.000329	0.000433	0.000208	2.49	0.57	0.54	0.16
3/13/95	22	18.3	0.000313	0.000443	0.000149	2.82	0.56	0.57	0.12
3/14/95	23	18.2	0.000303	0.000429	0.000256	2.78	0.54	0.55	0.20
3/22;AM-I	24	18.0	0.000349	0.000449	0.000352	2.86	0.64	0.59	0.28
3/22;AM-II	25	18.6	0.000342	0.000454	0.000236	2.95	0.63	0.60	0.19
3/22;PM	26	18.5	0.000338	0.000449	0.000248	2.96	0.62	0.59	0.20
3/23/95	27	18.4	0.000340	0.000417	0.000209	3.01	0.63	0.55	0.17
3/27/95	28	18.1	0.000332	0.000383	0.000160	3.06	0.61	0.51	0.13
3/27/95	29	18.5	0.000328	0.000361	0.000234	3.00	0.60	0.47	0.19
3/28/95	30	18.1	0.000322	0.000326	0.000199	3.01	0.59	0.43	0.16
3/28/95	31	18.2	0.000341	0.000385	0.000283	2.87	0.62	0.50	0.22
3/29/95	32	18.0	0.000347	0.000409	0.000169	2.88	0.63	0.53	0.13
3/29/95	33	17.9	0.000353	0.000419	0.000151	2.87	0.64	0.55	0.12
3/31/95	34	17.2	0.000240	0.000377	0.000124	3.40	0.45	0.51	0.10
4/3/95	35	18.1	0.000344	0.000400	0.000340	3.07	0.64	0.53	0.28
4/4/95	36	18.3	0.000362	0.000440	0.000291	3.46	0.70	0.61	0.25
4/10/95	37	18.7	0.000371	0.000258	0.000339	3.34	0.71	0.35	0.28
4/11/95	38	18.3	0.000345	0.000223	0.000247	4.79	0.78	0.36	0.24
4/13/95	39	17.9	0.000344	0.000389	0.000356	3.56	0.67	0.54	0.30

based on the system in place at Penn State and the information that was learned from operating it during the SCCWS and ABB CE programs (see Section 4.0). The design packages are intended to be used for soliciting bids from engineering/construction firms for completion of the detailed design, construction, and start-up of the candidate DOD boiler.

Section 5.0 contains summaries of the designs. The complete design packages are contained in Volume 2. The design packages include system descriptions, mass and energy balances, instrument lists, major equipment lists, electrical lists, building lists, compressed air consumption, drawing lists, cost summaries, vendor literature and quotes, and reduced copies of the blueprints.

5.1 Site Description

As discussed in Section 2.0, the boiler chosen for the design is located at the Crane Naval Surface Warfare Center (NSWC). Factors used in the selection process included geographic location, site specific parameters, and size and configuration in regards to total population. This facility is located in southern Indiana approximately 30 miles southwest of Bloomington, Indiana. The host boiler (Boiler #1) is located in building 150, along with two similar boilers. The boiler was installed in 1989 and is used to produce steam for weapons production and general building heating. The weapon production steam is used for a bomb assembly line and a mine filling area.

5.2 Boiler Description

The host boiler is a Cleaver-Brooks watertube boiler model D-42-LH. It has a design capacity of 20,000 lb/h saturated steam at 125 psig and was originally designed to fire natural gas, #2, or #6 fuel oil. The boiler has fired natural gas and #2 fuel oil. The boiler occupies this building with two other boilers; one is a twin of the unit and the other is a Cleaver-Brooks D-type with a capacity of 15,000 lb/h steam. Typically, the boilers are operated nine months of the year on a cycling basis, each boiler being utilized approximately three months per year. The annual fuel consumption per boiler is approximately 35,000 MM Btu. The boiler's normal production rate is approximately 80% of its maximum continuous rating. If additional steam is required, a second boiler is put into service.

The boiler is a two drum, bent tube D-type boiler. The inside and outside furnace walls and the floor and roof, are of tangent tube construction. The front and rear walls are also of tangent tube construction, but are refractory covered.

Base personnel are not normally at the site during routine operation of the boilers. The existing boiler controls are relatively simple and operate without an operator in attendance. A roving operator checks on the boilers in the building once or twice a day. The only existing boiler alarm is that of low steam pressure. All of the boilers on site are tied into phone line to a remote operations center.

5.3 Design Approach

The goals established for the retrofit designs were to maintain operational simplicity, low

operations cost, and to minimize any negative impact on boiler performance. Specific concerns to be addressed by the retrofit designs with respect to boiler performance included ash deposition and coal combustion efficiency.

Several features have been incorporated into the design to address these concerns. The coal will be micronized to increase the combustion efficiency and reduce the tendency of the ash to settle in the boiler system. Combustion efficiency will be further enhanced by preheating the combustion air to 400°F. To keep the system free of ash deposition, a compressed air ash reentrainment system will be installed in the furnace floor and an existing sootblower, in the convective pass, will also be utilized. The air heater is equipped with a sootblower to control ash deposition.

Each conversion includes a fuel preparation system (for the DMC option only), fuel delivery and handling systems, low-NO_x burner, baghouse, FD fan, combustion air preheaters, ID fan, ash silo, stack, and control system. The systems are all designed to minimize operator attention and maintenance requirements. Each of these systems are discussed in the following sections.

5.4 DMC System

The DMC retrofit design includes a fuel delivery and handling system, low-NO_x burner, baghouse, FD fan, combustion air preheaters, ID fan, ash silo, stack, and control system, each of which is described in the following subsections. See Figure 5-1 for the process flow diagram. This diagram demonstrates the functional relationship between the components of the system. Figure 5-2 presents an isometric view of the DMC retrofit facility with the various ancillary systems as designed for the Crane demonstration unit.

5.4.1 Fuel Unloading/Handling System

Coal will arrive at the facility in 20-ton conventional coal trucks. The system is based on a design coal from the Indiana VII seam (higher heating value of 11,898 Btu/lb). The coal will be received as a 2"x0 product. The coal will have less than 1.2 lb SO_2/million Btu and an ash content of 4.3 wt.% as received.

The DMC unloading and handling system will consist of an unloading building, coal receiving hopper, vibratory feeder, Z-belt conveyor, and coal storage silo. The system is sized to handle 20 tons/h or approximately one coal truck per hour. The coal will be delivered to the coal unloading building where the truck will dump into the coal receiving hopper. The unloading building will be a pre-fabricated metal building (22'L x 16'W x 20'H) and will be equipped with a dust collection system. The coal receiving hopper will be constructed of 304 stainless steel and have a capacity of 980 ft^3. The capacity includes the coal in and piled on the hopper. A vibratory feeder located underneath the hopper transfers the coal from the hopper to the roll crusher. The vibratory feeder will meter the coal flow from the hopper to the crusher. The vibratory feeder is equipped with a 0.5 HP TEXP motor and a magnet to capture any ferrous material. The roll crusher is powered by a 30 HP TEXP motor and will reduce the coal from 2"x0 to 3/4"x0. The

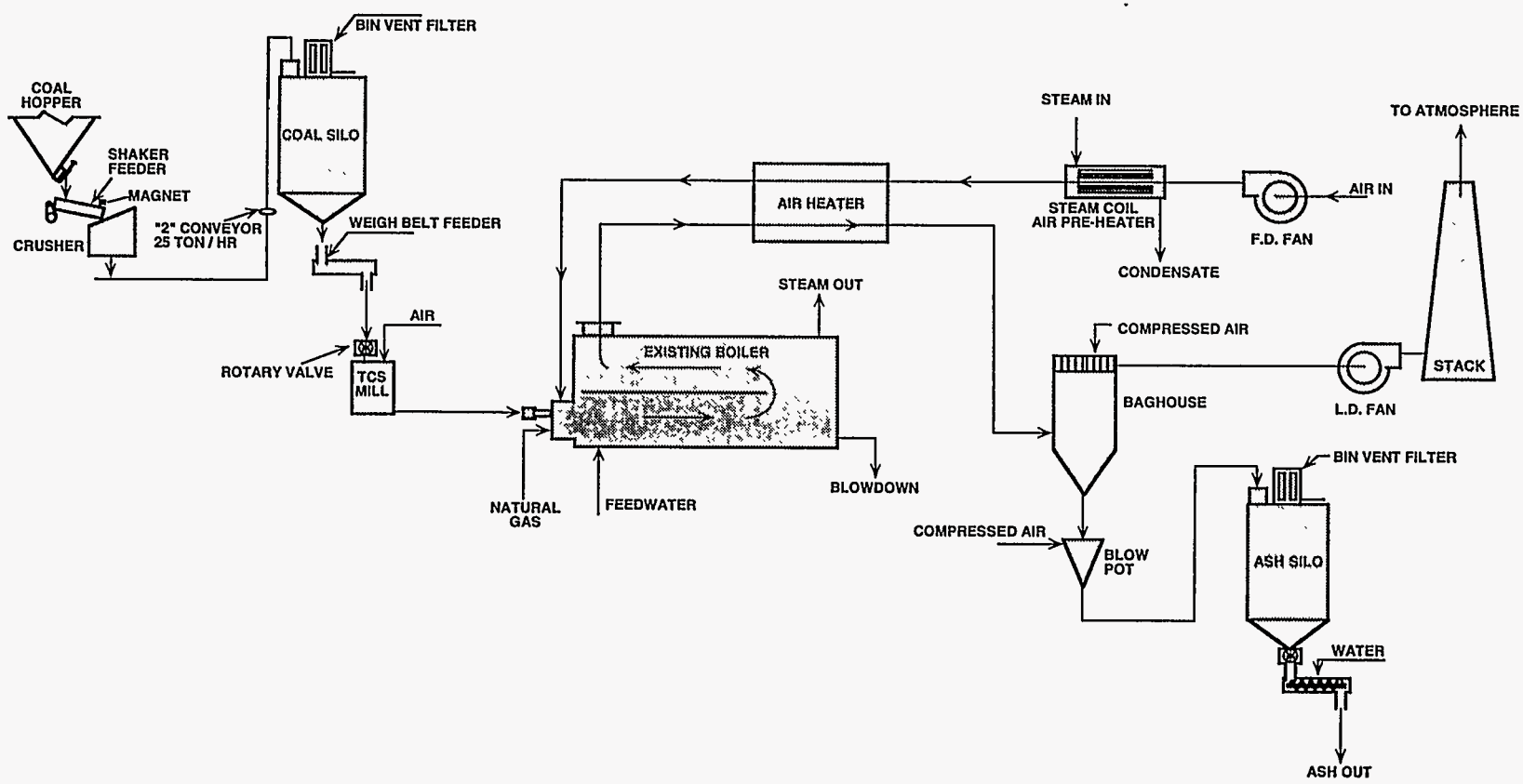

Figure 5-1. PROCESS FLOW DIAGRAM FOR THE DMC SYSTEM

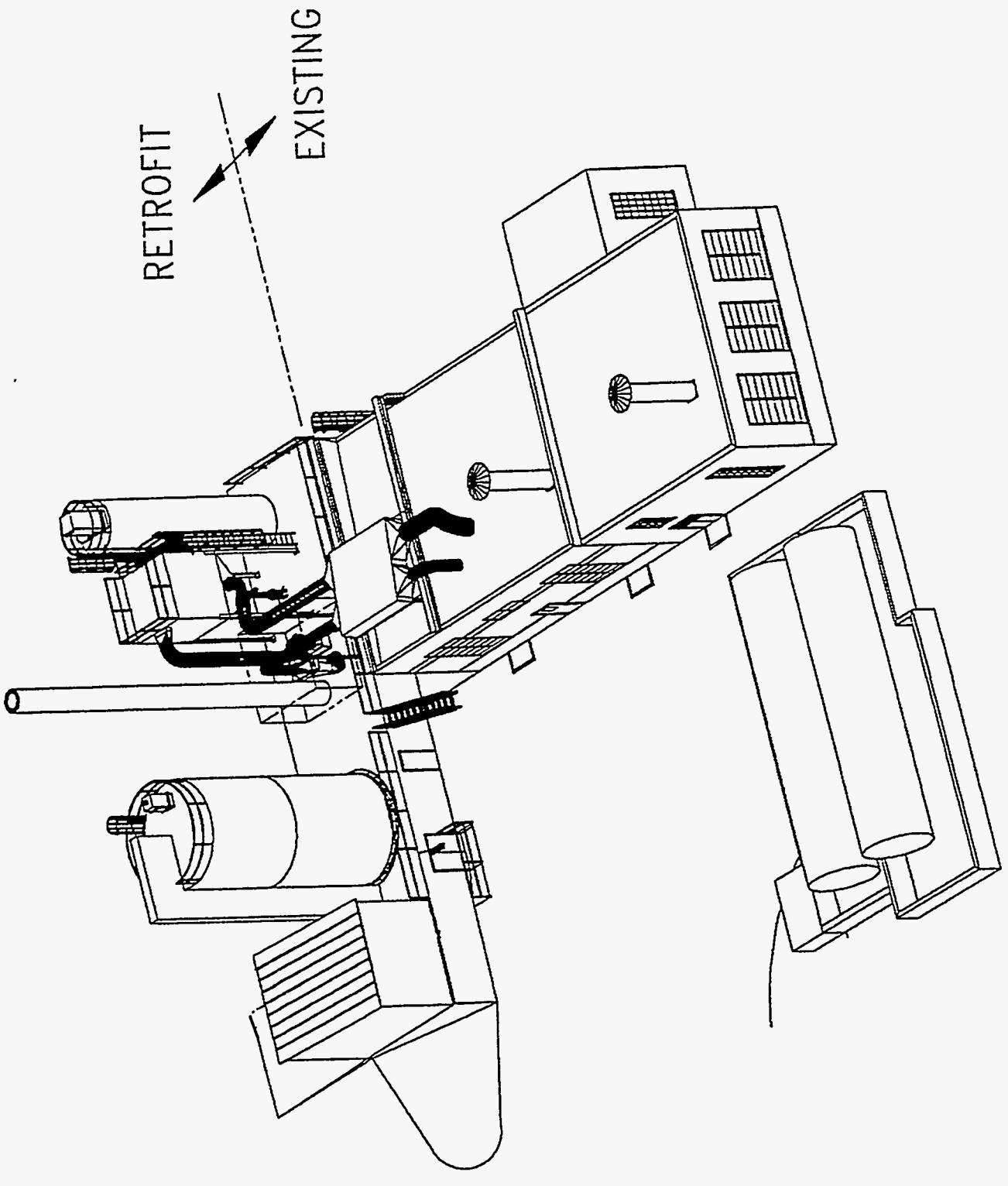

Figure 5-2. ISOMETRIC VIEW OF THE DMC RETROFIT FACILITY

crusher is designed to minimize fines production. The crusher will discharge into an enclosed Z-belt conveyor which transports the coal into the coal storage silo. The Z-belt conveyor will be equipped with a 36" wide continuous bucket belt and a 7.5 HP motor. The coal storage silo (16' D x 32' H - including 40° cone) will have a capacity of 4,100 ft^3 to provide the required five day on-site fuel reserve. The silo will be equipped with an air cannon that will operate when there is a loss of coal feed, bin vent filter, and high level alarms to prevent overfilling. The coal storage silo will also be equipped with a fire detection and CO_2 suppression system. Magnets will be used throughout the system to remove any ferrous material that may be entrained in the coal.

5.4.2 Fuel Delivery System

The DMC burner system will consist of a gravimetric weigh-belt feeder, rotary feeder, coal micronizing mill, and the coal delivery piping. Coal will be discharged from the coal storage silo onto the metering weigh-belt feeder. The feeder will have a capacity of 2,400 lb/h and be equipped with a 24" belt. The feeder, constructed of stainless steel, will be equipped with a DC drive to control the flow to the micronizing mill and, in turn, to the boiler. The National Fire Protection Association (NFPA) code requires that in pulverized coal feed systems all equipment from two feet above the coal feeder to the burners must be rated to withstand a 50 psig burst. An NFPA rated rotary feeder will be installed at the inlet to the mill to meet NFPA code requirements. By installing the rotary feeder, the explosion protection requirements will be limited two feet above the inlet of the valve, allowing the use of a standard weigh-belt feeder. The rotary feeder will be constructed of stainless steel and equipped with a 1.5 HP TEXP motor. The rotary feeder will discharge the coal into the micronizing mill.

The micronizing mill will take the coal from 3/4"x0 to 80% through 325 mesh (45 μm). The micronizing mill is equipped with a rotary classifier and provides the primary combustion air to transport the micronized coal to the burner. The mill has a capacity of 2,400 lb/h and is driven by a 125 HP TEXP motor. The mill is protected from tramp metal by magnets and a metal detector with diverter valve at the outlet of the weigh-belt feeder.

5.4.3 Burner

The burner will be a FlamemastEER™ burner that will fire natural gas to bring the boiler up to operating temperature then switch to DMC. A sectional view of the burner is shown in Figure 5-3. The DMC will be injected down the center of the burner and six spuds will deliver natural gas through the secondary air zone. The FlamemastEER™ burner is designed for long life and uses an innovative air flow control mechanism that eliminates complex linkages and gears.

The key functional features of the FlamemastEER™ burner design includes:

- Combustion air supply through separate secondary air (SA) and tertiary air (TA) passages;
- Variable SA/TA flow distribution;
- Variable SA and TA swirl;
- Low micronized coal velocity; and

CRANE NAVAL SURFACE WARFARE CENTER

EER DMC BURNER
MODEL 4AF-25.2-18.75

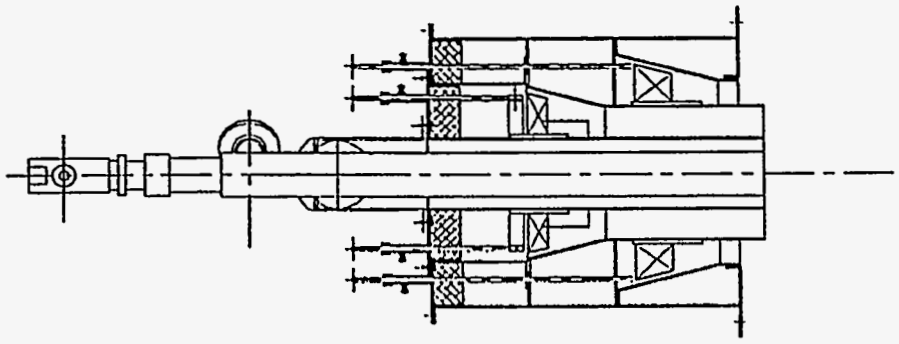

SECTIONAL TOP VIEW

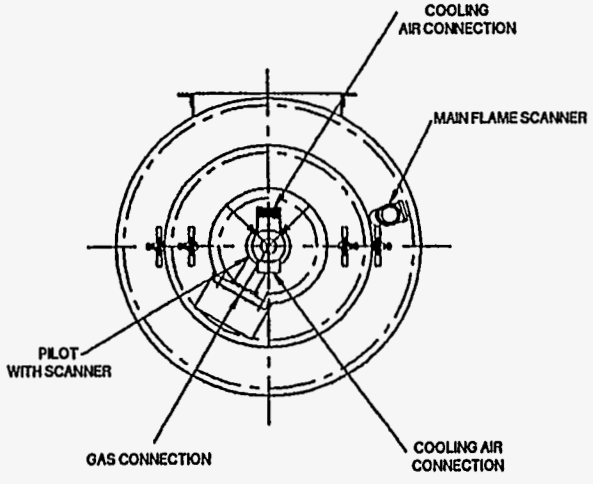

FRONT VIEW

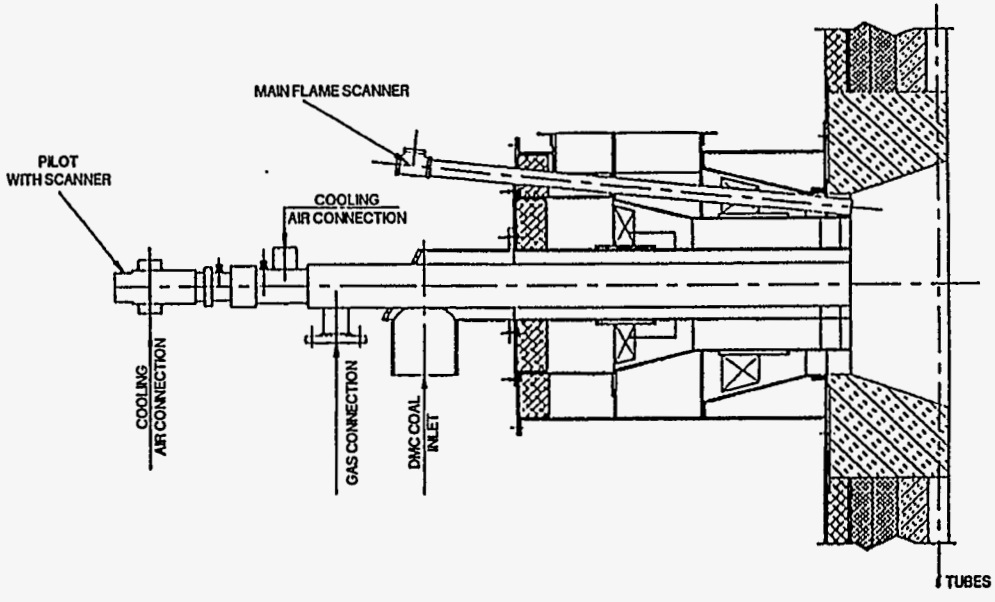

SECTIONAL FRONT VIEW

Figure 5-3. SECTIONAL VIEW OF THE DMC BURNER

- Flameholder attached to the coal nozzle.

The low primary air/coal velocity and flameholder are designed to provide good flame stability and acceptable flame characteristics for a wide range of operating conditions and fuel characteristics. The flameholder establishes local recirculation zones and promotes local mixing between the coal and the secondary air. This leads to rapid devolatilization of the coal and liberation of fuel nitrogen in a low excess air environment resulting in reduced NO_x formation.

Mechanically, the burner has been designed to minimize the number of moving parts. Those parts which do move slide axially, eliminating complex linkages and gears. The secondary and tertiary air swirl control vanes, called turbolators, move back and forth within conical passages of the burner. As the turbolators are moved toward the narrow end of the cone, more air passes through the vanes increasing the amount of swirl. As the turbolator is moved in the opposite direction, the air follows the path of least resistance and by-passes the vanes, resulting in less swirl. The moving parts are located away from the high heat flux environment in order to reduce warpage and binding. The parts of the burner which are subjected to a high heat flux are fabricated from a high strength heat resistant alloy.

5.4.4 Combustion Air Preheaters

The retrofit will include two combustion air preheaters. The first is a steam coil air preheater designed to heat 0°F ambient air to 200°F, to prevent corrosion in the flue gas system. The heater will have a rating of 1.4 MM Btu/h, and will be located in the combustion air duct work just after the discharge of the FD fan. The second combustion air heat exchanger is a heat pipe flue gas heat exchanger that will be located on the roof of the building. The flue gas will leave the boiler at 500°F and will exit the heat exchanger at 350°F. Simultaneously, the combustion air will be heated to 400°F. The heater has a rating of 7 MM Btu/h. The flue gas heat exchanger will be equipped with a sootblower to clean the flue gas side of the exchanger.

5.4.5 Ash Handling System

The ash handling system will consist of a baghouse to collect the particulate matter in the flue gas stream, pneumatic conveying system, ash storage silo, and an ash unloading screw conveyor. The baghouse was sized for a 3.5:1 air-to-cloth ratio and specified with Nomex bags and a fire detection/suppression system. The bags will be cleaned via compressed air pulses. The pneumatic conveying system will transfer the ash from the baghouse into the ash storage silo. The ash storage silo (8' D x 33' H) has a capacity of 12 tons and is constructed of carbon steel. The silo is sized to handle five days storage. The silo has a bin vent filter to capture fugitive dust from the pneumatic conveying system and a level sensor to prevent overfilling. The ash silo is also equipped with a fire detection system. The ash screw conveyor will unload the silo into trucks. The screw conveyor has a capacity of 1,200 ft^3/h and is equipped with a 5 HP variable frequency drive. Water injection nozzles are installed in the screw conveyor to condition the ash to prevent fugitive dust emissions. The screw conveyor is heat traced and insulated to prevent acidic

corrosion and freezing. Heat tracing was selected over a steam jacket since steam is not always available at the site.

5.4.6 Design Specifications

This section will present the design basis used in the preliminary design of the boiler retrofits to the Crane boiler. These criteria are based upon accepted engineering practices, vendor recommended parameters for their equipment, experience from operating the Penn State demonstration boiler system, and EER's experience. Also presented in this section is the boiler nameplate data and design operating parameters.

Design Specifications - DMC Retrofit

Boiler Manufacture	Cleaver-Brooks
Boiler Model No.	D-42-LH
Unit No.	W-3482
Steam Capacity	20,000 lb/h
Pressure Vessel Design	260 psig
Operating Pressure	125 psig
Heat Input	25.22 MM Btu/h
Pilot Gas	350 SCFH @ 7" H_2O to 1 psig
Main Gas	25,220 SCFH @ 1,000 Btu/ft^3

General Information on the DMC Retrofit System

1. DMC turndown is 3:1.
2. Natural gas turndown is 10:1.
3. Design carbon conversion is 99%.
   Minimum allowable carbon conversion is 98%.
4. The excess air is to be 25%.
5. The baghouse will have a minimum collection efficiency of 99.5%.
6. The pressure drop through the burner is less than 8" H_2O.
7. The combustion air preheater is to increase the combustion air temperature to 400°F.
8. All electric motors are to be of a TEFC design.
9. Electric motors larger than 1 HP are to be 480V/3PH/60HZ.
10. Electric equipment in an explosion proof area is to meet Class 2 Division 1.
    If explosion proof is required, this supersedes the TEFC requirement.
11. Allowable velocities:

Service	Velocity, ft/m
Air heater (air side)	1,000-5,000
Compressed air	1,500-2,000
Forced draft ducts	1,500-3,600
Air heater (flue gas side)	1,000-5,000
Induced draft flues and breaching	2,000-3,500
Stack	2,000-5,000

12. The minimum allowable flue gas temperature is 300°F while firing DMC.
13. Allowable compressed air velocities in braided nonlined flexible is 120 ft/s. If this is to be exceeded, consult the factory. All installation arrangements are to be factory specifications.
14. All liquid piping outside of the boiler house is to be heat traced and insulated to prevent freezing.
15. Boiler purge air exchange requirements is five times the total volume from FD fan to ID fan.
16. The baghouse is designed to have an air-to-cloth ratio of approximately 3.5 to 1. The baghouse will be equipped with Nomex type bags. The baghouse is to be insulated

and have a heated hopper.

17. The ash storage silo is to be designed to store five days worth of ash.

Information on the Coal Fuel System

1. Fuel storage capacity requirements is to be 75% boiler load on DMC for 120 hours.
2. Fuel analysis is 14% moisture, 4.3% ash, 31.2% volatile matter, 50.5% fixed carbon, less than 1.1 lb SO_2/million Btu, and a higher heating value of 11,898 Btu/lb.
3. The raw coal delivered size is 2" x 0.
4. The crusher is to reduce the coal from 2"x0 to 3/4"x0.
5. The bulk density of the coal is 45-48 lb/ft^3. This includes void factor.
6. The boiler is to be capable of firing 100% natural gas or 100% DMC and any combination within the turndown ranges.
7. The nominal DMC loaded primary air velocity is in the range of 3,000 to 5,000 ft/m.
8. The primary air flow is 10% of the total combustion air.
9. All DMC piping is to be schedule 80 carbon steel (3/8" wall thickness).
10. The stainless steel hoppers are to have an included angle of 60° and be equipped with an air blast system. The lining will have a 2B finish.
11. The coal storage silo will have a stainless steel lining with a 2B finish on the bottom with an included angle of 40°. The will also have a bin vent filter and two manways, one on the top and one on the side.
12. The truck unloading circuit is to be designed for 20 tons/h.
13. The combustion air steam coil is to operate with 100 psig saturated steam.
14. The combustion air steam coil is to increase the combustion air from 0 to 200°F.

5.5 MCWM System

The MCWM retrofit design includes a MCWM preparation, delivery and handling systems, low-NO_x burner, baghouse, FD fan, combustion air preheaters, ID fan, ash silo, stack, and control system, each of which is described in the following subsections. MCWM preparation will be off-site (see Section 5.5.1). See Figure 5-4 for the process flow diagram of the retrofit at Crane. This diagram demonstrates the functional relationship between the components of the system. Figure 5-5 presents an isometric view of the DMC retrofit facility with the various ancillary systems as designed for the Crane demonstration unit.

5.5.1 Fuel Preparation

Two conceptual MCWM preparation circuits were designed as part of AMAX Coal Company's Minnehaha Mine coal preparation plant that is currently operating near the Crane facility. Since the MCWM will be produced off-site, it was not included as part of the retrofit design package contained in Volume 2.

Figures 5-6 and 5-7 are layouts of the Minnehaha Mine coal preparation plant with MCWM preparation circuits attached. The coal preparation plant cleans approximately 750 tons/h of coal; consequently, the MCWM preparation circuits use slipstreams of coal from the cleaning circuit. The design shown in Figure 5-6 assumes that no further coal cleaning is required prior to MCWM preparation. In this scenario, a slipstream of 28x100 mesh coal coming off of the coal spirals is sent to the MCWM preparation circuit. The design in Figure 5-7 assumes that further coal cleaning is required prior to MCWM preparation. In this scenario, a slipstream of 3/16"x0 coal from the

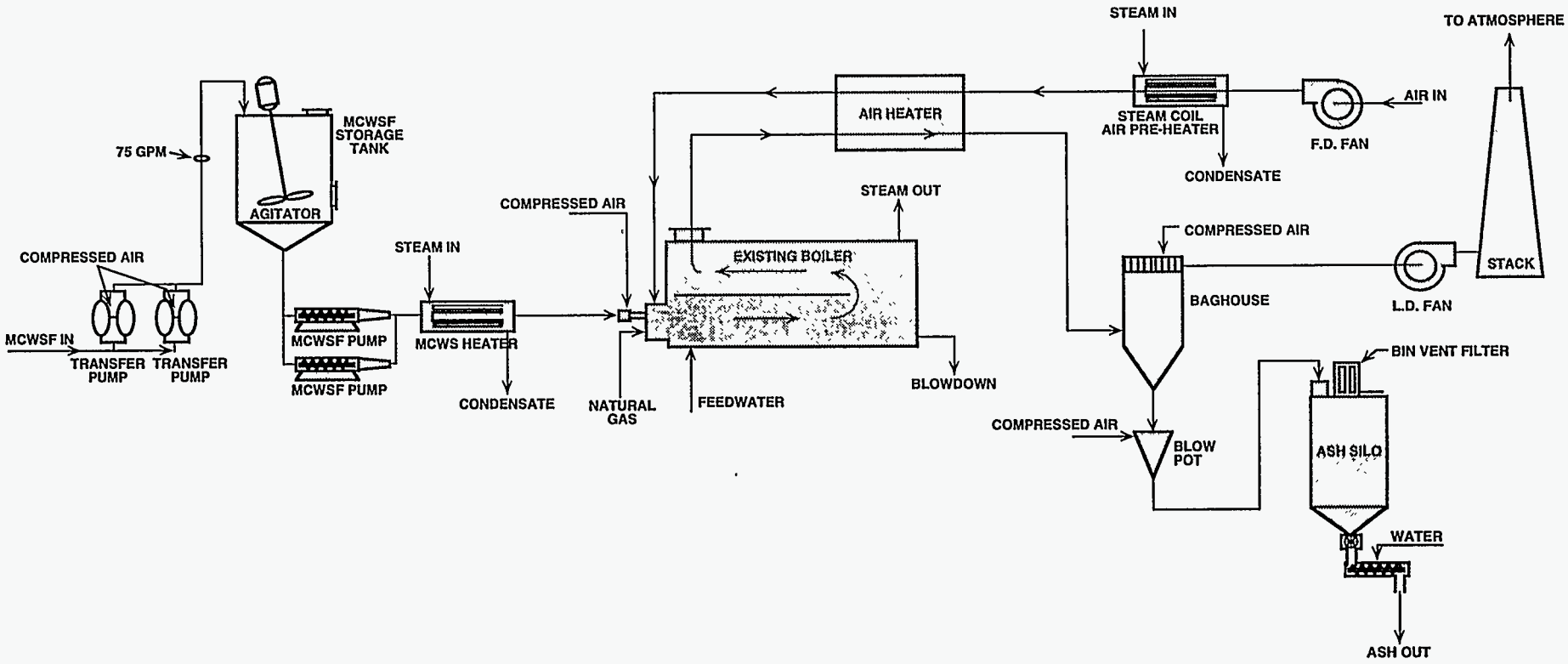

Figure 5-4. PROCESS FLOW DIAGRAM FOR THE MCWM SYSTEM

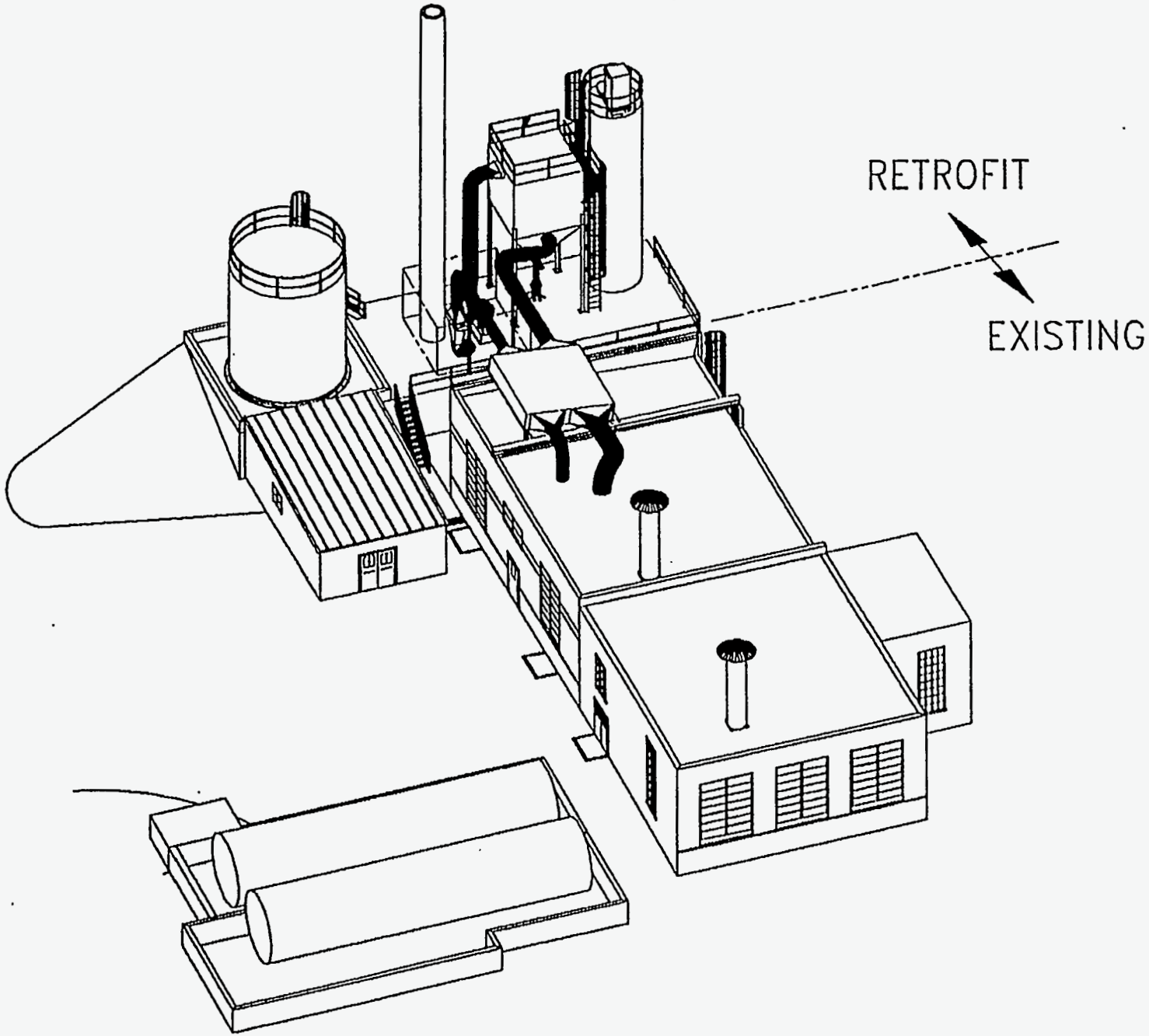

Figure 5-5. ISOMETRIC VIEW OF THE MCWM RETROFIT FACILITY

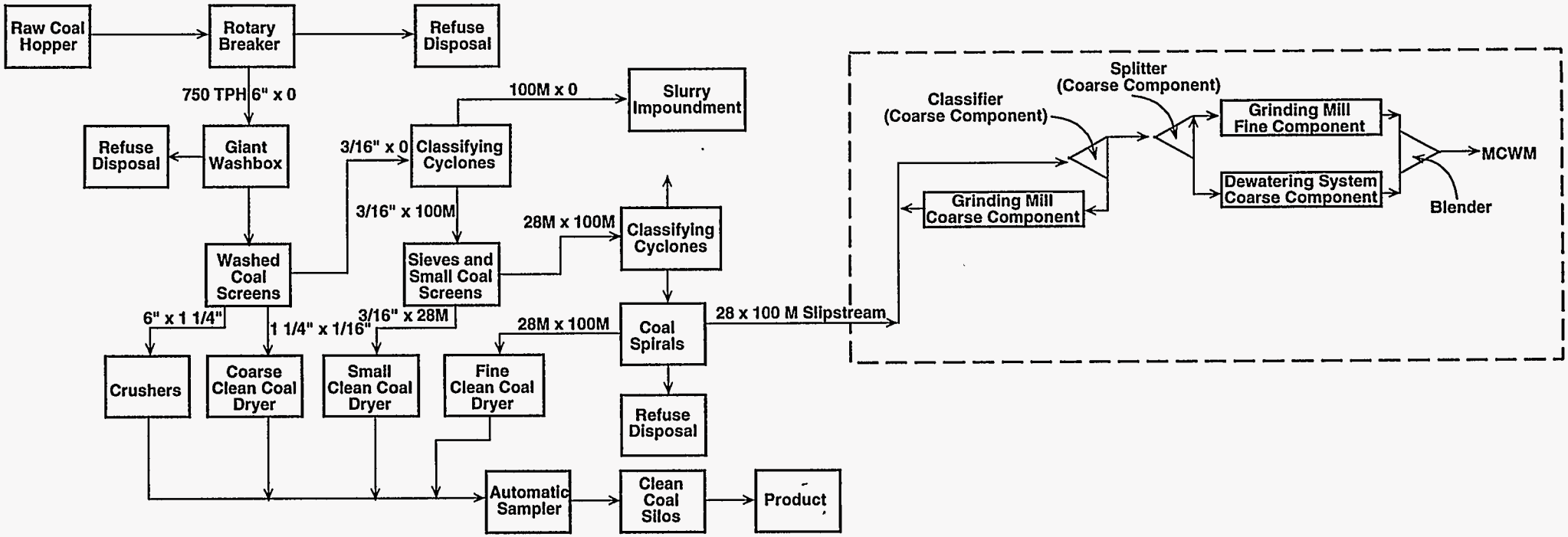

Figure 5-6. CONCEPTUAL MCWM PREPARATION CIRCUIT WHICH UTILIZES A SLIPSTREAM OF 28 x 100M COAL FROM AN OPERATING COAL PREPARATION PLANT NEAR THE CRANE FACILITY. IT IS ASSUMED THAT THE COAL SLIPSTREAM DOES NOT REQUIRE FURTHER CLEANING DURING MCWM PREPARATION.

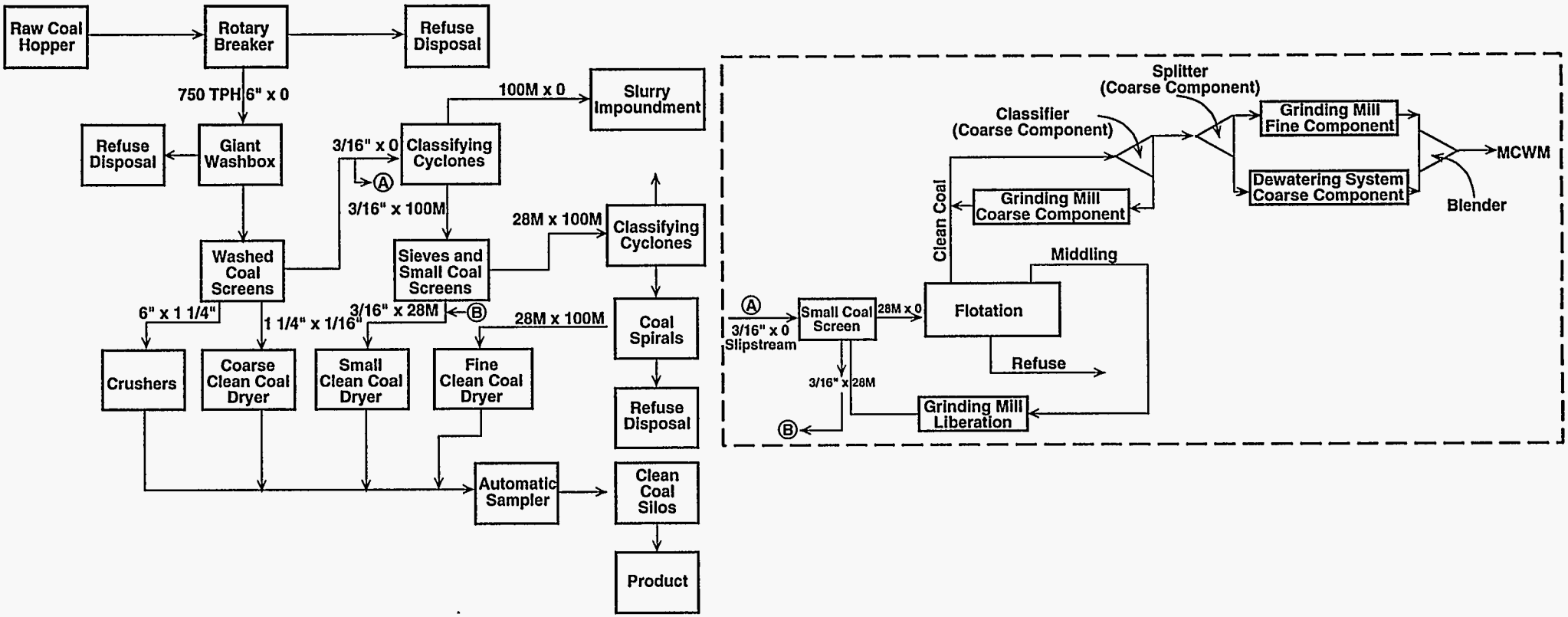

Figure 5-7. CONCEPTUAL MCWM PREPARATION CIRCUIT WHICH UTILIZES A SLIPSTREAM OF 3/16" x 0 COAL FROM AN OPERATING COAL PREPARATION PLANT NEAR THE CRANE FACILITY. IT IS ASSUMED THAT THE COAL SLIPSTREAM REQUIRES FURTHER CLEANING WHICH IS DONE BY FLOTATION DURING MCWM PREPARATION.

classifying cyclones is screened, the 28 mesh x 0 coal is then cleaned by flotation and then sent to the MCWM preparation circuit.

5.5.2 Fuel Unloading System

The MCWM will be produced off-site and will arrive at the facility in stainless steel tankers. The MCWM will have a solids loading of 60%, a heating value of approximately 8,300 Btu/lb, less than 1.2 lb SO_2/million Btu, and an ash content of 3 wt.%, as received. The parent coal of the MCWM is from the Indiana VII seam.

The MCWM unloading system will consist of an air operated diaphragm pump to unload the tanker. This system will have a redundant pump as back-up. The air operated pumps will be protected from foreign material by a set of simplex strainers. The system will be sized to unload a 4,000 gallon tank in one hour. The unloading circuit will be designed to automatically flush all of the slurry transport lines. The unloading system will also be capable of unloading the MCWM storage tank into tankers, if required.

The steel MCWM storage tank (16' D x 18' H) will have a capacity of 28,000 gallons. This capacity was a requirement of the host site to provide on-site fuel storage supply of five days. The tank will be dish bottomed and equipped with a roof mounted paddle mixer, baffles to promote better mixing, and level sensors. The MCWM storage tank will also be insulated and equipped with a heater capable of maintaining the slurry at 40°F. An air blast system will be located at the outlet of the tank to provide a means of breaking up the slurry should settling occur in the discharge.

5.5.3 Fuel Delivery System

The MCWM delivery system will consist of two progressive cavity pumps with variable speed drive motors, basket strainers, flow sensor, steam heater, and piping to the burner front. The MCWM will flow from the bottom of the MCWM storage tank through strainers for pump protection, and into the progressive cavity pumps. The pumps will have variable speed drive to control slurry flow to match boiler load following requirements. Both of the slurry injection pumps will be in operation at all times, therefore, in the event that one pump should fail the other pump will boost its output to match the boiler demand. Each of the MCWM pumps are designed to provide 6 gal/m of MCWM to the boiler. These pumps are protected from over-pressure by a high pressure switch located at the pump discharge. After the progressive cavity pumps, the MCWM flows through an indirect steam heater to increase the temperature to 250°F. The MCWM then enters strainers to prevent atomizer pluggage, followed by a mass flow meter. This meter will also measure the slurry temperature and density. The MCWM then flows to the twin fluid atomizer for injection into the boiler. The atomizer is of the internal mix design and manufactured from a wear-resistant material. In addition to the system described above, there will be a slurry recirculation loop and flush equipment to prevent settling of the MCWM.

5.5.4 Burner

Similar to the DMC design, the burner will be a FlamemastEER™ burner that will fire natural gas to bring the boiler up to operating temperature then switch to MCWM. A sectional view of the burner is shown in Figure 5-8. The MCWM atomizer will be located in the center of the burner and the natural gas injection will be adjacent to the MCWM. The FlamemastEER™ burner is designed for long life and uses an innovative air flow control mechanism that eliminates complex linkages and gears.

The key functional features of the FlamemastEER™ burner design includes:

- Combustion air supply through separate secondary air (SA) and tertiary air (TA) passages;
- Variable SA/TA flow distribution; and
- Variable SA and TA swirl.

The burner is designed to provide good flame stability and acceptable flame characteristics for a wide range of operating conditions and fuel characteristics. The burner establishes local recirculation zones and promotes local mixing between the coal and the secondary air. This leads to rapid devolatilization of the coal and liberation of fuel nitrogen in a low excess air environment resulting in reduced NO_x formation.

Mechanically, the burner has been designed to minimize the number of moving parts. Those parts which do move slide axially, eliminating complex linkages and gears. The secondary and tertiary swirl control vanes, called turbolators, move back and forth within conical passages of the burner. As the turbolators are moved toward the narrow end of the cone, more air passes through the vanes increasing the amount of swirl. As the turbolator is moved in the opposite direction, the air follows the path of least resistance and by-passes the vanes, resulting in less swirl. The moving parts are located away from the high heat flux environment in order to reduce warpage and binding. The parts of the burner which are subjected to a high heat flux are fabricated from a high strength heat resistant alloy.

5.5.5 Combustion Air Preheaters

The retrofit will include two combustion air preheaters. The first is a steam coil air preheater designed to heat 0°F ambient air to 200°F, to prevent corrosion in the flue gas system. The heater will have a rating of 1.4 MM Btu/h, and will be located in the combustion air duct work just after the discharge of the FD fan. The second combustion air heat exchanger is a heat pipe flue gas heat exchanger that will be located on the roof of the building. The flue gas will leave the boiler at 500°F and will exit the heat exchanger at 350°F. Simultaneously, the combustion air will be heated to 400°F. The heater has a rating of 7 MM Btu/h. The flue gas heat exchanger will be equipped with a sootblower to clean the flue gas side of the exchanger.

5.5.6 Ash Handling System

The ash handling system will consist of a baghouse to collect the particulate matter in the flue gas stream, pneumatic conveying system, ash storage silo, and an ash unloading screw

CRANE NAVAL SURFACE WARFARE CENTER

EER MCWM BURNER
MODEL 4AF-25.2-18.75

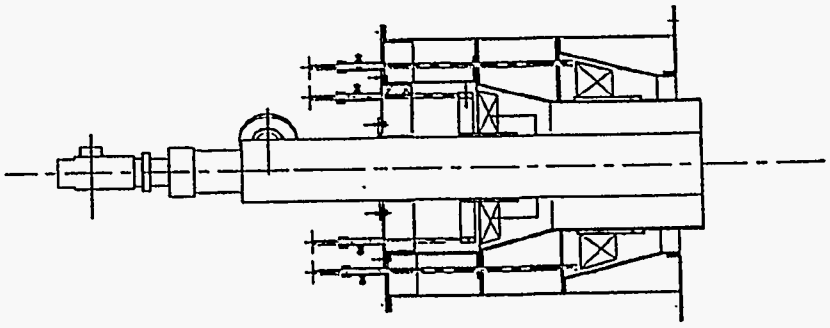

SECTIONAL TOP VIEW

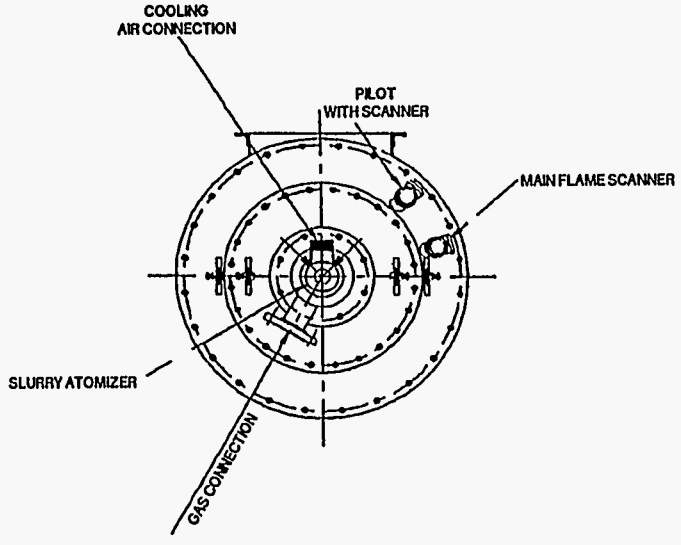

FRONT VIEW

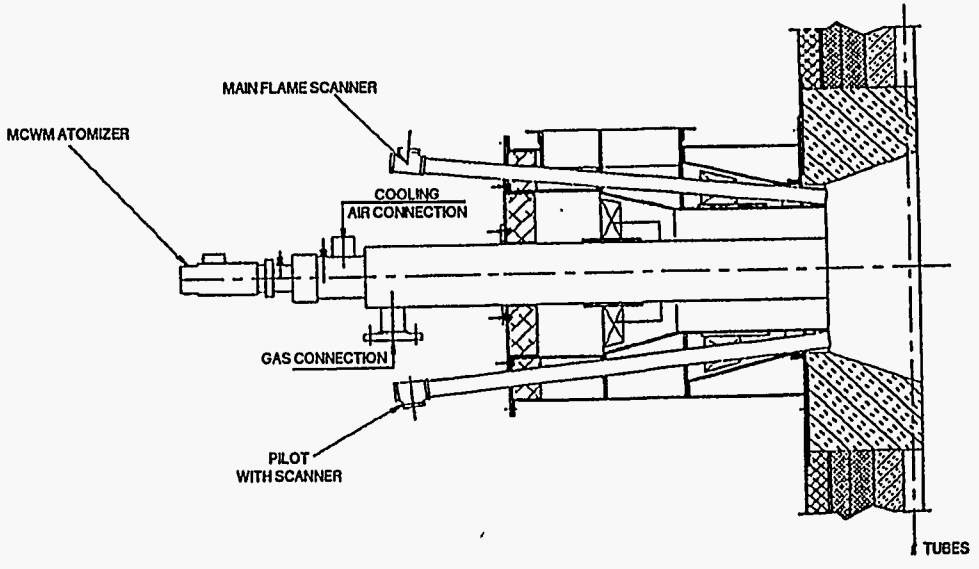

SECTIONAL FRONT VIEW

Figure 5-8. SECTIONAL VIEW OF THE MCWM BURNER

conveyor. The baghouse was sized for a 3.5:1 air-to-cloth ratio and specified with Nomex bags and a fire detection/suppression system. The bags will be cleaned via compressed air pulses. The pneumatic conveying system will transfer the ash from the baghouse into the ash storage silo. The ash storage silo (8' dia. x 33' H) has a capacity of 12 tons and is constructed of carbon steel. The silo is sized to handle five days storage. The silo has a bin vent filter to capture fugitive dust from the pneumatic conveying system and a level sensor to prevent overfilling. The ash silo is also equipped with a fire detection system. The ash screw conveyor will unload the silo into trucks. The screw conveyor has a capacity of 1,200 ft^3/h and is equipped with a 5 HP variable frequency drive. Water injection nozzles are installed in the screw conveyor to condition the ash to prevent fugitive dust emissions. The screw conveyor is heat traced and insulated to prevent acidic corrosion and freezing. Heat tracing was selected over a steam jacket since steam is not always available at the site.

5.5.7 Design Specifications

This section will present the design basis used in the preliminary design of the boiler retrofits to the Crane NSWC boiler. These criteria are based upon accepted engineering practices, vendor recommended parameters for their equipment, experience from operating the Penn State demonstration boiler system, and EER's experience. Also presented in this section is the boiler nameplate data and design operating parameters.

Design Specifications - MCWM Retrofit

Boiler Manufacture	Cleaver-Brooks
Boiler Model No.	D-42-LH
Unit No.	W-3482
Steam Capacity	20,000 lb/h
Pressure Vessel Design	260 psig
Operating Pressure	125 psig
Heat Input	25.22 MM Btu/h
Pilot Gas	350 SCFH @ 7" H_2O to 1 psig
Main Gas	25,220 SCFH @ 1,000 Btu/ft^3

General Information for the Retrofit System

1. MCWM turndown is 3:1.
2. Natural gas turndown is 10:1.
3. Design carbon conversion is 99%.
   Minimum allowable carbon conversion is 98%.
4. The excess air is to be 25%.
5. The baghouse will have a minimum collection efficiency of 99.5%.
6. The pressure drop through the burner is less than 8" H_2O.
7. The combustion air preheater is to increase the combustion air temperature to 400°F.
8. All electric motors are to be of a TEFC design.
9. Electric motors larger than 1 HP are to be 480V/3PH/60HZ.
10. Electric equipment in an explosion proof area is to meet Class 2 Division 1.
    If explosion proof is required, this supersedes the TEFC requirement.

11. Allowable velocities:

Service	Velocity, ft/m
Air heater (air side)	1,000-5,000
Compressed air	1,500-2,000
Forced draft ducts	1,500-3,600
Air heater (flue gas side)	1,000-5,000
Induced draft flues and breaching	2,000-3,500
Stack	2,000-5,000

12. The minimum allowable flue gas temperature is 300°F while firing MCWM.
13. Allowable compressed air velocities in braided nonlined flexible is 120 ft/s. If this is to be exceeded, consult the factory. All installation arrangements are to be factory specifications.
14. All liquid piping outside of the boiler house is to be heat traced and insulated to prevent freezing.
15. Boiler purge air exchange requirements is five times the total volume from FD fan to ID fan.
16. The baghouse is designed to have an air-to-cloth ratio of approximately 3.5 to 1. The baghouse will be equipped with Nomex type bags. The baghouse is to be insulated and have a heated hopper.
17. The ash storage silo is to be designed to store five days worth of ash.

Information for the Coal Fuel System

1. Fuel storage capacity requirements is to be 75% boiler load on DMC for 120 hours.
2. Fuel analysis is 40% moisture, 3% ash, 21.8% volatile matter, 35.2% fixed carbon, less than 1.2 lb SO_2/million Btu, and a higher heating value of 8,302 Btu/lb.
3. MCWM density is 1.2 kg/l or 10 lb/gal.
4. Viscosity of the MCWM is 1,000 cp at 100/s.
5. The boiler is to be capable of firing 100% natural gas or 100% MCWM and any combination within the turndown ranges.
6. The required MCWM pressure at the burner is 115 psig.
7. The required atomizing pressure is 115 psig.
8. The required atomizing air-to-fuel ratio is 0.5 lb air/lb MCWM.
9. Allowable MCWM velocity range is 1-3 ft/s.
10. All slurry piping is to be schedule 80 carbon steel.
11. The tanker unloading circuit is to be designed for 75 gal/m.
12. The transfer pump is to have wetted parts capable of withstanding abrasion from the slurry. The seats, balls, and diaphragms will be made from neoprene.
13. The MCWM storage tank is to have a dished bottom.
14. The MCWM storage tank is to be heated, insulated, and equipped with a mixer. It will also have two manways, one on the top and the one on the side.
15. The slurry preheater is to operate with 100 psig steam.
16. The slurry preheater is to increase the slurry temperature from 40 to 250°F.
17. The combustion air steam coil is to operate with 100 psig saturated steam.
18. The combustion air steam coil is to increase the combustion air from 0 to 200°F.

6.0 ENGINEERING AND ECONOMIC ANALYSIS

Section 6.0 presents the results of an engineering and economic analysis of the technology modifications at the Naval Surface Warfare Center at Crane, Indiana. The methodology used in identifying the appropriate cost estimating techniques used in the analysis is presented in Section 6.1. Then two reviews of facility economics are provided. The first, in Section 6.2, provides an extensive process analysis of the attractiveness of the alternative coal utilization technologies. Section 6.3 is a cost-engineering analysis of the comparative economics of MCWM and DMC at

the Crane facility. Section 6.4 is a report on the costs of transporting coal to Crane as either a MCWM or dry coal for on-site micronizing. Section 6.5 contains an examination of the environmental regulations applicable in the Crane area and their effects on coal conversion. Section 6.6 discusses the impacts of coal conversion on the economy in the region surrounding Crane.

The engineering and economic analysis was conducted concurrently with the engineering design of the retrofits at Crane. Consequently, the facility economics used in determining the process analysis and comparative economics analysis, Sections 6.2 and 6.3, respectively, were conducted using prefinal cost estimates for capital equipment. Cost estimates from the SCCWS program[123] and preliminary cost data from EER during the design stage[124] were used to set up the spreadsheet analyses and identify the factors which influence the analyses. Although the capital cost estimates used in the analyses were preliminary (final cost estimates are contained in the design package in Volume 2), the final conclusions remain unchanged.

6.1 Identify Appropriate Cost Estimating Methodologies

A major consideration in the adoption of new energy technologies is economic viability. While many factors are relevant, both on-site and off-site, a fundamental question is the cost of delivering a given unit of output, such as steam equivalent. This must, of course, be juxtaposed to the revenue (or broader benefits) stream before any final decision is made on the project.

A review of cost estimation alternatives and an assessment of their relative strengths and weaknesses as they relate to the estimation of new coal utilization technologies was previously discussed in detail[67]. This section discusses the assessment of the various estimation methods and the identification of the methods that were used in the cost analyses.

Assessment

An assessment of the various estimation methods is presented in Table 6-1. Each major cost estimation category is ranked on a three-part scale: Low (L), Moderate (M), or High (H), or some combination. Some criteria may be irrelevant to some of the methods. When this is the case, "none" is entered into the table. Note the convention used for scaling Cost and Data Needs, in columns 2 and 3, respectively. The rankings relate to how high the method ranks under the criterion. However, for some criteria such as cost, a low ranking is more desirable. For example, for the *Conference Method*, "Low" in the *cost* column means inexpensive; in actuality, this estimation method would rank "high" in terms of the desirability of this attribute. The reader is encouraged to note this carefully in examining the table.

Noted in the last column of the table is the applicability of the estimation method in terms of three stages of the development process: Pilot, Demonstration, and Commercial Deployment. Finally, the table pertains to the application of the techniques to both capital and operating cost estimation, acknowledging the differences arising in the two contexts.

As expected, a strong correlation prevailed between *Cost* and *Data Needs*, and almost as

Table 6-1. Assessment of Cost Estimation Methods

Estimation Method	Criteria						Technology Application
	Accuracy	Cost[a]	Data Needs[a]	Flexibility	Optimization	Stochastic	
Conference	Low	(Low)	(Low)	Moderate	None	Low	Pilot
Factor	Low	(Low)	(Low)	Moderate	None	None	Pilot-Demo
Analytical	M-H	(Moderate)	(M-H)	M-H	Moderate	Low	Deployment
Compartmentalized	Moderate	(L-M)	(L-H)	M-H	None	None	Demo-Deploy
Historical	M-H	(L-M)	(Moderate)	Low	Low	None	Deployment
Definitive	M-H	(M-H)	(M-H)	M-H	None	None	Deployment
Process	High	(High)	(High)	High	High	None	All
Stochastic	High	(High)	(M-H)	M-H	M-H	High	All

[a]Parentheses indicate that scores, from the standpoint of desirability, should be interpreted as inverse of those listed, e.g., a "Low" cost is "High" in desirability.

strong a correlation between *Accuracy* and *Flexibility*. At the same time, an inverse correlation exists between the first two criteria and the last two. Also, special stochastic and optimization properties are limited to estimation methods intended to focus on them.

Since the survey was limited to widely-employed costing techniques, all those considered are appropriate under some circumstances. Some of these methods are much better suited than others. The choice is based on a combination of the nature of the problem being studied and the available expertise. On the problem side, new technologies are being dealt with in which limited experience is available. On the expertise, the project involves cooperation between engineers who are leaders in developing knowledge about the technologies and economists familiar with the relevant principles of investment analysis and the tools available to implement such analyses.

A definitive method by definition is always preferable if feasible. The needs for a "definitive" estimate cannot be met for new technologies such as the subject of this project. Thus, the feasibility criterion cannot be met for the definitive approach. Moreover, the review should have made apparent that no estimate is truly definitive. Outcomes depend on forces such as future prices, technical developments, and public policy beyond the control of or predictability by an analyst. Thus, formal techniques of process model optimization and stochastic analyses are essential to show the implications of these uncertainties.

Similarly, reliance on broader surveys (the conference method), analogies (the historical method), and extensive reviews of experience (the analytic method) is inappropriate because again the needed material does not exist.

Under these circumstances, emphasis will be on process and stochastic analyses as defined here. At times, factor methods at both the gross and compartmentalized level will be employed. As the review showed, perils are associated with relying on these rules. The key problem is lack of clear guidance about the appropriateness of alternative rules for a particular situation. Thus, all uses will be made cautiously.

The goal is to provide the most complete possible economic analysis. Such an analysis has four key elements. The first is compilation of as much critical technical and economic data as possible on the venture being appraised. As previously mentioned, work done by Penn State and EER was used[123, 124]. The second is determining the uncertainties attached to critical cost and performance estimates. Here the EFRC/EER's expertise on technical issues can be combined with the Department of Mineral Economics' understanding of the market and public policy uncertainties. The third is using the well established technique of present value analysis [67] to combine the data into estimates of the range of possible outcomes. The fourth is use of analytic techniques such as linear programming and other optimization methods, as well as Monte Carlo simulations to provide further insights. Such techniques were used in Sections 6.2 and 6.3. A Monte Carlo Simulation approach was developed and employed.

6.2 Estimate Basic Costs of New Technologies

This section describes basic economics of retrofitting the single 25.2 MM Btu/hr boiler located at Crane, Indiana, to fire either MCWM or DMC. The analysis of the MCWM technology is extended to consider varying the MCWM preparation facility, which is separate from the boiler site, to produce fuel up to the equivalent of fifty Crane boilers. The analysis represents a 'first-pass' at evaluating the viability of conducting further retrofits of commercial-scale and industrial-scale boilers.

MCWM AND DMC Conversion Technology Overview

The MCWM and DMC technologies utilize the particular form of the feed coal to minimize solids handling problems and minimize boiler derating. Both technologies under development by the EFRC require premium quality coal fuels, one difference between the two being the physical form of the fuel as delivered to the boiler. DMC is delivered to the boiler site as crushed coal (nominal 2"x0) and reduced to the necessary micron size at the boiler site. MCWM, on the other hand, is transported, stored, handled, and fired in the boiler in slurry form.

Crane Boiler Characteristics

The Crane boiler being evaluated for the retrofit was described in Section 5.2. This case study considers only six month operation of the retrofitted boiler corresponding to the heating season. The basic boiler retrofit assumptions are:

- Boiler rated capacity — 25.2 MM Btu/hr
- Annual hours of operation — 4,383
- Boiler load during operation — 100%
- Coal requirement (operating) — 0.90 tons per hour (d.b.)
- Annual coal requirement — 3,945 tons (d.b.)

The annual operating hours assumes that the retrofitted boiler is used during a typical six-month heating season at rated capacity. Additional steam requirements for DOD users are met by adding boilers to the system. This arrangement of smaller, modular, boilers follows a normal DOD facilities planning philosophy that emphasizes maximization of system reliability under adverse conditions and standardized designs. Industrial- and commercial-scale boiler tend to be larger in order to minimize per unit cost of steam.

MCWM Supply

This subsection presents and reviews work performed by EER on the preliminary design and estimation of capital costs for the MCWM retrofit at Crane. Crane-specific operation and maintenance (O&M) costs have not yet been developed. Additional discussion of capital and O&M costs can be found in Section 6.3. This section also presents preliminary estimates for the cost of MCWM delivered to the Crane boiler.

The MCWM fuel form, as a slurry, has some potential advantages over DMC. First, since the fuel is handled as a slurry it can be easily pumped into the system, stored, and sent to the burner for atomization into the boiler. Also, the slurried fines pose little problem with the

generation of airborne dust (as long as splashing and spillage are avoided). Supply of the slurry may, potentially, come from a variety of relatively low cost sources as compared to other coal-forms. Since the slurry is delivered to the boiler at the proper size, the relatively capital and O&M cost intensive grinding mills for each boiler that is converted to fire the coal fuel are not necessary. Finally, cost advantages could be derived from the installation of a single slurry preparation system to supply several converted boilers.

One disadvantage of MCWM is that boiler may require derating due to the presence of inorganic material in the coal and the limited residence time of the boiler. Storage of the slurry can also be problematic due to a tendency of the solids in the slurry to settle and form a 'hard' or 'soft' pack. This settlement problem requires the development of specialized slurry preparation techniques and chemical additive packages.

MCWM Conversion Estimated Capital Costs

At the time this analysis was conducted, the final cost estimate generated by EER upon completion of the retrofit design (Section 5.0) was not available (see Volume 2 for the final cost estimate). Rather, preliminary cost data (+40/-20 %) which was provided by EER[124] was used. A summary of these results is presented in Table 6-2.

The five most expensive cost items for materials in the estimate are, in decreasing order: 1) Instrumentation ($200,000); 2) Electrical ($105,000); 3) Air Heater ($85,000); 4) Baghouse ($51,000); and 5) Burner Assembly ($50,000). The remaining items include the storage tank, duct work, miscellaneous new structures, pumps, and piping.

A basic difference governing the economics of fuel supply between MCWM and DMC technologies is that the form of the fuel delivered to the boiler is not readily available from an existing market source. Coal is not generally produced for delivery to customers in slurry form. In fact, state-of-the-art production of a MCWM with the requisite handleability, storage, and atomizing qualities is limited in terms of total quantity produced annually and in the number of potential suppliers. In addition, there can be substantial variation in the quality of slurry produced by the different suppliers. For that reason, the MCWM retrofit option must consider the costs of production and delivery of slurry to the Crane boiler.

MCWM Factored Cost Estimate

A factored cost estimate for the production and transportation of MCWM to the Crane boiler was developed to aide in comparing this fuel to DMC. At the present time, no specific coal source has been identified. The production and transportation analysis presented here is loosely based on using AMAX Coal Company's Minnehaha operation (located about 40 miles from the Crane boiler) to site the MCWM preparation plant.

Creation of a market for MCWM potentially addresses a problem faced by nearly every coal preparation plant operation, namely the disposition of coal fines. Coal fines are difficult to clean and dry to a level of acceptable moisture content. Even when recovered and dried to acceptable

Table 6-2. MCWM Capital Cost Estimate Summary (Including Contingency, 1993$)

	Sub Amount	% Sub	Category Amount	% Category	$/MM Btu
MATERIALS					
Civil/Structrual	59,746	6.3			
Instrumentation	28,344	3.0			
Mechanical	864,281	90.8			
		100.0			
Subtotal Materials			952,371	26.0	38,095
LABOR					
Civil/Structural	238,135	40.2			
Mechanical	354,215	59.8			
		100.0			
Subtotal Labor			592,350	16.2	23,694
SUBCONTRACTS					
Electrical	137,914	32.2			
Instrumentation	289,931	67.8			
		100.0			
Subtotal Subcontracts			427,845	11.7	17,114
MANAGEMENT/ENGINEERING/OTHER					
Project/Const. Mgmnt.	894,052	52.8			
Engineering	498,693	29.4			
Other	301,844	17.8			
		100.0			
Subtotal Mgmnt/Engineering/Other			1,694,589	46.2	67,784
TOTAL			$3,667,155	100.0	146,686

levels, conventional handling methods tend to cause fines to become easily airborne, representing both a loss of product and the creation of a potential health hazard. Both of the above problems can be addressed by producing and transporting the fines in a slurried fuel. Bearing this in mind, the feed to a MCWM production process can come from a variety of sources including: 1) existing coal impoundments; 2) existing operating coal preparation plants; and 3) conventionally mined coal.

Considerable uncertainty surrounds the recovery of coal from existing coal impoundments due to the difficulties of locating appropriate impoundments, the adequate characterization of the distribution of coal (and potential contaminants), and the higher expected costs associated with reclamation/dredging of the coal. An impoundment must be able to provide an inexpensive product possessing the rather stringent quality specifications. Mixtures of the desired coal with other coals and contaminants in the impoundment complicates the beneficiation and slurry production processes.

The surest method of providing the MCWM fuel is from coal obtained from the market (2"x0) that already possesses the desired quality specifications. The size reduction and slurrying required can then be carried out in a straight-forward manner. The disadvantages of this method are the expected higher cost of coal, as compared to the alternatives, and the extra equipment and effort required to reduce the +2"x0 coal the size required for MCWM.

A third option exists for producing MCWMs from slurry refuse streams in an existing coal preparation plant. Here, the characteristics of individual refuse streams in the conventional preparation plant can be utilized with little variation expected in the stream compositions over time (when cleaning the same coal). Since coal is recovered from process streams that would normally be discarded, the marginal cost of feed coal and refuse disposal for the slurry production plant would be zero. In fact, an economic benefit can be derived by reducing the quantity of solids requiring disposal.

A specific preparation plant was not identified for a detailed engineering/economic analysis. The MCWM production plant speculated here, however, makes use of this last scenario by providing what may be considered typical slurry preparation plant equipment. A MCWM production plant for the Crane boiler may be sized as follows:

- MCWM plant production rate — 2 tons per hour (d.b.)
- Annual operating hours — 1,972
- Annual production — 3,,945 tons of coal (d.b.)
- Annual maximum rated capacity — 14,026 tons MCWM

As can be seen, the slurry plant is oversized relative to the boiler requirement. The MCWM sizing reflects: 1) difficulties associated with the problems in differentiating between processes with capacities in the range of one to three tons per hour; 2) a built-in margin for the large uncertainty in the capital equipment requirement; and 3) a production rate sufficient to provide for preparation plant down time while the boiler operates 24 hours per day, seven days a week. The

maximum annual capacity of the MCWM production plant assumes a plant availability of 80 percent and the existence of a market for all of the production.

A simple factored capital cost estimate is provided in Table 6-3. The equipment list provides allowances for a single mill, conventional flotation cells, spirals (or the equivalent in other cleaning equipment), pumps, and a 25,000 gallon slurry storage tank, with an additional 10 percent allowance for miscellaneous equipment items. The electrical load of the equipment was estimated at 94 horsepower. The estimated equipment costs and electrical loads were generated after reviewing several sources[125-128] and applying standard cost estimating methodologies to account for inflation, at 4 percent, and scale[129]. The slurry plant described here purposely avoids the use of advanced fine coal cleaning methods reflecting an emphasis upon locating refuse streams that require minimum effort to recover coal fines of the required quality.

The total capital requirement is estimated to be $993,000. As can be seen from the equipment list, by far the largest capital outlay is by the mill. This item also represents the greatest proportion of the estimated horsepower due to the demanding grinding regime. The equipment list, and associated costs, are considered speculative due to the incomplete knowledge of the feed stream characteristics.

The plant cost factor used for determining the installed plant cost was generated using the Chilton method. The selection of this method was due to ease of use and consideration of the fact that the MCWM plant is an addition to an existing coal preparation facility. That advantage, along with the simple to implement approach, is somewhat offset by the relatively small size of the plant and the speculative nature of the estimate. The factor derived and presented above of 3.39 is less than the simpler Lang factor of 3.63 for solid-fluid plants.

Annualized capital and operation & maintenance (O&M) costs are presented in the Table 6-4. The MCWM cost, f.o.b. the slurry preparation plant, is estimated to be $90.6/ton coal (d.b.) or 3.23 $/MM Btu. This cost includes all capital, operation and maintenance charges.

O&M labor is assumed to be marginal to the existing coal preparation plant operation. An allowance of one person at $20/hr is provided. Maintenance materials and supplies are estimated at four percent of total plant cost. Both feed and refuse disposal costs are considered as marginal to the existing preparation plant operation and therefore equal to zero (no benefit assumed to be derived from avoided disposal to an impoundment pond). Consumption of grinding media is estimated to be 0.68 lb media per ton coal (d.b.) at $0.50/lb. An allowance is made for flotation reagents at $0.16/ton flocculant and 2 lb fuel oil per ton of coal at $0.20/lb. Electrical power consumption for the state of Indiana is taken at 4 cents/kWh[130]. Capital charges are calculated at a 15 percent cost of capital with a payback period of 7 years. At this level of the analysis, the use of government funds to build the MCWM plant (and a 4 percent discount rate) is not assumed in order to provide an additional margin, and to allow for sizing the plant for multiples of Crane (as discussed below).

Table 6-3. MCWM Factored Capital Costs (1993$)

Mill	176,000
Flotation Cells	30,000
Spirals	14,000
Pumps	13,000
Tankage	33,000
Miscellaneous Items (@ 10%)	27,000
Equipment Cost (Delivered)	$293,000
Total Plant Cost Factor (Chilton Method)	3.39
Total Installed Plant Cost	$993,000

Table 6-4. MCWM Annualized Capital and O&M Costs (1993$)

	Annual Cost $	$/ton Clean Coal (d.b.)	$/MMBtu
FIXED O&M COSTS:			
O&M Labor	$39,447	10.00	0.36
Maintenance Materials & Supplies	39,708	10.07	0.36
VARIABLE O&M COSTS:			
Feed Coal	0		
Refuse Disposal	0		
Grinding Media	1,341	0.34	0.01
Flotation Reagents Allowance	2,209	0.56	0.02
Additive Package	30,453	7.72	0.28
Electrical Power	5,509	1.40	0.05
Capital Charges:	238,606	60.49	2.16
TOTAL O&M AND CAPITAL CHARGES	$357,273	90.57	3.23

The additive package costs primarily consist of a dispersant to avoid the formation of agglomerates that pose problems for storage and atomization of the slurry by the burner. The additive package considered here is the same as that proposed by McHale et. al.[127]. The dispersant is estimated as 0.6 wt.% to coal at a cost of $0.55/lb (active ingredient). A base is also used in conjunction with the dispersant in order to adjust slurry pH. The costs for using the base are estimated as 0.4 wt.% to coal at a cost of $0.14/lb. It is recognized that several additive packages exist which may provide acceptable results. Physical slurry preparation techniques may also substantially reduce the amount of dispersant required.

A sensitivity analysis of MCWM costs, f.o.b. the slurry preparation plant, was conducted using a methodology similar to that accomplished for the Crane base case. The results of this analysis are presented in Figure 6-1. The figure shows that the $/MM Btu cost of coal decreases substantially with an increasing number of oil-designed boilers converted over to fire MCWM. At a coal requirement equivalent to 10 boilers the size of Crane, the MCWM cost is $1.03/MM Btu and drops to $0.67/MM Btu at 50 Crane boiler equivalents. The analysis presented here does not imply that this many boiler conversions will be undertaken. Indeed, only a few industrial or commercial-sized boilers would need to be converted to create an equivalent level of demand.

It should be noted that throughout the analysis of MCWM costs the capital charges are not amortized over a significant fraction of maximum rated slurry plant capacity. Since the demand is assumed to be only for a six month heating season, the slurry plant with all its capital equipment, sits idle for half of the year, regardless of the type of fuel supply.

Another consideration of using MCWM as a boiler fuel is the relatively high costs of transport that ranges from $0.87 to $1.45/MM Btu as shown in Section 6.4. A significant factor in the slurry transportation costs is the weight and bulk penalty of transporting up to 40 wt.% of water with the coal. Any slurry fuel system that reduces the weight being transported from the source to the point of use would reduce slurry transportation charges. Consideration might be given to transporting MCWM with the highest solids loading possible and then adding the necessary quantity of water at the boiler site. This fuel form also tends to produce higher costs due the necessity of using tanker versus dry bulk trucks. Extending the previous concept, the MCWM might be transported in covered trucks as filter cake and then slurried at the boiler site.

DMC Fuel Supply

This subsection presents and reviews some results of the work performed by EER on the preliminary design and estimation of capital costs for the DMC retrofit at Crane. Crane-specific operation and maintenance (O&M) costs have not yet been developed. Additional discussions of capital and O&M costs can be found in Volume 2 and Section 6.4.

DMC Conversion Estimated Capital Costs

Similar to the MCWM capital cost estimate, the DMC cost estimate used in this analysis was a preliminary estimate. A summary of the estimate is presented in Table 6-5.

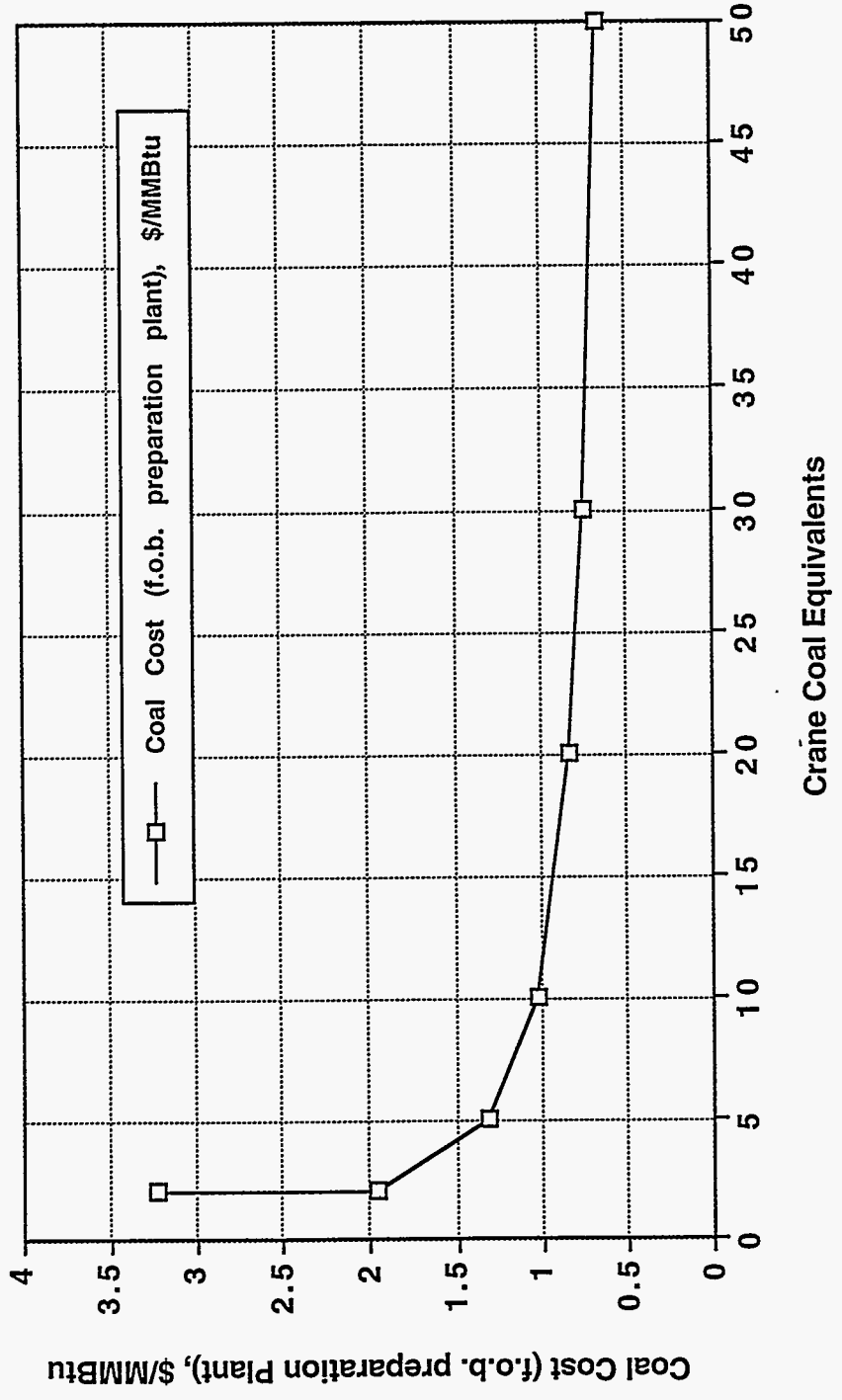

Figure 6-1. MCWM COSTS AS A FUNCTION OF CRANE BOILER EQUIVALENTS

Table 6-5. DMC Capital Cost Estimate Summary (Including Contingency, 1993$)

	Sub Amount	% Sub	Category Amount	% Category	$/MMBTU
MATERIALS					
Civil/Structrual	63,793	4.4			
Instrumentation	243,128	16.7			
Mechanical	1,146,331	78.9			
		100.0			
Subtotal Materials			1,453,252	27.9	58,130
LABOR					
Civil/Structural	402,127	37.9			
Electrical	176,586	16.7			
Mechanical	481,493	45.4			
		100.0			
Subtotal Labor			1,060,206	20.3	42,408
SUBCONTRACTS					
Instrumentation	290,458	100.0			
		100.0			
Subtotal Subcontracts			290,458	5.6	11,618
MANAGEMENT/ENGINEERING/OTHER					
Project/Const. Mgmnt.	1,274,880	52.9			
Engineering	709,154	29.4			
Other	426,881	17.7			
		100.0			
Subtotal Mgmnt/Engineering/Other			2,410,915	46.2	96,437
TOTAL			$5,214,831	100.0	208,593

The five most expensive cost items for materials in the estimate are, in decreasing order: 1) Instrumentation ($200,000); 2) Electrical ($160,000); 3) TCS Mill ($125,000); 4) Air Heater ($85,000); and 5) Coal Silo ($77,800). In addition, the Dust Control System, Coal Hoppers, and the Baghouse are all more expensive than the Burner Assembly (at $50,000). The remaining items include a crusher, duct work, miscellaneous new structures, pumps, and piping.

DMC Fuel Supply Considerations

A DMC fuel supply system, as contemplated for Crane, enjoys a number advantages over the MCWM supply system. These advantages include: 1) ready availability of the coal of the proper specifications from nearby suppliers; and 2) readily available, and lower cost, transport methods. Due to the expected market availability of DMC fuel, and the small market share of even 50 equivalent Crane conversion, it is assumed in the supply analysis that costs per ton of coal would not change with a larger number of retrofits.

Assuming a premium price charged for this coal at $35/ton, the f.o.b. preparation plant price is $1.25/MM Btu coal (d.b.). With coal transportation charges of 13.8 to 17.1 cents/MM Btu, as discussed in Section 6.4, the delivered cost of coal to a Crane boiler converted to fire DMC is $1.39 to $1.42/MM Btu. By comparison, MCWM, with a minimum transportation charge of 86.9 cents/MM Btu, does not match DMC's delivered cost of coal even when considering a MCWM supplying 50 Crane equivalents at $0.67/MM Btu for a minimum delivered cost of 1.54 $/MM Btu. This comparison between the two fuel forms points out the critical consideration of transportation costs, and in the cases where such a disparity in rates exists, to consider the possibility of alternate transportation scenarios.

Implications of DMC Versus MCWM Costs on Boiler Conversion Capital Costs

The delivered cost of coal fuel to a converted boiler is not the only consideration in assessing the trade-offs between MCWM and DMC fuels. The capital costs required to convert a boiler to fire DMC are higher than those required to convert a boiler to fire MCWM. This differential in the capital costs of conversion is due to the additional equipment required to handle and store DMC safely, and in an environmentally acceptable manner, and to reduce the coal to the micron size level necessary for firing in the boiler.

An analysis of the differential fuel costs was carried out at varying discount factors and MCWM market levels. The analysis considers the present value of the differential fuel costs over a 7 year operating period, with the delivered costs of MCWM at 1, 10, and 50 Crane coal market levels. The results of the analysis are shown in Figure 6-2. At the worst case for MCWM , one Crane coal market and zero percent discount factor, the DMC technology has a cost advantage of $2.1 million (1993$). It can be seen that MCWM market levels cause the largest variation in the present value of differential fuel costs. At a 4% discount rate the advantage of firing DMC over MCWM falls to $314,000 at a 10 Crane coal market level, and $92,000 at a 50 Crane coal market level.

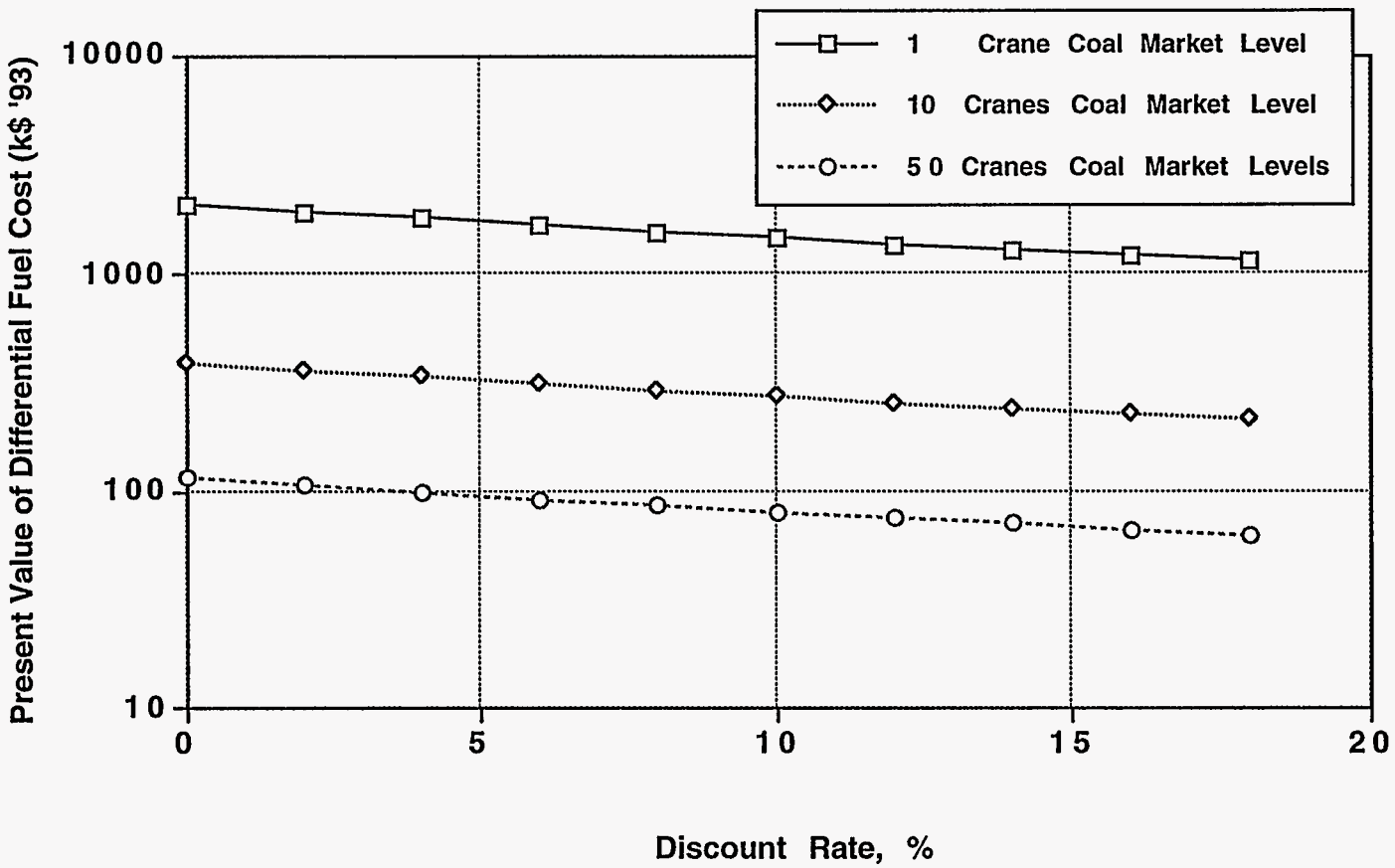

Figure 6-2. PRESENT VALUE OF DIFFERENTIAL FUEL COSTS AT VARYING DISCOUNT FACTORS FOR DMC v. MCWM (Over a 7 Year Period)

The differential in fuel costs can be treated as the maximum allowable premiums in capital and O&M costs for the conversion of a boiler to DMC over the MCWM conversion technology. Included in the DMC capital and O&M costs of conversion are the crusher, mill and dust suppression system.

Conclusion

The speculative costs of providing MCWM and DMC fuels that are developed here are intended to provide a preliminary evaluation of the merits of the two conversion technologies for the Crane boiler. It was shown that the DMC fuel holds a cost advantage over MCWM fuel as delivered to the boiler. This cost advantage for DMC held for MCWM market levels equivalent to 50 times the Crane boiler requirement, with the major reason being the difference in the transportation rates between the two fuels. It was then shown that the differential fuel cost could be translated into a capital and O&M cost premium for DMC boiler technology over the MCWM boiler technology. A complete benefit-cost analysis comparison requires an estimate of both boiler conversion capital and O&M costs and consideration of the future anticipated number of boiler conversions to be performed.

6.3 Process Analysis of MCWM and DMC

Section 6.3 provides a process analysis of the attractiveness of the alternative coal utilization technologies. A general case study and a Crane site evaluation were conducted. The general case study was conducted based on cost information from Penn State's demonstration boiler[123] and work done by Combustion Engineering, Inc.[131]. The general case study was done to develop the spreadsheet model for the Crane site evaluation, and to identify the critical influences such as fuel prices, boiler derating, utilization rates, boiler life, and cost of capital on the sensitivity of profitability. A discussion of the general case study is not presented here; a detailed discussion of is found elsewhere[67].

Process Analysis -- Crane Case Study for the MCWM Retrofit

The spreadsheet model, which was a convex cost curve model (this model reflects the condition of diminishing returns), was applied to the Crane boiler. The following analysis looks at how net present value (NPV) varies with different total capital requirements (TCRs), boiler derated capacities (BDCs), discount rates, boiler uses, and differential fuel costs (DFCs). This is to identify situations in which retrofitting is attractive. The EER preliminary TCR cost estimate of $3,667,192 for the Crane retrofit[124] was used and a 20 year boiler life was assumed.

Spreadsheet Model Application -- Sensitivity Analyses

Figure 6-3 shows NPV variation with TCR at different discount rates, when a $1.00 DFC, 80% BDC, and 100% boiler use (i.e., full year) are assumed. Only the 4% discount rate presents a feasible scenario for TCRs up to $1,300,000. NPV is seen to decrease with increasing discount rates.

Figure 6-4 shows the same variation with a new DFC of $1.50/MM Btu. Crane cannot be

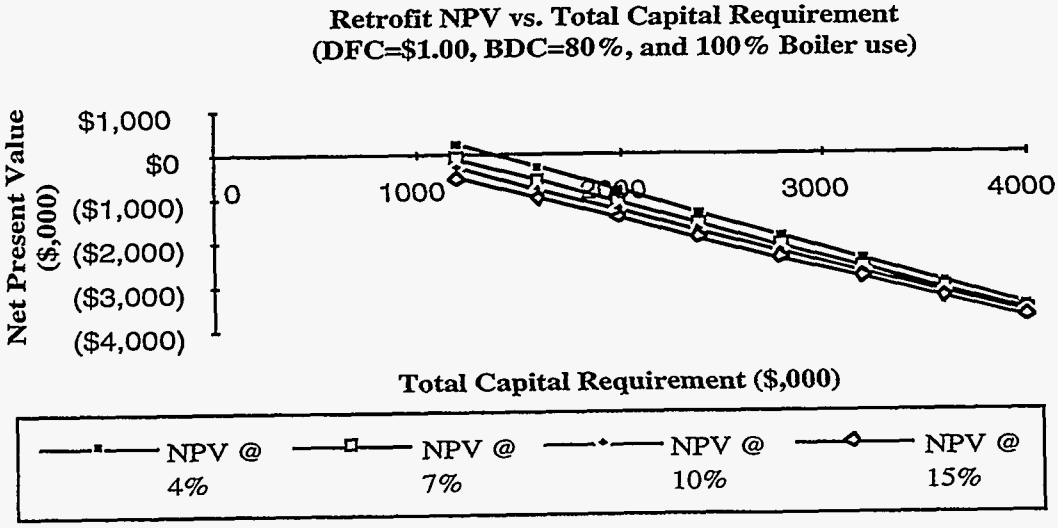

Figure 6-3. RETROFIT NPV vs. TOTAL CAPITAL REQUIREMENT ($1.00 DFC, 80% BDC, 100% Boiler use)

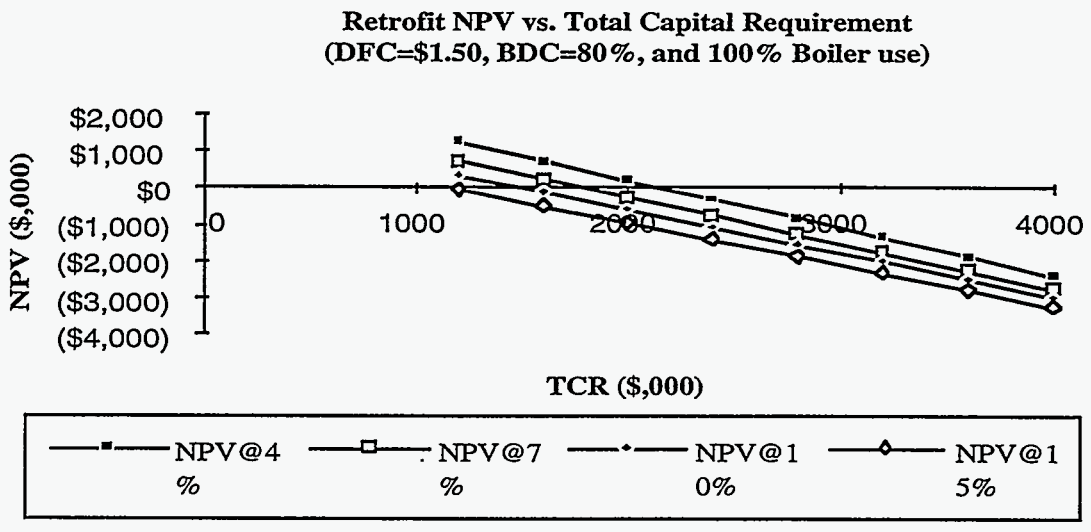

Figure 6-4. RETROFIT NPV vs. TOTAL CAPITAL REQUIREMENT ($1.50 DFC, 80% BDC, 100% Boiler use)

retrofitted commercially since negative NPVs are obtained for the 15% discount rate. At this new DFC, and 4% financing, the maximum TCR is $2,100,000. In addition NPV is seen to increase with increase in DFC.

Figure 6-5 shows NPV variation with TCR at different discount rates for a 50,000 lb steam/hr boiler, when a $1.50 DFC, 80% BDC, and 100% boiler use (i.e., full year) are assumed. This shows a break even TCR of almost $3,000,000 for a commercial retrofit. Currently, the MCWM retrofit technology is not feasible commercially.

Figure 6-6 shows the effect of boiler use on NPV. The scenario is the same as in Figure 6-4 with the exception of a boiler use decrease from 100% to 75%. The maximum TCR at 4% financing reduces from $2.1 million to $1.7 million dollars. Again commercial discount rates would render the retrofit unfeasible. This suggests that the 50% boiler use (six months in the year) makes the Crane retrofit seem rather unfeasible (The Crane boilerhouse operates the equivalent of one boiler for ~7 months per year.). NPV decreases with decreasing boiler use.

Figures 6-7 and 6-8 show NPV variation with TCR at 80% and 90% BDCs, when 100% boiler use and 4% financing are assumed, for a $1.00/MM Btu DFC and a $1.50/MM Btu DFC respectively. The break even TCR increase with in BDC and DFC. This shows that NPV increases with increasing BDC.

Figures 6-9 and 6-10 show NPVs quite similar to Figures 6-7 and 6-8. The difference is that whereas boiler use and discount rate were kept constant previously, DFC and discount rate are here kept constant at $1.50/MM Btu and 4%, respectively. The NPV-TCR curves are studied at 80% and 90% BDCs, and boiler use at 50, 75, and 100%. The break even TCR increases with increase in BDC and DFC. This shows that NPV increases with increasing BDC and decreases with boiler use.

Stochastic Analysis

Stochastic analyses of the Crane boiler were performed using a program called Crystal Ball. The focus was again on the variables which affected NPV the most. Initially, TCR, discount rate and boiler use were set at $3,667,000, 4% and 50%, respectively. BDC, boiler plant life and DFC were allowed to vary. BDC was assumed to have a modified normal distribution with mean of 80% and range 78-100%. Boiler plant life was assumed to have a uniform distribution from 18-25 years, and DFC a modified normal distribution with mean 1.2 and range $1.00-1.50/MM Btu per annum. Both payback period and NPV were set as forecasts. The outcome was a mean payback period of 48 years, which is much longer than the assumed boiler life, and of course a negative mean NPV, i.e., a loss of about $5,000,000.

In a second set of runs, all the previous assumptions were maintained and additionally, the TCR was given a uniform distribution over the range $1,360,000-3,668,000. The output improved somewhat but still indicated a mean payback period of 30 years, again longer than the assumed life of the boiler. Mean NPV was a loss of almost $2,000,000.

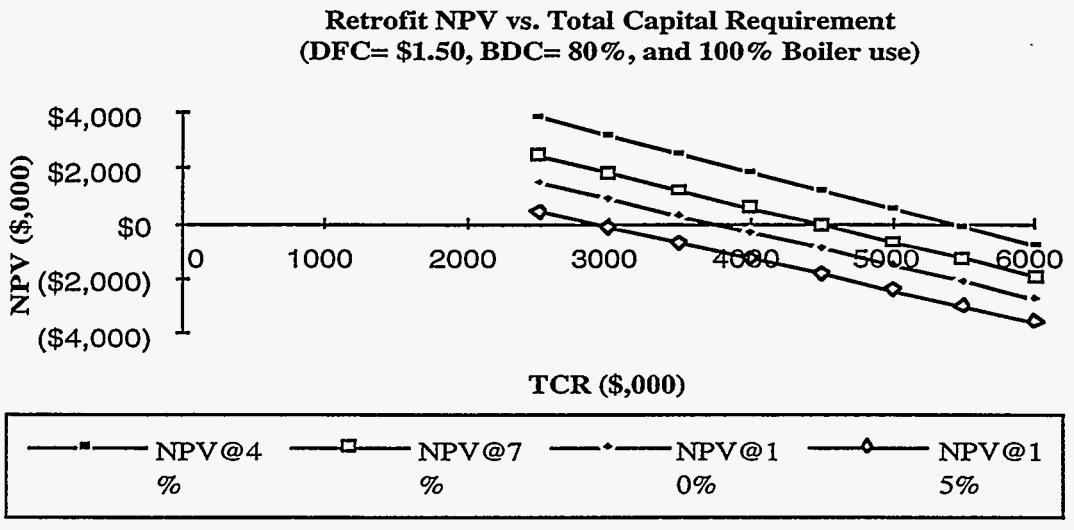

Figure 6-5. RETROFIT NPV vs. TOTAL CAPITAL REQUIREMENT FOR A 50,000 LB STEAM / HOUR BOILER ($1.50 DFC, 80% BDC, 100% Boiler use)

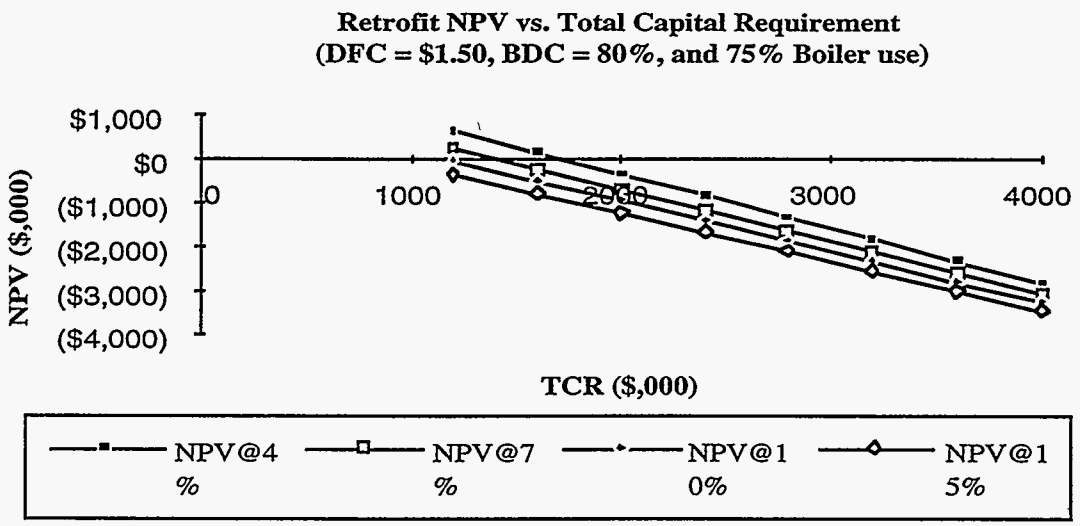

Figure 6-6. RETROFIT NPV vs. TOTAL CAPITAL REQUIREMENT ($1.50 DFC, 80% BDC, 75% Boiler use)

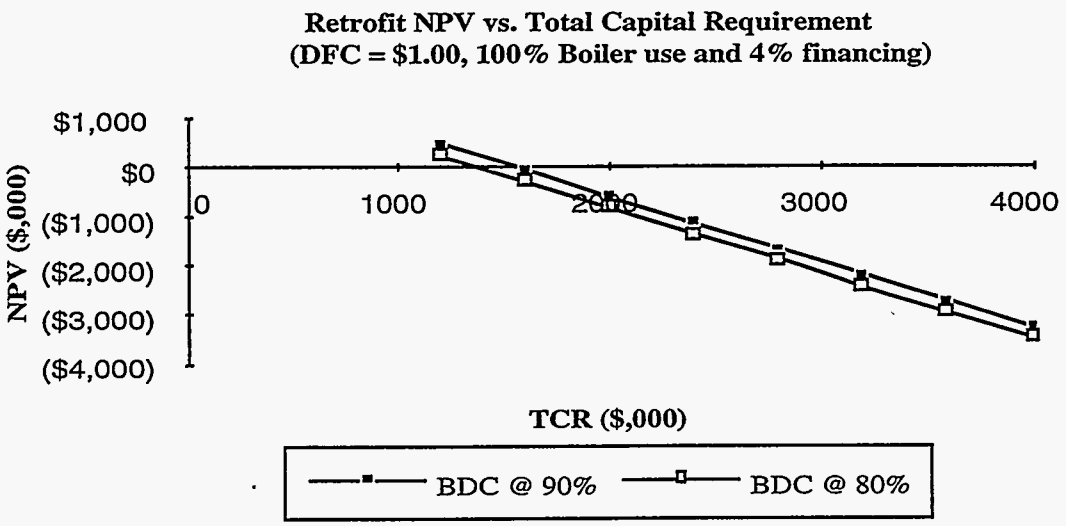

Figure 6-7. RETROFIT NPV vs. TOTAL CAPITAL REQUIREMENT ($1.00 DFC, 100% Boiler use, 4% Financing)

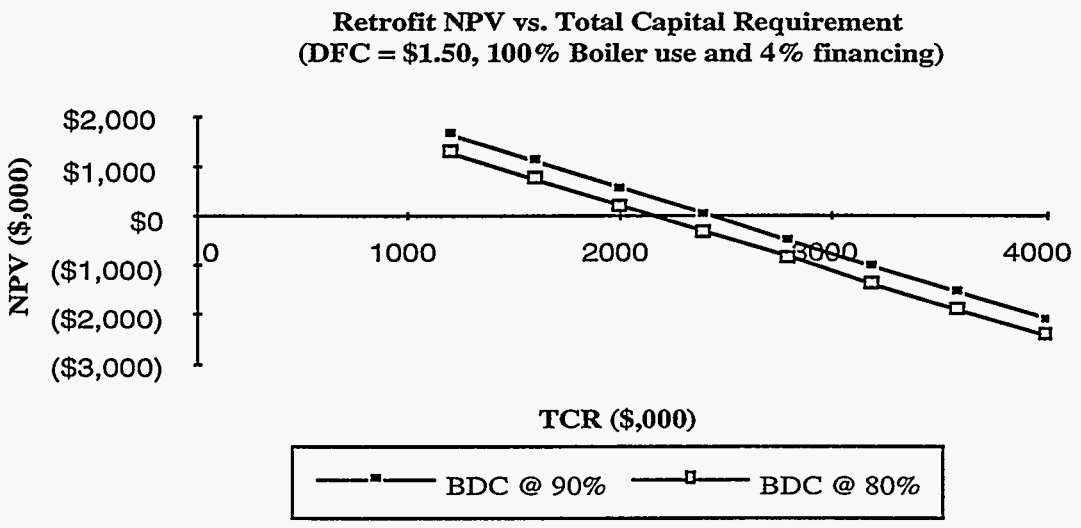

Figure 6-8. RETROFIT NPV vs. TOTAL CAPITAL REQUIREMENT ($1.50 DFC, 100% Boiler use, 4% Financing)

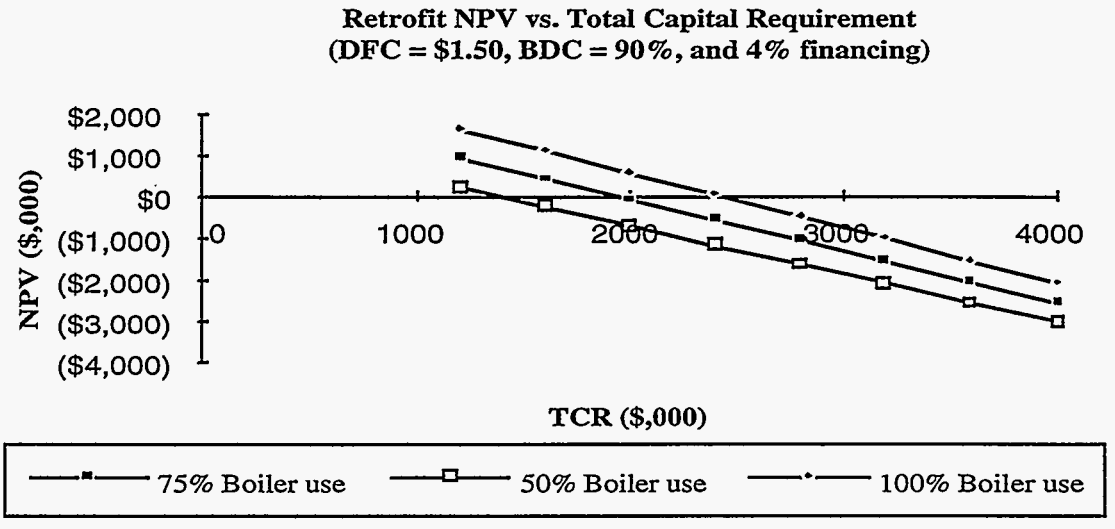

Figure 6-9. RETROFIT NPV vs. TOTAL CAPITAL REQUIREMENT ($1.50 DFC, 90% BDC, 4% Financing)

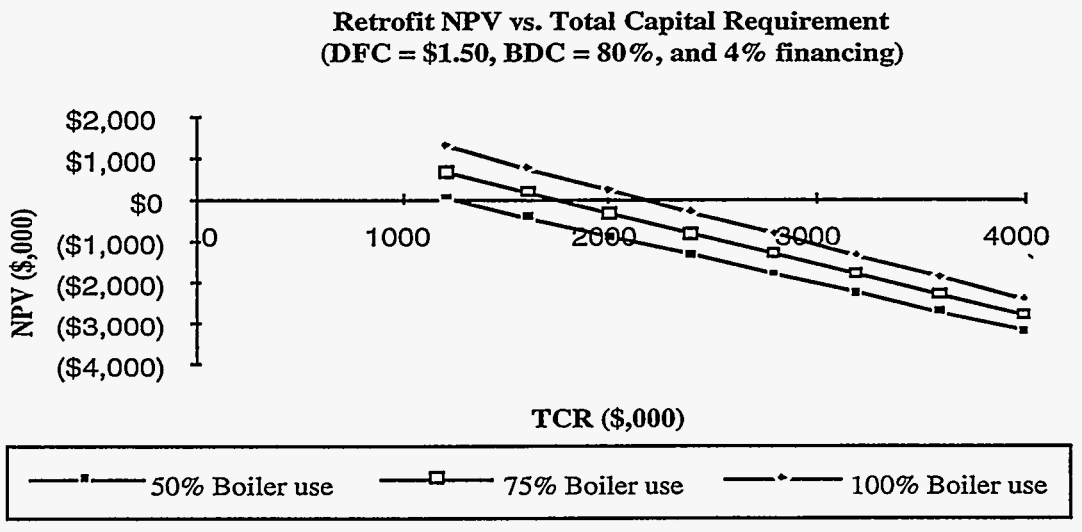

Figure 6-10. RETROFIT NPV vs. TOTAL CAPITAL REQUIREMENT ($1.50 DFC, 80% BDC, 4% Financing)

Conclusions

It must be noted that certain strong assumptions are implicit in the models. These are that the variables and inputs stay constant over the life of the plant. A crucial consideration is the MCWM assumed for the analysis. The MCWM considered here did not require flue gas desulfurization. In addition, the modeling of TCR as a function of BDC may not be fixed. The experience of the Penn State facility showed improved performance in terms of increased BDC with time. Such improvements can be characterized as movements closer to or towards the constant cost curve. This suggests that a more realistic modeling of TCR as a function of derating should incorporate a learning curve to account for such improvements.

The variables that most strongly influence the economic feasibility of retrofitting to fire MCWM are the differential fuel cost (DFC), the expected life of the boiler plant, its size (or capacity), total capital requirement (TCR), boiler derated capacity (BDC), and the discount rate. Feasibility (in terms of NPV) increases with increasing DFC, and also with increasing expected boiler life. There are economies of scale in retrofitting. Feasibility decreases with increasing discount rate. TCR is independent of BDC in the spreadsheet model and therefore seems to indicate that feasibility increases with increasing BDC.

A sensitivity analysis showed that the MCWM price had the most influence on the analysis. This really translates to mean that the DFC has the most influence since fuel oil price was kept constant. A DFC of at least $1.50/MM Btu is preferred. The current oil prices suggest that the delivered MCWM price must be at most $1.50/MM Btu. This can probably be achieved if coal cleaning, MCWM preparation, and DOD sites are close to each other and MCWM is prepared on a large scale.

The models show that some boilers will realize a net benefit from retrofitting while others will not. The differences in net benefits with size suggest that DOD can consider gains from a retrofitting distribution scheme in which the gains from retrofitting large (and more economic) boilers are given to boiler plants that will realize some operational gains by retrofitting but cannot afford the capital costs.

The payback period can be reduced with increases in the differential fuel cost. Payback periods decrease with increasing boiler size. Depending on the sizes of DOD boiler plants, it may well be the case that DOD will have to set a desirable payback period close to the useful plant life. Given the uncertainties in a study of this kind, the desirable payback period should be considerably or significantly less than the useful plant life.

Economics and Discussions

The key economic variables in this work are the differential fuel cost, discount rate, expected boiler plant life, boiler derated capacity, the boiler plant size, and the total capital requirement. Before plunging into an economic analysis of retrofitting it is important to note that there are several uncertainties in an analysis of this kind. The major uncertainty has to deal with

fuel price projections (both fuel oil and MCWM delivered). It is common knowledge that oil price fluctuations thwart the effort of analysts in making projections. Also, the absence of an existing MCWM commercial production facility means that delivered MCWM price can only be estimated. In this work, the price of oil is held constant at $3.00/MM Btu, and the delivered MCWM price varied between $1.50-2.00/MM Btu.

The next major uncertainty is with the boiler load factor or boiler derated capacity (BDC) as it is referred to in this section. The true BDC and other performance data can only be obtained in actual plant practice, however the model developed permits a sensitivity analysis varying BDC. It is important to note that the models are limited in the sense that any scenario depicted applies only to the type of MCWM fuel (and/or the source coal) considered in this analysis. The MCWM considered is the same as that used in the Penn State demonstration tests.

A survey of oil-fired boilers on DOD installations has shown that there are about 5-6 thousand such boilers on over 300 installations. This is encouraging, showing that there is a market for MCWM or other coal-based fuels. However, there are other factors to consider, such as proximity to suppliers, availability of supplies, environmental regulations in the respective regions, etc.. Even if the boiler conversion costs can be kept low, these factors could escalate the costs of operating the boiler on MCWM. For MCWM to have a clear advantage over the other coal-based fuels, the benefits from retrofitting significantly and substantially outweigh the costs [132,133].

The current state-of-the-art of MCWM is such that no major technical problems are apparent. Tests and demonstrations have proved that existing formulations of MCWM can be burned in existing boilers supplying reliable steam to industrial processes. MCWM has been demonstrated as a potential replacement for No. 6 fuel oil as a boiler fuel and can be fired economically. The question of a widespread retrofitting to fire MCWM is still one of economics. The main concern is the impact of oil prices on DFC and consequently on the economics of retrofitting. This is due to the fact that the cost savings in retrofitting is almost entirely made up of fuel cost savings. Congressional directives (and other forms of government interventions) will not drive the development of a market for slurries. A much better driving force is the differential fuel cost coupled with a low enough total capital requirement of retrofitting specific boiler units.

Oil price increases would increase the cost differential assuming MCWM prices remain the same, and would make MCWM attractive as an alternative fuel. MCWM has been predicted to economically replace oil if the price of No. 6 oil reaches $20/barrel. Others have predicted the growth of a MCWM market if the price of No. 6 fuel oil reaches $31/barrel. These predictions remain to be seen given the current trend in oil prices.

MCWM delivered cost price could be reduced with reduction in transportation and production costs. These are in part dependent on the transportation industry and technological improvements which lead to reduced cost of coal cleaning and slurry preparation, as well as ease in

transport. Reduction of boiler capacity losses with improvement in the retrofit technology would also lead to increased net benefits of retrofitting[132, 133].

If industrial, utility, and export demand for MCWM is created, then a market would evolve. This demand would encourage mass MCWM production which would lead to a MCWM cost reduction. However, such demand resulting in the creation of a market could bring about competition in the energy market and a probable decline in oil prices. There is the uncertainty of the success of a MCWM market to consider. The MCWM industry is likely to be very vulnerable to other energy sources, especially oil and gas. This can only be offset by reductions in coal price and technological improvements in MCWM manufacture and delivery. The perception of risk, in this case uncertainty or unknowns about fuel dependability, quality control, transportation, handling and storage, future environmental regulations, etc., could have retarding effects on the development of a market and its growth.

To a potential consumer of MCWMs (a DOD installation or other), there would be sufficient incentive to retrofit from firing oil to firing MCWM if the price differential between the two would yield significant savings. This translates, for DOD installations, to mean that there is less likelihood to prolong compliance with or oppose Congress' directives. MCWM would gain a foot-hold in the energy market if oil prices increase or technology improvements permit MCWM price decreases with falling oil prices such that the price differential sustains the MCWM market.

DMC Retrofit Evaluation

An evaluation was conducted investigating the profitability of retrofitting the Crane boiler to fire DMC. The methodology was similar to that for the MCWM option. Particular attention was given to the sensitivity of profitability to critical influences as fuel prices, boiler derating, utilization rates, boiler life, and the cost of capital.

The total capital required to retrofit the boiler to fire DMC includes provisions for a fuel preparation facility on site, whereas for the MCWM retrofit, the MCWM was delivered to the site. This means retrofitting to fire DMC has a higher total capital requirement than the case of MCWM. The critical pieces of equipment include coal handling pulverizing equipment. DMC preparation on site is necessary because of the difficulties in transporting fine coal.

The TCR for DMC retrofitting is higher than for MCWM retrofitting. Reasons for this are:

1. Increased equipment for the DMC application - coal handling, storage, and micronizing;
2. The MCWM supply system is simpler because the MCWM is pumpable; and
3. The cost of boiler modifications for MCWM can be less than for DMC especially when a cleaned coal is used.

The variables that influence the economic feasibility of retrofitting to fire DMC are the DFC, the expected boiler plant life, TCR, BDC, boiler use, and the discount rate. The coal used had the same characteristics as that for the MCWM. In this evaluation, a 20% derating is assumed as a base case. That is, the boiler will operate at a BDC of 80%. EER's preliminary TCR estimate

of $5.215 million was used as the base. A base 4% discount rate, and a 50% boiler use are assumed. A base case expected life of 20 years is used. In addition, a sensitivity analysis varying all the variables was performed.

The results show that:

- NPV increases with increasing DFC;
- NPV increases with BDC;
- NPV increases with increasing expected boiler life;
- NPV decreases with increasing discount rate;
- NPV decreases with increasing TCR; and
- NPV increases with increasing boiler use.

The main conclusion is that retrofitting the Crane boiler to fire DMC is not viable. Only at low TCRs does the retrofit show viability. Therefore, MCWM retrofitting seems to be more economical and is recommended for the Crane boiler.

6.4 Analyze/Identify Transportation Cost of Commercial Sources of MCWM and Cleaned Coal for DMC Production

This section provides an overview of transportation costs for the Crane case. In general, transportation costs are dependent upon the distance traveled, shipment size, frequency of travel, length of contract, availability of carriers, and some other side factors such as environment and safety. Transportation costs can be set for a given area by developing quotations for the specific set of transportation circumstances that exist at that point in time.

Selection of Transportation Mode

There are four types of MCWM transportation modes: truck, rail, pipeline, and barge. Rail transport is used for handling large volumes on a regular schedule. Barge transport is a cost-effective method for bulk fuel movements providing that the shipping and receiving locations have appropriate water access. Pipelines are used for high volume, continuous point-to point shipment of fluids, including slurries of various types. Only two such pipelines have been built for transporting coal in the U.S. and only one of these is operating in 1994. Truck transportation is considered most economic for low volume, short distance, and high frequency commodity movements. Extensive industry experience in shipping MCWM has been limited to rail, barge, and truck.

For this study, the Minnehaha mine was used. Given that Minnehaha and other mines are very close to Crane (within 40 miles) and that the slurry requirement is a small amount, estimated to be less 7,000 tons in total (using 25.2 MM Btu/h @ 6 months/year requires 1,275,456 gallons or 6,630 tons of MCWM), the only feasible choice is trucking. Standard MC-312 semitrailers could be used, with a nominal tank capacity of 3,500 to 5,500 gallon range. This capacity is normally reduced to meet the bridge Formula Compliance Code. These tanks are usually constructed with interior heavy duty shells.

Alternatives for the Crane Case

Theoretically, the transportation route would be from the coal source to a deep or conventional cleaning plant to a MCWM preparation plant and then to the boiler at Crane; however, in practice, the MCWM plant has to be located close to a cleaning plant and a coal mine. Actually there is a cleaning plant at the Minnehaha mine in Sullivan county; the capacity of that plant is 800 tons/h. There are 15 cleaning preparation plants in the state of Indiana according to the 1993 preparation plant census, some of them are located between the Minnehaha mine and Crane.

There are three alternatives: 1) build the MCWM preparation plant close to Minnehaha (in the case study, this mine is chosen); 2) build the plant somewhere between the mine and Crane (there are other mines with cleaning preparation plants in the surrounding area); and 3) use DMC technology at Crane. If the first and second alternatives are chosen, no coal transportation problems arise, since only MCWM will be transported. If the third alternative is picked, no MCWM transportation problems occur, since only 2"x0 coal will be transported. The total coal required at Crane will be around 5,038 tons (using 25.2 million Btu/h @ 6 months/year, 10,925 Btu/lb considering 19% moisture level, and 4,368 hours for the 6 months).

Transportation Rates

Trucking firms are regulated for service areas. To be a qualified carrier, the trucking company must have intrastate authority in Indiana and tank-truck carriers services.

The slurry and coal transportation rates from the Minnehaha mine to the military base at Crane were provided by AMAX Coal Company. The MCWM requirement used for Crane base was approximately 8,000 gallon per day, based upon the slurry heating value of 8,300 Btu/lb. Given the assumption of constant fuel input and the 4,000 gallon per tank limit, MCWM delivery requirement would be approximately two tanks per day. Based on the information provided by AMAX Coal Company, the following are MCWM transportation rates from Minnehaha to Crane (assuming slurry is prepared in Minnehaha and considering 40 miles of distance):

	Cents/Gallon	Cents/MM Btu	$/Tank Load
Lower range	7.5	86.9	300
Higher range	12.5	144.8	500

The cost of shipping coal from Minnehaha to Crane using 24-ton trucks is one dollar for the first mile and seven cents for each additional mile. Assuming 40 miles of distance from Minnehaha to Crane the cost is $3.73/ton. This translates into 13.84 cents/MM Btu for the lower range case and 17.07 cents/MM Btu for the higher range case.

Several reasons can be cited to account for the difference between MCWM and coal transportation rates. First, the additional cost of cleaning the MCWM tanks after being used is included in the transportation rate. Another reason is the amount of water in the slurry (approximately 35% of total weight); this extra weight increases the cost in cents/MM Btu.

According to AMAX Coal Company, the coal and slurry handling costs are not included in the transportation rates cited above. In general, coal handling costs are higher than slurry handling costs. Thus, including handling costs in addition to transportation costs will further reduce the difference between coal and slurry costs.

Estimating the MCWM economic rate directly is impossible at this stage due to limited information. Studies in this field also are very limited. An attempt to obtain data directly from trucking firms through telephone and questionnaire surveys was not very successful. The only comprehensive study found is the one conducted by EPRI[134]. Comparing the rates mentioned above with the rates estimated by EPRI can provide some insights about the reliability of MCWM transportation rates. However, a caveat is needed at the outset since the factors considered for rate estimations are different. For example, the EPRI study includes only the unloading facilities in the estimation of capital cost based on the assumption that utilities are operators of transportation systems with transportation facilities leased.

The results of the EPRI study (first three rows) and the simulation of Minnehaha-Crane transportation rates (last three rows) are summarized in Table 6-6. From this table, it is clear that the transportation rate depends upon the total distance delivered. Five cases are analyzed in the EPRI study. The Virginia Electric Power case, with a delivery distance of 43 miles, is very similar to the current project (last column in Table 6-6). Delivery costs given in $/ton-mile were first converted to $/MM Btu/mile for each case using the slurry heating value of 8,300 Btu/lb (fourth row of Table 6-6). Then, this fourth row was multiplied by 40 to obtain the MCWM transportation cost for each case to simulate the Minnehaha-Crane situation. Finally, these delivery rates were adjusted for inflation (see last row of Table 6-6).

Thus, based on the EPRI study, the slurry transportation rate estimated for the Virginia Electric Power case (which covers a similar distance as Minnehaha-Crane) would be around $0.85/MM Btu, which in fact is quite similar to the rate provided by AMAX Coal Company from Minnehaha to Crane ($0.87/MM Btu).

To confirm the MCWM rates, milk transportation costs were also investigated. The rationale for this is that milk tanks can easily be used for the slurry transportation, and the market for bulk-milk transportation is very competitive. For this reason, it would be reasonable to assume that the bulk-milk transportation rate is the minimum rate that can be found for the MCWM if the comparison is based on similar bases. According to the information provided by OMNI North America, the hauling cost from Altoona, Pennsylvania to State College, Pennsylvania (a distance of approximately 40 miles) is $295 per load. This rate is also similar to the lower range MCWM transportation rate provided by AMAX Coal Company, which is $300/load.

Conclusions

The coal transportation costs between Minnehaha, Indiana and Crane, Indiana range between 0.14 and $0.17/MM Btu. Transportation costs for MCWM are much higher, ranging

Table 6-6. MCWM Transportation Costs for Different Cases According to the Distance (Based on the EPRI Study)

Destinations	Boston Edison	Delmarva Power	Florida P&L	Houston L&P	Virginia E&P
One Way Mileage	564	234	134	349	43
Delivery cost in $/Ton/Mile (1985 dollars)	0.121	0.187	0.153	0.165	0.242
Delivery cost converted used Crane Slurry data ($/MMBtu/Mile)	0.007289	0.011265	0.009216	0.009940	0.014578
Delivery Cost as it were from Minnehaha to Crane ($/MMBtu/Mile)	0.2915	0.4506	0.3687	0.3976	0.5831
Delivery cost as it were from Minnehaha to Crane in $/MMBtu, assuming 40 miles, and adjusted by inflation (1994 dollars)	0.425	0.658	0.538	0.580	0.851

between 0.87 and $1.45/MM Btu. Surprisingly, the low limit of MCWM rates turned out to be consistent not only with the EPRI study, but also with the survey result conducted on bulk-milk transportation. Although there might be room for further MCWM transportation rate reduction, the potential would not be very high for the Crane case.

Trucking seems to be the most appropriate transportation mode for the Crane case. However, this mode is considered practical for only low annual quantities and short distances (less than 250,000 tons per year)[134]. The operation of a truck transportation system for a large quantity of MCWM or crushed coal will create environmental problems such as the impact of noise and safety upon the public of routing large number of trucks. This constraint in trucking transportation capacity will be considered in Phases II and III work, in which the transportation model will be generalized.

The costs that were found for transporting MCWM appear to be high and would constitute a significant percentage of the delivered cost of coal to a retrofitted boiler. For that reason, consideration should be given to alternative truck types. For instance, a local hauler of liquid mine wastes, which are designated as hazardous by the Department of Transportation, was contacted. The likely transportation rates using the type of trucks that they employ would be 2.8 to 4.2 cents/gallon or 32.4 to 48.6 cents/MM Btu. This results in a significant cost savings for MCWM supply and it is highly recommended that this trucking method be investigated.

Other cost savings may be realized in the transportation of MCWM. A large percentage of the costs with MCWM transportation involve the slurry loading and unloading times. If the trailer could also be utilized as a storage tank at the boiler site then the trucking firm could then deliver a full trailer and take away the empty trailer without tying up the driver and truck. The cost for this type of service, using the lower cost trailers are estimated to be 12.5 cents/MM Btu/mile or about 1.6 cents/MM Btu for the Crane case. The benefit obtained from this method of MCWM delivery would be offset to an unknown degree by other costs and would therefore require a more detailed benefit-cost analysis.

6.5 Determine Community Spillovers

Associated with the extraction, processing, and combustion of any fossil fuel are externalities (spillover effects) and emissions now recognized as hazardous, detrimental to the environment, or unpleasant to live by. Among the predominant fossil fuels - oil, coal, and natural gas - coal is recognized as the most harmful to the environment, and its adoption as a fuel source in lieu of oil or natural gas will incur added environmental and compliance costs and regulatory burden. This activity will review the environmental damage associated with coal mining, processing, transportation, and combustion and the federal and state regulations governing each stage. Outside field studies provide some estimates of the environmental and compliance costs.

The extraction and use of any fossil fuel is accompanied by environmental and regulatory costs. Any facility currently using oil or natural gas is already incurring some regulatory costs,

and it should be remembered that the production and use of oil and gas has its own set of environmental hazards and effects. Consequently, the appropriate costs to consider for a facility contemplating a switch from oil or gas to coal are the marginal costs associated with coal over and above the costs already associated with oil or natural gas.

A detailed review was conducted which concentrated on the environmental aspects of coal production and use[67]. In it, the environmental damage associated with coal and the Federal and Indiana state regulations governing its use were reviewed. A summary of the review which includes coal mining and processing, transportation, and combustion is presented.

Coal Mining and Processing

Mineral deposits are fixed and mining can only occur where a deposit already exists. Mines cannot be uniformly designed and consistently located in unobjectionable and "environmentally safe" areas.

Types of damage include destruction of the landscape (including subsidence and erosion), degradation of the visual environment, disturbance of water courses and sedimentation, acid mine drainage, damage to or destruction of agricultural, forest, or recreational lands, noise pollution, fugitive dust and coal fines, truck traffic, vibration from blasting and air blasts, tailings disposal, mining accidents and health hazards, and burning refuse banks and abandoned-mines fires.

Regulation of mining is a patchwork and uneven affair. Both federal and state regulations exist, involving many different agencies and significant overlap.

Federal agencies whose jurisdictions can involve mining include The Bureau of Land Management, The Forest Service, The Office of Surface Mining, The National Parks Service, The Bureau of Indian Affairs, The Bureau of Reclamation, The Fish and Wildlife Service, and The Environmental Protection Agency.

Applicable regulations include The Safe Drinking Water Act, The Clean Air Act, The Toxic Substances Control Act, The National Environmental Policy Act, The Comprehensive Environmental Liability Act and The Superfund Amendments and Reauthorization Act, The Clean Water Act, The Resources Conservation and Recovery Act, and The Surface Mine Control and Reclamation Act.

Compliance and effectiveness depends on not only on the nature and existence of environmental regulations but also on their enforcement.

The largest fraction of environmental costs expended during a mining project are for reclamation.

Coal Transportation

All stages of coal transport - loading, en route, and unloading - involve some environmental impacts. The effects are felt by 'natural' systems such as agriculture, forests, and waterways, by humans, and by structures and installations.

Environmental damage assessments for coal transport in general are incomplete and not

well known. All estimates are subject to substantial inaccuracies.

Coal Combustion

The most notable environmental impacts associated with coal combustion are the emission of air pollutants and the creation of ash which requires disposal. The quantity and nature of the effluents emitted is determined by both the composition of the fuel and the method of combustion.

Air emissions associated with coal combustion include sulfur oxides, nitrogen oxides, carbon monoxide, carbon dioxide, particulates, volatile organic compounds, polycyclic aromatic hydrocarbons, trace metals and radionuclides.

Associated with these emissions are acid rain, urban smog, ozone, global climate change, and a variety of pulmonary and respiratory diseases.

Most recent Federal legislation concerning emissions is the Clean Air Act amendments of 1990. It includes marketable permits and performance standards and regulates particulates, ozone, VOCs, NO_x, air toxics, NO, and sulfur dioxides.

Solid wastes associated with coal combustion are fly ash, bottom ash, slag, and scrubber sludge. All are disposed on land. Some are classified as hazardous materials. Data from one study found no major environmental effects from the disposal of coal combustion wastes.

Summary

Most detrimental impacts occur during combustion. Many of the environmental costs associated with coal use are not included in the market price of the fuel, although more are internalized now than prior to the environmental legislation of the 1970s, 1980s, and 1990s. Most single industrial boilers will be able to meet federal and state regulations with standard pollution control devices.

6.6 Regional Market Considerations and Impacts

A comprehensive regional economic impact analysis was conducted. A detailed discussion of a methodology for determining the total regional economic impacts of new coal technologies was presented elsewhere[67]. In this section, this methodology was applied to the analysis of the regional economic impacts of MCWM and DMC boiler retrofits at the Crane site. The three separate cases analyzed are summarized below:

Scale	MCWM	DMC
One Unit	7,000 tons/year	5,000 tons/year
Five Units	35,000 tons/year	25,000 tons/year
Fifty Units	350,000 tons/year	250,000 tons/year

A number of regional economic indicators are worthy of study, but attention will be confined to output (sales) and employment. Not only were the direct impacts at the site estimated, but so was ascertaining the multiplier effects on other sectors in the Crane Region economy. Note

that because detailed data on boiler operations were not available at the time of this writing, the impacts of construction costs were only simulated. An analysis of operating costs will be included later.

Also note that the construction costs associated with even the largest scenario is relatively small compared to the Crane Regional economy as a whole. However, the analysis is able to identify strengths and weaknesses of the methodology for application to other cases, including those where impacts are likely to be more prominent.

Sectoral Disaggregation of Combustion Technology Data

In order to perform an impact analysis, it is necessary to make basic engineering data on the technologies compatible to data in the regional economic model. This involves three steps:

- Obtain disaggregated construction (retrofit) cost data;
- Map the engineering categories into Bureau of Economics Analysis Industrial Classifications used in the Crane Region input-output table; and
- Distinguish between total direct engineering requirements and those that can be supplied by producers within the region (and will thus be able to further stimulate the regional economy).

Capital Costs and Regional Purchases

EER provided construction estimates of DMC and MCWM technologies for the DOD coal retrofit[124]. In order to evaluate the impacts that these costs would have on the region, it was necessary to first organize the data in such a way that it could easily be inputted into the U.S. Government's Impact Analysis for Planning (IMPLAN) modeling system for impact analysis; consequently Tables 6-7 and 6-8 were created using the information provided. The initial step in creating these tables was to assign Standard Industrial Classification (SIC) codes to each component of the DMC and MCWM technologies. Afterwards, SIC codes were translated into Bureau of Economic Analysis (BEA) Industry codes and components were grouped at the 2-digit BEA classification level. Finally, IMPLAN codes (which are basically a renumbering of BEA codes) were assigned, allowing for data input into the IMPLAN computer system.

Costs were distributed to components as specified by EER; however, these "Listed Costs" were not ready to be input into IMPLAN due to data adjustments specified in the "Summary of Project Costs" part of the reports. Adjustments reflect changes from: (1) a 20% upward revision in the value of labor (initial labor estimate considered low); (2) an estimating accuracy allowance (equipment/material) of 20%; (3) a labor contingency of 20%; and (4) a material contingency of 15%. The column labeled "Modified Costs" reflects all adjustments made to the "Listed Cost" of each component.

In addition to costs directly associated with the material and labor costs of the components, there are a number of other costs. These include freight, engineering, home office, field supervision, construction overhead and fee, project management, construction management, start

Table 6-7. MCWM Capital Cost Estimate

REF #	Component	Cost Item	SIC Code	BEA Code	IMPLAN Code	Modified Cost	Percent of Total
	Labor						
	Specified Labor			11.0300	50	$726,611	0.198
144	Heat-Light-Fire Surp		3569	11.0300	50	$12,080	0.003
144	Heat Light-Fire Surp		3569	11.0300	50	$6,041	0.002
	Construction overhead and fee		8741	11.0300	50	$332,344	0.091
	Construction management		8741	11.0300	50	$265,970	0.073
	Labor Subtotal					$1,343,045	0.366
	Materials						
115	Stack	Paint	2850	30.0000	200	$190	0.000
119	Air Compressor Equip	Paint	2850	30.0000	200	$46	0.000
140	Slurry Storage Tank	Paint	2850	30.0000	200	$1,689	0.000
115	Stack	Equipment	3251	36.0200	233	$13,192	0.044
123	Concrete Building	Civil Sitework	3271	36.1000	242	$13,753	0.004
124	Retaining Wall	Civil Sitework	3271	36.1000	242	$5,970	0.002
126	Concrete Slab	Civil Sitework	3273	36.1200	244	$9,307	0.003
127	Concrete Roof	Civil Sitework	3273	36.1200	244	$6,009	0.002
133	Run-off Drain	Civil Sitework	3273	36.1200	244	$541	0.000
134	Concrete Pipeway	Civil Sitework	3273	36.1200	244	$889	0.000
140	Slurry Storage Tank	Insulation	3296	36.2000	251	$9,855	0.003
128	Air and FG Ductwork	Insulation	3296	36.2000	251	$9,855	0.003
132	2" Slurry Trans. Pipe	Insulation	3296	36.2000	251	$3,863	0.001
146	A.H. Sootblower Piping	Insulation	3296	36.2000	251	$1,379	0.000
129	A.H. Support Steel	Equipment	3312	37.0101	254	$6,523	0.002
127	Concrete Roof	Steelwork	3312	37.0101	254	$7,248	0.002
108	Air Preheater Steam	Equipment	3443	40.0600	284	$14,497	0.004
113	Air Heater	Equipment	3443	40.0600	284	$123,221	0.034
140	Slurry Storage Tank	Equipment	3443	40.0600	284	$61,900	0.017
147	Burner	Equipment	3443	40.0600	284	$72,483	0.020
122	Metal Prefab. Bldg.	Civil Sitework	3448	40.0901	287	$16,030	0.004
128	Air and FG Ductwork	Piping	3498	41.0800	303	$42,605	0.012
132	2" Slurry Trans. Pipe	Piping	3498	42.0800	303	$26,808	0.007
146	A.H. Sootblower Piping	Piping	3498	42.0800	303	$826	0.000
118	Ash Screw Conveyor	Equipment	3535	46.0200	315	$12,322	0.003
138	Slurry (Moyno) Pump	Equipment	3561	49.0100	332	$18,845	0.005
119	Air Compressor Equip	Equipment	3563	49.0100	332	$24,064	0.007
143	Air Compressor	Equipment	3563	49.0100	332	$24,644	0.007
148	Slurry Unloading Pump	Equipment	3561	49.0100	332	$2,174	0.001
110	ID Fan	Equipment	3564	49.0300	334	$26,978	0.007
111	FD Fan	Equipment	3564	49.0300	334	$17,106	0.005
112	Bag House	Equipment	3564	49.0300	334	$73,932	0.020

Table 6-7. MCWM Capital Cost Estimate (cont.)

REF #	Component	Cost Item	SIC Code	BEA Code	IMPLAN Code	Modified Cost	Percent of Total
114	Sootblower Modification	Equipment	3564	49.0300	334	$7,248	0.002
116	Floor Air Blast System	Equipment	3564	49.0300	334	$14,497	0.004
121	Pitot Grid-Comb Air	Equipment	3564	49.0300	334	$4,349	0.001
145	A.H. Sootblowers	Equipment	3564	49.0300	334	$14,497	0.004
142	Slurry Heater	Equipment	3567	49.0600	337	$4,639	0.001
141	Slurry Tank Mixer	Equipment	3569	49.0700	338	$23,194	0.006
136	Slurry Strainer	Equipment	3569	49.0700	338	$4,349	0.001
144	Heat-Light Fire Surf	Equipment	3569	49.0700	338	$12,080	0.003
139	Flow Element Slurry	Equipment	3569	49.0700	338	$10,148	0.003
131	Electrical Work	Equipment	3621	53.0400	357	$152,214	0.042
144	Heat-Light-Fire Surp	Equipment	3621	53.0400	357	$6,041	0.002
130	Instrumentation	Equipment	3823	62.0100	403	$289,931	0.079
132	2" Slurry Trans. Pipe	Instrumentation	3823	62.0100	403	$28,268	0.008
146	A.H. Sootblower Piping	Instrumentation	3823	62.0100	403	$75	0.000
	Material Subtotal					$1,224,180	0.334
	Other						
	Freight		4731	65.0701	440	$51,420	0.014
	Engineering		8711	73.0302	506	$498,693	0.136
	Home Office		8711	73.0302	506	$57,449	0.016
	Field supervision		8741	73.0105	508	$72,058	0.020
	Project management		8741	73.0105	508	$166,231	0.045
	Start up		8741	73.0105	508	$132,985	0.036
	Field		8741	73.0105	508	$132,985	0.036
AREA	Piping System Testing		8741	73.0105	508	$3,654	0.001
	Taxes, Permits		9311			$59,990	0.016
	Other Subtotal					$1,048,509	.0270
	MCWSF Project Total					$3,667,154	1.000

Tabel 6-8. DMC Capital Cost Estimate

REF #	Component	Cost Item	SIC Code	BEA Code	IMPLAN Code	Modified Cost	Percent of Total
	Labor						
	Specified Labor			11.0300	50	$1,053,856	0.202
135	Lights, Heat, and Fire		3569	11.0300	50	$12,102	0.002
135	Lights, Heat & Fire		3569	11.0300	50	$6,052	0.001
	Construction overhead and fee		8741	11.0300	50	$473,072	0.091
	Construction management		8741	11.0300	50	$378,216	0.073
	Labor Subtotal					$1,923,298	0.369
	Materials						
100	Coal Hoppers	Paint	2850	30.0000	200	$610	0.000
115	Stack	Paint	2850	30.0000	200	$190	0.000
119	Air Compressor Eqpt	Paint	2850	30.0000	200	$46	0.000
115	Stack	Equipment	3251	36.0200	233	$13,216	0.003
123	Concrete Bldg	Civil/Sitework	3271	36.1000	242	$21.601	0.004
124	Retaining Wall	Civil/Sitework	3271	36.1000	242	$5,981	0.001
126	Concrete Slab	Civil/Sitework	3273	36.1200	244	$10,576	0.002
127	Concrete Roof	Civil/Sitework	3273	36.1200	244	$6,731	0.001
133	Run-Off Drain	Civil/Sitework	3273	36.1200	244	$542	0.000
134	Concrete Pipeway	Civil/Sitework	3273	36.1200	244	$890	0.000
128	Air & FG Ductwork	Insulation	3296	36.2000	251	$13,787	0.003
132	6" Coal Transport Pipe	Insulation	3296	36.2000	251	$1,683	0.000
137	Soot Blower Piping	Insulation	3296	36.2000	251	$1,522	0.000
127	Concrete Roof	Steelwork	3312	37.0101	254	$7,261	0.001
129	AH Support Steel	Equipment	3312	37.0101	254	$6,535	0.001
100	Coal Hoppers	Equipment	3443	40.0600	284	$92,947	0.018
108	Air Preheater Steam	Equipment	3443	40.0600	284	$14,523	0.003
113	Air Heater	Equipment	3443	40.0600	284	$123,445	0.024
120	Air Rcvr Tanks	Equipment	3443	40.0600	284	$2,033	0.000
138	Burner	Equipment	3443	40.0600	284	$72,614	0.014
104	Coal Silo	Equipment	3448	40.0901	287	$112,988	0.022
122	Metal Prefab Bldg	Civil/Sitework	3448	40.0901	287	$10,211	0.002
128	Air & FG Ductwork	Piping	3498	42.0800	303	$42,683	0.008
132	6" Coal Transport Pipt	Piping	3498	42.0800	303	$7,295	0.001
137	Soot Blower Piping	piping	3498	42.0800	303	$855	0.000
102	Coal Crusher	Equipment	3532	45.0200	312	$58,527	0.011
105	Weight Belt	Equipment	3532	45.0200	312	$21,784	0.004
106	Tass Mill	Equipment	3532	45.0200	312	$181,536	0.035
101	Screw Conveyor	Equipment	3535	46.0200	315	$13,361	0.003
103	Bucket Conveyor	Equipment	3535	46.0200	315	$18,008	0.003
118	Ash Screw Conveyor	Equipment	3535	46.0200	315	$12,344	0.002

Table 6-8. DMC Capital Cost Estimate (Cont.)

REF #	Component	Cost Item	SIC Code	BEA Code	IMPLAN Code	Modified Cost	Percent of Total
117	Air Compressor	Equipment	3563	49.0100	332	$14,523	0.003
119	Air Compressor Eqpt	Equipment	3563	49.0100	332	$13,942	0.003
107	Silo Bin Vent Filter	Equipment	3564	49.0300	334	$5,809	0.001
109	Dust Control System	Equipment	3564	49.0300	334	$110,374	0.021
110	ID Fan	Equipment	3564	49.0300	334	$27,027	0.005
111	FD Fan	Equipment	3564	49.0300	334	$17,137	0.003
112	Baghouse	Equipment	3564	49.0300	334	$74,067	0.014
114	Soot Blower Modification	Equipment	3564	49.0300	334	$7,261	0.001
116	Floor Air Blast System	Equipment	3564	49.0300	334	$14,523	0.003
121	Pitot Grid-Comb Air	Equipment	3564	49.0300	334	$4,357	0.001
136	AH Soot Blowers	Equipment	3564	49.0300	334	$14,523	0.003
135	Lights, Heat & Fire	Equipment	3569	49.0700	338	$12,102	0.002
135	Lights, Heat & Fire	Equipment	3621	53.0400	357	$6,052	0.001
131	Electrical Work	Equipment	3621	53.0400	357	$232,366	0.045
130	Instrumentation	Equipment	3823	62.0100	403	$290,458	0.056
132	6" Coal Transport Pipe	Instrumentation	3823	62.0100	403	$3,911	0.001
137	Soot Blower Piping	Instrumentation	3823	62.0100	403	$799	0.00
	Materials Subtotal					$1,725,556	0.331
	Other						
	Freight		4731	65.0701	440	$72,036	0.014
	Engineering		8711	73.0302	506	$709,154	0.136
	Home office		8711	73.0302	506	$81,695	0.016
	Field supervision		8741	73.0105	508	$105,512	0.020
	Project Management		8741	73.0105	508	$236,385	0.045
	Start Up		8741	73.0105	508	$189,108	0.036
	Field		8741	73.0105	508	$81,695	0.016
AREA	Hydrotesting		8741	73.0105	508	$5,569	0.001
AREA	Electrical Circuit Testing		8741	73.0105	508	$781	0.000
	Taxes, permits		9311			$84,042	0.016
	Other Subtotal					$1,493,941	0.270
	DMC Project Total					$5,214,831	1.000

up, field, taxes, and permits. These costs are located at the end of each table.

Operating Costs and Regional Purchases

These data were not available.

Single Boiler Impacts

The construction of each type of coal retrofit, either for MCWM or DMC, will have various impacts upon the nine-county Crane Region economy. These impacts include direct, indirect, and induced effects. Direct effects stem from the actual construction of the retrofit. Indirect effects represent business activity from the many rounds of "upstream" supplies of construction materials. Induced effects represent not only spending activity resulting from the income and profits created initially through direct and indirect effects but also from additional rounds of business activity they generate. The overall total impacts of a coal retrofit include all three types of effects.

Direct Impacts

Of the $3.6 million in direct construction expenditures only the $1.1 million spent within the Region will have any impacts on its economy. This difference of $2.5 million attributable to import leakages is estimated by IMPLAN with the use of regional purchase coefficients, measures of the ability of businesses within the region to satisfy regional demand of products. In constructing the coal combustion retrofit, the region is able to satisfy a portion of each of several inputs, and there are items such as Pumps and Compressors that the region cannot provide at all.

Table 6-9 illustrates the distribution of direct expenditures associated with the construction of the MCWM coal retrofit and the calculated regional expenditures (remaining inputs are satisfied by sources outside the region). The sectors that satisfy the largest regional demand are: Business and Professional Services, Scientific and Controlling Equipment, and Electrical Industrial Equipment. Together they account for 51.0% of direct local expenditures. Nearly 11 jobs out of a total of 20 are estimated to be generated in these sectors.

Table 6-9 also illustrates the distribution of expenditures associated with the DMC coal retrofit. The largest sectors are: Business and Professional Services, Electrical Industrial Equipment, and Scientific and Controlling Equipment. Together these account for 48.0% of expenditures. The direct expenditures associated with these sectors are estimated to generate 15 of the total of 29 new jobs.

Total Impacts

The $1.1 million in direct regional construction expenditures associated with the MCWM Technology will circulate throughout the economy stimulating additional economic activity. Indirect expenditures of $176,500 will be generated, creating 3 new jobs. Furthermore, $398,900 in induced expenditures will create 9 additional jobs. Total regional impacts associated with the MCWM coal retrofit are expected to be $1,678,600 in total output, an overall regional increase of 0.015%. The output multiplier is 1.53 ($1,678,600/$1,100,000), which means that indirect and induced benefits are expected to be 53% of direct expenditures. The corresponding increase in

Table 6-9. Direct Construction Expenditures

MCWM Technology

Sector	Total Direct Expenditures	Regional Direct Expenditures
Business and Professional Services	$988,519	$402,414
Scientific Controlling Equipment	$318,274	$91,981
Electrical Industrial Equipment	$158,524	$67,389
Transportation Services	$51,420	$17,210
Materials Handling Machinergy	$12,322	$8,195
Other Fabricated Metal Production	$70,240	$4,889
Fabricated Plate Work	$272,100	$2,639
Stone and Clay Products	$78,518	$58
Primary Iron and Steel Manufacturing	$13,772	$28
Paints and Allied Products	$1,925	$6
Prefabricated Metal Buildings	$16,030	$0
General and Industrial Machinergy	$213,017	$0
Pumps and Compressors	$69,728	$0
Construction Laboor and Management	$1,074,436	$505,500 [a]
Taxes	$328,599	$0
Totals	$3,667,154	$1,100,309

DMC Technology

Sector	Total Direct Expenditures	Regional Direct Expenditures
Business and Professional Services	$1,409,899	$572,911
Electrical Industrial Equipment	$238,418	$101,352
Scientific and Controlling Equipment	$295,168	$85,304
Mining Machinery	$261,847	$29,144
Materials Handling Machinery	$43,713	$29,074
Transportation Services	$72,036	$24,110
Other Fabricated Metal Production	$50,833	$3,538
Fabricated Plate Work	$305,562	$2,964
Stone and Clay Products	$76,529	$69
Blast Furnaces and Steel Mills	$13,796	$28
Paints and Allied Products	$846	$3
General Industrial Machinery	$287,180	$0
Prefabricated Metal Buildings	$123,199	$0
Pumps and Compressors	$28,465	$0
Construction Labor and Management	$1,538,638	$724,000 [a]
Taxes and Permits	$468,702	$0
Totals	$5,214,831	$1,572,497

[a] Expenditures here are distributed over all sectors in the region in impact analysis

employment is 33 new jobs, an increase of 0.018%. The employment multiplier is 1.65 (33/20).

Table 6-10 shows the total impacts associated with the MCWM coal retrofit. Sectors which display the greatest total impacts on the region are: Business and Professional Services, Real Estate and Rental, Wholesale and Retail Trade, and Health, Education, and Social Services. Together they account for $1,083,700 of the total change in output (or 64%). Furthermore, 22 of the total of 33 new jobs are created by these sectors.

The $1.5 million in direct regional construction expenditures associated with the DMC Technology will stimulate additional economic activity throughout the region. Indirect expenditures of $255,700 will be generated creating 5 new jobs. In addition induced expenditures of $569,600 will be generated creating 13 jobs. Total impacts associated with the DMC retrofit is expected to be $2,400,400 in total output, an overall regional increase of 0.002%. The output multiplier is calculated to be 1.60 ($2,400,400/$1,500,000). Once again this means that indirect and induced benefits are expected to be about 60% of direct expenditures. The total number of new jobs created is 47, so the employment multiplier is 1.62 (47/29).

Table 6-10 also shows the total impacts associated with the DMC coal retrofit. The largest impacts are to be felt in the following sectors: Business and Professional Services, Real Estate and Rental, Wholesale and Retail Trade, and Health, Education, and Social Services. Together they account for $1,548,200 of the total change in output (or 64%),as well as 31 out of the 47 new jobs associated with these sectors.

Scaling The Results

The basic economic impacts from a single boiler retrofit can be used to evaluate impacts on a broader scale. Considering the Crane retrofit as a base case, impacts from a scenario considering five Crane equivalents and another considering fifty Crane equivalents can be estimated. Table 6-11 lists total change in output and employment for both technologies at each scale considered. Note that at 50-equivalent scale-up, the employment impacts would be very significant, amounting to a 0.9% increase in the region in the MCWMs case and a 1.4% increase in the DMC case.

It should be noted that since the base case scenario is based on the nine-county Crane Region, larger scale-ups will continue to reflect economic conditions affecting the nine-county Crane Region, where the overall average regional purchase coefficient is 0.3. Thus, regions that have higher RPCs would experience greater impacts. There is, of course, the possibility that a large construction effort would attract proportionally more direct and indirect suppliers into the region, thereby raising the RPCs and the overall impacts. Such "agglomeration" effects are not uncommon. Lastly, it should once again be noted that these impacts only consider capital costs and not the operating costs of the retrofit, which would obviously add to the impacts.

Conclusion

By developing either of the MCWM or DMC technologies at the Crane Naval Surface Warfare Center, the surrounding nine-county Crane Region economy will be stimulated and will

Table 6-10. Total Impacts

MCWM Technology

Sector	Total Change in Output	Total Change in Employment
Business and Professional Services	$483,100	10.98
Real Estate and Rental	$212,800	0.50
Wholesale and Retail Trade	$211,600	6.70
Health, Educ., Soc. Services	$176,200	3.69
Scientific Controlling Equipment	$95,300	1.30
Finance and Insurance	$72,400	1.26
Electrical Industrial Equipment	$69,200	1.00
Transportation Services	$38,200	0.96
Hotels, Personal Services	$35,400	1.35
Repair and Maintenance	$26,600	0.57
Eating and Drinking	$18,500	1.24
Subtotal of top sectors	$1,439,300	29.55
Totals	$1,678,600	33.04

DMC Technology

Sector	Total Change in Output	Total Change in Employment
Business and Professional Services	$688,200	15.69
Real Estate and Rental	$304,600	0.71
Wholesale and Retail Trade	$303,300	9.58
Health, Educ., Soc. Services	$252,100	5.25
Electrical Industrial Equipment	$104,500	1.51
Finance and Insurance	$103,500	1.81
Scientific and Controlling Equipment	$89,900	1.22
Transportation Services	$54,700	1.35
Hotels, Personal Services	$50,500	1.98
Repair and maintenance	$38,600	0.82
Eating and Drinking	$26,400	1.77
Subtotals of top sectors	$2,016,300	41.69
Totals	2,400,400	47.21

Table 6-11. Total Impacts at Various Scales

Scale	MCWM		DMC	
	Total Change in Output	Total Change in Employment	Total Change in Output	Total change in Employment
Base Case Crane	$1,678,600	33	$2,400,400	47
5 Crane Equivalents	$8,393,000	165	$12,002,000	235
50 Crane Equivalents	$83,930,000	1650	$120,020,000	2350

show changes in total output and employment. This creation of jobs and increased output is obviously of concern to both those directly and indirectly associated with the developing technology within the regions where it may be implemented.

By obtaining construction estimates and with the use of IMPLAN, regional impacts have been estimated. Of course, these impacts only represent part of the whole picture because of the lack of operating costs at the time of this writing. Nevertheless, the expenditures show an increase of 47 new jobs for the DMC technology and 33 for the MCWM technology. Corresponding increases in output are $2,400,400 and $1,678,600 respectively. More important are the potential impacts that these technologies may have if implemented on a much broader scale. In the case where 50 Crane Case equivalents are considered, 2,350 new jobs associated with the DMC technology are estimated and 1,650 new jobs for the MCWM technology. Corresponding increases in output are $120,020,000 and $83,930,000 respectively. All in all, the potential for economic growth as a result of the implementation of either technology is significant.
Finally, some caveats are noted with regard to the model used in this section. The nine-county Crane Region I-O table is based on 1990 technology and industrial structure. It also allows for only limited substitution of inputs and assumes perfectly elastic supply curves for all primary factors and intermediate goods. Still, these assumptions are not likely to pose any serious limitations with respect to estimating the impacts of a single boiler retrofit or a five-unit scale up. The capital inputs required would not lead to supply bottlenecks that would cause prices to rise and spur substitution among various inputs. Technologies, other than the boilers in question, are not likely to change much between 1990 and 1994, nor are they likely to change in any relevant way in any of the scenarios. The fifty-unit scale up might be somewhat more problematic, and the results here should be taken as a linear approximation of the possible impacts. Still, even this deviation is muted by the likelihood that all fifty units would not be constructed in one year, but phased over a number of years, thereby limiting bottlenecks in this case as well. In general, the I-O methodology is adequate to the task of generating reasonably accurate assessments of the impact of a modest number of boiler retrofits, such as when the number of sites is limited to military installations.

6.7 Integrated Analysis

The integration of economic research for Phase I began at the design stage. In essence, a case study of a single site was performed. Data was utilized on technology design and cost from other members of the Project Team for the DMC and MCWM installations at the Crane Center. The individual activities for engineering design and cost/economic analysis utilized a common set of parameters and assumptions relating to this site.

Members of the Mineral Economics Team visited the site to collect data and gain perspective on this focal point. In addition to the primary data collected and site-specific data gleaned from other members of the Project Team and from the literature, state and national data was adapted to the Crane site.

Below are summaries of the activities, including some generalization of the results:

Identify Appropriate Cost-Estimating Methodologies

- Standard economic concepts of investment appraisal must be used.
- Use of standard techniques (e.g., regression, linear programming, and Monte Carlo Simulations) of data analysis is desirable.
- Rules of thumb for generating rough estimates of input costs of standard economic concepts of investment and analysis are available but tricky to use.
- A more formal linear programming, Monte Carlo Simulation approach is preferable (one was developed and employed).

Estimate Basic Costs of New Technologies

- The capital cost (preliminary) to retrofit the Crane boiler to fire MCWM is $3.67 million or $147,000/MM Btu. The final capital cost was $2.89 million or $116,000/MM Btu.
- The capital cost (preliminary) to retrofit the Crane boiler to fire DMC is $5.21 million or $209,000/MM Btu. The final capital cost was $3.23 million or 130,000/MM Btu.
- The differential fuel cost of DMC and MCWM can be large and varies greatly depending upon demand levels (see below). The result is that at a 4% discount factor over a seven-year payback period, the DMC retrofit technology enjoys almost a $2 million (1993$) net present value advantage in fuel costs relative to MCWM. This provides DMC with a total $0.5 million cost advantage over the MCWM.
- The MCWM retrofit technology is the least cost alternative, when considering cost of fuels alone, when discount rates are increased, or demand levels are increased. At a demand level equivalent to ten Crane boilers and at 4% discount rate, the net present value advantage to firing DMC for any individual boiler falls to $314,000. MCWM then has a $1.2 million total cost advantage over DMC for the Crane Site. A fifty Crane boiler demand level and four percent discount rate increases MCWM's cost advantage over DMC to $1.4 million.
- Coal for preparing DMC is readily available from existing market sources for delivery by coal truck to a boiler site. Its price and availability would be set and would fluctuate closely with conditions in the general coal market.
- Fuel for MCWM is not currently available from market sources at a large scale. Its supply would not be as closely linked to the general coal market and is likely to be set according to a 'cost plus fee' contract.
- Fuel cost, as delivered to a DMC retrofitted boiler, is estimated to be $1.25/MM Btu which includes transportation charges of $0.138 to $0.171/MM Btu.
- Costs for preparation of MCWM were estimated at $3.23/MM Btu (f.o.b. preparation plant) for just the one Crane boiler. However, economies of scale exist for MCWM production that would significantly lower its per unit cost. MCWM preparation costs drop to $0.67/MM Btu (f.o.b. preparation plant) at an annual demand equivalent to fifty Crane boilers, or only a few (larger) industrial/commercial boilers.
- Current estimates for transportation costs of MCWM vary from $0.87 to $1.45/MM Btu. The difference in transportation costs is due to the use of 'special' tank trucks instead of conventional coal trucks.

Process Analysis of MCWM and DMC

- The variables that most strongly influence the economic feasibility of retrofitting to fire MCWM or DMC are the differential fuel cost (DFC), the expected life of the boiler plant, its size (or capacity), total capital requirement (TCR), boiler derated capacity (BDC), boiler use, and the discount rate.
- With respect to direct capital and operating cost considerations, *new* DMC and MCWM technology for industrial boilers are economically not viable. Viability improves with increases in DFC, expected boiler life, boiler use, and BDC. Viability also improves with decreases in the discount rate and TCR.
- With respect to direct capital and operating cost considerations, retrofit MCWM and DMC

technology boilers are not economically viable. MCWM retrofits become viable with economies of scale in fuel preparation (e.g., at 10 Crane size equivalents). The viability of ***retrofit*** DMC technology is uncertain due to the high TCR involved. Viability improves with increases in DFC, expected boiler life, boiler use, and BDC. Viability also improves with decreases in the discount rate and TCR. In the case of MCWM, viability can go both ways with variation in BDC.

- A sensitivity analysis showed that the DFC has the most influence on the analyses. A DFC of at least $1.50 is preferred for MCWM.
- It is important to note that there are several uncertainties in an analysis of this kind. The major uncertainty has to deal with fuel price projections. The next major uncertainty is with the boiler load factor or boiler derated capacity. The true BDC and other performance data can only be obtained in actual plant practice, however the model developed in this permits a sensitivity analysis varying BDC.
- For economic viability in retrofitting, the benefits must significantly and substantially outweigh the costs. The question of a widespread retrofitting is still one of economics. The main concern is the impact of oil prices on DFC and consequently on the economics of retrofitting. This is due to the fact that the cost savings in retrofitting is almost entirely made up of fuel cost savings.

Analyze/Identify Transportation Cost of Commercial Sources of MCWM and Cleaned Coal for Dry, Micronized Coal Production

- Transportation cost is the major inhibiting factor to the economic viability of MCWM technology. DMC delivered fuel costs are insensitive to fuel demand level.
- Transportation costs can also be improved by developing a lower cost system of transportation dedicated solely to coal.

Determine Community Spillovers

Nature of the Task

- Associated with extraction and use of coal are externalities and emissions now recognized as hazardous, detrimental to the environment, or unpleasant to live by.
- Among the predominant fossil fuels - oil, coal, and natural gas - coal is recognized as the most harmful to the environment.
- This activity reviews the environmental damage associated with coal and the Federal and Indiana state regulations governing its use.

Findings

Coal Mining and Processing

- Mineral deposits are fixed and mining can only occur where a deposit already exists. Mines cannot be uniformly designed and consistently located in unobjectionable and "environmentally safe" areas.
- Types of damage include destruction of the landscape (including subsidence and erosion), degradation of the visual environment, disturbance of water courses and sedimentation, acid mine drainage, damage to or destruction of agricultural, forest, or recreational lands, noise pollution, fugitive dust and coal fines, truck traffic, vibration from blasting and air blasts, tailings disposal, mining accidents and health hazards, and burning refuse banks and abandoned-mines fires.
- Regulation of mining is a patchwork and uneven affair. Both federal and state regulations exist, involving many different agencies and significant overlap.
- Federal agencies whose jurisdictions can involve mining include The Bureau of Land Management, The Forest Service, The Office of Surface Mining, The National Parks Service, The Bureau of Indian Affairs, The Bureau of Reclamation, The Fish and Wildlife Service, and The Environmental Protection Agency.
- Applicable regulations include The Safe Drinking Water Act, The Clean Air Act, The Toxic Substances Control Act, The National Environmental Policy Act, The Comprehensive Environmental Liability Act and The Superfund Amendments and

Reauthorization Act, The Clean Water Act, The Resources Conservation and Recovery Act, and The Surface Mine Control and Reclamation Act.

- Compliance and effectiveness depends on not only on the nature and existence of environmental regulations but also on their enforcement.
- The largest fraction of environmental costs expended during a mining project are for reclamation.

Coal Transportation

- All stages of coal transport - loading, en route, and unloading - involve some environmental impacts. The effects are felt by 'natural' systems such as agriculture, forests, and waterways, by humans, and by structures and installations.
- Environmental damage assessments for coal transport in general are incomplete and not well known. All estimates are subject to substantial inaccuracies.

Coal Combustion

- The most notable environmental impacts associated with coal combustion are the emission of air pollutants and the creation of ash waste which requires disposal.
- Air emissions associated with coal combustion include sulfur oxides, nitrogen oxides, carbon monoxide, carbon dioxide, particulates, volatile organic compounds, polycyclic aromatic hydrocarbons, trace metals and radionuclides.
- Associated with these emissions are acid rain, urban smog, ozone, global climate change, and a variety of pulmonary and respiratory diseases.
- Most recent Federal legislation concerning emissions is the Clean Air Act amendments of 1990. It includes marketable permits and performance standards and regulates particulates, ozone, VOCs, NO_x, air toxics, NO, and sulfur dioxides.
- Solid wastes associated with coal combustion are fly ash, bottom ash, slag, and scrubber sludge. All are disposed on land. Some are classified as hazardous materials.
- Data from one study found no major environmental effects from the disposal of coal combustion wastes.

Summary

- Most detrimental impacts occur during combustion.
- Many of the environmental costs associated with coal use are not included in the market price of the fuel, although more are internalized now than prior to the environmental legislation of the 1970s, 1980s, and 1990s.
- Most single industrial boilers will be able to meet federal and state regulations with standard pollution control devices.

Regional Market Considerations and Impacts

- A number of excellent methodologies exist for determining the total regional economic impacts of new coal combustion technologies. An input-output (I-O) model is adequate to the task of estimating the impacts of a small number of retrofits. A computable general equilibrium (CGE) model is best-suited for analysis of the impacts of widespread technology adoption and to simulate the impacts of major policies affecting coal.
- An independent verification of the U.S. Government's Impact Analysis for Planning (IMPLAN) Modeling System indicated the database and input-output model construction methodology were sufficiently accurate to be reliable for small region impact analyses.
- A Pennsylvania Computable General Equilibrium Model, incorporating several advances relating to energy use, regional accounts, and factor mobility was developed.
- A case study was undertaken of the total regional economic impacts of boiler retrofits at the Crane (Indiana) Naval Surface Warfare Center and surrounding areas. The major findings are:
    - Only about 30% of the total capital expenditures for both MCWM and DMC technologies are used to purchase inputs within the nine-county Crane Region. The three major sectors most directly affected by these purchases are Business and Professional Services, Scientific Controlling Equipment, and Electrical Industrial Equipment. These three sectors comprise about 50% of direct local

expenditures for each technology.

- The total output multiplier impact for the MCWM technology was 1.53 of the direct regional expenditures, and for the DMC technology was 1.60 of the direct regional expenditures. These multiplier ratios would not vary with scale.
- The sectors most greatly impacted indirectly are Real Estate and Rental, Wholesale and Retail Trade, and Health/Education/Social Services.
- Employment impacts of individual boiler retrofits are trivial. However, for the case of 50 retrofits, there is the potential for the MCWM technology to generate 1,650 jobs and for the DMC technology to generate 2,350 jobs. These would represent 0.9% and 1.4%, respectively, of the Crane Region's employment base. This would mean a decrease in unemployment of 15% and 20%, respectively.
- The military can enhance the local impacts by making greater efforts to purchase local inputs.

7.0 REFERENCES

1. Schanche, G., Personal communication, DOD/DOE Coal Utilization Project Meeting No.1, Pittsburgh, Pennsylvania, October 23, 1992.

2. PON, Program Opportunity Notice for Superclean Coal Water Slurry (SCCWS) Combustion Testing in Oil-Designed Industrial Boilers, PON No. DE-PS22-88PC88697, 1989, U.S. Department of Energy, Pittsburgh Energy Technology Center.

3. Miller, B. G., Scaroni, A. W., Britton, S. A., Clark, D. A., Morrison, J. L., Pisupati, S. V., Poe, R. L., Walsh, P. M., Wincek, R. T., Xie, J., Patel, R., Thornock, D. and Borio, R., Coal-Water Slurry Fuel Combustion Testing in an Oil-Fired Industrial Boiler, Final Report, U.S. Department of Energy, Federal Energy Technology Center, No. DE-FC22-89PC88697, December 20, 1996.

4. RFP, Request for Proposal (RFP) for Development and Testing a High Efficiency Advanced Coal Combustor, RFP No. DE-RP22-90PC90162, 1990, U.S. Department of Energy, Pittsburgh Energy Technology Center.

5. Patel, R. L., Borio, R., Scaroni, A. W., Miller, B. G. and McGowan, J. G., Development and Testing of a High Efficiency Advanced Coal Combustor Phase III Industrial Boiler Retrofit, Proof of Concept Testing Summary (Task 3.0), U.S. Department of Energy, Pittsburgh Energy Technology Center, No. DE-AC22-91PC91160, March 1995.

6. Miller, B. G., Scaroni, A. W., Hogg, R., Chander, S., Ityokumbul, M. T., Klima, M. S., Luckie, P. T., Rose, A., Considine, T. J., Gordon, R. L., McClain, K., Walsh, P. M., Painter, P. C., Rini, M. J., Jha, M., Morrison, D., Melick, T. and Sommer, T. M., The Development of Coal-Based Technologies for Department of Defense Facilities, Semiannual Technical Progress Report for the Period 09/28/1992 to 03/27/1993, DOE/PETC, No. DE-FC22-92PC92162, May 13, 1993.

7. Miller, B. G., Morrison, J. L., Sharifi, R., Shepard, J. F., Scaroni, A. W., Hogg, R., Chander, S., Ityokumbul, M. T., Klima, M. S., Luckie, P. T., Rose, A., Addy, S., Considine, T. J., Gordon, R. L., McClain, K., Walsh, P. M., Xie, J., Painter, P. C., Veytsman, B., Rini, M. J., Jha, M., Morrison, D., Melick, A. and Sommer, T. M., The Development of Coal-Based Technologies for Department of Defense Facilities, Interim Report for the Period 03/27/1993 to 07/30/1993, DOE/PETC, No. DE-FC22-92PC92162, September 24, 1993.

8. Gottfried, B. S., Luckie, P. T. and Tierney, J. W., Computer Simulation of Coal

Preparation Plants, Final Report, Department of Energy, No. PC/30144-T7, 1982.

9. Klima, M. S. and Killmeyer, R. P., Baseline Performance Evaluation of Micronized-Magnetite Cycloning, Topical Report, Department of Energy, No. DOE/PETC/TR-91/9, 1991.

10. Mengelers, J., The Influence of Cyclone Diameter on Separating Performance and Economy, *Ninth Int. Coal Prep. Cong.*, New Delhi, India, 1982, pp. 1-10.

11. King, R. P. and Juckes, A. H., Cleaning of Fine Coals by Dense-Medium Cyclones, Powder Technology, 40, pp. 147-160, 1984.

12. Chedgy, D. G., Watters, L. A. and Higgins, S. T., Heavy-Media Cyclone Separations at Ultralow Specific Gravity, *Tenth Int. Coal Prep. Cong.*, Edmonton, Alberta, Canada, 1986, pp. 60-79.

13. He, Y. B. and Laskowski, J. S., Effect of Dense Medium Properties on the Separation Performance of a Dense-Medium Cyclone, Minerals Engineering, 7, pp. 209-221, 1994.

14. Davis, J. J. and Napier-Munn, J. T., The influence of Medium Viscosity on the Performance of Dense Medium Cyclones in Coal Preparation, *Third Int. Conf. on Hydrocyclones*, Oxford, 1987, pp. 1155-1165.

15. Austin, L. G., Lee, C. H., Concha, F. and Luckie, P. T., Hindered Settling and Classification Partition Curves, *Minerals and Metallurgical Proc. 9*, 1992, 4, pp. 161-168.

16. Cho, H. and Klima, M. S., Application of a Batch Hindered-Settling Model to Dense-Medium Separations, Coal Prep, 14, pp. 166-184, 1994.

17. Lee, C. H., Modeling of Batch Hindered Settling, Ph.D. Thesis, 1989, Pennsylvania State University.

18. Zanker, A., Hydrocyclones: Dimensions and Performance, Chem. Eng., 84, pp. 122-125, 1977.

19. Schubert, H. and Neesse, T., The Role of Turbulence in Wet Classification, *10th Int. Min. Proc. Cong.*, London, 1973, pp. 213-240.

20. Klima, M. S. and Luckie, P. T., Use of an Unsteady-State Pulp Partition Model to Investigate Multiple Variable Interactions, Coal Prep., 8, pp. 185-193, 1990.

21. Walker, M. S., Devernoe, A. L. and Urbanski, W. S., Separation of Non-Magnetic Minerals using Magnetic Fluids in a Flow-Through MHS Rotor, *Trans. SME-AIME*, 1990, 288, pp. 209-214.

22. Dowling, E. C., Klimpel, R. R. and Aplan, F. F., Model Discrimination in the Flotation of a Porphyry Copper Ore, *Minerals and Metallurgical Processing*, 1985, 2, pp. 87-101.

23. Huber-Panu, I., Ene-Danalache, E. and Cojocariu, D. G., *Mathematical Models of Batch and Continuous Flotation,* in "A.M. Gaudin Memorial Volume", ed., 1976, New York, pp. 675-724.

24. Klimpel, R. R., *Selection or Chemical Reagents for Flotation,* in "Mineral Processing Plant Design", Mular, A. L. and Bhappu, R. B., ed., 1980, AIME: New York, pp. 907-934.

25. Meyer, W. C. and Klimpel, R. R., Rate Limitations in Froth Flotation, *Trans. AIME*, 1984, 274, pp. 1852-1858.

26. Diao, J., Fuerstenau, D. W. and Hanson, J. S., Kinetics of Coal Flotation, *SME-AIME Annual Meeting*, Pheonix, Arizona, 1992, pp. 92-200.

27. Lay, W. C. and Bell, G. M., *Analysis of Operating Flotation Plants,* in "Froth Flotation", ed., 1962, AIME: New York.

28. Rastogi, R. C. and Aplan, F. F., Coal Flotation as a Rate Process, *Trans, AIME*, 1985, 2, pp. 137-145.

29. Gahl, R., History of the Flotation Process at Inspiration, *Trans. AIME*, 1916, 55, pp. 576-630.

30. Anon, Flotation Column Due for Mill Tests in Canada, *Eng. Min*, 1965, 166, pp. 76-80.

31. Dobby, G. S. and Finch, J. A., Flotation Column Scale-up and Modelling, CIM Bull, 78, pp. 89-96, 1986.

32. Bensley, C. N., Roberts, T. and Nicol, S. K., Column Flotation for the Treatment of Fine Coal, *Proc. 3rd. Australian Coal Prep. Conf.*, Wollonong, New South Wales, 1985, pp. 18-21.

33. Luttrel, G. H., Weber, A. T., Adel, G. T. and Yoon, R. H., Microbubble Flotation of Fine Coal, *Column Flotation '88*, Littleton, Colorado, 1988, 21, pp. 205-211.

34. Parekh, B. K., Bland, A. E., Groppo, J. G. and Yingling, J., A Parametric Study of Column Flotation For Fine Coal Cleaning, Coal Prep., 8, pp. 49-60, 1990.

35. Ityokumbul, M. T., A New Modelling Approach to Flotation Column Design, Minerals Engineering, 5, pp. 585-595, 1992.

36. Ityokumbul, M. T., A Mass Transfer Approach to Flotation Column Design, Chem. Eng. Sci., 47, pp. 3605-3612, 1992.

37. Mills, P. J. T. and O'Connor, C. T., The Modelling of Liquid and Solids Mixing in a Flotation Column, Minerals Engineering, 3, pp. 567-576, 1990.

38. Mills, P. J. T., Yiannatos, J. B. and O'Connor, C. T., The Mixing Characteristics of Solid and Liquid Phases in a Flotation Column, Minerals Engineering, 5, pp. 1195-1205, 1992.

39. Xu, M. and Finch, J. A., Solids Mixing in the Collection Zone of Flotation Columns, Minerals Engineering, 5, pp. 1029-1039, 1992.

40. Ityokumbul, M. T., A Gaussian-Convection Model for Solid Dispersion in Slurry Bubble Columns, Chem. Eng. Process, 31, pp. 321-325, 1992.

41. Espinosa-Gomez, R., Johnson, N. W., Pease, J. D. and Munro, P. D., The Commissioning of the First Flotation Column at Mount Isa Mine Limited, 1989, Oxford: Pergamon Press, pp. 293-302.

42. Ityokumbul, M. T., Selection of Recovery Zone Height in Flotation Column Design, Chem. Eng. Process, 32, pp. 87-92, 1993.

43. Xu, M. and Finch, J. A., Effect of Sparger Surface Area on Bubble Diameter in Flotation Columns, Can. Metall. Quart, 28, pp. 1-6, 1990.

44. Ityokumbul, M. T., Maximum Gas Velocity in Column Flotation, Minerals Engineering, 6, pp. 1279-1286, 1993.

45. Raymond, D. R. and Zieminski, S. A., Mass Transfer and Drag Coefficients on Bubbles Rising in Dilute Aqueous Solutions, *AIChE J.*, 1971, 17, p. 57.

46. Ityokumbul, M. T., Salama, A. I. A. and Al Taweel, A. M., Estimation of Bubble Size in Flotation Columns,, *Minerals Engineering '95*, Lake Tahoe, Nevada, 1994, pp. 26-28.

47. Mehrotra, V. P., Sastry, K. V. S. and Morey, W. B., Review of Oil Agglomeration Techniques for Processing of Fine Coals, *Int. J. of Min. Proc.*, 1983, 11, (3), pp. 175-201.

48. Capes, C. E., Hazlett, J. D. and Ignasiak, B. L., Novel Application of Oil Agglomeration Technology for Coal Preparation, Upgrading of Low Quality Fuels and Environmental Clean-up, *Eleventh Int. Coal Prep. Cong.*, Tokyo, Japan, 1990, pp. 22-25.

49. Pawlak, W., Szymocha, K., Briker, Y. and Ignasiak, B., High-Sulfur Coal Upgrading by Improved Oil Agglomeration, *Third Int. Conf. on Proc. and Util. of High-Sulfur Coals*, Ames, Iowa, 1989.

50. Simmons, F. J. and Keller, D. V., Two Ton-Per-Day Production Otisca T-Process Ultra-Clean Coal/Water Slurry, *Tenth Int. Coal Prep. Cong.*, Canada, 1986.

51. Wei, D., Chander, S. and Hogg, R., Distribution of Wettability of Coal, Coal Preparation, 10, pp. 37-45, 1992.

52. Satoh, Experimental Study on Coal Water Slurry Preparation With a 26 T/H Scale Facility, *Proc. 13th Int. Conf. on Coal & Slurry Tech.*, Denver, Colorado, 1988, pp. 57-68.

53. Miller, B. G., Morrison, J. L., Sharifi, R., Shepard, J. F., Scaroni, A. W., Hogg, R., Chander, S., Cho, H., Ityokumbul, M. T., Klima, M. S., Luckie, P. T., Rose, A., Addy, S., Considine, T. J., Gordon, R. L., McClain, K., Schaal, A. M., Walsh, P. M., Xie, J., Painter, P. C., Veytsman, B., Rini, M. J., Jha, M., Morrison, D., Melick, T. and Sommer, T. M., The Development of Coal-Based Technologies for Department of Defense Facilities, Semiannual Technical Progress Report for the Period 03/28/1993 to 09/27/1993, DOE/PETC, No. DE-FC22-92PC92162, December 17, 1993.

54. Cross, M., Prediction of the Voidage of Packed Beds, *Agglomeration '85 Proceedings of the 4th International Symposium on Agglomeration*, Toronto, Canada, 1985.

55. Tangsathitkulchai, C., The Effect of Slurry Density and Rheology on Wet Grinding Characteristics in a Tumbling Ball Mill, Ph.D. thesis, 1986, Pennsylvania State University.

56. Klimpel, R. R., Laboratory Studies of the Grinding and Rheology of Coal-Waters Slurries, Powder Technology, 32, pp. 267-277, 1982.

57. Henderson, C. B. and Scheffee, R. S., The Optimum Particle-Size Distribution of Coal for Coal-Water Slurries, *Am. Chem. Soc.*, 1983, 28, pp. 1-11.

58. Link, T., Killmeyer, R. P., Elstrodt, R. and Haden, N., Initial Study of Dry Ultrafine Coal Benefication Utilizing Triboelectrostatic Charging with Subsequent Electrostatic Separation, Topical Report, Department of Energy, No. DOE/PETC/TR-90/11, 1990.

59. Guichard, J. C., *Aerosol Generating Using Fluidized Beds,* in "Fine Particles: Aerosol Generation, Measurement, Sampling, and Analysis", Liu, B. Y. H., ed., 1976, Academic Press: Minneapolis, Minnesota, pp. 173-193.

60. Willeke, K., Lo, C. S. K. and Whitby, K. T., Particulate Dispersion by Means of a Fluidized Bed, *Aerosol Science*, 1974, 5, p. 449.

61. Marple, V. A., Liu, B. Y. H. and Rubow, K. L., A Dust Generator for Laboratory Use, *Am. Ind. Hyg. Assoc. J.*, 1978, 39, pp. 26-32.

62. Furnas, C. C., Grading Aggregates, I-Mathematical Relations for Beds of Broken Solids of Maximum Density, Ind. Eng. Chem., 23, pp. 1052-1058, 1931.

63. Cumberland, D. J. and Crawford, R. J., The Packing of Particles, 1987, Amsterdam: Elsevier.

64. Skolnik, E. G., Scheffee, R. S. and Henderson, C. B., Effect of Particle Size Distribution on Viscosity of Coal Water Fuels, *Proc. of the 8th Int. Symp. on Coal Slurry Fuels Prep. and Util.*, Orlando, Florida, 1986, pp. 25-36.

65. Sadler, L. Y. and Sim, K. G., Minimize Solid-Liquid Mixture Viscosity By Optimizing Particle Size Distribution, Chemical Engineering Progress, pp. 68-71, 1991.

66. Hussaini, M. Y., Kumar, A. and Voigt, R. G., Major Research Topics in Combustion, 1992, New York: Springer-Verlag Inc.

67. Miller, B. G., Morrison, J. L., Sharifi, R., Shepard, J. F., Scaroni, A. W., Hogg, R., Chander, S., Cho, H., Ityokumbul, M. T., Klima, M. S., Luckie, P. T., Rose, A., Addy, S., Considine, T. J., Gordon, R. L., Lazo, J., Li, P. C., McClain, K., Schaal, A. M., Szczesniak, P., Walsh, P. M., Xie, J., Painter, P. C., Veytsman, B., Morrison, D., Englehardt, D. and Sommer, T. M., The Development of Coal-Based Technologies for Department of Defense Facilities, Semiannual Technical Progress Report for the Period 09/28/1993 to 03/27/1994, DOE/PETC, No. DE-FC22-92PC92162, November 30, 1994.

68. Miller, B. G., Bartley, D. A., Hatcher, P., Knicker, H., McConnie, J., Moulton, B., Morrison, J. L., Pisupati, S. V., Poe, R. L., Sharifi, R., Shepard, J. F., Xie, J., Xu, G., Scaroni, A. W., Hogg, R., Chander, S., Cho, H., Ityokumbul, M. T., Klima, M. S., Luckie, P. T., Rose, A., Addy, S., Chidley, P., Considine, T. J., Gordon, R. L., Harley, K., Jung, G. C., Kocagil, A. E., Lazo, J., Li, P. C., McClain, K., Schaal, A. M., Painter, P. C., Veytsman, B., Morrison, D., Englehardt, D. and Sommer, T. M., The Development of Coal-Based Technologies for Department of Defense Facilities, Semiannual Technical Progress Report for the Period 09/28/1994 to 03/27/1995, DOE/PETC, No. DE-FC22-92PC92162, October 15, 1996.

69. Schack, A., The Theory and Application of the Suction Pyrometer, *Journal of the Institute of Fuel*, 1939, 12, pp. S30-S38.

70. Mullikin, H. F., *Gas-Temperature Measurement and the High-Velocity Thermocouple,* in "Temperature: Its Measurement and Control in Science and Industry", Standards, American Institute of Physics with National Bureau of Standards, ed., 1941, Reinhold Publishing Corp.: New York, pp. 775-829.

71. Mullikin, H. F. and Osborn, W. J., *Accuracy Tests of the High-Velocity Thermocouple,* in "Temperature: Its Measurement and Control In Science and Industry", Standards, American

Institute of Physics with National Bureau of Standards, ed., 1941, Reinhold Publishing Corp: New York, pp. 805-829.

72. Marsh, J. S., *Significance of Air Temperature in Open Hearth Operation,* in "American Iron and Steel Institute, Year Book", ed., 1951, pp. 185-207.

73. Barber, R., Jackson, R., Land, T. and Thurlow, G. G., A Suction Pyrometer for Measuring Gas Exit Temperatures from the Combustion Chambers of Water-tube boilers, *Journal of Institute of Fuel,* 1954, pp. 408-416.

74. Land, T., Suction Pyrometry, Instrumentation and Automation, 29, pp. 1314-1317, 1956.

75. Gupta, A. K., Lilly, D. G. and Syred, N., Swirl Flows, 1984, ABACUS Press.

76. Levenspiel, O., Chemical Reaction Engineering, 1962, New York, New York: Wiley.

77. Palmer, H. B. and Beer, J. M., Combustion Technology: Some Modern Developments, 1974, New York and London: Academic Press.

78. Rao, S. T. R., Aerodynamics of Incinerator Combustion Process: Experimental Determination of Stirring Factors in Isothermal Combustion Chamber Models, 1970, The Pennsylvania State University.

79. Rao, S. T. R., Kuo, T. J. and Essenhigh, R. H., Combustion and Emission Phenomena in Incinerators: Characterization of Stirring Factors by Cold Model Simulation, *4th National Incinerator Conference, ASME,* 1970.

80. Rao, S. T. R. and Essenhigh, R. H., Experimental Determination of Stirring Factors Generated by Straight and Swirling Jets in Isothermal Combustion Chamber Models, *Thirteenth Symp. (Int.) on Combustion, The Combustion Institute,*, Pittsburgh, Pennsylvania, 1971, pp. 603-615.

81. Beer, J. M. and Chigier, N. A., Combustion Aerodynamics, 1972, London: John Wiley and Sons.

82. Holve, D. J. and Self, S. A., An Optical Particle Sizing Counter for In Situ Measurements; Parts I and II., *Journal of Apllied Optics,* 1979, 18, (10), pp. 1632-1652.

83. Holve, D. J., In Situ Optical Particle Sizing Technique, *Journal of Energy,* 1980, 4, (4), pp. 176-183.

84. Holve, D. J., Transit Timing Velocimetry (TTV) for Two Phase Reacting Flows, *Combustion and Flame,* 1982, 48, pp. 105-108.

85. Holve, D. J., In Situ Measurements of Flyash Formation from Pulverized Coal, *Combust. Sci. and Tech.*, 1986, 44, pp. 269-288.

86. Sharifi, R., Miller Falcone, S., Scaroni, A. W., Koopmann, G. H. and Chen, W., In Situ Monitoring of the Acoustic Agglomeration of Fly Ash Particles, *ASME Cogen Turbo Power Conference*, Portland, Oregon, 1994.

87. Sharifi, R. and Scaroni, A. W., Comparative Analysis of Two Commercial, Low NOx Pulverized Coal Swirl Burners, *Joint Technical Meeting April 23-26,* San Antonio, Texas, 1995.

88. Whaley, H. and Whalen, P., Burner Nozzle Wear During Coal-Oil Mixture (COM) Combustion Trials in a Small Utility Boiler, *The Int. Corrosion Forum*, Toronto, Ontario, Canada, 1981, 84.

89. Bruno, L., Deshpande, A. S. and Whaley, H., Coal/Oil Slurry Combustion and Tribology - A Canadian Experience, *Symposium, Coal Slurry Combustion*, Orlando, Fla., 1982, pp.

90. Raask, E., Erosion Wear in Coal Utilization, 1988, Hemisphere Publishing Corporation.

91. Militzer, J., Shiu, D. T. and Watts, K. C., Transactions of the ASME, *Engineering for Gas Turbines and Power*, 1988, 110, pp. 712-713.

92. Finnie, I., Wear, 3, pp. 87-103, 1960.

93. Bitter, J. G. A., Wear, 6, pp. 169-190, 1963.

94. Tilly, G. P., Wear, 23, pp. 87-96, 1973.

95. Hockey, B. J., Wiederhorn, S. M. and Johnson, H., *Erosion of Brittle Materials by Solid Particle Impact,* in "Fracture Mechanics of Ceramics", Bradt, R. C., Hasselman, D. P. H., and Langes, F. F., ed., 1978, Plenum Press: New York, pp. 379-402.

96. Hutchings, I. M., The Erosion of Materials by Liquid Flow, Materials Technology Institute.

97. Levy, A. V., Wear, 108, pp. 1-21, 1986.

98. Sundararajan, G., A Comprehensive Model for the Solid Particle Erosion of Ductile Materials, Wear, 149, pp. 111-127, 1991.

99. van Vlack, L. H., Elements of Materials Science and Engineering, 1989.

100. FLUENT, v. 4.25, 1994, Users Guide, FLUENT Inc.

101. Shepard, J. F., M.S., 1995, The Pennsylvania State University.

102. Ott, L., An Introduction to Statistical Methods and Data Analysis, 1988, Boston: PWS-KENT.

103. Sundararajan, G. and Shewmon, P. G., Wear, 84, pp. 237-258, 1983.

104. Sundararajan, G., Wear, 84, pp. 217-235, 1983.

105. Tirupataiah, Y., Venkataraman, B. and Sundararajan, G., Materials Science and Engineering, A124, pp. 133-140, 1990.

106. Tirupataiah, Y. and Sundararajan, G., *Mech. Phys. Solids*, 1991, 39, pp. 243-271.

107. Brach, R., *Impact Eng.*, 1988, 7, pp. 37-53.

108. MathCad 3.1, 1991, MathSoft Inc., Cambridge, MA.

109. Walsh, P. M., Xie, J., Poe, R. L., Miller, B. G. and Scaroni, A. W., Erosion by Char and Ash Particles and Deposition of Ash on Carbon Steel in the Convective Section of an Industrial Boiler, Corrosion, 50, pp. 82-88, 1994.

110. Jennings, P. L., Borio, R. W., Miller, B. G., Scaroni, A. W. and McGowan, J. G., Installation and Intial Testing of Micronized Coal in a Gas/Oil-Designed Package Boiler, *Proc. of the 19th Int. Tech. Conf. on Coal Util. & Fuel Systems*, Washington, DC, 1994, p. 63.

111. Miller, B. G., Bartley, D. A., Poe, R. L. and Scaroni, A. W., A Comparison between Firing Coal-Water Slurry Fuel and Dry, Micronized Coal in an Oil-Designed Industrial Watertube Boiler, *Proc. of the 20th Int. Tech. Conf. on Coal Util. & Fuel Systems*, Washington, DC, 1995, pp. 267-278.

112. Mitchell, R. E., Hurt, R. H., Baxter, L. L. and Hardesty, D. R., Compilation of Sandia Coal Char Combustion Data and Kinetic Analyses, Milestone Report, Sandia National Laboratories, No. SAND92-8208, UC-361, 1992.

113. Xie, J. and Walsh, P. M., Erosion-Corrosion of Carbon Steel by Products of Coal Combustion, Wear, 99, 1995.

114. Xie, J. and Walsh, P. M., Erosion-Corrosion of Carbon Steel in the Convection Section of an Industrial Boiler Cofiring Coal-Water Fuel and Natural Gas, *Trans. ASME, Journal of Engineering for Gas Turbines and Power*, 1993, (Paper No. 93-JPGC-PWR-23, ASME).

115. Xie, J. and Walsh, P. M., Erosion-Corrosion of Carbon Steel in the Convection Section of an Industrial Boiler, *Engineering Foundation Conference on The Impact of Ash Deposition on Coal-Fired Plant*, 1994, pp. 735-746.

116. Israel, R. and Rosner, D., Use of a Generalized Stokes Number to Determine the Aerodynamic Capture Efficiency of Non-Stokesian Particles from a Compressible Gas Flow, Aerosol Science and Technology, 2, pp. 45-51, 1983.

117. Serafini, J. S., Impingement of Water Droplets on Wedges and Double-Wedge Airfoils at Supersonic Speeds, National Advisory Committee for Aeronautics, No. 1159, 1954.

118. Walsh, P. M., Beer, J. M. and Sarofim, A. F., Estimation of Aerodynamic Effects on Erosion of a Tube by Ash, *Effects of Coal Quality on Power Plants*, 1988, pp. 2-19 – 2-34.

119. Xie, J., Walsh, P. M., Miller, B. G. and Scaroni, A. W., Evaluation of Erosion-Corrosion and Ash Deposition in the Convection Section of an Industrial Watertube Boiler Retrofitted to Fire Coal-Water Fuel, *Proc. of the 19th Int. Tech. Conf. on Coal Util. & Fuel Systems*, Washington, D.C., 1994, pp. 721-732.

120. Stultz, S. C. and Kitto, J. B., ed. STEAM: Its Generation and Use. 40 ed. 1992, Babcock & Wilcox.

121. Miller, B. G., Bartley, D. A., Morrison, R., Poe, R. L., Sharifi, R., Shepard, J. F., Xu, G., Scaroni, A. W., Hogg, R., Chander, S., Cho, H., Ityokumbul, M. T., Klima, M. S., Luckie, P. T., Rose, A., Addy, S., Considine, T. J., Gordon, R. L., Lazo, J., Li, P. C., McClain, K., Schaal, A. M., Szczesniak, P., Walsh, P. M., Xie, J., Painter, P. C., Veytsman, B., Morrison, D., Englehardt, D. and Sommer, T. M., The Development of Coal-Based Technologies for Department of Defense Facilities, Interim Report for the Period 03/27/1994 to 07/30/1994, DOE/PETC, No. DE-FC22-92PC92162, November 30, 1994.

122. Miller, B. G., Bartley, D. A., Morrison, R., Poe, R. L., Sharifi, R., Shepard, J. F., Xu, G., Scaroni, A. W., Hogg, R., Chander, S., Cho, H., Ityokumbul, M. T., Klima, M. S., Luckie, P. T., Rose, A., Addy, S., Considine, T. J., Gordon, R. L., Lazo, J., Li, P. C., McClain, K., Schaal, A. M., Szczesniak, P., Walsh, P. M., Xie, J., Painter, P. C.,

Veytsman, B., Morrison, D., Englehardt, D. and Sommer, T. M., The Development of Coal-Based Technologies for Department of Defense Facilities, Semiannual Report for the Period 03/28/1994 to 09/27/1994, DOE/PETC, No. DE-FC22-92PC92162, April 14, 1995.

123. Miller, B. G., Pisupati, S. V., Poe, R. L., Morrison, J. L., Xie, J., Walsh, P. M., Wincek, R. T., Clark, D. A. and Scaroni, A. W., Superclean Coal-Water Slurry Combustion Testing in an Oil-Fired Boiler, Semiannual Technical Progress Report for the Period 08/15/1992 to 02/15/1993, DOE/PETC, No. DE-FC22-89PC88697, April 21, 1993.

124. Englehardt, D. A., Personal Communication, 1993.

125. Huettenhain, H. H., Venkatachari, M. K. and Schall, A. M., Advanced Physical Fine Coal Cleaning, Final Report, Bechtel National, Inc., DOE/PETC, No. DE-AC22-85-PC81205, September 1988.

126. Wan, E. I. and Fraser, Low-Sulfur Coal-Water Fuel to Retrofit a Coal Fired Utility Boiler to Comply with U.S. Clean Air Act Amendments of 1990, *18th Int. Tech. Conf. on Coal Util. & Fuel Systems*, Clearwater, Florida, 1993.

127. McHale, E. T., Paul, A. D. and Bartis, J. T., Integrated Coal Preparation and CWF Processing Plant: Conceptual Design and Costing, Final Technical Report, DOE/PETC, No. DE-AC22-89-PC88400, December 1992.

128. Sheng, R., Development of Screening and Life Cycle Cost Models for New Pulverized Coal-Fired Heat Plants, Final Technical Report, Institute of Gas Technology, U.S. Army Corps of Engineers, No. December 1992.

129. Jelen, F. C. and Black, J. H., Cost and Optimization Engineering, 1983, New York: McGraw-Hill Book Company.

130. (EIA), Electric Power Monthly, DOE/EIA, Office of Coal, Nuclear, Electric and Alternative Fuels, No. DOE/EIA-0226 (93/04), April 1993.

131. Combustion, Engineering., Combustion and Fuel Characterization of Coal-Water Fuels, Final Report, DOE, No. DE-AC22-82PC50271, February 1989.

132. Alderman, J. K., An Integrated Approach to Coal-Water Mixture Production, Coal Liquid Mixtures: The Pathway to Commercialization, Pasha Publications Inc.

133. Weston, M. D. and Hill, R. A., Planning a Large Coal Slurry Project, *Proc. of the Eighth Int. Conf. on Slurry Transportation*, 1983.

134. EPRI, Coal-Water-Slurry Transportation Alternatives, Texas Eastern Engineering, Ltd., No. CS-5053, 1987.

8.0 SELECTED NOMENCLATURE

E = dimensionless erosion rate of the orifice surface

n = strain hardening exponent

C = constant characterizing the temperature dependence of the flow stress, K^{-1}

V = impact velocity, m s^{-1}

$F(t)$ = material constant

C_p = specific heat, J kg^{-1} K^{-1}

e = coefficient of restitution

Greek Letters

α = impact angle

μ = friction coefficient of particle/surface system

μ_c = critical friction coefficient

λ = particle shape factor; $0 \leq \lambda \leq 3$

9.0 ACKNOWLEDGMENTS

Funding for the work was provided by the U.S. Department of Defense (via an interagency agreement with the U.S. Department of Energy) and the Commonwealth of Pennsylvania under Cooperative Agreement No. DE-FC22-92PC92162. The project is being managed by the U.S. Department of Energy, Federal Energy Technology Center (FETC) at Pittsburgh, Pennsylvania. Anthony Mayne of FETC is the project manager.

The following Penn State staff were actively involved in the program: Michael Anna, David A. Bartley, Abigail Bitner, Scott Briton, David Clark, Paul Colose, David DeCapria, Glenn Decker, Howard R. Glunt, Sam Gross, Kathleen Gummo, Gregory Hargrove, Michael Hill, Robert Klemz, John Kovalchick, Ruth Krebs, Scott Lyons, Bradley Maben, Penny Maben, Carl Martin, Susan Rockey, Christopher Snyder, Anthony Stempkowski, Joseph Suefert, Ronald Wasco, Robert Wells, Timothy Wilkinson, Ronald T. Wincek, and Guheng Xu.

The following Penn State graduate research assistants contributed to this research effort: Mohamed Fofana, Sian Hu, Bruce Kim, Miriam Leffler, Udayini Pendyala, Hurriyet Polat, Mehmet Polat, Jayanta Sarkar, Russell Smith, Robert Weiland, and DaoDe Xu.